NASA Contractor Report 4257
DOT/FAA/CT–87/22

An Experimental Method for Measuring Water Droplet Impingement Efficiency on Two- and Three-Dimensional Bodies

M. Papadakis, R. Elangonan, G.A. Freund, Jr.,
M. Breer, G.W. Zumwalt, and L. Whitmer

GRANT NAG3–566
NOVEMBER 1989

National Aeronautics and
Space Administration

NASA Contractor Report 4257
DOT/FAA/CT–87/22

An Experimental Method for Measuring Water Droplet Impingement Efficiency on Two- and Three-Dimensional Bodies

M. Papadakis
Wichita State University
Wichita, Kansas

R. Elangonan, G.A. Freund, Jr., and M. Breer
Boeing Military Airplanes
Wichita, Kansas

G.W. Zumwalt
Wichita State University
Wichita, Kansas

L. Whitmer
Boeing Military Airplanes
Wichita, Kansas

Prepared for
Lewis Research Center and
the Federal Aviation Administration
under Grant NAG3–566

National Aeronautics and
Space Administration

DOCUMENT AVAILABILITY CHANGE NOTICE

NASA Contractor Report 4257

An Experimental Method for Measuring Water Droplet Impingement Efficiency on Two- and Three-Dimensional Bodies

M. Papadakis, R. Elangonan, G.A. Freund, Jr., M. Breer, G.W. Zumwalt, and L. Whitmer

November 1989

ABSTRACT

An experimental method has been developed to determine the droplet impingement characteristics on two and three-dimensional bodies. The experimental results provide the essential droplet impingement data required to validate water droplet trajectory codes, which are used in the analysis of aircraft icing.

A body, whose water droplet impingement characteristics are required, is covered at strategic locations by thin strips of moisture absorbing (blotter) paper, and is exposed to an air stream containing a water-dye solution spray cloud. Water droplet impingement data are extracted from the dyed blotter strips by measuring the optical reflectance of the dye deposit on the strips, using an automated reflectometer.

Models tested include a 4 inch diameter cylinder, a NACA 65_2015 airfoil section, a MS(1)-0317 supercritical airfoil section, three simulated ice shapes, an axisymmetric inlet and a Boeing 737-300 inlet model.

Detailed descriptions of the dye-tracer technique, instrumentation, data reduction method and the results obtained are presented in this report. Analytical predictions of collection efficiency characteristics for most test configurations are included for comparison.

FOREWORD

The authors wish to acknowledge the cooperation and assistance they have received from many quarters; in particular, they would like to express their appreciation to the NASA Lewis Research Center and the Federal Aviation Administration (FAA) Technical Center for funding this research.

The authors would like to express their special thanks to: Dr. J. Kim, Mr. W. Seibel and Mr. M. Smith of Boeing Military Airplanes (BMA), Wichita, for providing analytical trajectory data used in this study; and the Optics Laboratory personnel of BMA who provided important help and information on the method of data reduction.

Thanks are due to: Dr. J. Riley of the FAA for his encouragement and support, Dr. R. J. Shaw and Mr. J. Newton of NASA Lewis for helping with the tests and for supplying the data on droplet distributions; Dr. W. Olsen of NASA Lewis for his comments and the use of some unpublished material; the NASA Lewis Icing Research Tunnel personnel for their help with the wind tunnel tests; and Mr. R. Nussle of NASA Lewis for his technical assistance throughout the testing.

The authors would also like to thank: Mr. A. Porter of Wichita State University who manufactured and helped with the design of the various components used in the tests; Mrs. J. Combs of BMA for her help in preparing many of the computer plots of the analysis results; Mrs. E. Chrisco of BMA for her help in data reduction; and Giao Vu, for typing the original manuscript.

Finally, the authors would like to acknowledge those who read the manuscript and commented on it.

TABLE OF CONTENTS

TABLE OF CONTENTS

TABLE OF CONTENTS

TABLE OF CONTENTS

TABLE OF CONTENTS

EXECUTIVE SUMMARY

The design of ice protection systems requires knowledge of the droplet impingement characteristics of the surface to be protected. Computer codes capable of predicting trajectories of particles impinging on internal and external surfaces of two-dimensional, axi-symmetric, and three-dimensional bodies have recently been developed by National Aeronautics and Space Administration (NASA), industry, and universities. The application of these codes to icing analysis requires validation against experimental data. Prior to the work described in this report, water droplet trajectory codes were evaluated by comparison with two-dimensional data on cylinders and airfoils generated by the National Advisory Committee for Aeronautics (NACA) in the 1950's using a dye tracer technique and colorimetric analysis. This data base was limited in scope and, in particular, was confined to low-speed studies of airfoil sections of interest to the aviation community in the 1940 to 1955 time period. No experimental impingement data were available for modern airfoil sections, engine inlets, or other three-dimensional configurations.

To provide the experimental data base required today, a joint Wichita State - Boeing Military Airplanes research program sponsored by the NASA and the Federal Aviation Administration was initiated in August 1984. The specific accomplishments of this project are listed below:

1. Development of a laser reflectance method for measuring local droplet impingement efficiency on a variety of aerodynamic surfaces in two-dimensional and three-dimensional flows. This method is accurate and more efficient than colorimetric analysis.

2. Experiments were performed to verify the accuracy of the laser reflectance method.

3. Testing of several modern airfoil sections as well as wing and engine inlet geometries for inclusion in a comprehensive experimental data base.

4. Development of an automated data reduction system to make practical the acquisition and reduction of large amounts of data.

5. Correlation of the experimental data with computer code predictions.

1.0 INTRODUCTION

Aircraft flying at subsonic speeds through clouds below about 8000 meters can be subject to ice formation on critical aerodynamic surfaces. Ice accretion results from very small supercooled droplets (droplets cooled below freezing), usually 5 to 50 microns in diameter, which can freeze upon impact with the aircraft surface. The local and total rates of droplet impingement as well as the extent of the impingement are important design considerations for aircraft ice protection systems.

Ice usually is accreted on the forward facing surfaces only, giving a few centimeters thickness on the front (approximately two percent) of the wing chord. However, this can be enough to cause flow separation and decrease lift, particularly if the aircraft slows or maneuvers. In addition, drag may increase enough to exhaust fuel reserves or cause flight instability. Helicopter rotors are even more vulnerable to the detrimental effects of ice, and engine inlet diffusers (internal surfaces) require icing protection to a greater degree than lifting surfaces (external surfaces). Thus, aircraft must be designed with the necessary equipment required for ice removal or prevention. Basically, ice protection systems can be classified as either de-icing or anti-icing.

The de-icing (or ice removal) principle involves the periodic removal of a layer of ice by mechanical, thermal or chemical means. This is accomplished by destroying the adhesion strength between the ice and the aircraft surfaces. De-icing systems have low energy requirements; however, periodic ice-removal results in higher aerodynamic penalties. The anti-icing (or ice prevention principle) involves the prevention of ice formation on the protected area at all times by using thermal energy or Freezing Point Depressant (FPD). These methods minimize aerodynamic losses but either require large amounts of energy or substantial weight penalty. Examples of de-icing and anti-icing systems and typical applications are shown in Table 1.

The choice between anti-icing and de-icing techniques depends upon the component geometry, energy requirements and its function. Verification of these techniques and methods for testing can be found in Reference 1. Other factors such as the energy source utilized, the sensitivity of the component and the total energy available for ice protection must be considered.

The design of de-icing systems requires knowledge of the extent and shape of the ice accreted as well as the allowable level of ice accretion, before removal of ice is necessary. This information is directly related to droplet impingement characteristics of the surface to be de-iced. Anti-icing systems are designed based on information of local as well as total droplet impingement intensities in order to evaluate the necessary energy requirements. Thus, the determination of water droplet impingement characteristics on aircraft surfaces is a fundamental task in determining aircraft icing protection requirements.

TABLE 1

TYPICAL EXAMPLES AND APPLICATIONS OF ANTI-ICING AND DE-ICING AIRCRAFT SYSTEMS

SYSTEM	SOURCE	TYPICAL AIRCRAFT APPLICATION
(a) anti-icing	electrothermal	propellers, windshield
	hot air (bleed air)	wings, engine inlets
	chemical (freezing point depressants)	wings, propellers
(b) de-icing	pneumatic boot	wings, empennage
	electrothermal	helicopter rotor blades
	electromagnetic impulse	wings, engine inlets
	chemical (freezing point depressants)	wings

Advances in computer technology in recent years have led to the development of analytical codes capable of performing icing analyses. These computer programs are used by industry as a cost effective tool for evaluating icing protection requirements of aircraft components. The codes can also be used to assist in the testing and certification of aircraft.

Computer codes capable of predicting trajectories of particles impinging on internal and external surfaces of two-dimensional, axisymmetric, and three-dimensional bodies have been developed by NASA, industry and universities. The application of these codes to icing analysis requires validation against experimental data. Historically, water droplet trajectory codes have been evaluated by comparison with available two dimensional data on cylinders and airfoils generated by NACA in the 1950's using a dye tracer technique (Reference 2). In general, the codes appear to give reasonably good agreement with experimental results which themselves may be subject to some appreciable errors. However, this data base is limited in scope and, in particular, is confined to low speed studies of airfoil sections of interest to the aviation community in the 1940 to 1955 time period. No experimental water droplet impingement data are available for modern technology airfoil sections. Such data are obviously required to validate trajectory codes for current wing and airfoil configurations.

In addition, it should be pointed out that almost no water droplet impingement data exist for inlet configurations. Modern aircraft inlets

have complex geometries which result in highly three dimensional flows. Droplet trajectory codes must be extensively validated against experimental data obtained for such geometric flow conditions. The validation of these codes for water droplet calculations will also enhance their application to the design and analysis of VSTOL engine inlet sand particles separators (Reference 3) and engine blade erosion studies. No method has been proposed for experimentally determining solid particle collection coefficients. However, since the equations for solid and liquid particles differ only in the density, a liquid droplet code which is validated by experiment gives credance to the use of the code for solid particles.

To provide the required experimental data base, a joint Wichita State University (WSU) - Boeing Military Airplanes (BMA) research program sponsored by the National Aeronautics and Space Administration (NASA) and the Federal Aviation Administration (FAA) was initiated in August 1984. The specific objectives of this research project are listed below:

a. Develop an efficient and accurate method of measuring local droplet impingement efficiency on a variety of aerodynamic surfaces in two-dimensional and three-dimensional flows.

b. Develop experiments to verify the method.

c. Test several state-of-the-art airfoil sections as well as wing and engine inlet geometries to produce a comprehensive experimental data base.

d. Develop an automated data reduction system to make practical the acquisition and reduction of a large mass of data.

e. Correlate experimental data with analytical results.

Models tested in this study include a 4 inch diameter cylinder, a NACA 65_2015 airfoil, an axisymmetric engine inlet, a supercritical airfoil and a three-dimensional Boeing 737-300 engine inlet model which represents the most difficult test case. All tests were conducted in the NASA Lewis Icing Research Tunnel (IRT) in June and September 1985.

This report presents detailed descriptions of the experimental method developed, instrumentation, models tested, test conditions, data reduction system and experimental data. In addition, correlations of analytical and experimental data are provided for most test cases.

2.0 EQUATIONS OF DROPLET MOTION AND IMPINGEMENT PARAMETERS

The phenomenon of droplet impingement on a body is better understood by examining the various parameters that influence the droplet trajectories. In the next section, the non-dimensional droplet trajectory equations are presented together with the main assumptions made in deriving these equations. In addition, some non-dimensional impingement parameters which are commonly used in the presentation of theoretical and experimental impingement data are discussed. The dependent impingement parameters are defined for clouds with uniform and nonuniform droplet size distributions.

2.1 Differential Equation of Particle Trajectory

The forces on a small spherical droplet moving in the steady flow of air are droplet drag, weight and buoyancy. The predominant force acting on a droplet is the fluid dynamic drag arising from the relative (slip) velocity of air with respect to the droplet (Reference 4). The particle equation of motion in non-dimensional form is (Appendix D):

$$\frac{dU_i}{dt} = \frac{C_D(R_v) \cdot R_v \cdot (V_i - U_i)}{24K} - \frac{(1-\sigma)gL\delta_{i2}}{V_\infty^2} \qquad (2\text{-}1)$$

where:

$K = \rho_p V_\infty d^2/18\mu L$, inertia parameter of droplet.

t = time , dimensionless with L/V_∞.

$\sigma = \rho/\rho_p$, density ratio of air to particle.

L = Characteristic dimension of body.

R_v = Relative Reynolds number of droplet.

U_i = i^{th} directional component of particle velocity, dimensionless with V_∞.

V_i = i^{th} directional component of air velocity, dimensionless with V_∞.

($i = 1$ x – direction, $i = 2$ y – direction, $i = 3$ z – direction)

The derivation of Equation (2-1) is based on the following assumptions:

-- Single phase (air) flow about the body; air flow is not disturbed by the presence of droplets

-- Quasi-steady-state approximation: at each instant and position the steady-state drag and other forces act on the particle

-- Compressible or incompressible potential flow field of the gas phase about the body

-- Particles of spherical shape

-- Viscous flow effects such as thick boundary layer formation and flow separation are not considered.

The above mathematical model is a valid approximation for typical icing conditions within the intermittent and continuous maximum icing envelopes of the FAA (Reference 5). The maximum concentration and mean volumetric diameter (MVD) of droplets for these conditions are:

INTERMITTENT MAXIMUM		CONTINUOUS MAXIMUM	
LWC Max	3.0 g/m^3	LWC Max	0.8 g/m^3
MVD Max	50 μm	MVD Max	40 μm

For the concentrations and sizes of droplets expected to occur within icing clouds, the assumptions of undisturbed airflow and spherical shape (due to surface tension) of droplets are quite valid.

Given an expression for $C_D(R_V)$, the drag coefficient of the droplet as a function of the relative Reynolds number of the droplet, Equation (2-1) can be integrated numerically to find the particle trajectory path.

An example of C_D as a function of R_V is given below (Reference 4). This function is used in the computer code discussed in Section 6 of this report.

$$C_D(M,R_v)=C_{D_{inc}}(R_v)/G(M/R_v) \tag{2-2}$$

where:

$C_{D_{inc}}$ = Incompressible sphere drag coefficient.

$G(M/R_v)$ = Cunningham drag correction factor.

The algebraic expressions for the above terms are (References 4 and 6):

(a) $$C_{D_{inc}}(R_v)=C_{D_{Stokes}}(R_v)(1+R_v^{2/3}/6) \tag{2-3}$$

where:

$C_{D_{Stokes}}(R_v) = 24/R_v$

This equation agrees to within about 5 percent of the standard sphere drag curve in the range $0 \leq R_V \leq 1000$ and for particles of diameter less than or equal 1 mm.

(b) $$G(M/R_v) = A/B \tag{2-4}$$

where:

$$A = 1 + \left(M/R_v\right)\left[3.82 + 1.28\exp\left(-1.25R_v/M\right)\right] \tag{2-5}$$

$$B = 1 + \exp\left(-0.427\,M^{-4.63} - 3.0\,R_v^{-0.88}\right)$$

The numerator (A) in Equation (2-4) represents the drag reduction factor to account for the incompressible drag due to the molecular slip or rarefaction effects.

The denominator (B) in Equation (2-4) is the additional correction to account for the Mach number (M) dependence of the particle drag (compressibility) in continuum flow.

Once the droplet trajectories have been calculated, the points of impingement on the body surface can be determined. These impingement points are used to evaluate the impingement parameters described in the following sections.

The trajectory equation can be used to clarify the effect of various flow variables and body geometries on droplet trajectories. In the vicinity of the body, the flow field streamlines deviate from their original straight line paths and flow around the body. A droplet owing to its inertia tends to maintain its original straight line path toward the body and the drag force imposed by the slip velocity of air with respect to the droplet tends to cause the droplet to follow the air streamline around the body. The droplet trajectory is determined by the combined effect of inertial and drag forces. Consider the particle trajectory Equation (2-1) with negligible buoyancy and gravity forces,

$$\frac{dU_i}{dt} = \frac{C_D(R_v) \cdot R_v \cdot (V_i - U_i)}{24K} \tag{2-6}$$

The inertia parameter K is the ratio of inertia force to drag force. For the case of small droplet size, K is small and drag force will exceed that of the inertia force ($K \to 0$, $U_i = V_i$). Hence, the droplets

will tend to follow the streamlines around the body and consequently, many of the droplets which were originally directly ahead of the frontal projected area of the body will miss the body entirely. For large droplets, the inertia force is greater than that of the drag force (K is large and as $K \rightarrow \infty$, U_i = constant). The droplets will tend to maintain their original straight line path and many of the droplets directly ahead of the body will hit the body.

2.2 Impingement Parameters

The main dependent impingement parameters are listed below and their definitions will be given in this section.

a. Local impingement efficiency

b. Total impingement efficiency

c. Maximum limits of impingement

The above parameters are affected by the following:

a. Free stream velocity

b. Body size and shape

c. Body orientation with respect to the flow direction

d. Air density

e. Air viscosity

f. Droplet size (diameter)

g. Droplet distribution

h. Droplet density

2.2.1 Definition of Impingement Parameters for Uniform Droplet Size

2.2.1.1 Local Impingement Efficiency (β)

Consider the flight of a three-dimensional body through a cloud of water droplets of uniform size (monodispersed). Referring to Figure 2.1, the local impingement efficiency (β) for any point on the body surface is defined as local droplet flux rate at the body surface normalized to the free-stream flux rate. Analytically, (β) is simply the ratio of that infinitesimal freestream area (dA_∞) to the corresponding impingement area on the body surface (dA_S), Equation (2-7). This definition follows from the continuity of droplet mass flow.

$$\beta = dA_\infty / dA_s \tag{2-7}$$

A second definition of local impingement efficiency used by experimentalists is given by equation (2-8).

$$\beta = \left\{ \frac{\text{Amount of water caught on infinitesimal area of surface in a given unit of time}}{\text{Amount of water which could be caught in that time on that area if the trajectories were straight lines parallel to the free-stream velocity direction and if the area was oriented to be perpendicular to the trajectories}} \right\} \tag{2-8}$$

It should be noted here that Equation (2-8) applies to non-uniform as well as monodispersed droplet distributions.

2.2.1.2 Total Impingement Efficiency (E)

The total impingement efficiency (E) for an arbitrary three-dimensional body in a cloud of uniform droplet size is defined as:

$$E = \frac{1}{A_f} \int \beta \, dA_s = \frac{1}{A_f} \int \frac{dA_\infty}{dA_s} dA_s = \frac{A_{\infty,m}}{A_f} \tag{2-9}$$

where:

$A_{\infty,m}$ = Total area through which all the droplets impinging on the body must pass at some point at a large distance ahead of the body

A_f = Projected frontal area of the body

Both $A_{\infty,m}$ and A_f are taken perpendicular to the free-stream direction.

2.2.1.3 Impingement Limits (s_m/L)

Droplet trajectories for a two-dimensional body are shown in Figure 2.2. Droplets which start out at progressively larger initial ordinates (y_∞'s) measured from the reference line will strike the body progressively farther back along the surface until a maximum value

($y_{\infty,m}$) is obtained. The trajectory originating at $y_{\infty,m}$ will be tangent to the surface of the body at point P. Droplets starting at ordinates greater than $y_{\infty,m}$ will miss the body entirely. Thus, the distance s_m measured along the body surface from a reference point on the body to point P is called the limit of impingement. This distance is usually expressed in dimensionless form by dividing s_m by the characteristic length (L) of the body.

In two-dimensional flows, there are two impingement limits, an upper and a lower or an outer and an inner, depending on whether the flow is wholly external (e.g., airfoil section) or partly internal (e.g., engine inlet). For three-dimensional bodies, the limits of impingement may vary circumferentially along the body surface as shown in Figure 2.3.

2.2.2 Clouds with Non-Uniform Droplet Distribution

Both natural and artificial icing clouds consist of droplets of various sizes and droplet number densities. The main parameters commonly used to describe a cloud of droplets, for the purpose of droplet impingement characteristics, are:

a. Liquid Water Content (LWC)

b. Cloud Droplet Distribution

c. Droplet Mean Volumetric Diameter (MVD)

2.2.2.1 Liquid Water Content

The liquid water content (LWC) of a cloud is the amount of water contained in a given volume of cloud. LWC is usually given in grams of water per cubic meter of cloud. Typical LWC_{Max} values for icing clouds are listed in Section 2.1.

For a cloud which is artificially produced, the amount of water injected into the airstream is fixed by the water and/or air pressures of the given spray system which produces the cloud.

2.2.2.2 Cloud Droplet Distribution

The distribution of droplets in a cloud can be expressed in various graphical forms. The four types of distributions which are most commonly used are:

a. Number density of droplets versus droplet diameter

b. Percent of liquid water content versus droplet diameter

c. Percent of liquid water content versus droplet diameter normalized to mean volumetric diameter.

d. Percent cumulative liquid water content versus droplet diameter normalized to mean volumetric diameter.

It is relatively easy to transform one distribution into any one of the others. For the last two distributions, however, the mean volumetric diameter must be known. The above distributions can be given in discrete or continuous form. Examples of the distributions listed above are shown in Figure 2.4. For convenience and computational efficiency, a discrete form of Figure 2.4d is commonly used for analysis.

A uniform cloud is one with a spacially invariant LWC and droplet distribution. Clouds with spacially invariant droplet distributions, however, do not necessarily have a uniform LWC distribution. This is true for naturally and artificially produced clouds. For example, it is thought that the spray cloud in the NASA Lewis IRT does not exhibit a completely uniform LWC, while it does have a spacially uniform droplet distribution. This is sufficient to determine impingement efficiency in the IRT if the free-stream LWC is measured at appropriate locations as was done in actual testing.

A distribution which has been employed in various analytical studies is the Langmuir "D". This distribution (see Figure 2.5) and other similar ones were established by Langmuir (Reference 8) by matching the data from natural-icing cloud measurements made on Mt. Washington. The rate of deposition of ice on slowly rotating cylinders exposed to supercooled clouds blowing over the summit was correlated with that of theoretical calculations (Reference 2). Comparisons of Langmuir "D" distribution and the droplet distributions produced by the spray nozzles used in this test are given in Appendix E.

2.2.2.3 Mean Volumetric Diameter

By definition, the mean volumetric diameter (MVD) of a droplet distribution is that droplet diameter for which half the total liquid water content is contained in droplets larger than the mean and half in droplets smaller than the mean.

Given a droplet distribution as shown in Figure 2.5, the MVD can be calculated as follows. For a continuous distribution, if n(d) is known as a function of d and assuming unit cloud volume then MVD can be calculated from

$$\frac{\frac{\pi}{2}\rho_w \int_{d_{min}}^{MVD} n(x) \cdot x^2 \cdot dx}{\frac{\pi}{2}\rho_w \int_{d_{min}}^{d_{max}} n(x) \cdot x^2 \cdot dx} = 0.5 \qquad (2\text{-}10)$$

where x is the droplet diameter d.

If a discrete distribution is given with N discrete groups of droplets such that $n_i(d_i)$ is the number of particles in group i having diameters between d_i and $d_i + \delta d$ then Equation (2-10) can be written as:

$$\frac{\frac{\pi}{6}\rho_w \sum_{i=1}^{K} n_i(d_i) \cdot d_i^3}{\frac{\pi}{6}\rho_w \sum_{i=1}^{N} n_i(d_i) \cdot d_i^3} = 0.5 \qquad (2\text{-}11)$$

where d_K, the diameter of group K, is equal to MVD and ρ_w is the density of water.

2.2.3 Definition of Impingement Parameters for Clouds of Non-Uniform Droplet Size

The dimensionless dependent impingement parameters β, E and s_m/L are defined in this section for a cloud of non-uniform droplet size. It is assumed that the droplet distribution, in discrete or continuous form, and the liquid water content of the cloud are known.

2.2.3.1 Local Impingement Efficiency ($\bar{\beta}$)

For a continuous distribution, the impingement efficiency is given by Equation (2-12).

$$\bar{\beta} = \frac{1}{w_t} \int_0^{w_t} \beta \cdot dw \qquad (2\text{-}12)$$

where β is a function of drop size and therefore can be expressed as a function of w, the liquid water content for a given drop size.

For a discrete cloud distribution such as the one shown in Figure 2.4d, $\bar{\beta}$ is defined as the weighted average of the local impingement efficiencies due to each droplet group in the cloud. Let w_t be the liquid water content of the cloud, Δw_i be the partial liquid water content contained in the droplets of size (d_i), in the group (i) of the distribution, and N be the total number of discrete size droplet groups available.

For a body exposed to a cloud with such a droplet distribution, the local impingement efficiency due to a single droplet group of size d_i is β_i, where β is defined by Equation (2-7) or (2-8). The local impingement efficiency due to all N groups in the distribution over an infinitesimal area of the body is given by Equation (2-13).

$$\bar{\beta} = \frac{1}{w_t} \sum_{i=1}^{N} \beta_i \cdot \Delta w_i \qquad (2\text{-}13)$$

2.2.3.2 Total Impingement Efficiency ($\bar{E}$)

The total impingement efficiency of a three dimensional body exposed to a cloud with a given droplet distribution is

$$\bar{E} = \frac{1}{A_f} \int \bar{\beta} \cdot dA_s \qquad (2\text{-}14)$$

where:

A_f is the projected frontal area of the body

dA_s is an infinitesimal impingement area on the surface of the body.

In order to integrate Equation (2-14), $\bar{\beta}$ must be known as a function of surface location. Such a function can be defined from experimental or analytical results.

2.2.3.3 Impingement Limits $(s_m/L)_{max}$

A droplet distribution consists of droplets of diameters varying from d_{min} to d_{max}. For each droplet diameter, impingement limits can be established for a given body and flow conditions as explained in Section 2.2.1.3. Clearly, distributions with larger droplets will result in larger impingement limits. This defines the maximum impingement limits which are denoted by $(s_m/L)_{max}$.

2.3 Local Impingement Rate

To calculate the amount of water collected on a small area of the body where the local impingement efficiency value is known, the following equation can be used.

$$\bar{W}_\beta = 0.3296\, V_\infty w_t \bar{\beta} \qquad (2\text{-}15)$$

where:

$\bar{W}_\beta$ – Local impingement rate ~ lb/hr ft^2

V_∞ = Free stream velocity ~ mph

w_t = Total liquid water content ~ g/m^3

$\bar{\beta}$ = Local impingement efficiency

0.3296 = Conversion factor for units used.

2.4 Concluding Remarks

The evaluation of the dependent impingement parameters can be done by analytical or experimental means. The experimental approach is taken in this work in order to produce a data base for the validation of trajectory computer codes.

To summarize, experimentally determining the water droplet impingement characteristics on an aerodynamic surface traveling through a cloud requires determination of:

a. Local collection efficiency distributions including limits of impingement as a function of droplet size.

b. The liquid water content and droplet size distribution contained within the icing cloud.

The development of an experimental method to accurately and efficiently acquire a validation data base for water droplet trajectory codes is a very difficult task. The complex flow fields and geometries involved and the problems associated with measuring droplet size and distribution in a cloud constitute part of the problem. Capturing droplets of the size of 5 to 50 microns on a surface without disturbing the local flow and evaluating the local water accumulation rates for a large variety of test conditions make the problem even more involved. Of all aircraft components, the three dimensional engine inlet represents the most challenging case, due to of variations in local geometry, inlet mass flows and angle of attack effects.

Finally, consideration must also be given to the method to be employed for reducing to engineering units the large amount of data that would be produced from such tests. The technique must be time efficient and versatile enough to handle all test cases under consideration. In addition, there is a need to test many models to develop a comprehensive data base.

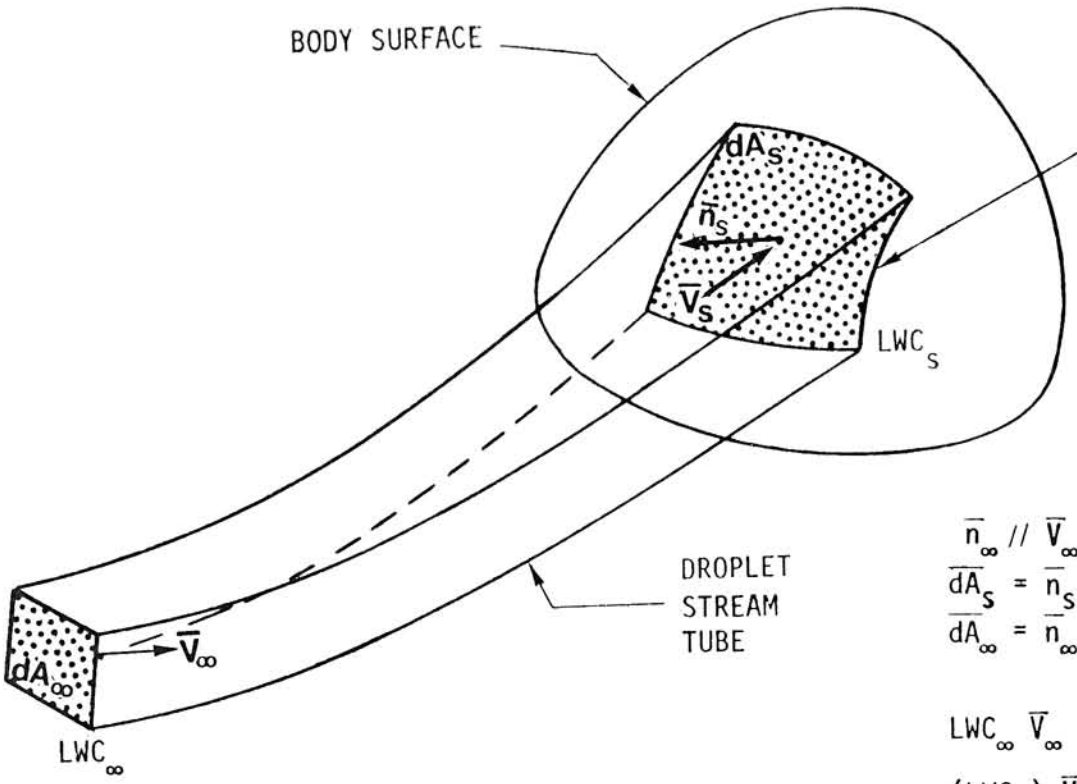

$$\bar{n}_\infty \,//\, \bar{V}_\infty$$

$$\overline{dA_s} = \bar{n}_s dA_s$$

$$\overline{dA_\infty} = \bar{n}_\infty dA_\infty$$

$$LWC_\infty \, \bar{V}_\infty \cdot \overline{dA_\infty} = LWC_s \, \bar{V}_s \cdot \overline{dA_s}$$

$$(LWC_\infty) \, \bar{V}_\infty \cdot \overline{dA_\infty} = LWC_s (-\bar{n}_s \cdot \bar{V}_s) dA_s$$

$$\beta = \frac{dA_\infty}{dA_s} = \frac{LWC_s(-\bar{n}_s \cdot \bar{V}_s)}{LWC_\infty \, V_\infty}$$

FIGURE 2.1

DEFINITION OF LOCAL IMPINGEMENT EFFICIENCY (β) FOR A THREE-DIMENSIONAL BODY IN A CLOUD OF UNIFORM DROPLET SIZE

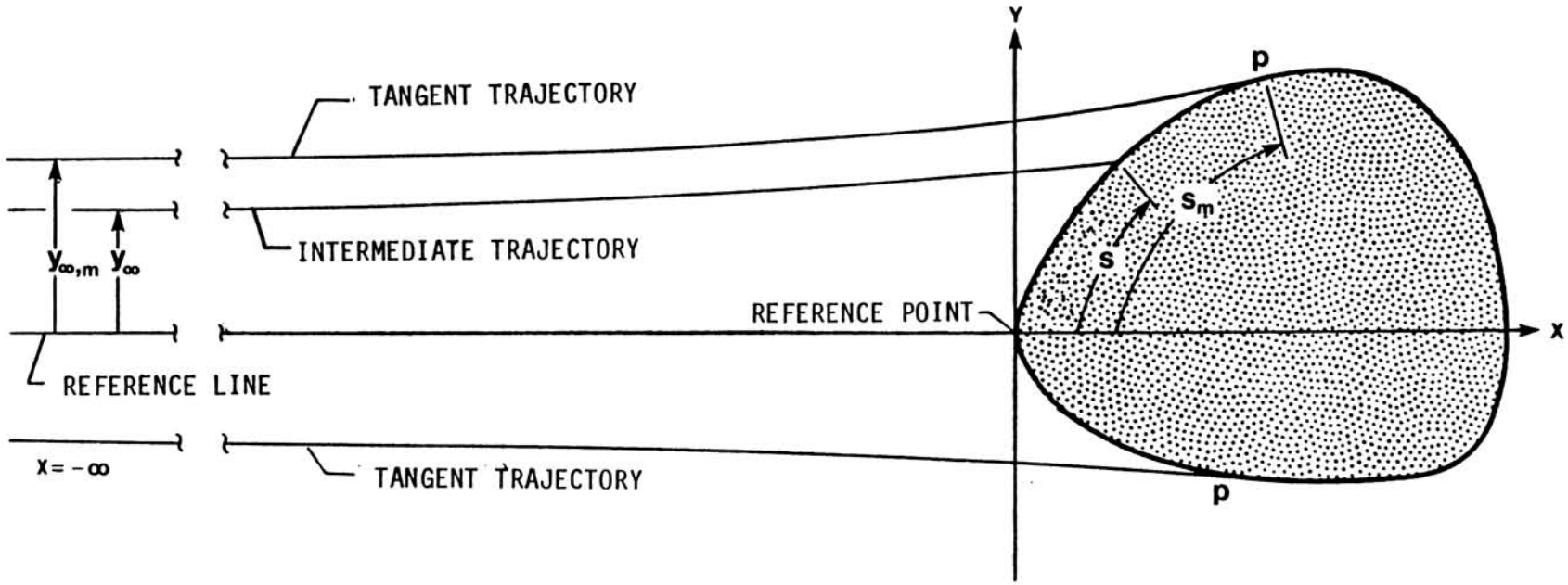

FIGURE 2.2

DROPLET TRAJECTORIES FOR A TWO-DIMENSIONAL BODY IN A CLOUD OF UNIFORM DROPLET SIZE

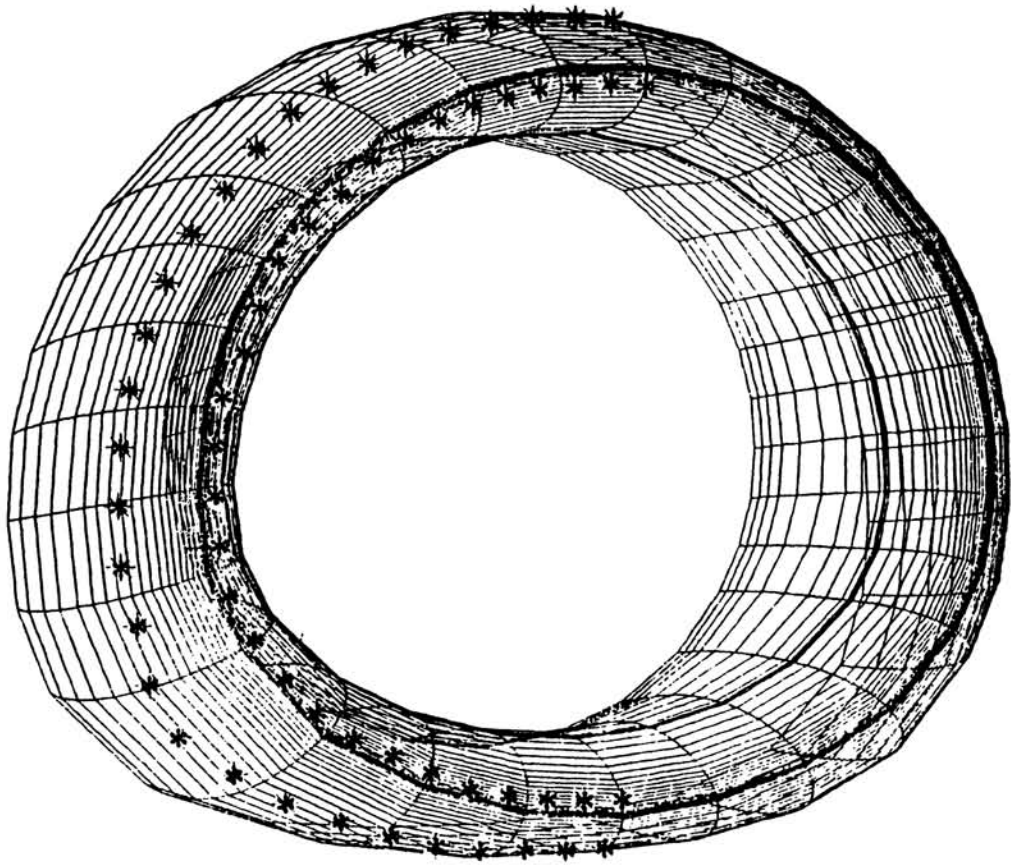

FIGURE 2.3

IMPINGEMENT LIMITS FOR AN ENGINE INLET AT $\alpha = 0°$

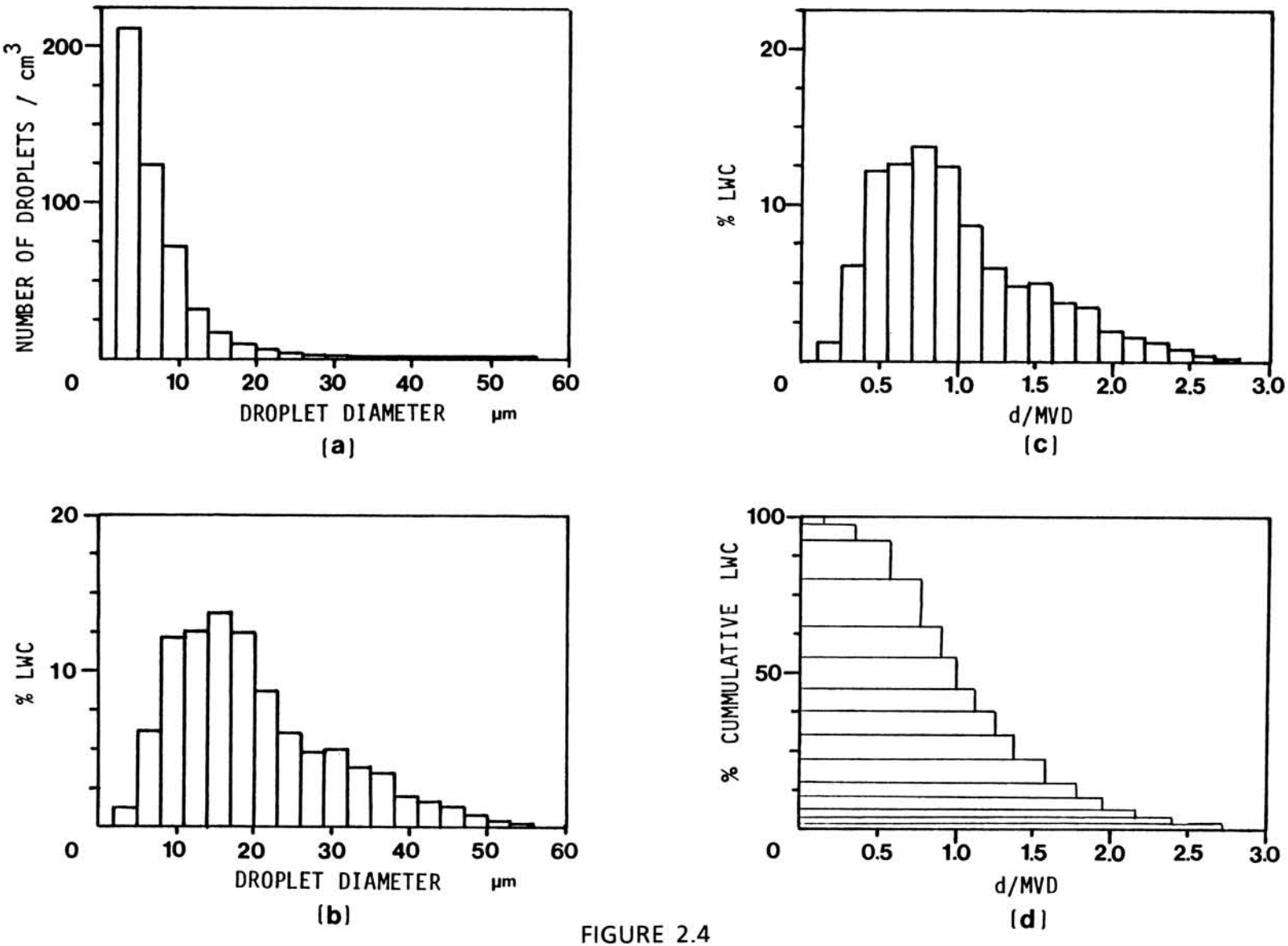

FIGURE 2.4

TYPES OF DISCRETE CLOUD DROPLET DISTRIBUTIONS

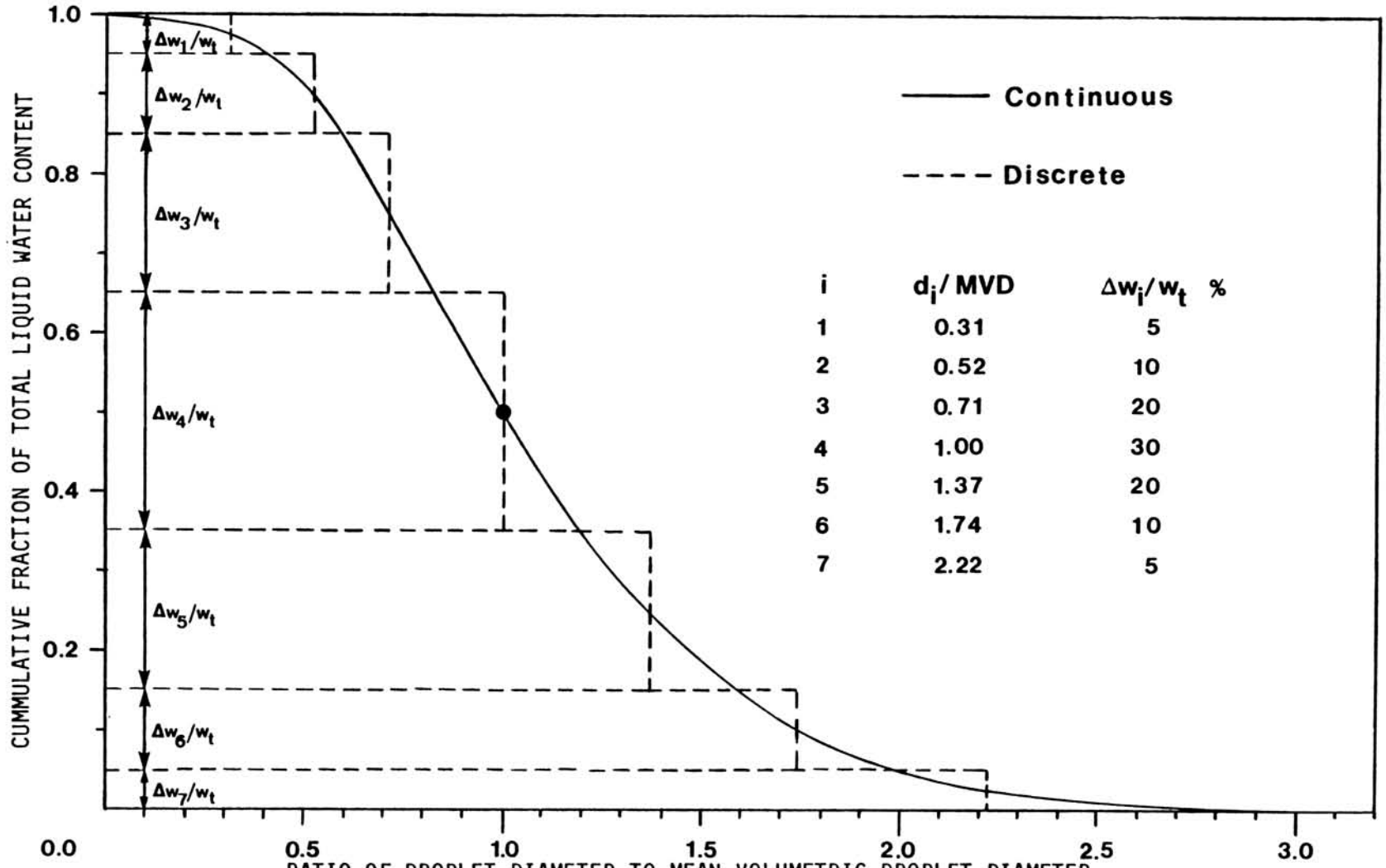

FIGURE 2.5

LANGMUIR "D" DIMENSIONLESS DISTRIBUTION OF DROPLET SIZES

3.0 EXPERIMENTAL METHOD

3.1 Dye-Tracer Technique

A dye-tracer technique of measuring local impingement efficiency on a number of two-dimensional aerodynamic surfaces and some axisymmetric bodies at small angles of attack was developed by NACA in the 1950's (Reference 2).

In this technique, water containing a small amount of water-soluble dye was injected in the form of droplets into the air stream ahead of the body by means of spray nozzles. The surface of the body was covered with an absorbent material upon which the dyed water impinged and was absorbed. At the point of impact and droplet absorption, a permanent dye deposit (dye trace) was obtained. The amount of dye per unit area deposited in a measured time interval was determined by colorimetric analysis.

The impingement limits were obtained directly from the rearmost dye trace on the absorbent material. The dye analysis consisted of removing the dye impregnated absorbent material from the body and punching out small segments of the material for the determination of local impingement characteristics (see Figure 3.1). The dye was dissolved out of each segment in a known quantity of water. The weight of dye in this solution was determined by the amount of light of a suitable wavelength transmitted through the solution by use of a calibrated colorimeter (see Section 5.3.3). From knowledge of the original concentration of the dye in the water droplets, the weight of dye collected per unit area was converted into the weight of water which impinged at any surface location per unit time. This conversion assumes no evaporation of the droplets occurred in the air stream.

The liquid water content in the cloud was determined using an aspirating device (Reference 2). This device consisted essentially of a tube which sucked in the approaching air and cloud droplets at the free stream velocity (inlet velocity ratio 1.0) so that both the air streamlines and droplets entered the tube along straight-line paths. All the dyed droplets were deposited on a filter mounted within the tube, leaving a dye trace which could be analyzed using colorimetric analysis.

The droplet size distribution was determined by comparing experimental local impingement rates on cylinders of different sizes with theoretical predictions of droplet trajectories and impingement points using a differential analyzer.

For most test cases, the NACA method is found to be sufficiently accurate. The error in evaluating maximum local impingement efficiency varied from 10 percent to 25 percent (Reference 7). The major limitation of the method stems from the technique used to determine the amount of dye in the absorbent material. Dye extraction from each ribbon was so time consuming and the required sample size (punched segment) was so large that the method was impractical for complicated

geometries or flow conditions. Thus, the method was limited to two-dimensional flows and some basic axisymmetric flows.

The NACA method is the only published experimental method for the purpose of measuring droplet impingement characteristics.

3.2 Present Test Method

A dye tracer technique similar to the one used by NACA in the 1950's is employed in the present testing. Distilled water containing a small amount of blue water-soluble dye is injected into the airstream of the wind tunnel in the form of droplets, using a specially designed spray system installed in the IRT plenum chamber. The forward surface of the model being tested is covered at selected locations with thin strips of blotter paper which absorbs the impinging droplets. The amount of dye trace, on the blotter, obtained in a given time interval can be determined using a laser reflectance method. A detailed description of the reflectance method can be found in Section 5 of this report. Given the amount of dye at a given location on the blotter paper, the amount of water impinged at that location is found from knowledge of the dye concentration in the solution.

To calculate the amount of impinging water from measured dye mass per unit area, an accurate measurement of LWC is required. But in practice, perfect uniformity of the cloud is very difficult to obtain in a wind tunnel. So a local LWC value is needed. The method chosen to minimize the uncertainty in local LWC value was to insert a small reference collector at each location in the empty tunnel at which a blotter strip will be placed on the model. This must be done for each test condition of airflow and water spray. The reference collector shape was chosen to give a nearly 100 percent collection efficiency (Reference 14). Even very small collectors have less than 100 percent, and the reference collector must have a blotter surface large enough to measure its reflectance by the laser beam method.

The collection efficiency of the small reference collector was determined by the following procedure. First, a droplet trajectory computer code was used to predict $\bar{\beta}$. To provide a check on this, a symmetrical airfoil at zero angle of attack was tested and compared with the reference collector measurements. Such an airfoil provides a flow field which is easily computed with accuracy, since separation or three-dimensional effects are prevented, and the larger size makes laser reflectance measurements easier. Second, rime ice collection on the reference collector had previously been measured which permits comparison (Reference 14). Thus, a local measurement could be made which represented LWC with a high degree of confidence. This served as a standard for calculation at each tunnel location and run condition.

Using a reference collector mechanism and the laser reflectance method, the amount of dye per unit area of the free stream per unit time can be determined. This amount of dye is converted into liquid water content in the cloud since the dye concentration in the water is known;

therefore, the local impingement efficiency ($\bar{\beta}$) of the model at a given location is found from:

$$\bar{\beta} = \frac{\text{Measured amount of dye/unit surface area/unit time on model at a given location}}{\text{Measured amount of dye/unit flow area/unit time in free stream for a collector whose } \beta = 1}$$

The main differences between the present test method and the method developed by NACA in the 1950's are summarized in Table 3.1. These differences will be explained in detail in the sections that follow.

TABLE 3.1

MAIN DIFFERENCES BETWEEN PRESENT TEST METHOD AND NACA METHOD

ITEM	NACA	PRESENT
Data Reduction Method	Colorimetric Analysis	Reflectance Spectroscopy
Measurement of Liquid Water Content	Aspirating Device	Collector Mechanism (see Section 3.7)
Spraying Time	3 – 10 seconds. Dye penetration into absorbent material was allowed, saturation was avoided.	1 – 3 seconds. Dye penetration must be minimized.
Solution Concentration	0.005 – 0.01 by weight (red dye)	0.0002 – 0.0005 by weight (blue dye)

Prior to all tests, the position of the spray nozzles in the plenum chamber was determined so as to give a nearly uniform water distribution over a cross-sectional area in the test section greater than the frontal area of the largest model (engine inlet) A nearly uniform distribution of dye in the spray cloud minimizes errors in local impingement rates on models that would be attributed to a nonuniform cloud ahead of the model. The process used to achieve dye uniformity in the spray cloud is described in Section 3.5.

Water droplet sizes and distribution in the cloud are required inputs to particle trajectory computer codes. Tests must be performed to establish these cloud parameters prior to testing models so that experimental results can be correlated with analytical calculations.

After the tests described above were completed, tests of the actual models were conducted. The model was positioned in the test section and strips of blotter paper were attached to the forward facing areas of

interest on the model. Air and water pressures in the spray system were adjusted and the tunnel conditions (air speed, temperature) were set. The spray system was activated for a few seconds (typically 1 to 3 seconds) and a dye deposit obtained on the blotter strips. The test was repeated for all required variations of test parameters such as: angle of attack, engine inlet mass flow and water droplet size. Each set of test conditions was repeated three times to allow a meaningful statistical average of efficiency distributions to be determined, due to variation in flow conditions attributed to tunnel turbulence, spray system performance, etc.

Once all tests of a given model were completed, the model was removed from the tunnel and the collector mechanism described in Section 3.7 was placed in the same location as the model and a series of calibration tests were performed which were used to determine the liquid water content of the cloud. The tunnel conditions and spray system pressures and spray times were identical to the ones used for model testing.

For all engine inlets tested, surface pressure measurements were obtained prior to water droplet impingement tests. It should be noted that all pressure survey tests were run with the spray system off. The surface pressure measurements are required when comparing theoretical and experimental flow field results. Since water droplet trajectories depend on the flow field, matching of experimental and analytical flow fields enhances the credibility of correlations between analytical and experimental results.

A detailed description of the experimental procedure is given in the following sections.

3.3 IRT Wind Tunnel

All tests described in this report were conducted in the NASA Lewis Icing Research Tunnel (IRT) (see Figure 3.2). The IRT built in 1942-1944 is the largest icing wind tunnel in North America (Reference 15). The tunnel has a 6 ft. high by 9 ft. wide by 20 ft. long test section; a top airspeed of 300 mph (empty tunnel); a refrigeration plant which produces total air temperatures down to -30^{o} F and which provides for year-round operation; an air atomizing water nozzle spray system which produces simulated icing clouds with liquid water contents from 0.5 to over 2 g/m^3. The IRT test section operates from sea level (at 0 mph) to 3000 ft. altitude (at 300 mph).

The present tests were conducted at a tunnel total air temperature of approximately 50^{o} F (i.e. no icing) and at an indicated airspeed of approximately 175 mph and 165 mph for the airfoils and engine inlets respectively. The IRT spray system was not used in these tests. Instead, a specially designed spray system was employed for reasons explained in Section 3.4. However, the tunnel spray system proved useful in establishing a high humidity level of the air in the tunnel. A high humidity level is required to avoid evaporation of the water droplets during the travel from the spray nozzles to the body. Droplet evaporation can alter the original concentration of dye in the droplet solution. By spraying water for a short period of time prior to

a test, the humidity in the tunnel air can be brought to a desired level.

Tunnel choice was based on availability, size of test section (a large test section was required to accommodate the large engine inlet models), requirements for a suction system to simulate various engine mass flow conditions and facilities for spraying.

3.4 Spray System

A schematic of the spray system employed in the present experimental study is shown in Figure 3.3. The system consists of a 9 gallon aluminum alloy tank, containing the dye solution, which is connected to 12 nozzle assemblies (only two are shown in Figure 3.3). Each nozzle assembly consists of (see Figure A.4, Appendix A):

a. A two-way, fast action, normally-closed solenoid valve

b. A NASA standard icing spray nozzle

c. The nozzle housing which contains the atomizing air inlet

The nozzles are of the same type as those currently used in the main icing spray system of the IRT and are mounted in the tunnel plenum chamber (see Figure 3.4). Each nozzle assembly was adjustable as to its orientation, to aid in obtaining a nearly uniform spray cloud in the IRT test section.

Since the spray interval is very short to avoid saturating the blotters (usually 1 to 3 seconds), the spray on-and-off response time was kept to a minimum by reducing the volume in the nozzle housing down stream of the solenoid valve (Appendix A, Section A.1). The housings of the air atomizing water nozzles normally in use in the IRT are not designed for this purpose.

The dye solution in the tank was pressurized to approximately 106 psig. From the tank, the solution passes through a filter and fittings and then through rubber hoses to each individual nozzle assembly. The air pressure for the spray nozzles was varied from 65 to 80 psig. The air was ducted through rubber hoses to a steel pipe attached to the housing. A two-way fast action normally-closed solenoid valve was used to turn on and off the main air supply. Just before exit through the nozzle, discharge orifice air and dye solution are mixed under pressure to produce a spray cloud with droplets whose mean volumetric diameter (MVD) varies as a function of air-to-water pressure ratio. The pressure ratios used during all tests and the corresponding droplet MVD's are given in Section 3.6.

Prior to installation in the IRT, a typical nozzle assembly was tested over the pressure operating envelope to determine:

a. The time required for the nozzle to spray after the control solenoid valve was activated and

b. The time required for the spray to completely die off after the solenoid valve was closed.

The timings were estimated using a video camera to record the spray system response from the moment the system was turned on to the moment the nozzle stop spraying. By counting video frames, the times mentioned above were determined to be 0.05 sec and 0.66 sec for items a and b, respectively.

Before each test the air and dye-solution pressures were set using pressure regulators. The dye-solution pressure was monitored at the tank and before the entry to the nozzle housing (Figure 3.4). Pressure gauges (oil-filled) were used to help adjust the pressure manually and electrical transducers were used to check the pressure in the system during each test (Figure 3.5). The air manifold pressure was monitored using two gauges (oil-filled) at the pressure regulator (Figure A.3, Appendix A). All pressures were checked before and after each test. The solenoid valves which controlled the spray duration were linked to an electronic timer by means of which the duration of the spray was repeatable to $\pm$ 0.01 second.

Detailed descriptions of the spray system, its operation, exact location of nozzle assemblies, nozzle housing design and system components are given in Appendix A.

3.5 Uniformity Test

In calculating local impingement efficiency, it is assumed that both test model and the reference collector device that measures the liquid water content (LWC) are exposed to a droplet cloud with uniform dye distribution. The ratio of dye accumulation on the model to corrected dye accumulation on the reference collector, assuming unit area and unit time of exposure, gives the value for local impingement efficiency ($\bar{\beta}$) on the model. Considerable local variations in dye distribution will seriously affect the calculated value of ($\bar{\beta}$) given by the above ratio. In addition, a non-uniform distribution of dye can complicate the data reduction process for large test models. In the last case, it would be very difficult to differentiate between variations in local impingement efficiency caused by the flow field and variations caused by local changes in dye distribution.

The degree of cloud uniformity depends on the number and position of nozzles used and the extent of cross-sectional area in the tunnel over which cloud uniformity is required. Factors such as tunnel turbulence and nozzle discharge patterns can cause small random changes in cloud uniformity which cannot be easily accounted for.

Achieving a completely uniform cloud would require a large number of nozzles. A large number of nozzles will provide too high LWC, thus

resulting in a very short exposure time to limit dye penetration to less than 40 percent, and to avoid saturation of blotter strips. Also, extensive testing would be needed to determine the optimum nozzle positions in the plenum chamber. The aim in the present tests was to obtain a water droplet cloud where variations in dye distribution were within 10 percent of the mean value over the area of interest.

The 10 percent variation is based upon a sensitivity analysis performed on the data reduction method to determine the effect of small dye variation in calculating local water droplet impingement efficiency.

During preliminary tests on some two dimensional models carried out in June 1985, a spray system with 8 nozzles was employed positioned as shown in Figure 3.6. The decision on the number and position of the nozzles was based on early NACA work (Figure 3.7). This configuration was tested three times and found to give a uniform cloud over a 1 foot high by 2 feet wide area centered in the tunnel cross-section. Variations of dye distribution were within 10 percent of the mean. The engine inlet tests were performed in September 1985; however, cloud uniformity over a larger cross-sectional area was required. This area was determined from the size of the engine inlet models and it was found to be 2 feet high by 3 feet wide.

To achieve the required uniformity level within this larger area, a 12 nozzle system was designed. To determine the best location and nozzle orientation in the plenum chamber, 36 uniformity tests were performed prior to all inlet model tests. An additional 4 tests were performed after all engine inlet models were tested, to verify that cloud uniformity had not changed during testing.

To determine the cloud uniformity, a grid was placed in the tunnel test section and 1.25 inch square blotter pieces were mounted on the grid at regular intervals. Spacing between the blotter squares was 6 inches and the array of (5X7) blotter squares covered an area 2 feet high by 3 feet wide centered in the tunnel test section. The grid with the blotter squares is shown in Figure 3.8. The spray system air and dyed water pressures were adjusted to the required level (see Appendix A); the tunnel air speed, temperature and humidity were set. The spray system was activated for approximately 1 to 3 seconds depending on air/dyed-water pressure ratio used. The blotters were removed from the grid and were allowed to dry. The dye deposits on the blotters were measured after the test using a laser reflectivity method. If the reflectivity (dye deposit) of the squares at any location varied more than 10 percent from the mean, positions of the nozzles in the plenum chamber were adjusted and the test repeated. The uniformity test conditions and data can be found in Appendix G. Typical uniformity results are given in Table 3.2.

3.6 Droplet Sizing

The validation of computer codes requires knowledge of droplet diameter and distribution. Droplet size distribution data for the spray system pressure ratios (P_{air}/P_{water}) used in the present trajectory tests were

TABLE 3.2

TYPICAL UNIFORMITY DATA
(UNIFORMITY TESTS 1 AND 3 9/25/85; PAGE 1 OF 2)

GRID ROW ↓	→ GRID COLUMN	1	2	3	4	5	6	7
1	Test 1	.3997	.4202	.4257	.4063	.4026	.3847	.3976
	Test 3	.4128	.4276	.4079	.4089	.4000	.3833	.4072
2	Test 1	.3943	.4063	.4115	.3860	.3596	.3906	.3982
	Test 3	.3966	.3932	.4572	.4146	.3775	.3995	.4196
3	Test 1	.3977	.4026	.4310	.4076	.4043	.4129	.3990
	Test 3	.4360	.4395	.4608	.4166	.4480	.4302	.4278
4	Test 1	.3823	.3921	.3743	.4053	.4076	.3727	.3923
	Test 3	.4315	.3952	.3847	.4323	.4282	.3708	.4160
5	Test 1	.3920	.3997	.4059	.4072	.3813	.3786	.4065
	Test 3	.3935	.4149	.4209	.4116	.3771	.3428	.3991

NOTES:
1. Grid locations looking downstream.
2. Vertical and horizontal locations are 6 inches apart.
3. Location 11 (Row = 1, Column = 1) is at 12 inches above and 18 inches to the left with respect to the tunnel centerline.
4. Tunnel test section center is at location 34.
5. Voltage ratio (V1 / V2) values are shown (see Section 5).

TABLE 3.2

TYPICAL UNIFORMITY DATA
(REFLECTIVITY PERCENT DEVIATION FROM THE MEAN FOR UNIFORMITY TEST 1; PAGE 2 OF 2)

BARE WHITE PAPER VOLTAGE RATIO = 1.1450
AVERAGE NORMALIZED REFLECTIVITY = 0.3478

STRIP LOCATION	VOLTAGE RATIO (V1 / V2)	NORMALIZED REFLECTIVITY (V1 / V2 / 1.145)	REFLECTIVITY % DEVIATION FROM MEAN
11	0.39969	0.3491	0.3699
12	0.42017	0.3670	5.5147
13	0.42569	0.3718	6.8997
14	0.40627	0.3548	2.0240
15	0.40260	0.3516	1.1019
16	0.38465	0.3359	-3.4058
17	0.39757	0.3472	-0.1612
21	0.39432	0.3444	-0.9786
22	0.40628	0.3548	2.0259
23	0.41151	0.3594	3.3381
24	0.38598	0.3371	-3.0713
25	0.35956	0.3140	-9.7058
26	0.39062	0.3411	-1.9082
27	0.39818	0.3478	-0.0077
31	0.39969	0.3491	0.3714
32	0.40261	0.3516	1.1044
33	0.43095	0.3764	8.2193
34	0.40760	0.3560	2.3570
35	0.40427	0.3531	1.5199
36	0.41289	0.3606	3.6860
37	0.39904	0.3485	0.2066
41	0.38227	0.3339	-4.0030
42	0.39205	0.3424	-1.5490
43	0.37425	0.3269	-6.0178
44	0.40525	0.3539	1.7661
45	0.40756	0.3559	2.3459
46	0.37274	0.3255	-6.3982
47	0.39225	0.3426	-1.4969
51	0.39196	0.3423	-1.5708
52	0.39967	0.3491	0.3660
53	0.40586	0.3545	1.9207
54	0.40716	0.3556	2.2475
55	0.38127	0.3330	-4.2547
56	0.37856	0.3306	-4.9363
57	0.40652	0.3550	2.0847

provided by NASA Lewis. Table 3.3 gives the droplet MVD for each pressure ratio used.

TABLE 3.3

CLOUD DROPLET MVD FOR EACH PRESSURE RATIO USED IN THE PRESENT TRAJECTORY TESTS.

PAIR (PSIG)	PWATER (PSIG)	PRESSURE RATIO	MVD (MICRONS)
80	100	0.80	16.45
65	100	0.65	20.36

Droplet size distribution data are presented in Appendix E. Details of the methods for determining spray cloud properties can be found in References 2, 16 and 17.

3.7 Measurement of LWC

To determine the liquid water content (LWC) in the free stream spray cloud, a "reference collector mechanism" was used (Figures 3.9 - 3.11). The mechanism consists of a telescopic beam of airfoil cross-section, a wedge shaped part ("the collector") and a steel rod which is free to rotate and is attached to a stepper motor on the lower end and to the collector on the upper end. The stepper motor is housed within the larger airfoil section beam and is controlled by a computer (Commodore VIC 20). The stepper motor was used during preliminary investigations but it was not employed during the LWC tests.

The dimensions of the wedge-shaped collector which was mounted on the top of the mechanism are given in Figure 3.12. The small size of the wedge minimizes disturbance to the flow and enables it to have a collection efficiency near unity. The height of the wedge can be adjusted from 32 inches to 38 inches above its base.

After testing a given model, the collector was positioned close to the location where the model had been installed and was exposed to the spray cloud under tunnel conditions identical to those for the model itself. Spraying times of various lengths, usually in the range of 0.5 to 3 seconds were used to calibrate the collector. A rectangular blotter strip (0.2 X 1.5 inch) mounted on the upper part of the wedge was used to collect dye during each test. The calibration curves for the collector for 0.65 and 0.8 air/water pressure ratios showing dye-mass ($\mu g/cm^2$) accumulated versus time in seconds are shown in Figure 3.13 and were used with all two-dimensional flow models. The upper part of the

collector mechanism was modified for engine inlets as shown in Figure 3.14 to measure LWC at four different locations simultaneously. This was done to record variations in cloud uniformity and therefore liquid water content (LWC) over the projected area of the inlet. When calculating the local impingement efficiency ($\bar{\beta}$) on different locations on the inlet surface, local variations in LWC must be considered. The calibration for the four blade collector is shown in Figure 3.15.

The number of tests performed to calibrate the collector and the corresponding test conditions are given in Appendix G.

As explained in Section 3.2, the collector does not capture all the particles travelling within its frontal area. To calculate the water droplet cloud LWC, the collector local impingement efficiency must be determined first. The method and code of Reference 18 were employed to develop a theoretical local impingement efficiency curve versus droplet mean volumetric diameter for the collector. The results are shown in Figure 3.16 and 3.17. For large particle droplet size (MVD = 20.36, P_{air}/P_{water} = 0.65), the collector efficiency is 0.89 (89 percent). For the smaller droplets (MVD = 16.45, P_{air}/P_{water} = 0.80), the collector efficiency is 0.86 (86 percent).

To determine the LWC, the amount of dye per unit time of collector exposure given by Figure 3.13 or 3.15 is divided by the collector local impingement efficiency determined from Figure 3.16 and 3.17 (given the MVD of the cloud) and by the concentration of the dye solution.

$$\text{LWC} = \frac{\text{mass of dye per unit time on collector blotter strip} / \bar{\beta} \text{ collector for given MVD}}{\text{concentration of dye solution}}$$

3.8 Mass Flow Measurements

The flowfield around an engine inlet depends on free stream conditions and engine inlet mass flow. For illustrative purposes, consider a thin-walled circular air inlet with no center body and a means of regulating air flow through the inlet. Also incompressible flow has been assumed so that

$$\frac{V_{inlet}}{V_{\infty}} = \frac{A_{\infty}}{A_{inlet}}.$$

Figure 3.18 shows the three possible situations that can arise:

a. $A_{\infty 1} > A_{inlet}$ (capture ratio $A_{\infty 1}/A_{inlet} > 1$, $V_{inlet}/V_{\infty} > 1$) corresponds to a large engine inlet mass flow, typical of take-off power settings.

b. $A_{\infty 2} = A_{inlet}$ (capture ratio $A_{\infty 2}/A_{inlet} = 1$, $V_{inlet}/V_{\infty} = 1$), the diameter of the inlet air stream tube is equal to the inlet diameter. The air mass flow through the inlet is less than in the case above if V_{∞} = constant.

c. If the engine mass flow is reduced further then $A_{\infty 3} < A_{inlet}$ which corresponds to a capture ratio $A_{\infty 3}/A_{inlet}$ of less than 1 and a velocity ratio V_{inlet}/V_{∞} of less than 1, typical of holding, climb and descent flight conditions.

Clearly the water droplet impingement characteristics, all other flow conditions being equal, depend considerably on engine inlet mass flow. Thus, to provide a complete data base, the inlets must be tested at various mass flows.

To provide the required inlet mass flow variations, the suction system of the IRT was used. The system consists of a very large vacuum system located outside the tunnel and a long 24 inch internal diameter (ID) pipe that connects the vacuum system to the tunnel test section. The vacuum is maintained by means of remote vacuum pumps. A regulating valve which can be opened or closed electrically from the tunnel control room is used to adjust the suction required. In order to connect the engine inlet to the vacuum system, a 12 inch ID rubber hose and a steel elbow arrangement were designed and manufactured (see Figure 3.19). The rubber hose was found to be the easiest way for allowing engine inlet angle of attack to vary.

The suction system had to be calibrated prior to engine inlet testing since no mass flow measuring method existed. Details of the calibration system and procedure are given in Appendix B. Basically, the mass flow in the suction duct was measured using a KURZ velocity and temperature probe inserted in the NASA 24 inch ID duct. The calibration curve for the probe showing volts versus mass flow in lbm/min is given in Appendix B. The mass flow was measured by means of a digital voltmeter connected to the probe. The voltmeter was located in the tunnel control room. Voltmeter readings, corresponding mass flows converted to lbm/sec obtained from the calibration curve and corresponding inlet capture ratios are given in Table 3.4.

TABLE 3.4

MASS OF EXHAUSTED AIR

VOLMETER READING (VOLTS)	MASS FLOW (LBM/SEC)	APPROXIMATE CAPTURE RATIOS FOR INLET MODELS
5.2	22.97	1.00
3.9	17.22	0.75
2.6	11.47	0.50

3.9 Model Aerodynamic Data Acquisition

Particle trajectories depend on the flow field about a given body. When comparing experimental and analytical water droplet trajectory data, it is important to verify that the experimental and analytical flow fields are in good agreement. This is particularly true in the case of a large body, such as an engine inlet, being tested in a wind tunnel. The effect of tunnel walls and tunnel turbulence on the flow field about the body must be considered and appropriate corrections for such effects must be applied.

Prior to acquiring droplet impingement data for the two engine inlet models, the pressure distributions on the surface of the models were measured. Pressure measurements were performed at an indicated air speed of 165 mph, two angles of attack and two inlet mass flows with the spray system off. Three sets of pressure measurements were obtained for each configuration to establish repeatability of the data. A total of 34 static pressure taps were available on the axisymmetric inlet and 88 static pressure taps on the 737-300 inlet. The locations of the pressure taps are given on Figure 3.20. The test configurations for each inlet are summarized in Table 3.5.

TABLE 3.5

ENGINE INLET TEST CONFIGURATIONS FOR AERODYNAMIC DATA ACQUISITION

INLET	ANGLE OF ATTACK (DEGREES)	MASS FLOW (LBM/SEC)	REPEATS
AXISYMMETRIC 34 PRESSURE TAPS	0	17.20	3
		22.96	3
	15	17.20	3
		22.96	3
737-300 88 PRESSURE TAPS	0	17.20	3
		22.96	3
	15	17.20	3
		22.96	3

To measure the pressure distribution, spaghetti tubes (small plastic pneumatic tubes 0.1 inch in diameter) were used to connect the static pressure taps on the inlet to the automated pressure data acquisition system available at the NASA IRT. Each spaghetti tube was blown out and checked after installation using compressed air. The tubes were carried

out of the test section through a four inch diameter cylindrical pipe mounted on top of the engine inlet supporting body (see Figure 3.19). Before the start of an engine inlet aerodynamic test, a set of pressure measurements were taken at zero airspeed to verify that the pressure data acquisition system was working properly. The pressures were recorded and printed out using a microcomputer.

To test for pressure distribution, the angle of attack of the inlet was set to the required value, the tunnel airspeed (indicated) was brought to 165 mph, and the engine mass flow adjusted to the desired level. Once all conditions were stable the surface pressures were recorded. Each set of pressure measurements took a few seconds to complete.

Example measurements for both inlets are given in Section 6.3 where experimental data are plotted and compared to analytical pressure distributions.

3.10 Model Impingement Data Acquisition

In this section, the sequence of steps used to obtain water droplet impingement data of the test geometries considered is described:

a. The pressures for air and dyed water of the spray system were set to the required levels. Typically, these pressures were 100 psig (at the nozzle) for water and 65 or 80 psig for air, depending on droplet size desired (Table 3.3).

b. The timer which activates the water solenoid valve was set to 2 or 2.5 seconds depending on the air/water pressure ratio used. The shorter time period corresponds to the smaller pressure ratio (higher LWC). A short spray time is required to avoid blotter saturation.

c. Blotter strips typically 1.5 inches wide and of various length, depending on the model being tested, were attached to the forward (upstream) facing surface of the model at strategic locations. Blotter strips have a smooth and a rough side. Care must be taken when positioning the strip on the model so that the rough side of the blotter is against the surface of the body being tested. A strip identification code appropriate to the test being conducted was written on the rough side of the blotter strip. The strip was attached to the body by means of aluminum tape. Figures 3.21, 3.22 and 3.23 show examples of blotter strip locations for the engine inlet models tested.

d. The following tunnel conditions were set prior to each impingement test:

   - airspeed
   - temperature
   - humidity (approximately)

and the following test variables were recorded (see Appendix G):

- Tunnel indicated airspeed (mph)
- Tunnel air, static (psia) and dynamic pressures (inches of water)
- Air average total temperature measured at three different locations upstream of spray bar system(°F)
- Dew point temperature (°F)
- Spray system pressures from electric transducers and pressure gauges (psig)
- Spraying time = time water solenoid valve remains open + 0.33 seconds (see Appendix G)
- Dyed water concentration (typically 0.5 μg dye/1 liter of water)
- Test identification number

e. This step applies to engine inlets only. The engine inlet air mass flow was adjusted to the required level by opening or closing the air regulating valve of the suction system. A precalibrated digital voltmeter was used to record engine inlet mass flow (see Appendix B).

f. The spray system was activated and a dye deposit was obtained on the blotters. The tunnel airspeed was reduced to about 10 mph (idle speed), the blotter strips were carefully removed from the model and were taken out of the tunnel. The strips were allowed to dry and then they were placed in envelopes for storage. Each envelope was labeled appropriately for future reference.

g. Before the next test began, the surface of the model was wiped dry and new blotter strips were placed on the model.

Test times varied depending on model. Two dimensional models required approximately 5 to 10 minutes per test while engine inlets tests took 20 to 30 minutes to complete.

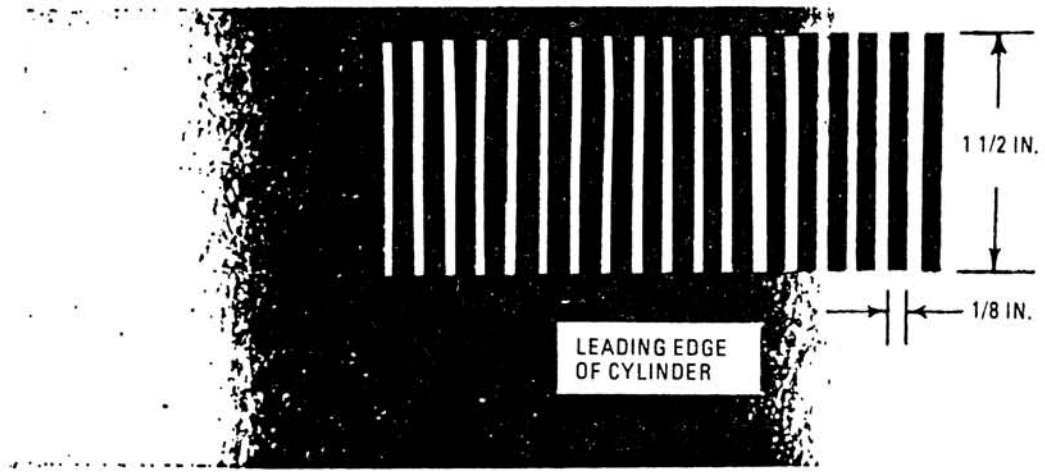

FIGURE 3.1

TYPICAL BLOTTER RECORD FROM CYLINDER WITH PUNCHED SEGMENTS REMOVED
FOR COLORIMETRIC ANALYSIS AFTER EXPOSURE TO
DYED WATER CLOUD, AS DONE BY NACA (REFERENCE 2)

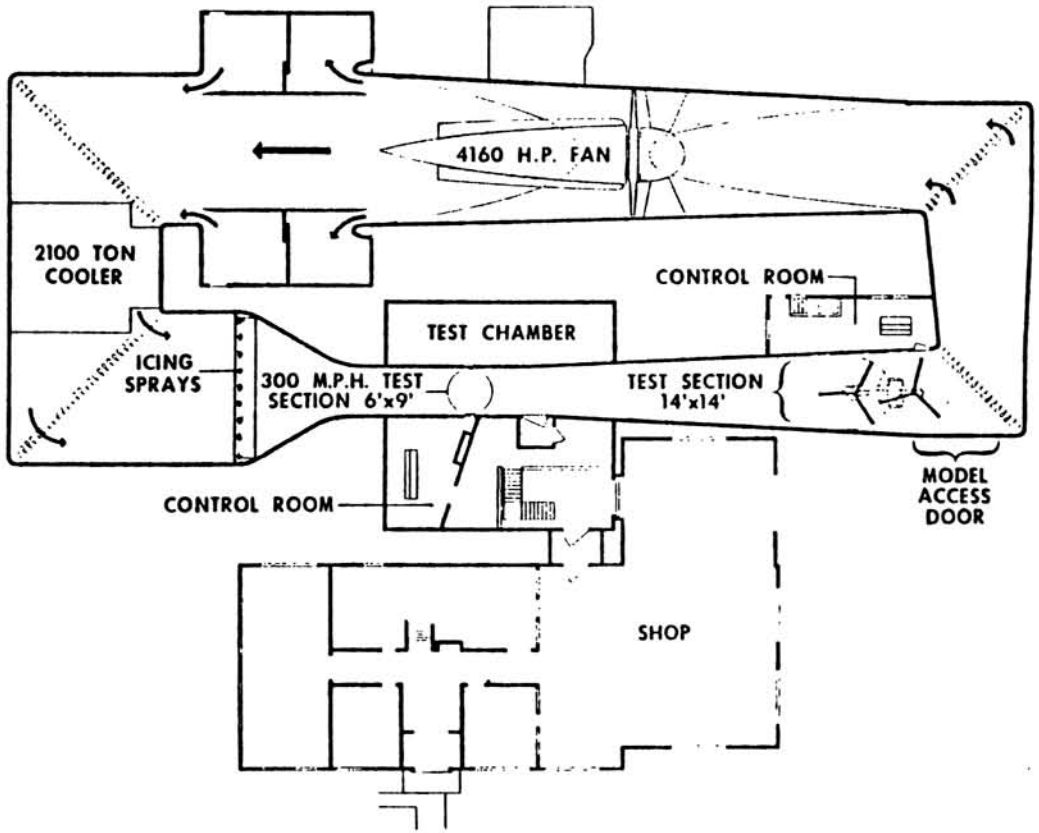

FIGURE 3.2

SCHEMATIC DIAGRAM OF NASA-LEWIS ICING RESEARCH TUNNEL.

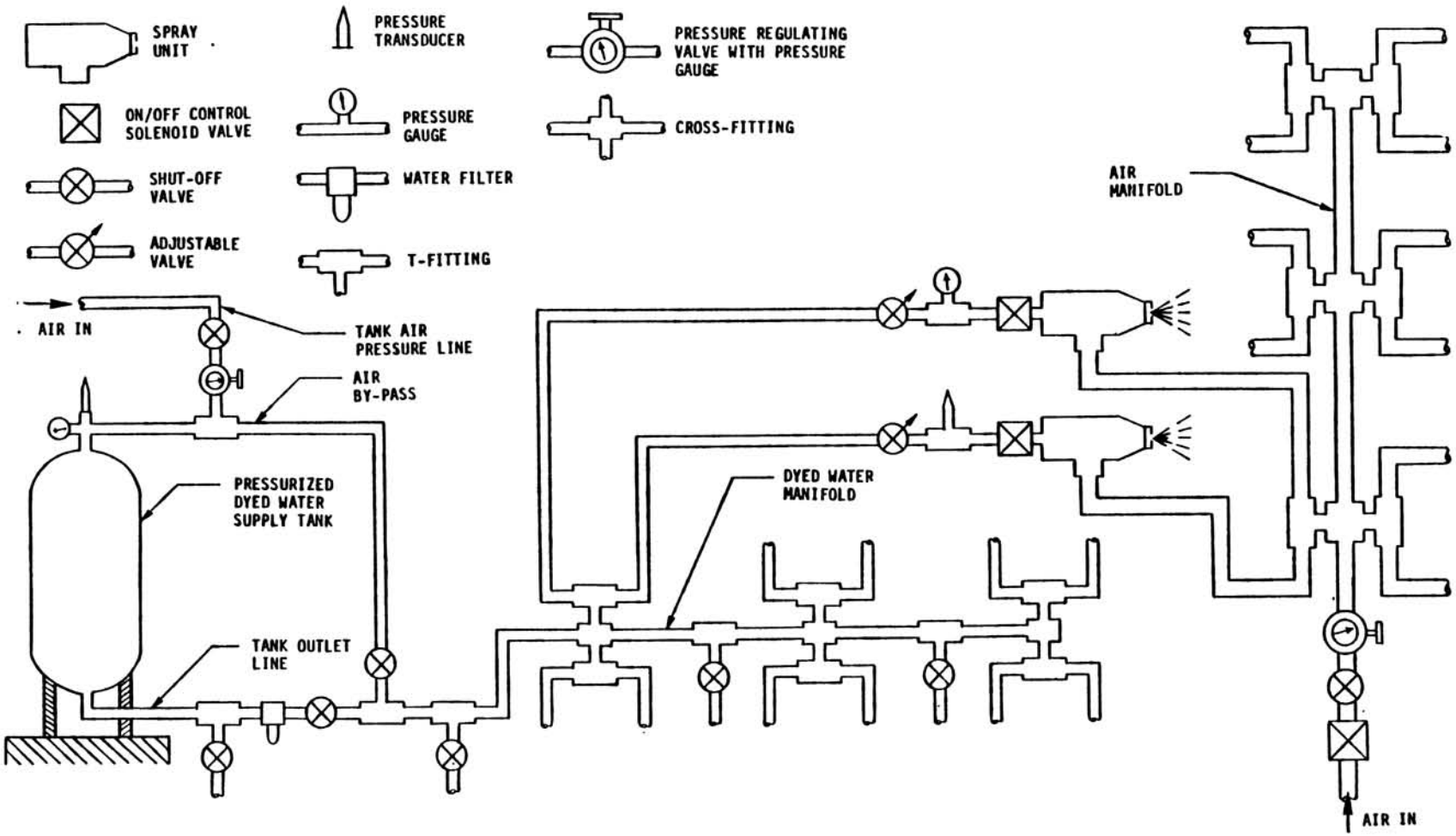

FIGURE 3.3

SCHEMATIC DIAGRAM OF SPRAY SYSTEM.

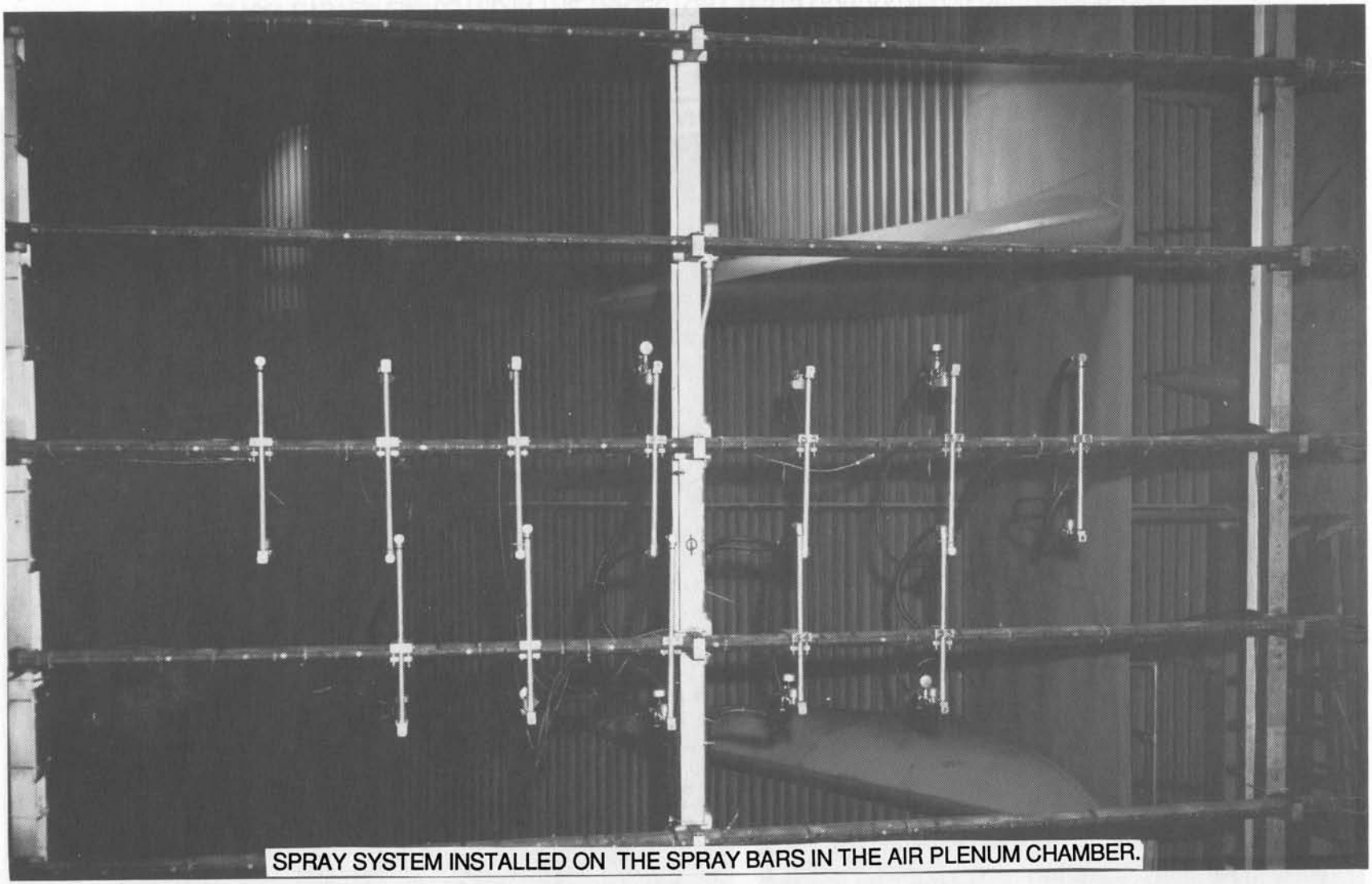

FIGURE 3.4
SPRAY SYSTEM EMPLOYED IN THE TRAJECTORY TESTS CONDUCTED IN SEPTEMBER 1985.
(PAGE 1 OF 2)

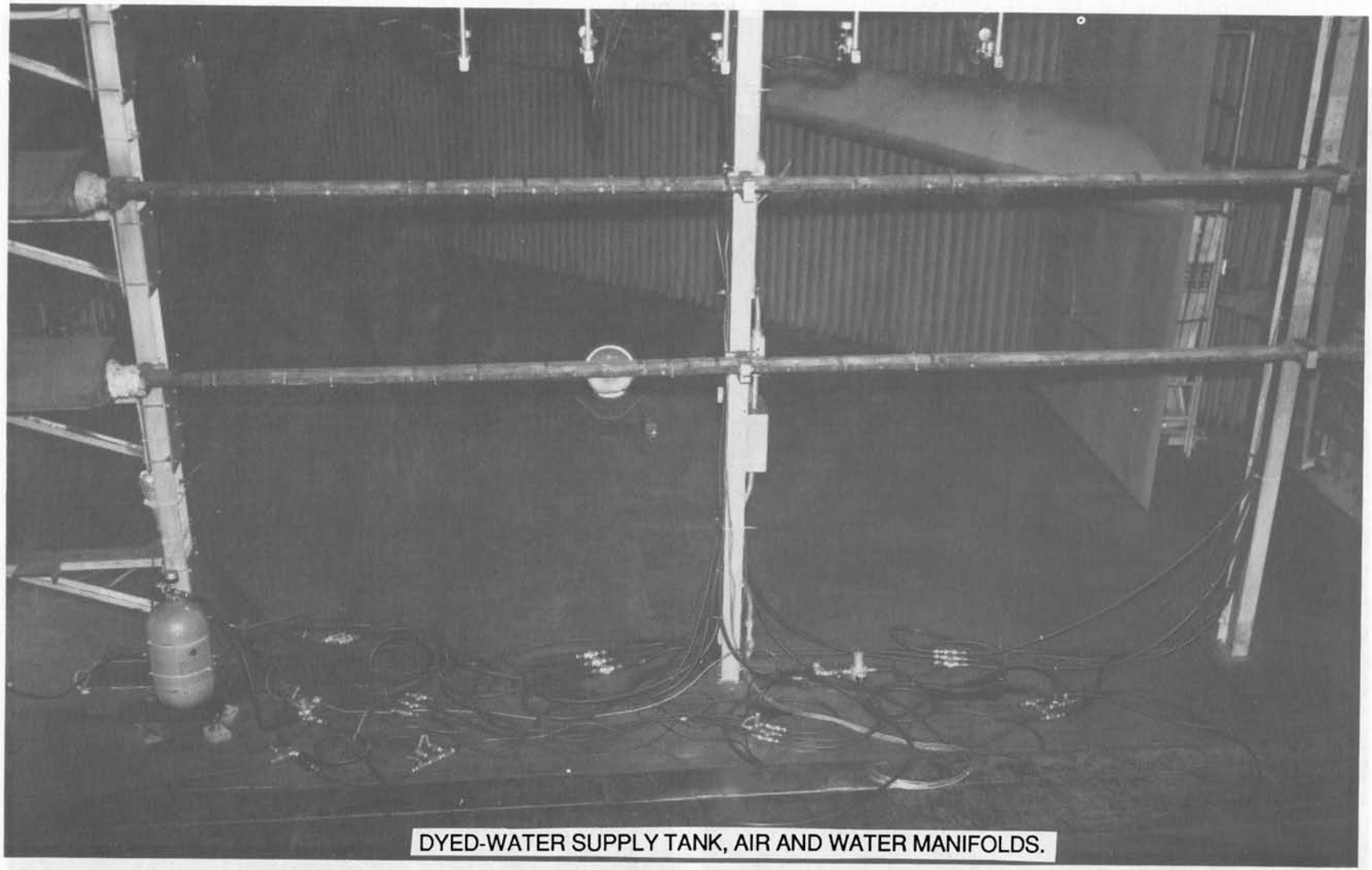

DYED-WATER SUPPLY TANK, AIR AND WATER MANIFOLDS.

FIGURE 3.4
SPRAY SYSTEM EMPLOYED IN THE TRAJECTORY TESTS CONDUCTED IN SEPTEMBER 1985.
(PAGE 2 OF 2)

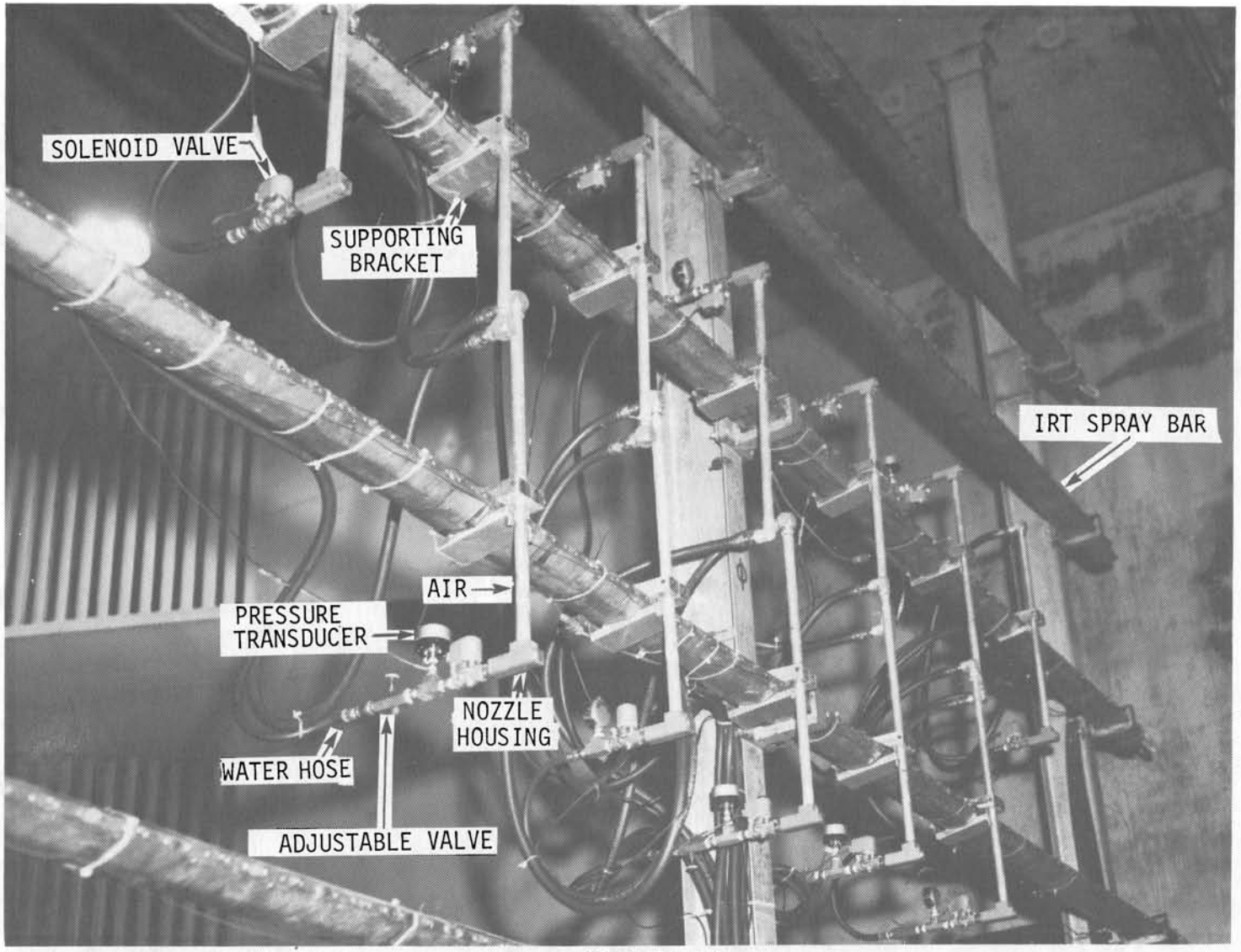

FIGURE 3.5

COMPONENTS OF SPRAY NOZZLE ASSEMBLIES.

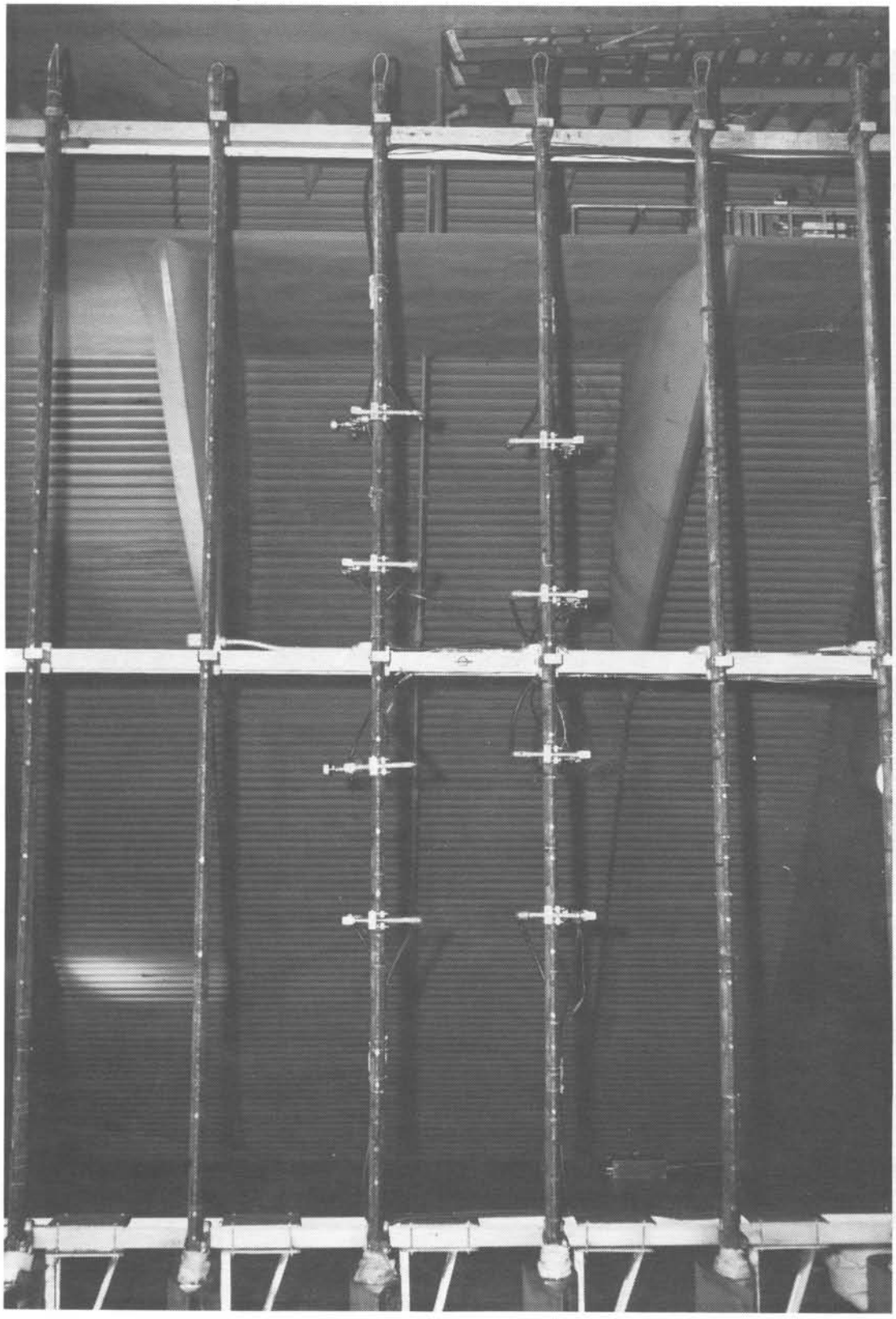

FIGURE 3.6

SPRAY SYSTEM EMPLOYED IN THE TRAJECTORY TESTS CONDUCTED IN JUNE 1985.

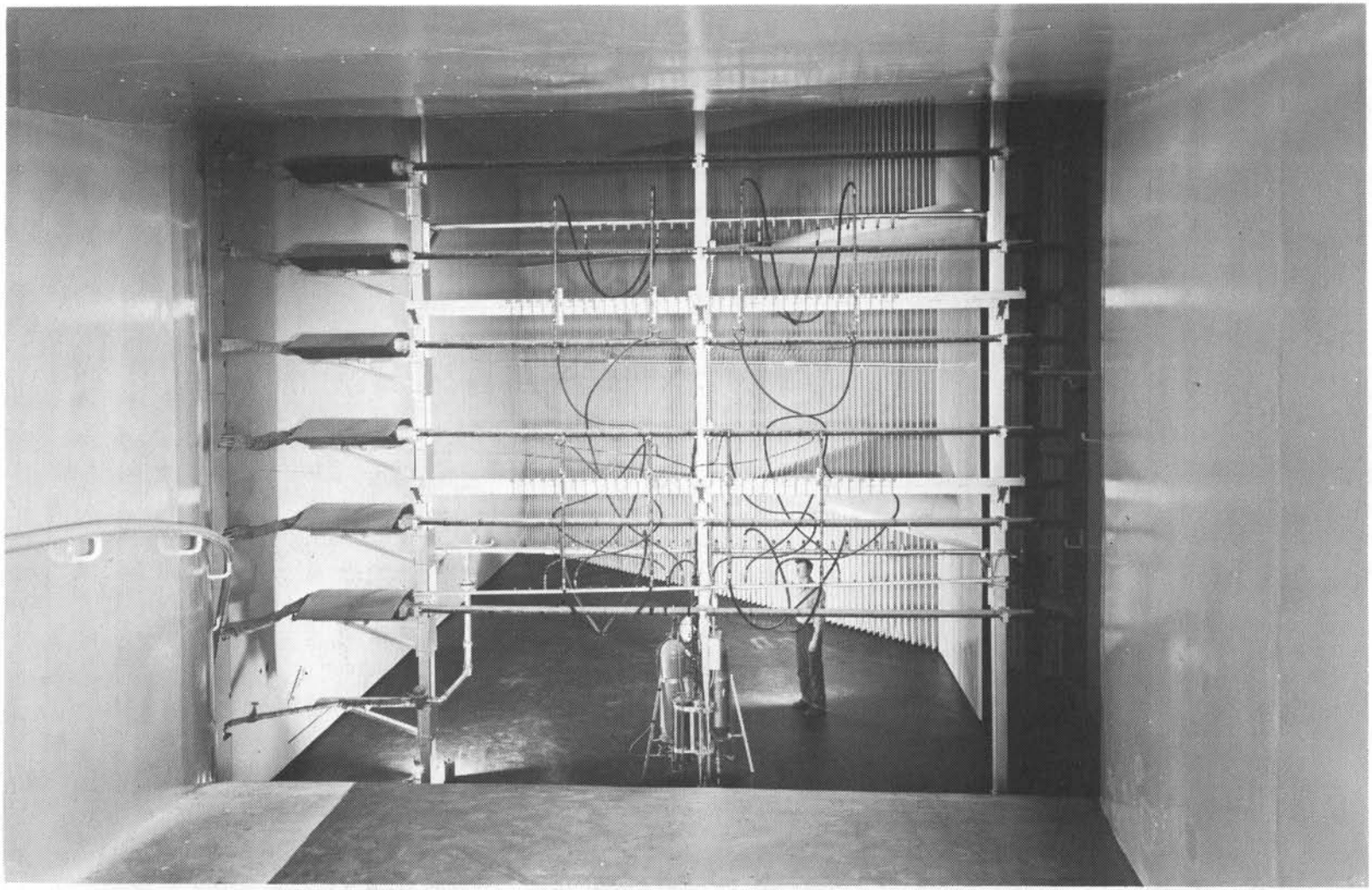

FIGURE 3.7

SPRAY SYSTEM USED IN THE TRAJECTORY TESTS CONDUCTED BY NACA IN 1956
(SHAW, R. J., PERSONAL COMMUNICATION, NASA-LEWIS RESEARCH CENTER).

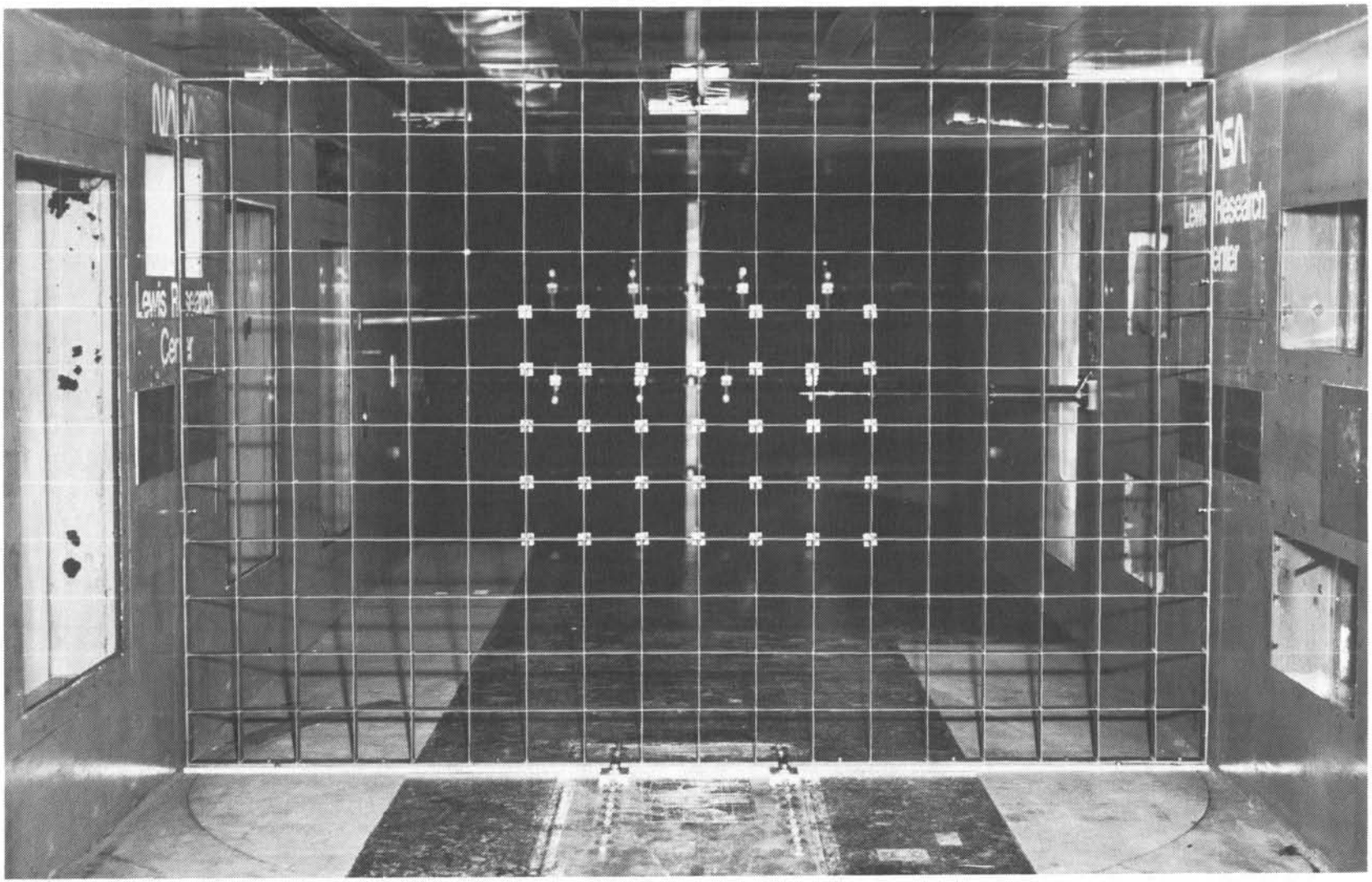

FIGURE 3.8

UNIFORMITY GRID WITH BLOTTER SQUARES INSTALLED (LOOKING UPSTREAM).

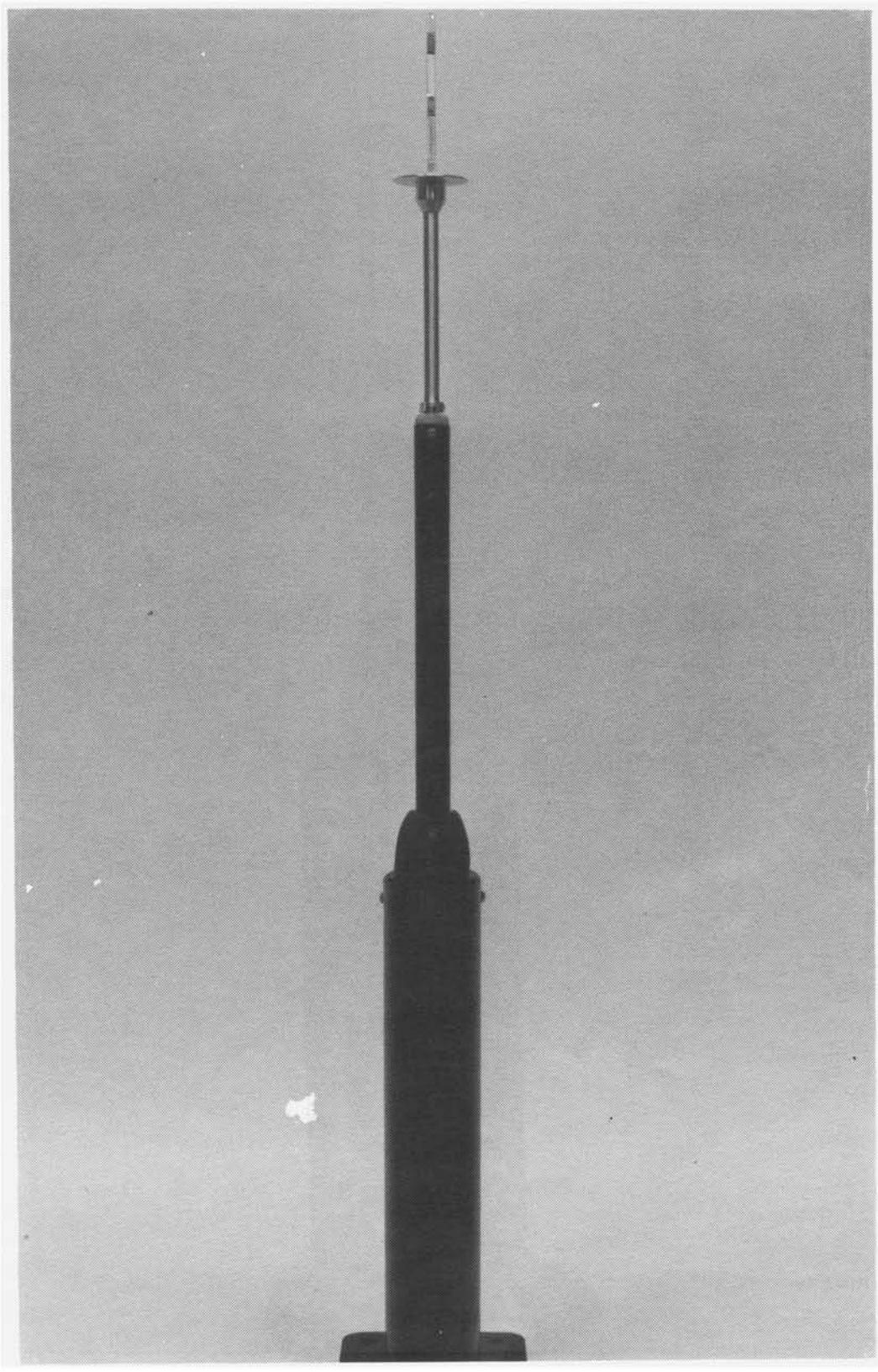

FIGURE 3.9

SINGLE BLADE REFERENCE COLLECTOR MECHANISM, FRONT VIEW.

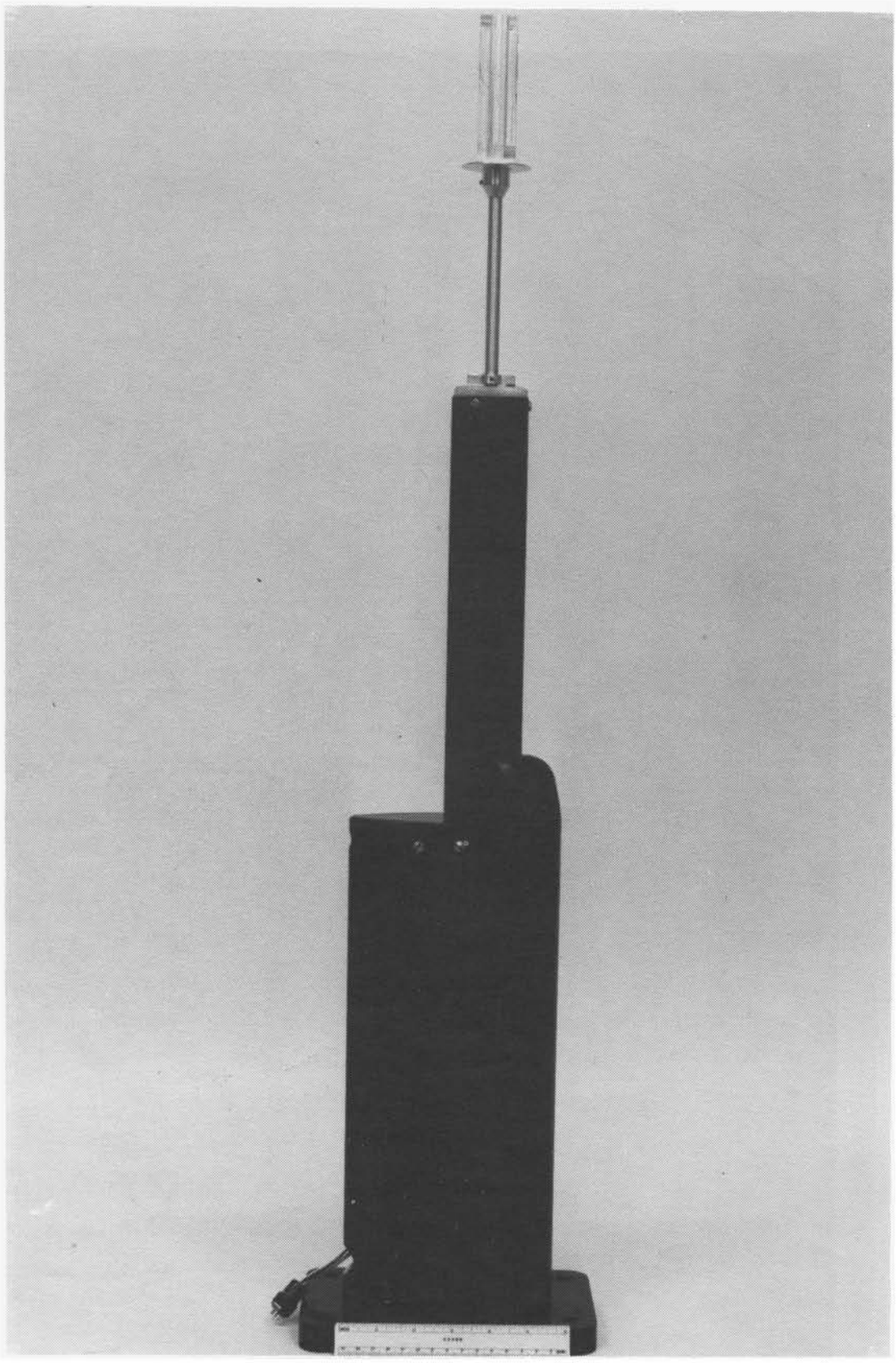

FIGURE 3.10

SINGLE BLADE REFERENCE COLLECTOR MECHANISM, SIDE VIEW.

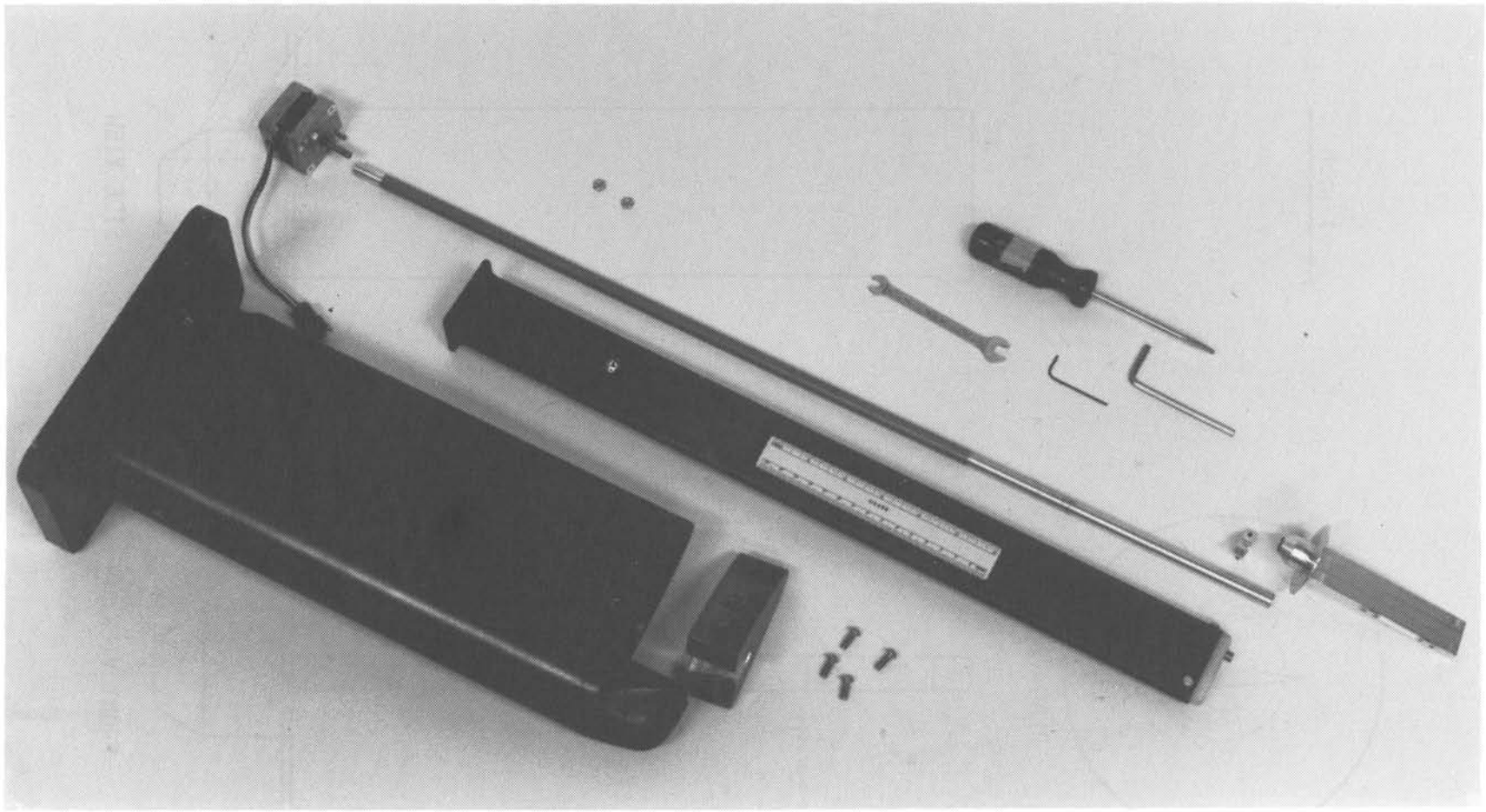

FIGURE 3.11.

COMPONENTS OF REFERENCE COLLECTOR MECHANISM.

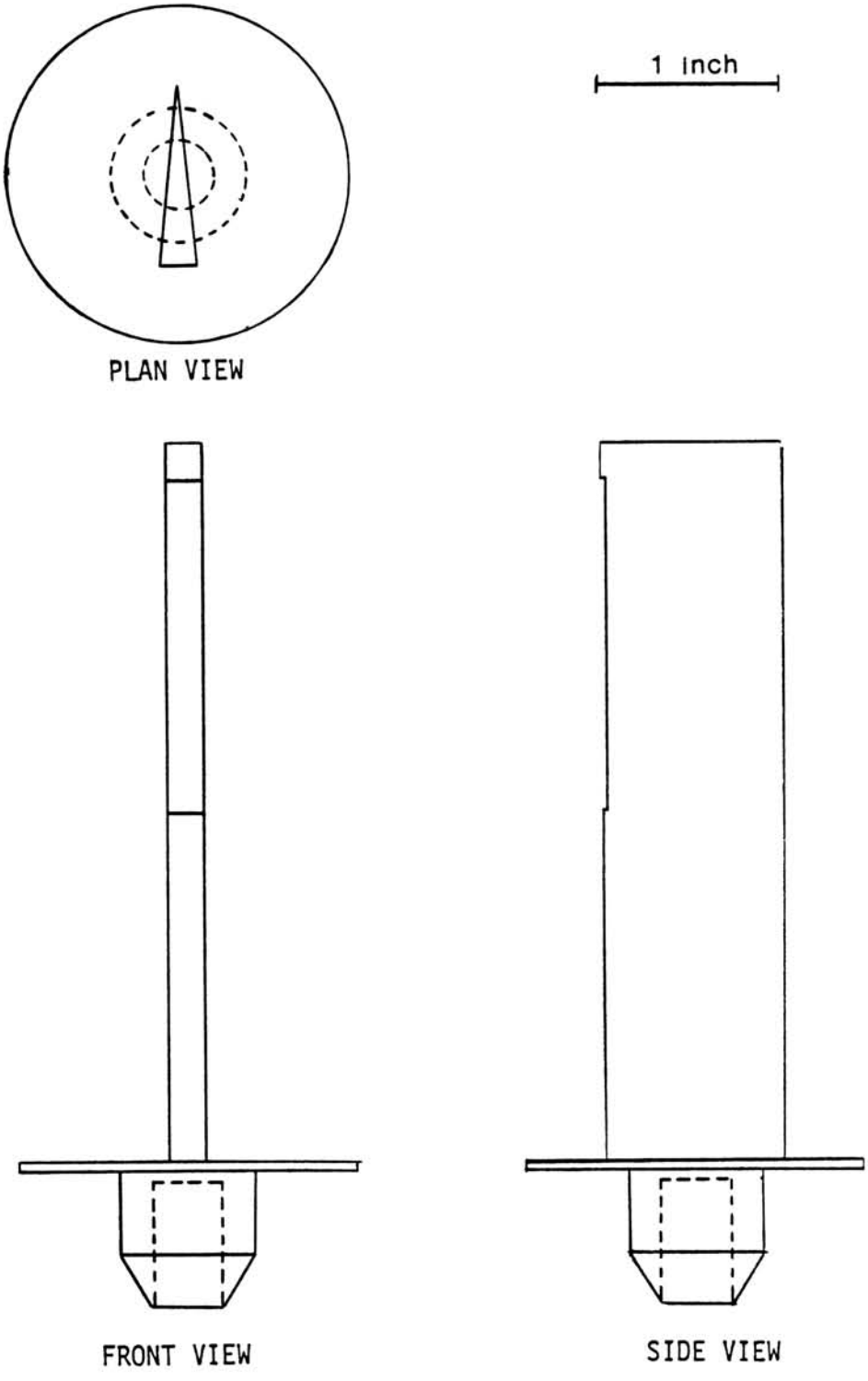

FIGURE 3.12

REFERENCE COLLECTOR BLADE.

LEAST SQUARES CALIBRATION LINES

1 Dye Mass Density ($\mu g/cm^2$) = 0.7601 * Time (sec) + 0.2460 , MVD = 20.36 µm , 36* inches •

2 Dye Mass Density ($\mu g/cm^2$) = 0.6735 * Time (sec) + 0.0620 , MVD = 16.45 µm , 36* inches o

3 Dye Mass Density ($\mu g/cm^2$) = 0.7236 * Time (sec) + 0.1560 , MVD = 20.36 µm , 32* inches ▼

4 Dye Mass Density ($\mu g/cm^2$) = 0.5607 * Time (sec) + 0.1578 , MVD = 16.45 µm , 32* inches x

* Above tunnel floor.

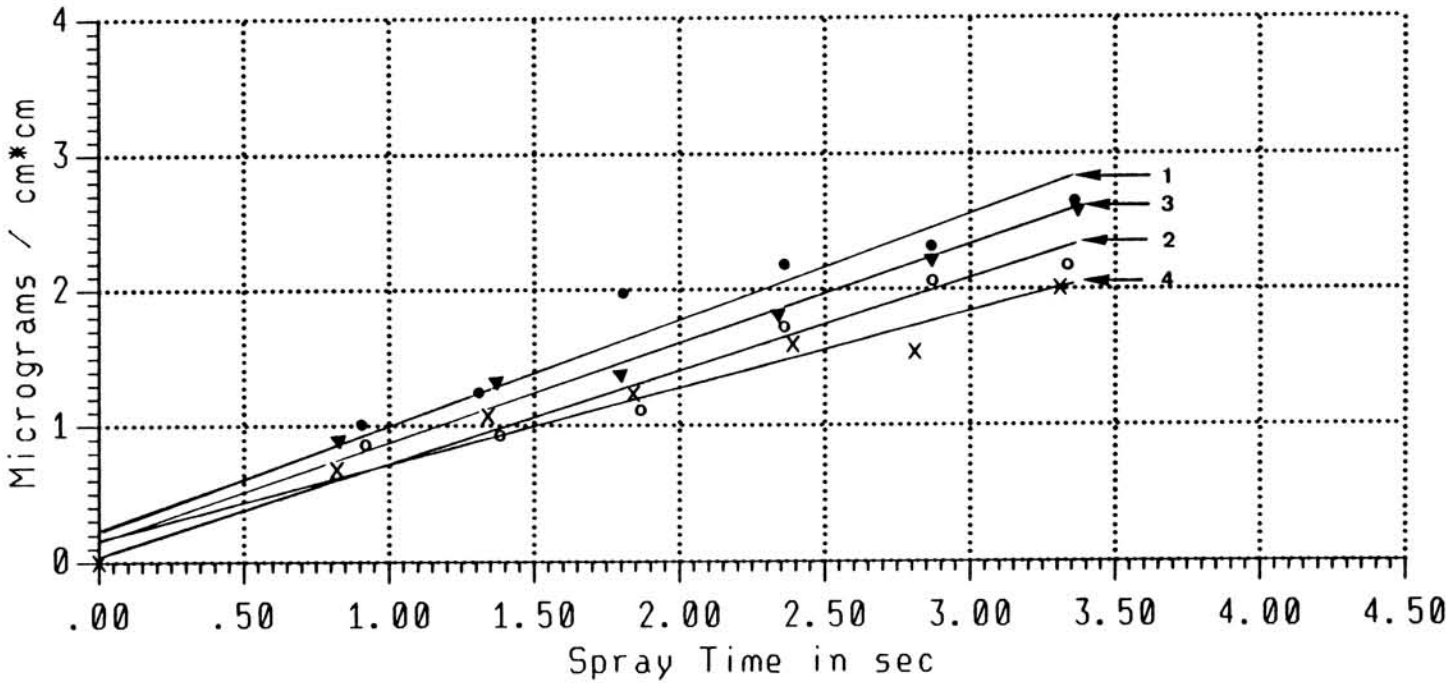

FIGURE 3.13

SINGLE BLADE COLLECTOR CALIBRATION CURVES
(USED WITH ALL TWO-DIMENSIONAL TEST MODELS).

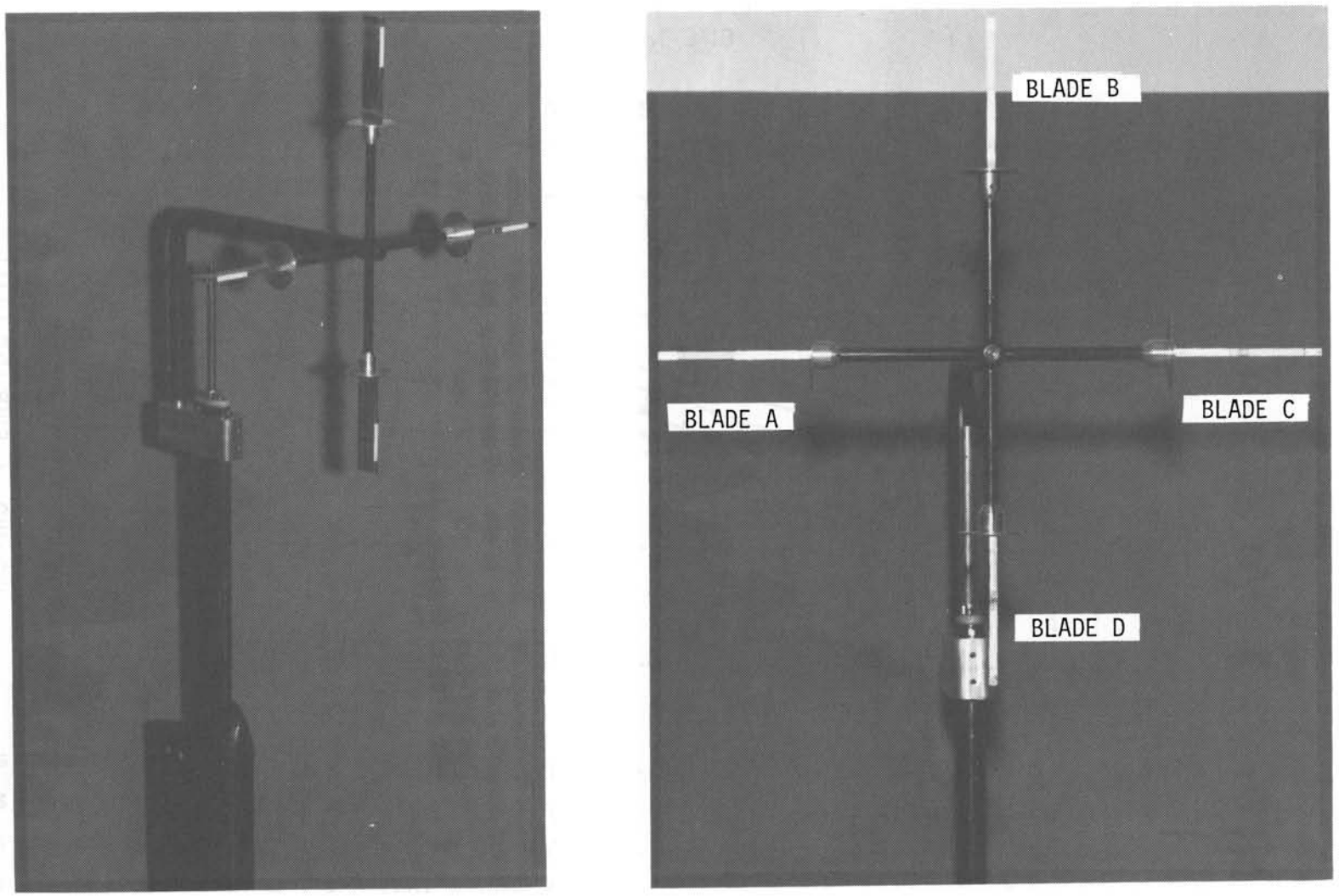

FIGURE 3.14

FOUR BLADE REFERENCE COLLECTOR MECHANISM.

LEAST SQUARES CALIBRATION LINES

Blade-A , Dye Mass Density ($\mu g/cm^2$) = 0.8031 * Time (sec) + 0.0125

Blade-B , Dye Mass Density ($\mu g/cm^2$) = 1.1449 * Time (sec) + 0.0046

Blade-C , Dye Mass Density ($\mu g/cm^2$) = 0.7241 * Time (sec) + 0.0261

Blade-D , Dye Mass Density ($\mu g/cm^2$) = 0.8272 * Time (sec) + 0.0203

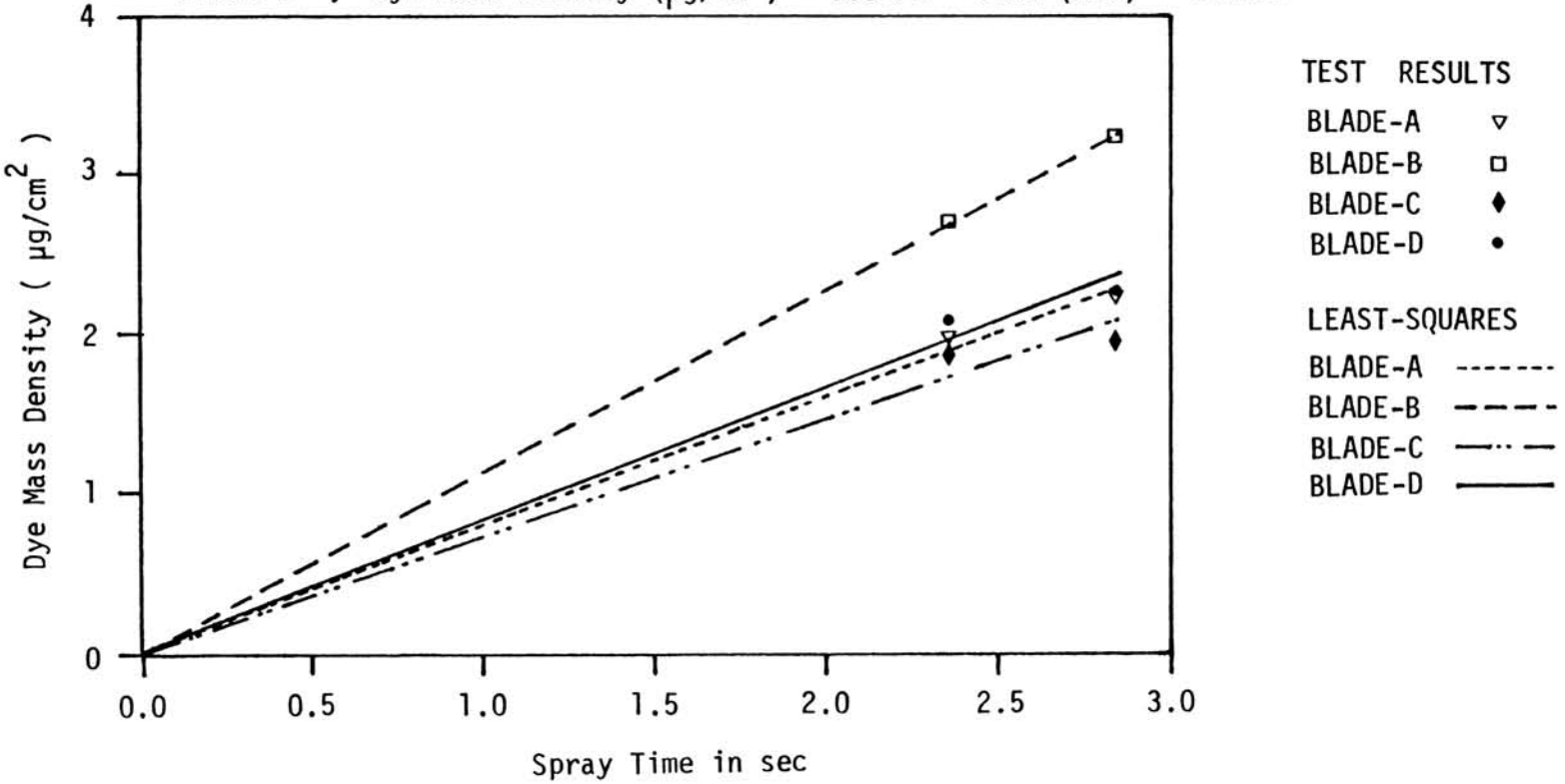

(a) MVD = 20.36 microns - Alpha = 0 Deg., Collector Runs 13,14,15,16,17,18 .

FIGURE 3.15

FOUR BLADE COLLECTOR CALIBRATION CURVES
(USED WITH ALL ENGINE INLET MODELS)
(PAGE 1 OF 4).

LEAST SQUARES CALIBRATION LINES

Blade-A , Dye Mass Density ($\mu g/cm^2$) = 0.6874 * Time (sec) + 0.0157

Blade-B , Dye Mass Density ($\mu g/cm^2$) = 0.9068 * Time (sec) + 0.0106

Blade-C , Dye Mass Density ($\mu g/cm^2$) = 0.6142 * Time (sec) + 0.0160

Blade-D , Dye Mass Density ($\mu g/cm^2$) = 0.6884 * Time (sec) + 0.0115

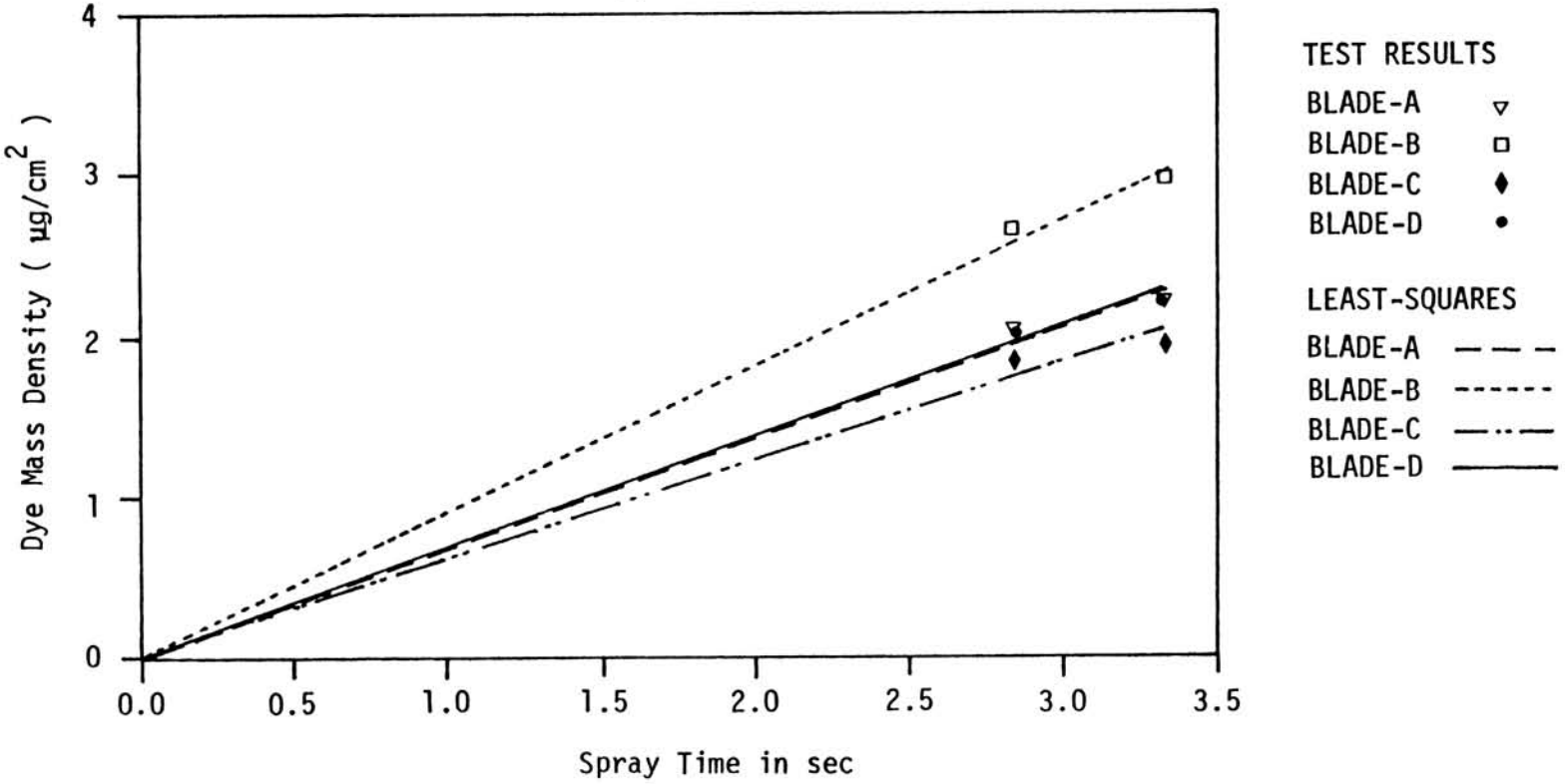

(b) MVD = 16.45 microns - Alpha = 0 Deg., Collector Runs 19,20,21,22,23,24.

FIGURE 3.15

FOUR BLADE COLLECTOR CALIBRATION CURVES
(USED WITH ALL ENGINE INLET MODELS)
(PAGE 2 OF 4).

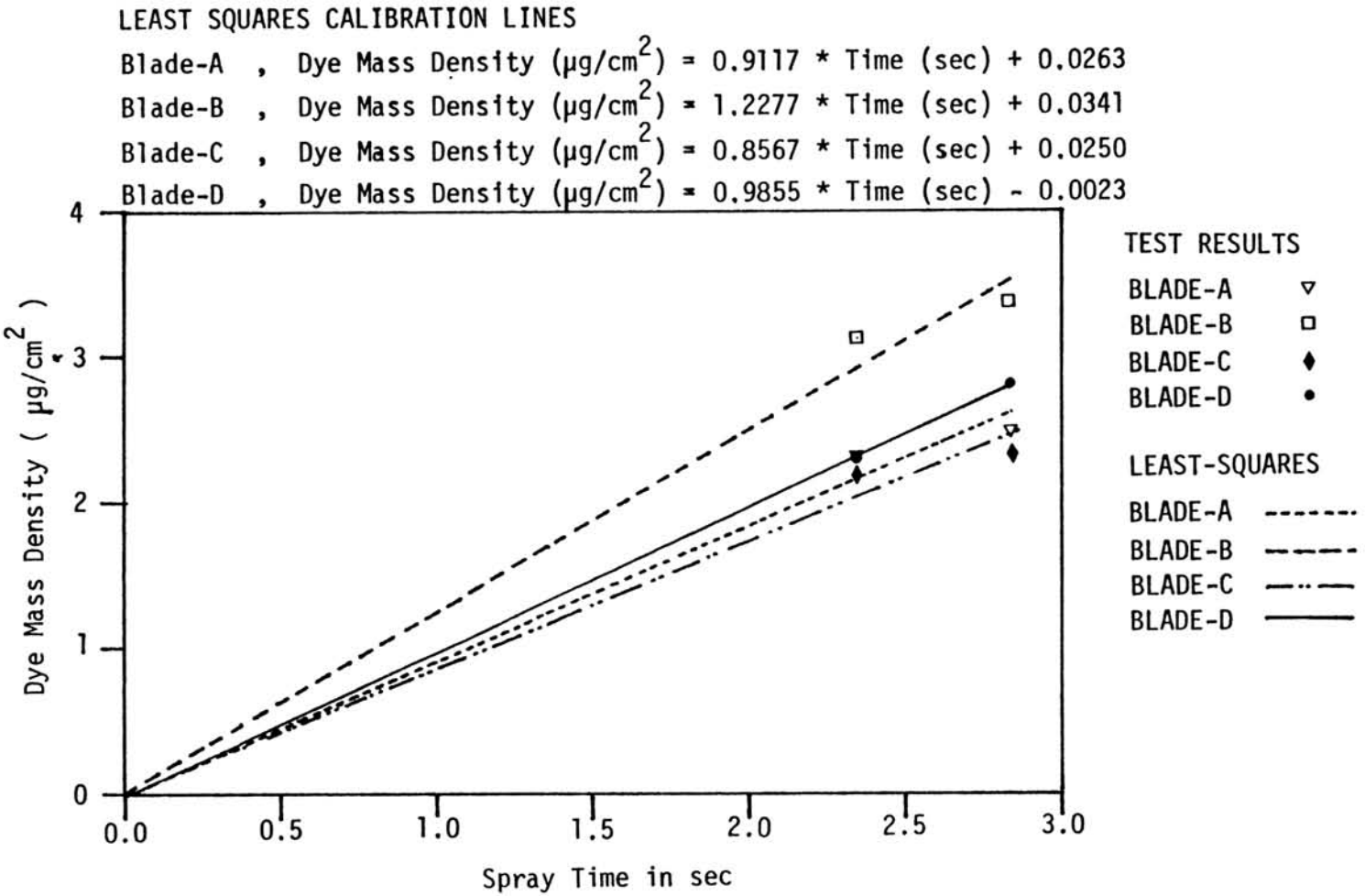

(c) MVD = 20.36 microns - Alpha = 15 Deg. , Collector Runs 1,2,3,4,5,6,7.

FIGURE 3.15

FOUR BLADE COLLECTOR CALIBRATION CURVES
(USED WITH ALL ENGINE INLET MODELS)
(PAGE 3 OF 4).

LEAST SQUARES CALIBRATION LINES

Blade-A , Dye Mass Density ($\mu g/cm^2$) = 0.7392 * Time (sec) + 0.0098

Blade-B , Dye Mass Density ($\mu g/cm^2$) = 0.9740 * Time (sec) + 0.0128

Blade-C , Dye Mass Density ($\mu g/cm^2$) = 0.6586 * Time (sec) + 0.0275

Blade-D , Dye Mass Density ($\mu g/cm^2$) = 0.7408 * Time (sec) + 0.0230

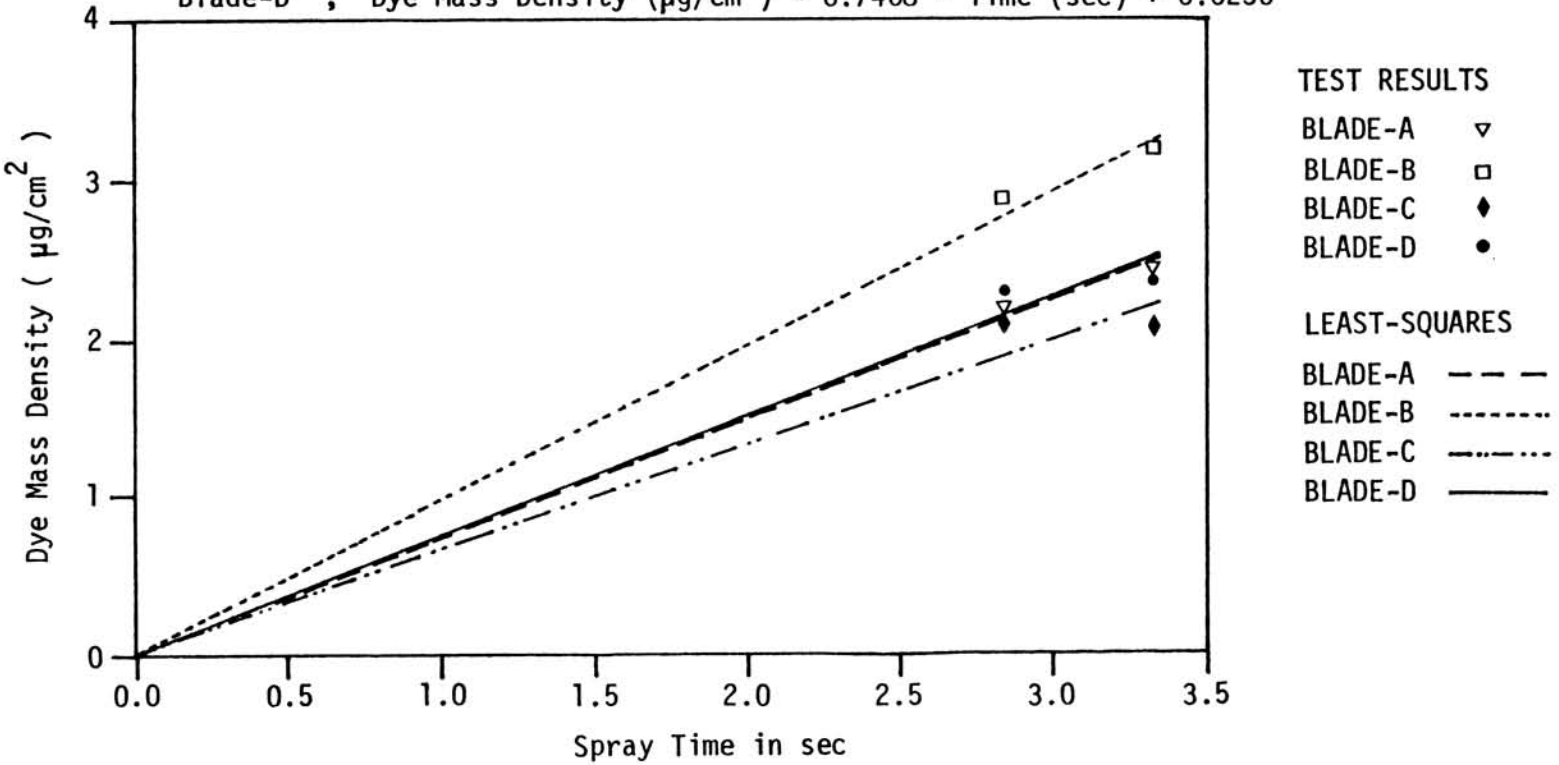

(d) MVD = 16.45 microns - Alpha = 15 Deg. , Collector Runs 8,9,10,11,12.

FIGURE 3.15

FOUR BLADE COLLECTOR CALIBRATION CURVES
(USED WITH ALL ENGINE INLET MODELS)
(PAGE 4 OF 4).

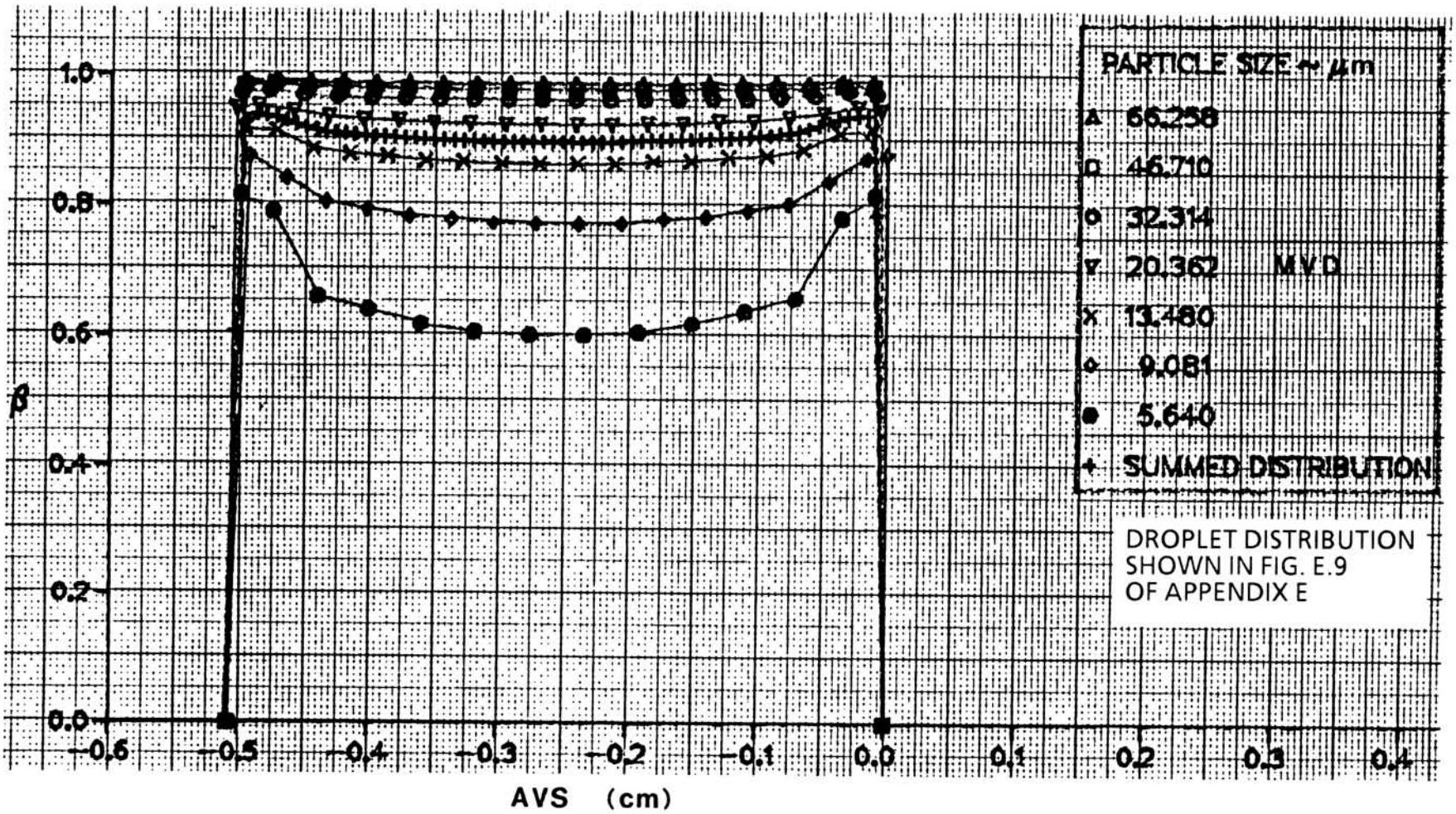

FIGURE 3.16

THEORETICAL IMPINGEMENT EFFICIENCY OF COLLECTOR BLADE
(MVD = 20.36 MICRONS, PRESSURE RATIO = 0.65).

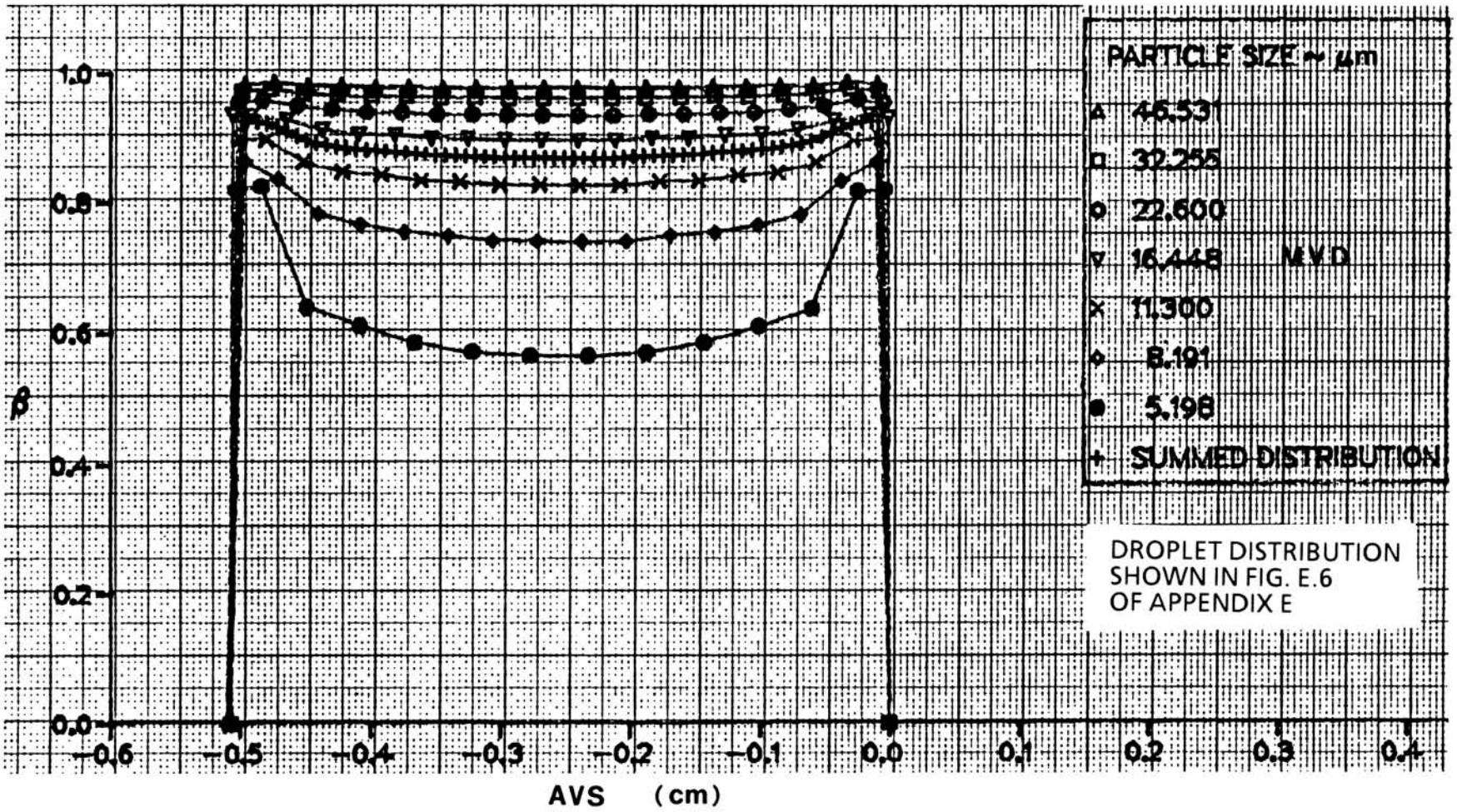

FIGURE 3.17

THEORETICAL IMPINGEMENT EFFICIENCY OF COLLECTOR BLADE
(MVD = 16.45 MICRONS, PRESSURE RATIO = 0.80).

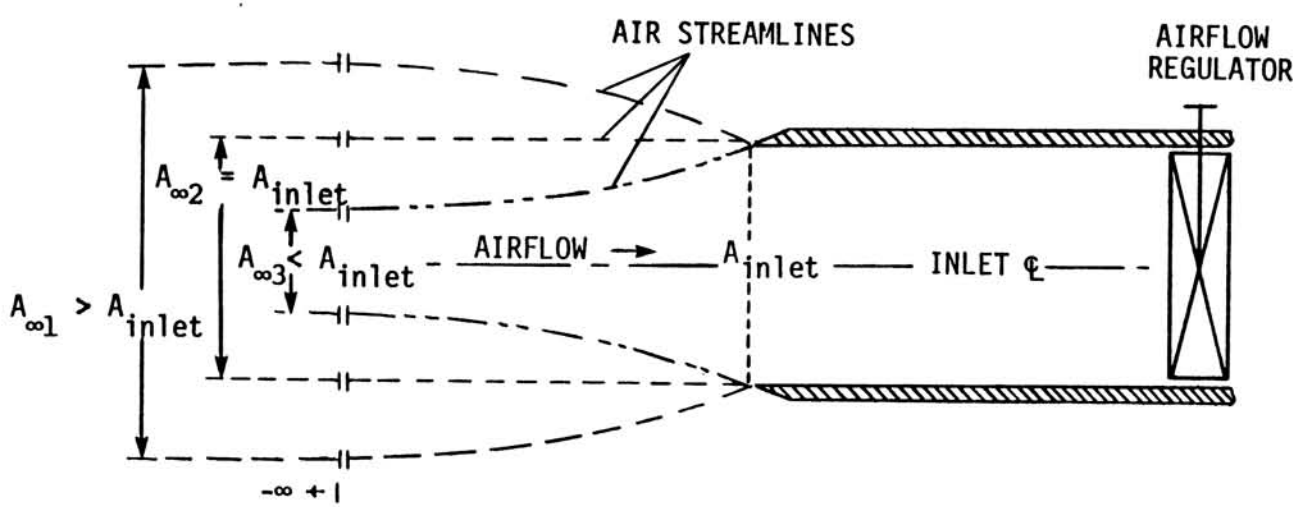

FIGURE 3.18

SCHEMATIC OF INLET CAPTURE AREA RATIOS AT VARIOUS SUCTION FLOWS.

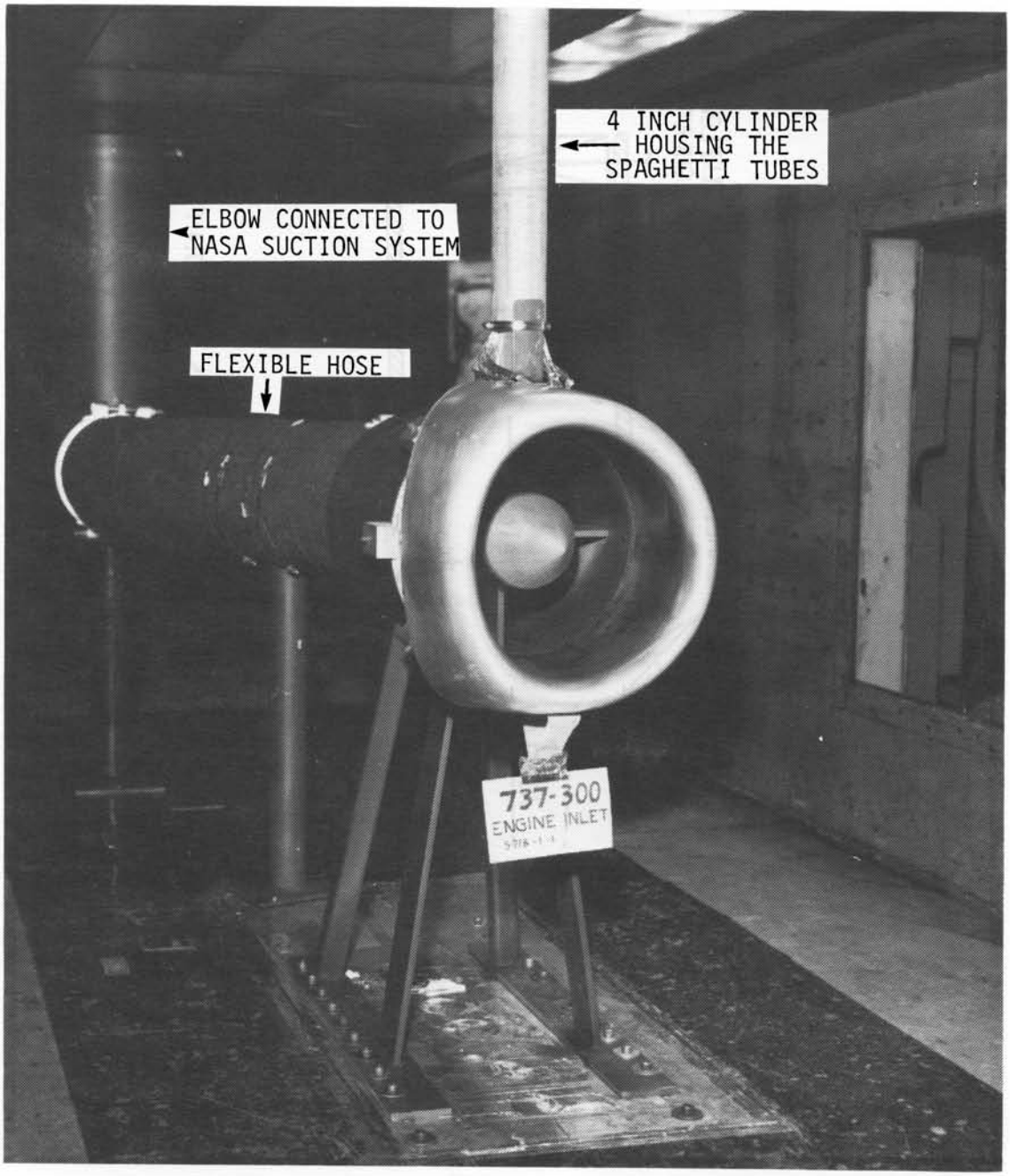

FIGURE 3.19

INSTALLATION OF BOEING 737-300 INLET IN THE IRT TEST SECTION (LOOKING DOWNSTREAM).

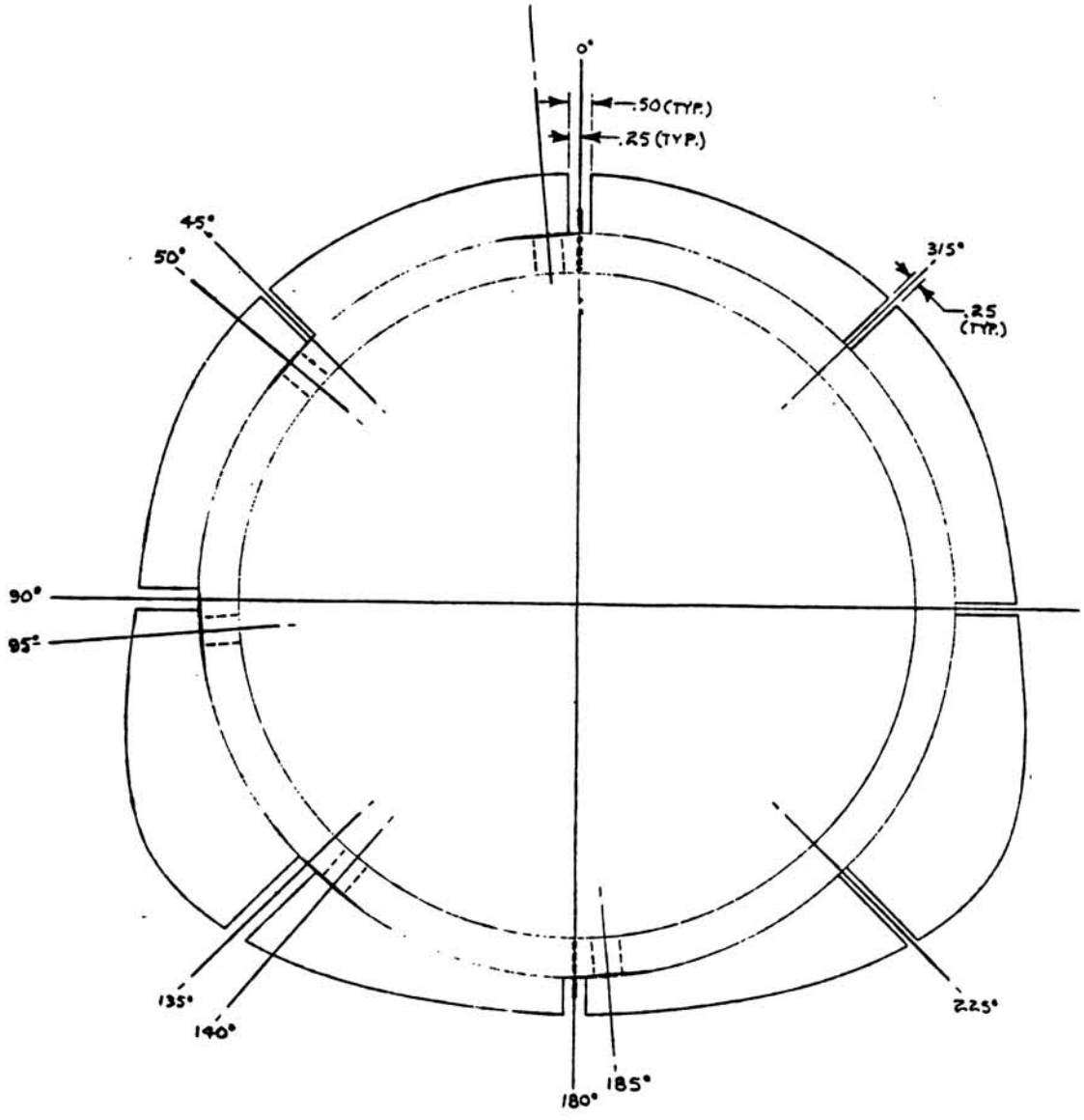

BOEING 737-300 INLET

FIGURE 3.20

STATIC PRESSURE TAP LOCATIONS FOR AXISYMMETRIC AND BOEING 737-300 INLETS (PAGE 1 OF 3).

737-300 (RB-432) INLET MODEL

COWL STATIC PRESSURE INSTRUMENTATION, CONFIG. 1

	FULL SCALE STATION*	0°**	45°	90°	135°	180°	225°	270°	315°
	-14.0	CWA1							
	-10.8	CWA2							
	-7.8	CWA3							
↑	-5.0	CWA4							
	-3.0	CWA5							
	-1.6	CWA6							
EXTERNAL	-0.8	CWA7							
HILITE	0	CWA8	CWB1	CWC1	CWD1	CWE1	CWF1	CWG1	CWH1
INTERNAL	.8	CWA9		CWC2	CWD2	CWE2			
	1.6	CWA10		CWC3	CWD3	CWE3			
	3.0	CWA11		CWC4	CWD4	CWE4			
↓	4.7	CWA12		CWC5	CWD5	CWE5			
	6.8	CWA13	CWB2	CWC6	CWD6	CWE6	CWF2	CWG2	CWH2
	9.4	CWA14		CWC7	CWD7	CWE7			
	12.0	CWA15		CWC8	CWD8	CWE8			
	14.5	CWA16		CWC9	CWD9	CWE9			
	17.0	CWA17		CWC10	CWD10	CWE10			
	21.4	CWA18		CWC11	CWD11	CWE11			
	26.0	CWA19	CWB3	CWC12	CWD12	CWE12	CWF3	CWG3	CWH3
	30.4	CWA20		CWC13	CWD13	CWE13			
	35.0	CWA21		CWC14	CWD14	CWE14			
	39.5	CWA22		CWC15	CWD15	CWE15			
	43.0	CWA23							
	FAN FACE	CWA24	CWB4	CWC16	CWD16	CWE16	CWF4	CWG4	CWH4

*FULL SCALE STATION IS AXIAL DISTANCE AS MEASURED ALONG INLET CENTERLINE.

**ANGLES MEASURED CLOCKWISE, LOOKING DOWNSTREAM

SCALE FACTOR = 7.5/29.45

BOEING 737-300 INLET

FIGURE 3.20

STATIC PRESSURE TAP LOCATIONS FOR AXISYMMETRIC AND BOEING 737-300 INLETS (PAGE 2 OF 3).

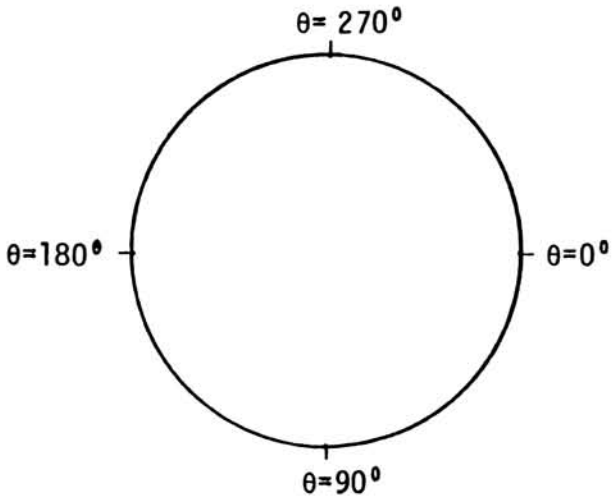

STATION X in.	θ = 0 Deg.	θ = 90 Deg.	θ = 180 Deg.	θ = 270 Deg.
0.56	A-14		A-28	
0.32	A-13		A-27	
0.16	A-12		A-26	
0.00	A-01	A-29	A-15	A-32
0.16	A-02		A-16	
0.36	A-03		A-17	
0.64	A-04		A-18	
1.04	A-05		A-19	
1.52	A-06		A-20	
2.08	A-07	A-30	A-21	B-01
2.40	A-08		A-22	
3.04	A-09		A-23	
6.08	A-10	A-31	A-24	B-02
8.40	A-11		A-25	

Notes:
1. Angles measured clockwise looking downstream.
2. High light at X = 0.
3. Outer cowl X = .56 to X = 0.
4. Inner cowl X = .0 to X = 8.40

AXISYMMETRIC INLET

FIGURE 3.20

STATIC PRESSURE TAP LOCATIONS FOR AXISYMMETRIC AND BOEING 737-300 INLETS (PAGE 3 OF 3).

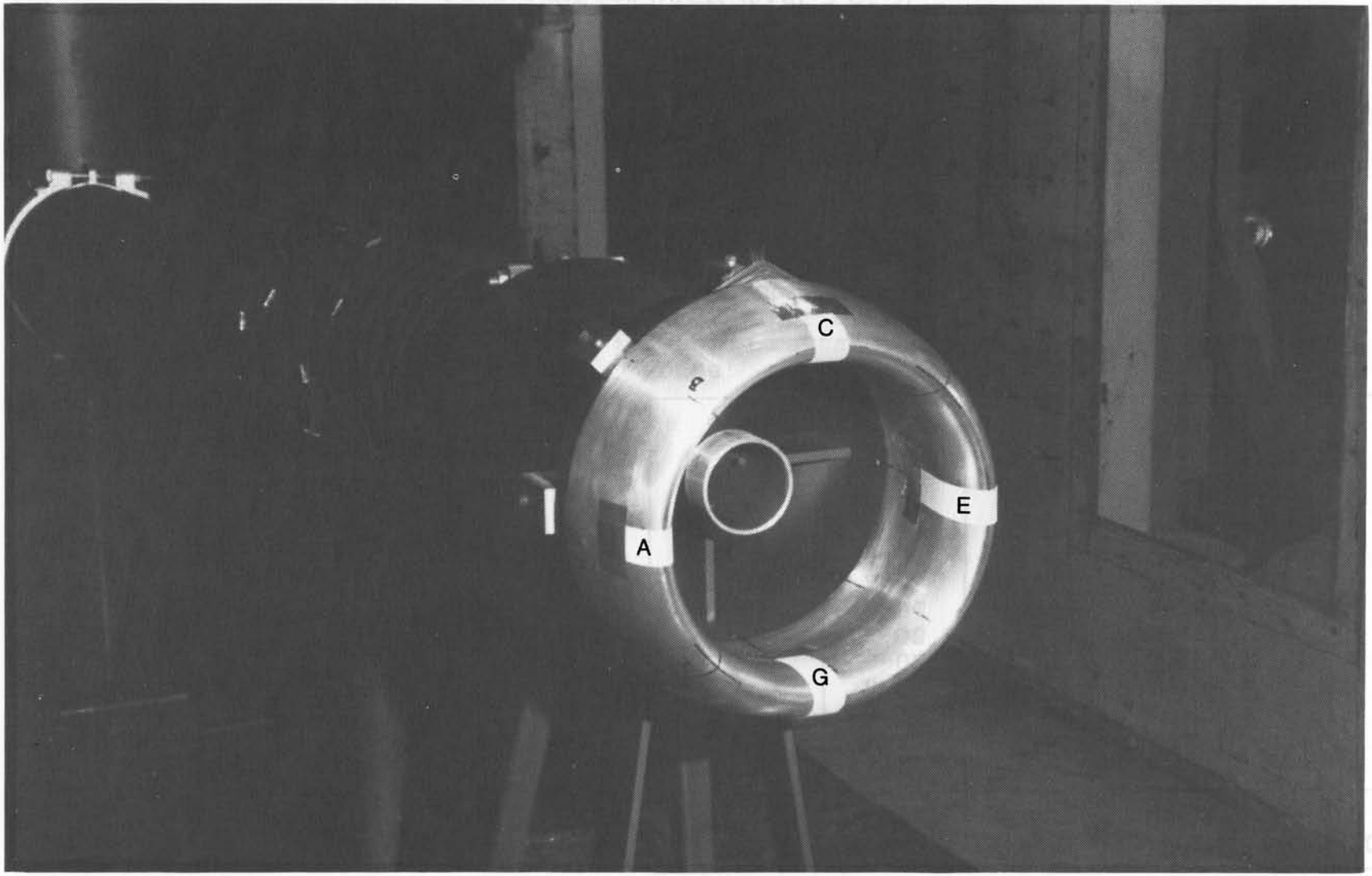

FIGURE 3.21

BLOTTER STRIP LOCATIONS ON AXISYMMETRIC INLET FOR $\alpha = 0°$.

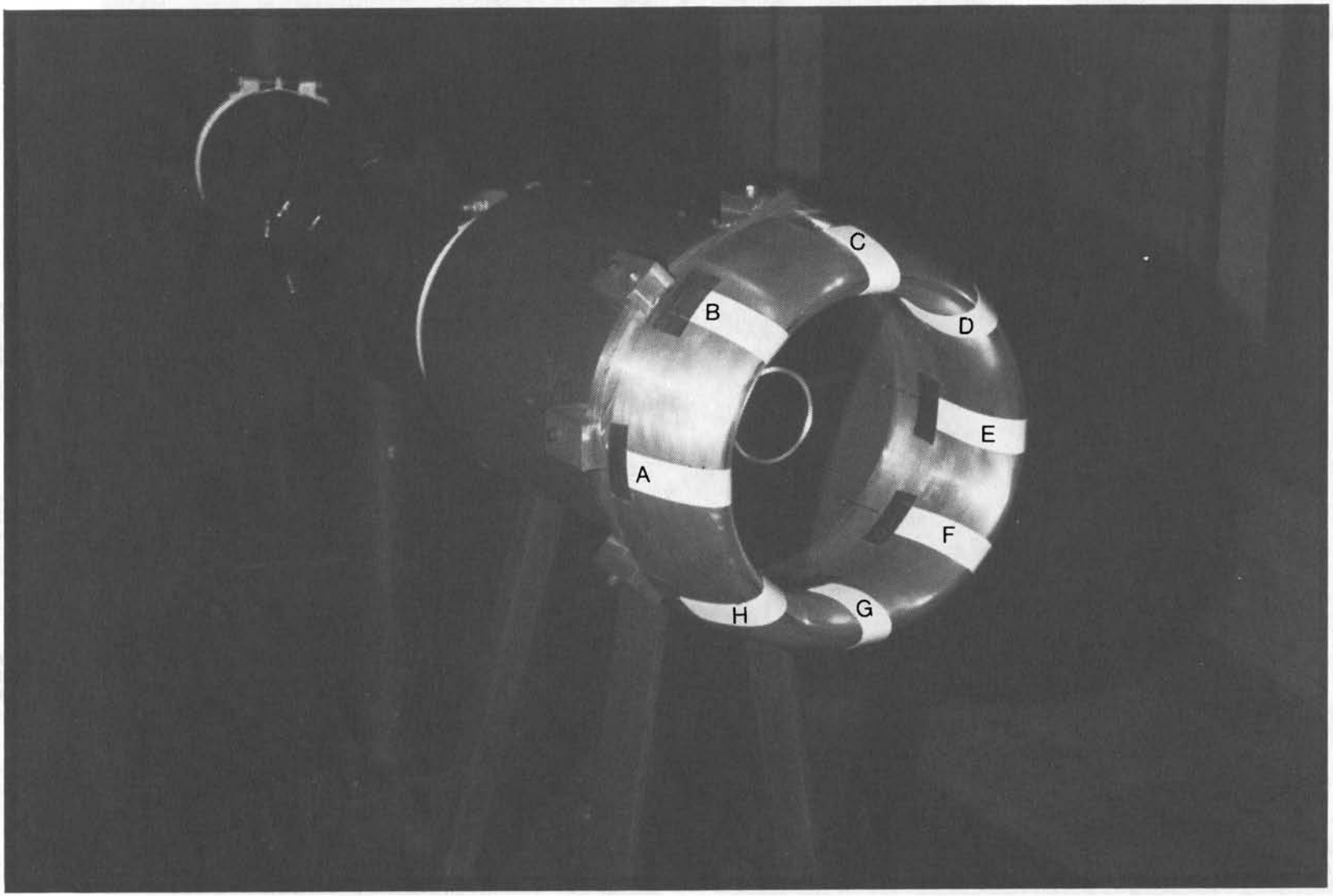

FIGURE 3.22

BLOTTER STRIP LOCATIONS ON AXISYMMETRIC INLET FOR $\alpha = 15°$.

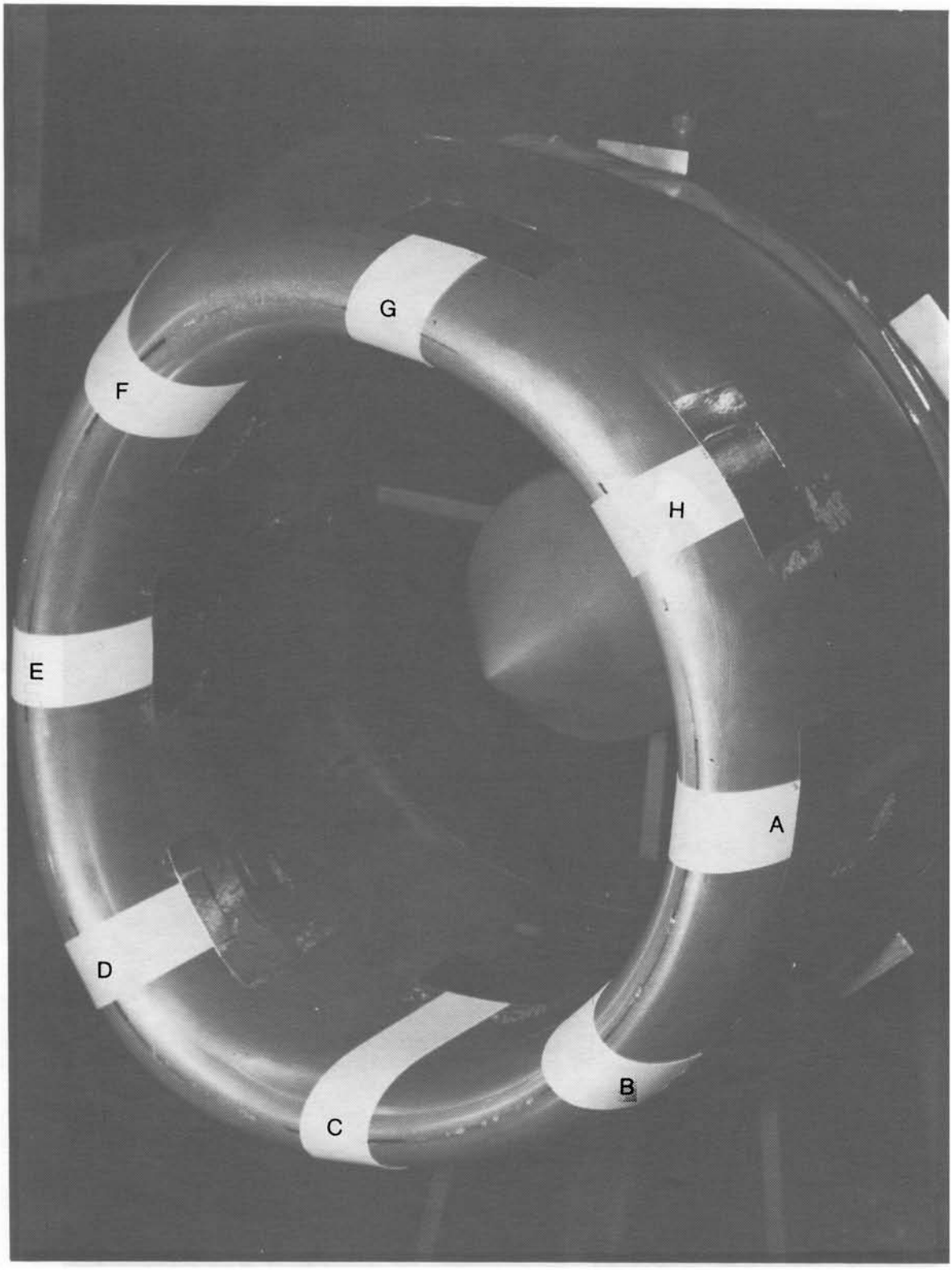

FIGURE 3.23

BLOTTER STRIP LOCATIONS ON BOEING 737-300 INLET
FOR α = 0° AND α = 15° TESTS.

4.0 TEST MODELS AND CONDITIONS

Descriptions of the test models, model location in the tunnel test section and test conditions are given in this section.

4.1 Two-Dimensional Flow Models

The two-dimensional models tested are listed in Table 4.1. Their streamwise sections are presented in Figure 4.1. The coordinates for the NACA 65_2015 airfoil, MS(1)-0317 airfoil and ice shapes are given in Figure 4.2. The airfoils and the four inch cylinder spanned the 6-foot height of the tunnel. All ice shapes were 18 inches in span and were mounted on a two inch cylinder as shown in Figure 4.1.

TABLE 4.1

TWO-DIMENSIONAL TEST MODELS

MODEL	CHORD LENGTH IN STREAMWISE DIRECTION, INCHES	SPAN, INCHES	REMARKS
CYLINDER	4	72	STEEL PIPE MOUNTED AT CENTER OF TURNTABLE.
65_2015	13	72	WOODEN MODEL. LEADING EDGE WAS 5 INCHES AHEAD OF TURNTABLE CENTER.
MS(1)-0317	36	72	WOODEN MODEL. LEADING EDGE WAS 14.75 INCHES AHEAD OF TURNTABLE CENTER.
3-ICE SHAPES	2*	18	SMALL GLAZE, LARGE GLAZE AND RIME. ALL ICE SHAPES WERE MOUNTED ON A 2-INCH DIAMETER CYLINDER. THE CYLINDER WAS 72 INCHES IN SPAN.

* CHORD REFERENCED TO THE UNACCRETED BODY

The locations of the airfoil sections with respect to the tunnel turntable center are shown in Figure 4.3. The leading edge of each of the two-dimensional models was about 200 inches downstream from the entrance to the test section.

The cylinders and the 65_2015 models were chosen so that results obtained with the present method can be compared with existing data taken during NACA tests of the 1950's. In addition, analytical predictions of

droplet impingement are easy to generate for these models for comparison with experimental data.

The MS(1)-0317 airfoil was chosen because it is representative of the family of supercritical airfoils. Such airfoil sections are used on modern high speed transport aircraft.

Computer trajectory codes (Reference 18) are often used to determine impingement characteristics of bodies with ice growth. The ice shapes and accumulation are important factors in such studies. The simulated ice shapes tested are representative of the types often encountered on aircraft surfaces.

4.2 Engine Inlets

The axisymmetric inlet and the Boeing 737-300 (0.2547 scale) model, employed in this test, were provided by the Boeing Commercial Airplane Company. These models were chosen because they: (a) represent modern inlet designs, (b) have well defined surface geometries so that accurate flow field data can be obtained from analytical codes and (c) have a sufficient number of built-in static pressure taps for measuring surface pressure distributions.

The fan face, throat and highlight areas for the axisymmetric and Boeing 737-300 inlets are given in Table 4.2. Brief geometry definitions for the two inlets are given in Figures 4.4 and 4.5. Complete 737-300 geometry is available on computer tape (Shaw, R.J., NASA, Lewis Research Center). The center body for the 737-300 inlet is shown in Figure 4.6. No center body was used with the axisymmetric inlet.

TABLE 4.2

FAN FACE, THROAT AND HIGHLIGHT AREAS FOR AXISYMMETRIC AND BOEING 737-300 INLETS

GEOMETRY	737-300 INLET	AXISYMMETRIC INLET
FAN FACE AREA ~ IN^2	149.77	176.71
THROAT AREA ~ IN^2	143.01	141.95
HIGHLIGHT AREA ~ IN^2	185.58	181.70

The 737-300 inlet, support assembly and mass flow connections were shown earlier in Figure 3.19. A close up view of the aluminum brackets used to attach the inlet to its cylindrical support is given in Figure 4.7. The axial locations of the engine inlet vertical plane and compressor face with respect to the tunnel axis are shown in Figure 4.8.

4.2.1 Axisymmetric Geometry - Axisymmetric Flow

An axisymmetric inlet at an angle of attack of zero degrees represents the simplest flow case for an engine inlet. Test results obtained for this case can be used to validate existing codes (see for example References 18 and 19) which can only handle simple geometries and axisymmetric flow fields.

4.2.2 Axisymmetric Geometry - Three Dimensional Flow

A number of computer codes capable of predicting three dimensional flow fields have only axisymmetric geometry capability and thus cannot handle complex three dimensional geometries. To help validate such codes an axisymmetric inlet model was tested at an angle of attack of 15 degrees and two different mass flows (Table 4.3). The angle of attack produces a three dimensional flow field around the axisymmetric inlet.

4.2.3 Three Dimensional Geometry - Three Dimensional Flow

For this test case, a Boeing 737-300 inlet was tested at various mass flows and two angles of attack as indicated in Table 4.3. This inlet has a complex three dimensional geometry, a three dimensional flow field and can be analyzed by some recently developed codes (Reference 4). The data base produced from the present tests can be used to validate these codes which are capable of predicting particle trajectories about inlets with complex geometries in three dimensional flows.

4.3 Test Condition Matrix

Models tested, individual test conditions, test configurations and number of blotter strips used for each configuration are shown in Table 4.3. The tests produced a total number of 550 blotter strips (including 120 reference collector strips). Data from these strips were reduced by scanning along the length of each strip at three different width locations (see Figure 5.12) using the automated data processing system discussed in Section 5.

A variety of test models and conditions were selected to provide an extensive data base. The angle of attack of the NACA 65_2015 and supercritical MS(1)-0317 airfoils was limited to 8 degrees to avoid flow separation. The engine inlet angle of attack was limited to 15 degrees to keep the inlet models well within the uniformity region of the IRT tunnel (see Figure 4.8). The flow about the inlet was attached as can be seen from the test pressure data presented in Section 6.

The spray pressure ratios chosen (0.8 and 0.65) correspond to water droplet clouds with an MVD of approximately 16.45 and 20.36 microns which are representative of realistic icing cloud conditions.

Engine inlet mass flows of 22.96 lbm/sec, 17.2 lbm/sec and 11.47 lbm/sec correspond to capture ratios of 1, 0.75, and 0.5 respectively. These capture ratios are representative of various flight conditions as shown in Table 4.4.

TABLE 4.3

TEST CONDITION MATRIX (PAGE 1 OF 2)

TEST MODEL	ANGLE OF ATTACK	PRESSURE RATIO	MVD	INLET MASS FLOW	NUMBER OF TESTS	SPRAY TIME	BLOTTER STRIPS PER TEST	TOTAL NO. OF BLOTTER STRIPS	TEST DATE	TEST ID
	~ DEG.	AIR / WATER ~PSIG / ~PSIG	~ MICRONS	~ LBM/SEC		~ SEC				
FOUR INCH DIAMETER CYLINDER	NA	0.65	20.36	NA	4	2.0	2	16	9/18/85	CYL-1,2,3,8
		0.80	16.45		4	2.5	2			CYL-4,5,6,7
NACA $65_2$015 AIRFOIL SECTION 13 INCH CHORD	0.0	0.65	20.36	NA	3	2.0	2	12	9/26/85	1,2,3-015-0
		0.80	16.45		3	2.5	2			4,5,6-015-0
	8.0	0.65	20.36	NA	3	2.0	2	12	9/26/85	7,8,9-015-8
		0.80	16.45		3	2.5	2			10,11,12-015-8
MS(1)-0317 SUPERCRITICAL AIRFOIL SECTION 36 INCH CHORD	0.0	0.65	20.36	NA	3	2.0	2	12	9/26/85	1,2,3-SUP-0
		0.80	16.45		3	2.5	2			4,5,6-SUP-0
	8.0	0.65	20.36	NA	3	2.0	2	12	9/26/85	7,8,9-SUP-8
		0.80	16.45		3	2.5	2			10,11,12-SUP-8

TABLE 4.3

TEST CONDITION MATRIX (PAGE 2 OF 2)

TEST MODEL	ANGLE OF ATTACK	PRESSURE RATIO	MVD	INLET MASS FLOW	NUMBER OF TESTS	SPRAY TIME	BLOTTER STRIPS PER TEST	TOTAL NO. OF BLOTTER STRIPS	TEST DATE	TEST ID
	~ DEG.	AIR / WATER ~PSIG / ~PSIG	~ MICRONS	~ LBM/SEC		~ SEC				
RIME ICE SHAPE	0.0	0.65	20.36	NA	2	2.0	1	2	9/26/85	1,2-RIME
SMALL GLAZE ICE SHAPE	0.0	0.65	20.36	NA	2	2.0	1	2	9/26/85	1,2-SG
LARGE GLAZE ICE SHAPE	0.0	0.65	20.36	NA	2	2.0	1	2	9/26/85	1,2-LG
AXISYMMETRIC ENGINE INLET	0.0	0.65	20.36	22.96	3	2.0	4	48	9/21&23/85	13,14,15-AXI-0
				17.20	3	2.0	4		9/23/85	16,17,18-AXI-0
		0.80	16.45	22.96	3	2.5	4		9/23/85	19,20,21-AXI-0
				17.20	3	2.5	4		9/23/85	22,23,24-AXI-0
	15.0	0.65	20.36	22.96	3	2.0	8	96	9/21/85	1,2,3-AXI-15
				17.20	3	2.0	8		9/21/85	4,5,6-AXI-15
		0.80	16.45	22.96	3	2.5	8		9/21/85	7,8,9-AXI-15
				17.20	3	2.5	8		9/21/85	10,11,12-AXI-15
BOEING 737-300 ENGINE INLET	0.0	0.65	20.36	22.96	3	2.0	8	96	9/23/85	1,2,3-737-0
				17.20	3	2.0	8		9/23/85	4,5,6-737-0
		0.80	16.45	22.96	3	2.5	8		9/23/85	7,8,9-737-0
				17.20	3	2.5	8		9/23/85	10,11,12-737-0
	15.0	0.65	20.36	22.96	3	2.0	8	120	9/23/85	13,14,15-737-15
				17.20	3	2.0	8		9/23/85	16,17,18-737-15
		0.80	16.45	22.96	3	2.5	8		9/24/85	19,20,21-737-15
				17.20	3	2.5	8		9/24/85	22,23,24-737-15
				11.47	3	2.5	8		9/24/85	25,26,27-737-15

TABLE 4.4

747 ANTI-ICING FLIGHT CONDITIONS (REFERENCE 20)

ALTITUDE ~ FT.	FLIGHT CONDITION	MACH NUMBER	CAPTURE AREA RATIO
0	TAKE-OFF	0.24	2.05
5,000	CLIMB	0.60	0.84
10,000	HOLD	0.40	0.82
15,000	CLIMB	0.73	0.76
15,000	DESCENT	0.68	0.49

Each set of conditions was repeated three times to obtain a statistical average. For the cylinders, the tests were repeated four times per condition.

The single blade reference collector was calibrated using six different exposure times, two locations and two droplet sizes giving a total of 24 tests. This collector was used to determine the cloud liquid water content for the 4 inch cylinder, airfoils and ice shapes.

The four blade reference collector was calibrated using two exposure times, two locations, and two droplet sizes and three repeats giving a total of 24 tests. The results obtained from the four blade collector tests were used to determine the cloud liquid water content for engine inlets.

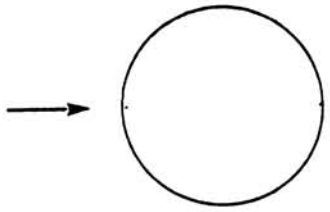

(A) 4 INCH CYLINDER

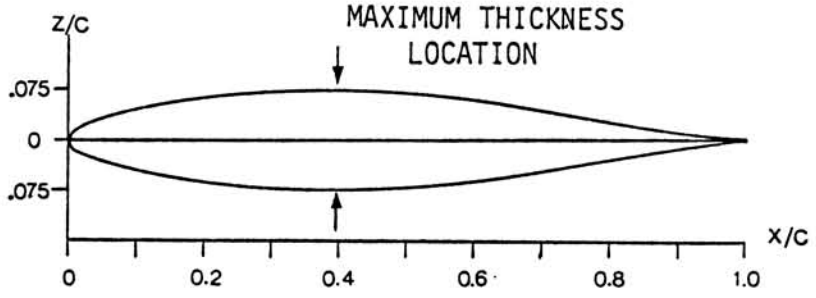

(B) 65_2015 AIRFOIL

FIGURE 4.1

TWO-DIMENSIONAL TEST MODEL SECTIONS
(PAGE 1 OF 3).

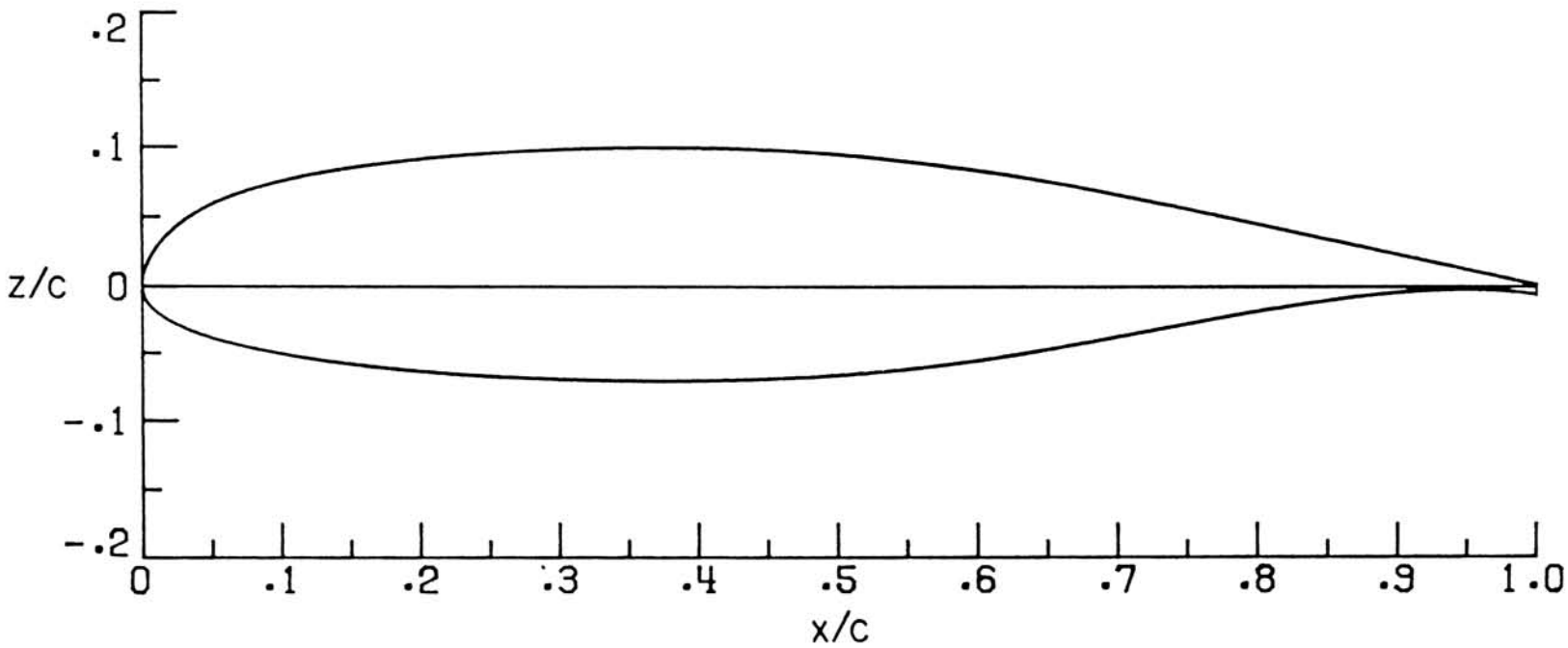

(C) MS(1)-0317 SUPERCRITICAL AIRFOIL

FIGURE 4.1

TWO-DIMENSIONAL TEST MODEL SECTIONS
(PAGE 2 OF 3).

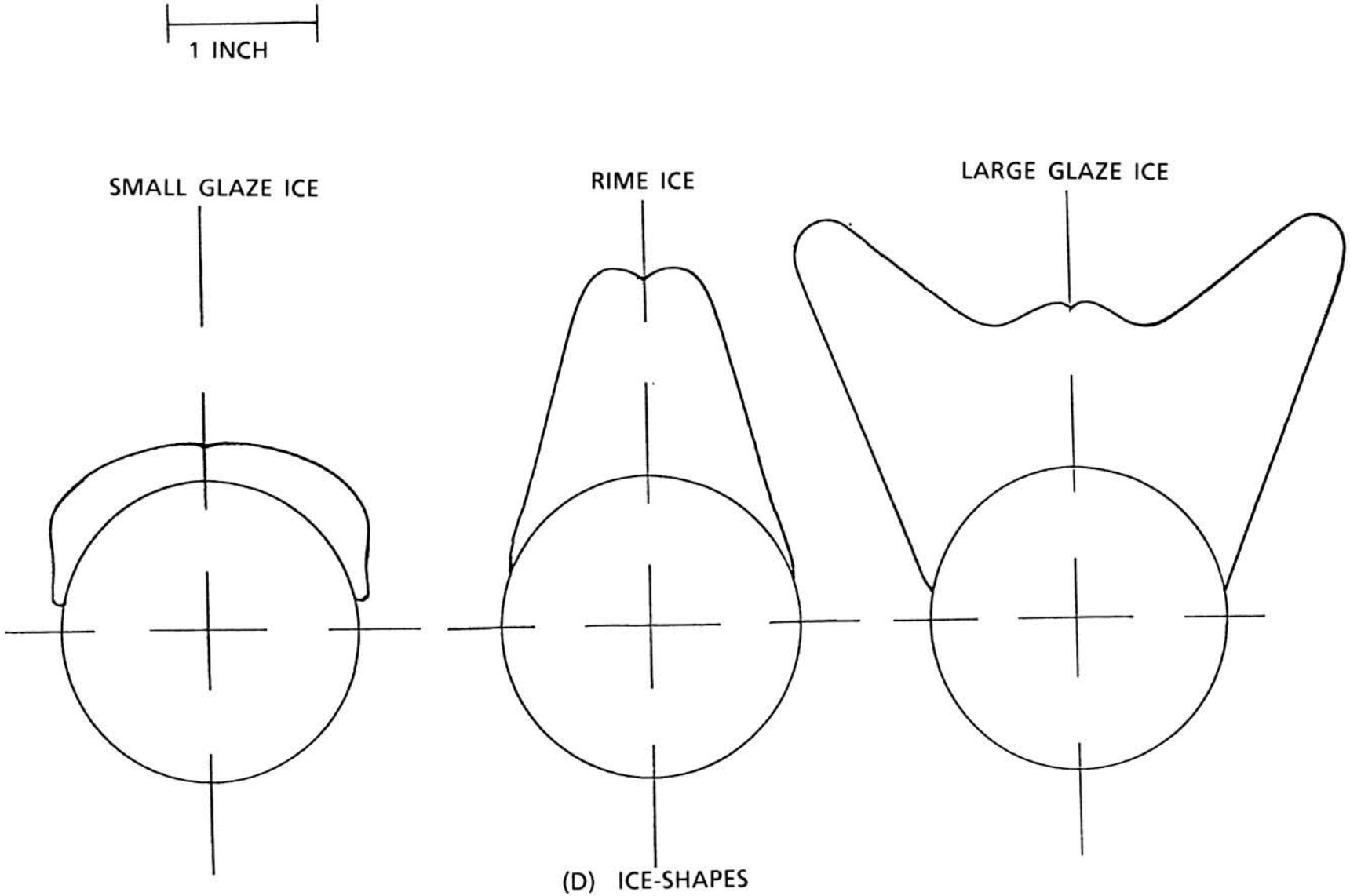

FIGURE 4.1

TWO-DIMENSIONAL TEST MODEL SECTIONS
(PAGE 3 OF 3).

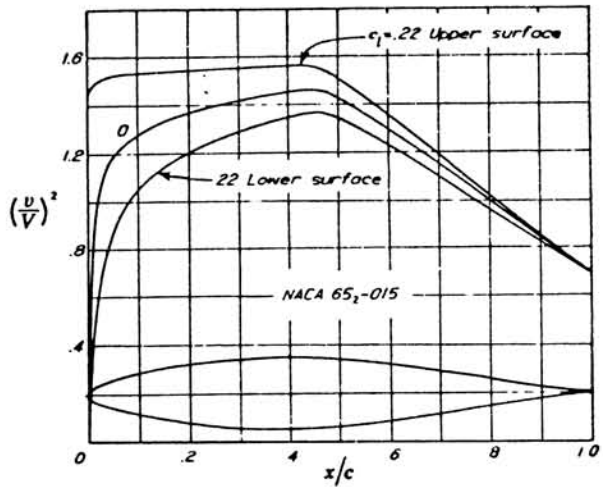

x (per cent c)	y (per cent c)	$(v/V)^2$	v/V	$\Delta v_s/V$
0	0	0	0	2.038
0.5	1.124	0.654	0.809	1.729
0.75	1.356	0.817	0.904	1.390
1.25	1.702	0.939	0.969	1.156
2.5	2.324	1.063	1.031	0.920
5.0	3.245	1.184	1.088	0.682
7.5	3.959	1.241	1.114	0.563
10	4.555	1.281	1.132	0.487
15	5.504	1.336	1.156	0.393
20	6.223	1.374	1.172	0.334
25	6.764	1.397	1.182	0.290
30	7.152	1.418	1.191	0.255
35	7.396	1.438	1.199	0.227
40	7.498	1.452	1.205	0.203
45	7.427	1.464	1.210	0.184
50	7.168	1.433	1.197	0.160
55	6.720	1.369	1.170	0.143
60	6.118	1.297	1.139	0.127
65	5.403	1.228	1.108	0.109
70	4.600	1.151	1.073	0.096
75	3.744	1.077	1.038	0.078
80	2.858	1.002	1.001	0.068
85	1.977	0.924	0.961	0.052
90	1.144	0.846	0.920	0.038
95	0.428	0.773	0.879	0.026
100	0	0.697	0.835	0
L.E. radius: 1.505 per cent c				

NACA 65_2015 AIRFOIL COORDINATES

FIGURE 4.2

GEOMETRY OF TWO-DIMENSIONAL TEST MODELS (PAGE 1 OF 5).

MS(1)-0317 AIRFOIL COORDINATES

x / c	z / c, UPPER	z / c, LOWER
0.00000	0.00099	0.00099
.00200	.01248	−.00857
.00500	.01950	−.01366
.01250	.03099	−.02105
.02500	.04322	−.02866
.03750	.05210	−.03423
.05000	.05893	−.03865
.07500	.06840	−.04541
.10000	.07511	−.05058
.12500	.08033	−.05477
.15000	.08454	−.05817
.17500	.08805	−.06099
.20000	.09096	−.06330
.22500	.09339	−.06527
.25000	.09536	−.06685
.27500	.09694	−.06812
.30000	.09815	−.06909
.32500	.09901	−.06978
.35000	.09952	−.07021
.37500	.09972	−.07036
.40000	.09956	−.07019
.42500	.09909	−.06967
.45000	.09826	−.06880
.47500	.09700	−.06755
.50000	.09535	−.06591
.52500	.09323	−.06389
.55000	.09073	−.06138
.57500	.08777	−.05845
.60000	.08448	−.05501
.62500	.08079	−.05106
.65000	.07672	−.04674
.67500	.07232	−.04214
.70000	.06763	−.03735
.72500	.06269	−.03255
.75000	.05755	−.02780
.77500	.05225	−.02309
.80000	.04687	−.01857
.82500	.04132	−.01433
.85000	.03576	−.01049
.87500	.03013	−.00719
.90000	.02444	−.00460
.92500	.01873	−.00289
.95000	.01302	−.00232
.97500	.00720	−.00324
1.00000	.00125	−.00597

FIGURE 4.2

GEOMETRY OF TWO-DIMENSIONAL TEST MODELS (PAGE 2 OF 5).

COORDINATES FOR 2 MINUTE GLAZE ICE ACCRETION
(NOTE: DATA FROM NASA - LEWIS)

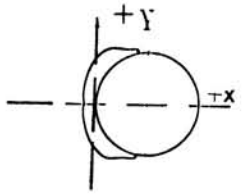

C = .0508 m = 2.0"

X/C

1.0000000	0.9980649	0.9922500	0.9825492	0.9689901	0.9516240
0.9310589	0.9071791	0.8801693	0.8502499	0.8188995	0.7850649
0.7489684	0.7108700	0.6710334	0.6297538	0.5873248	0.5440689
0.4999999	0.4759901	0.4524940	0.4290000	0.4054999	0.3820097
0.3584803	0.3355491	0.3122243	0.2890708	0.2673995	0.2446043
0.2220708	0.1991948	0.1762047	0.1531397	0.1303445	0.1108405
0.0909448	0.0724606	0.0558996	0.0394547	0.0247559	0.0099842
-0.0042106	-0.0170197	-0.0281004	-0.0373091	-0.0450689	-0.0515197
-0.0580197	-0.0644389	-0.0698149	-0.0747105	-0.0804842	-0.0849507
-0.0852500	-0.0850000	-0.0850000	-0.0854055	-0.0842637	-0.0799999
-0.0839192	-0.0852854	-0.0850196	-0.0853640	-0.0842637	-0.0813838
-0.0760491	-0.0694646	-0.0637953	-0.0585098	-0.0538406	-0.0481850
-0.0410039	-0.0333346	-0.0256988	-0.0163307	-0.0048189	0.0073898
0.0204154	0.0348799	0.0477657	0.0610098	0.0794842	0.0971141
0.1165746	0.1383858	0.1608444	0.1835490	0.2056909	0.2272854
0.2490747	0.2716141	0.2944901	0.3174704	0.3403739	0.3624055
0.3854153	0.4083858	0.4313503	0.4542657	0.4771495	0.4999999
0.5395039	0.5788838	0.6178936	0.6562834	0.6938090	0.7302244
0.7645295	0.7971752	0.8279586	0.8566948	0.8823385	0.9058799
0.9271240	0.9459153	0.9620984	0.9755492	0.9861495	0.9938051
0.9984390	1.0000000	0.0000000	0.0000000	0.0000000	0.0000000

Y/C

0.0000000	-0.0439291	-0.0876947	-0.1309448	-0.1733444	-0.2145551
-0.2533504	-0.2901789	-0.3247655	-0.3568247	-0.3851002	-0.4107795
-0.4336042	-0.4533602	-0.4698345	-0.4828699	-0.4923149	-0.4980550
-0.4999999	-0.4999999	-0.4999999	-0.4999999	-0.4999999	-0.4999999
-0.5004880	-0.4961358	-0.4949743	-0.4965157	-0.5057697	-0.5114841
-0.5181849	-0.5234605	-0.5227931	-0.5178602	-0.5121495	-0.4995293
-0.4870098	-0.4728503	-0.4561396	-0.4393857	-0.4210649	-0.4027755
-0.3840905	-0.3643640	-0.3437046	-0.3220746	-0.2999350	-0.2773307
-0.2547400	-0.2321455	-0.2092795	-0.1862951	-0.1634546	-0.1404801
-0.1170353	-0.0935157	-0.0700197	-0.0465000	-0.0231201	0.0000000
0.0231909	0.0460394	0.0690197	0.0919939	0.1148994	0.1376947
0.1599605	0.1819841	0.2042341	0.2265805	0.2490747	0.2712952
0.2931043	0.3147538	0.3364448	0.3573306	0.3772105	0.3966594
0.4155649	0.4334054	0.4524644	0.4709704	0.4846043	0.4993896
0.5114388	0.5179999	0.5230097	0.5255294	0.5205452	0.5124488
0.5052302	0.5008640	0.4998089	0.4999999	0.5000687	0.5055137
0.5050589	0.5053602	0.5052793	0.5042439	0.5024742	0.4999999
0.4984389	0.4937401	0.4859053	0.4749507	0.4609094	0.4438444
0.4242952	0.4021042	0.3774153	0.3503856	0.3222046	0.2919939
0.2599290	0.2261790	0.1909507	0.1544388	0.1168700	0.0784606
0.0394449	0.0000000	0.0000000	0.0000000	0.0000000	0.0000000

FIGURE 4.2

GEOMETRY OF TWO-DIMENSIONAL TEST MODELS (PAGE 3 OF 5).

COORDINATES FOR 15 MINUTE RIME ICE ACCRETION
(NOTE: DATA FROM NASA - LEWIS)

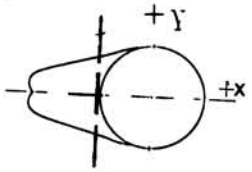

C = .0508 m = 2.0"

X/C

1.0000000	0.9955845	0.9822499	0.9605433	0.9307696	0.8934783
0.8493739	0.8019350	0.7490787	0.6915748	0.6303247	0.5662991
0.4999999	0.4750000	0.4499999	0.4250000	0.3999999	0.3749999
0.3500039	0.3271397	0.3048798	0.2812636	0.2604842	0.2397696
0.2181849	0.1949153	0.1713247	0.1478208	0.1242990	0.1004448
0.0768602	0.0531102	0.0286496	0.0051909	-0.0187087	-0.0430098
-0.0670748	-0.0905353	-0.1139252	-0.1379389	-0.1625649	-0.1870747
-0.2109507	-0.2345138	-0.2581850	-0.2820334	-0.3059940	-0.3301790
-0.3545334	-0.3786653	-0.4023188	-0.4257342	-0.4492283	-0.4728700
-0.4962854	-0.5190787	-0.5421200	-0.5655531	-0.5863090	-0.6073444
-0.6274232	-0.6372184	-0.6408148	-0.6402085	-0.6357145	-0.6269193
-0.6162440	-0.6050000	-0.6162440	-0.6269193	-0.6357145	-0.6402085
-0.6408148	-0.6372184	-0.6274232	-0.6073444	-0.5863090	-0.5655531
-0.5421200	-0.5190787	-0.4962854	-0.4728700	-0.4492283	-0.4257342
-0.4023188	-0.3786653	-0.3545334	-0.3301790	-0.3059940	-0.2820334
-0.2581850	-0.2345138	-0.2109507	-0.1870747	-0.1625649	-0.1379389
-0.1139252	-0.0905353	-0.0670748	-0.0430098	-0.0187087	0.0051909
0.0286496	0.0531102	0.0768602	0.1004448	0.1242990	0.1478208
0.1713247	0.1949153	0.2181849	0.2397696	0.2604842	0.2812636
0.3048798	0.3271397	0.3500039	0.3749999	0.3999999	0.4250000
0.4499999	0.4750000	0.4999999	0.0000000	0.0000000	0.0000000
0.5662991	0.6303247	0.6915748	0.7490787	0.8019350	0.0000000
0.8493739	0.8934783	0.9307696	0.9605433	0.9822499	0.9955845
1.0000000	0.0000000	0.0000000	0.0000000	0.0000000	0.0000000

Y/C

0.0000000	-0.0663148	-0.1320451	-0.1946692	-0.2538443	-0.3085038
-0.3576849	-0.3985392	-0.4335451	-0.4618404	-0.4827145	-0.4955845
-0.4999999	-0.4999999	-0.4999999	-0.4999999	-0.4999999	-0.4999999
-0.4976396	-0.4890904	-0.4781240	-0.4705846	-0.4572695	-0.4435846
-0.4314350	-0.4230944	-0.4154389	-0.4075805	-0.3997794	-0.3930590
-0.3854251	-0.3786239	-0.3746553	-0.3666751	-0.3602341	-0.3552341
-0.3493996	-0.3413443	-0.3331042	-0.3274290	-0.3243051	-0.3206338
-0.3142439	-0.3064743	-0.2990806	-0.2923386	-0.2859999	-0.2806004
-0.2758935	-0.2703640	-0.2630649	-0.2549054	-0.2469901	-0.2395098
-0.2314290	-0.2217145	-0.2126239	-0.2047302	-0.1912596	-0.1775905
-0.1633305	-0.1414644	-0.1167400	-0.0919152	-0.0675707	-0.0444941
-0.0220905	0.0000000	0.0220905	0.0444941	0.0675707	0.0919152
0.1167400	0.1414644	0.1633305	0.1775905	0.1912596	0.2047302
0.2126239	0.2217145	0.2314290	0.2395098	0.2469901	0.2549054
0.2630649	0.2703640	0.2758935	0.2806004	0.2859999	0.2923386
0.2990806	0.3064743	0.3142439	0.3206338	0.3243051	0.3274290
0.3331042	0.3413443	0.3493996	0.3552341	0.3602341	0.3666751
0.3746553	0.3786239	0.3854251	0.3930590	0.3997794	0.4075805
0.4154389	0.4230944	0.4314350	0.4435846	0.4572695	0.4705846
0.4781240	0.4890904	0.4976396	0.4999999	0.4999999	0.4999999
0.4999999	0.4999999	0.4999999	0.0000000	0.0000000	0.0000000
0.4955845	0.4827145	0.4618404	0.4335452	0.3985392	0.0000000
0.3576849	0.3085038	0.2538443	0.1946692	0.1320451	0.0663148
0.0000000	0.0000000	0.0000000	0.0000000	0.0000000	0.0000000

FIGURE 4.2

GEOMETRY OF TWO-DIMENSIONAL TEST MODELS (PAGE 4 OF 5).

COORDINATES FOR 15 MINUTE GLAZE ICE ACCRETION
(NOTE: DATA FROM NASA - LEWIS)

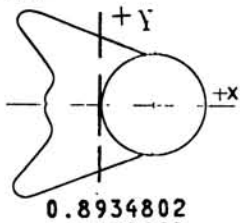

C = .0508 m = 2.0"

X/C

1.0000000	0.9955845	0.9822499	0.9605452	0.9307696	0.8934802
0.8493739	0.8019350	0.7490787	0.6915748	0.6303247	0.5662991
0.4999999	0.4750000	0.4499999	0.4250000	0.3999999	0.3749999
0.3515000	0.3279999	0.3044999	0.2810000	0.2574999	0.2339998
0.2104999	0.1869999	0.1635000	0.1399999	0.1164998	0.0929999
0.0695000	0.0460000	0.0225000	-0.0010000	-0.0245000	-0.0480000
-0.0714999	-0.0949998	-0.1184999	-0.1420000	-0.1654999	-0.1890000
-0.2124999	-0.2359999	-0.2595000	-0.2829999	-0.3064999	-0.3299999
-0.3534999	-0.3769999	-0.4004999	-0.4239998	-0.4474999	-0.4710000
-0.4944999	-0.5179999	-0.5415000	-0.5649999	-0.6299999	-0.6599998
-0.6899999	-0.7200000	-0.7549999	-0.7749999	-0.7749999	-0.7649999
-0.7499999	-0.7249998	-0.6899999	-0.6599998	-0.6299999	-0.5899999
-0.5500000	-0.5249999	-0.5049999	-0.4800000	-0.4650000	-0.4499999
-0.4399999	-0.4250000	-0.4199999	-0.4250000	-0.4349999	-0.4599999
-0.4800000	-0.4899999	-0.4899999	-0.4899999	-0.4750000	-0.4899999
-0.4899999	-0.4899999	-0.4800000	-0.4599999	-0.4349999	-0.4250000
-0.4199999	-0.4250000	-0.4399999	-0.4499999	-0.4650000	-0.4800000
-0.5049999	-0.5249999	-0.5500000	-0.5899999	-0.6299999	-0.6599998
-0.6899999	-0.7249998	-0.7499999	-0.7649999	-0.7749999	-0.7749999
-0.7549999	-0.7200000	-0.6899999	-0.6599998	-0.6299999	-0.5649999
-0.5415000	-0.5179999	-0.4944999	-0.4710000	-0.4474999	-0.4239998
-0.4004999	-0.3769999	-0.3534999	-0.3299999	-0.3064999	-0.2829999
-0.2595000	-0.2359999	-0.2124999	-0.1890000	-0.1654999	-0.1420000
-0.1184999	-0.0949998	-0.0714999	-0.0480000	-0.0245000	-0.0010000
0.0225000	0.0460000	0.0695000	0.0929999	0.1164998	0.1399999
0.1635000	0.1869999	0.2104999	0.2339998	0.2574999	0.2810000
0.3044999	0.3279999	0.3515000	0.3749999	0.3999999	0.4250000
0.4499999	0.4750000	0.4999999	0.0000000	0.0000000	0.0000000
0.5662991	0.6303247	0.6915748	0.0000000	0.0000000	0.0000000
0.7490787	0.8019350	0.8493739	0.8934783	0.9307696	0.9605452
0.9822499	0.9955845	1.0000000	0.0000000	0.0000000	0.0000000

Y/C

0.0000000	-0.0663148	-0.1320450	-0.1946691	-0.2538443	-0.3085057
-0.3576849	-0.3985392	-0.4335451	-0.4618403	-0.4827144	-0.4955844
-0.4999998	-0.4999998	-0.4999998	-0.4999998	-0.4999998	-0.4999998
-0.5092498	-0.5184999	-0.5277499	-0.5369998	-0.5462497	-0.5554978
-0.5647499	-0.5739939	-0.5832439	-0.5924940	-0.6017439	-0.6109939
-0.6202439	-0.6294938	-0.6387440	-0.6479939	-0.6572440	-0.6664939
-0.6757439	-0.6849939	-0.6942438	-0.7034940	-0.7127439	-0.7219899
-0.7312400	-0.7404900	-0.7497399	-0.7589900	-0.7682401	-0.7774881
-0.7867399	-0.7959899	-0.8052400	-0.8144898	-0.8237396	-0.8329887
-0.8422393	-0.8514891	-0.8607381	-0.8699996	-0.8999985	-0.8999985
-0.9099994	-0.8999985	-0.8799990	-0.8399983	-0.8149990	-0.7749998
-0.7449998	-0.6999997	-0.6649999	-0.6249998	-0.5899998	-0.5449998
-0.4949998	-0.4649999	-0.4349998	-0.3949998	-0.3649998	-0.3399999
-0.3099998	-0.2799997	-0.2449998	-0.2149999	-0.1849998	-0.1499999
-0.1149998	-0.0899997	-0.0600000	-0.0300000	0.0000000	0.0300000
0.0600000	0.0899997	0.1149998	0.1499999	0.1849998	0.2149999
0.2449998	0.2799997	0.3099998	0.3399999	0.3649998	0.3949998
0.4349998	0.4649999	0.4949998	0.5449998	0.5899998	0.6249998
0.6649999	0.6999997	0.7449998	0.7749998	0.8149990	0.8399983
0.8799990	0.8999985	0.9099994	0.8999985	0.8999985	0.8699996
0.8607381	0.8514891	0.8422393	0.8329887	0.8237396	0.8144898
0.8052400	0.7959899	0.7867399	0.7774881	0.7682401	0.7589900
0.7497399	0.7404900	0.7312400	0.7219899	0.7127439	0.7034940
0.6942438	0.6849939	0.6757439	0.6664939	0.6572440	0.6479939
0.6387440	0.6294938	0.6202439	0.6109939	0.6017439	0.5924940
0.5832439	0.5739939	0.5647499	0.5554978	0.5462497	0.5369998
0.5277499	0.5184999	0.5092498	0.4999998	0.4999998	0.4999998
0.4999998	0.4999998	0.4999998	0.0000000	0.0000000	0.0000000
0.4955844	0.4827144	0.4618403	0.0000000	0.0000000	0.0000000
0.4335451	0.3985392	0.3576849	0.3085057	0.2538443	0.1946691
0.1320450	0.0663148	0.0000000	0.0000000	0.0000000	0.0000000

FIGURE 4.2

GEOMETRY OF TWO-DIMENSIONAL TEST MODELS (PAGE 5 OF 5).

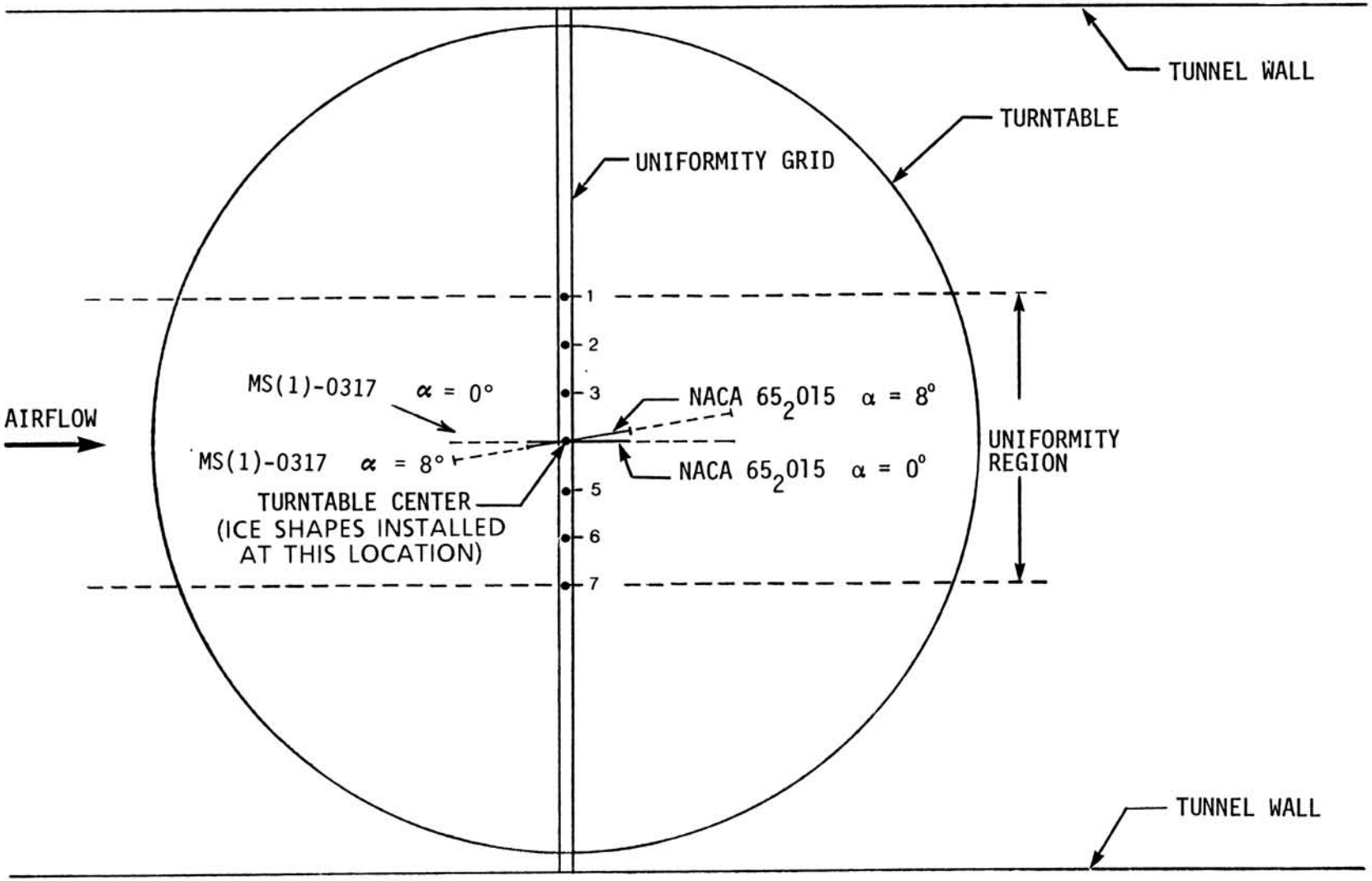

FIGURE 4.3

TWO-DIMENSIONAL TEST MODELS AND LOCATIONS IN THE IRT TEST SECTION (PAGE 1 OF 4).

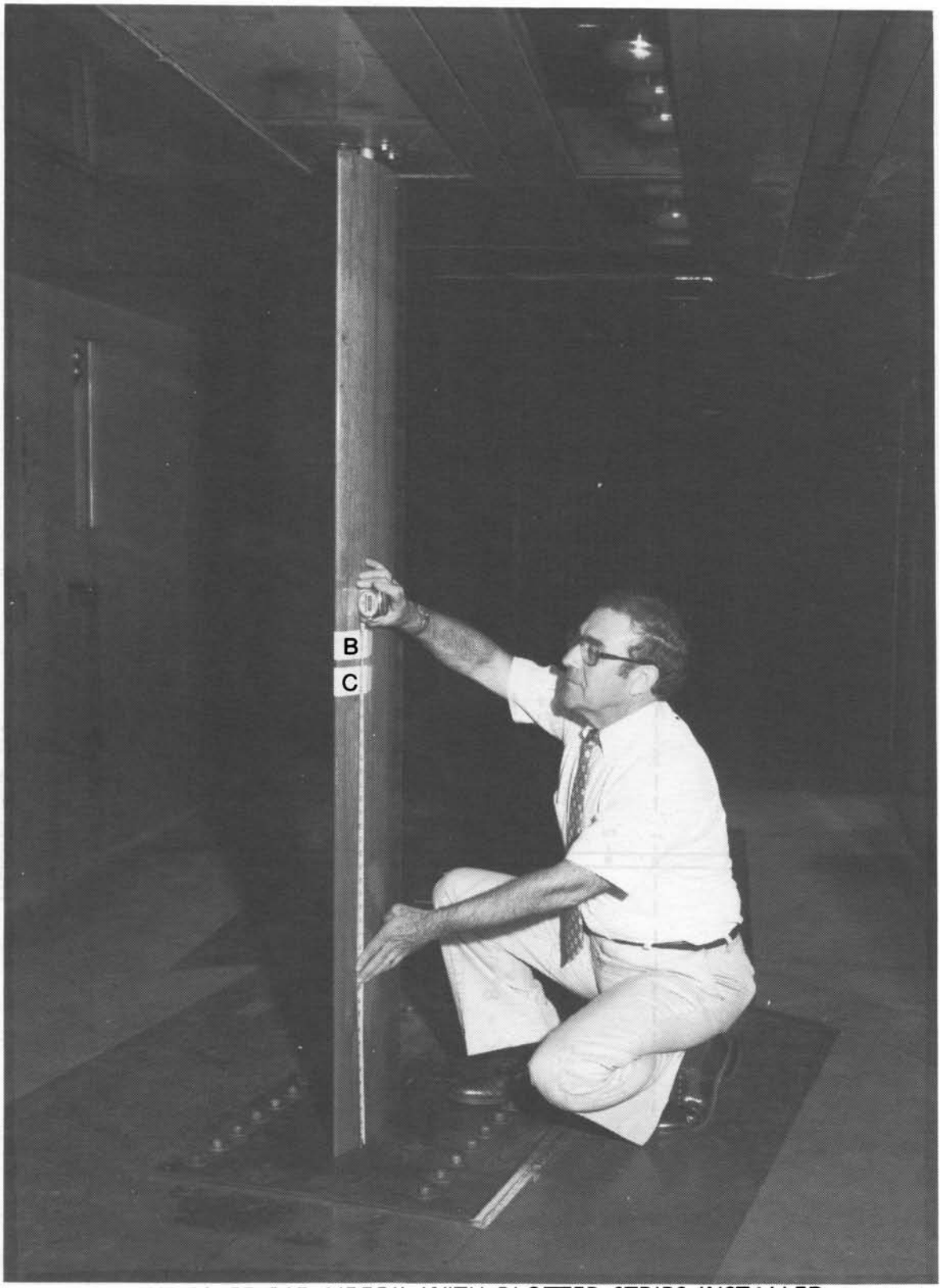

NACA 65_2015 AIRFOIL WITH BLOTTER STRIPS INSTALLED

FIGURE 4.3

TWO-DIMENSIONAL TEST MODELS AND LOCATIONS IN THE IRT TEST SECTION (PAGE 2 OF 4).

SUPERCRITICAL AIRFOIL MS(1)-0317

FIGURE 4.3

TWO-DIMENSIONAL TEST MODELS AND LOCATIONS IN THE IRT TEST SECTION (PAGE 3 OF 4).

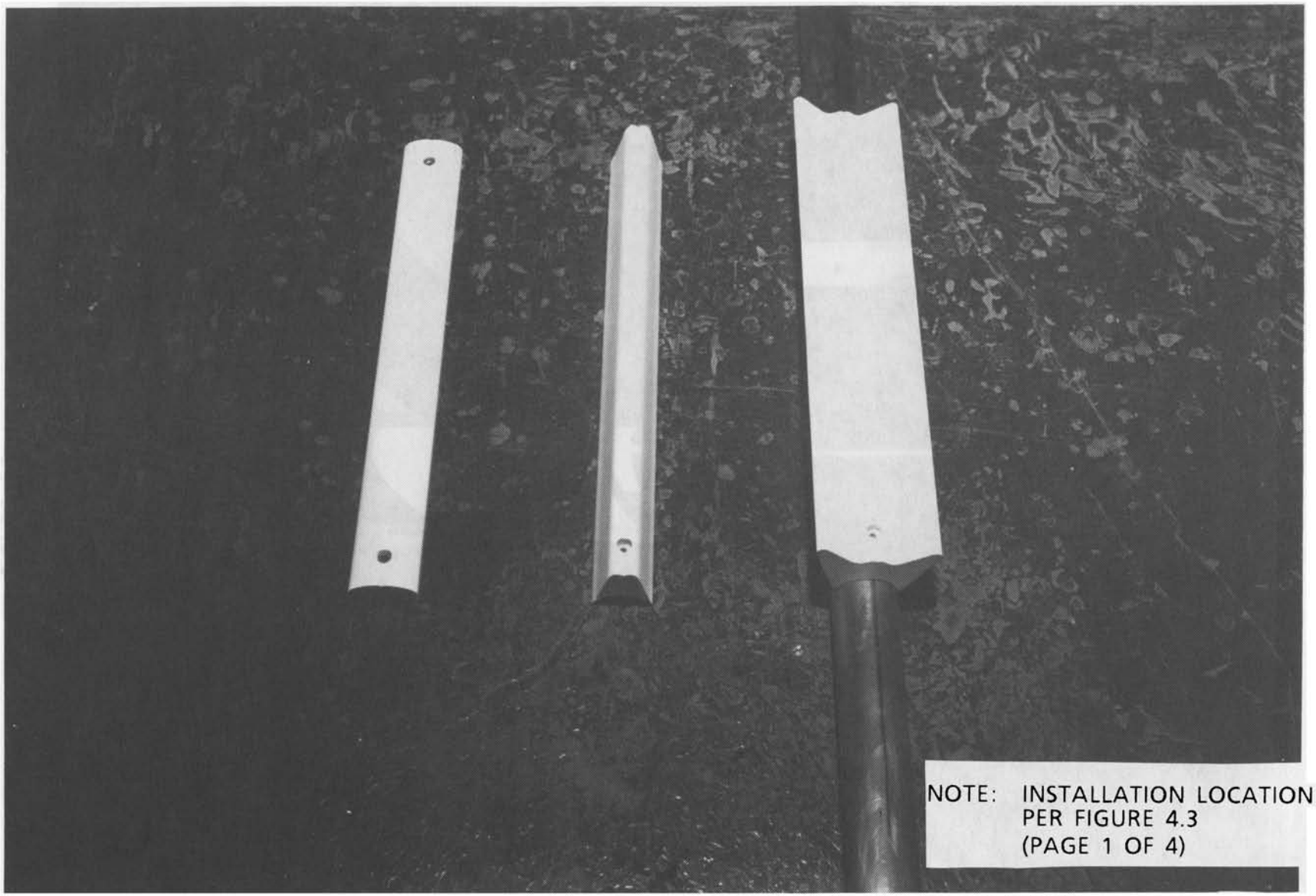

ICE SHAPES – FROM LEFT TO RIGHT: SMALL GLAZE, RIME AND LARGE GLAZE

FIGURE 4.3

TWO-DIMENSIONAL TEST MODELS AND LOCATIONS IN THE IRT TEST SECTION
(PAGE 4 OF 4).

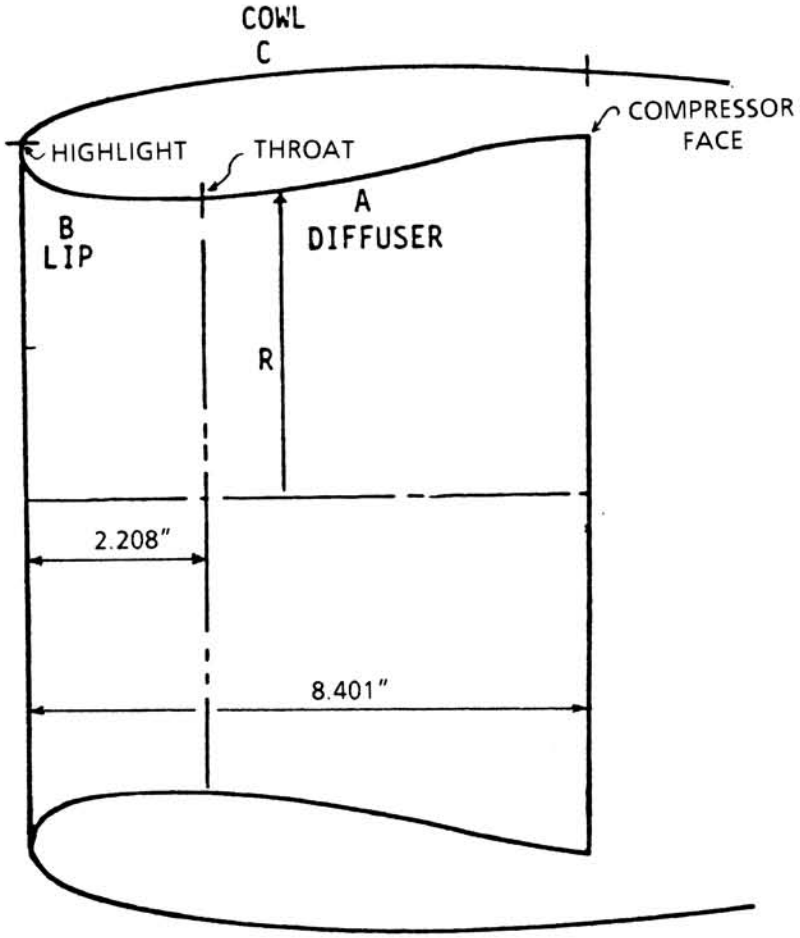

FIGURE 4.4

AXISYMMETRIC INLET
(PAGE 1 OF 4).

EXTERNAL COWL LINES (C)
AXISYMMETRIC REFERENCE INLET
$\cdot D_{HI}/D_{MAX} \approx .78$

X	R	DY / DX	RC
0	7.605	∞	.353
.1	7.915	1.5742	.827
.2	8.046	1.1113	1.185
.3	8.145	.9030	1.573
.4	8.229	.7773	1.988
.5	8.302	.6905	2.426
.6	8.368	.6257	2.884
.7	8.428	.5748	3.361
.8	8.483	.5333	3.854
.9	8.535	.4986	4.362
1.0	8.583	.4689	4.882
1.5	8.789	.3652	7.627
2.0	8.954	.3001	10.516
2.5	9.092	.2532	13.450
3.0	9.209	.2167	16.353
3.5	9.310	.1868	19.168
4.0	9.397	.1613	21.847
4.5	9.472	.1389	24.352
5.0	9.536	.1188	26.652
5.5	9.591	.1004	28.719
6.0	9.637	.0833	30.532
6.5	9.674	.0672	32.074
7.0	9.704	.0519	33.329
7.5	9.726	.0370	34.287
8.0	9.741	.0226	34.940
8.5	9.749	.0083	35.282
8.795	9.750	0	35.336

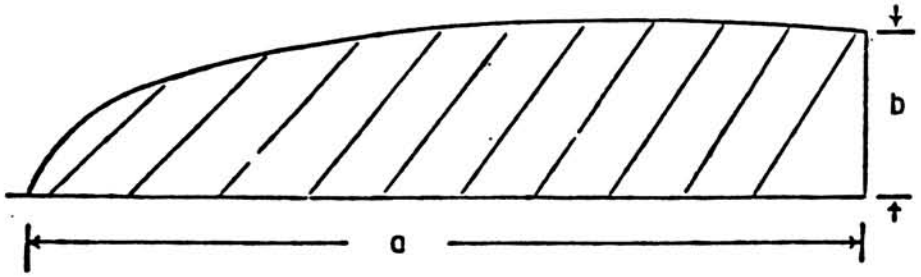

SUPER ELLIPSE:

$(x/a)^n + (y/b)^m = 1$

$n = 2.0$
$m = 1.96$
$a = 8.795$ INCHES
$b = 2.145$ INCHES

ZERO X-REFERENCE IS THE HILITE

RC = RADIUS OF CURVATURE
DY/DX = SLOPE
R = RADIUS (INCHES)
X = AXIAL DISTANCE (INCHES)

FIGURE 4.4

AXISYMMETRIC INLET
(PAGE 2 OF 4).

INLET LIP LINES (B)
AXISYMMETRIC REFERENCE INLET
C.R. 1.28

X	R	DY/DX	RC
0	7.605	1.3188	.353
.1	7.342	1.2834	.626
.2	7.238	.8746	.931
.3	7.161	.6868	1.256
.4	7.098	.5705	1.593
.5	7.045	.4882	1.936
.6	7.000	.4250	2.279
.7	6.960	.3740	2.618
.8	6.925	.3311	2.949
.9	6.894	.2941	3.269
1.0	6.866	.2614	3.575
1.1	6.841	.2320	3.865
1.2	6.819	.2052	4.135
1.3	6.800	.1804	4.386
1.4	6.783	.1572	4.615
1.5	6.769	.1353	4.820
1.6	6.756	.1145	5.001
1.7	6.746	.0945	5.156
1.8	6.737	.0752	5.284
1.9	6.731	.0563	5.385
2.0	6.726	.0378	5.458
2.1	6.724	.0195	5.503
2.2	6.722	.0014	5.519
2.208	6.722	0	5.519

ZERO X - REFERENCE IS THE HILITE

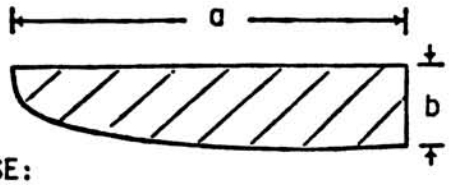

ELLIPSE:

$$\left(\frac{x}{a}\right)^{2.0} + \left(\frac{y}{b}\right)^{2.0} = 1$$

a = 2.208 INCHES
b = 0.883 INCHES

FIGURE 4.4

AXISYMMETRIC INLET
(PAGE 3 OF 4).

INLET DIFFUSER LINES (A)
AXISYMMETRIC REFERENCE. INLET

X	R	DY/DX	RC
0	6.722	0	5.519
.160	6.724	.0279	5.973
.320	6.731	.0536	6.563
.480	6.741	.0768	7.341
.640	6.755	.0975	8.395
.800	6.772	.1154	9.884
.960	6.792	.1305	12.126
1.120	6.814	.1424	15.867
1.280	6.837	.1511	23.346
1.440	6.862	.1566	45.763
1.600	6.887	.1584	∞
1.760	6.912	↑	↑
1.920	6.938	↑	↑
2.080	6.963	↑	↑
2.240	6.989	↑	↑
2.400	7.014	↑	↑
2.560	7.039	↑	↑
2.720	7.065	↑	↑
2.880	7.090	↑	↑
3.040	7.115	↑	↑
3.200	7.141	↑	↑
3.360	7.166	↑	↑
3.520	7.191	↑	↑
3.680	7.217	↑	↑
3.840	7.242	↑	↑
4.000	7.267	↓	∞
4.160	7.293	.1584	-67.695
4.320	7.318	.1571	-34.728
4.480	7.343	.1535	-23.750
4.640	7.367	.1477	-18.273
4.800	7.390	.1397	-15.001
4.960	7.412	.1297	-12.835
5.120	7.431	.1178	-11.304
5.280	7.449	.1043	-10.175
5.440	7.465	.0891	-9.319
5.599	7.478	.0725	-8.656
5.759	7.488	.0545	-8.138
5.919	7.495	.0354	-7.734
6.079	7.499	.0152	-7.500
6.193	7.500	0	

ZERO X REFERENCE IS THE THROAT

FIGURE 4.4

AXISYMMETRIC INLET
(PAGE 4 OF 4).

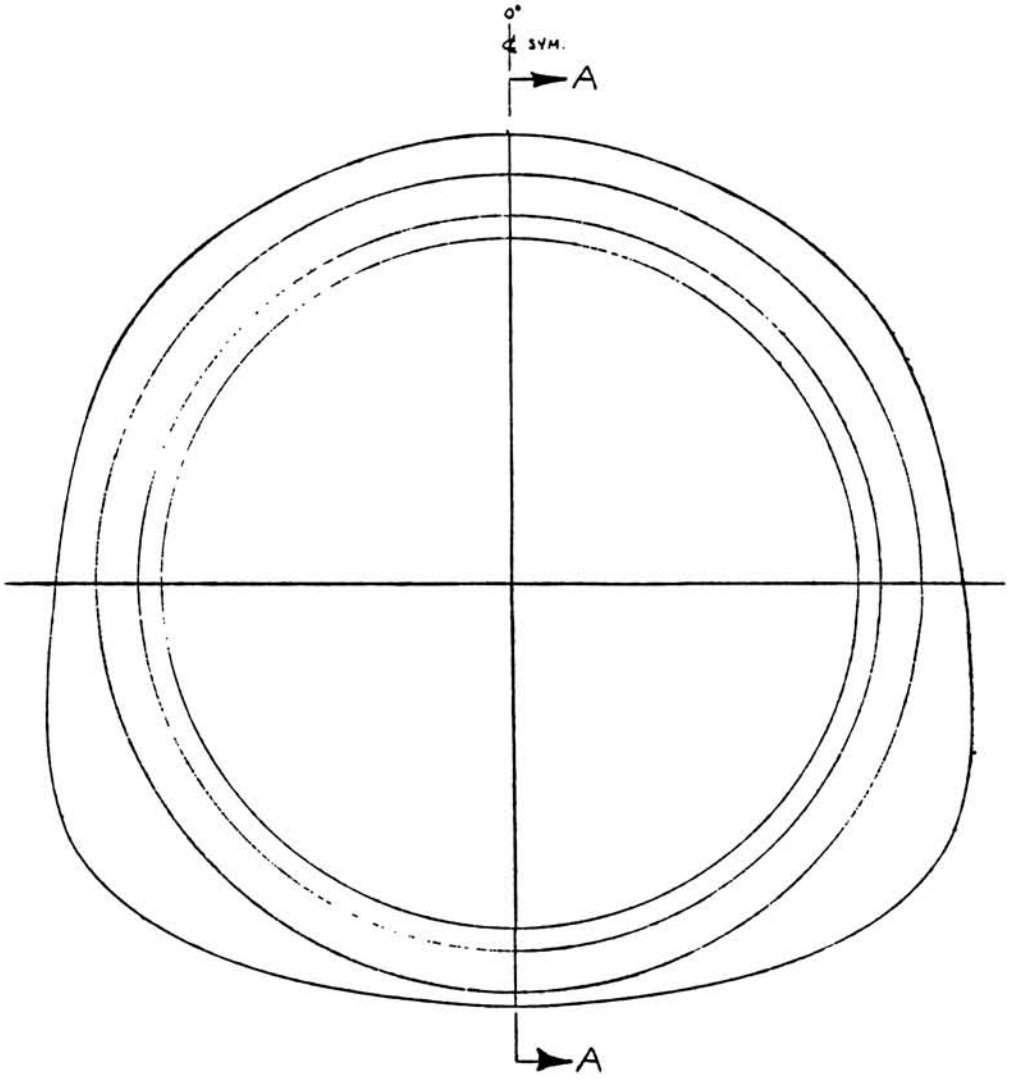

FIGURE 4.5

BOEING 737-300 INLET
(PAGE 1 OF 2).

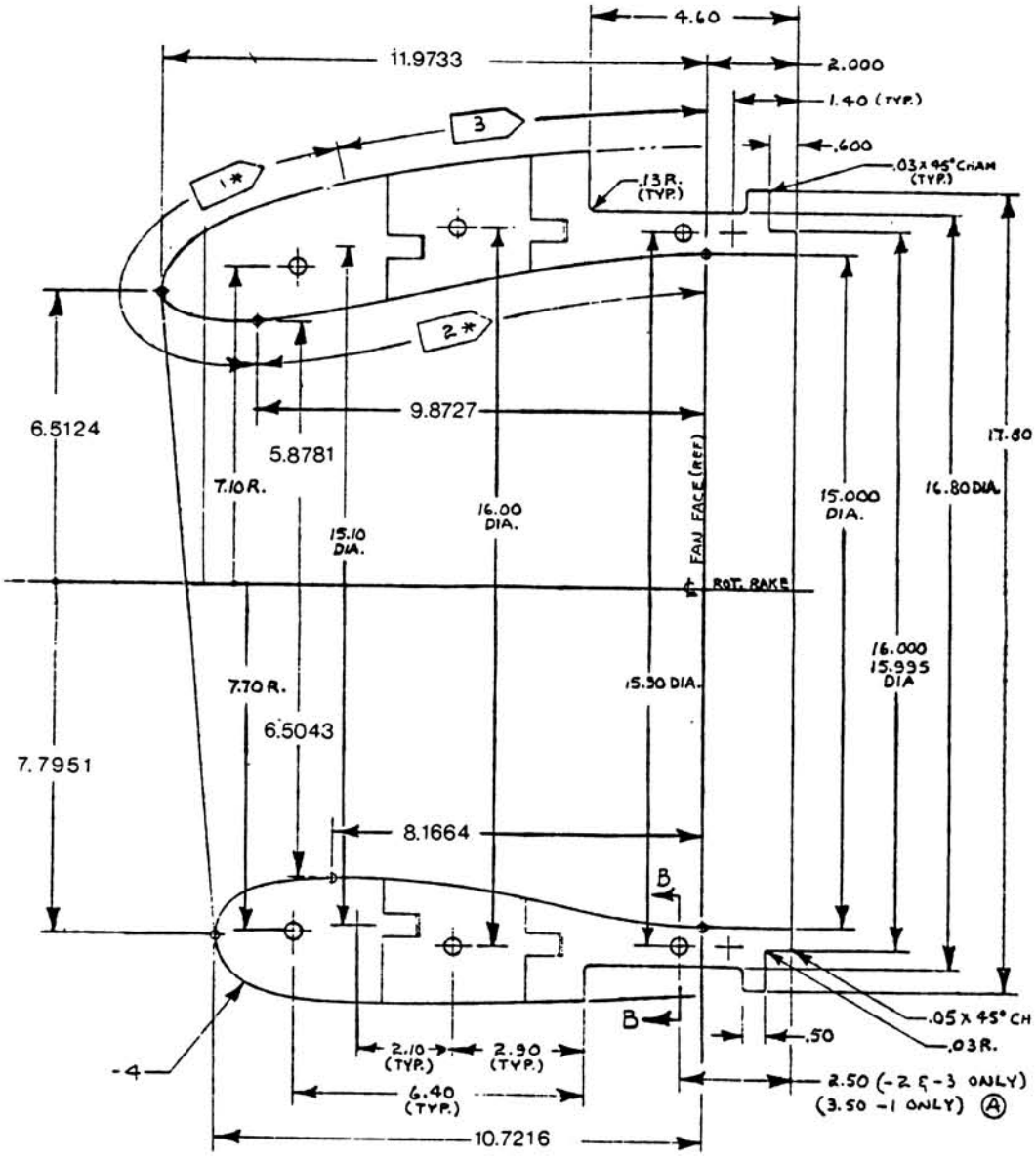

SEC A-A

All dimensions in inches

FIGURE 4.5

BOEING 737-300 INLET
(PAGE 2 OF 2).

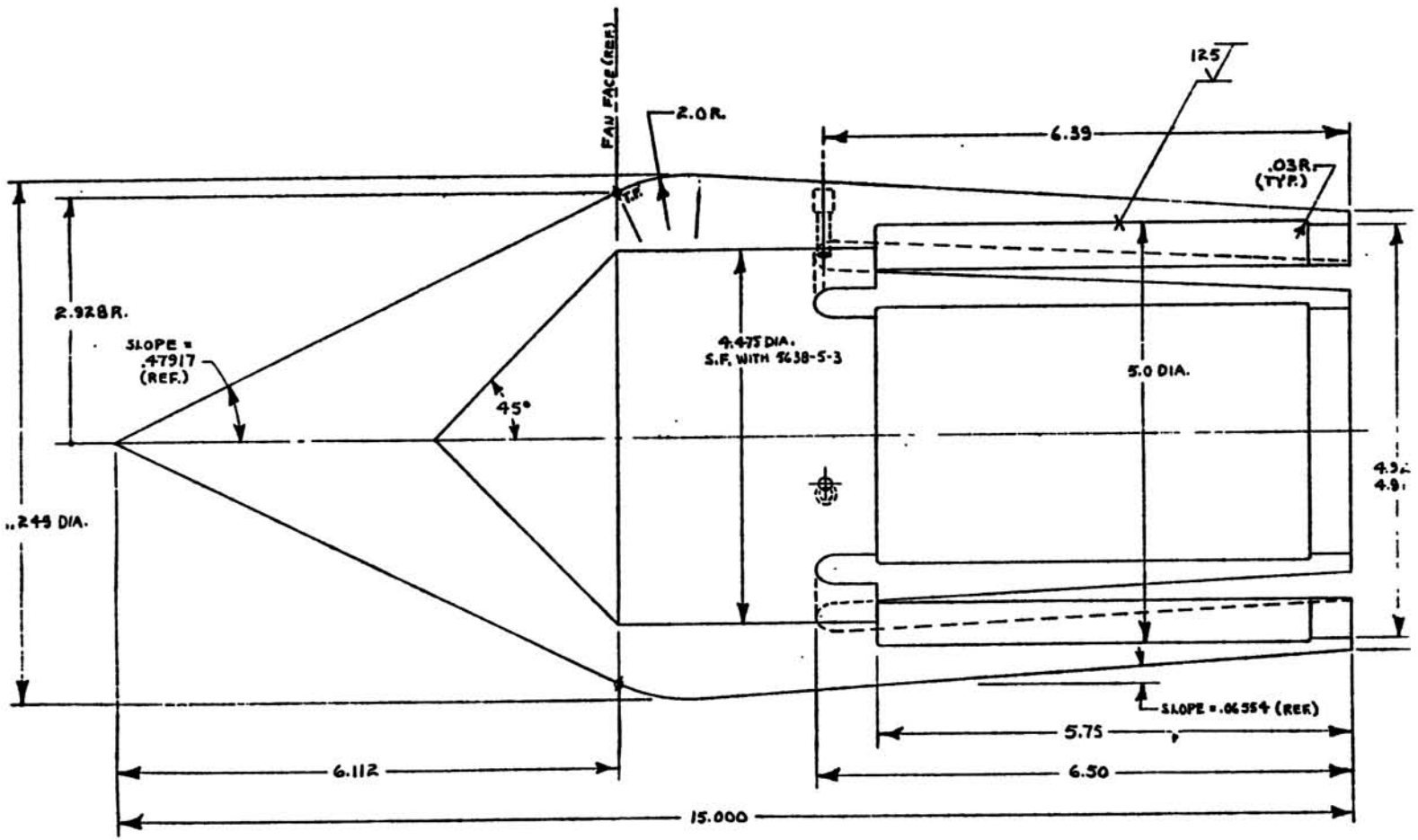

SEC·A-A

FIGURE 4.6

CENTER BODY FOR BOEING 737-300 INLET.

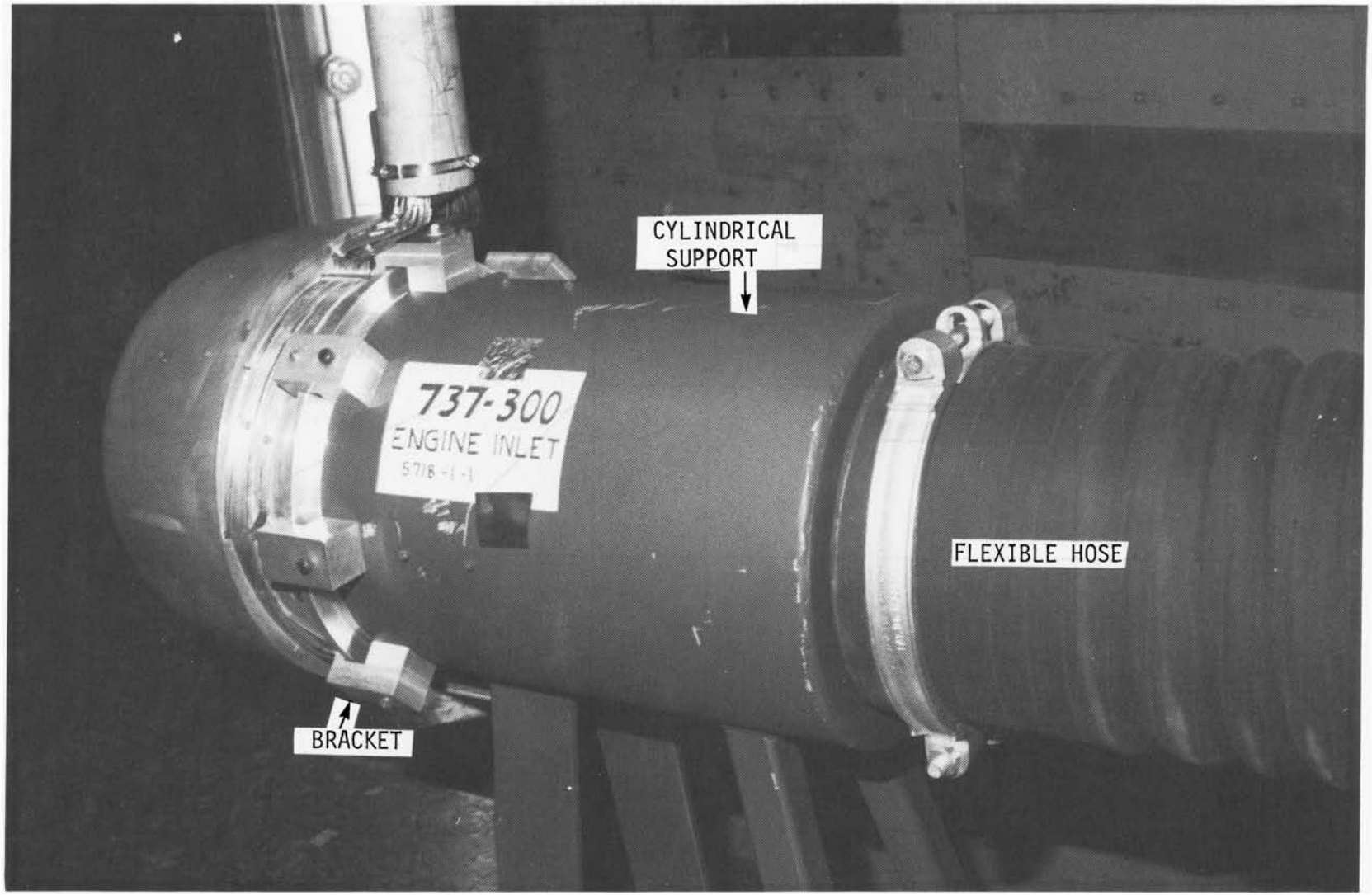

FIGURE 4.7

DETAIL VIEW OF BOEING 737-300 INLET AND CYLINDRICAL SUPPORT.

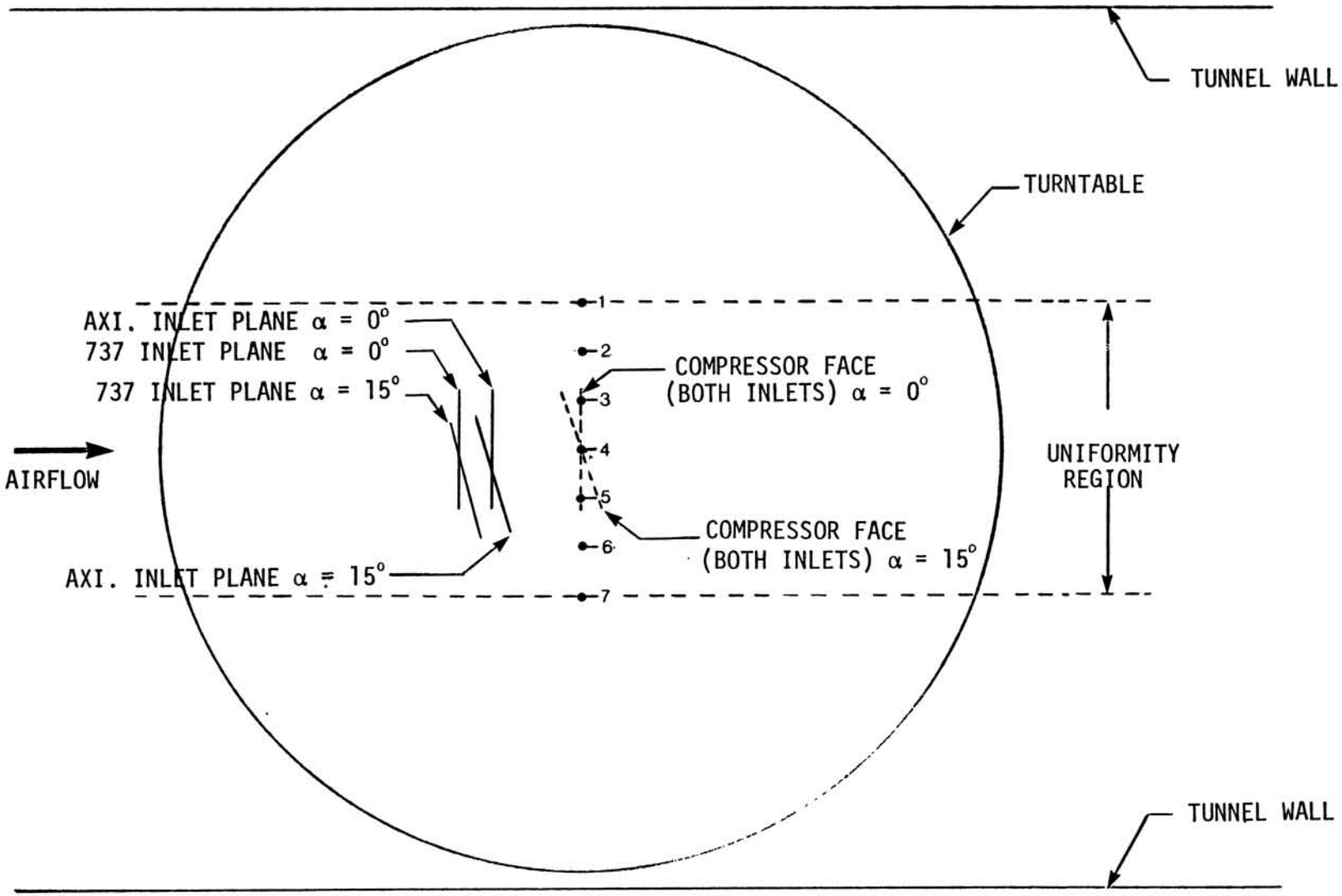

FIGURE 4.8

AXIAL LOCATIONS OF INLET PLANES IN THE IRT TEST SECTION

5.0 DATA REDUCTION METHOD

In the present dye-tracer technique, the spatial variations in the concentration of the dye on the blotter are determined by reflectance spectroscopy. The reflectance method is based on the assumption that the surface reflectance of the paper is a measure of the dye mass per unit area on the paper. Knowledge of the dye concentration in the spray water then gives water impingement.

The blotter paper strips are illuminated with light from a He-Ne laser. Light diffusely reflected from the paper is collected by a lens and focussed onto a silicon photodetector. The voltage from the silicon photodetector decreases as light is absorbed by the dye, the amount of absorption being related to the concentration of dye deposited on the paper. An automated reflectometer with digital data acquisition system was developed to extract the raw data from the blotter paper strips, calculate the impingement efficiency curves, print and plot the results. Details of the various aspects of the technique and data reduction are described in the remainder of this section.

5.1 Reflectance Spectroscopy

Reflectance from a surface can be considered either specular (or mirror-like) when the angle of the reflected beam makes the same angle to the normal as the incident beam; or diffuse when the reflected light is observed at any angle other than that of the specular reflection. Reflection from most real surfaces is a combination of specularly and diffusely reflected light. The blotter paper is primarily a diffuse reflector. This means that for any angle of incidence some of the diffusely reflected light will be detected at every angle within a hemisphere around the point of intersection between the beam of light and the paper. The diffuse reflectance of a non-absorbing mat surface can be expressed by

$$R = (I_0 / \pi) \cos\alpha \cos\theta \qquad (5\text{-}1)$$

where I_0 is the maximum intensity of the diffusely reflected light at perpendicular incidence, α is the angle of incidence and θ is the angle of observation (Reference 21). Figure 5.1 shows a typical reflectance curve for the blotter paper used in these experiments as a function of angle of observation.

5.1.1 Theory-Assumptions

The transmission and reflection of light in highly scattering media is usually modelled by the Kubelka-Munk theory. The theory considers two beams propagating normal to the surface of the material, a transmitted beam and a reflected beam (Figure 5.2). The intensity of the incident is I_0. This can be described by the following system of differential equations:

$$-\frac{di}{dx} = -(S + K)i + Sj$$

$$\frac{dj}{dx} = -(S + K)j + Si \qquad (5\text{-}2)$$

where:

i = intensity of light travelling inside the specimen towards its unilluminated surface

j = intensity of light travelling inside the specimen towards its illuminated surface

S = coefficient of scatter per unit depth or thickness

K = coefficient of absorption per unit depth or thickness

x = distance from the unilluminated surface of the specimen

The key assumptions of the Kublelka-Munk theory are the following:

a. The light beam is collimated and normal to the plane of the sample

b. The reflections and absorptions occur at infinitesimal distances and are constant over the frequency range of the light, the area illuminated by the beam and the depth of the sample.

c. The reflected light is backscattered (i.e., the reflected beam travels at 180 degrees to the incident beam).

d. The material is homogeneous in this way, that the optical inhomogeneities are incomparably smaller than the thickness of the specimen and uniformly distributed in the material.

e. The reflected or transmitted light is not reflected again to the specimen unless we consider a backing, reflecting the transmitted light in defined manner.

For a two component system consisting of a finitely thick specimen (blue dye layer) in contact with a backing (blotter paper), Equation (5-2) can be integrated over the whole thickness of the specimen to get (Appendix F):

$$R = \frac{1 - R_g(a - b\coth(bSX))}{a + b\coth(bSX) - R_g} \qquad (5\text{-}3)$$

where

R = J/I Light reflectance of a specimen or fraction of incident light reflected from the specimen (the specimen generally being in contact with a backing)

R_g = Reflectance of the backing

a = $\frac{S+K}{S} = \frac{1}{2}\left(\frac{1}{R_\infty} + R_\infty\right)$

b = $\sqrt{a^2 - 1} = \frac{1}{2}\left(\frac{1}{R_\infty} - R_\infty\right)$

$R_\infty = R_{X \to \infty}$ Light reflectivity of the specimen assuming infinite thickness

X = Thickness of specimen

Details of the Kubelka-Munk theory are given in References 22 and 23.

5.2 Selection of Blotter Paper, Dye and Laser

5.2.1 Blotter Paper

In order to obtain consistent results, the blotter paper should retain its texture as nearly as possible throughout the program of testing and chemically be inert to the dye and water. Several different types of paper were considered for use in these wind tunnel experiments. These were Whatman 3 MM, James River Paper Company Pulp Testing and James River Paper Company 100# Verigood Blotting Paper. The James River 100# Verigood Blotting Paper was found to be the best. Therefore, a box of 250 sheets, 19" x 24", of 100# Verigood blotting paper was purchased from Southwest Paper Company, a local distributor. Strips of desired sizes were cut from the large sheets and used in the calibration tests and wind tunnel tests. Penetration test conducted indicate that the dye/water solution penetrates less than 50 percent of the thickness of the paper. In most cases, for the short exposures used, the dye resides on the top surface of the paper with very little penetration.

5.2.2 Dye

The dye and laser must be considered in combination, since to be effective the dye must have a strong absorption at the wavelength of the laser radiation. The laser emits red light at 632.8 nm. This means that a blue dye would be appropriate. Blue food coloring (FD&C Blue No.

1 also known as Brilliant Blue FCF) has many of the properties essential to these experiments. It is soluble in water, moderately stable to oxidation and exposure to light and highly stable on exposure to heat. A plot of the absorption as a function of wavelength is shown in Figure 5.3. The peak of the absorption is at 629.5 nm which is quite close to the laser wavelength of 632.8 nm.

5.2.3 Laser

The laser used in this system is a Hughes model 3225H-PC He-Ne laser which emits light at 632.8 nm. Its output power is nominally 5mW and the output beam is polarized. A Spectra-Physics model 147 laser with unpolarized output was tried but found to be unsuitable because of the fluctuations in output over a period of time. A Hughes model 3225H-PC He-Ne laser gave a more stable output.

5.3 Calibration Procedure

To reduce the raw data, a reflectance vs. dye-concentration calibration curve was developed during the course of this research. This curve is a standard against which all strips are compared when the data are extracted from them by the automated reflectometer. The curve depends only on dye, blotter paper and laser used; therefore, it only needs to be defined once. The tests performed and the method used to produce the data required to define the calibration curve are described in this section.

5.3.1 Humidity Chamber

A set of test samples of blotter paper were prepared by spraying the dye/water solution into a chamber and allowing the spray to fall under gravity onto the paper. By varying the amount of solution sprayed into the chamber and the amount of time the paper was allowed to remain in the chamber, the exposure of the paper to the dye solution could be controlled. Fifteen samples were made in this chamber and ten of these, whose reflectivities ranged from 84 to 23 percent of the white blotter paper value, were selected for determining the calibration curve.

5.3.2 Small Wind Tunnel

A similar set of test samples were made in a small wind tunnel at Wichita State University by wrapping blotter paper strips around an elliptical airfoil section placed at 90 degrees to the airstream and spraying the dye/water solution into the tunnel. The tunnel speed was 60 mph. Eleven samples were made by this technique and used along with humidity chamber samples for determining the calibration curve. The reflectivities of the wind tunnel samples ranged from 63 to 29 percent of the white blotter paper reflectivity value.

The main reason for the wind tunnel tests was to study the effect of droplet penetration into the blotter paper due to droplet momentum. No significant change in penetration was found. In addition, the spraying

times required to avoid saturation of the blotter strips were established.

5.3.3 Elution of Dye

From the 26 test samples produced in the above tests, 18 were selected to cover the range of reflectivity required to define the calibration curve. The reflectivity of each blotter test sample was measured and a uniform reflectance region was identified on each blotter sample. From this uniform region, three 1 inch diameter discs were punched out giving a total of 54 discs. These discs were sent to the Wichita State University Chemistry Lab to determine the mass of dye contained in each disc using a photospectrometer.

The method of colorimetric analysis, similar to the one used by NACA during the 1950's impingement tests, was employed to measure the dye mass on each disc. First, a standard absorbance calibration curve (Figure 5.4) for the dye used was established for the wavelength where the dye absorbance is maximum (629.5 nm). Next, each disc provided was cut into 3 mm squares and the squares from each disc were carefully collected in a conical centrifuge tube. To each tube containing the squares from each disc, 2.5 ml of water were added to elute the material, a mixture of blotter paper and dye. Elution was carried out with occasional shaking for 24 hours. Thereafter, the contents were centrifuged and the liquid was passed through a special membrane having a pore diameter of 0.2 micrometer, with the help of syringe and needles. This procedure allowed quantitative removal of the fibrous particles which could interfere in the optical assay method. About 1 ml of solution from each extract was assayed at the 629.5 nm wavelength. The optical assay method involved measurement of the light absorbance through the 1 ml solution. The absorbance of each sample was compared to the standard absorbance calibration curve from which the dye mass per disc was established. The average reflectivity and dye mass corresponding to each set of three discs are shown in Table 5.1. These data plot on a single curve.

It should be noted here that this reflectance calibration procedure using colorimetric analysis needs to be done only once.

5.3.4 Standard Reflectance Calibration Curve

Figure 5.5 shows the reflectance calibration curve obtained by fitting a cubic spline to the data of Table 5.1. The measured reflectance, of the blotter paper - blue dye combination, is normalized to the reflectance of the bare blotter paper and is plotted vs. dye concentration measured in micrograms per square centimeter of blotter paper. Clearly, for the case where there is no dye on the blotter paper, the normalized reflectance is equal to one.

TABLE 5.1

AVERAGE DYE MASS AND NORMALIZED REFLECTIVITY VALUES FOR EACH DISC

HUMIDITY CHAMBER		SMALL WIND TUNNEL	
DYE MASS PER DISC ~ μg	NORMALIZED REFLECTIVITY	DYE MASS PER DISC ~ μg	NORMALIZED REFLECTIVITY
0.780	0.8443	1.810	0.6274
1.590	0.7037	3.060	0.5279
2.330	0.6196	4.060	0.4433
3.240	0.5193	5.840	0.3946
4.020	0.4507	5.940	0.3831
4.330	0.4232	5.937	0.3672
7.790	0.3603	9.693	0.3316
15.230	0.2643	11.400	0.3090
16.870	0.2320	13.870	0.2910

5.4 Error Analysis

Since the dye mass on the strip is determined from reflectance measurements, the relationship between normalized reflectance error and the corresponding dye concentration error must be established. In addition, the optimum concentration range over which to collect data in the wind tunnel experiments needs to be defined. From these studies, the combination of dye concentration and spray time duration required to keep the dye concentration on the blotter strip within the optimum range was determined.

An approximate relationship between the reflectivity and dye concentration errors can be obtained from Equation (5-3). The approximation is due to the fact that an exact correlation with the Kubelka-Munk theory was not established because S, the scattering coefficient, and K, the absorption coefficient for both the paper and the dye are not known. We also cannot measure these quantities accurately enough to determine them. This would require simultaneous measurements of the total transmitted and total (both specular and diffuse) reflected power. Furthermore, to spend much effort on this aspect of the problem did not seem justified, since whether the data follow the Kubelka-Munk formulas exactly or not, there are certain qualitative features of the calibration curve from which we can draw

some conclusions (Reference 24). Figure 5.6 shows a comparison between the standard reflectance calibration curve and that obtained from Equation 5-3 using K * X = 2.5, S * X = 3.5, R_g = 0.6. The scattering (S) and absorption (K) coefficients have been multiplied by the thickness (X) of the dye layer, since they always appear in combination. The values for K * X, S * X and R were established by matching the theoretical with the experimental data.

The absorption coefficient (K) for the dye material can be expressed by:

$$K = \alpha * c \tag{5-4}$$

where α is a constant of proportionality

c is the surface mass density of the dye

Equation (5-3) can now be differentiated with respect to c (Appendix F) to determine the relationship between the fractional error in dye mass density (dc/c) due to a given error (dR) in reflectance measurements.

Figure 5.7 shows plots of dc/c vs. R for three values of dR. Assuming 1 percent error in reflectivity (dR = 0.01), the result indicates that the minimum error in these measurements is slightly greater than 8 percent and that to restrict the dye mass error to less than 10 percent the reflectivity range for the dye - blotter combination should range from 31 to 87 percent. The shape of the error curve follows directly from the shape of the calibration curve. Near maximum reflectivity, dc is some discrete size and c is small resulting in a large relative error. On the flat side of the reflectivity curve, dc is large for a given value of dR and c is some discrete size resulting once again in a large error. In between these two extremes, dc/c decreases to some minimum value. Similar error curves derived numerically from the standard reflectivity curve of Figure 5.5 are shown in Figure 5.8. This is the actual curve used in this study.

5.5 Automated Data Processing

Due to the large number of strips produced from the wind tunnel tests, an automated data processing system was developed to help speed-up the process of data reduction. Other advantages of the automated process are consistency and elimination of possible human error. The automated processing system consists of an automated reflectometer and digital data acquisition system.

A schematic of the automated reflectometer and digital data acquisition system is shown in Figure 5.9. Photographs of the automated

reflectometer and data acquisition system are shown in Figures 5.10-5.11. The main components of the reflectometer are:

a. A Hughes 3225H-PC He-Ne laser

b. Two EG&G FND-100 silicon photodectors

c. A rotating drum with vertical translation

d. A convergent lens

e. Two noise filters with signal amplifiers

f. Power supplies for the various components

The digital acquisition system consists of:

a. A Hewlett Packard microcomputer with dual floppy disk drives

b. Two digital voltmeters

c. A Hewlett Packard plotter

d. A Hewlett Packard printer

In Figure 5.9, the blotter strip is positioned on the drum whose rotation and vertical translation are controlled by a stepper motor and a linear actuator, respectively. The stepper motor is capable of 800 steps per revolution. Since the drum radius is 68.26 mm (2.688 in), this corresponds to a movement of 0.54 mm (0.021 in) per step. This is approximately 0.57D where (D) is the laser beam diameter. The vertical motion of the drum is controlled by a linear actuator which moves the drum in 0.0254 mm (0.001 in) increments. Each blotter strip is scanned horizontally at three vertical locations H_1, H_2 and H_3 as shown in Figure 5.12. The length of each horizontal scan depends on the extent of dye impingement on the blotter strip. The vertical distance between horizontal scans is 5 mm (0.2 in) for the engine inlets blotter strips and 10 mm (0.4 in) for the airfoil and cylinder blotter strips.

The He-Ne laser illuminates the paper at an angle of 10^{o} with respect to the normal. The reflected (scattered) light is collected over a solid angle determined by the lens diameter and distance from the paper and is focused on an EG&G FND-100 silicon photodetector. The signal from the photodetector is input to an amplifier with gain 500 to 1. Filtering from high frequency electrical noise is also provided by the amplifier circuitry. This ensures that electrical noise comparable in magnitude to the signal is not a problem. The signal from the amplifier is directed to a digital voltmeter. The voltmeter reading (V1) is fed to the digital computer and stored on a floppy disk.

During the early stages of the reflectometer design, it was found that the intensity of the laser beam can vary over long periods of time.

This can affect the accuracy of the data reduction. The problem was eliminated using optical feedback. The optical feedback is accomplished by splitting off a portion of the beam as it exits the laser with a glass plate at an angle of approximately 45 degrees (Figure 5.13). The split beam is directed onto a second EG&G FND-100 silicon photodetector. The signal of the detector is passed through another amplifier with a high frequency noise filter and a gain of 10 to 1. The signal from the amplifier is directed to a second digital voltmeter. The reading (V2) from this voltmeter is also stored on floppy disk. During the data reduction, the microcomputer samples both digital voltmeters simultaneously and the two voltages are ratioed by the data acquisition system to take into account any drift in the output of the laser.

The reflectivity at any location on the strip is calculated from:

$$R = \frac{(V1/V2)_{\text{Dyed Blotter Paper}}}{(V1/V2)_{\text{Bare Blotter Paper}}} \qquad (5\text{-}5)$$

To determine $(V1/V2)_{\text{Bare Blotter Paper}}$ for each strip, a part of the strip which does not have any dye deposit is scanned.

Programs were developed to transform the measured voltages into reflectivity and then into dye mass using the standard reflectivity calibration curve. The software stores the raw data in files, processes the data into impingement efficiencies, and prints and plots the impingement efficiency data.

The complete optical and mechanical system with associated electronics and power supplies is conveniently mounted on two tiered aluminum plates. Both the instrument and the data acquisition/reduction system are completely portable. Tests conducted with this system indicate that the instrument itself will measure reproducibly to $\pm$ 0.3 percent. The largest uncertainty in extracting data from an individual strip comes from the blotter paper itself, which varies about $\pm$ 1.0 percent in addition to the instrument uncertainty.

Further details on the data reduction system and an example output can be found in Appendix C.

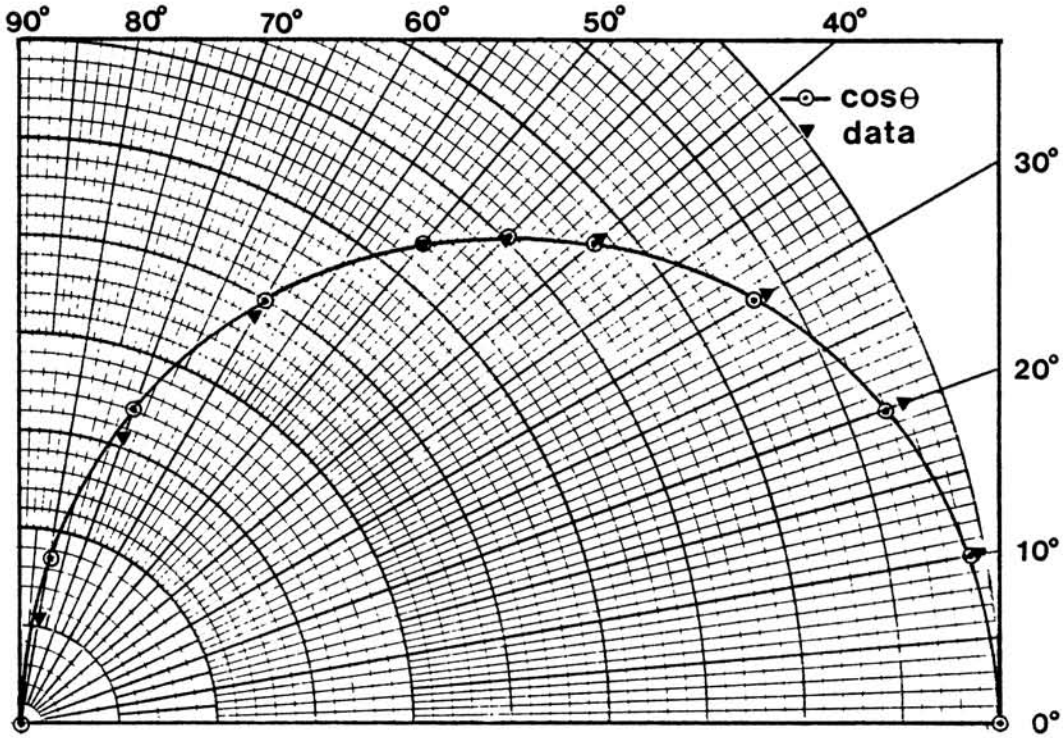

FIGURE 5.1

REFLECTANCE CURVE FOR THE BLOTTER PAPER
AS A FUNCTION OF ANGLE OF OBSERVATION θ.

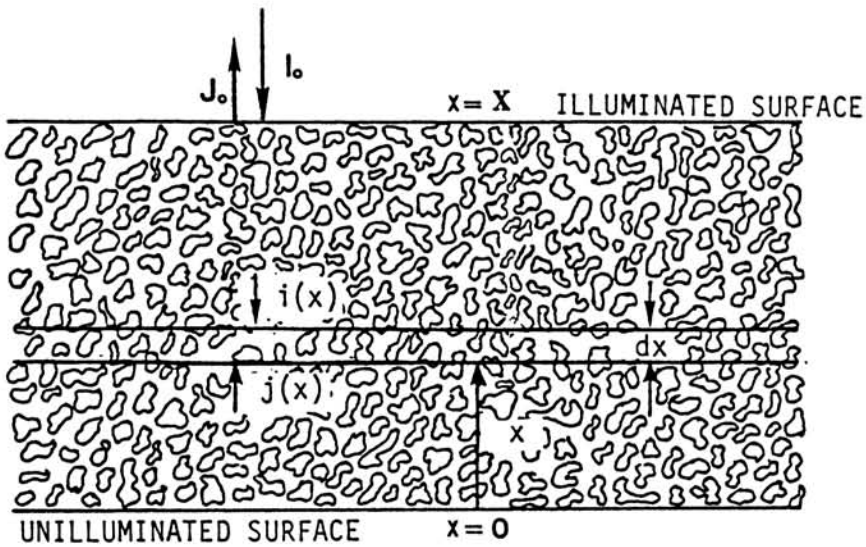

FIGURE 5.2

SCHEMATIC REPRESENTATION OF A LAYER OF
ABSORBING AND LIGHT-SCATTERING PARTICLES.

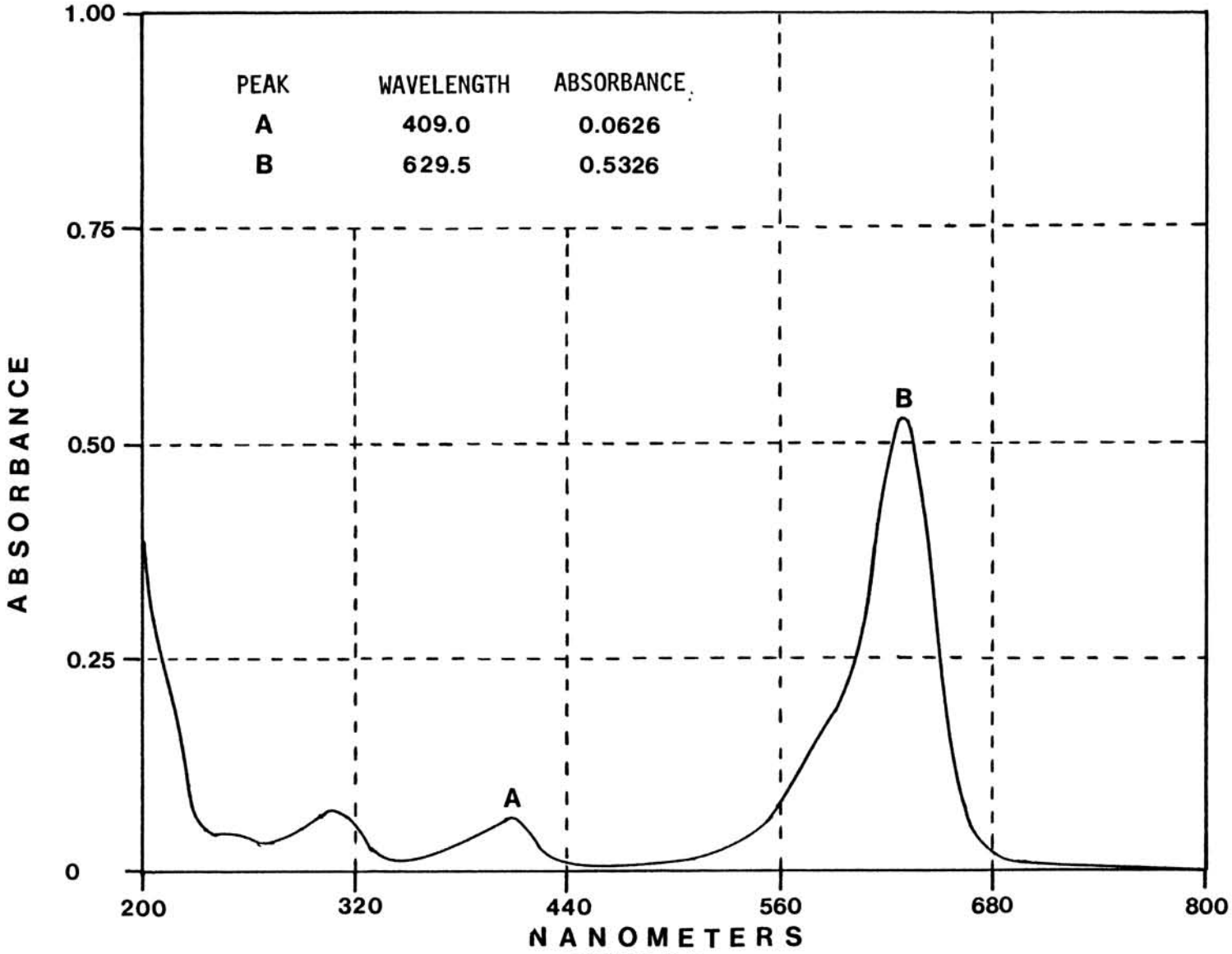

FIGURE 5.3

ABSORBANCE OF BRILLIANT BLUE FCF AS A FUNCTION OF WAVELENGTH.

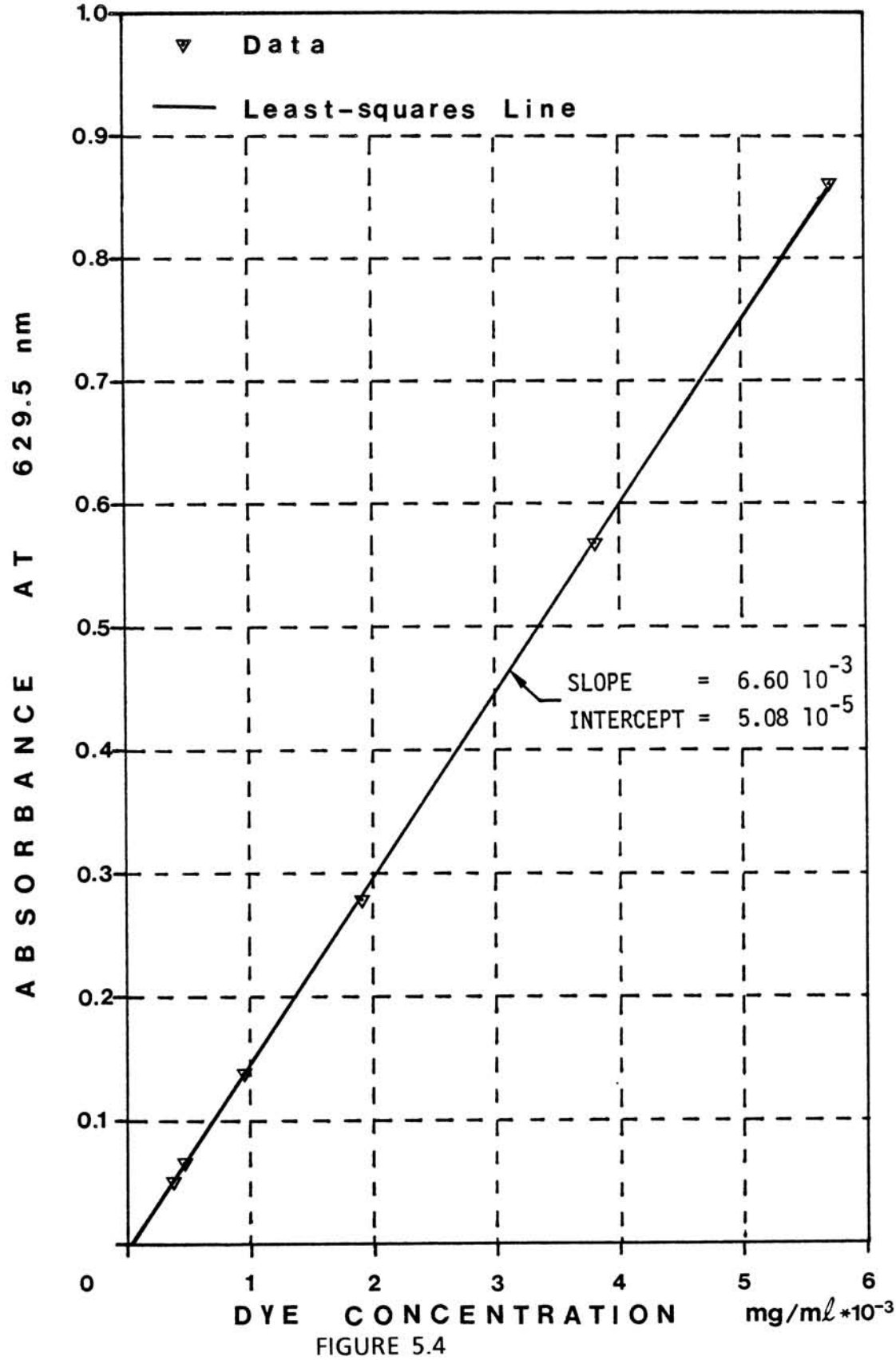

FIGURE 5.4

STANDARD ABSORBANCE CALIBRATION CURVE.

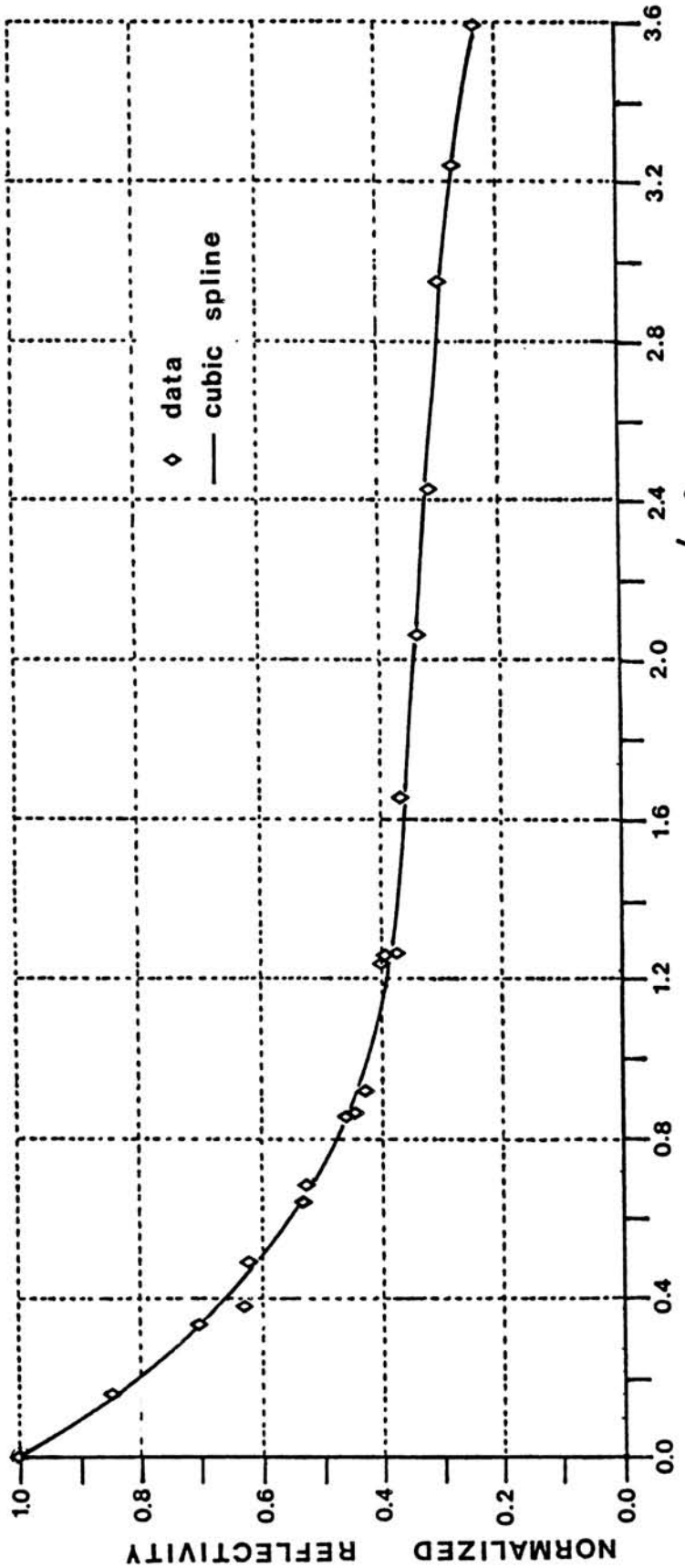

FIGURE 5.5

STANDARD NORMALIZED REFLECTIVITY CALIBRATION CURVE.

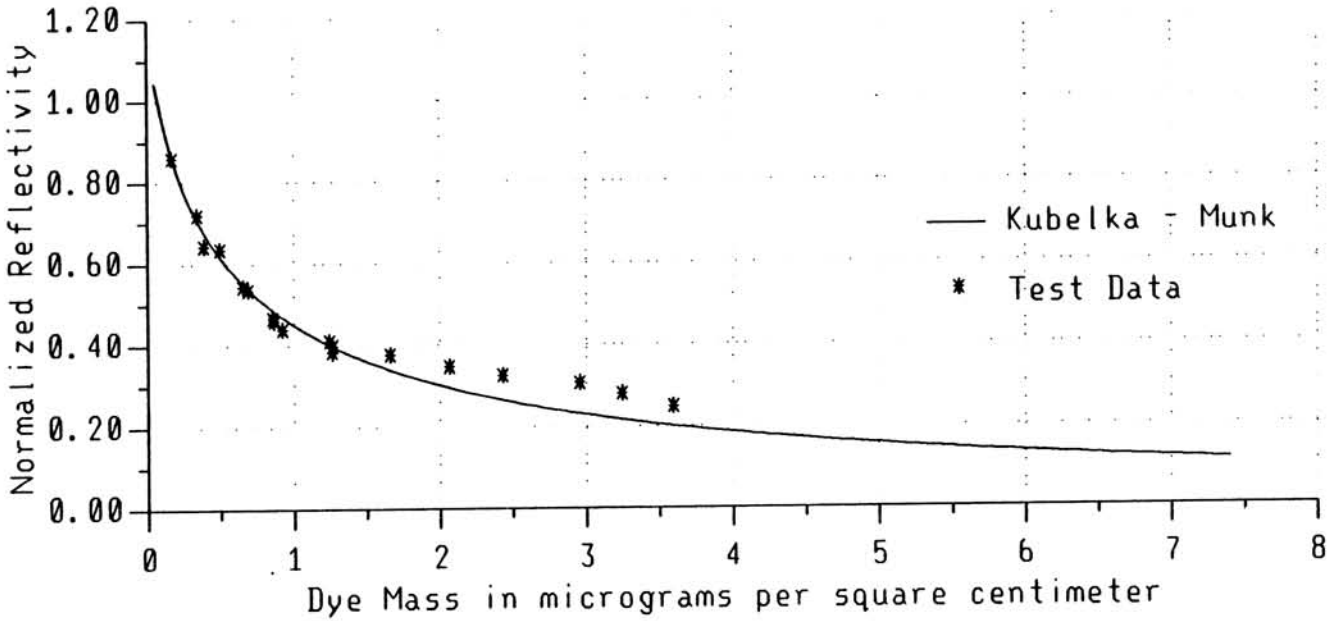

FIGURE 5.6

KUBELKA – MUNK NORMALIZED REFLECTIVITY CURVE
($K * X = 2.5$, $S * X = 3.5$, $R_g = 0.60$).

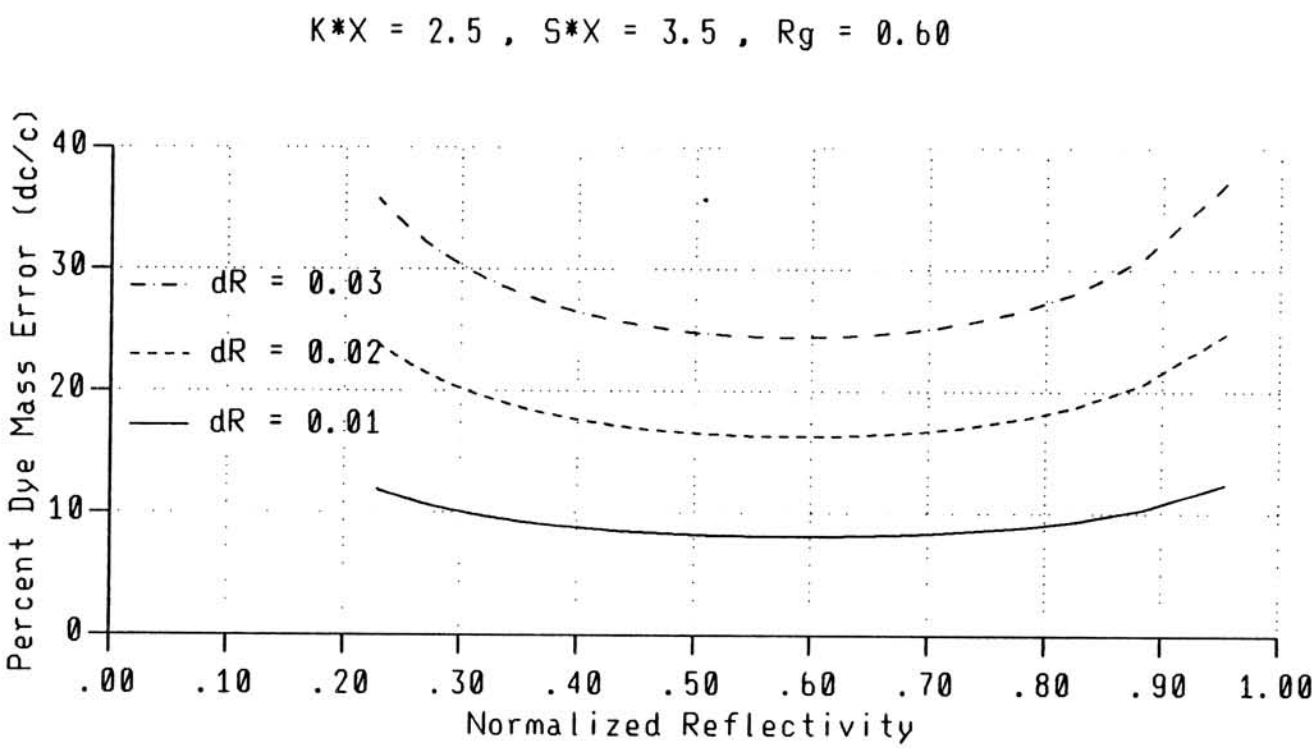

FIGURE 5.7

RELATIVE ERROR IN DYE MASS FROM AN ERROR OF dR
DERIVED FROM EQUATION 5-3.

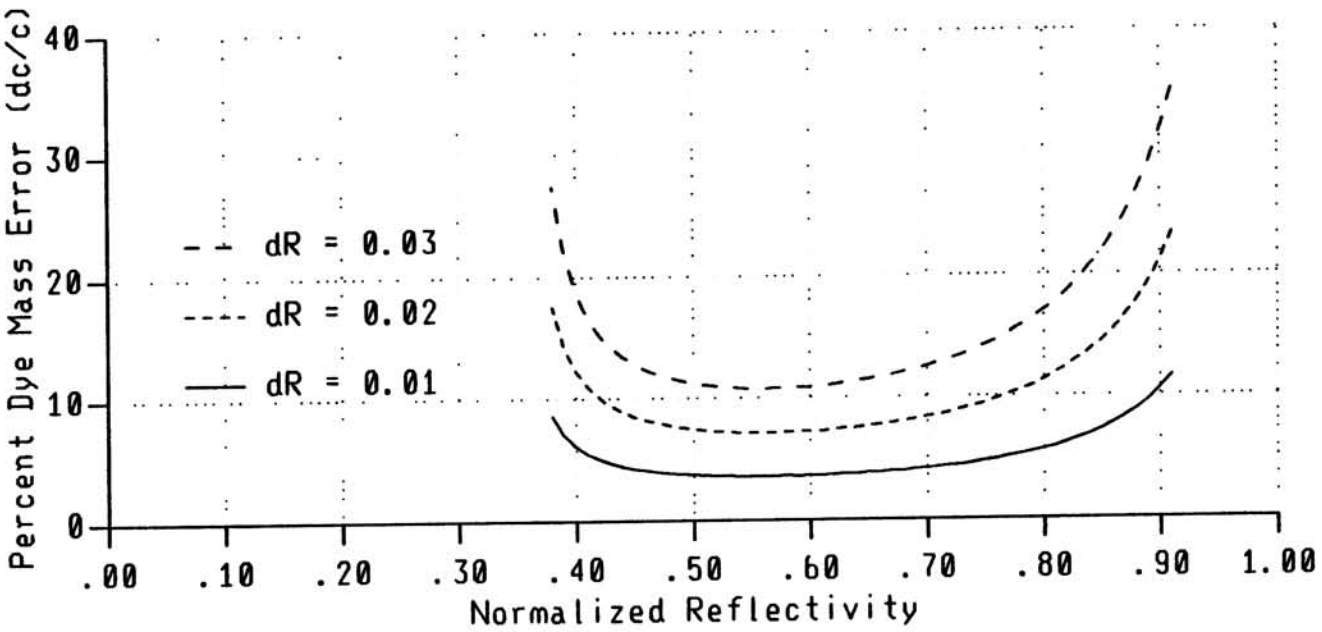

FIGURE 5.8

RELATIVE ERROR IN DYE MASS FROM AN ERROR OF dR
DERIVED NUMERICALLY FROM FIGURE 5.5.

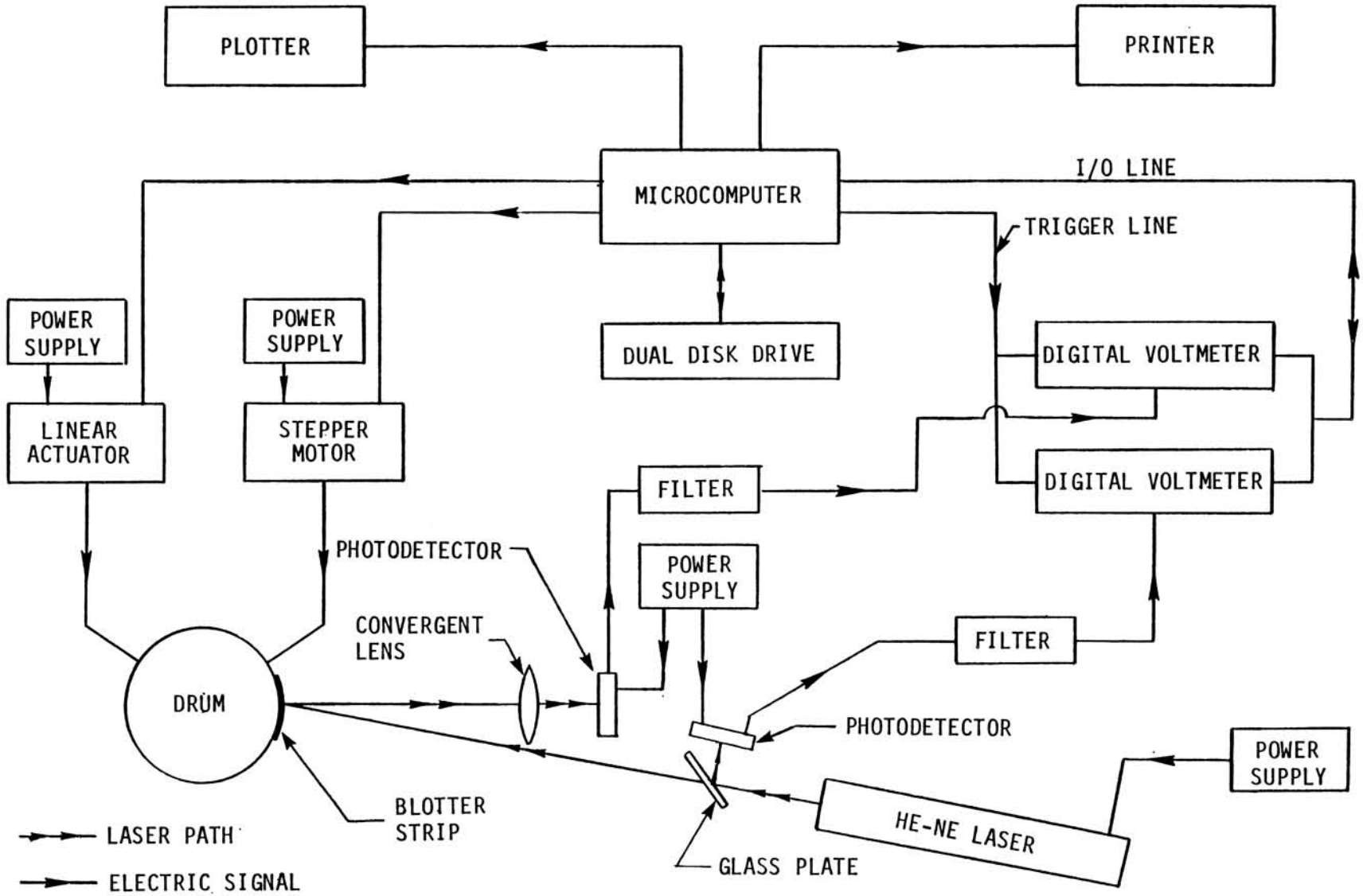

FIGURE 5.9

SCHEMATIC OF AUTOMATED REFLECTOMETER AND DIGITAL ACQUISITION SYSTEM.

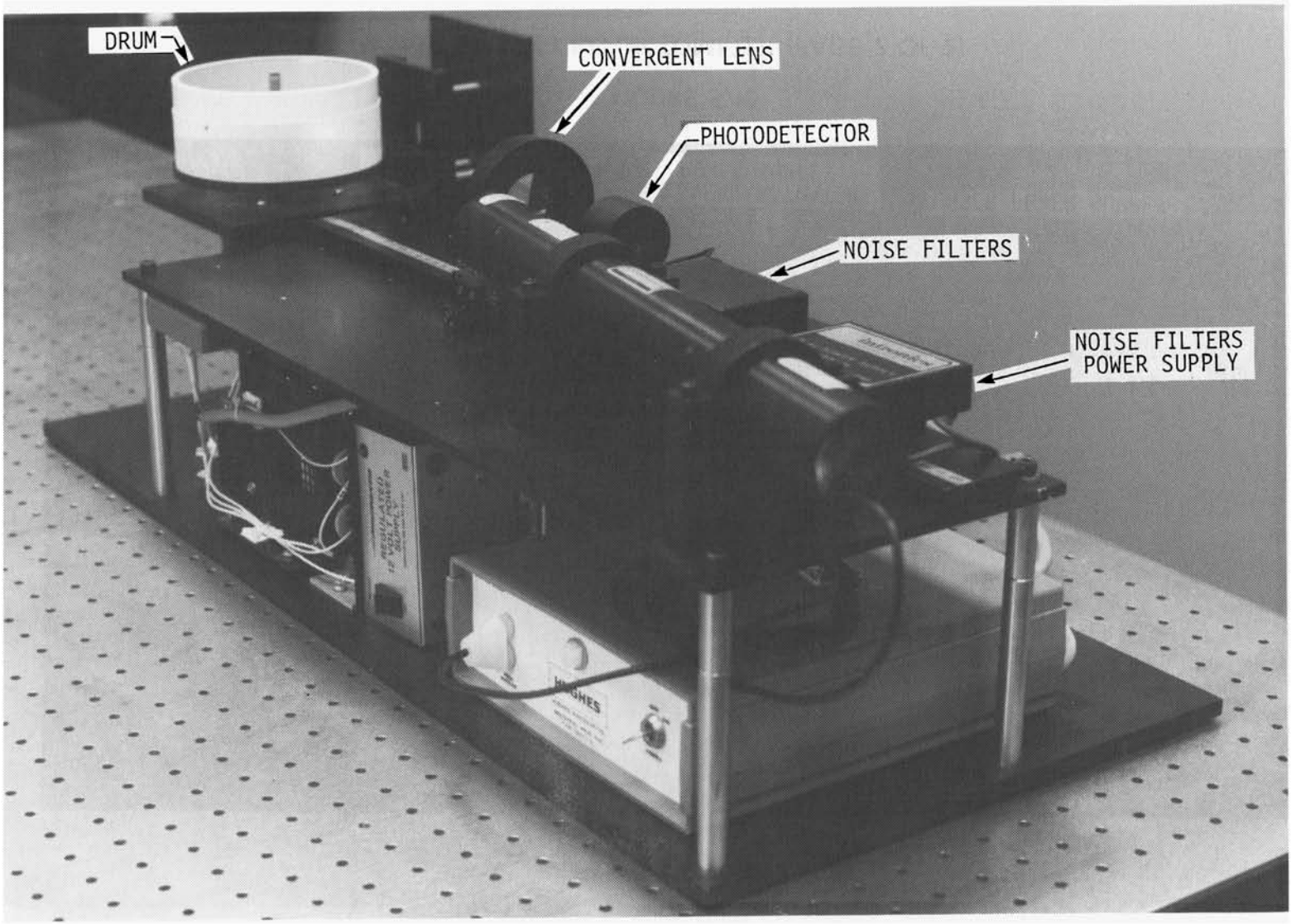

FIGURE 5.10

AUTOMATED REFLECTOMETER (PAGE 1 OF 2).

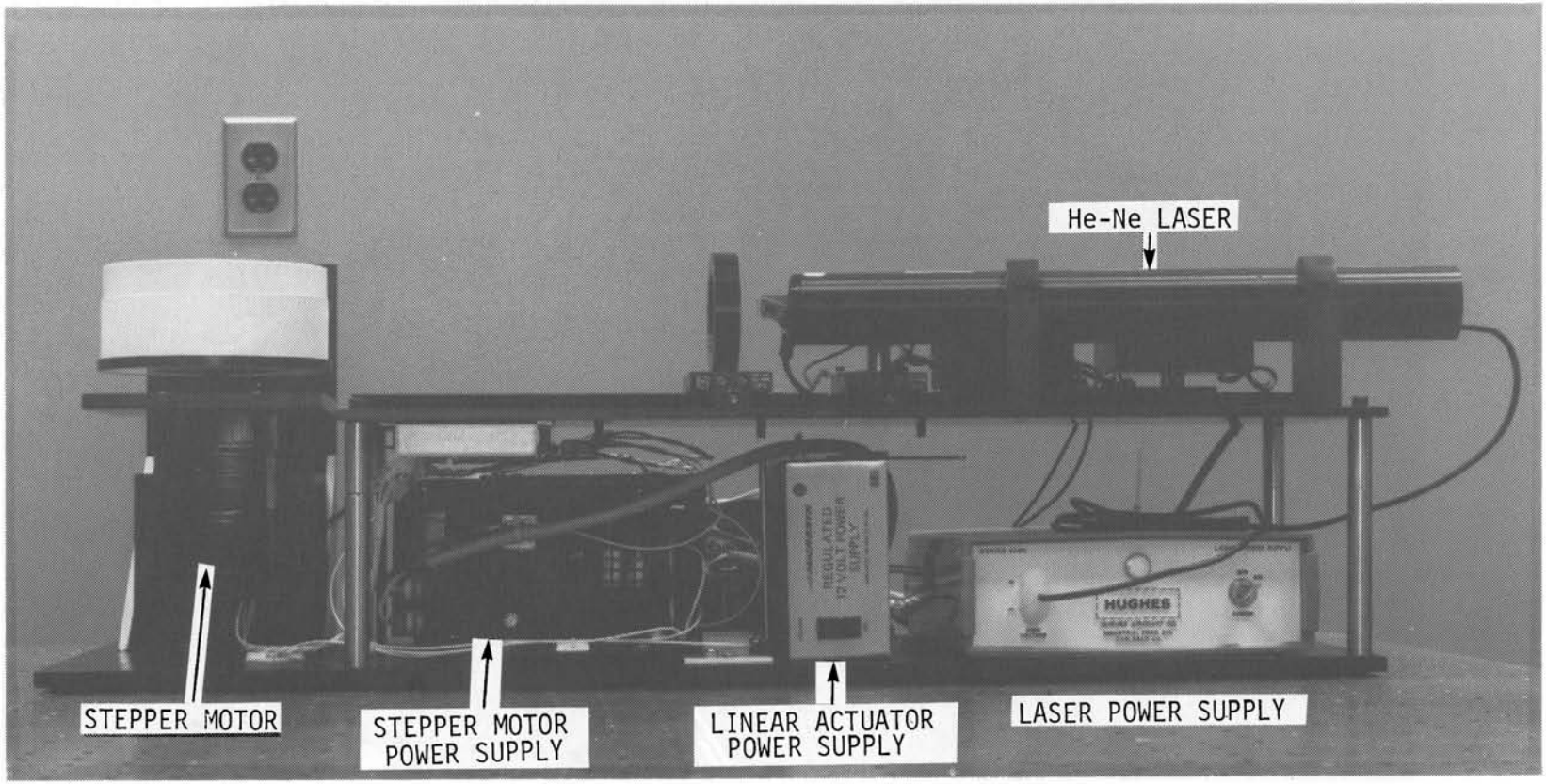

FIGURE 5.10

AUTOMATED REFLECTOMETER (PAGE 2 OF 2).

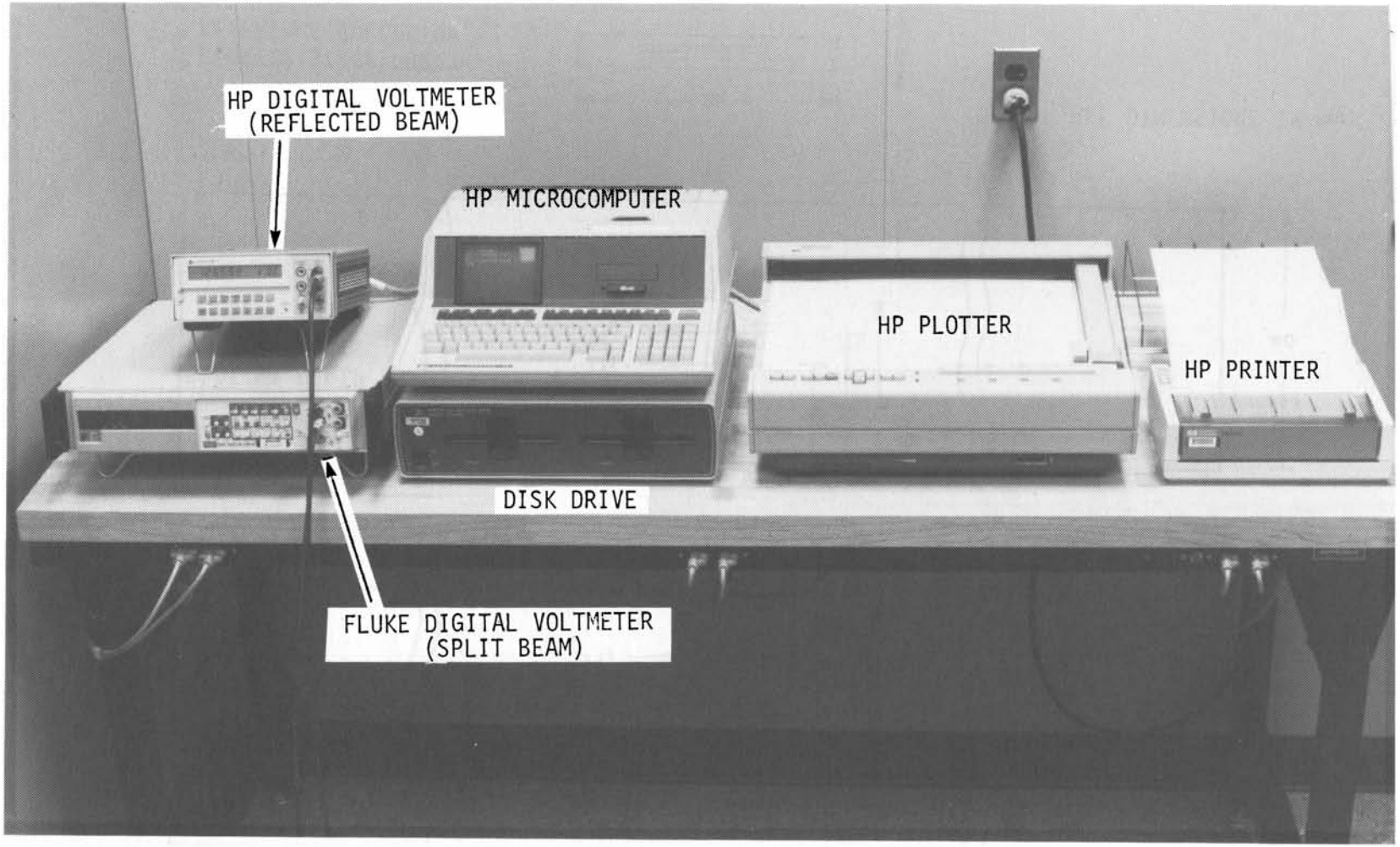

FIGURE 5.11

DIGITAL DATA ACQUISITION SYSTEM.

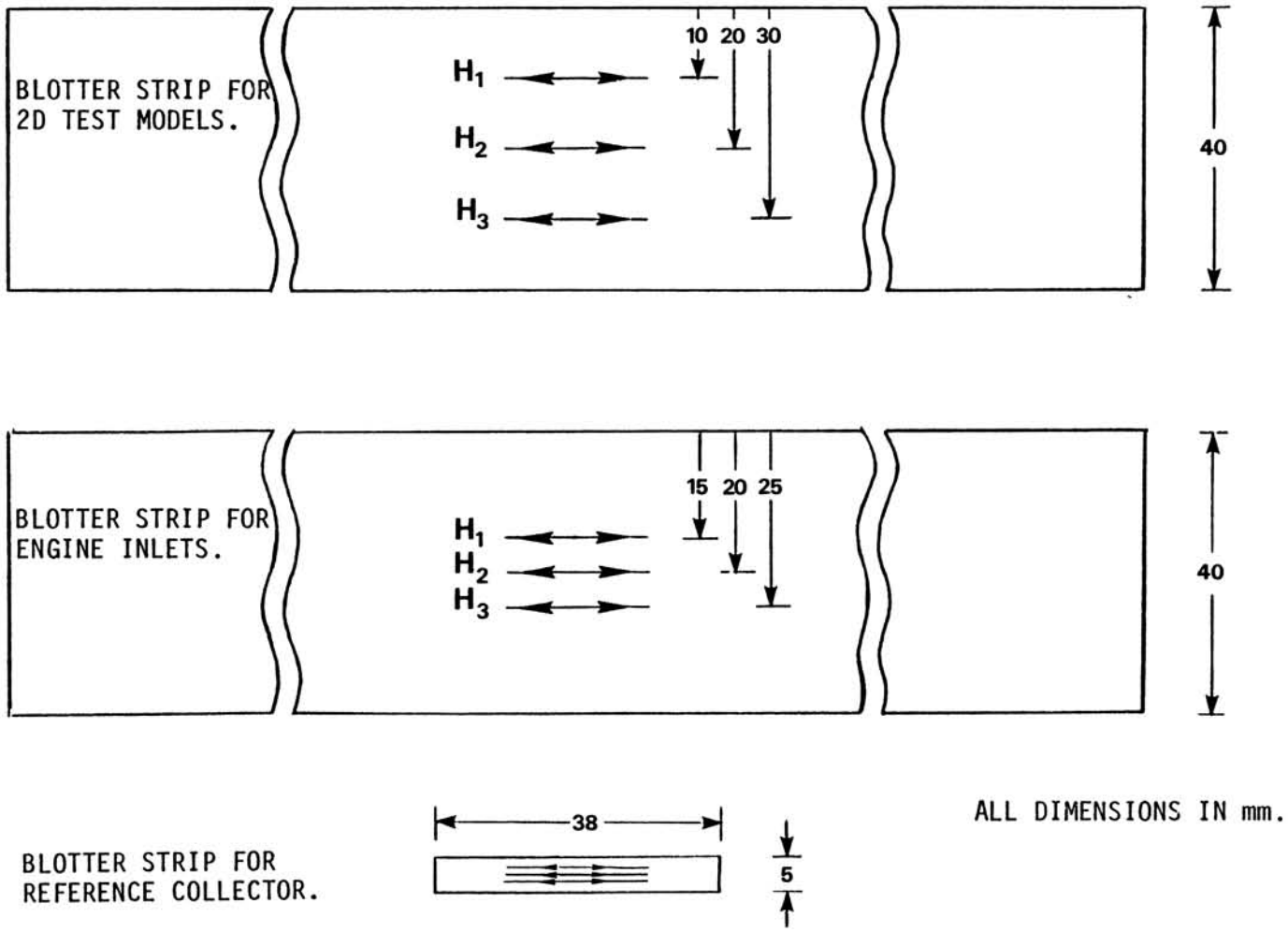

FIGURE 5.12

TYPICAL SCANNING LOCATIONS FOR BLOTTER STRIPS.

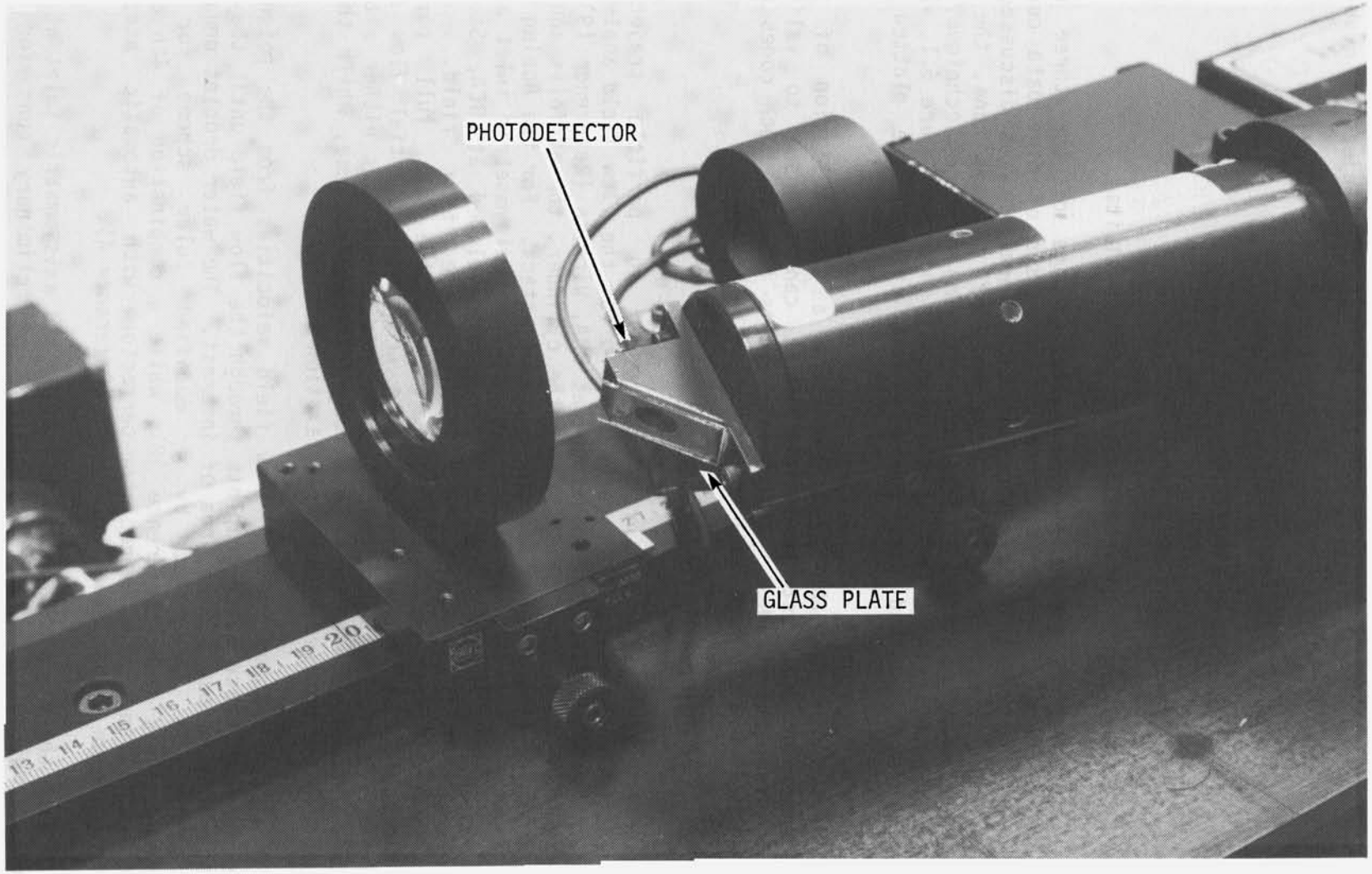

FIGURE 5.13

COMPONENTS OF OPTICAL FEEDBACK SYSTEM.

6.0 RESULTS AND DISCUSSION

Local impingement efficiency as a function of surface distance is the standard method for presenting droplet impingement trajectory results. The main features of the $\bar{\beta}$- curve are:

a. Curve overall shape

b. Magnitude of peak efficiency

c. Location of peak efficiency

d. Extent of the curve tails (impingement limits).

The $\bar{\beta}$- curves presented here are the average of the three runs performed (Note: Data from three runs consists of nine data curves since each blotter strip is scanned at three locations, as discussed in Section 5.5). Prior to averaging the data of repeated runs, the $\bar{\beta}$- values are smoothed using a three point moving average technique. A typical example of the effect of smoothing is shown in Figure 6.1, where unsmoothed and smoothed data for a 4 inch cylinder are plotted for comparison.

The $\bar{\beta}$ - curves included here represent a wide variation of test configurations and test conditions which can be used to validate existing trajectory codes. Analytical results from two such codes will be compared with the test data in the following sections.

6.1 Computer Codes Used for Comparison

Flow field analyses are required prior to particle trajectory calculations. Two separate codes were used for the flow field analyses. A 2D/axisymmetric flow code developed at BMA, Wichita (Reference 19) was used for the flow field analysis for the cylinder, the airfoils and the axisymmetric inlet at zero degrees angle of attack. For the Boeing 737-300 inlet (both angles of attack) and for the axisymmetric inlet at 15 degrees angle of attack, a 3D flow code developed at BCA, Seattle (Reference 25) was used to calculate the flow field. The 2D/axisymmetric and 3D potential codes solve the full partial differential equations of compressible transonic potential flow by a finite difference method. The 2D/axisymmetric code uses either a block successive over-relaxation or a strongly implicit scheme, while the 3D code uses a successive line over-relaxation scheme.

The trajectory codes utilize flow field velocities from the potential flow codes to trace water droplets through the flow field until they hit a body or pass out of the area of interest. The water droplet equation of motion is integrated by a modified Euler scheme for the 2D/axisymmetric code (Reference 18), while a combination of 4th order Runge-Kutta and Adams predictor-corrector with automatic stepsize control scheme is used for the 3D code (Reference 4).

To compare the axisymmetric and 3D codes, the axisymmetric inlet at zero degrees angle of attack was employed. Preliminary runs for this

configuration showed a 9 percent difference in maximum $\bar{\beta}$ between the two codes for identical flow conditions and particle distributions. After refining the potential flow grid mesh in both codes, nearly identical results were produced. The axisymmetric code was also tested using exact analytical flow field solutions for a cylinder. Good agreement between the numerical and exact solutions was obtained.

Clearly the degree of grid refinement is very important in calculating accurate $\bar{\beta}$ - distributions. When complex geometries are involved the program user must have considerable experience or utilize a proven grid generation computer code to determine how fine the grid should be. Extensive code validation against experimental data obtained using a variety of geometries, flow conditions and particle distribution, is required to help establish guide lines with respect to grid refinement.

6.2 Two-Dimensional Test Impingement Data

Results for the 4 inch cylinder, ice shapes (mounted on a 2 inch cylinder), 65_2015 airfoil section and MS(1)-0317 airfoil section are presented here. The highlight marks and surface distance convention for the 4 inch cylinder and the airfoils are shown in Figure 6.2. Two blotter strips were employed for both the 4 inch cylinder and airfoils at different spanwise locations while only one was employed on each of the three ice shapes. Strip locations (B, C) for the NACA 65_2015 and MS(1)-0317 airfoils are shown in Figure 4.3 of Section 4. Local impingement efficiency data on strips B and C should be identical in theory since the flow field is two-dimensional. In practice, small variations (See Figures 6.3-6.5) are expected due to local variation in dye uniformity.

Test repeatability for the 4 inch cylinder, the NACA 65_2015 airfoil at $\alpha = 0^o$ and $\alpha = 8^o$ is demonstrated in Figures 6.3 - 6.5. Averaged local water droplet impingement efficiency curves for all two-dimensional test configurations are shown in Figures 6.6 - 6.8. The strip identification letters and run identification numbers of curves averaged are shown at the top of each plot (RUN ID:) together with tunnel and spray test conditions. For the cases of symmetric airflow (4 inch cylinder, ice shapes and NACA 65_2015) about the model, symmetric $\bar{\beta}$ distributions are observed (Figures 6.6 -6.7), as expected. For the airfoils at 8^o angle-of-attack, test data shows that the shift in $\bar{\beta}_{max}$ position results from the shift in flow stagnation point and the increase in total water collected is due to the greater frontal projected area.

The analytical curves presented agree well with the test data for the 4 inch cylinder and the airfoils at $\alpha = 0^o$ and show similar trends. Fair agreement between test and theory is demonstrated for the NACA 65_2015 and MS(1)-0317 airfoil sections at $\alpha = 8^o$. The droplet distribution data employed to produce the analytical curves are presented in Appendix E (Tables E4 and E5).

6.3 Engine Inlets

For engine inlets, the effects of droplet size, mass flow, angle of attack and surface angular location on the $\bar{\beta}$ - curve are discussed in the following sections.

6.3.1 Aerodynamic Data

Aerodynamic data were obtained for the inlets prior to the water impingement efficiency testing. As explained in Section 3.9, comparison of experimental and analytical impingement data requires that analytical and experimental flow fields are in good agreement. In this section, all aerodynamic data are presented and compared to analytical results produced using the codes described in Section 6.1. Surface Mach numbers are plotted versus axial distance (X = 0 is highlight for axisymmetric inlet, X = 0 is compressor face for 737-300 inlet).

Results for two angles of attack ($\alpha = 0^{o}$ and $\alpha = 15^{o}$), two suction flows (17.2 and 22.96 lbm/sec) and various θ locations are presented for the axisymmetric inlet and the Boeing 737-300 inlet, Figures 6.9 and 6.10. These figures consist of summary data followed by detailed data. Good correlation between test and analytical data is demonstrated.

6.3.2 Water Impingement Efficiency Data

Averaged water impingement data are presented in this section for all inlet test configurations. Analytical results are also presented for comparison. The analytical local impingement efficiencies were calculated using the droplet distributions presented in Appendix E (Tables E4 and E5).

Surface distance, in all cases, is measured with respect to a reference point (highlight) and is positive along the inner cowl and negative along the outer cowl. Figures 6.11, 6.14 and 6.17 show the highlight marks, surface distance convention and strip locations for the axisymmetric and Boeing 737-300 inlets. These figures also show the dye mass density for the collector in $\mu g/cm^2$ for each inlet strip location. These collector masses are used in the calculation of the local impingement efficiency curves as explained in Appendix C. The collector masses for locations $\theta = 0^{o}$, 90^{o}, 180^{o} and 270^{o} are the average of three calibration runs performed using the four blade reference collector as described in Section 3.7. The calibration curves for the four blade reference collector are shown in Figure 3.15. The collector masses corresponding to locations $\theta = 45^{o}$, 135^{o}, 225^{o} and 315^{o} have been estimated.

6.3.2.1 Axisymmetric Geometry - Axisymmetric Flow

Results for the axisymmetric inlet at zero degrees angle of attack are presented in this section. Figure 6.12 shows typical repeatability results for locations $\theta = 90^{o}$ and 180^{o}. In theory, all locations should give identical results due to symmetry in airflow and geometry. The variations in $\bar{\beta}_{max}$ observed in Figure 6.12 are mainly due to non-uniformity effects. Overall, good agreement is demonstrated amongst

test $\bar{\beta}$ - curves for the two runs and two locations shown in Figure 6-12. A summary of the results for the axisymmetric inlet at zero degrees angle of attack are presented in Figure 6.13, detailed results are also given in Figure 6.13.

The results shown in Figure 6.13 are the average of 12 strips (3 runs, 4 locations per run). Agreement between test and analysis is good for all test configurations. Based on the test results, the following trends are observed:

a. For the same inlet mass flow, decreasing the MVD of the cloud reduces both $\bar{\beta}_{max}$ and impingement limits.

b. For the same cloud MVD, reducing the inlet suction flow reduces the value of $\bar{\beta}_{max}$ and shifts the peak location towards the inner cowl. No change in the extent of the impingement limits (s_{max} - s_{min}) is observed. However, both impingement limits shift slightly to the right.

c. For the high mass flow (capture area ratio = 1), the peak $\bar{\beta}$ - location is at the highlight.

d. Maximum $\bar{\beta}_{max}$ is approximately 0.58 and corresponds to MVD = 20.36 microns and inlet mass flow = 22.96 lbm/sec. Minimum $\bar{\beta}_{max}$ is approximately 0.47 and corresponds to MVD = 16.45 microns and inlet mass flow = 17.2 lbm/sec.

6.3.2.2 Axisymmetric Geometry - Three Dimensional Flow

Results for the axisymmetric inlet at 15 degrees angle of attack are discussed in this section. Typical repeatability results for various locations on the inlet and for two runs are shown in Figure 6.15. Good repeatability is demonstrated. Nearly identical $\bar{\beta}$ - distribution between C and G locations are observed in Figure 6.15 as expected. A summary of all test and analytical results is given in Figure 6.16. Detailed results of local impingement efficiency variation with inlet mass flow, cloud MVD and inlet surface location are presented in Figure 6.16. The flow field is symmetric with respect to a horizontal axis through locations A ($\theta = 180^{o}$) and E ($\theta = 0^{o}$). This means that the $\bar{\beta}$ - curves for strips B and H should be identical. Identical impingement results between strips C and G and for strips D and F are also expected.

The single averaged test $\bar{\beta}$ - curves presented for each test configuration in Figure 6.16 have been obtained from the following strips:

a. $\theta = 0^{o}$, E strip , three runs (total 3 strips)

b. $\theta = 45^{o}$, D and F strips, three runs (total 6 strips)

c. $\theta = 90^{o}$, C and G strips, three runs (total 6 strips)

d. $\theta = 135^{o}$, B and H strips, three runs (total 6 strips)

e. $\theta = 180^{o}$, A strip, three runs (total 3 strips).

Overall, good agreement between test and analysis is demonstrated for the majority of test configurations and inlet locations. The only noticeable disagreement occurs at $\theta = 0^{o}$ (E strip) for all test configurations.

The following trends are observed based on the test data:

a. For the same inlet mass flow and surface location, the larger the MVD of the cloud the greater the value of $\bar{\beta}_{max}$ and the impingement limits.

b. In most cases if MVD is kept constant, decreasing the inlet suction flow reduces $\bar{\beta}_{max}$ for corresponding inlet surface locations. In addition, the impingement limits and the peak of the $\bar{\beta}$- curve are slightly shifted towards the inner cowl (positive s).

c. For the same inlet mass flow and cloud MVD, the location of $\bar{\beta}_{max}$ shifts from the inner cowl at $\theta = 0^{o}$ to the highlight at $\theta = 90^{o}$ and then to the outer cowl at $\theta = 180^{o}$.

d. For all mass flows and droplet distributions the experimental maximum value of $\bar{\beta}_{max}$ occurs at $\theta = 135^{o}$ and the maximum impingement limits are observed at $\theta = 180^{o}$.

e. The maximum value of the experimental $\bar{\beta}_{max}$ is approximately 66 percent and corresponds to MVD = 20.36 microns, inlet mass flows = 22.96 and 17.2 lbm/sec and $\theta = 135^{o}$. The minimum $\bar{\beta}_{max}$ is about 38 percent and corresponds to MVD = 16.45 microns, inlet mass flow = 17.2 lbm/sec and $\theta = 0^{o}$.

6.3.2.3 Three Dimensional Geometry - Three Dimensional Flow

Water droplet local impingement efficiency curves for the Boeing 737-300 inlet at angles of attack 0 and 15 degrees are presented in this section. This inlet has a truly three dimensional geometry and the flow field about the inlet is also three dimensional at both angles of attack.

Typical test repeatability results are shown in Figures 6.18 and 6.20 for the inlet at $\alpha = 0^{o}$ and $\alpha = 15^{o}$, respectively. Averaged local impingement efficiency curves are presented in Figures 6.19 (α = 0 degrees) and 6.21 (α = 15 degrees). Variations in inlet mass flow, spray cloud MVD and inlet surface location give a total of 20 curves for $\alpha = 0^{o}$ and 25 curves for $\alpha = 15^{o}$. The greater number of curves for $\alpha = 15^{o}$ is due to the additional mass flow setting used in this case.

As in the case of the axisymmetric inlet, the flow is symmetric with respect to a horizontal plane through locations A ($\theta = 0^{o}$) and E ($\theta = 180^{o}$). Thus, in theory, identical results are expected for

a. Strips B and H

b. Strips C and G

c. Strips D and F

The single averaged test local impingement efficiency curves have been obtained by averaging experimental results from all three runs performed for each test configuration. The number of blotter strips used for each inlet location are:

a. $\theta = 0^o$, A strip, three runs (total 3 strips)

b. $\theta = 45^o$, B and H strips, three runs (total 6 strips)

c. $\theta = 90^o$, C and G strips, three runs (total 6 strips)

d. $\theta = 135^o$, D and F strips, three runs (total 6 strips)

e. $\theta = 180^o$, E strip, three runs (total 3 strips).

Overall, agreement between test and analysis for the Boeing 737-300 inlet is very good at α = 0 degrees and good at α = 15 degrees. The only case where correlation between analysis and test is poor corresponds to surface location $\theta = 0^o$ (strip A) at 15 degrees angle of attack. The reason for this discrepancy is not clear.

Based on the test results, the following general trends are observed:

1. In most cases, for the same inlet mass flow both $\overline{\beta}_{max}$ and impingement limits decrease with MVD as expected for corresponding θ locations. This is observed for both angles of attack.

2. For the same cloud MVD, decreasing the inlet mass flow results in a decrease in the value of $\overline{\beta}_{max}$ for corresponding θ locations. In addition, both the peak location of the $\overline{\beta}$-curve and the impingement limits are shifted towards the inner cowl. The lower the mass flow the greater the shift as shown in Figure 6.21. The mass flow effect is the same for both angles of attack.

3. For the same MVD, inlet mass flow and angle of attack, the only parameter affecting the $\overline{\beta}$- curve is surface location θ. The maximum value of $\overline{\beta}$ occurs at $\theta = 90^o$ for $\alpha = 0^o$. For $\alpha = 15^o$, the maximum value of $\overline{\beta}$ occurs at $\theta = 90^o$ and $\theta = 135^o$ depending on inlet mass flow and cloud MVD. For both angles of attack, the extent of impingement limits is maximum at $\theta = 135^o$.

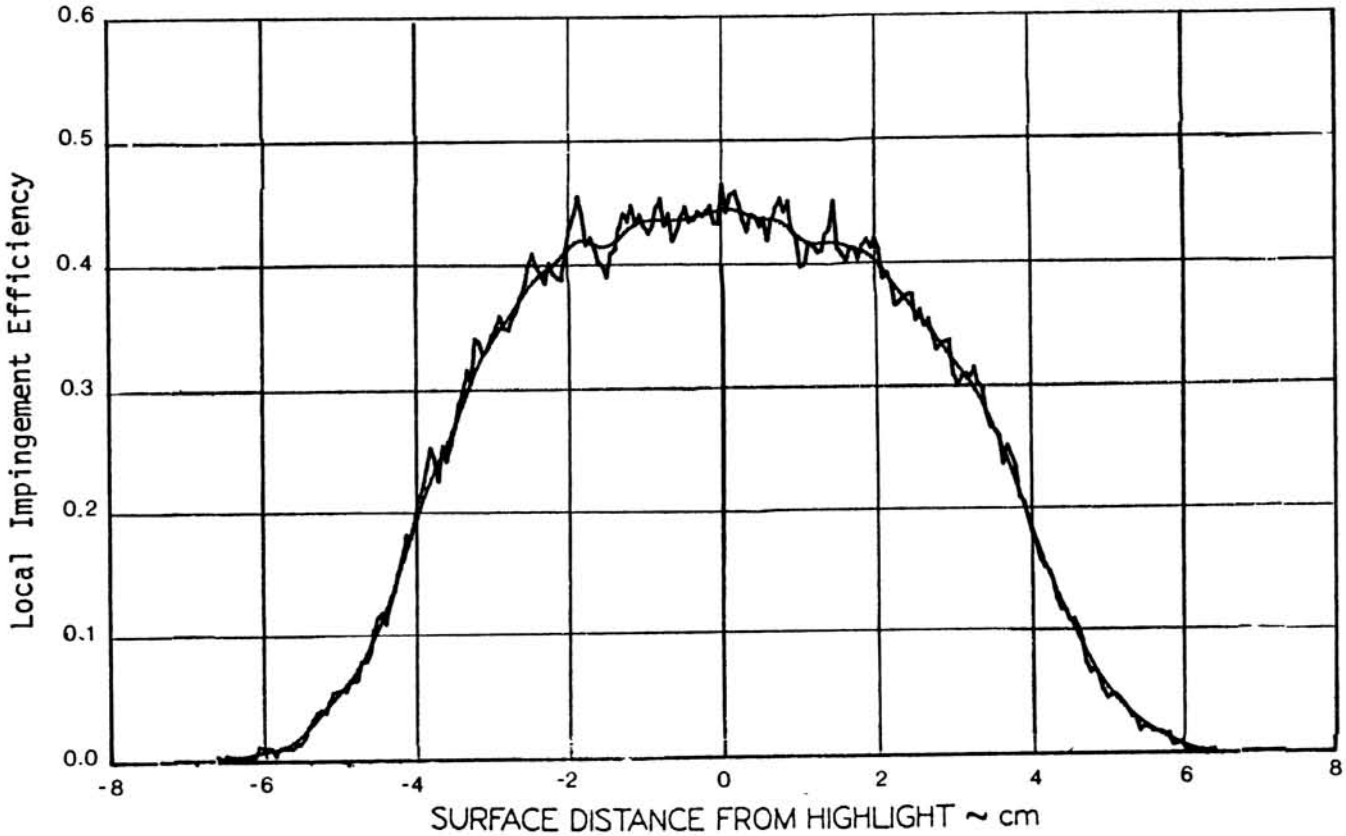

FIGURE 6.1

COMPARISON OF UNSMOOTHED AND SMOOTHED TEST DATA FOR 4 INCH CYLINDER.

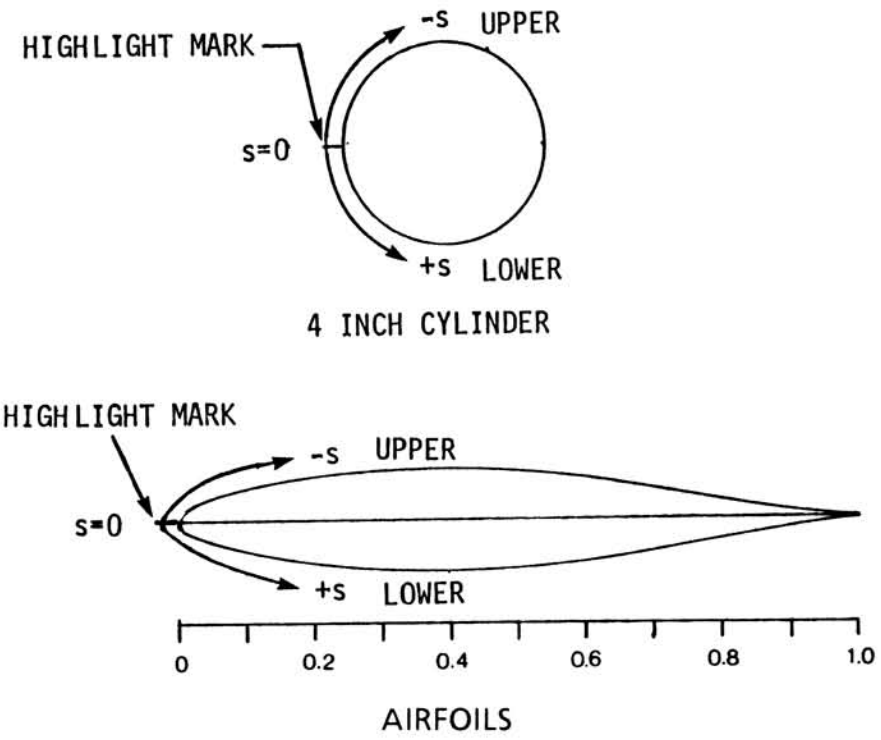

FIGURE 6.2

HIGHLIGHT MARKS AND SURFACE DISTANCE CONVENTION FOR TWO-DIMENSIONAL MODELS.

TEST RUN ID: 091885-2,3C-4IN-CYL 4 INCH CYLINDER

TRUE AIR SPEED	=	80.25 m/s	(179.51 mph)
TUNNEL TOTAL TEMP	=	7.9 C	(46.3 F)
TUNNEL STATIC PRESSURE	=	95.72 kPa	(13.89 psia)
AIR/WATER PRESSURE RATIO	=	0.65	
COLLECTOR EFFICIENCY	=	0.89	

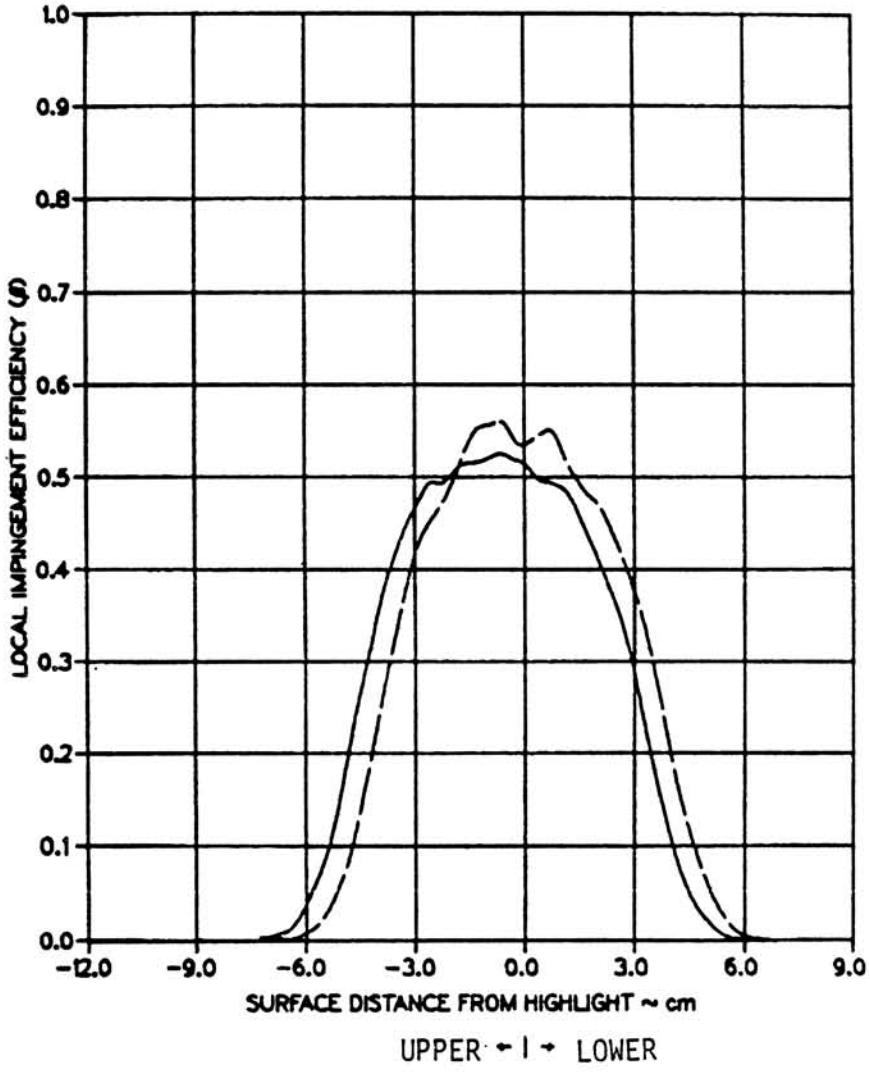

(A) MVD = 20.36 MICRONS

FIGURE 6.3

TEST REPEATABILITY FOR 4 INCH CYLINDER (PAGE 1 OF 2).

TEST RUN ID: 091885-5C,6BC-4IN-CYL 4 INCH CYLINDER

TRUE AIR SPEED	=	81.02 m/s	(181.22 mph)
TUNNEL TOTAL TEMP	=	8.2 C	(46.7 F)
TUNNEL STATIC PRESSURE	=	95.65 kPa	(13.88 psia)
AIR/WATER PRESSURE RATIO	=	0.80	
COLLECTOR EFFICIENCY	=	0.86	

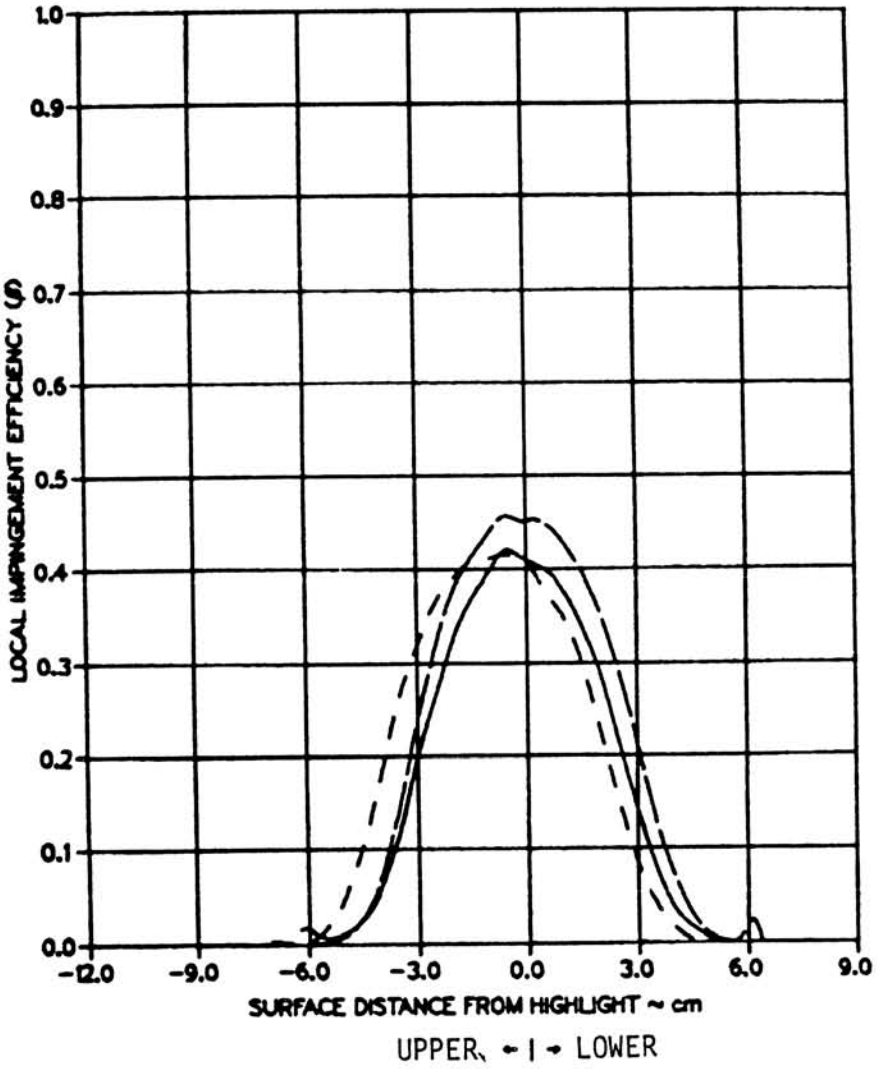

(B) MVD = 16.45 MICRONS

FIGURE 6.3

TEST REPEATABILITY FOR 4 INCH CYLINDER (PAGE 2 OF 2).

TEST RUN ID. 092685-1,2,3BC-015-0 NACA 65_2015

TRUE AIR SPEED	=	80.77 m/s	(180.68 mph)
TUNNEL TOTAL TEMP	=	8.9 C	(48.1 F)
TUNNEL STATIC PRESSURE	=	94.48 kPa	(13.71 psia)
AIR/WATER PRESSURE RATIO	=	0.65	
COLLECTOR EFFICIENCY	=	0.89	

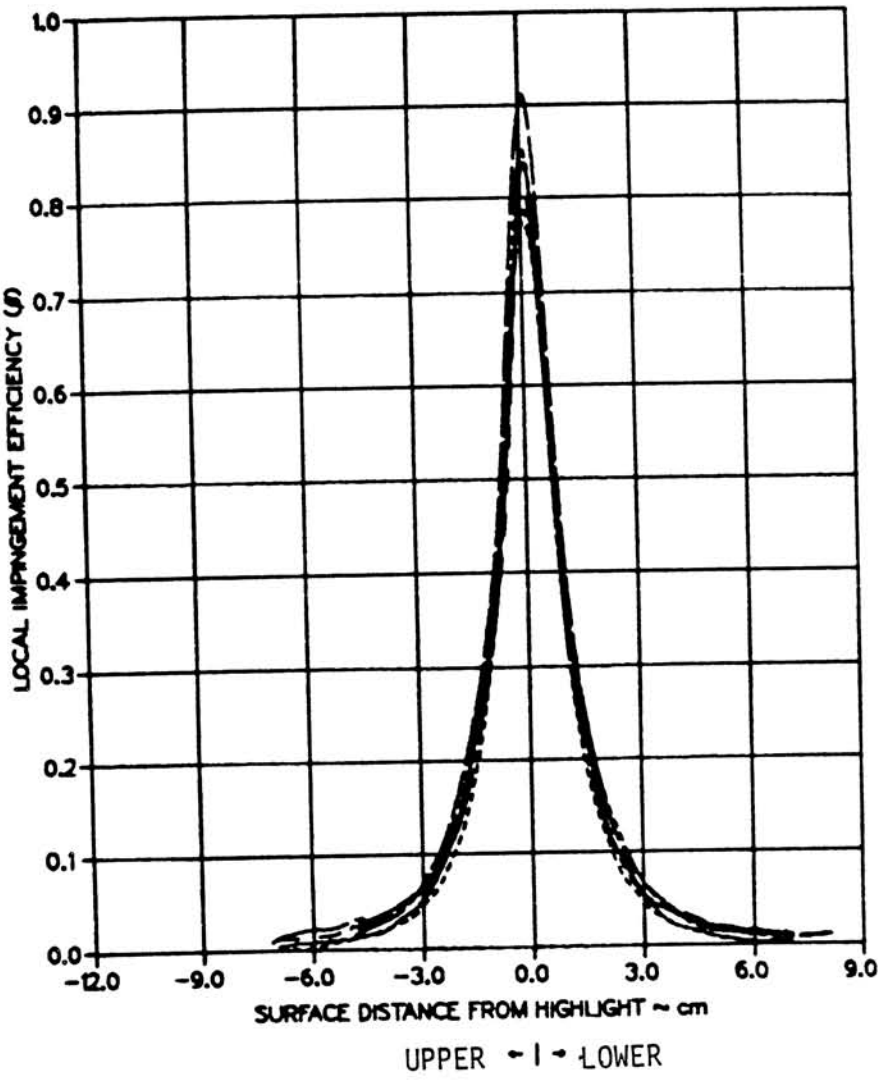

MVD = 20.36 MICRONS

FIGURE 6.4

TEST REPEATABILITY FOR NACA 65_2015 AIRFOIL AT $\alpha = 0°$.

TEST RUN ID: 092685-10C,11CB,12C-015-8 NACA 65_2015

TRUE AIR SPEED	=	81.26 m/s	(181.76 mph)
TUNNEL TOTAL TEMP	=	9.6 C	(49.2 F)
TUNNEL STATIC PRESSURE	=	94.54 kPa	(13.72 psia)
AIR/WATER PRESSURE RATIO	=	0.80	
COLLECTOR EFFICIENCY	=	0.86	

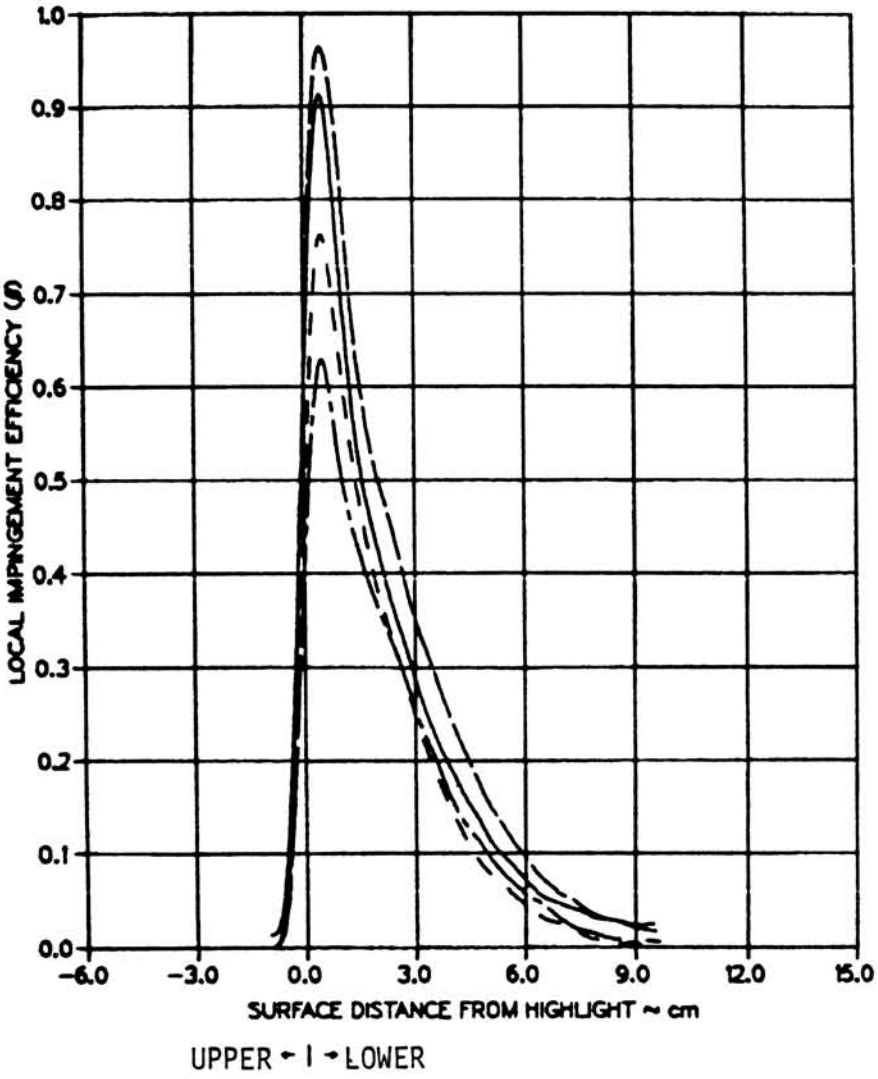

MVD = 16.45 MICRONS

FIGURE 6.5

TEST REPEATABILITY FOR NACA 65_2015 AIRFOIL AT $\alpha = 8°$.

TEST RUN ID: 091885—2,3C-4IN-CYL 4 INCH CYLINDER

TRUE AIR SPEED	=	80.25 m/s	(179.51 mph)
TUNNEL TOTAL TEMP	=	7.9 C	(46.3 F)
TUNNEL STATIC PRESSURE	=	95.72 kPa	(13.89 psia)
AIR/WATER PRESSURE RATIO	=	0.65	
COLLECTOR EFFICIENCY	=	0.89	

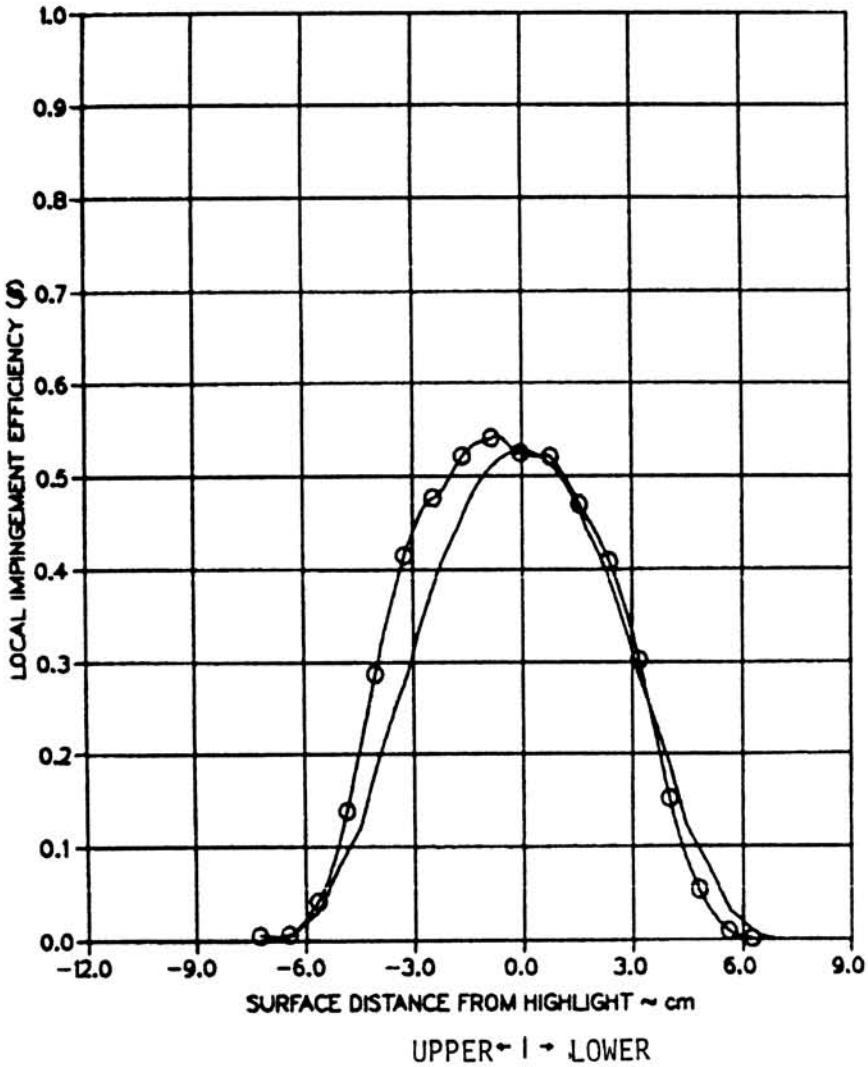

(A) MVD = 20.36 MICRONS

FIGURE 6.6

AVERAGED LOCAL WATER DROPLET IMPINGEMENT EFFICIENCY DATA FOR 4 INCH CYLINDER AND ICE SHAPES (MOUNTED ON 2 INCH CYLINDER) PAGE 1 OF 5.

TEST RUN ID: 091885-5C,6CB-4IN-CYL 4 INCH CYLINDER

TRUE AIR SPEED	=	81.02 m/s	(181.22 mph)
TUNNEL TOTAL TEMP	=	8.2 C	(46.7 F)
TUNNEL STATIC PRESSURE	=	95.65 kPa	(13.88 psia)
AIR/WATER PRESSURE RATIO	=	0.80	
COLLECTOR EFFICIENCY	=	0.86	

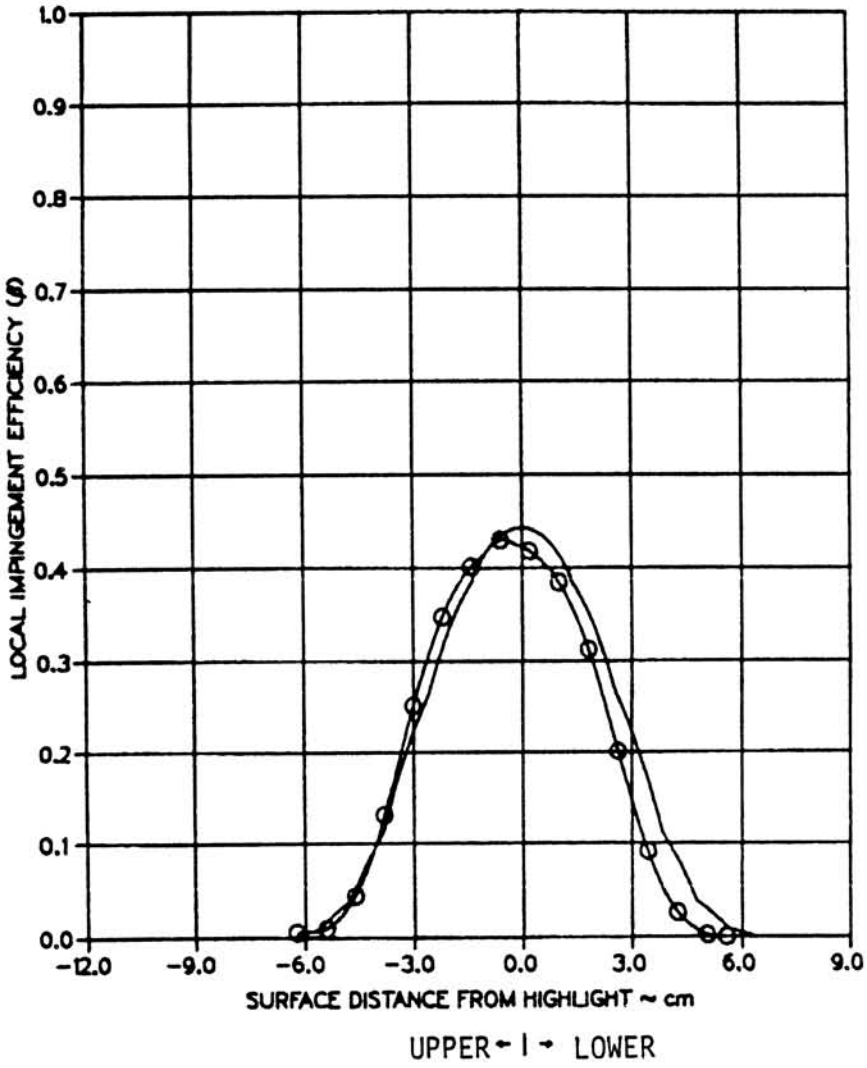

(B) MVD = 16.45 MICRONS

FIGURE 6.6

AVERAGED LOCAL WATER DROPLET IMPINGEMENT EFFICIENCY DATA FOR 4 INCH CYLINDER AND ICE SHAPES (MOUNTED ON 2 INCH CYLINDER) PAGE 2 OF 5.

TEST RUN ID: 092685-12-SG ICE SHAPE

TRUE AIR SPEED	=	80.96 m/s	(181.10 mph)
TUNNEL TOTAL TEMP	=	8.4 C	(47.2 F)
TUNNEL STATIC PRESSURE	=	94.48 kPa	(13.71 psia)
AIR/WATER PRESSURE RATIO	=	0.65	
COLLECTOR EFFICIENCY	=	0.89	

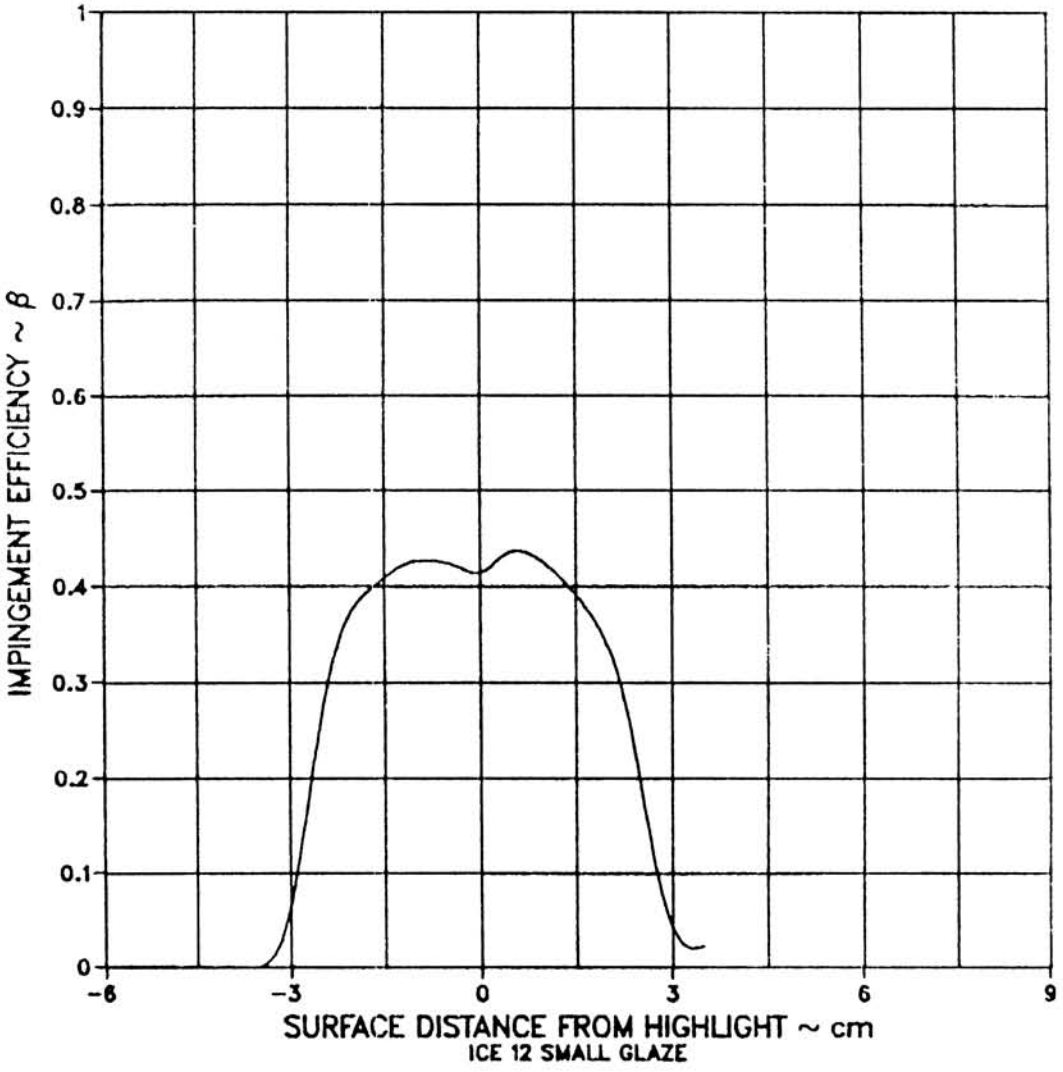

(C) MVD = 20.36 MICRONS

FIGURE 6.6

AVERAGED LOCAL WATER DROPLET IMPINGEMENT EFFICIENCY DATA FOR 4 INCH CYLINDER AND ICE SHAPES (MOUNTED ON 2 INCH CYLINDER) SG = SMALL GLAZE (PAGE 3 OF 5).

TEST RUN ID: 092685-12-RIME ICE SHAPE

TRUE AIR SPEED	=	81.15 m/s	(181.52 mph)
TUNNEL TOTAL TEMP	=	9.6 C	(49.3 F)
TUNNEL STATIC PRESSURE	=	94.48 kPa	(13.72 psia)
AIR/WATER PRESSURE RATIO	=	0.65	
COLLECTOR EFFICIENCY	=	0.89	

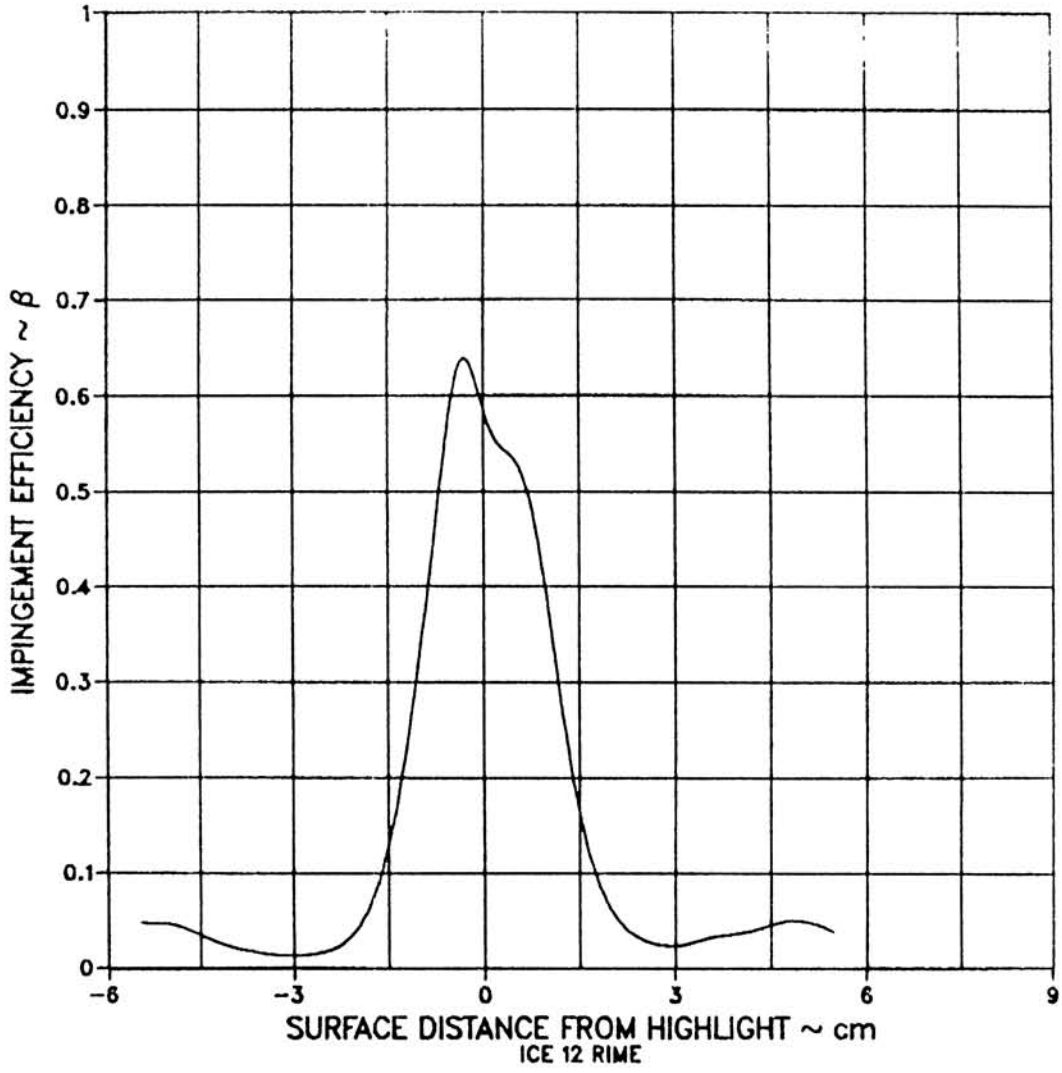

(D) MVD = 20.36 MICRONS

FIGURE 6.6

AVERAGED LOCAL WATER DROPLET IMPINGEMENT EFFICIENCY DATA FOR 4 INCH CYLINDER AND ICE SHAPES (MOUNTED ON 2 INCH CYLINDER) (PAGE 4 OF 5).

TEST RUN ID: 092685-12-LG ICE SHAPE

TRUE AIR SPEED	=	81.10 m/s	(181.41 mph)
TUNNEL TOTAL TEMP	=	10.3 C	(50.5 F)
TUNNEL STATIC PRESSURE	=	94.48 kPa	(13.71 psia)
AIR/WATER PRESSURE RATIO	=	0.65	
COLLECTOR EFFICIENCY	=	0.89	

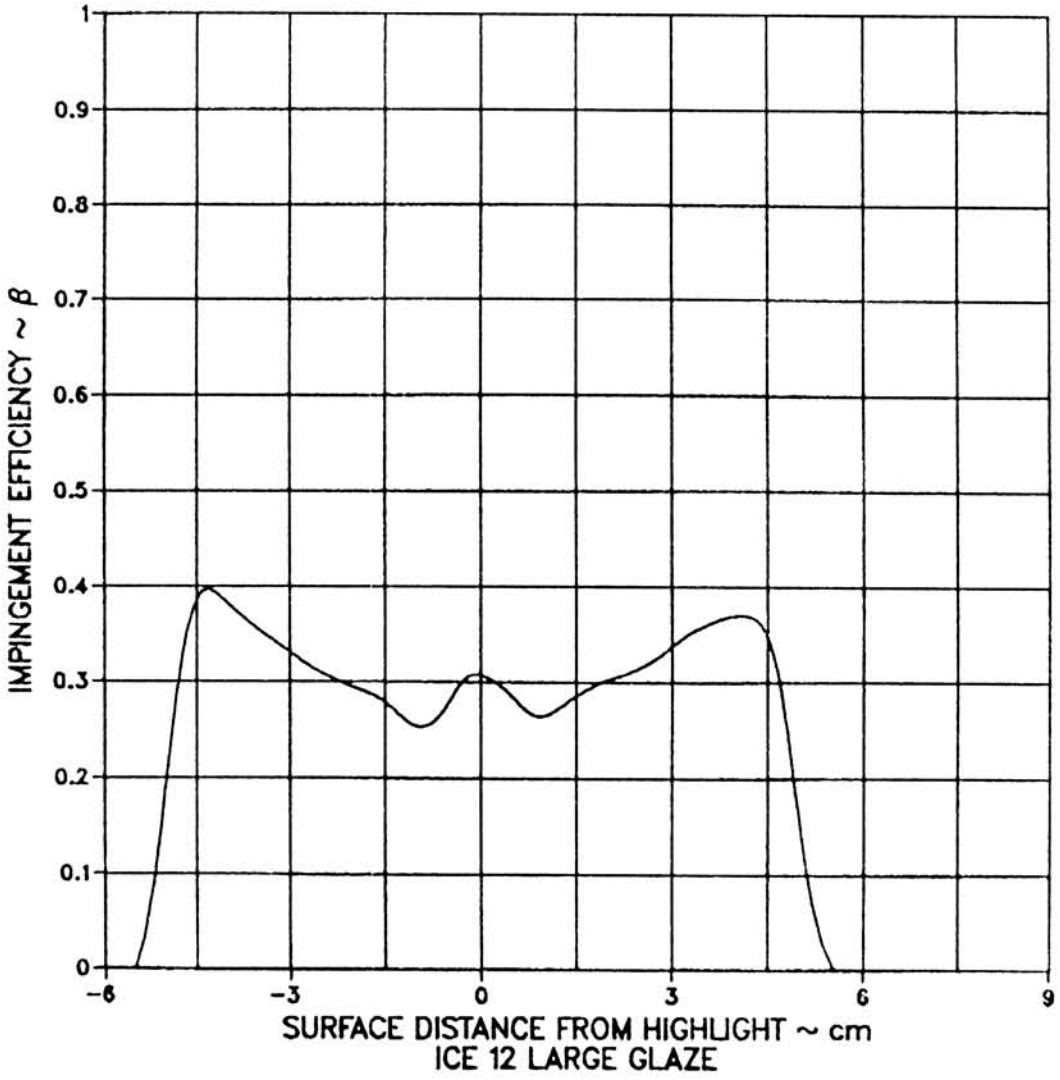

(E) MVD = 20.36 MICRONS

FIGURE 6.6

AVERAGED LOCAL WATER DROPLET IMPINGEMENT EFFICIENCY DATA FOR 4 INCH CYLINDER AND ICE SHAPES (MOUNTED ON 2 INCH CYLINDER) LG = LARGE GLAZE (PAGE 5 OF 5).

TEST RUN ID: 092685-1,2,3BC-015-0 NACA 65_2015

TRUE AIR SPEED	=	80.77 m/s	(180.68 mph)
TUNNEL TOTAL TEMP	=	8.9 C	(48.1 F)
TUNNEL STATIC PRESSURE	=	94.48 kPa	(13.71 psia)
AIR/WATER PRESSURE RATIO	=	0.65	
COLLECTOR EFFICIENCY	=	0.89	

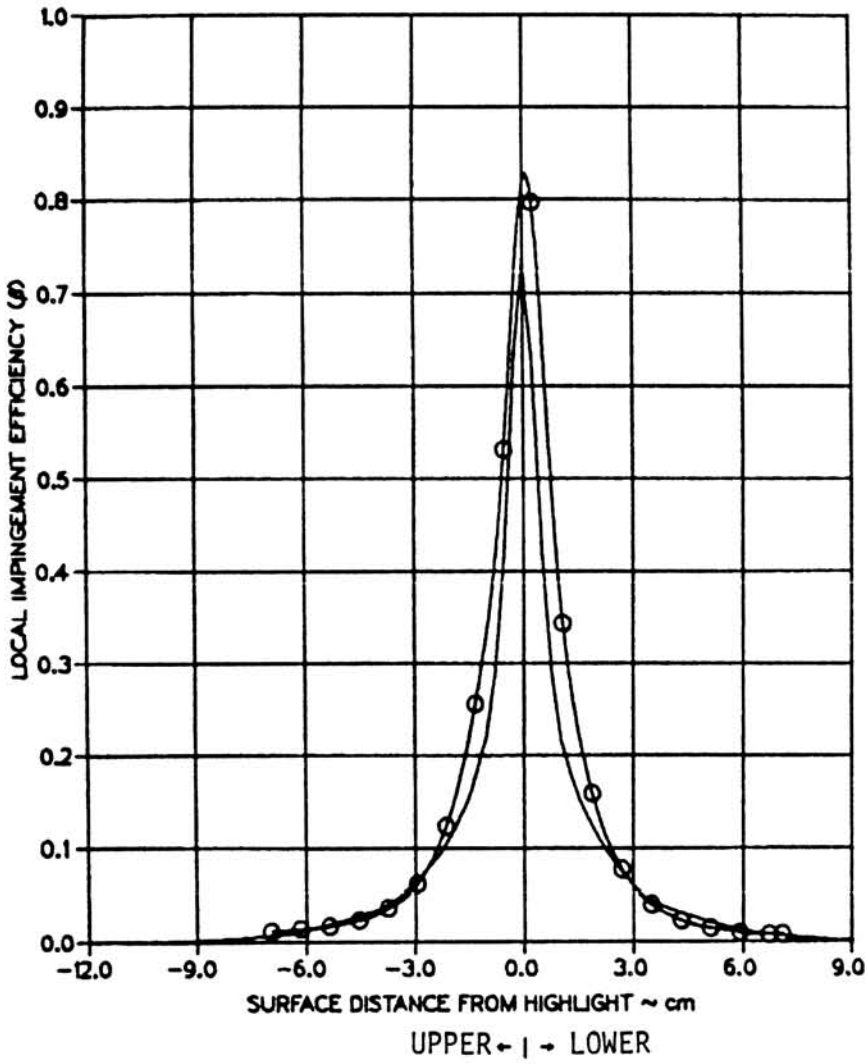

(A) MVD = 20.36 MICRONS

FIGURE 6.7

AVERAGED LOCAL WATER DROPLET IMPINGEMENT EFFICIENCY DATA FOR NACA 65_2015 AND MS(1)-0317 AIRFOILS AT $\alpha = 0°$ (PAGE 1 OF 4).

TEST RUN ID. 092685-4,5,6BC-015-0 NACA 65_2015

TRUE AIR SPEED	=	81.55 m/s	(182.40 mph)
TUNNEL TOTAL TEMP	=	9.4 C	(49.0 F)
TUNNEL STATIC PRESSURE	=	94.48 kPa	(13.71 psia)
AIR/WATER PRESSURE RATIO	=	0.80	
COLLECTOR EFFICIENCY	=	0.86	

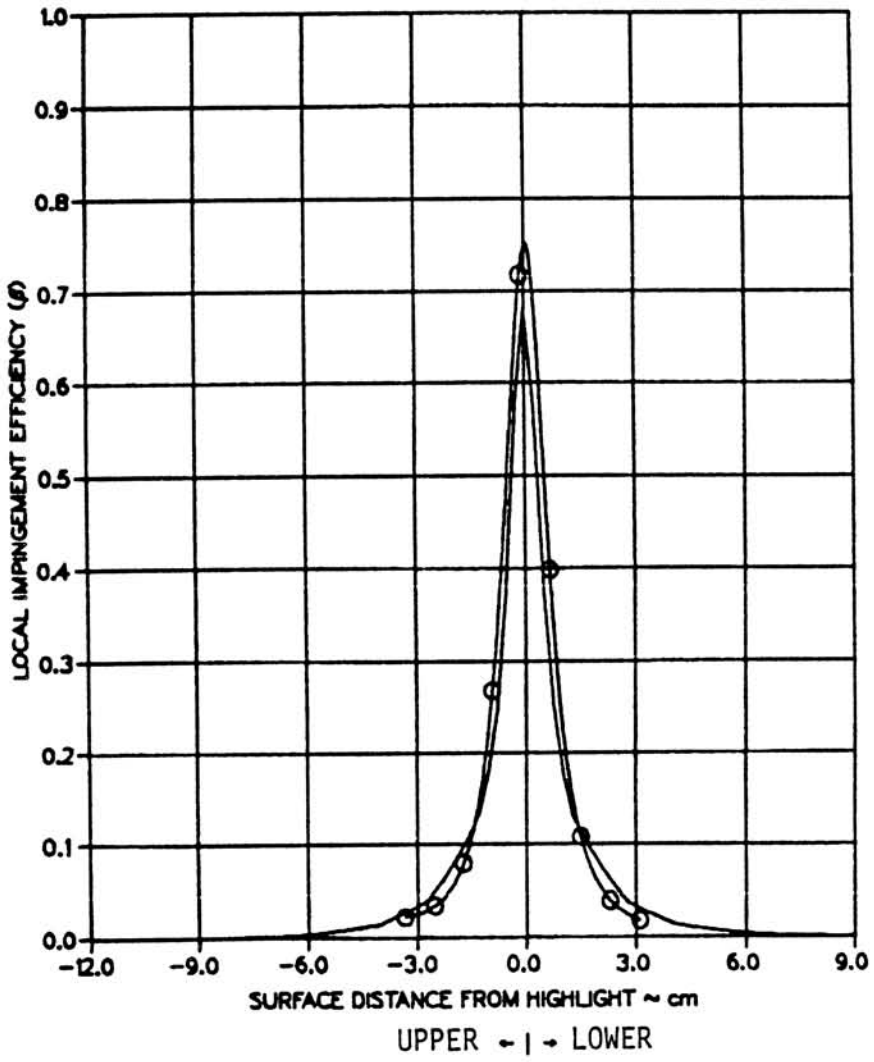

(B) MVD = 16.45 MICRONS

FIGURE 6.7

AVERAGED LOCAL WATER DROPLET IMPINGEMENT EFFICIENCY DATA FOR NACA 65_2015 AND MS(1)-0317 AIRFOILS AT $\alpha = 0°$ (PAGE 2 OF 4).

TEST RUN ID: 092685-1,2,3BC-SUP-0 SUPERCRITICAL AIRFOIL

TRUE AIR SPEED	=	80.81 m/s	(180.76 mph)
TUNNEL TOTAL TEMP	=	8.2 C	(46.8 F)
TUNNEL STATIC PRESSURE	=	94.34 kPa	(13.69 psia)
AIR/WATER PRESSURE RATIO	=	0.65	
COLLECTOR EFFICIENCY	=	0.89	

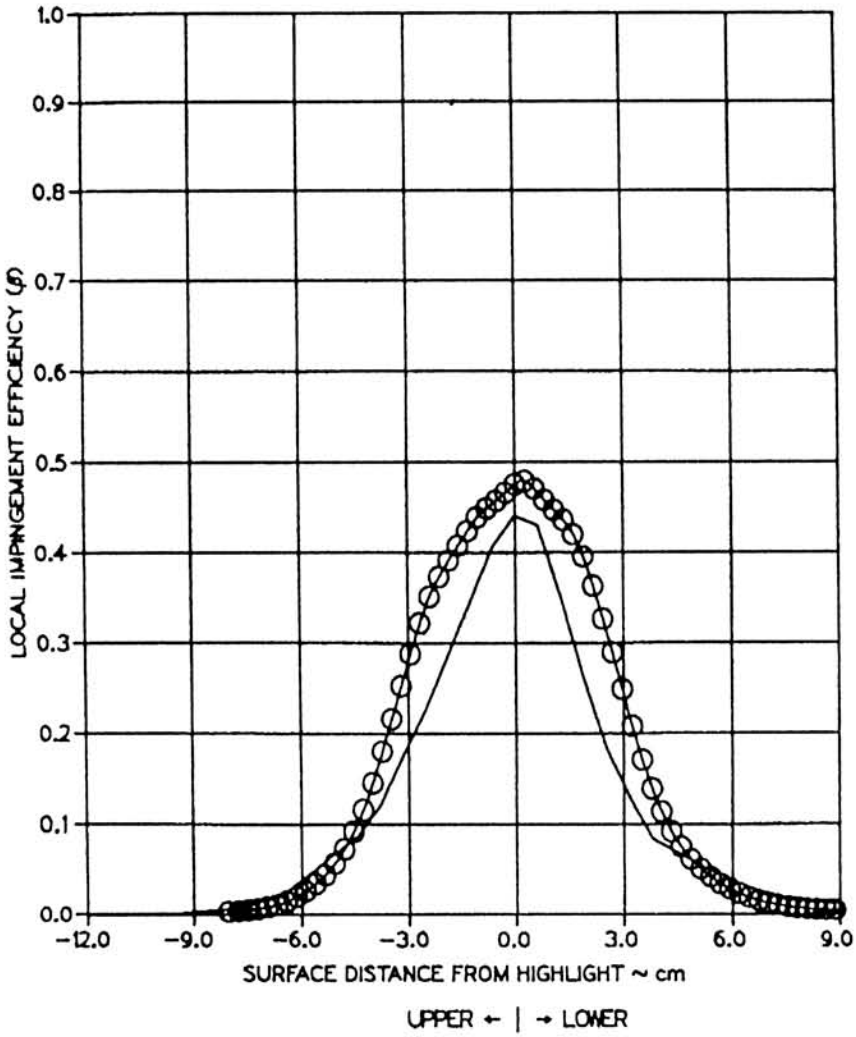

(C) MVD = 20.36 MICRONS

FIGURE 6.7

AVERAGED LOCAL WATER DROPLET IMPINGEMENT EFFICIENCY DATA FOR NACA 65_2015 AND MS(1)-0317 AIRFOILS AT $\alpha = 0°$ (PAGE 3 OF 4).

TEST RUN ID: 092685-4,5,6BC-SUP-0 SUPERCRITICAL AIRFOIL

TRUE AIR SPEED	=	81.13 m/s	(181.47 mph)
TUNNEL TOTAL TEMP	=	9.8 C	(49.6 F)
TUNNEL STATIC PRESSURE	=	94.48 kPa	(13.71 psia)
AIR/WATER PRESSURE RATIO	=	0.80	
COLLECTOR EFFICIENCY	=	0.86	

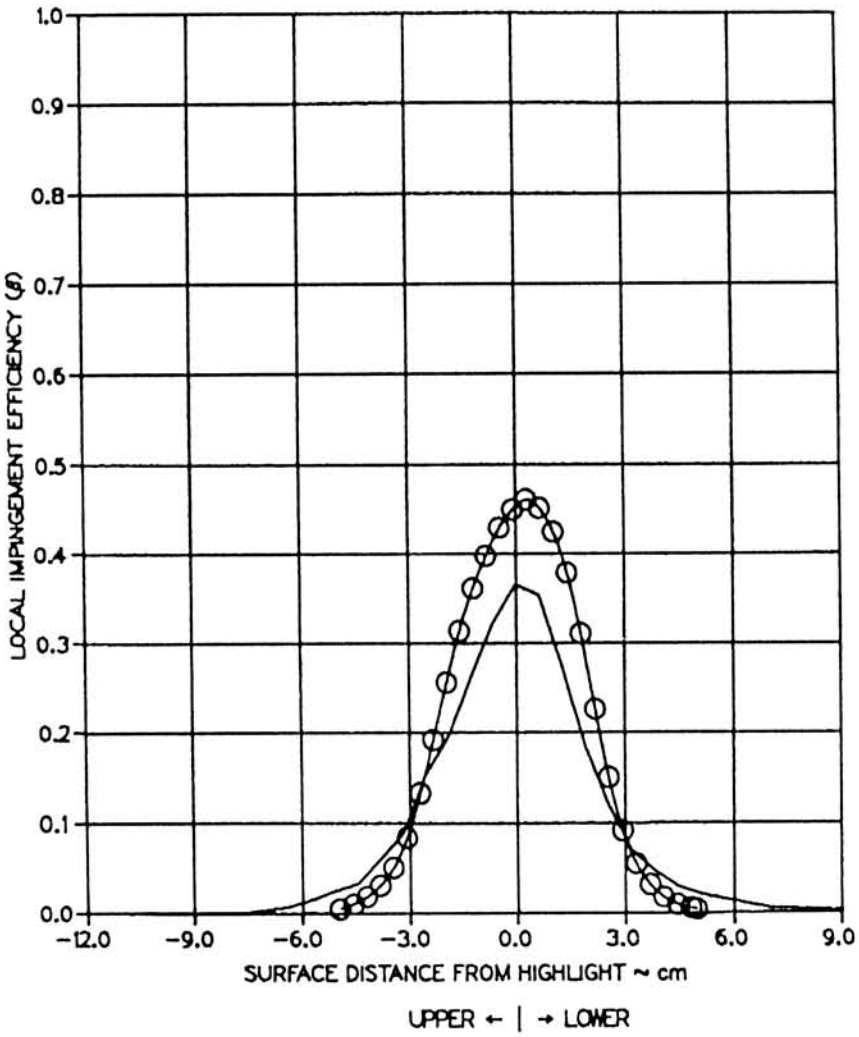

(D) MVD = 16.45 MICRONS

FIGURE 6.7

AVERAGED LOCAL WATER DROPLET IMPINGEMENT EFFICIENCY DATA FOR NACA 65_2015 AND MS(1)-0317 AIRFOILS AT $\alpha = 0°$ (PAGE 4 OF 4).

TEST RUN ID: 092685-7,8,9C-015-8 NACA 65_2015

TRUE AIR SPEED	=	81.07 m/s	(181.34 mph)
TUNNEL TOTAL TEMP	=	9.4 C	(48.9 F)
TUNNEL STATIC PRESSURE	=	94.54 kPa	(13.72 psia)
AIR/WATER PRESSURE RATIO	=	0.65	
COLLECTOR EFFICIENCY	=	0.89	

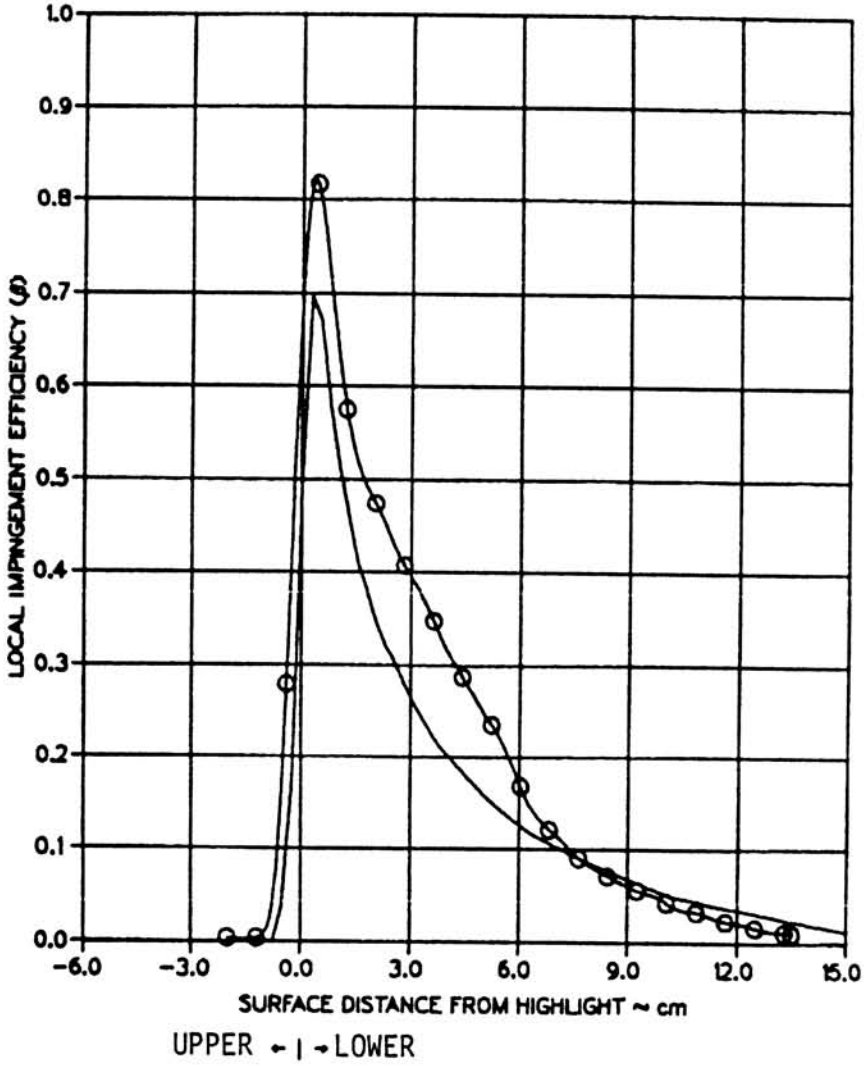

(A) MVD = 20.36 MICRONS

FIGURE 6.8

AVERAGED LOCAL WATER DROPLET IMPINGEMENT EFFICIENCY DATA FOR NACA 65_2015 AND MS(1)-0317 AIRFOILS AT α = 8° (PAGE 1 OF 4).

TEST RUN ID: 092685-10C,11CB,12C-015-8 NACA 65_2015

TRUE AIR SPEED	=	81.26 m/s	(181.76 mph)
TUNNEL TOTAL TEMP	=	9.6 C	(49.2 F)
TUNNEL STATIC PRESSURE	=	94.54 kPa	(13.72 psia)
AIR/WATER PRESSURE RATIO	=	0.80	
COLLECTOR EFFICIENCY	=	0.86	

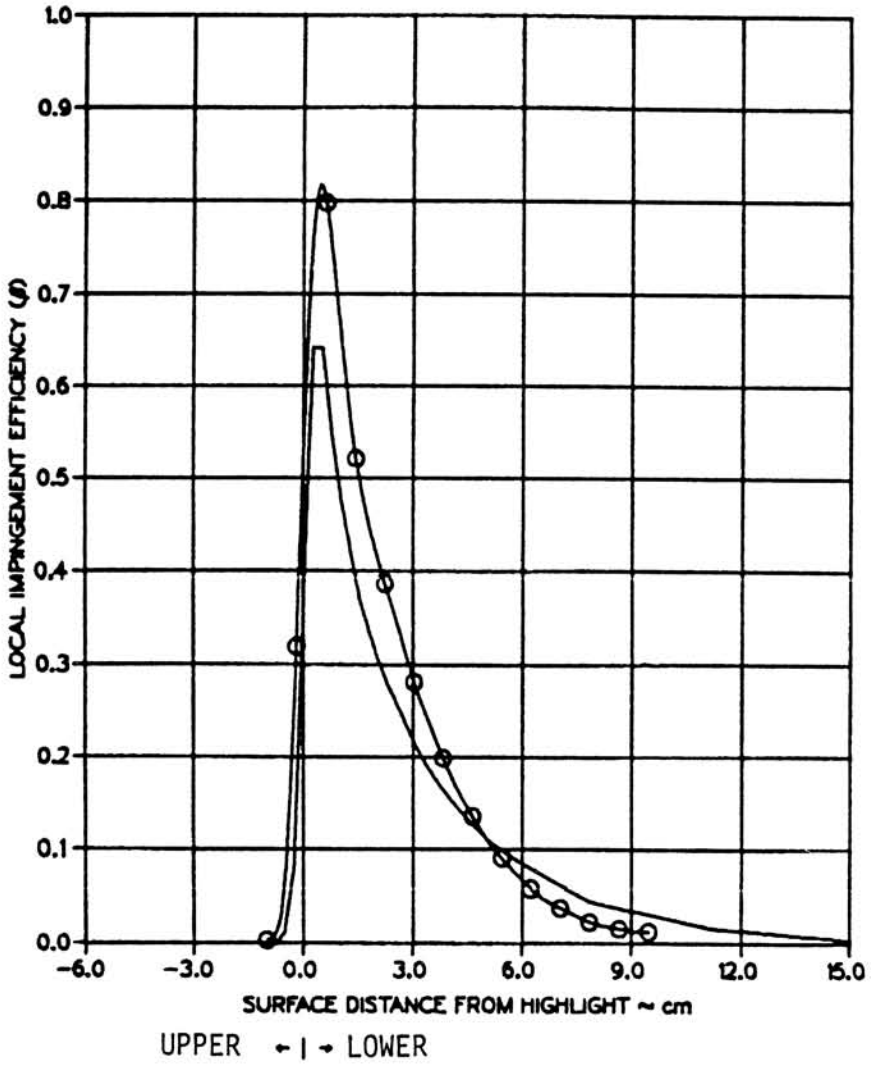

(B) MVD = 16.45 MICRONS

FIGURE 6.8

AVERAGED LOCAL WATER DROPLET IMPINGEMENT EFFICIENCY DATA FOR NACA 65_2015 AND MS(1)-0317 AIRFOILS AT α = 8° (PAGE 2 OF 4).

TEST RUN ID: 092685-7,8,9BC-SUP-8 SUPERCRITICAL AIRFOIL

TRUE AIR SPEED	=	80.55 m/s	(180.18 mph)
TUNNEL TOTAL TEMP	=	9.8 C	(49.7 F)
TUNNEL STATIC PRESSURE	=	94.48 kPa	(13.71 psia)
AIR/WATER PRESSURE RATIO	=	0.65	
COLLECTOR EFFICIENCY	=	0.89	

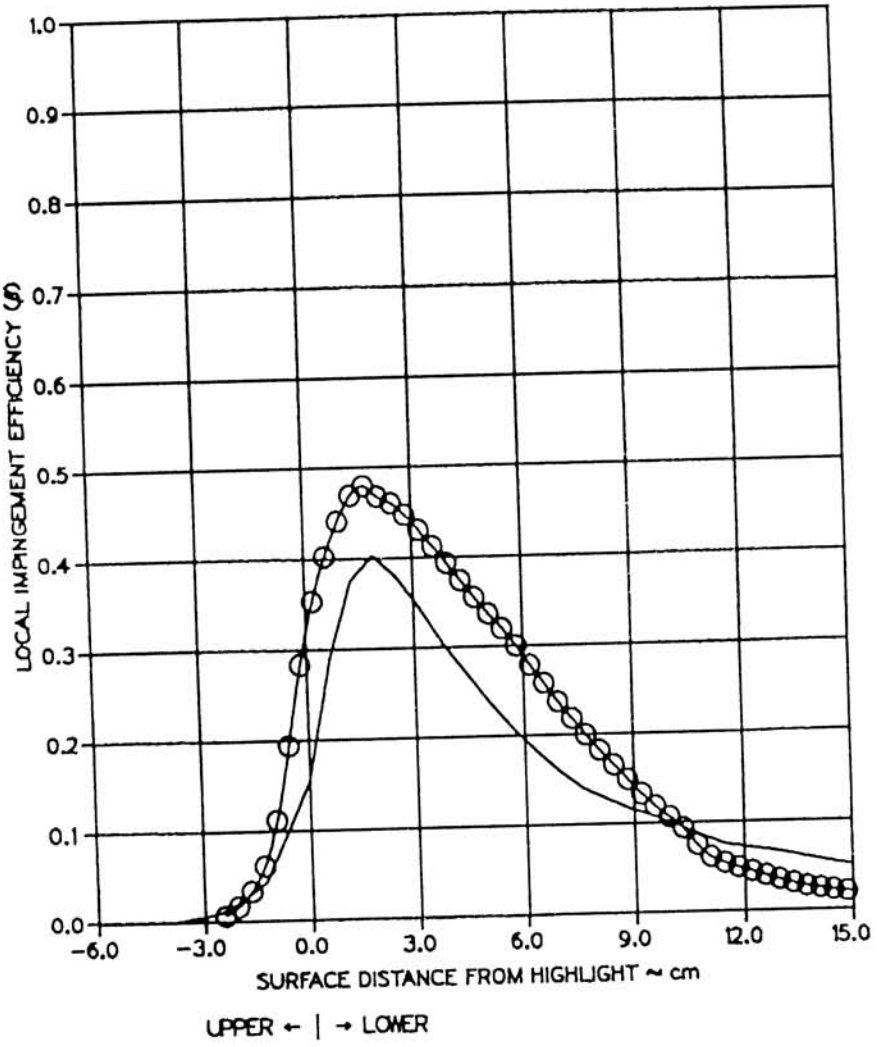

(C) MVD = 20.36 MICRONS

FIGURE 6.8

AVERAGED LOCAL WATER DROPLET IMPINGEMENT EFFICIENCY DATA FOR NACA 65_2015 AND MS(1)-0317 AIRFOILS AT α = 8° (PAGE 3 OF 4).

TEST RUN ID: 092685-10,11,12BC-SUP-8 SUPERCRITICAL AIRFOIL

TRUE AIR SPEED	=	80.90 m/s	(180.95 mph)
TUNNEL TOTAL TEMP	=	9.9 C	(49.8 F)
TUNNEL STATIC PRESSURE	=	94.54 kPa	(13.72 psia)
AIR/WATER PRESSURE RATIO	=	0.80	
COLLECTOR EFFICIENCY	=	0.86	

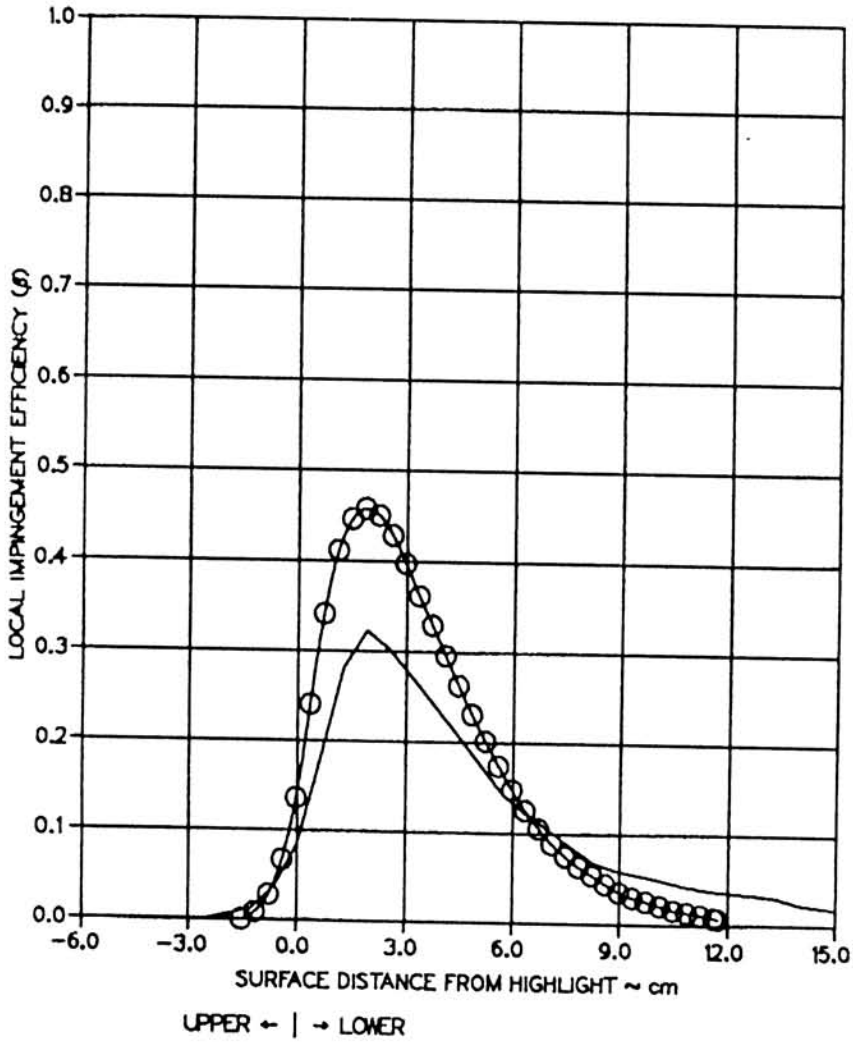

(D) MVD = 16.45 MICRONS

FIGURE 6.8

AVERAGED LOCAL WATER DROPLET IMPINGEMENT EFFICIENCY DATA FOR NACA 65_2015 AND MS(1)-0317 AIRFOILS AT α = 8° (PAGE 4 OF 4).

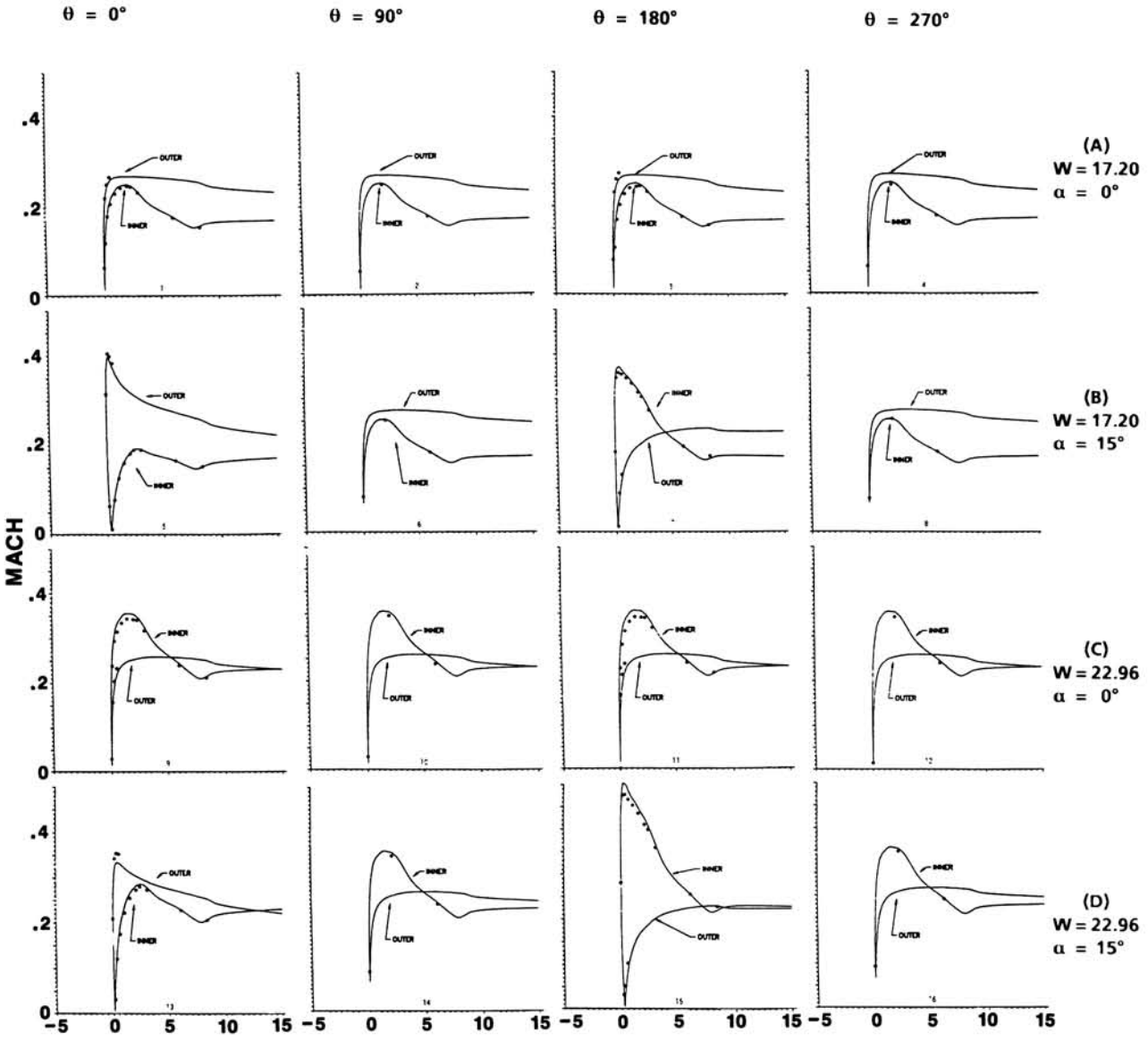

X ~ INCHES

NOTE: W ~ LBM / SEC
COMPRESSOR FACE @ X = 8.401

● TEST DATA
——— THEORY

SUMMARY OF RESULTS

FIGURE 6.9

EXPERIMENTAL AND ANALYTICAL SURFACE MACH NUMBERS FOR AXISYMMETRIC INLET (PAGE 1 OF 17).

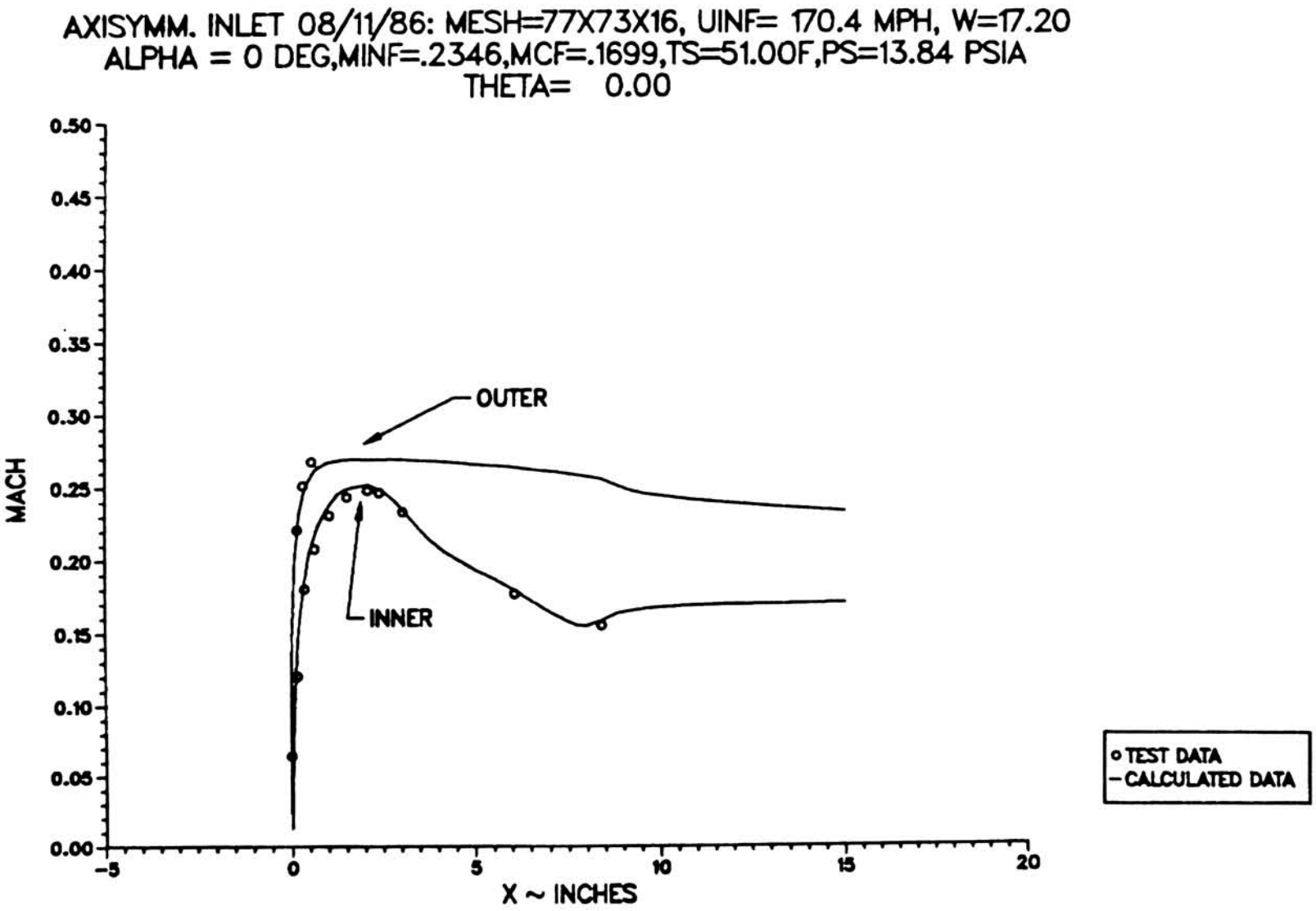

FIGURE 6.9

EXPERIMENTAL AND ANALYTICAL SURFACE MACH NUMBERS FOR AXISYMMETRIC INLET (A1) W = 17.20 LBM/SEC (PAGE 2 OF 17).

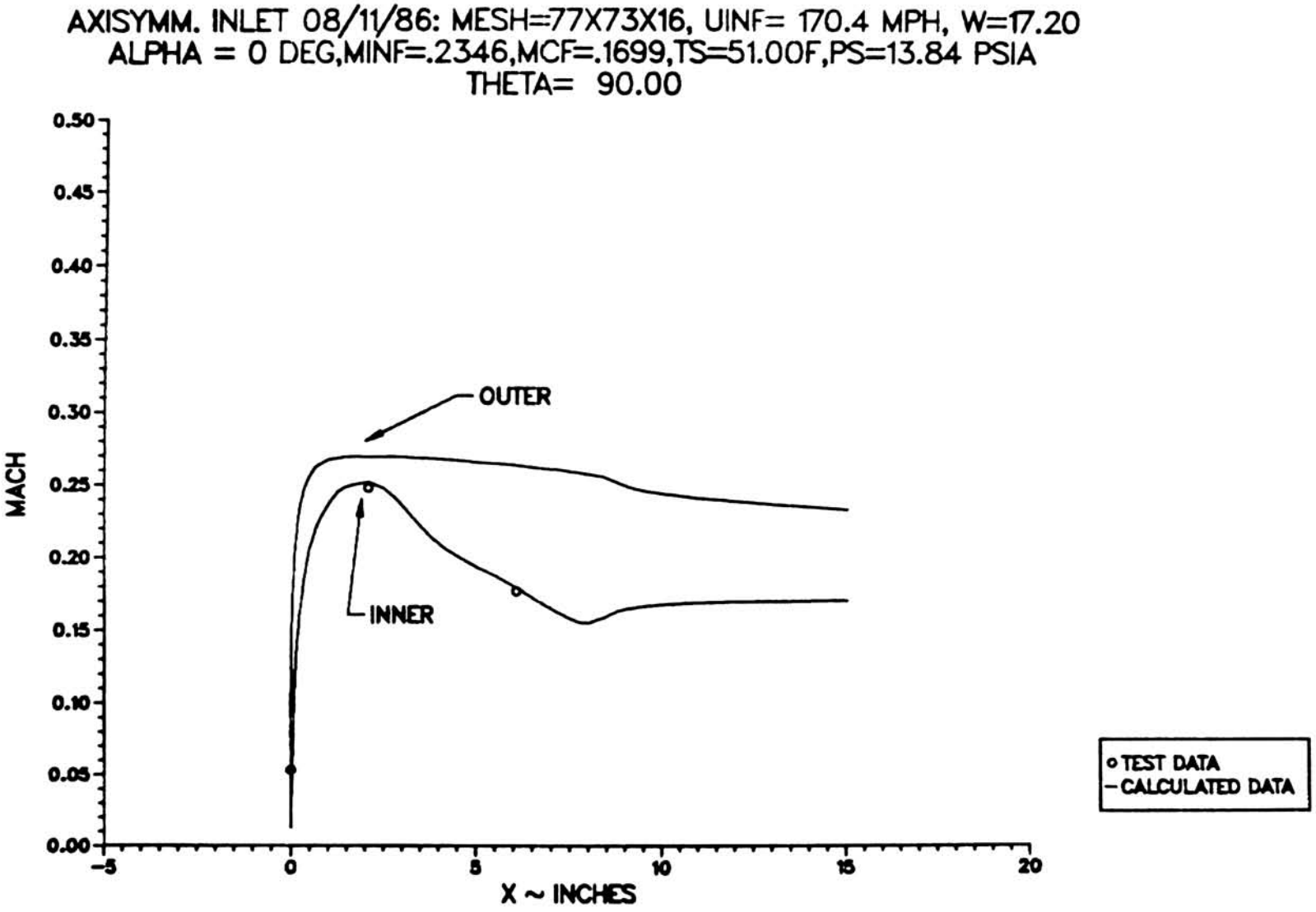

FIGURE 6.9

EXPERIMENTAL AND ANALYTICAL SURFACE MACH NUMBERS FOR AXISYMMETRIC INLET (A2) W = 17.20 LBM / SEC (PAGE 3 OF 17).

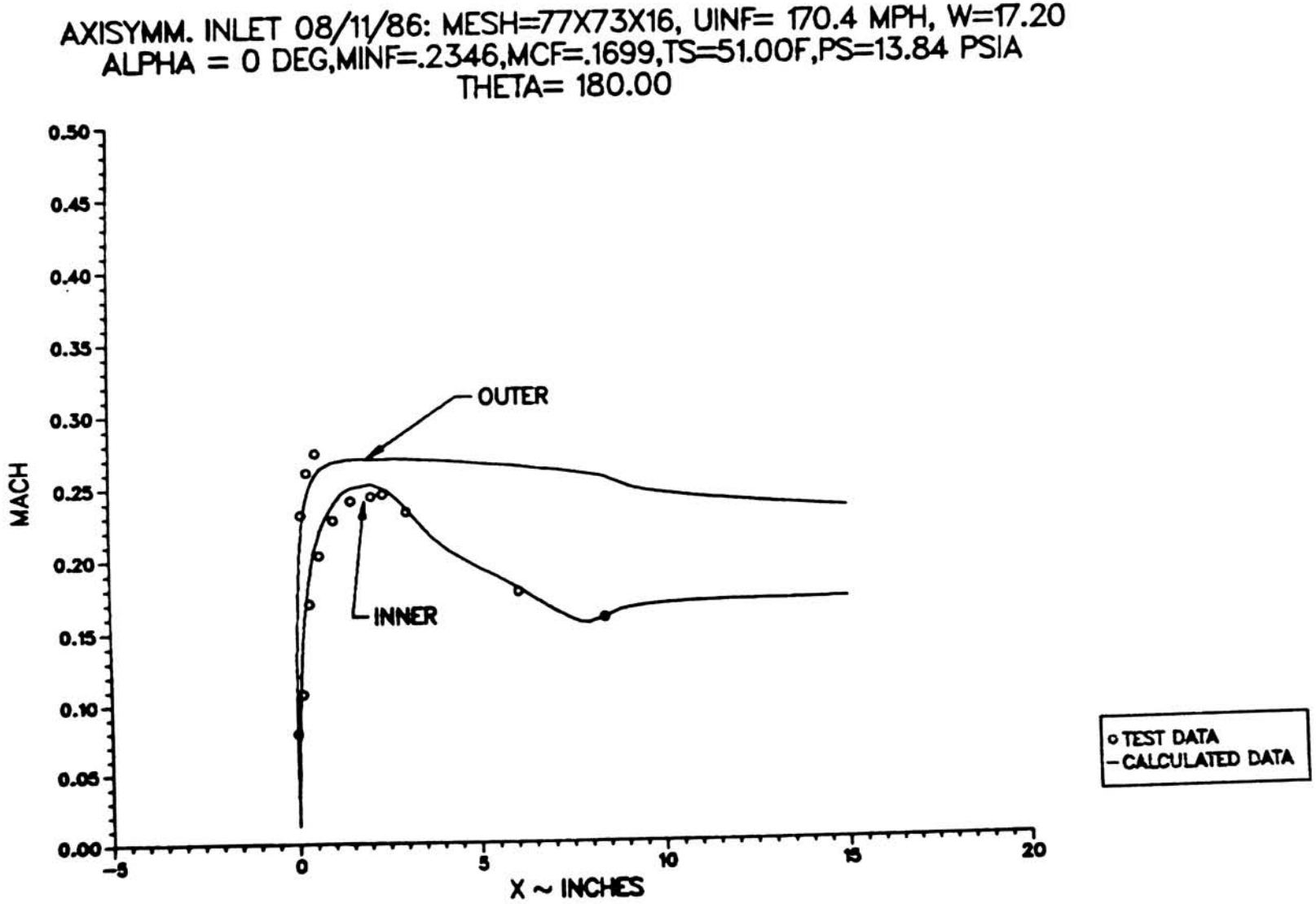

FIGURE 6.9

EXPERIMENTAL AND ANALYTICAL SURFACE MACH NUMBERS FOR AXISYMMETRIC INLET (A3) W = 17.20 LBM / SEC (PAGE 4 OF 17).

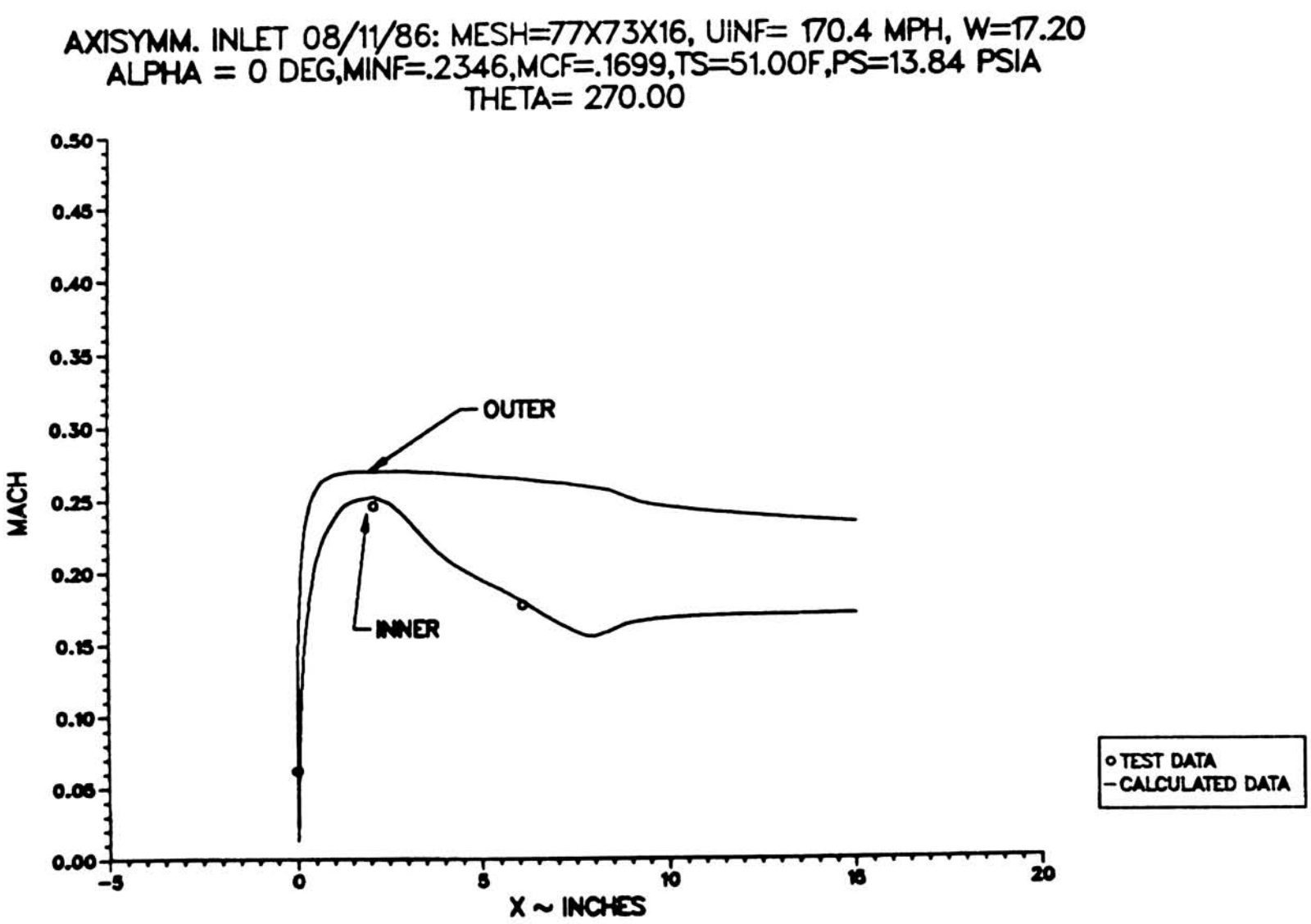

FIGURE 6.9

EXPERIMENTAL AND ANALYTICAL SURFACE MACH NUMBERS FOR AXISYMMETRIC INLET (A4) W = 17.20 LBM/SEC (PAGE 5 OF 17).

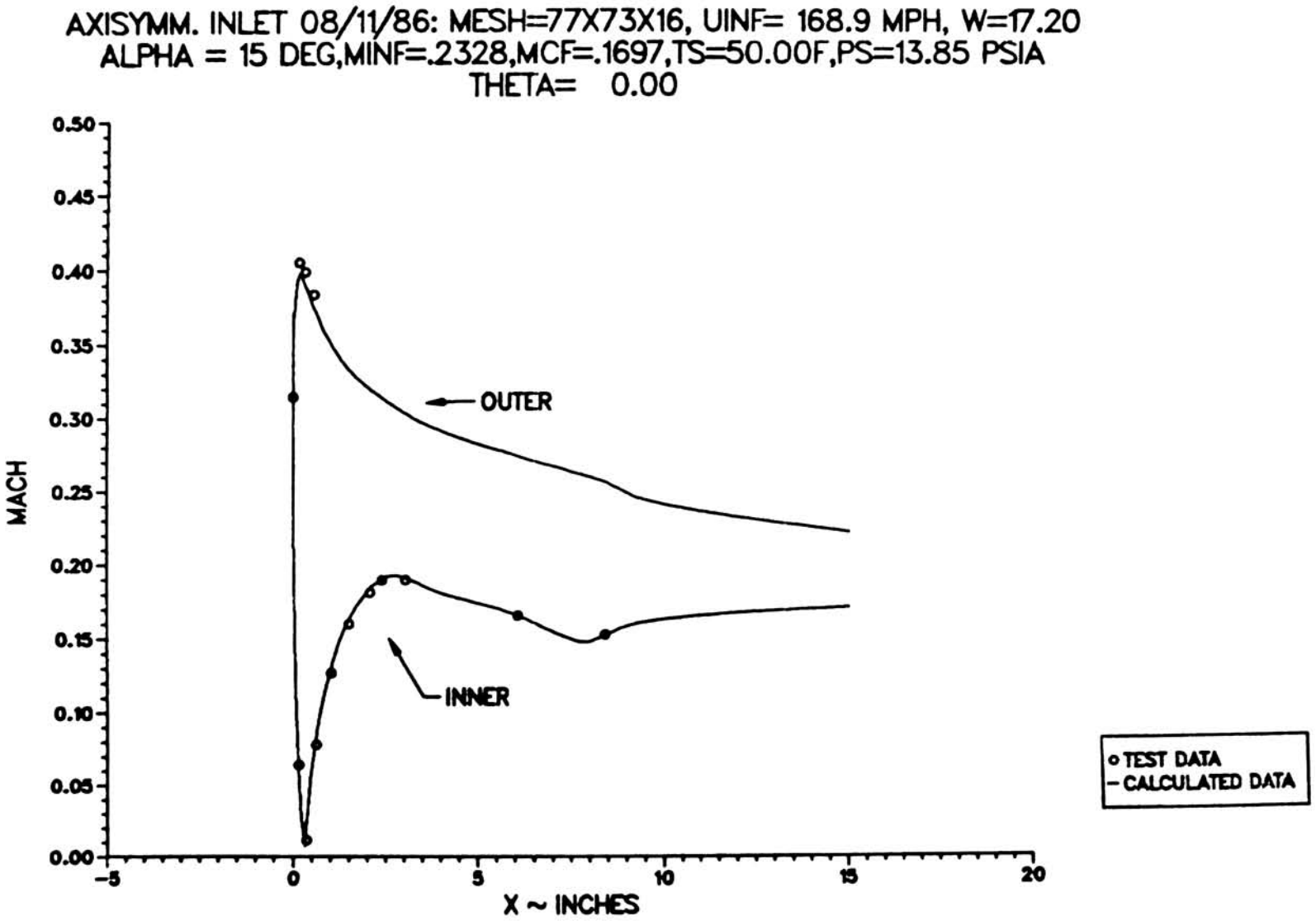

FIGURE 6.9

EXPERIMENTAL AND ANALYTICAL SURFACE MACH NUMBERS FOR AXISYMMETRIC INLET (B1) W = 17.20 LBM/SEC (PAGE 6 OF 17).

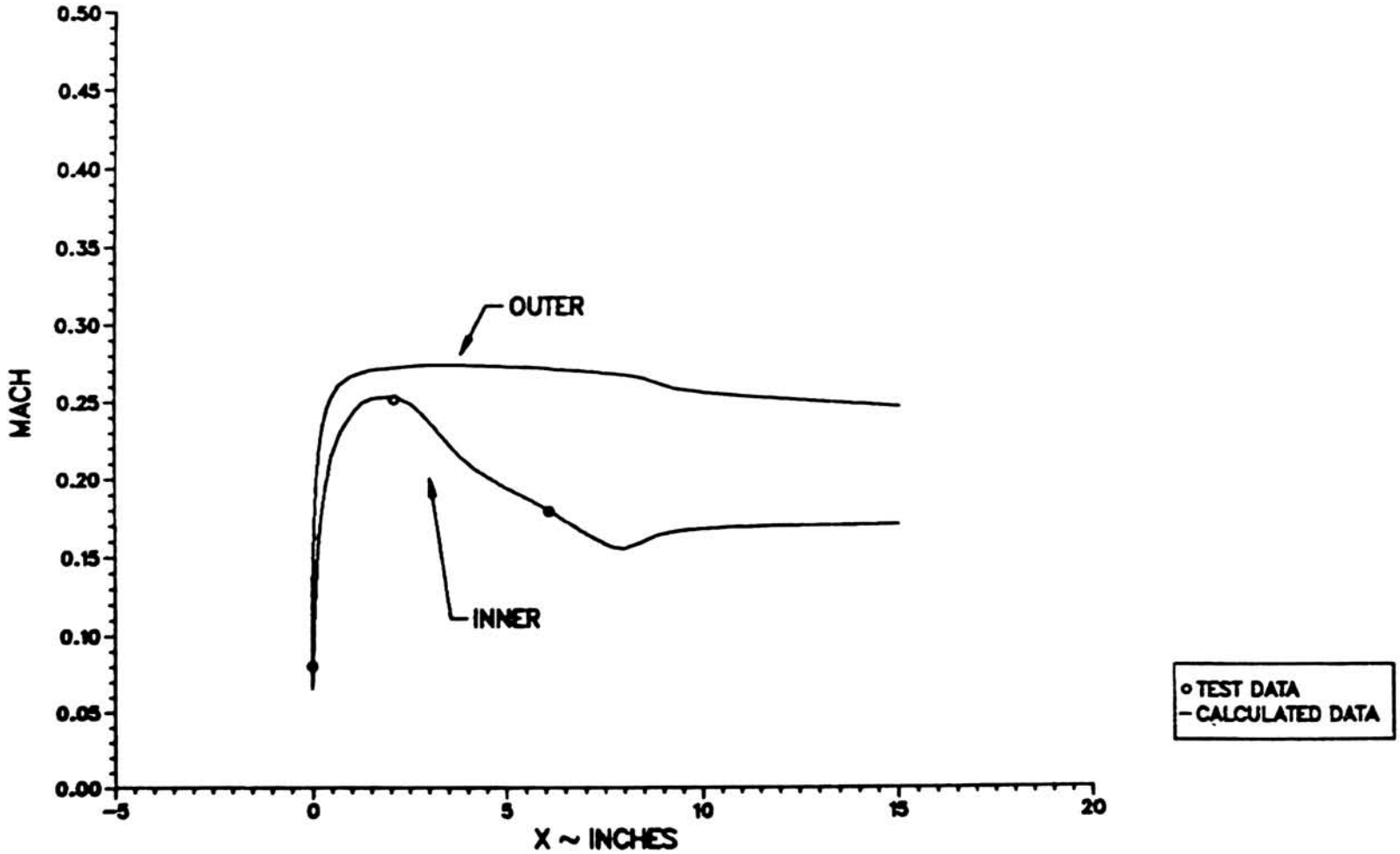

FIGURE 6.9

EXPERIMENTAL AND ANALYTICAL SURFACE MACH NUMBERS FOR AXISYMMETRIC INLET (B2) W = 17.20 LBM/SEC (PAGE 7 OF 17).

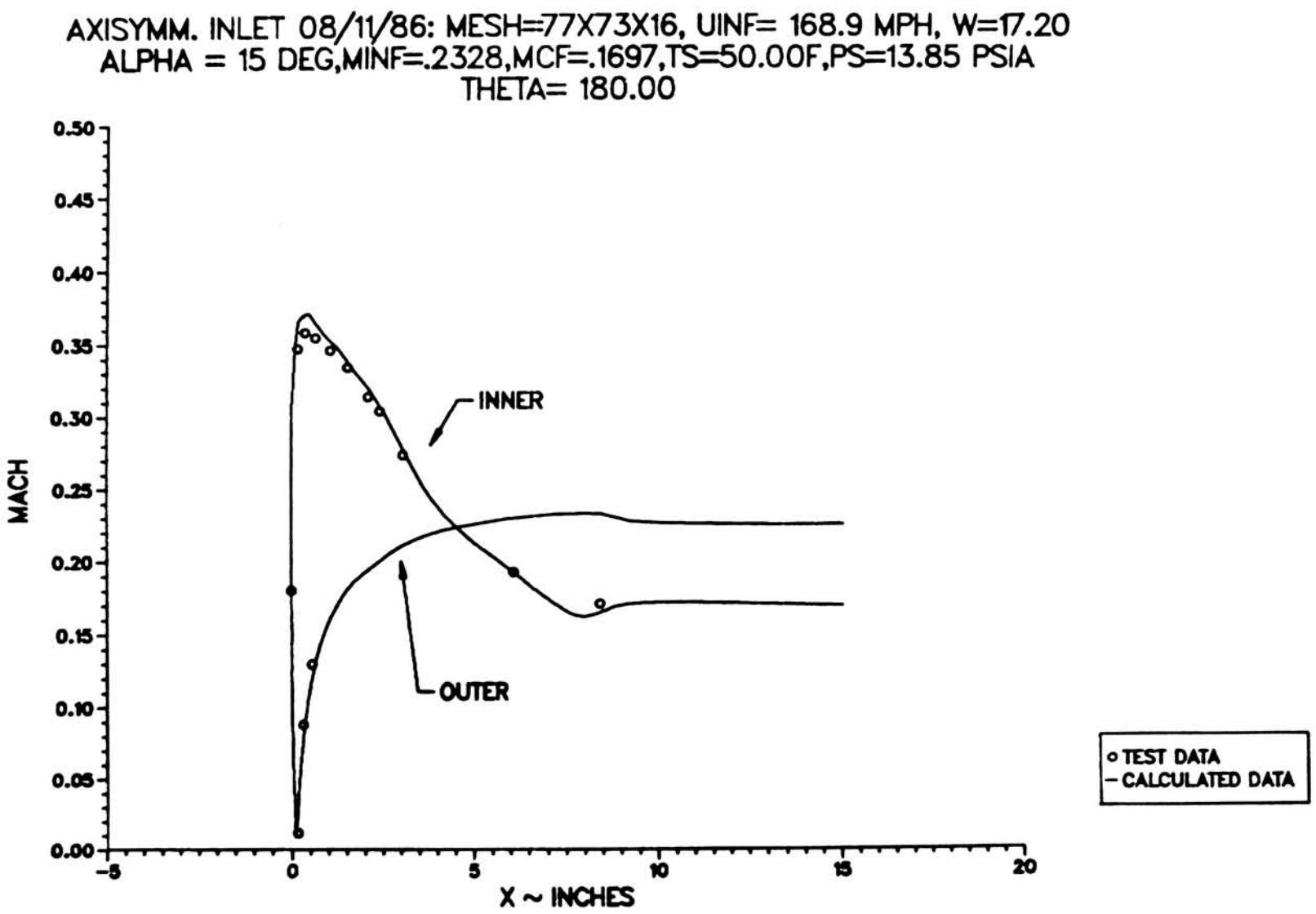

FIGURE 6.9

EXPERIMENTAL AND ANALYTICAL SURFACE MACH NUMBERS FOR AXISYMMETRIC INLET (B3) W = 17.20 LBM/SEC (PAGE 8 OF 17).

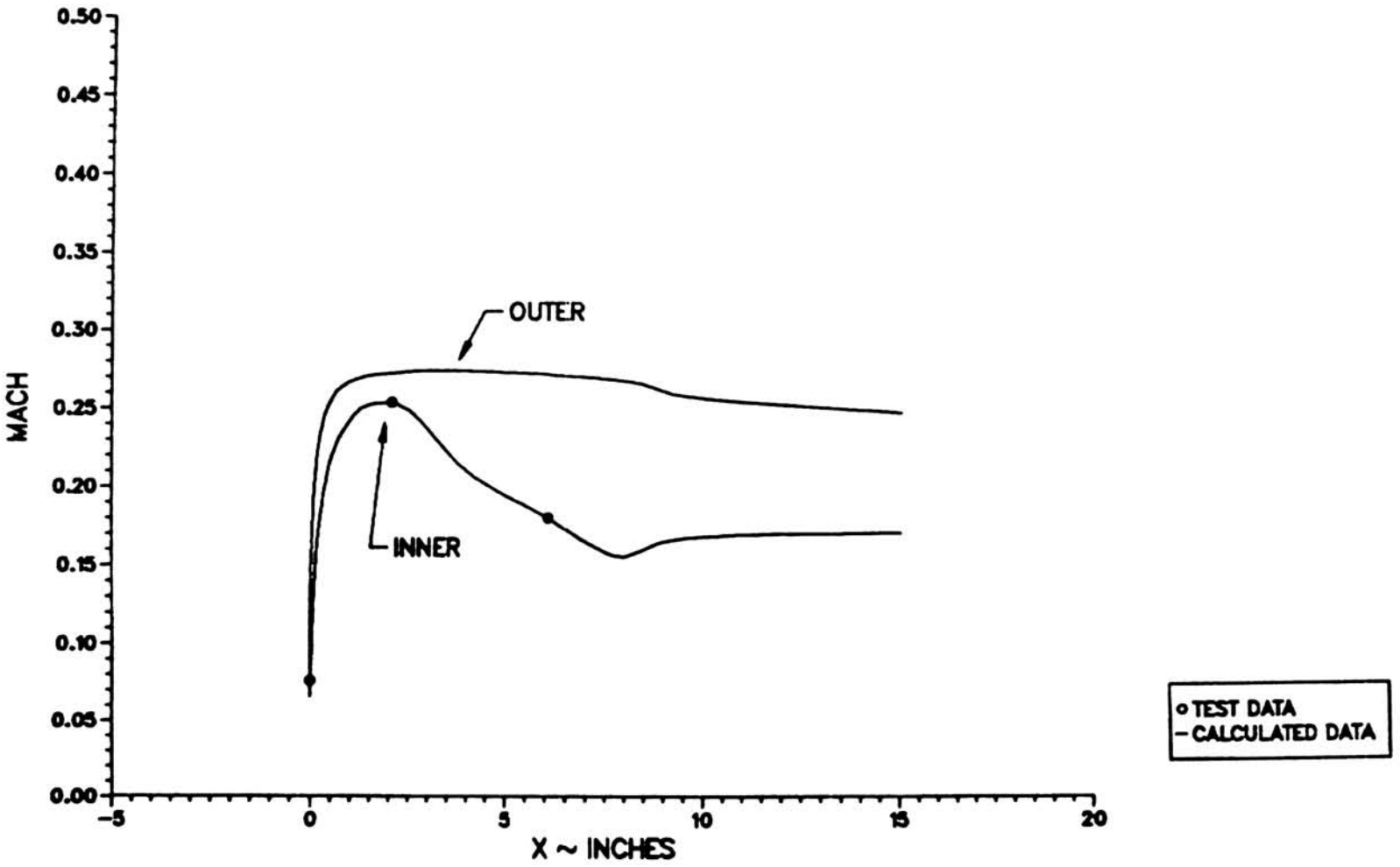

FIGURE 6.9

EXPERIMENTAL AND ANALYTICAL SURFACE MACH NUMBERS FOR AXISYMMETRIC INLET (B4) W = 17.20 LBM/SEC (PAGE 9 OF 17).

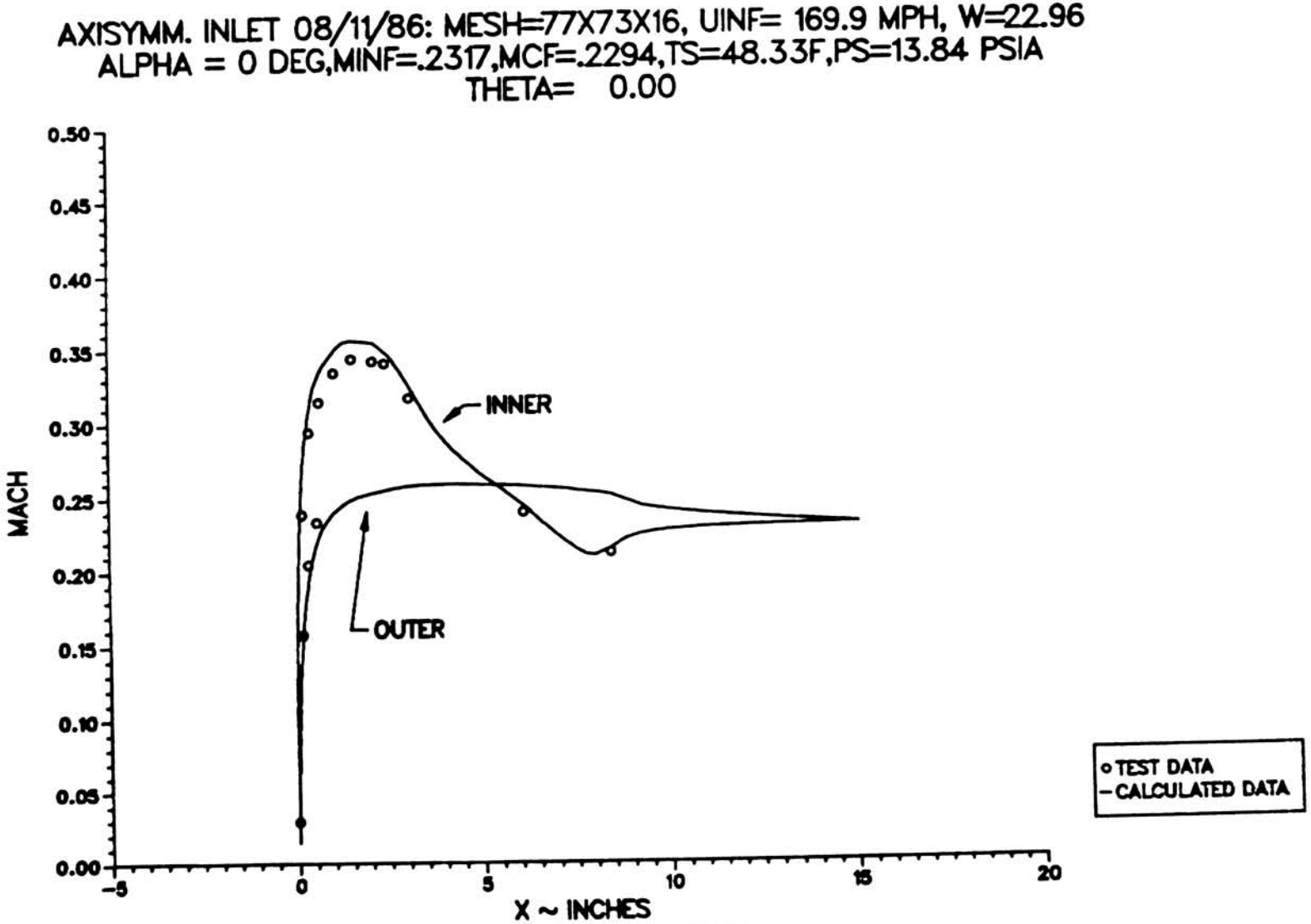

FIGURE 6.9

EXPERIMENTAL AND ANALYTICAL SURFACE MACH NUMBERS FOR AXISYMMETRIC INLET (C1) W = 22.96 LBM/SEC (PAGE 10 OF 17).

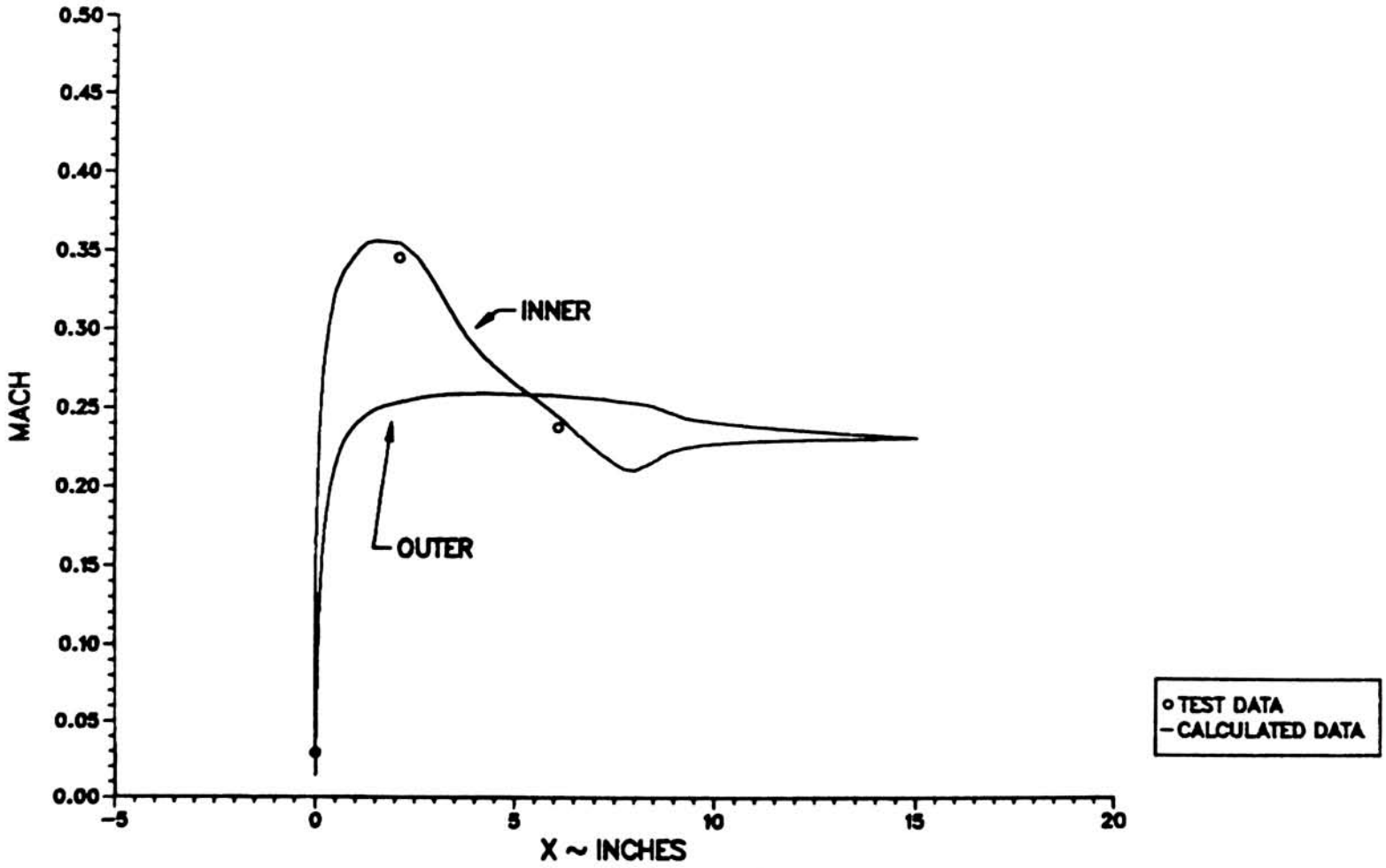

FIGURE 6.9

EXPERIMENTAL AND ANALYTICAL SURFACE MACH NUMBERS FOR AXISYMMETRIC INLET (C2) W = 22.96 LBM/SEC (PAGE 11 OF 17).

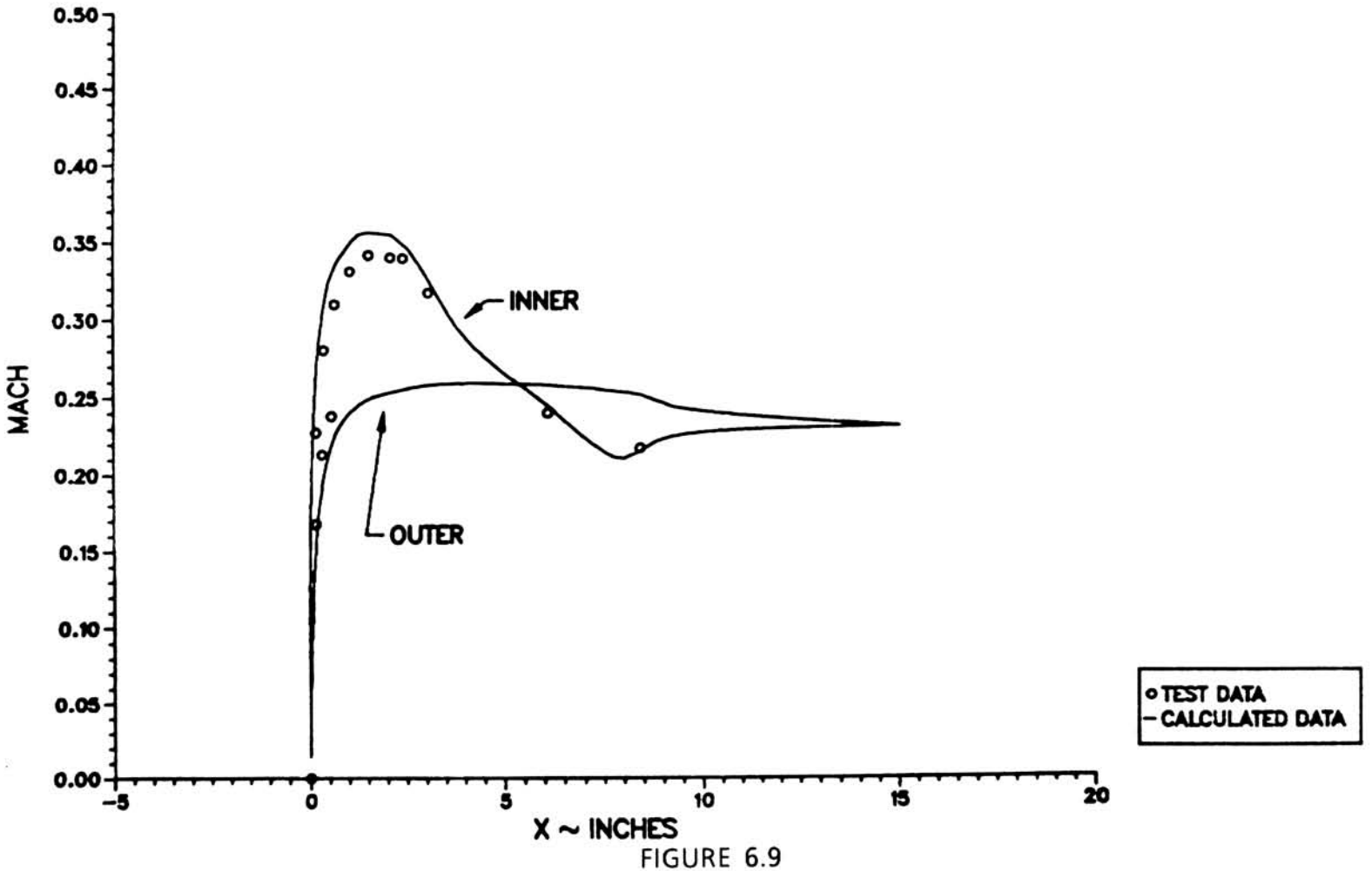

FIGURE 6.9

EXPERIMENTAL AND ANALYTICAL SURFACE MACH NUMBERS FOR AXISYMMETRIC INLET (C3) W = 22.96 LBM/SEC (PAGE 12 OF 17).

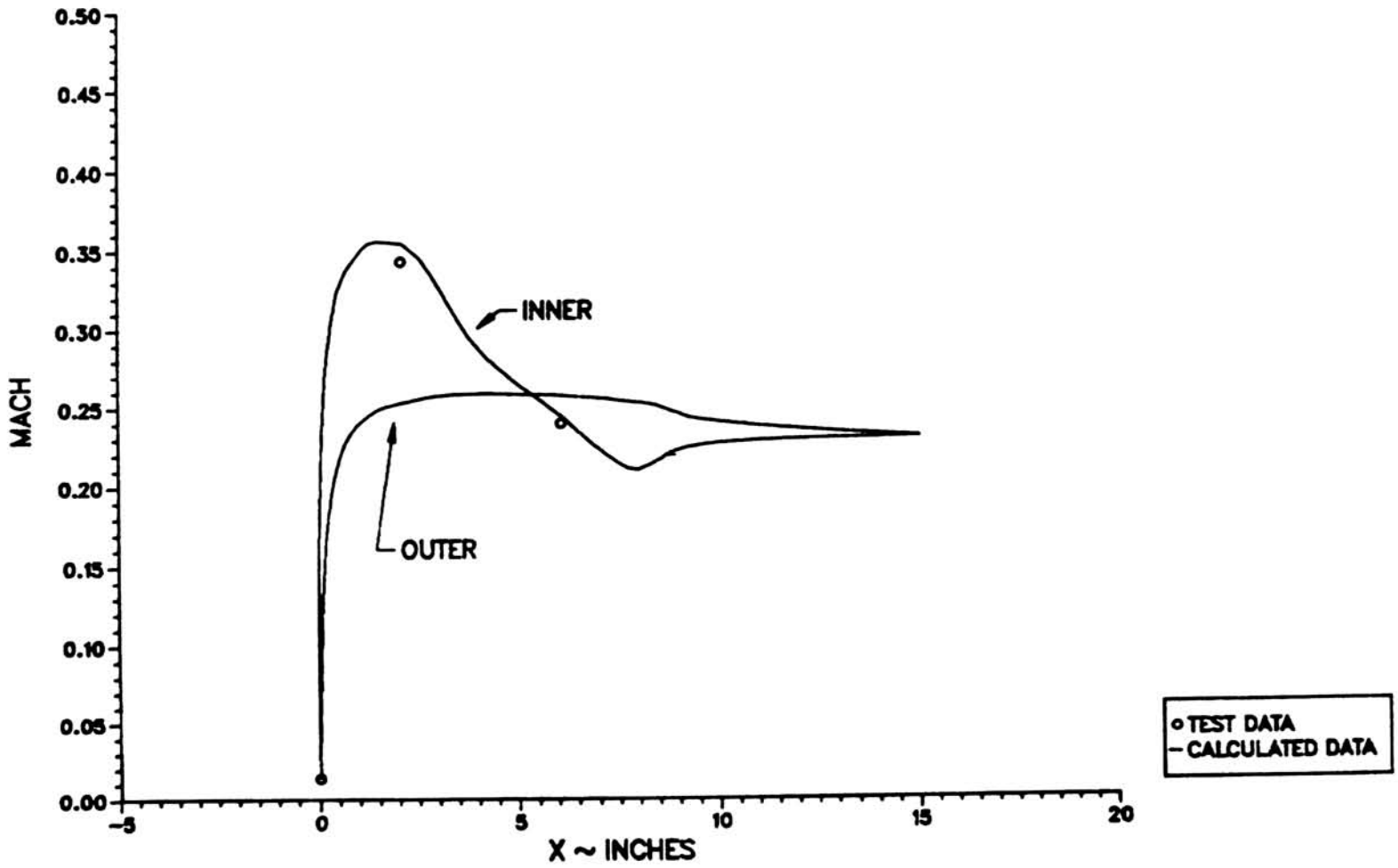

FIGURE 6.9

EXPERIMENTAL AND ANALYTICAL SURFACE MACH NUMBERS FOR AXISYMMETRIC INLET (C4) W = 22.96 LBM / SEC (PAGE 13 OF 17).

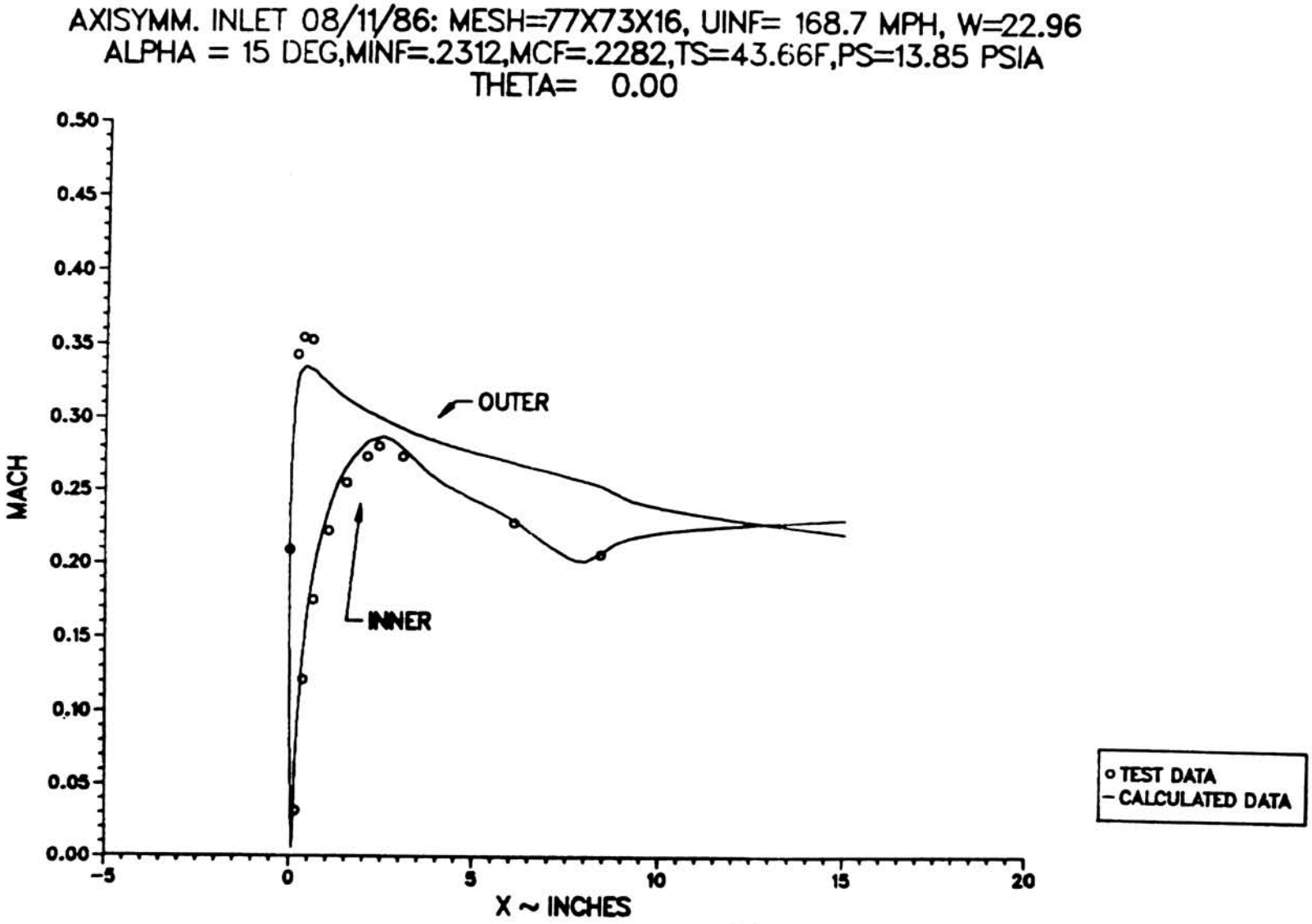

FIGURE 6.9

EXPERIMENTAL AND ANALYTICAL SURFACE MACH NUMBERS FOR AXISYMMETRIC INLET (D1) W = 22.96 LBM/SEC (PAGE 14 OF 17).

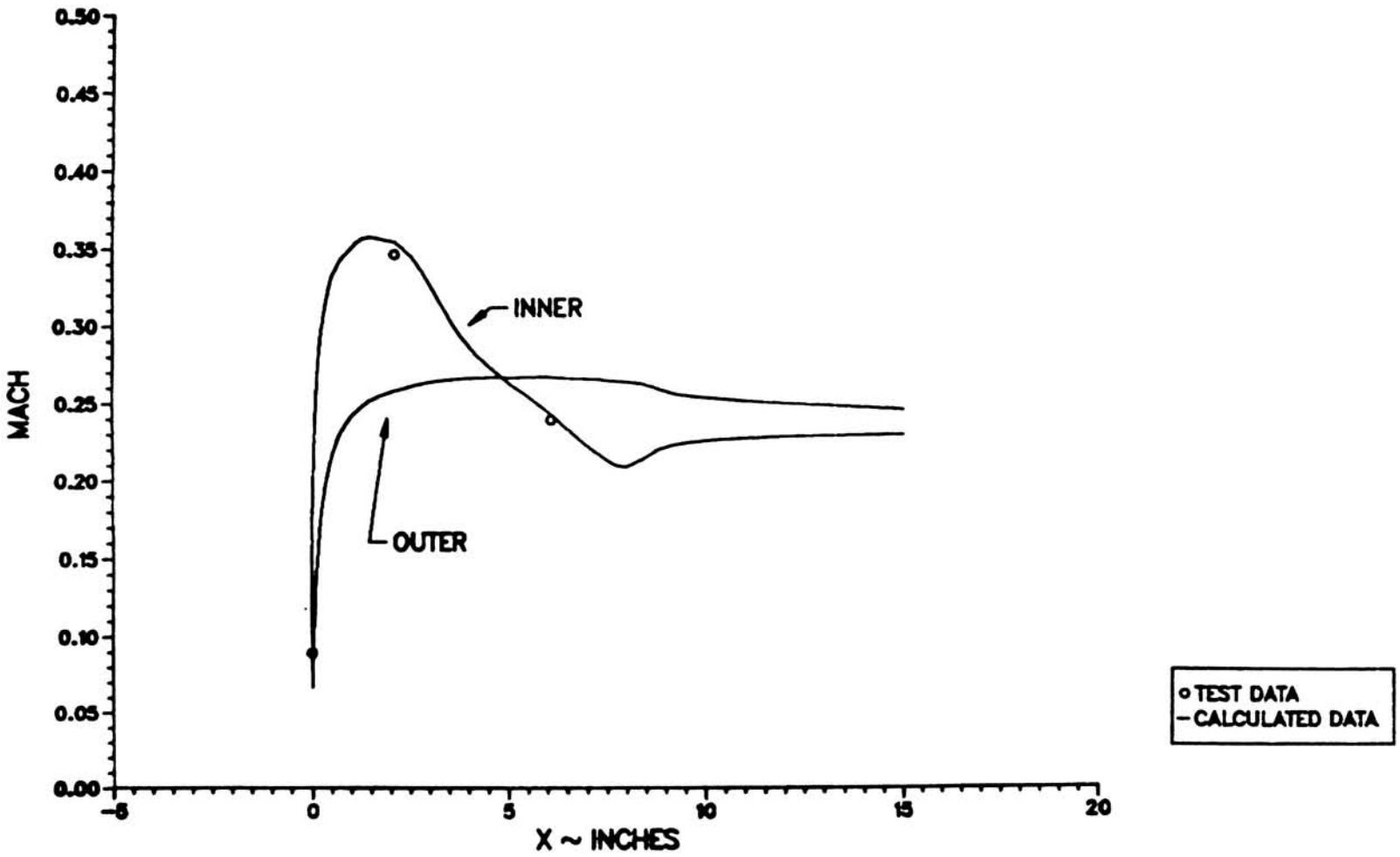

FIGURE 6.9

EXPERIMENTAL AND ANALYTICAL SURFACE MACH NUMBERS FOR AXISYMMETRIC INLET (D2) W = 22.96 LBM/SEC (PAGE 15 OF 17).

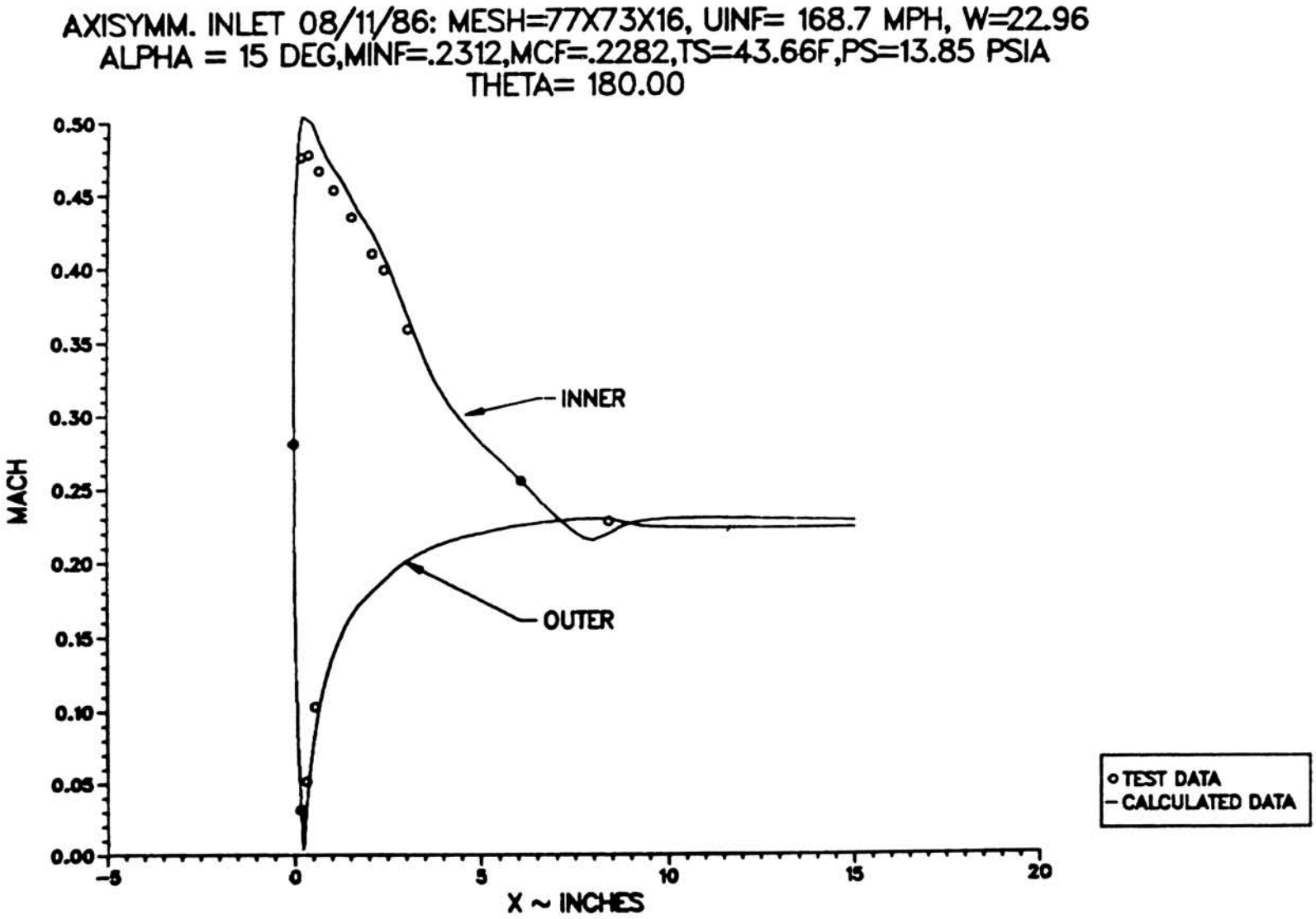

FIGURE 6.9

EXPERIMENTAL AND ANALYTICAL SURFACE MACH NUMBERS FOR AXISYMMETRIC INLET (D3) W = 22.96 LBM/SEC (PAGE 16 OF 17).

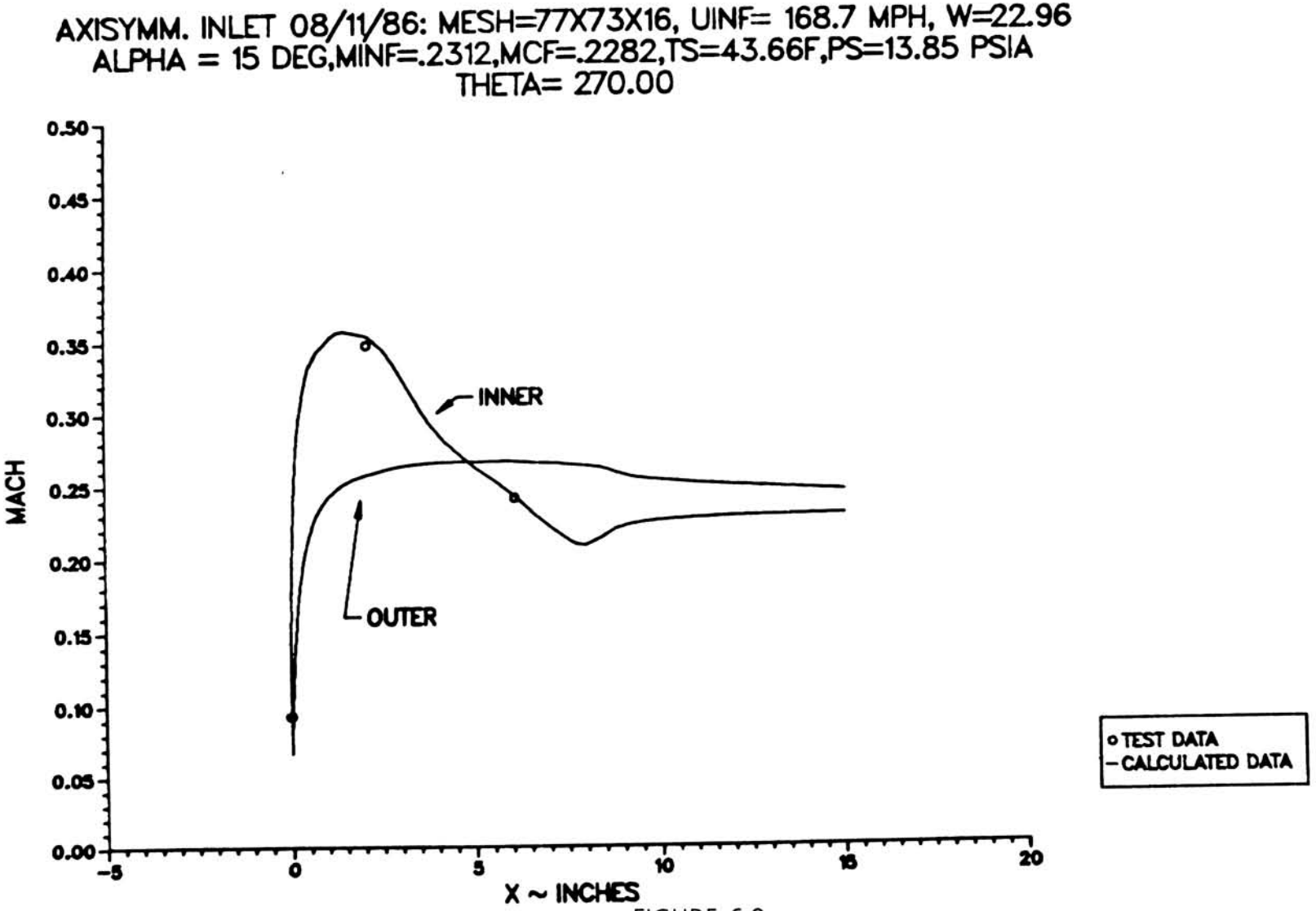

FIGURE 6.9

EXPERIMENTAL AND ANALYTICAL SURFACE MACH NUMBERS FOR AXISYMMETRIC INLET (D4) W = 22.96 LBM/SEC (PAGE 17 OF 17).

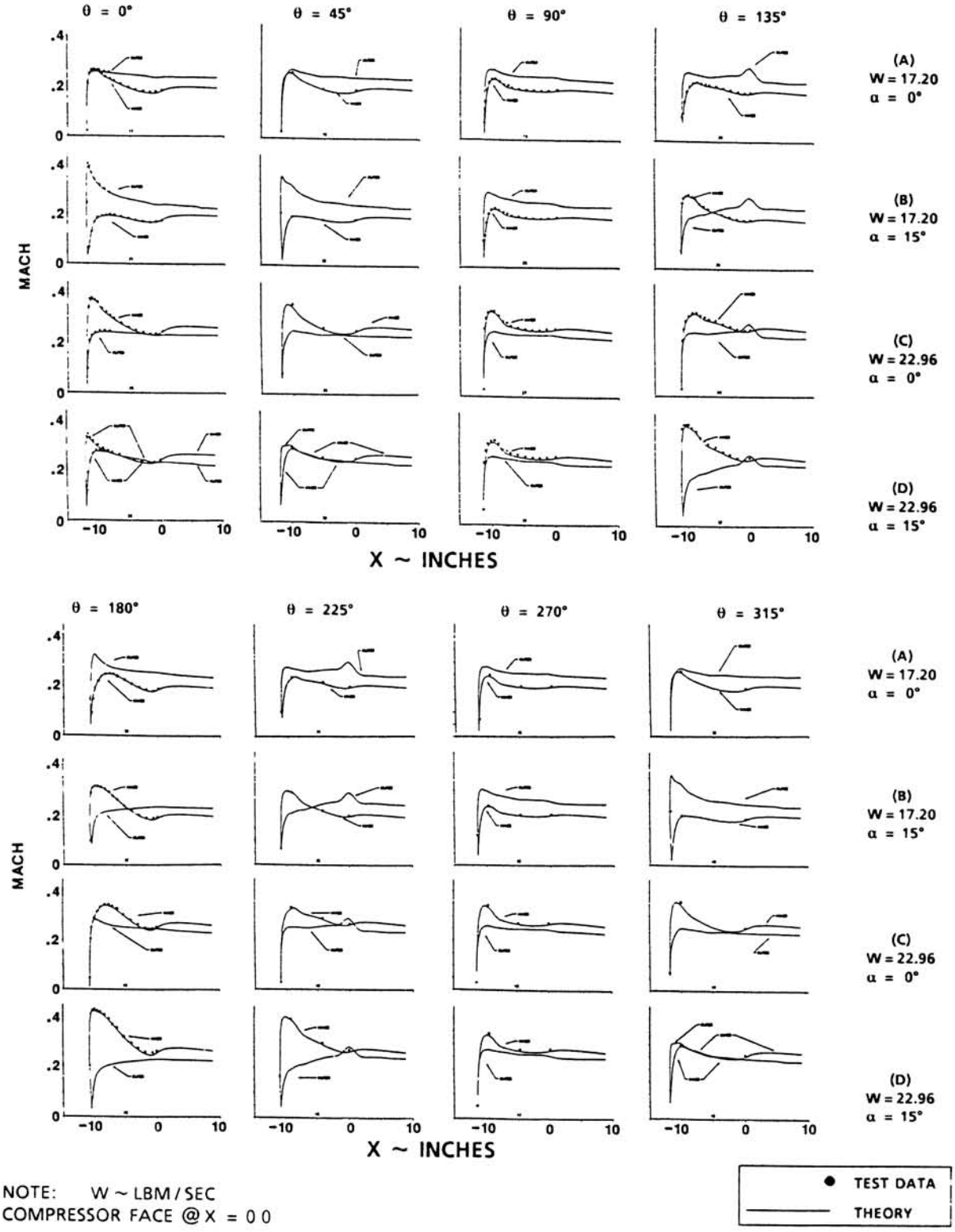

SUMMARY OF RESULTS

FIGURE 6.10

EXPERIMENTAL AND ANALYTICAL SURFACE MACH NUMBERS FOR BOEING 737-300 INLET (PAGE 1 OF 33).

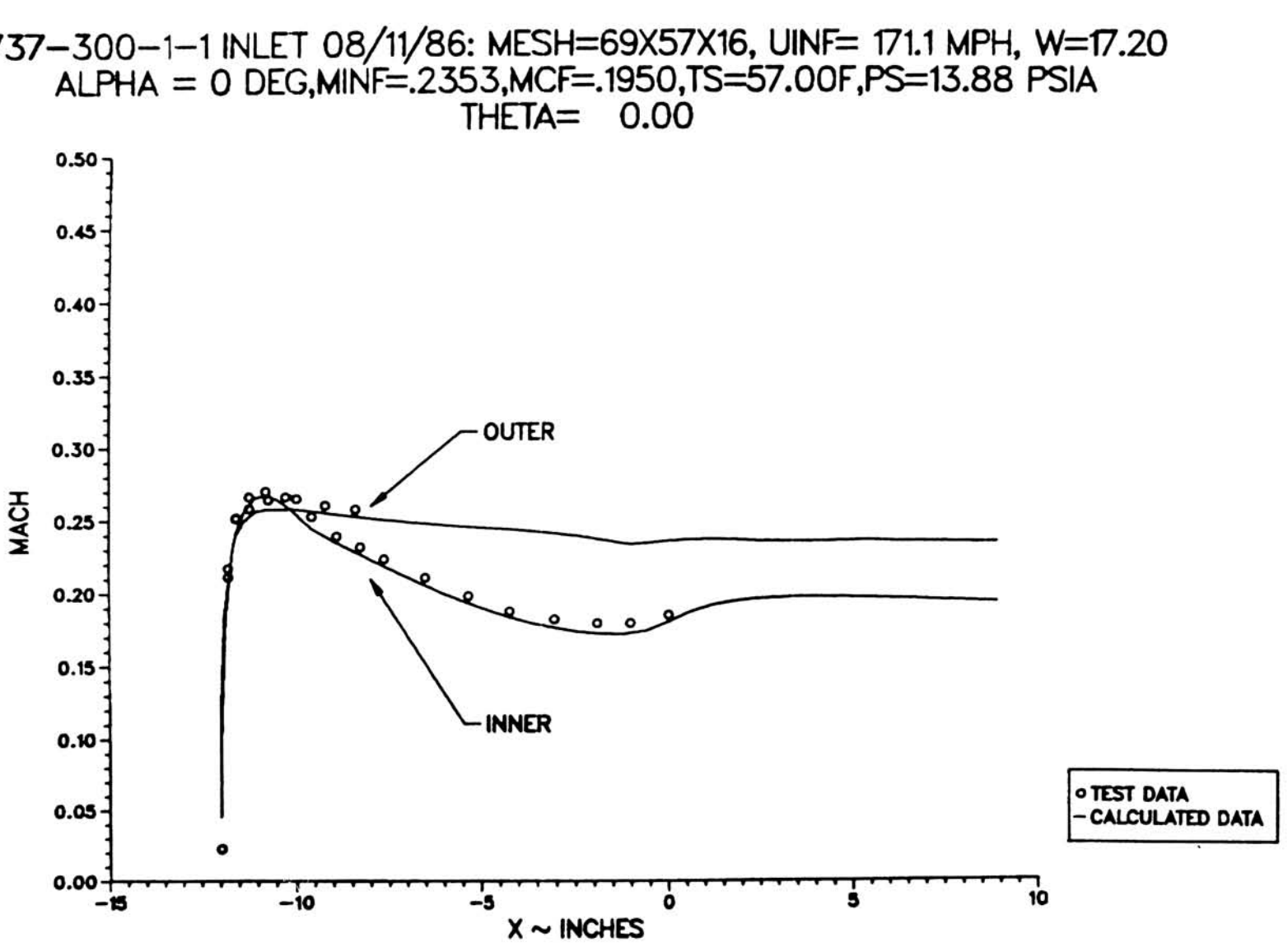

FIGURE 6.10

EXPERIMENTAL AND ANALYTICAL SURFACE MACH NUMBERS FOR BOEING 737-300 INLET (A1) W = 17.20 LBM/SEC, α = 0° (PAGE 2 OF 33).

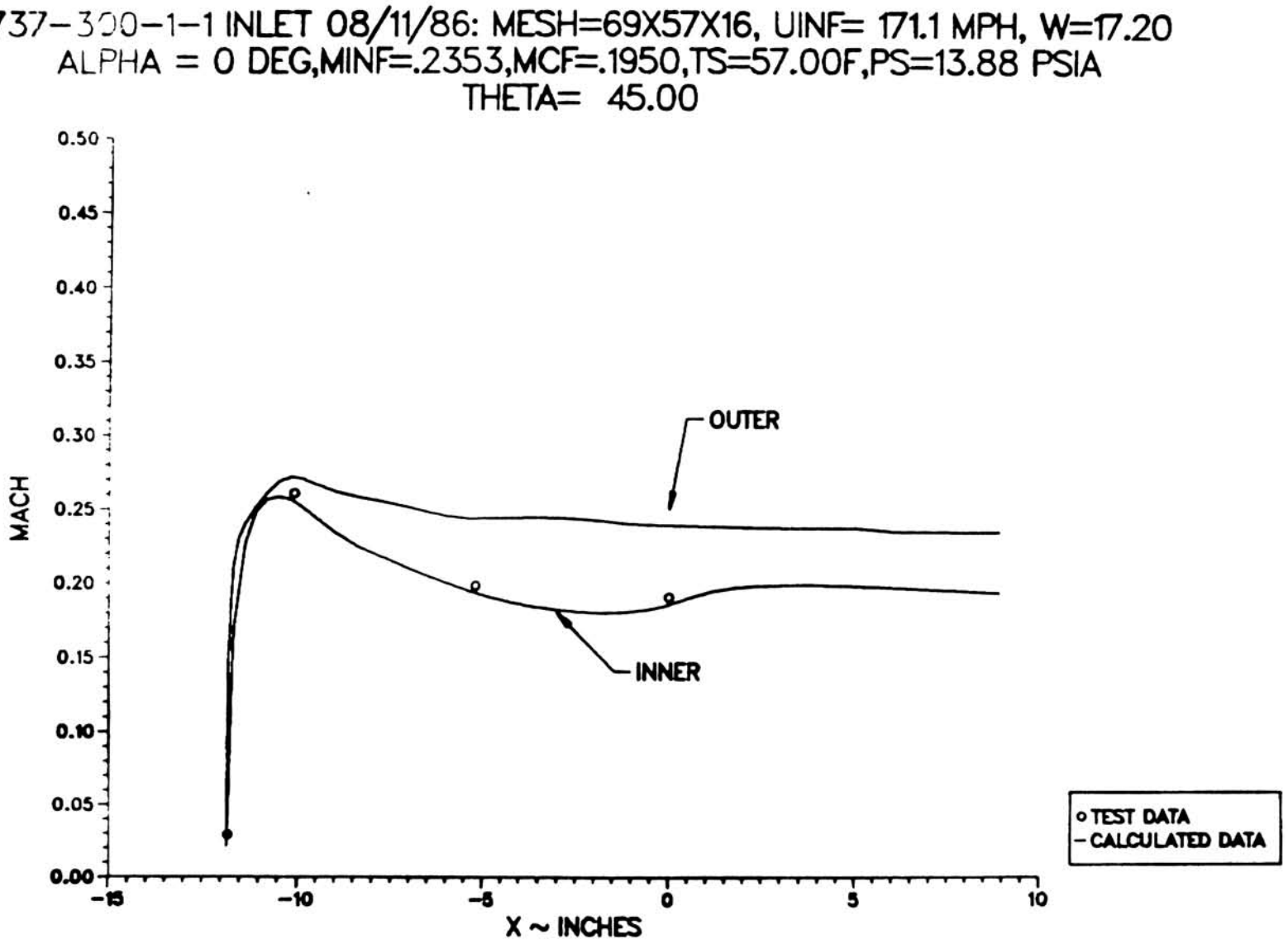

FIGURE 6.10

EXPERIMENTAL AND ANALYTICAL SURFACE MACH NUMBERS FOR BOEING 737-300 INLET (A2) W = 17.20 LBM/SEC, α = 0° (PAGE 3 OF 33).

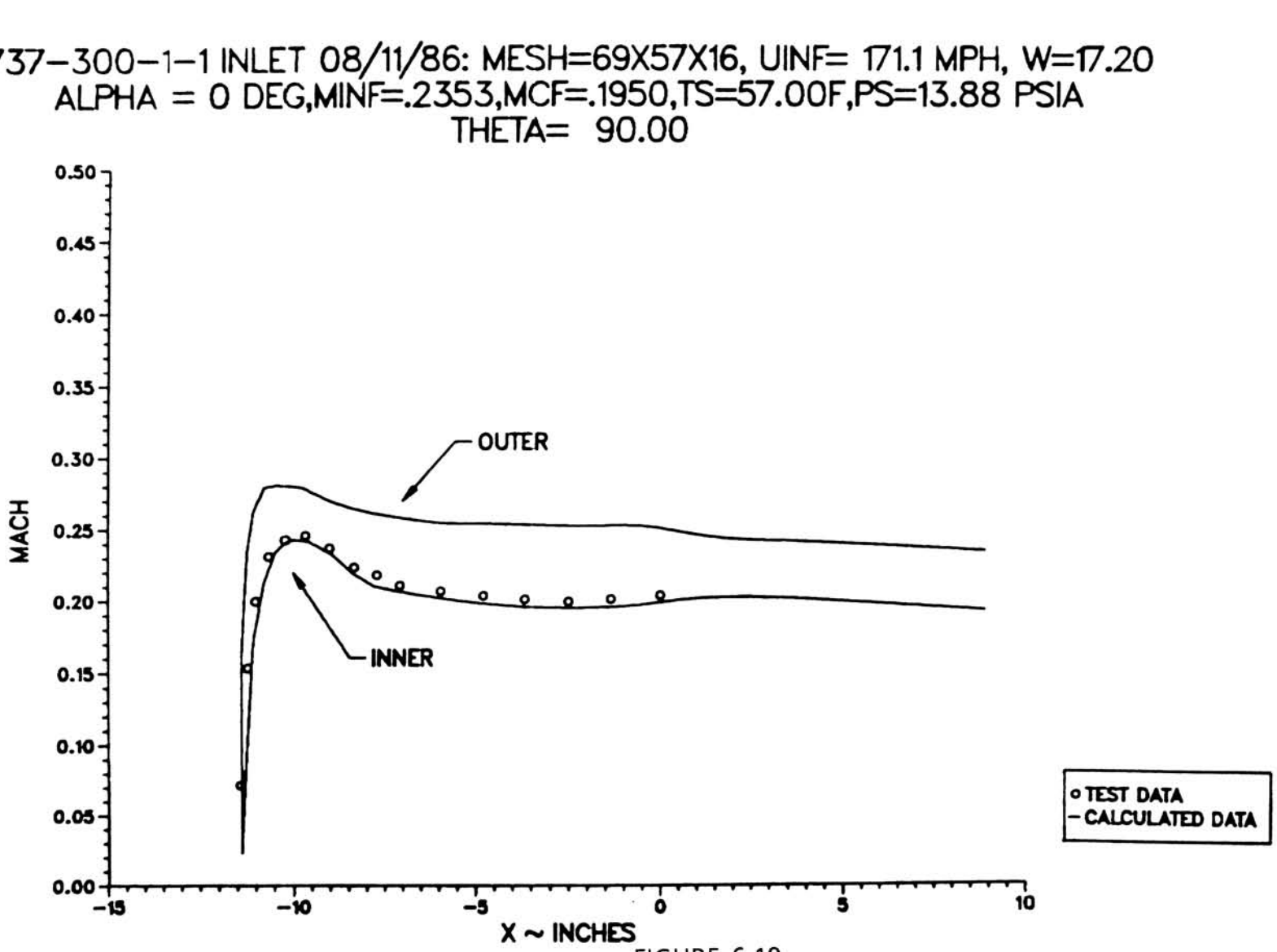

FIGURE 6.10

EXPERIMENTAL AND ANALYTICAL SURFACE MACH NUMBERS FOR BOEING 737-300 INLET (A3) W = 17.20 LBM/SEC, α = 0° (PAGE 4 OF 33).

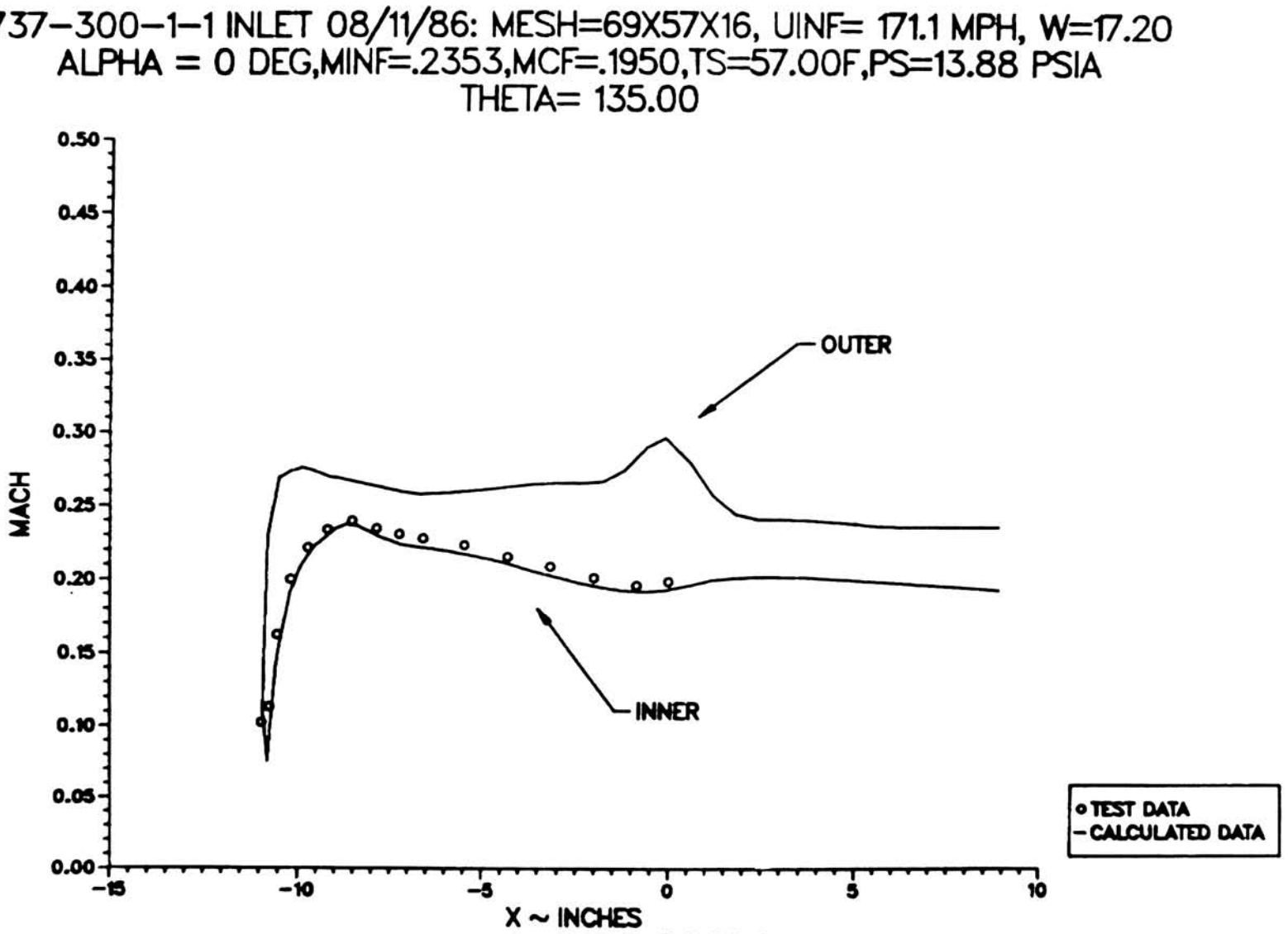

FIGURE 6.10

EXPERIMENTAL AND ANALYTICAL SURFACE MACH NUMBERS FOR BOEING 737-300 INLET (A4) W = 17.20 LBM/SEC, α = 0° (PAGE 5 OF 33).

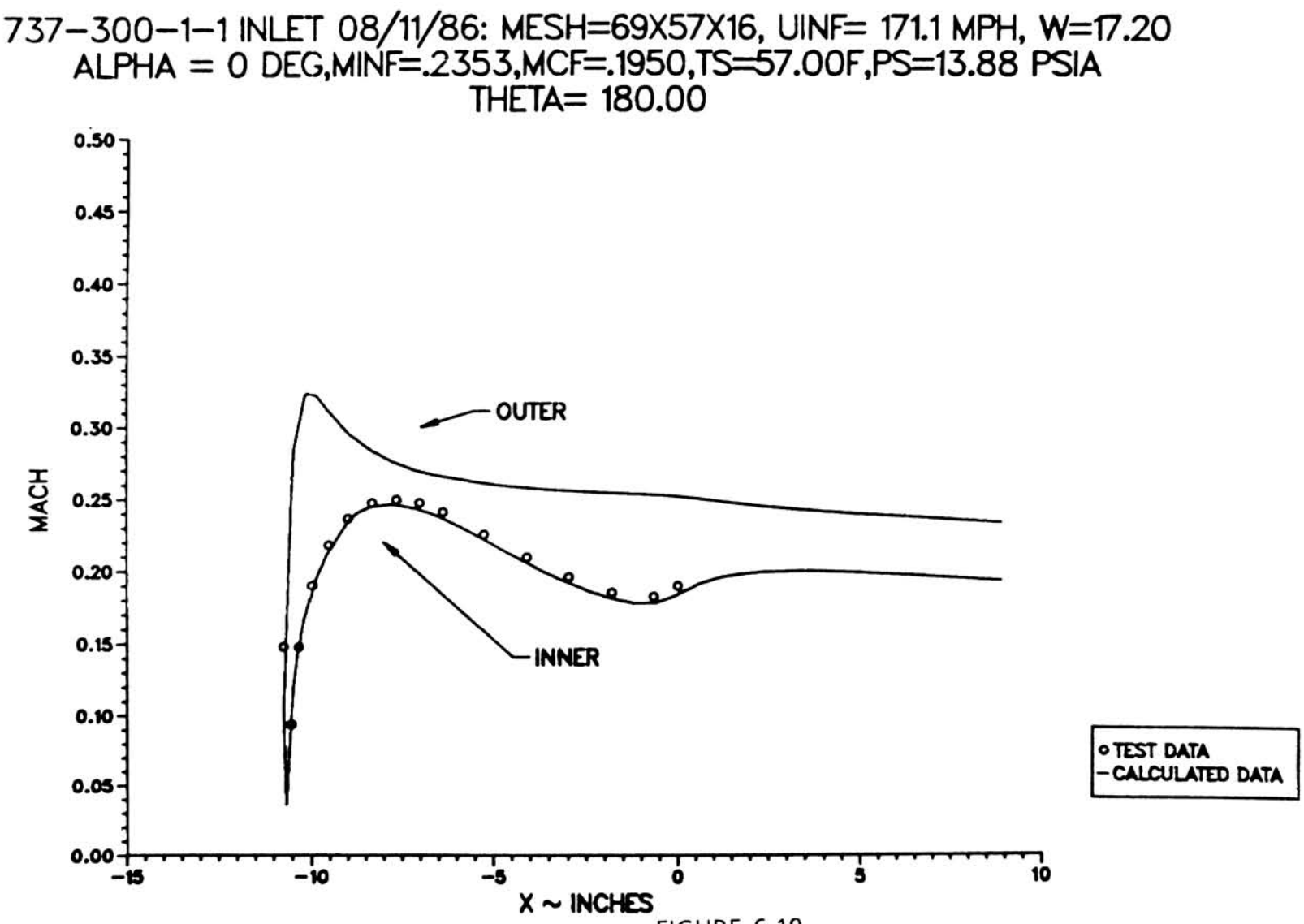

FIGURE 6.10

EXPERIMENTAL AND ANALYTICAL SURFACE MACH NUMBERS FOR BOEING 737-300 INLET (A5) W = 17.20 LBM / SEC, α = 0° (PAGE 6 OF 33).

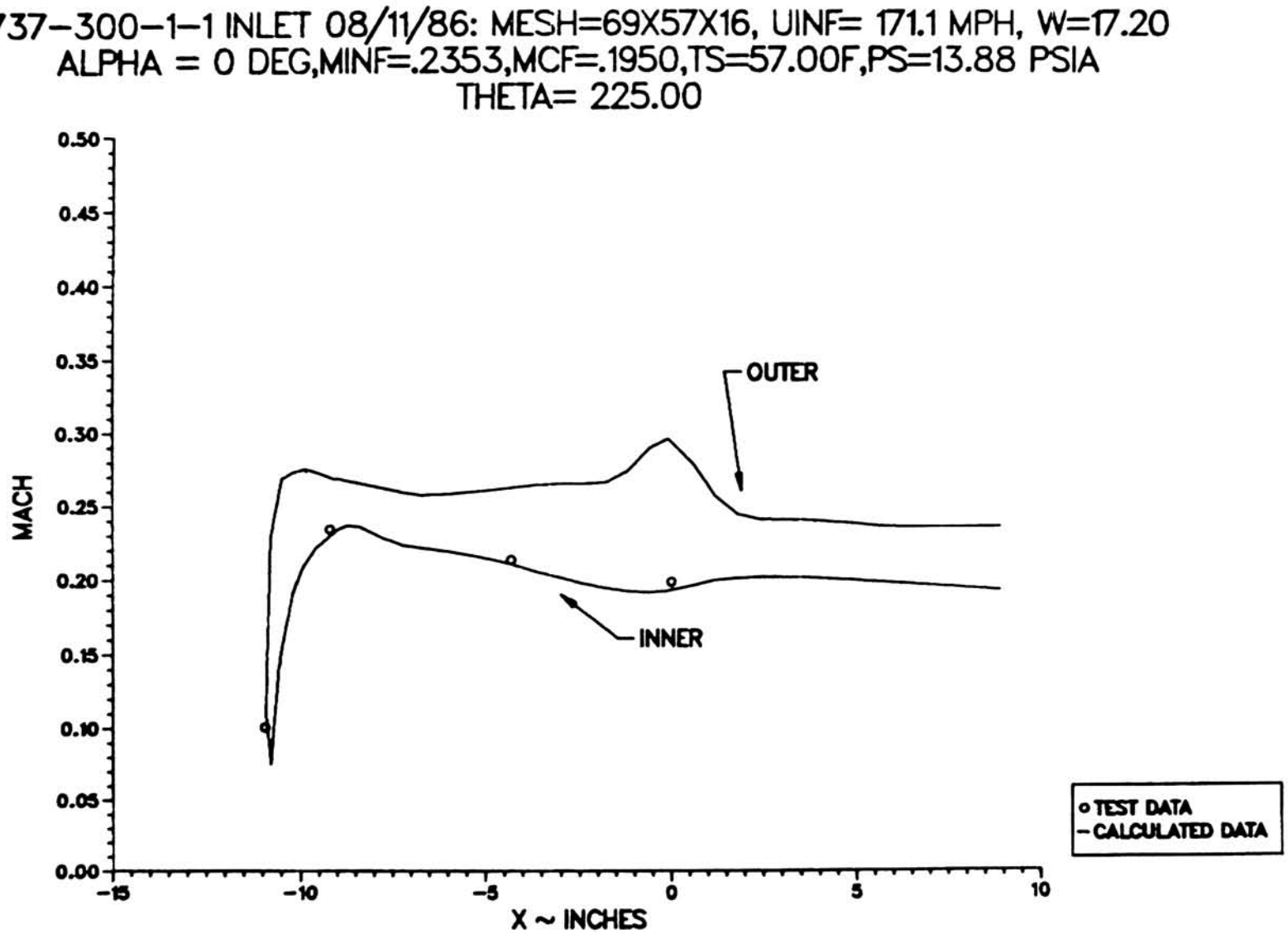

FIGURE 6.10

EXPERIMENTAL AND ANALYTICAL SURFACE MACH NUMBERS FOR BOEING 737-300 INLET (A6) W = 17.20 LBM/SEC, α = 0° (PAGE 7 OF 33).

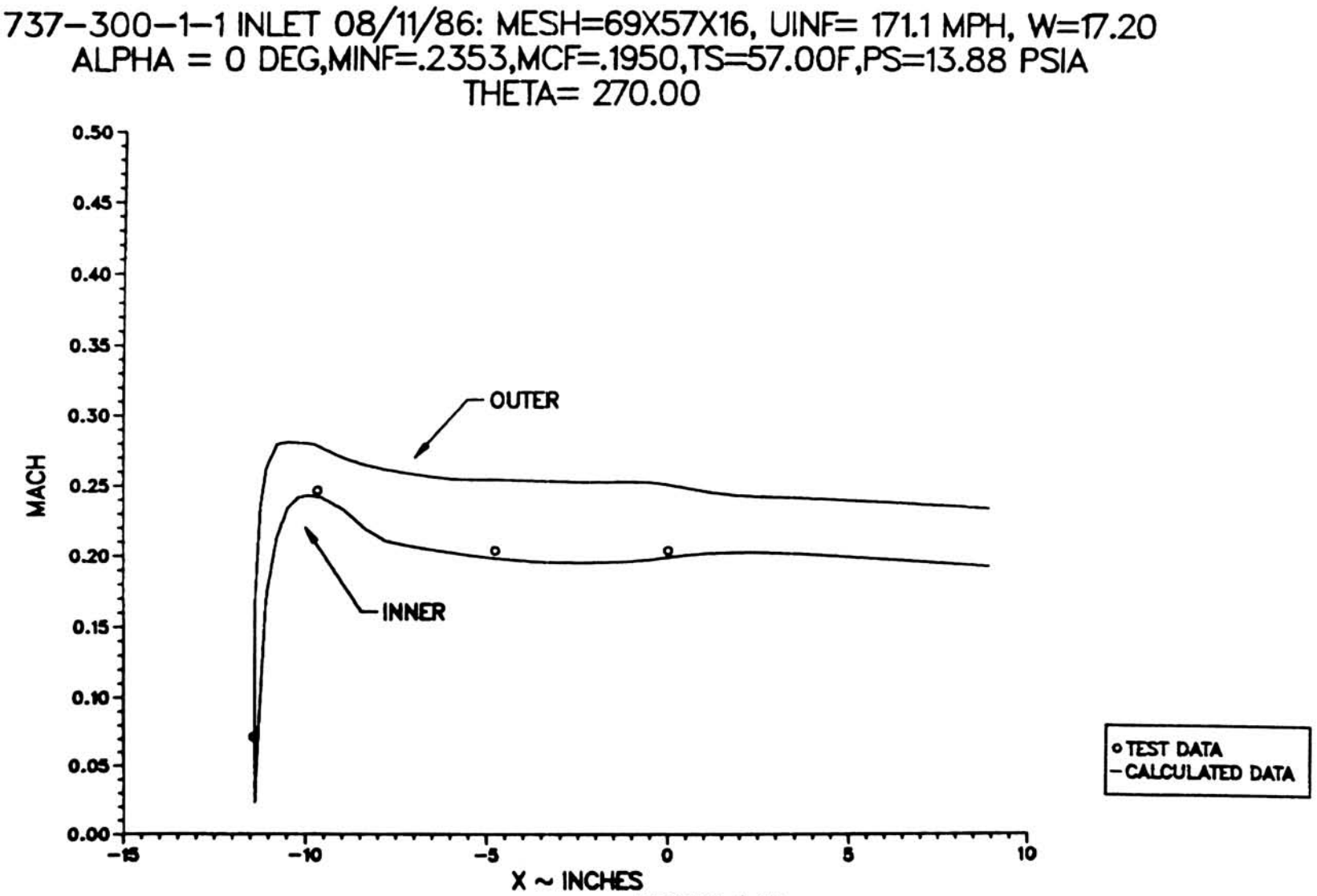

FIGURE 6.10

EXPERIMENTAL AND ANALYTICAL SURFACE MACH NUMBERS FOR BOEING 737-300 INLET (A7) W = 17.20 LBM/SEC, α = 0° (PAGE 8 OF 33).

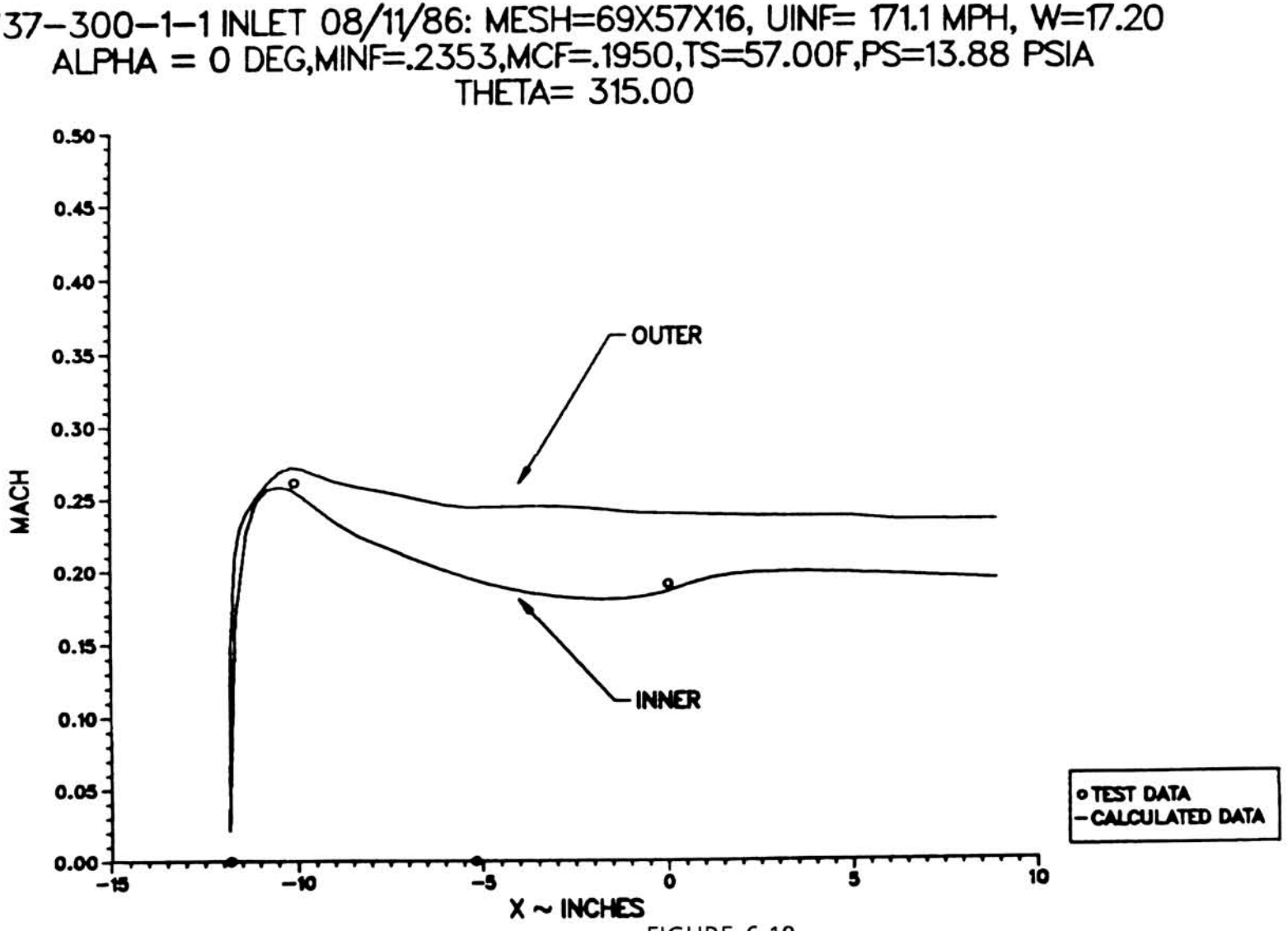

FIGURE 6.10

EXPERIMENTAL AND ANALYTICAL SURFACE MACH NUMBERS FOR BOEING 737-300 INLET (A8) W = 17.20 LBM/SEC, α = 0° (PAGE 9 OF 33).

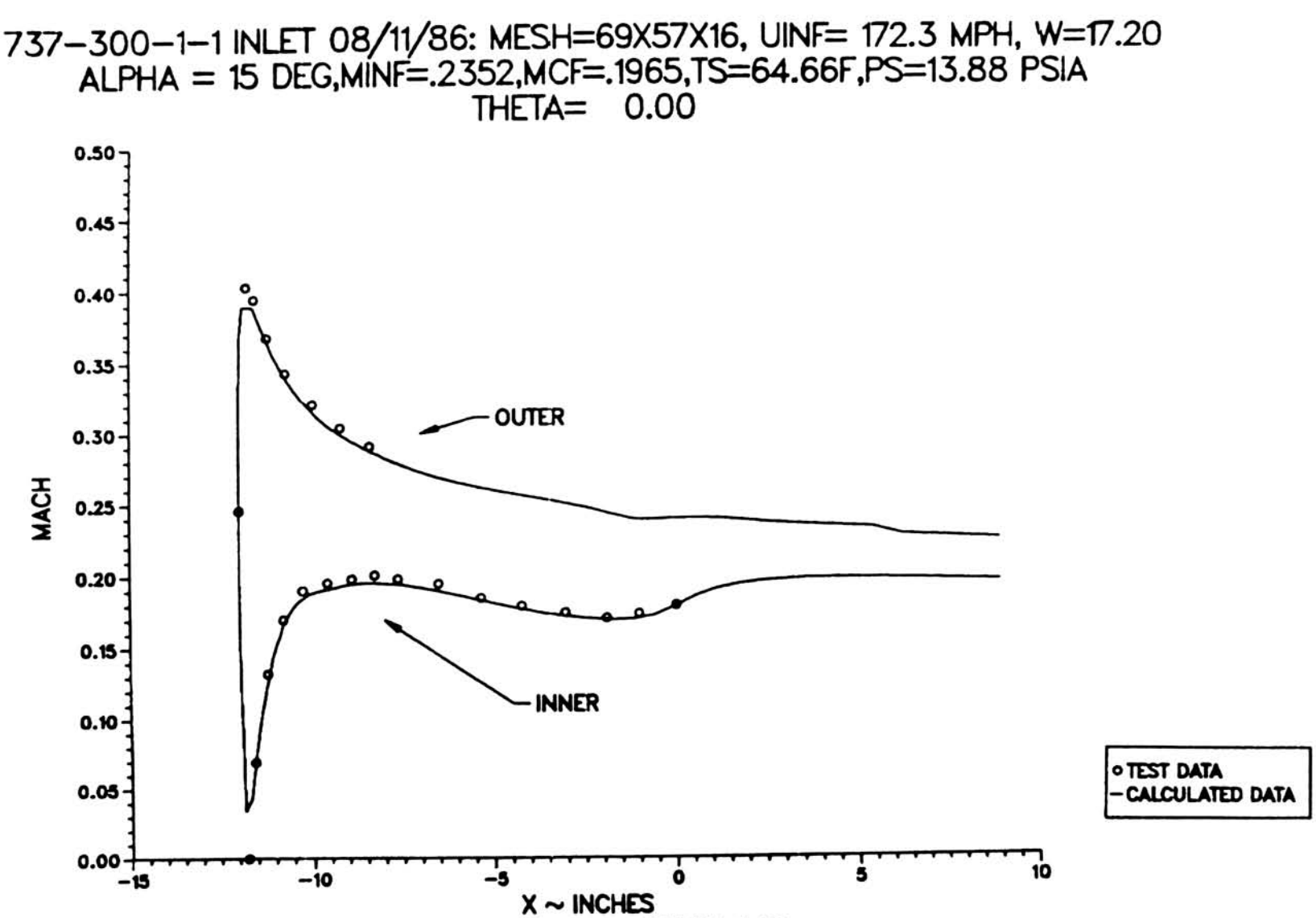

FIGURE 6.10

EXPERIMENTAL AND ANALYTICAL SURFACE MACH NUMBERS FOR BOEING 737-300 INLET (B1) W = 17.20 LBM/SEC, α = 15° (PAGE 10 OF 33).

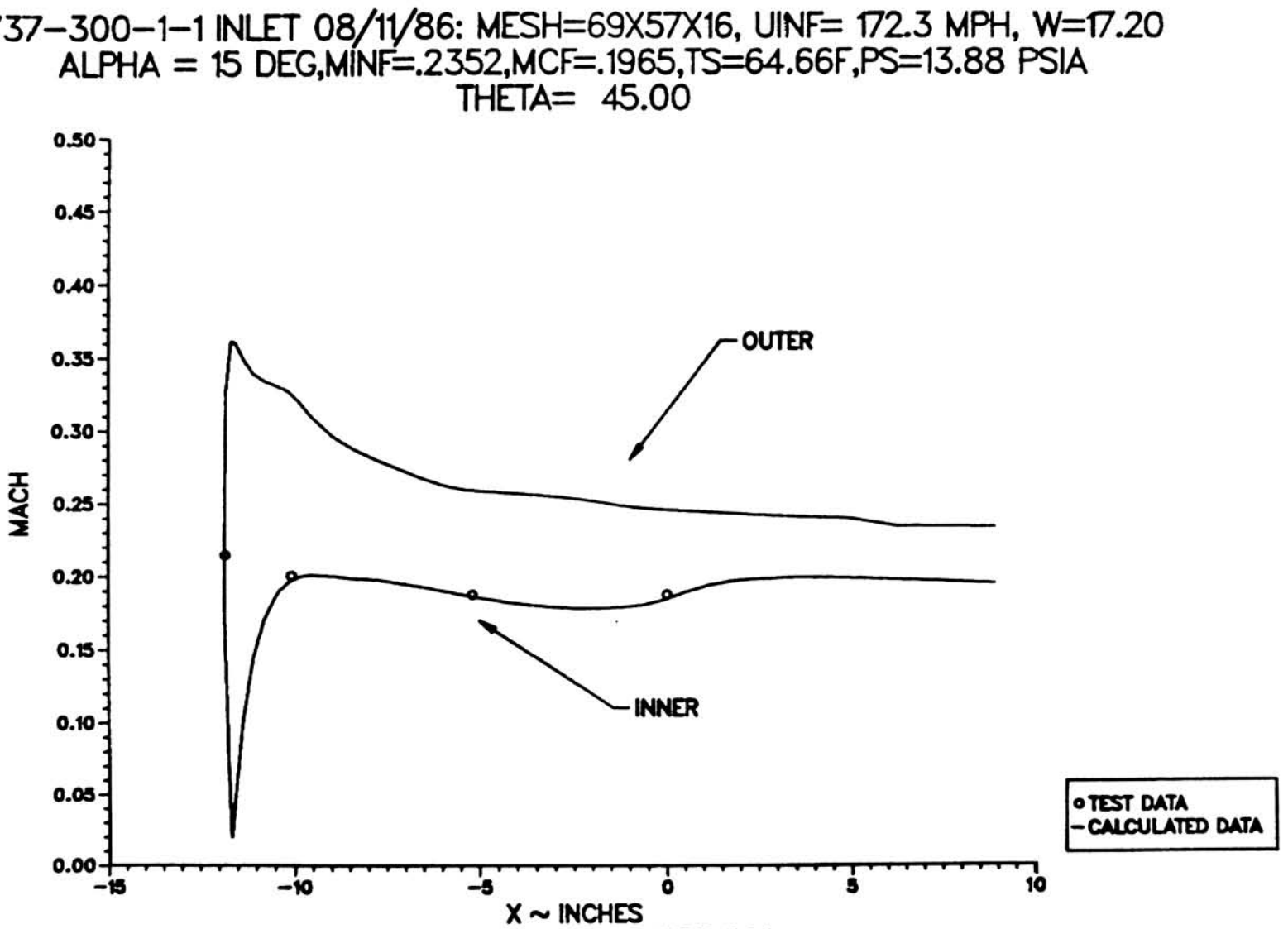

FIGURE 6.10

EXPERIMENTAL AND ANALYTICAL SURFACE MACH NUMBERS FOR BOEING 737-300 INLET (B2) W = 17.20 LBM/SEC, α = 15° (PAGE 11 OF 33).

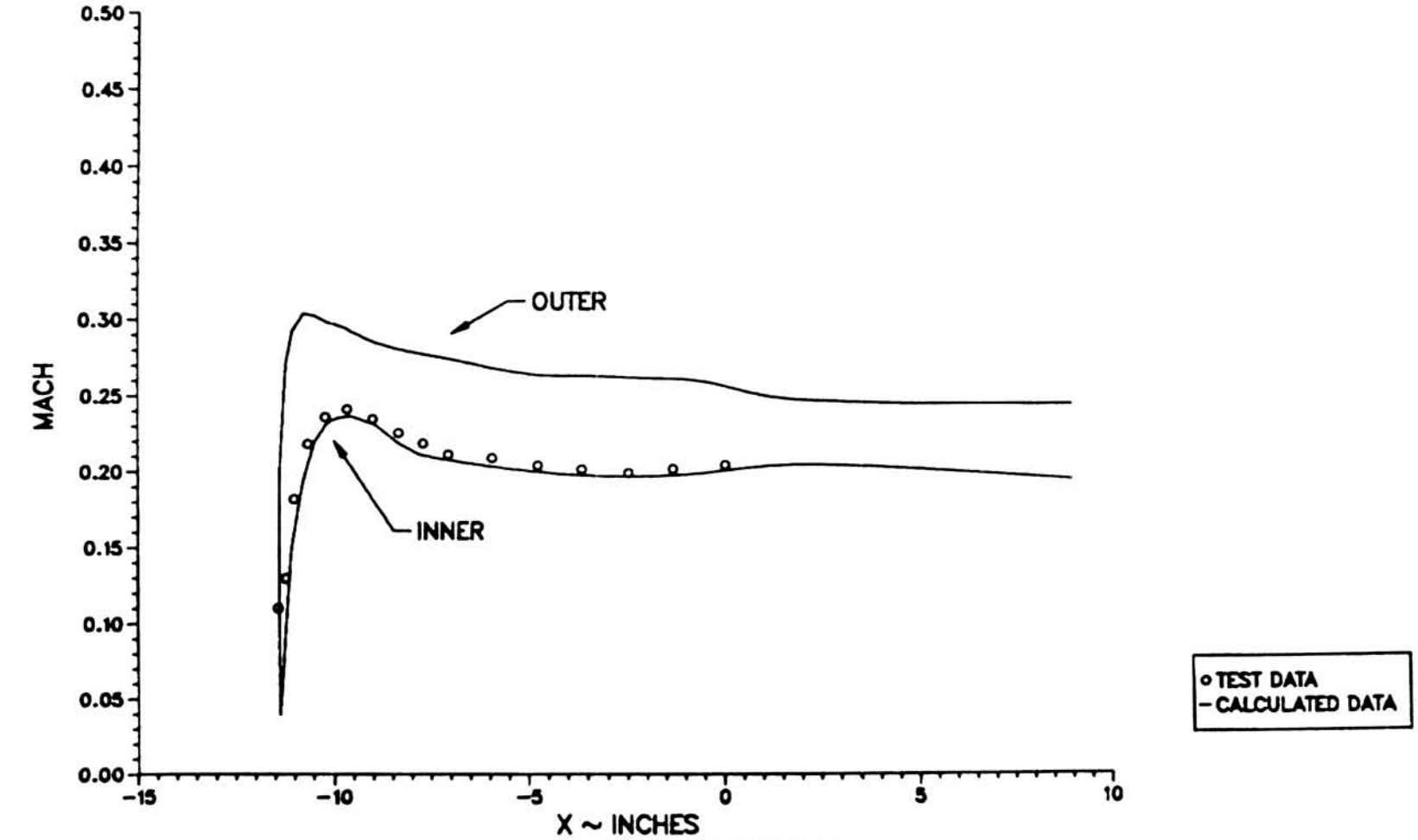

FIGURE 6.10

EXPERIMENTAL AND ANALYTICAL SURFACE MACH NUMBERS FOR BOEING 737-300 INLET (B3) W = 17.20 LBM/SEC, α = 15° (PAGE 12 OF 33).

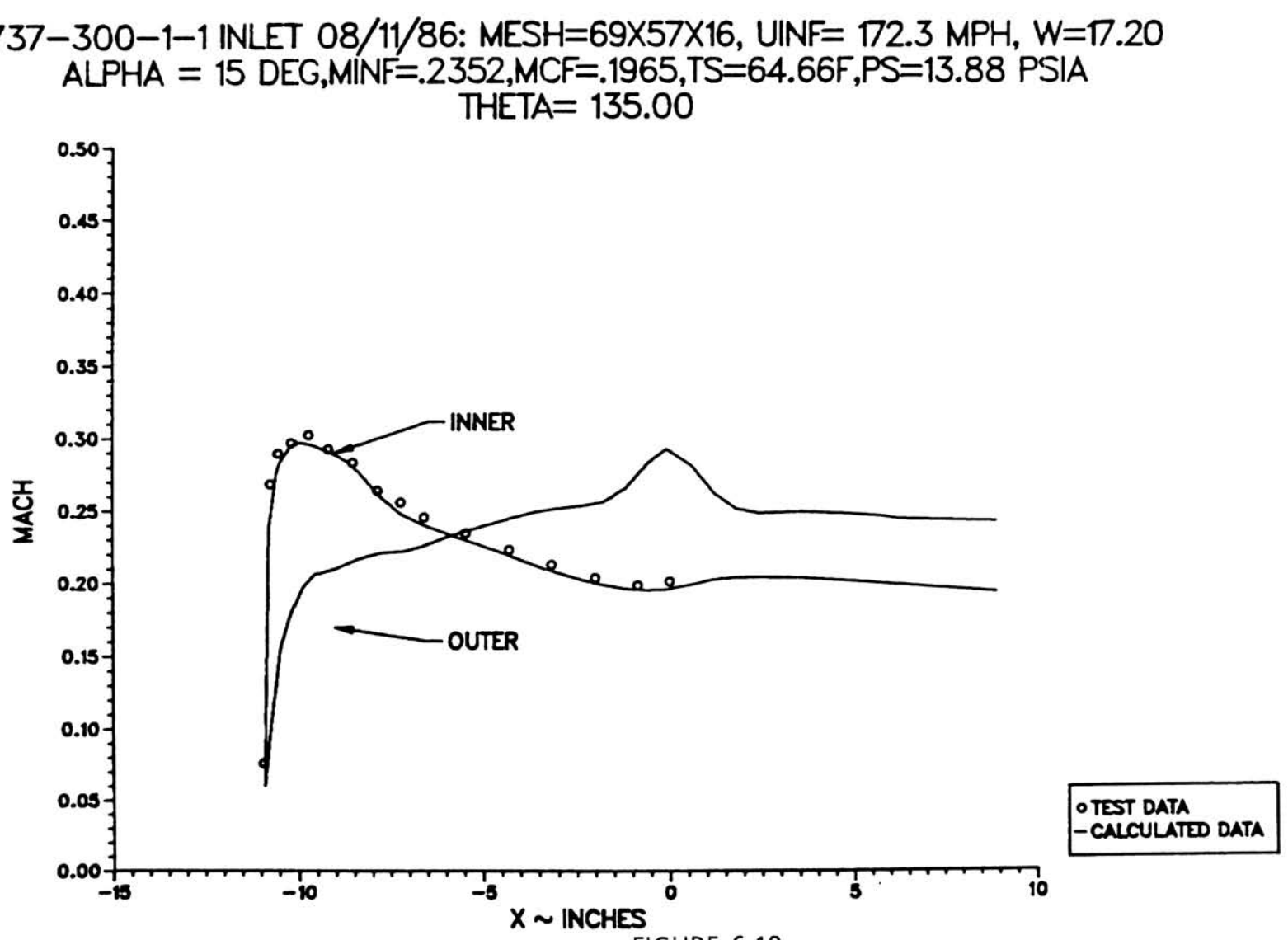

FIGURE 6.10

EXPERIMENTAL AND ANALYTICAL SURFACE MACH NUMBERS FOR BOEING 737-300 INLET (B4) W = 17.20 LBM/SEC, α = 15° (PAGE 13 OF 33).

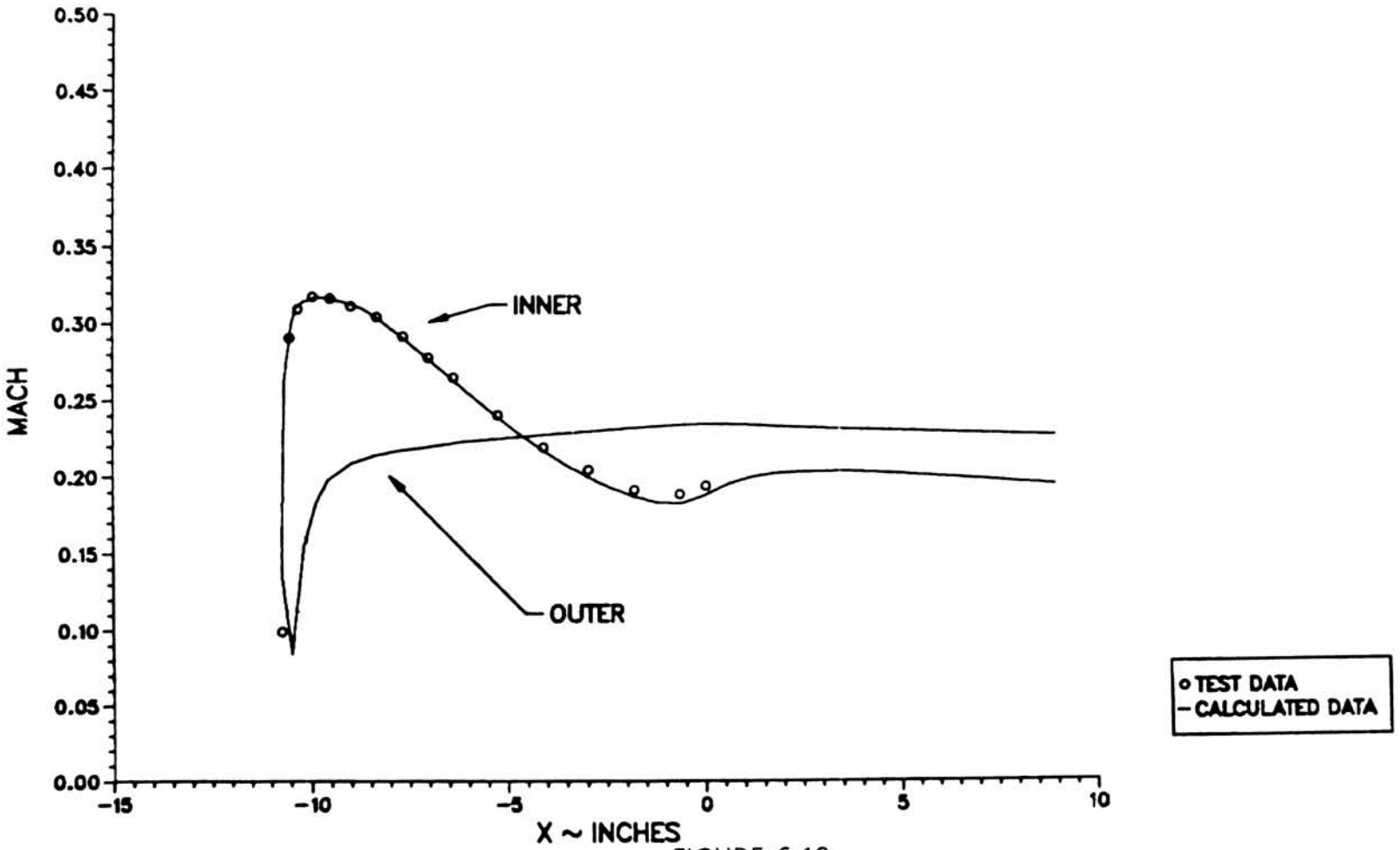

FIGURE 6.10

EXPERIMENTAL AND ANALYTICAL SURFACE MACH NUMBERS FOR BOEING 737-300 INLET (B5) W = 17.20 LBM/SEC, α = 15° (PAGE 14 OF 33).

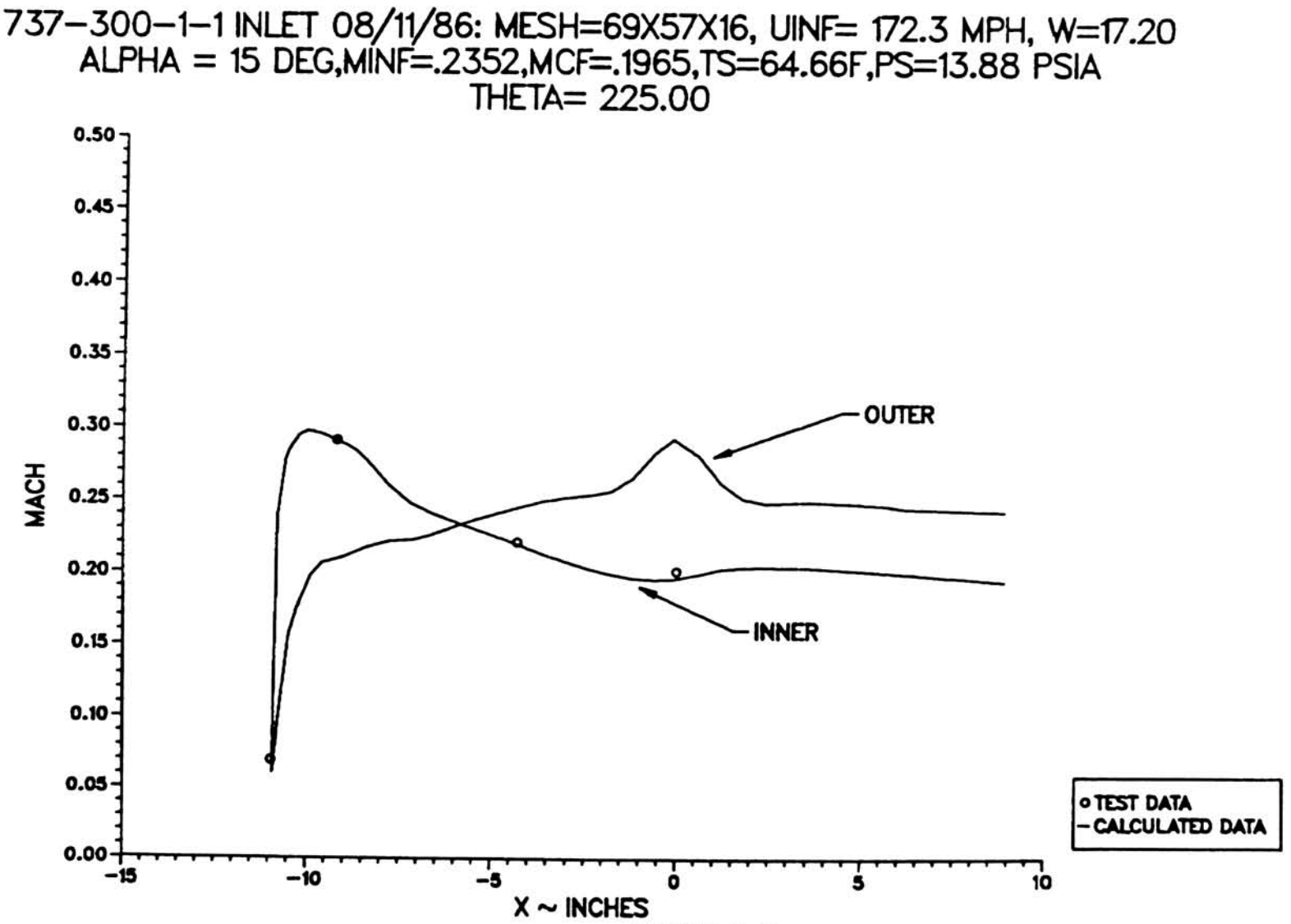

FIGURE 6.10

EXPERIMENTAL AND ANALYTICAL SURFACE MACH NUMBERS FOR BOEING 737-300 INLET (B6) W = 17.20 LBM / SEC, α = 15° (PAGE 15 OF 33).

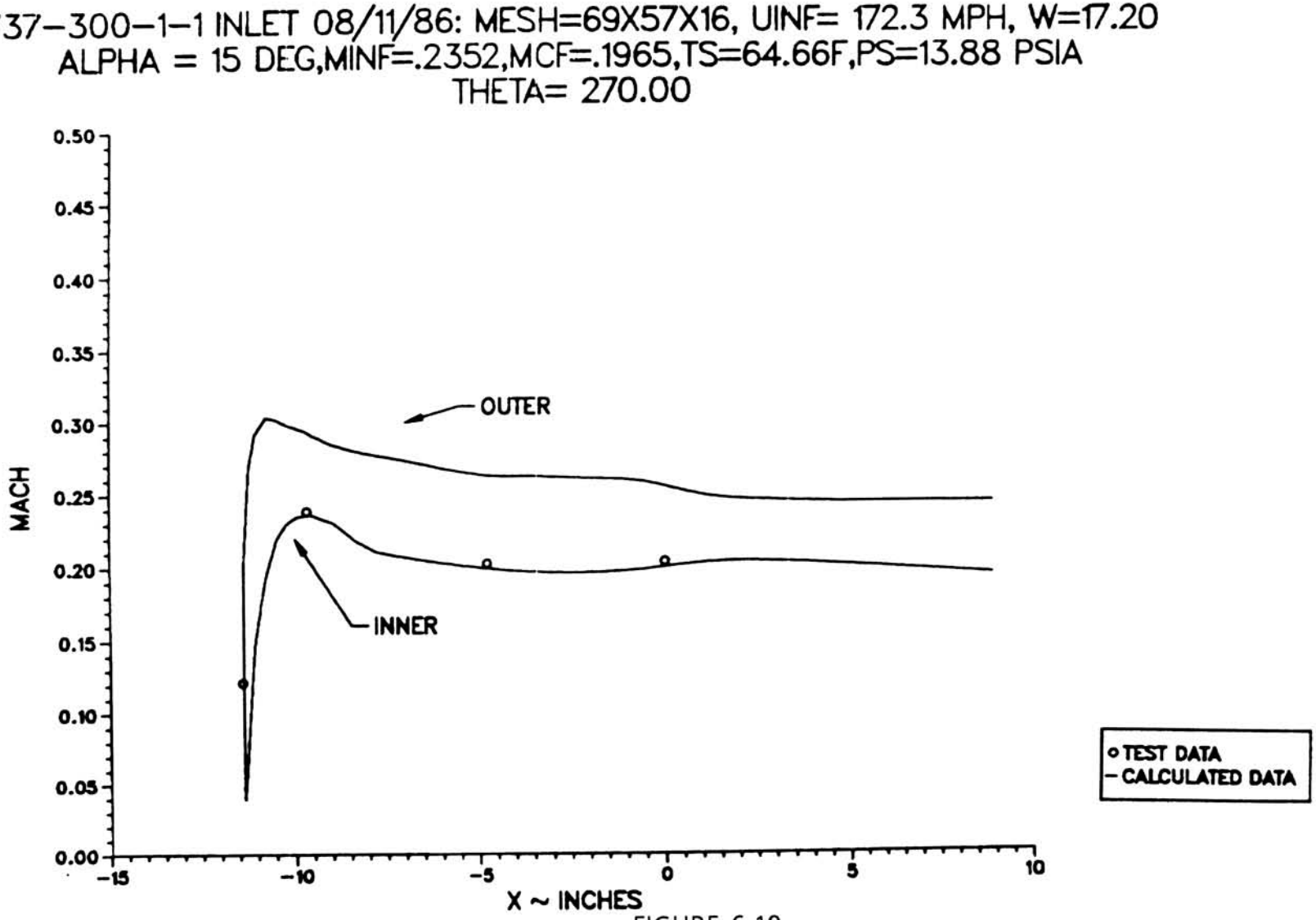

FIGURE 6.10

EXPERIMENTAL AND ANALYTICAL SURFACE MACH NUMBERS FOR BOEING 737-300 INLET (B7) W = 17.20 LBM/SEC, α = 15° (PAGE 16 OF 33).

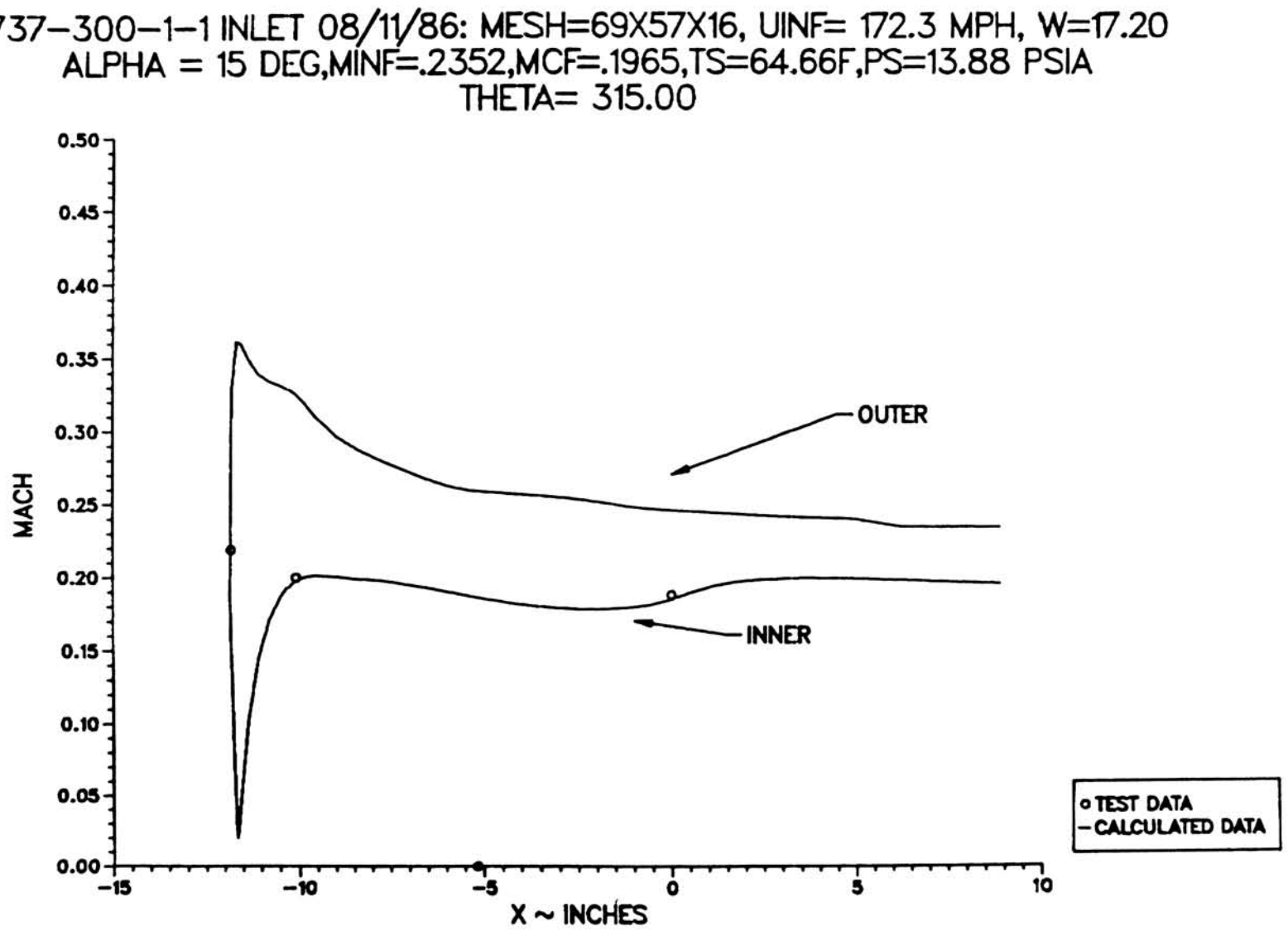

FIGURE 6.10

EXPERIMENTAL AND ANALYTICAL SURFACE MACH NUMBERS FOR BOEING 737-300 INLET (B8) W = 17.20 LBM/SEC, α = 15° (PAGE 17 OF 33).

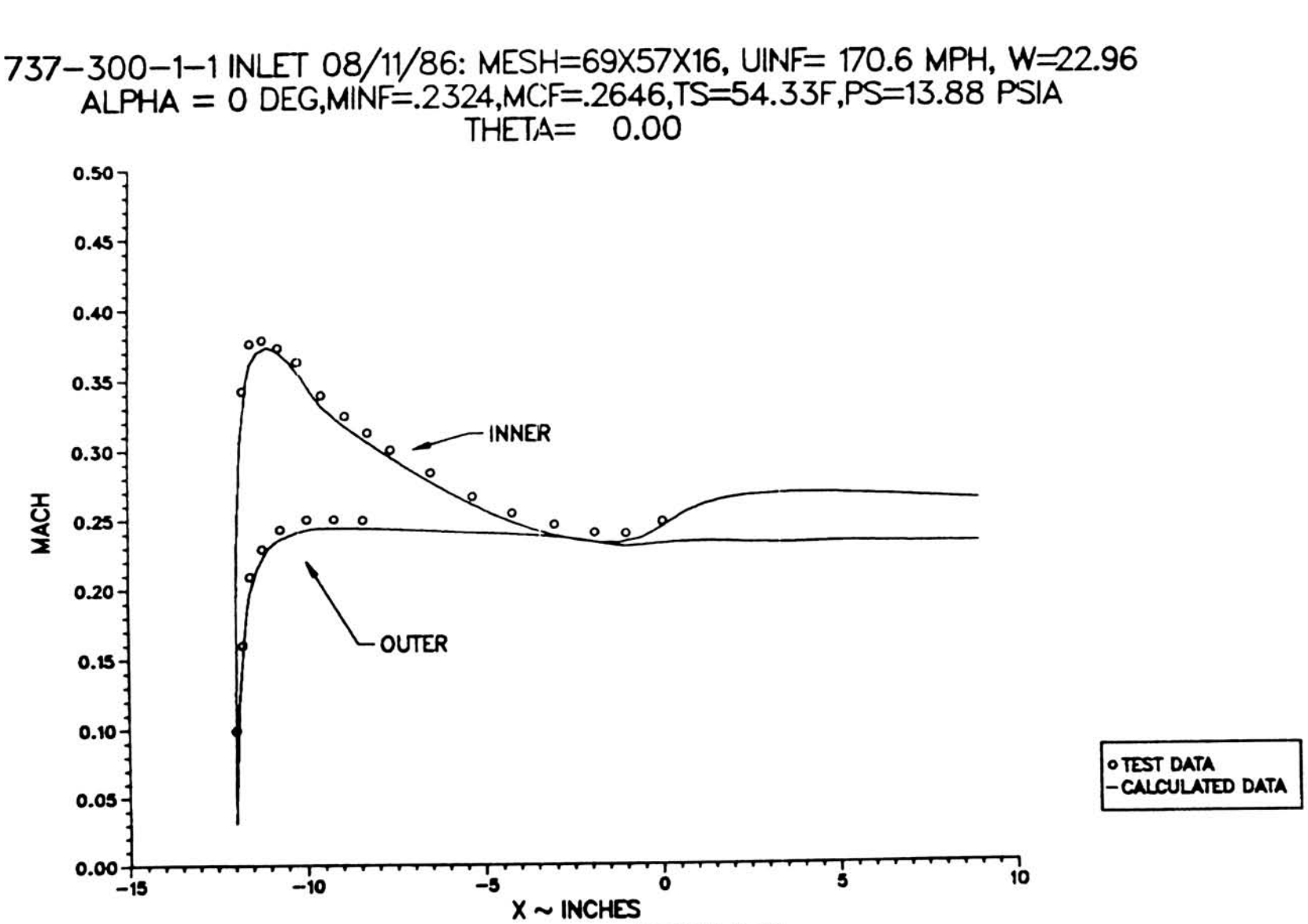

FIGURE 6.10

EXPERIMENTAL AND ANALYTICAL SURFACE MACH NUMBERS FOR BOEING 737-300 INLET
(C1) W = 22.96 LBM/SEC, α = 0° (PAGE 18 OF 33).

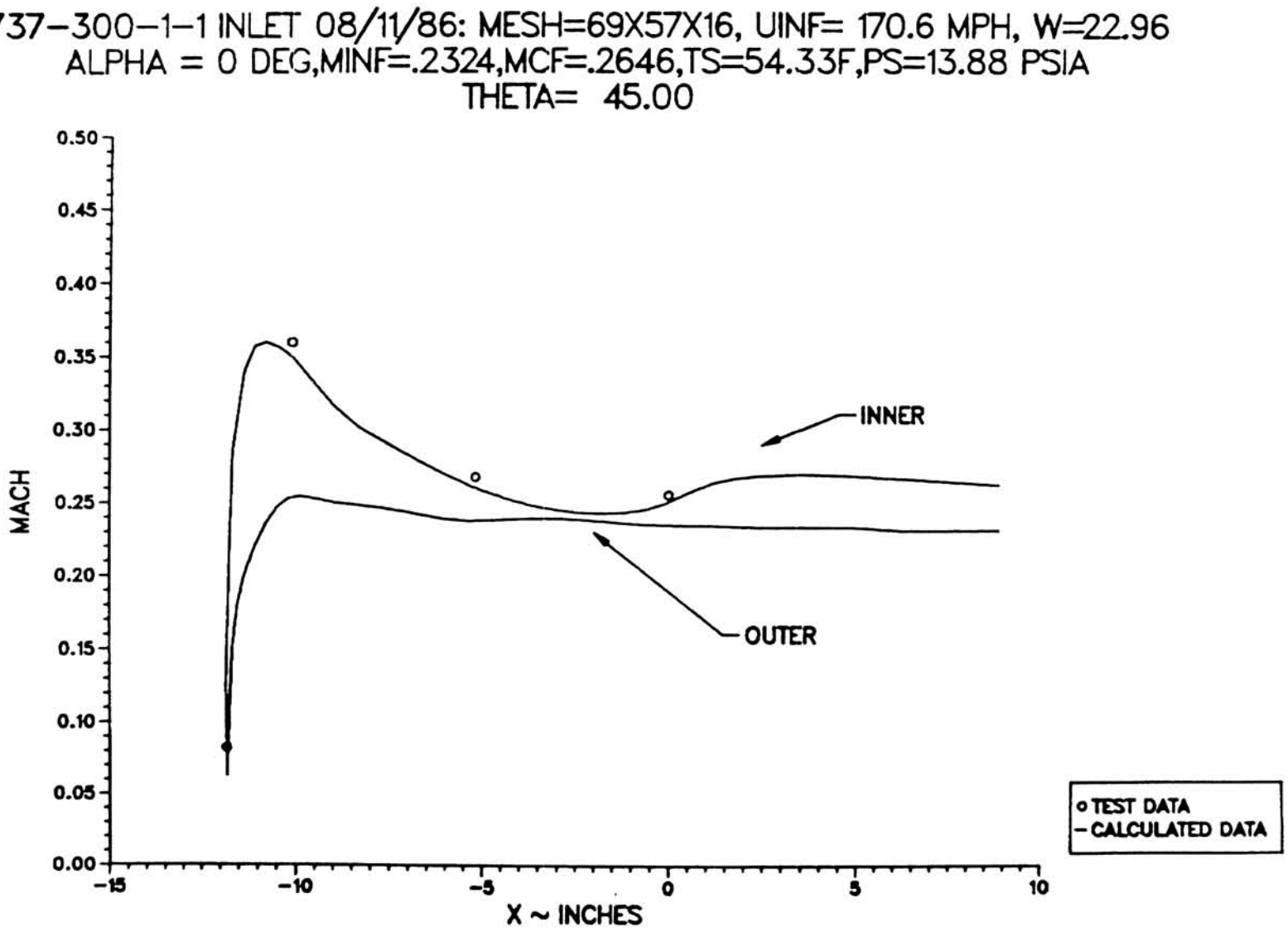

FIGURE 6.10

EXPERIMENTAL AND ANALYTICAL SURFACE MACH NUMBERS FOR BOEING 737-300 INLET (C2) W = 22.96 LBM/SEC, α = 0° (PAGE 19 OF 33).

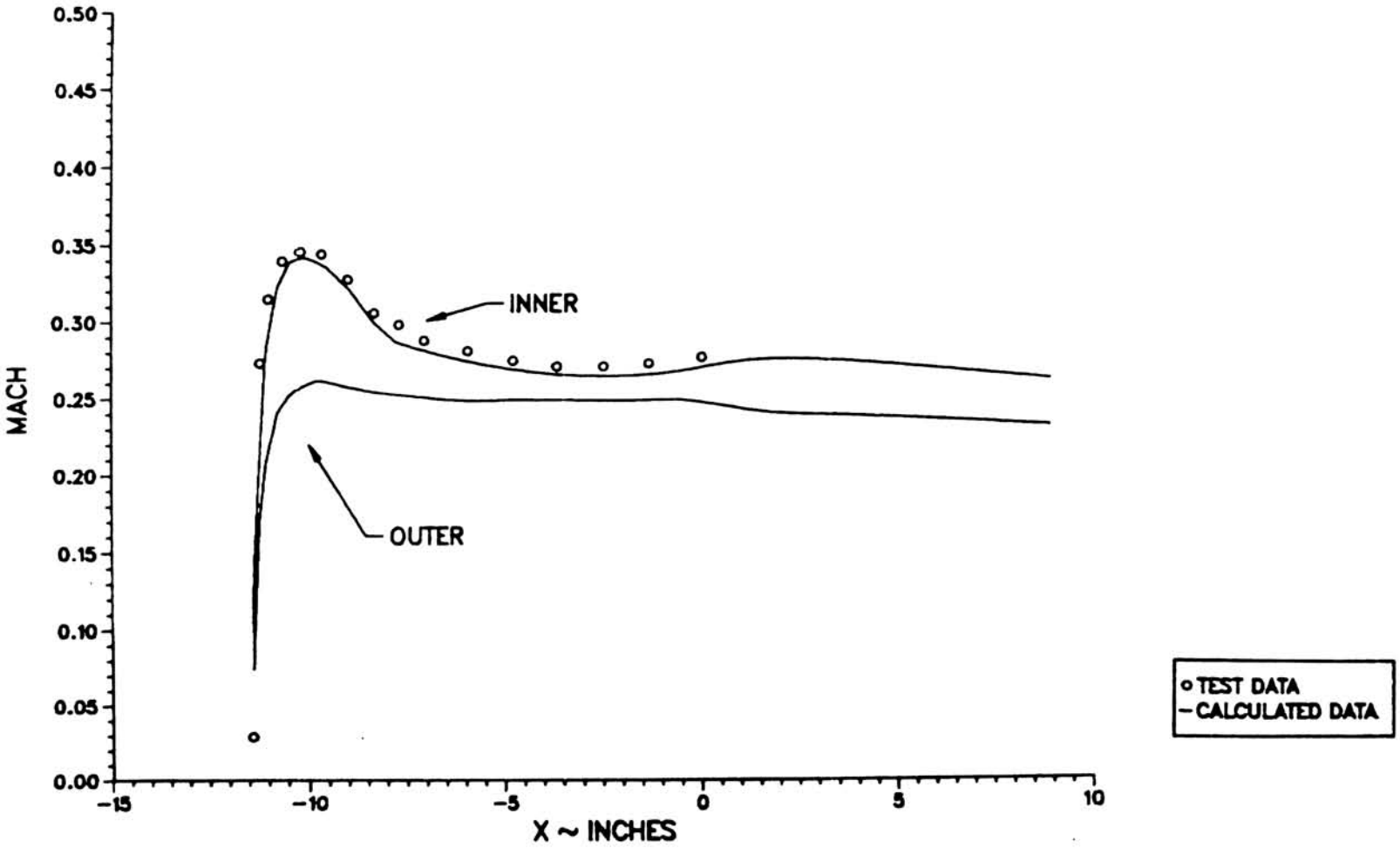

FIGURE 6.10

EXPERIMENTAL AND ANALYTICAL SURFACE MACH NUMBERS FOR BOEING 737-300 INLET (C3) W = 22.96 LBM/SEC, α = 0° (PAGE 20 OF 33).

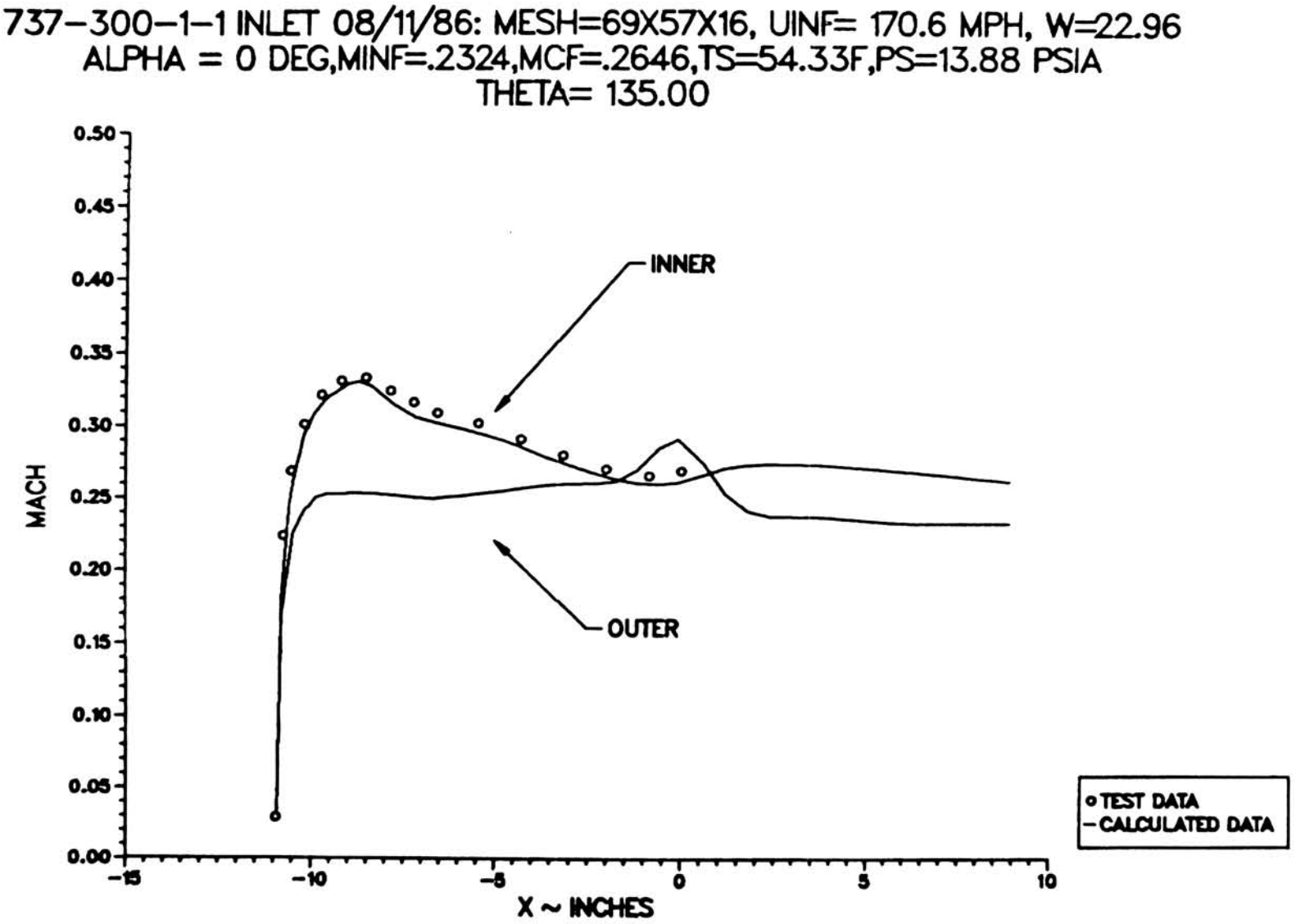

FIGURE 6.10

EXPERIMENTAL AND ANALYTICAL SURFACE MACH NUMBERS FOR BOEING 737-300 INLET (C4) W = 22.96 LBM/SEC, α = 0° (PAGE 21 OF 33).

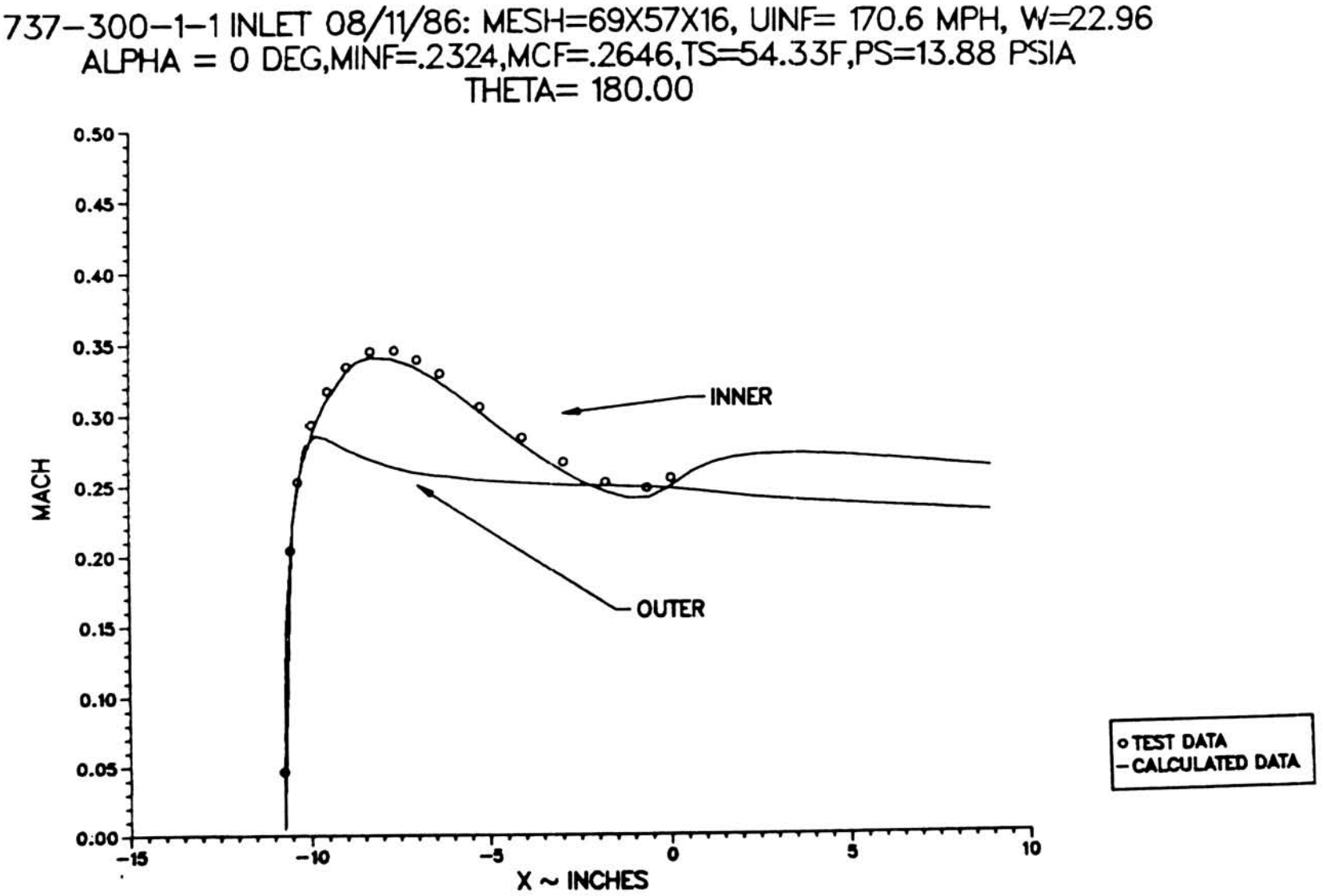

FIGURE 6.10

EXPERIMENTAL AND ANALYTICAL SURFACE MACH NUMBERS FOR BOEING 737-300 INLET
(C4) W = 22.96 LBM/SEC, α = 0° (PAGE 22 OF 33).

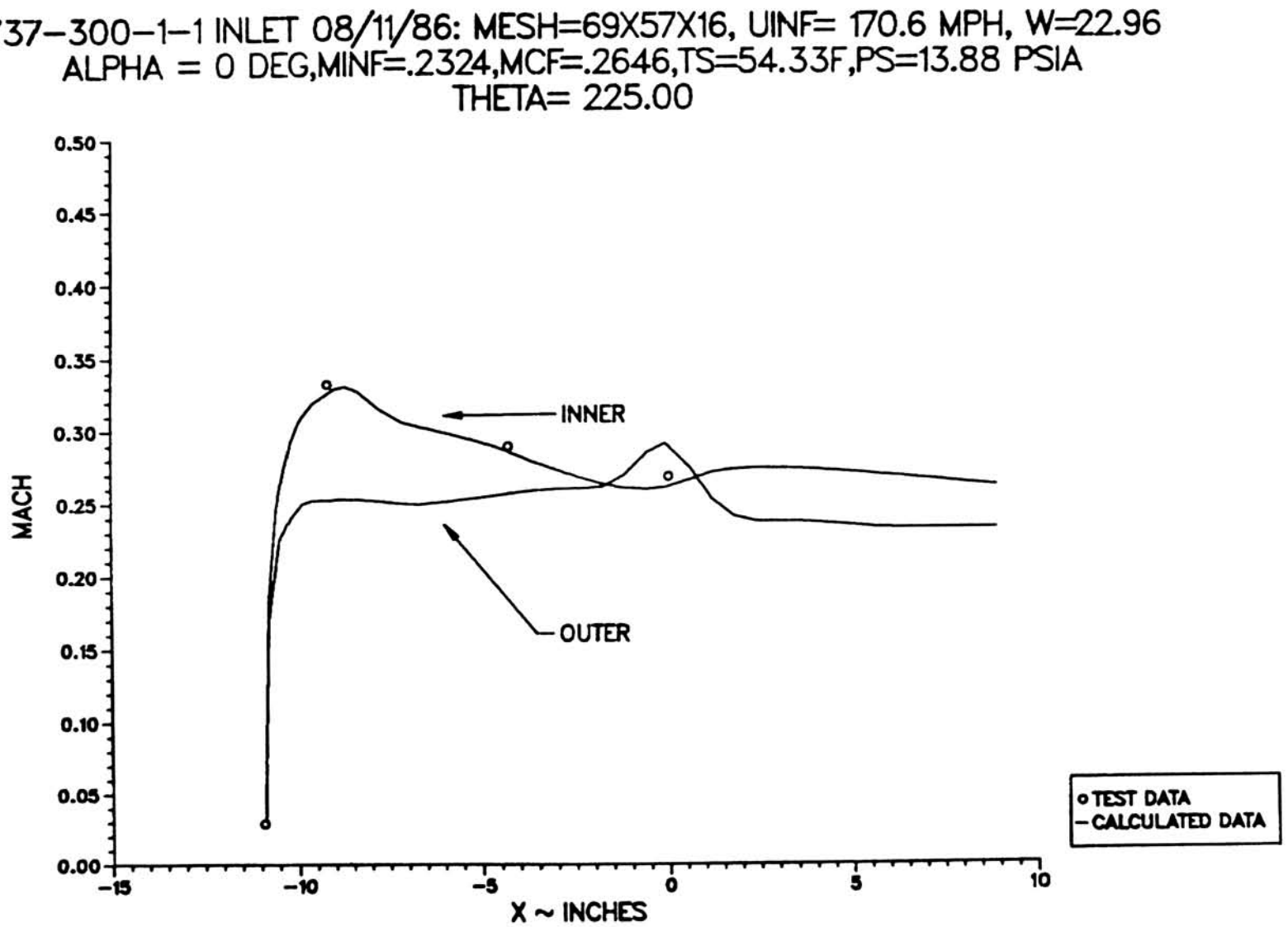

FIGURE 6.10

EXPERIMENTAL AND ANALYTICAL SURFACE MACH NUMBERS FOR BOEING 737-300 INLET (C6) W = 22.96 LBM/SEC, α = 0° (PAGE 23 OF 33).

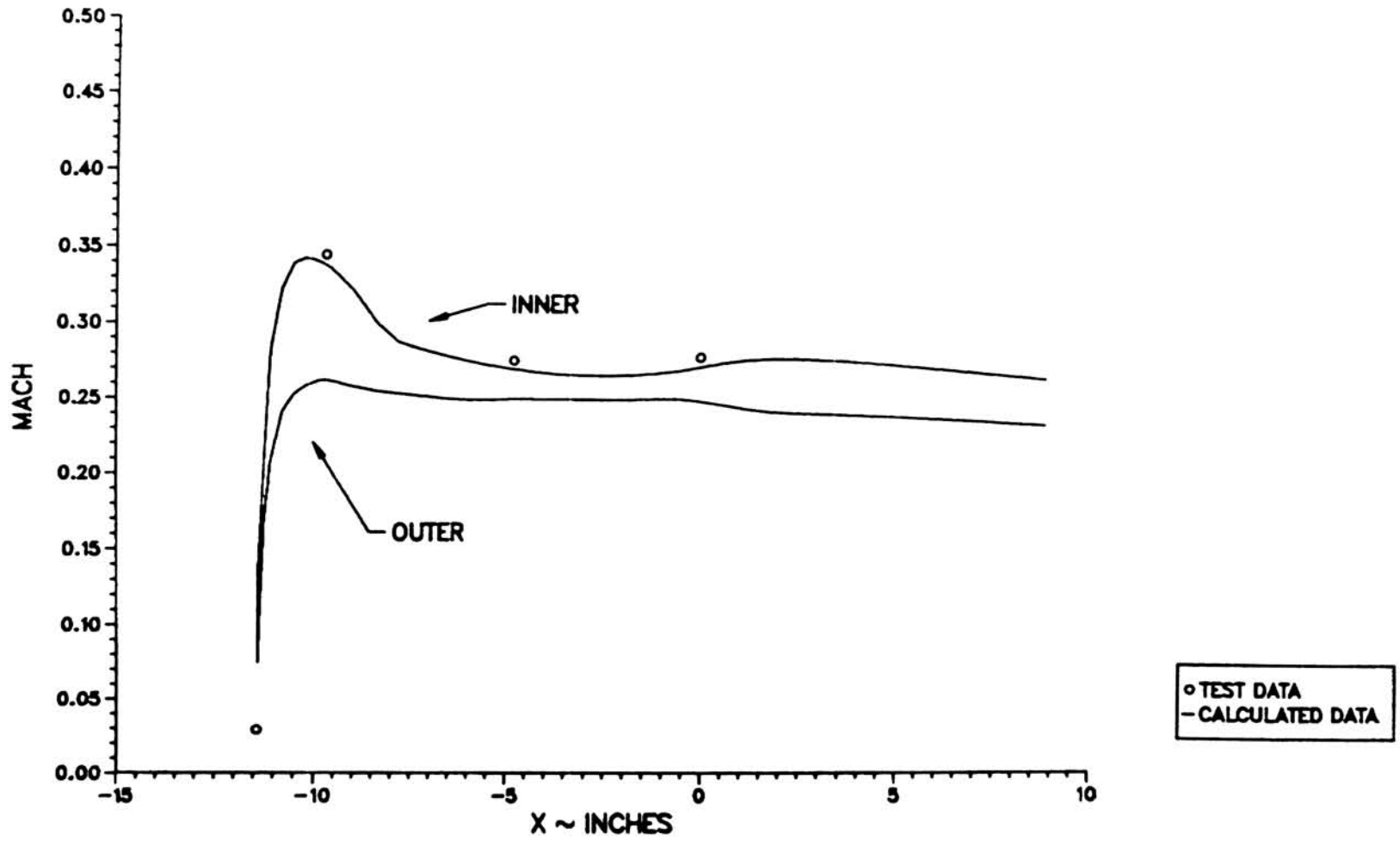

FIGURE 6.10

EXPERIMENTAL AND ANALYTICAL SURFACE MACH NUMBERS FOR BOEING 737-300 INLET (C7) W = 22.96 LBM/SEC, α = 0° (PAGE 24 OF 33).

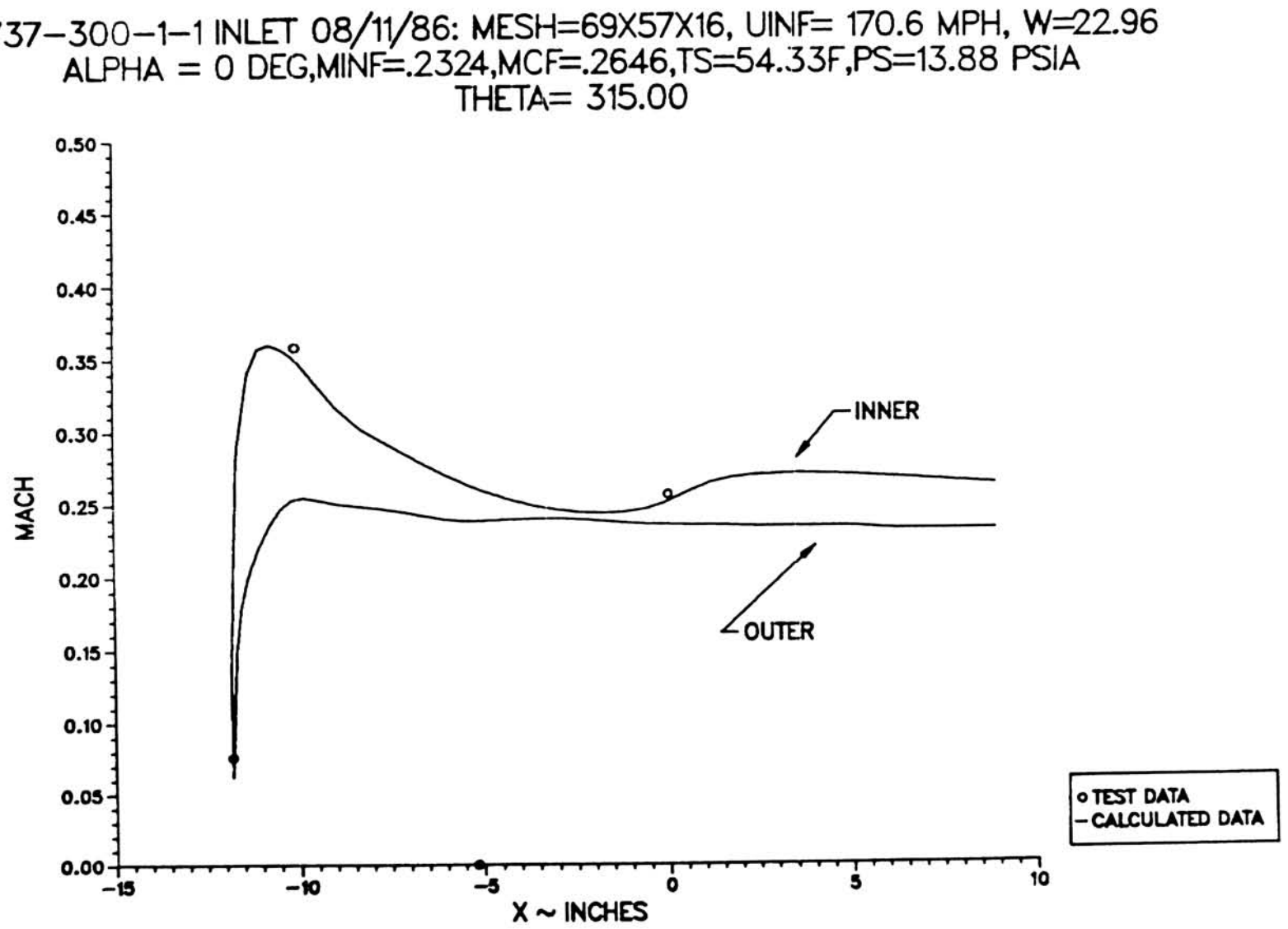

FIGURE 6.10

EXPERIMENTAL AND ANALYTICAL SURFACE MACH NUMBERS FOR BOEING 737-300 INLET (C8) W = 22.96 LBM / SEC, α = 0° (PAGE 25 OF 33).

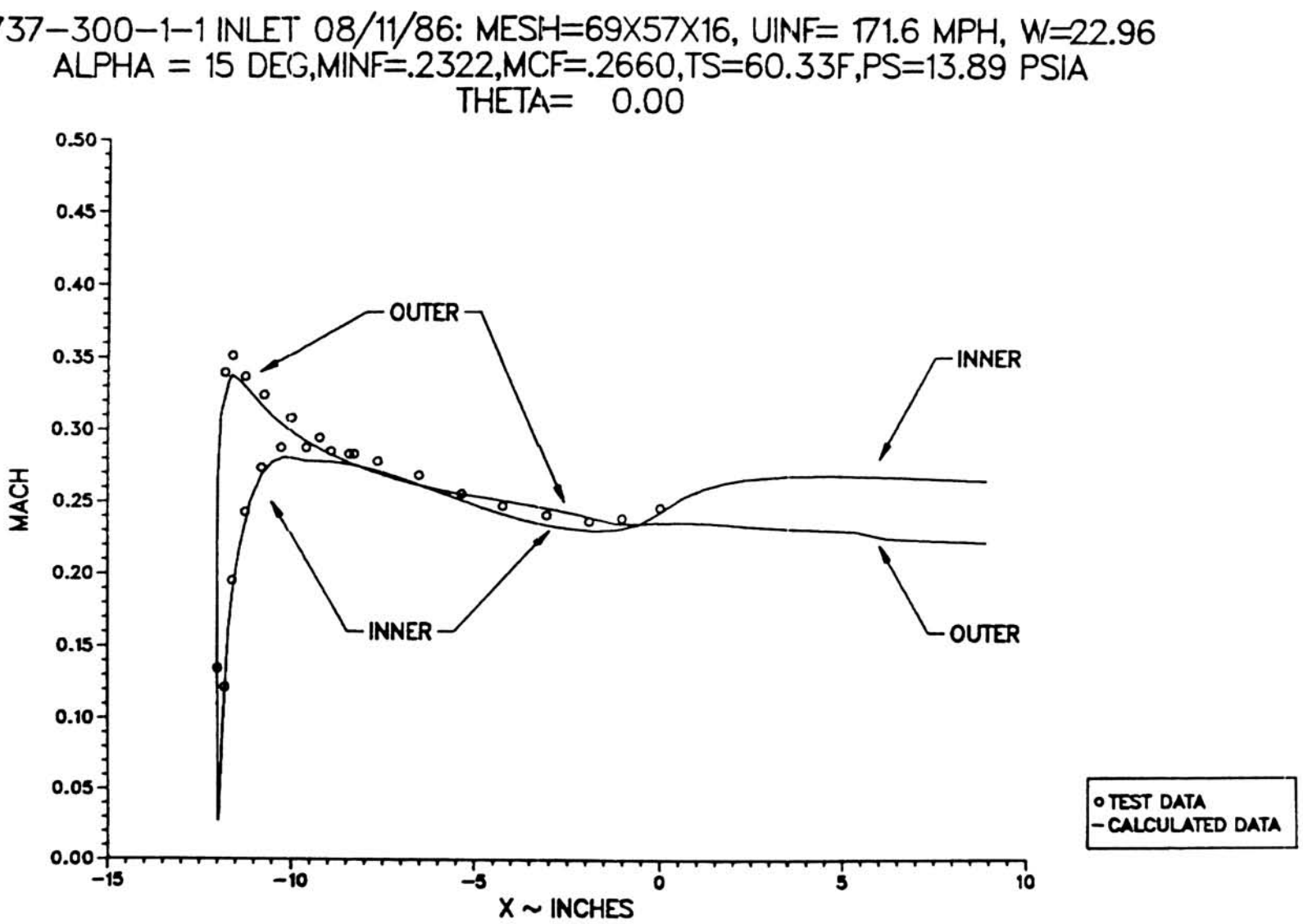

FIGURE 6.10

EXPERIMENTAL AND ANALYTICAL SURFACE MACH NUMBERS FOR BOEING 737-300 INLET (D1) W = 22.96 LBM/SEC, α = 15° (PAGE 26 OF 33).

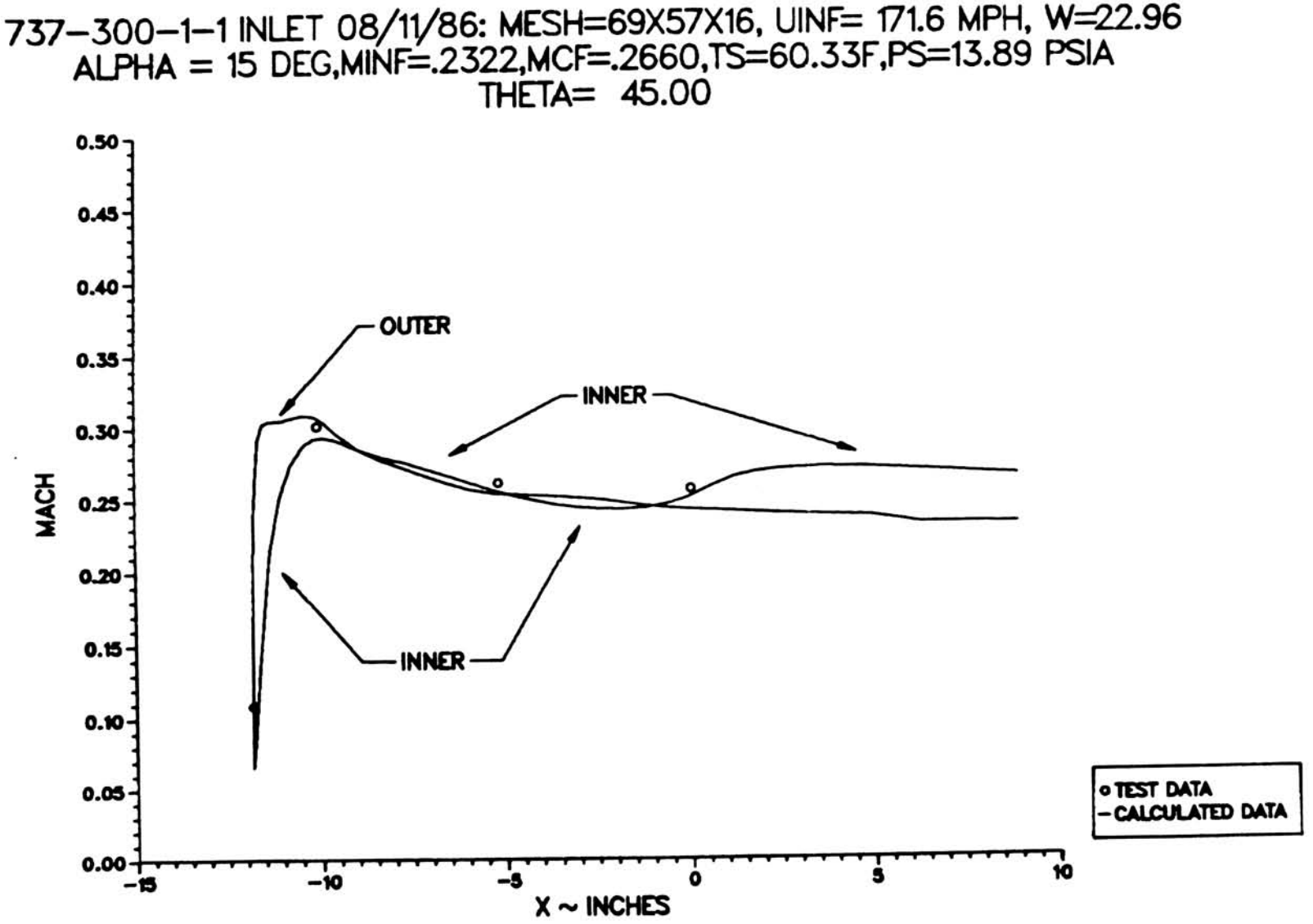

FIGURE 6.10

EXPERIMENTAL AND ANALYTICAL SURFACE MACH NUMBERS FOR BOEING 737-300 INLET (D2) W = 22.96 LBM/SEC, α = 15° (PAGE 27 OF 33).

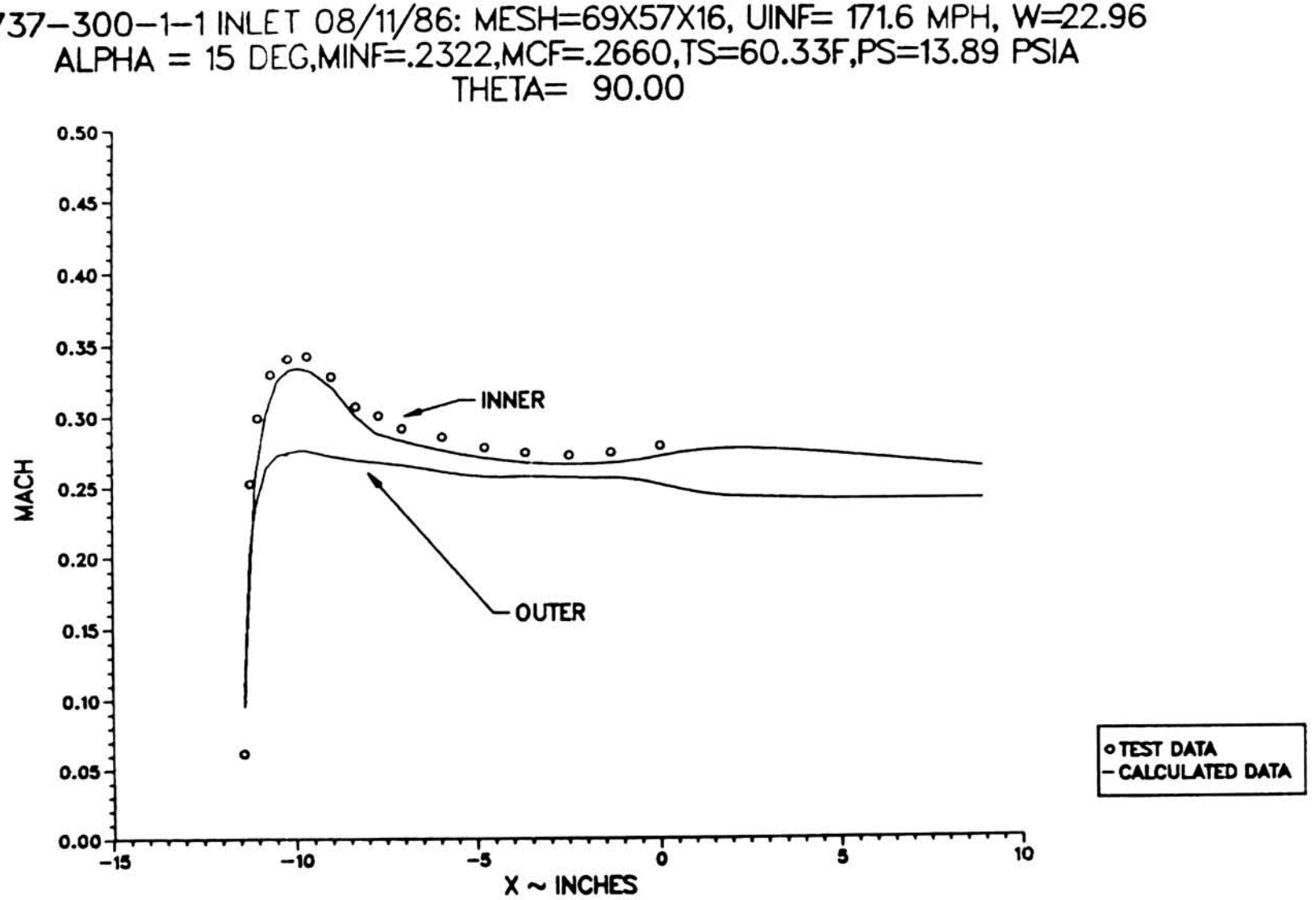

FIGURE 6.10

EXPERIMENTAL AND ANALYTICAL SURFACE MACH NUMBERS FOR BOEING 737-300 INLET (D3) W = 22.96 LBM/SEC, α = 15° (PAGE 28 OF 33).

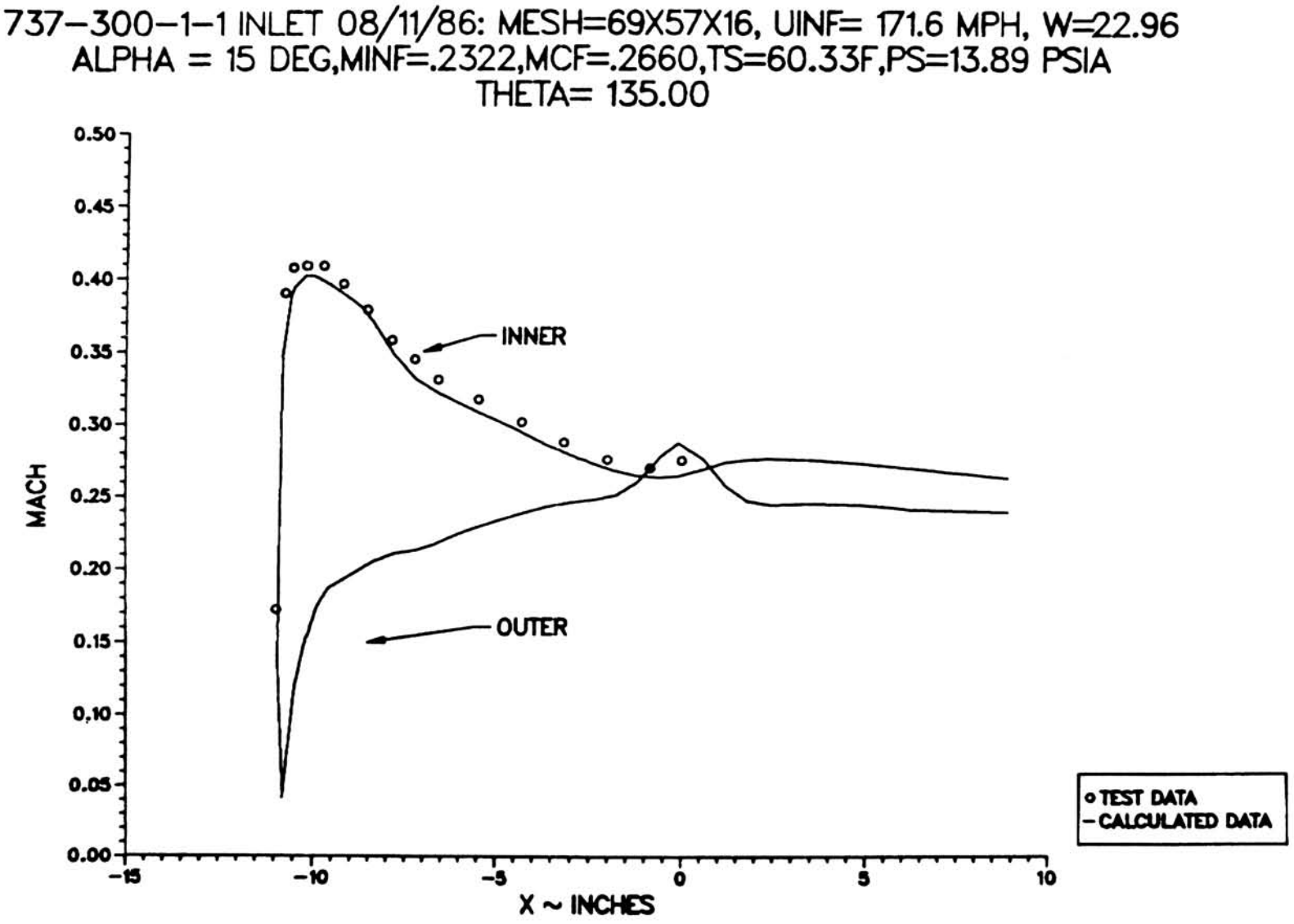

FIGURE 6.10

EXPERIMENTAL AND ANALYTICAL SURFACE MACH NUMBERS FOR BOEING 737-300 INLET (D4) W = 22.96 LBM/SEC, α = 15° (PAGE 29 OF 33).

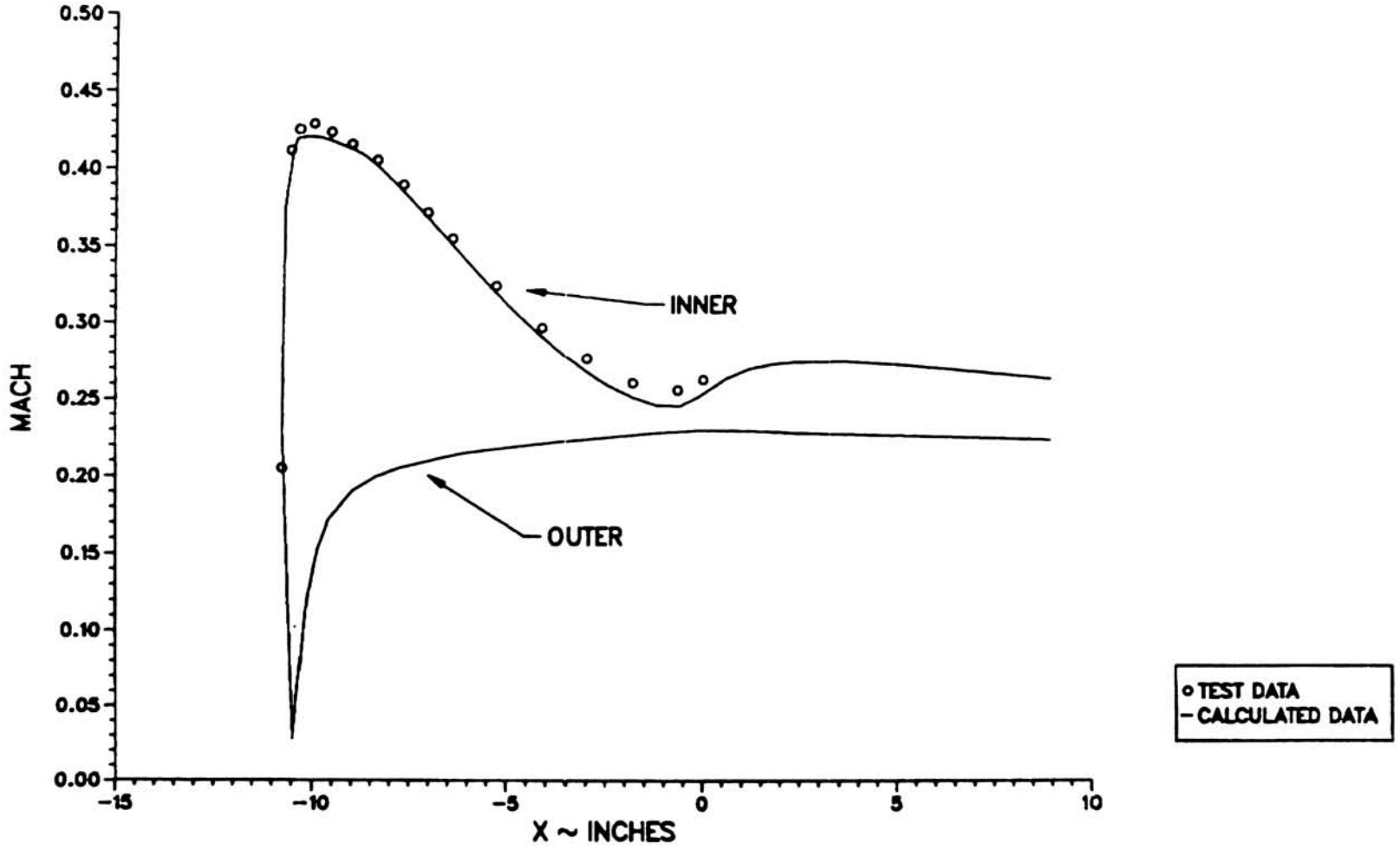

FIGURE 6.10

EXPERIMENTAL AND ANALYTICAL SURFACE MACH NUMBERS FOR BOEING 737-300 INLET (D5) W = 22.96 LBM/SEC, α = 15° (PAGE 30 OF 33).

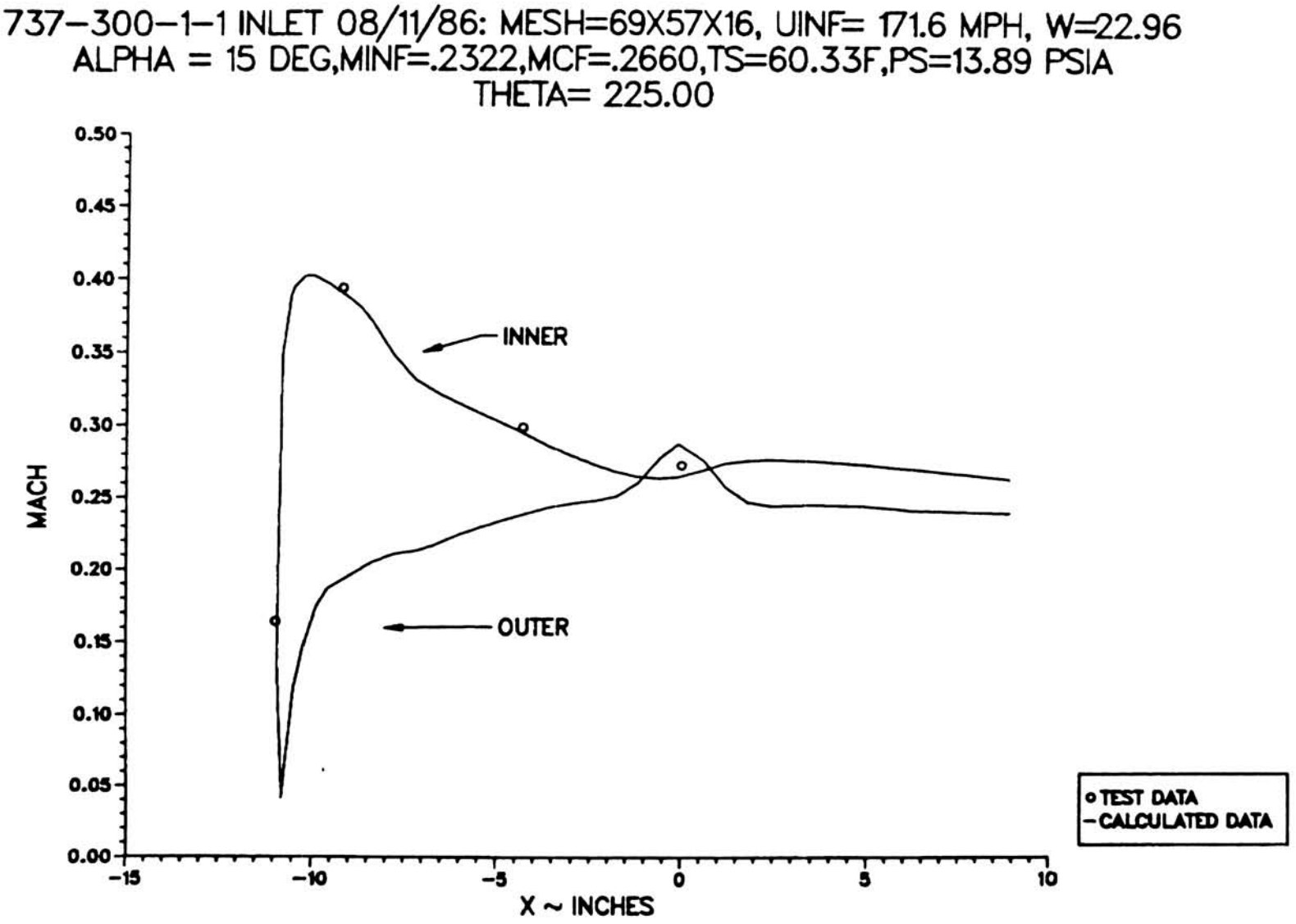

FIGURE 6.10

EXPERIMENTAL AND ANALYTICAL SURFACE MACH NUMBERS FOR BOEING 737-300 INLET (D6) W = 22.96 LBM/SEC, α = 15° (PAGE 31 OF 33).

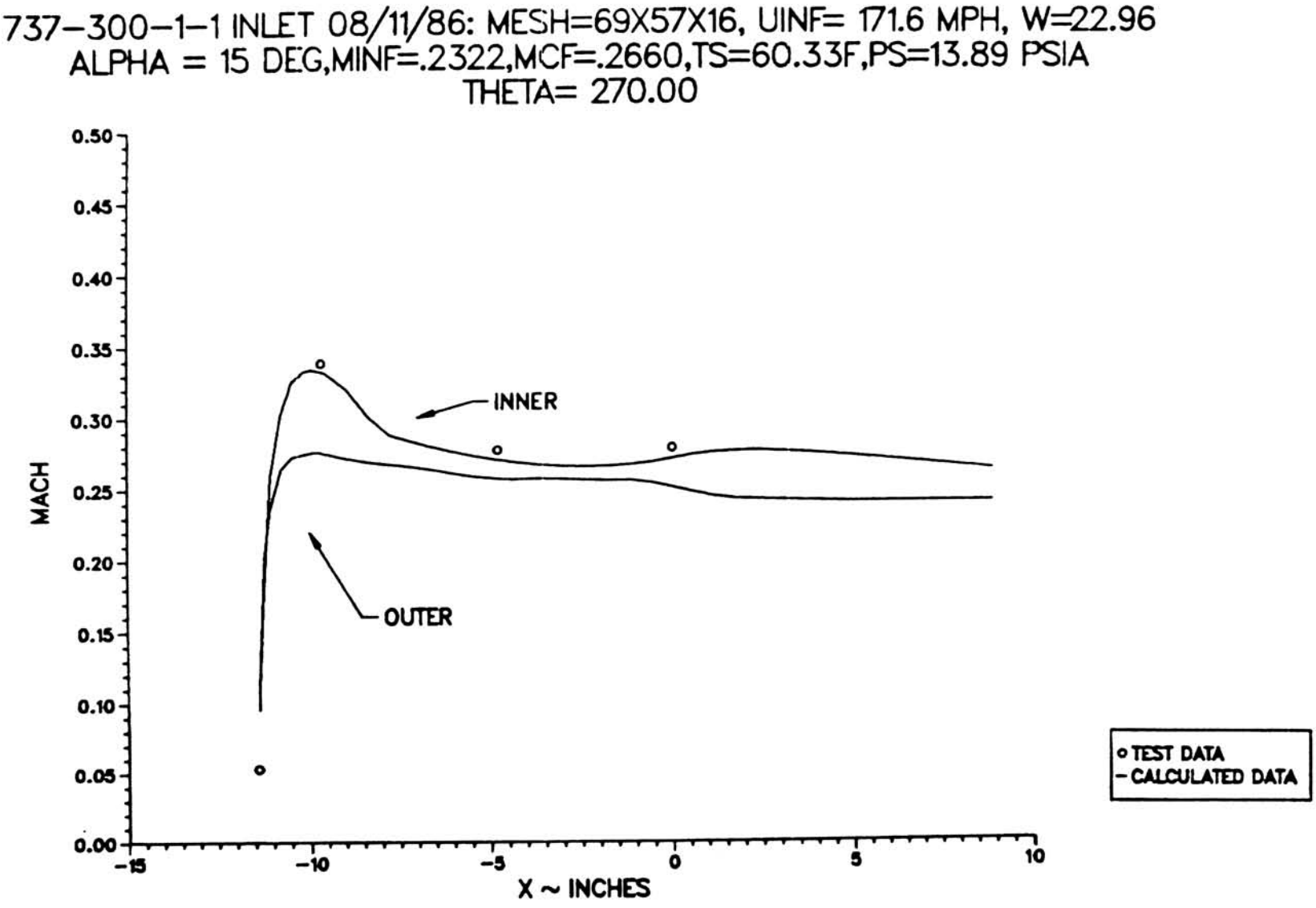

FIGURE 6.10

EXPERIMENTAL AND ANALYTICAL SURFACE MACH NUMBERS FOR BOEING 737-300 INLET (D7) W = 22.96 LBM/SEC, α = 15° (PAGE 32 OF 33).

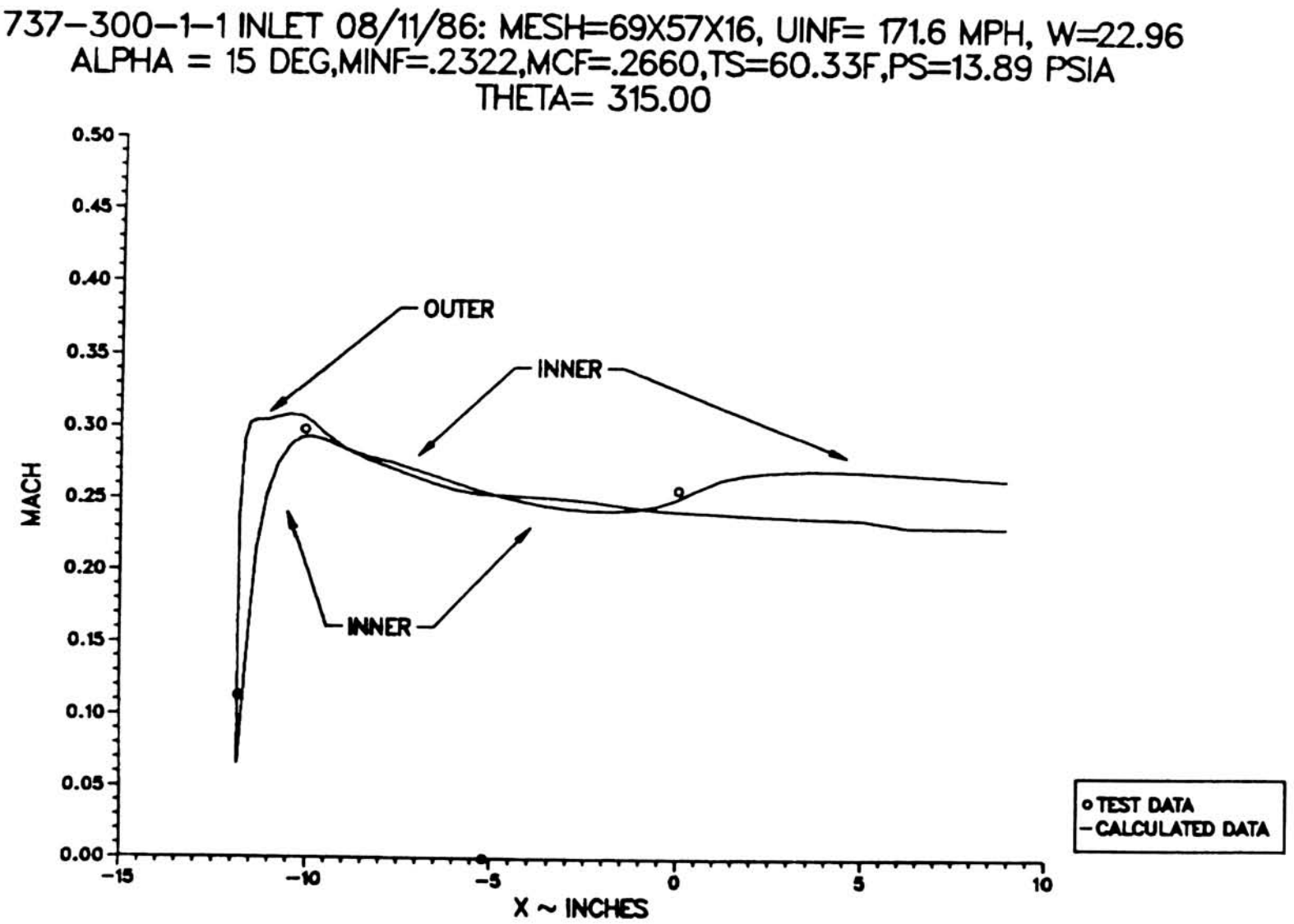

FIGURE 6.10

EXPERIMENTAL AND ANALYTICAL SURFACE MACH NUMBERS FOR BOEING 737-300 INLET (D8) W = 22.96 LBM/SEC, α = 15° (PAGE 33 OF 33).

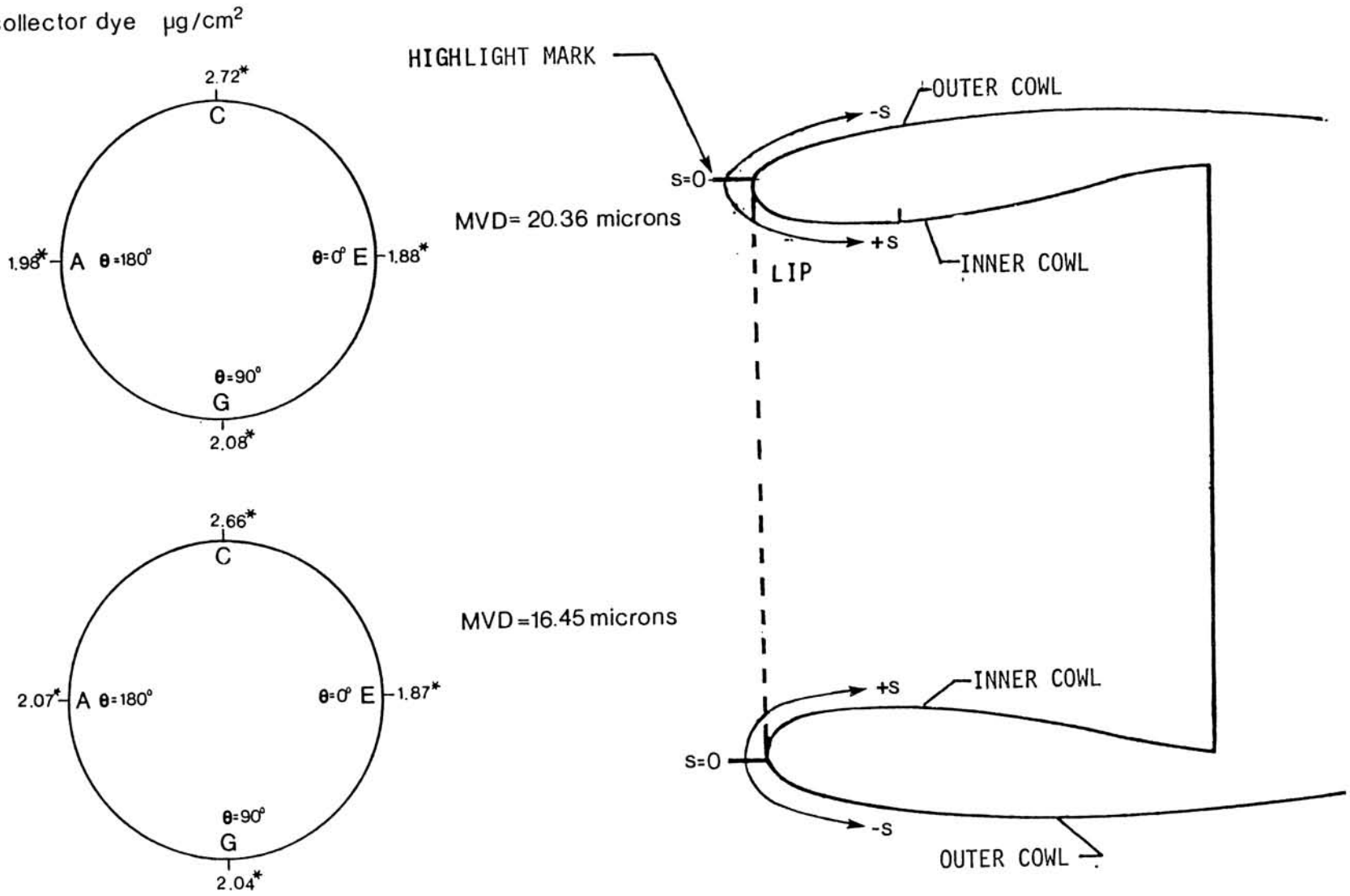

FIGURE 6.11

BLOTTER STRIP LOCATIONS, REFERENCE COLLECTOR DYE MASS, HIGHLIGHT MARK AND SURFACE DISTANCE CONVENTION FOR AXISYMMETRIC INLET AT $\alpha = 0°$.

TEST RUN ID: 092385-22,23AG-AXI-0 AXISYMMETRIC INLET

TRUE AIR SPEED	=	76.86 m/s	(171.92 mph)
TUNNEL TOTAL TEMP	=	11.8 C	(53.2 F)
TUNNEL STATIC PRESSURE	=	94.68 kPa	(13.74 psia)
AIR/WATER PRESSURE RATIO	=	0.80	
COLLECTOR EFFICIENCY	=	0.86	

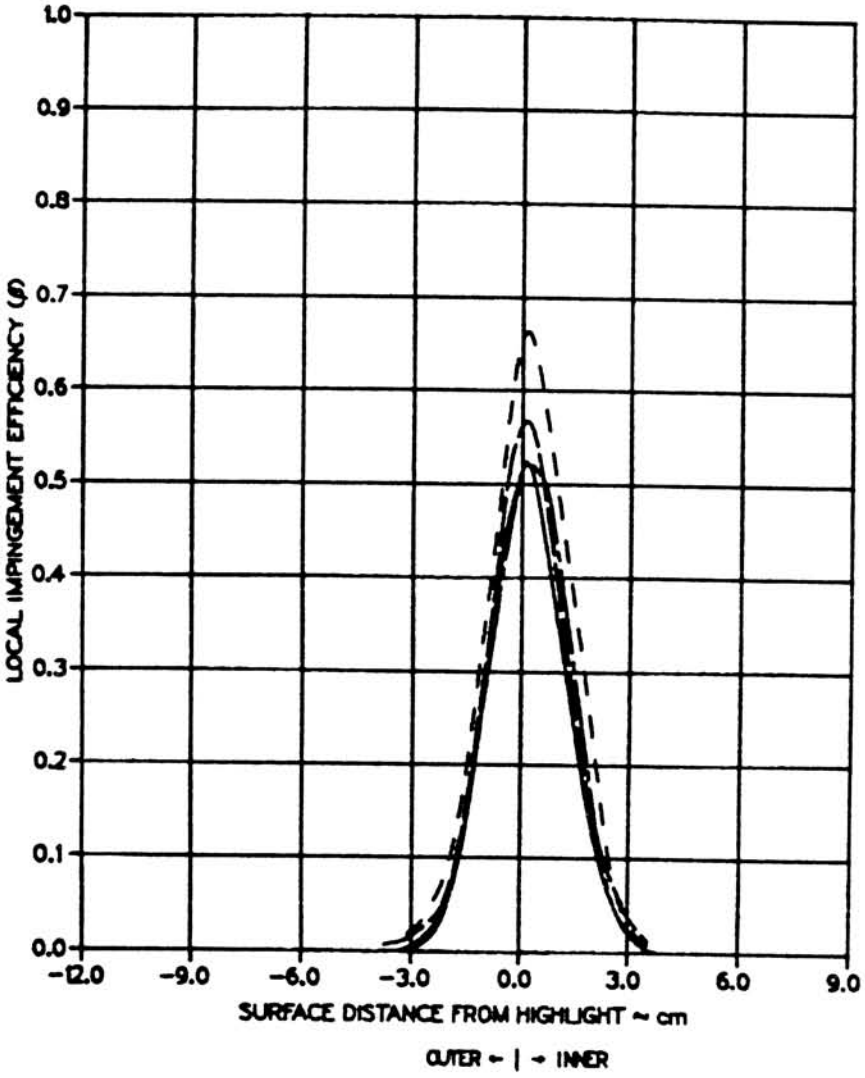

MVD = 16.45 MICRONS

FIGURE 6.12

TEST REPEATABILITY FOR AXISYMMETRIC INLET:
α = 0°, MASS FLOW 17.2 LBM/SEC.

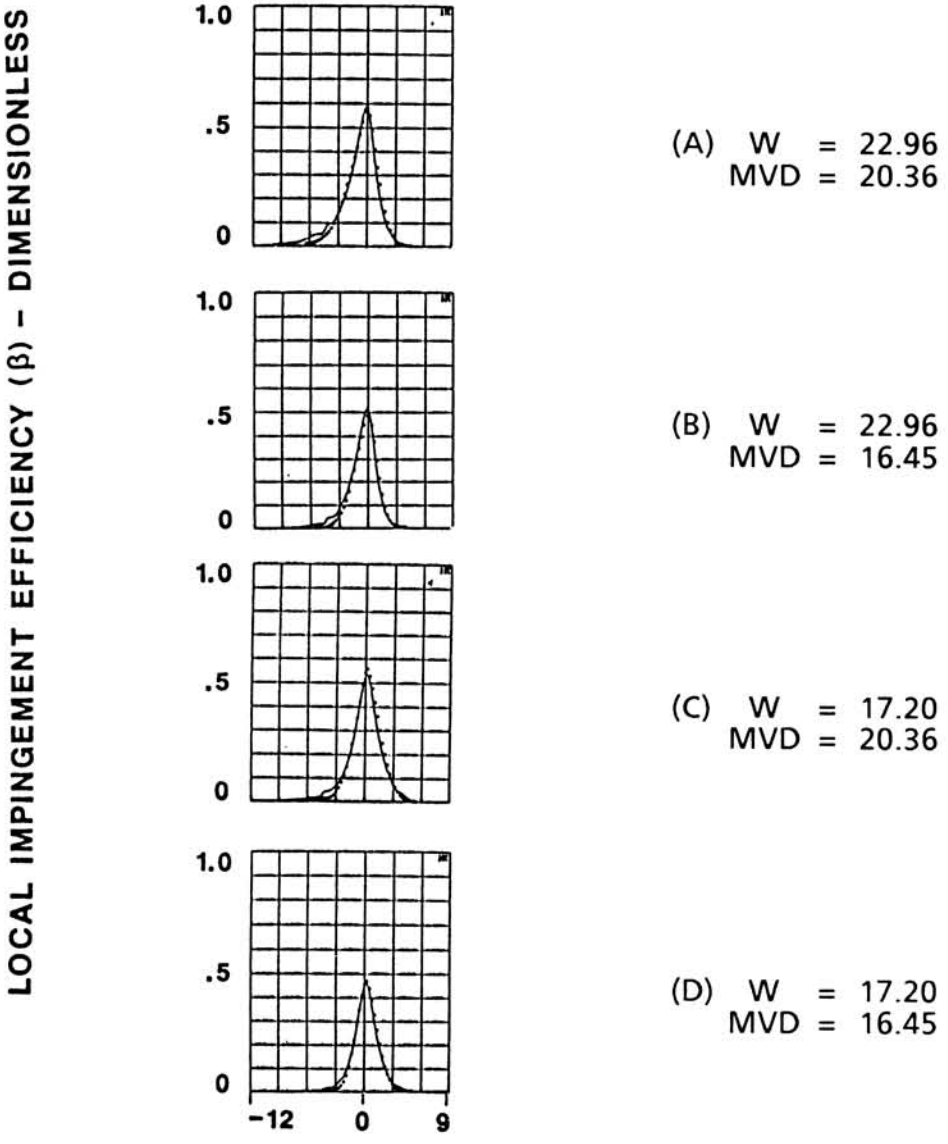

SUMMARY OF RESULTS

FIGURE 6.13

AVERAGED LOCAL WATER IMPINGEMENT EFFICIENCY DATA FOR AXISYMMETRIC INLET AT $\alpha = 0°$ (PAGE 1 OF 5).

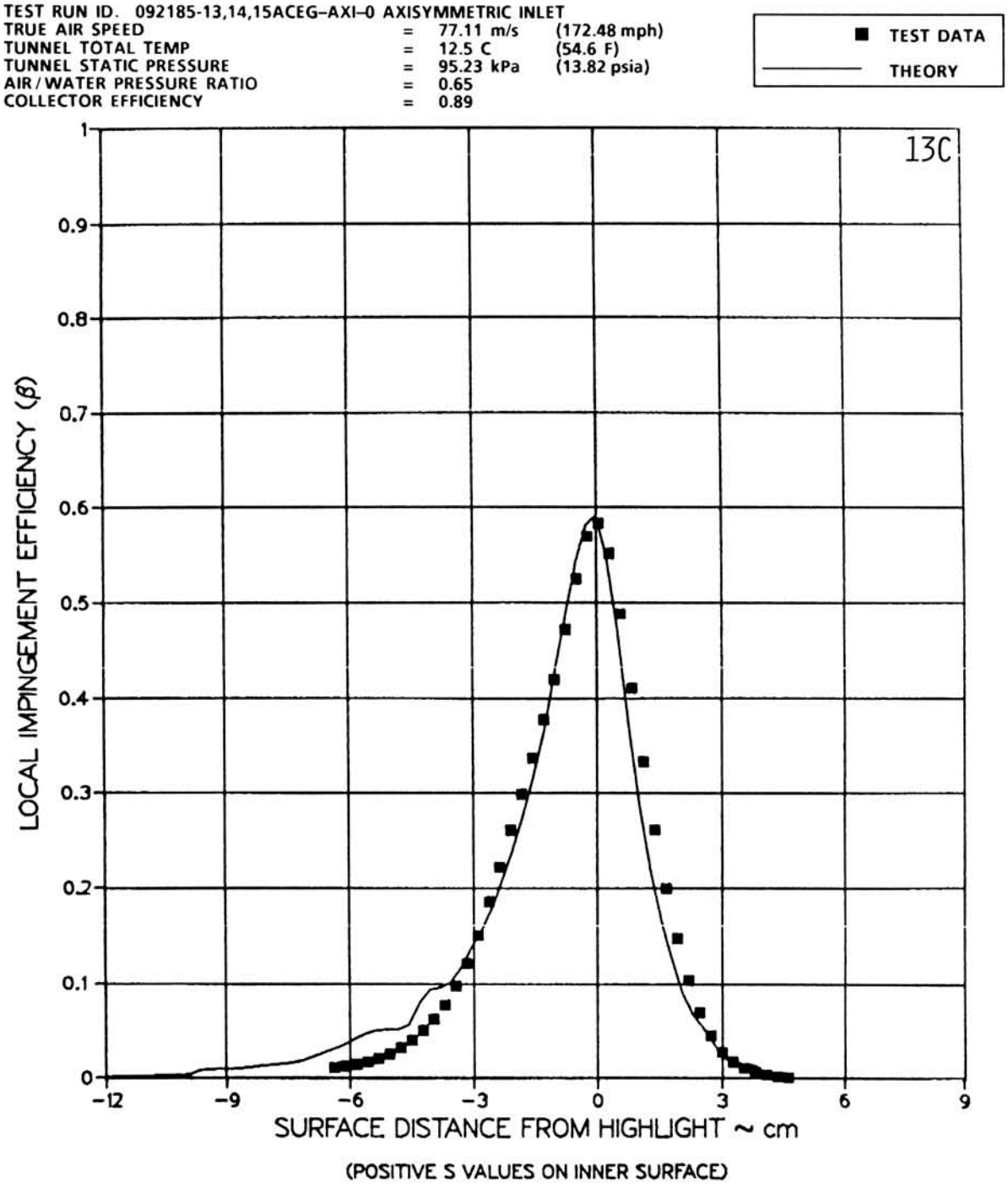

(A) MVD = 20.36 MICRONS, MASS FLOW = 22.96 LBM/SEC

FIGURE 6.13

AVERAGED LOCAL WATER IMPINGEMENT EFFICIENCY DATA FOR AXISYMMETRIC INLET AT $\alpha = 0°$ (PAGE 2 OF 5).

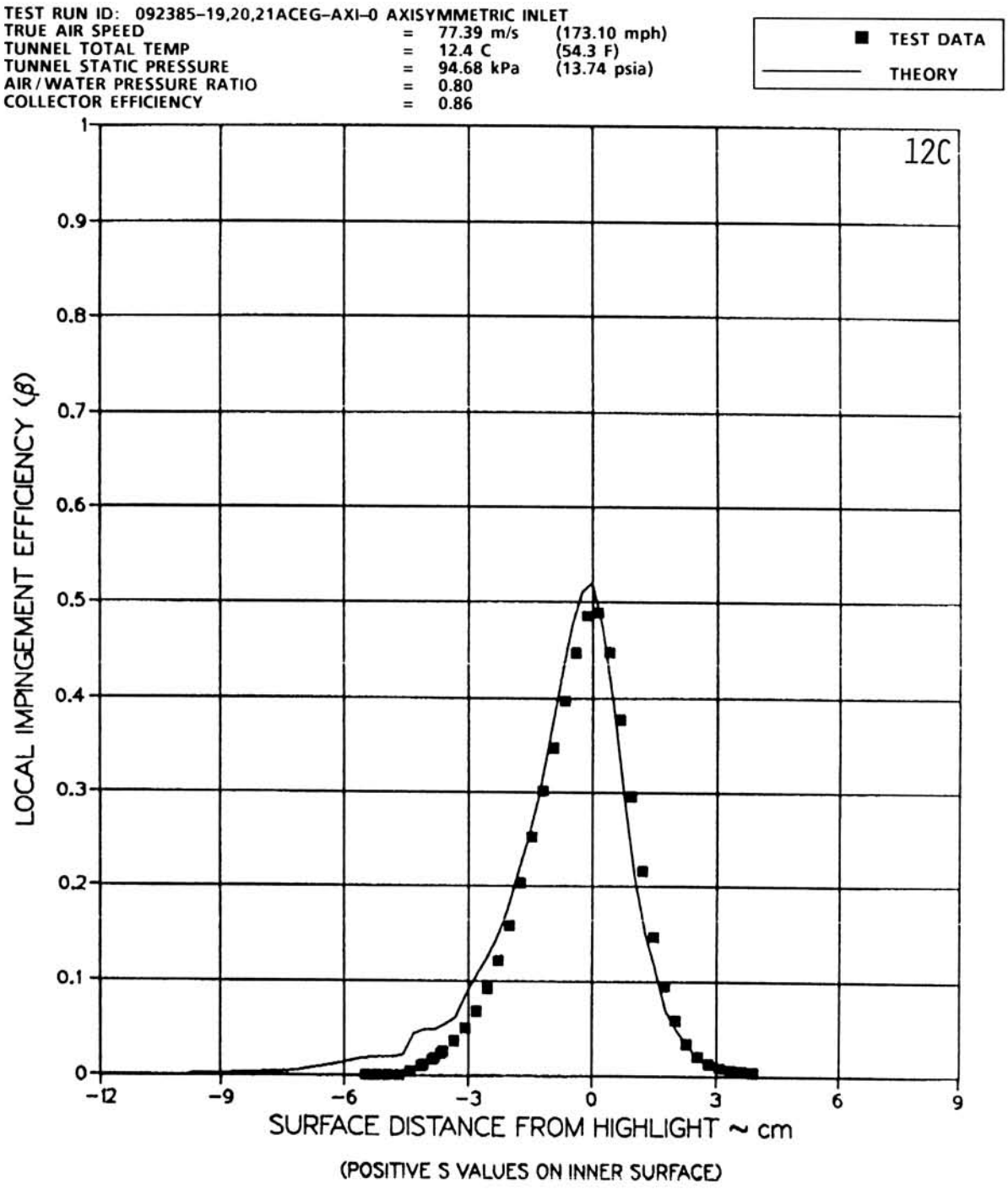

(B) MVD = 16.45 MICRONS, MASS FLOW = 22.96 LBM/SEC

FIGURE 6.13

AVERAGED LOCAL WATER IMPINGEMENT EFFICIENCY DATA FOR AXISYMMETRIC INLET AT $\alpha = 0°$ (PAGE 3 OF 5).

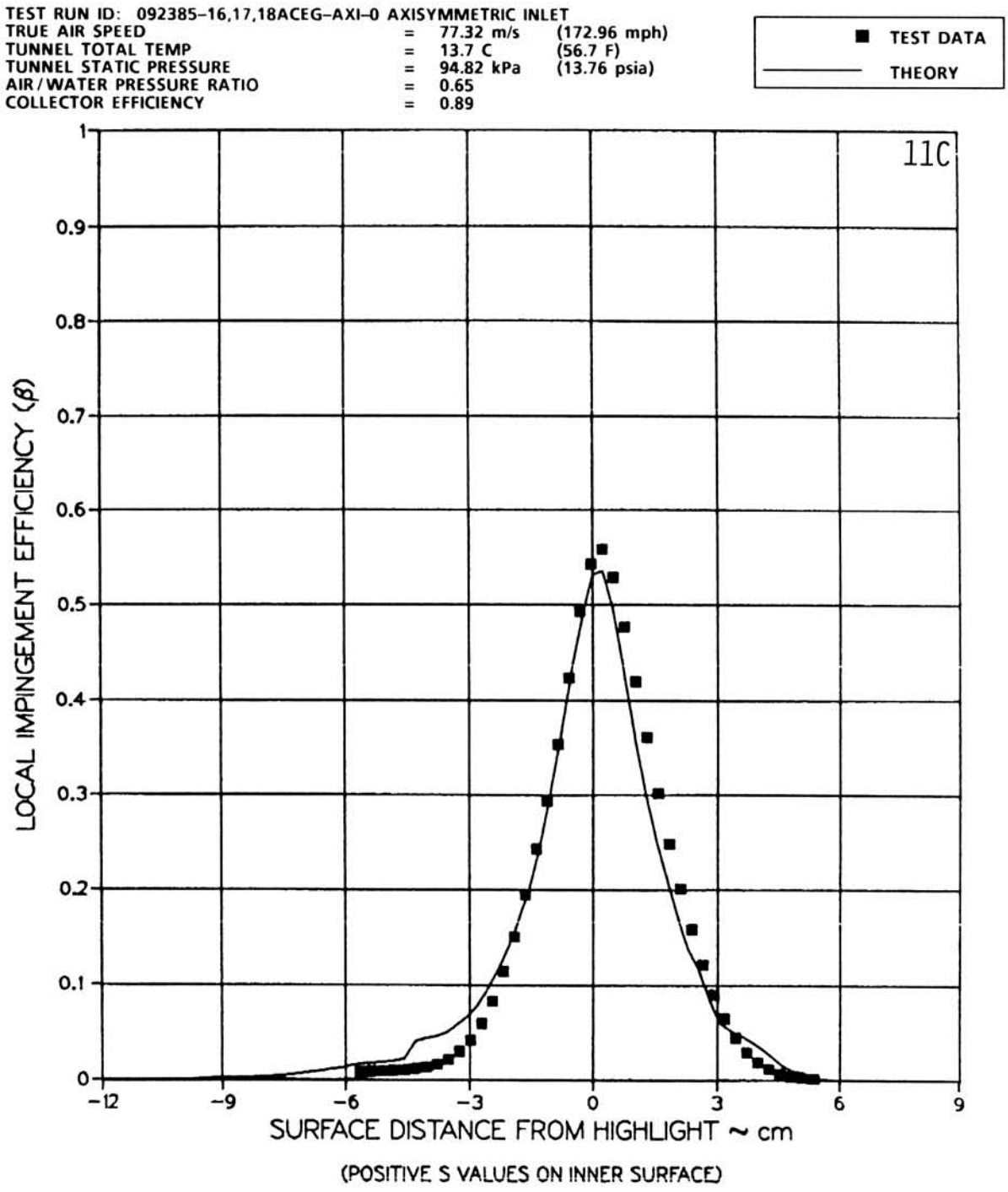

(C) MVD = 20.36 MICRONS, MASS FLOW = 17.20 LBM / SEC

FIGURE 6.13

AVERAGED LOCAL WATER IMPINGEMENT EFFICIENCY DATA FOR AXISYMMETRIC INLET AT $\alpha = 0°$ (PAGE 4 OF 5).

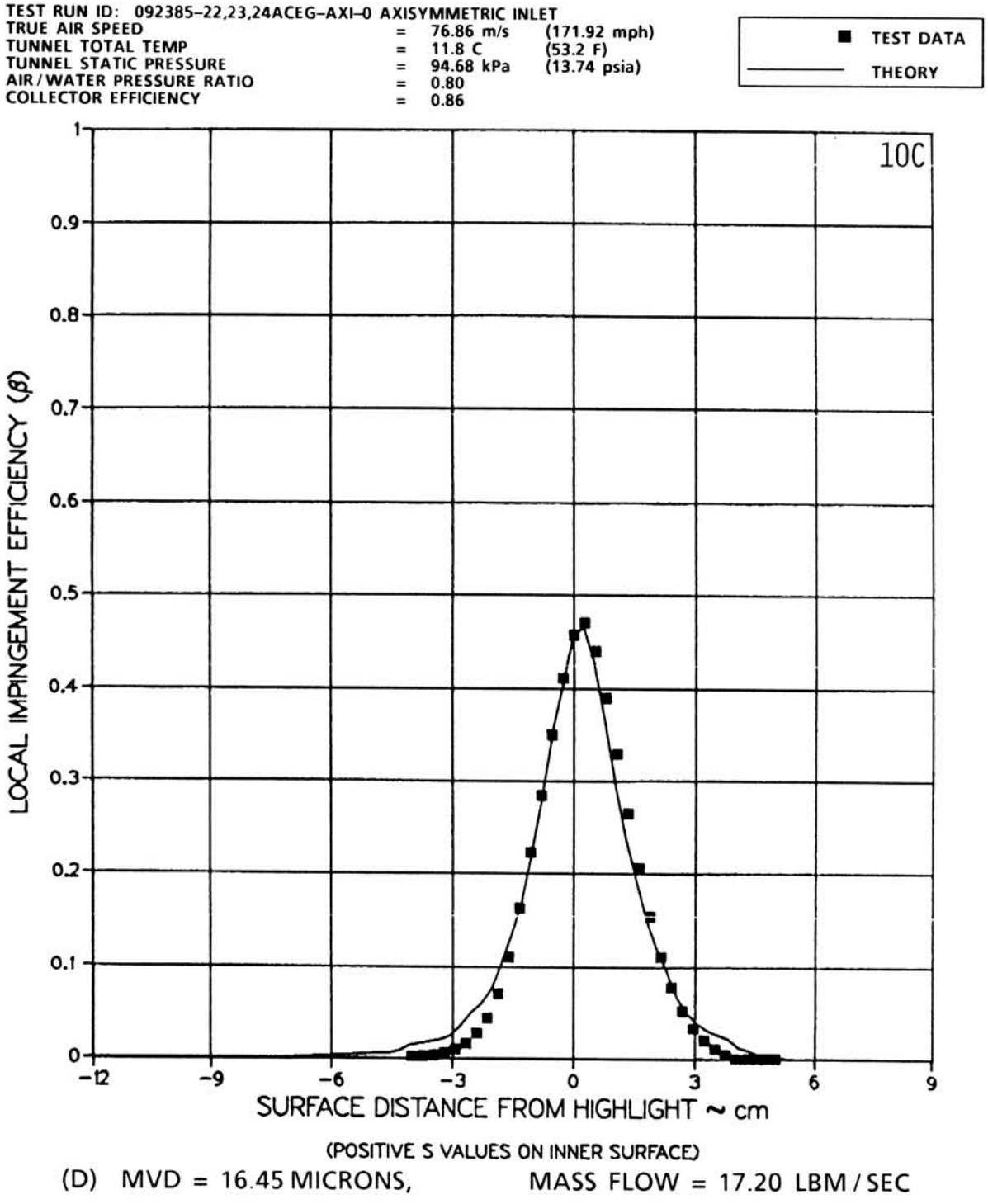

(D) MVD = 16.45 MICRONS, MASS FLOW = 17.20 LBM/SEC

FIGURE 6.13

AVERAGED LOCAL WATER IMPINGEMENT EFFICIENCY DATA FOR AXISYMMETRIC INLET AT $\alpha = 0°$ (PAGE 5 OF 5).

* COLLECTOR DYE $\mu g/cm^2$

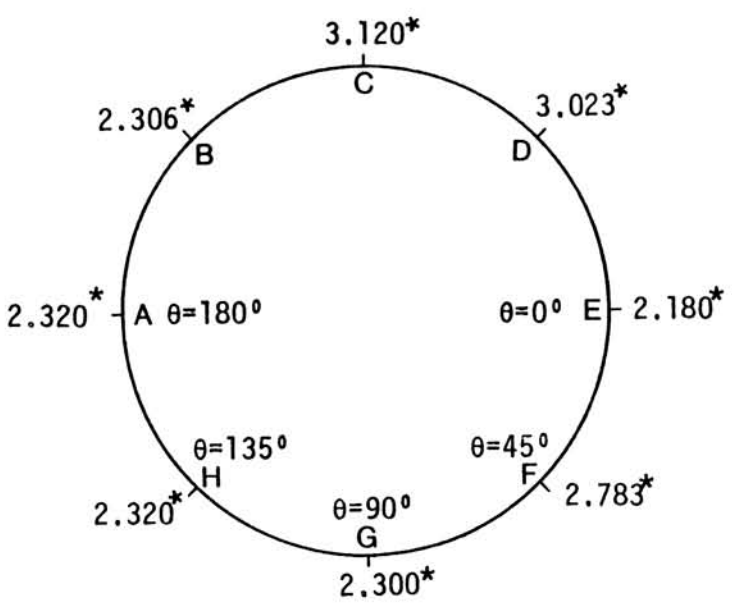

MVD = 20.36 microns

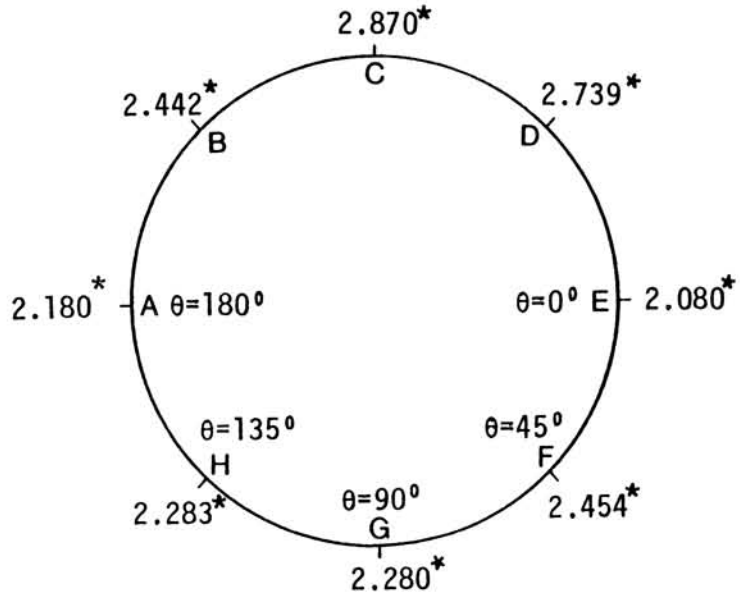

MVD = 16.45 microns

FIGURE 6.14

BLOTTER STRIP LOCATIONS AND REFERENCE COLLECTOR DYE MASS FOR AXISYMMETRIC INLET AT $\alpha = 15°$.

TEST RUN ID: 092185-7,9E-AXI-15 AXISYMMETRIC INLET

TRUE AIR SPEED	=	76.45 m/s	(171.00 mph)
TUNNEL TOTAL TEMP	=	11.7 C	(53.1 F)
TUNNEL STATIC PRESSURE	=	95.44 kPa	(13.85 psia)
AIR/WATER PRESSURE RATIO	=	0.80	
COLLECTOR EFFICIENCY	=	0,86	

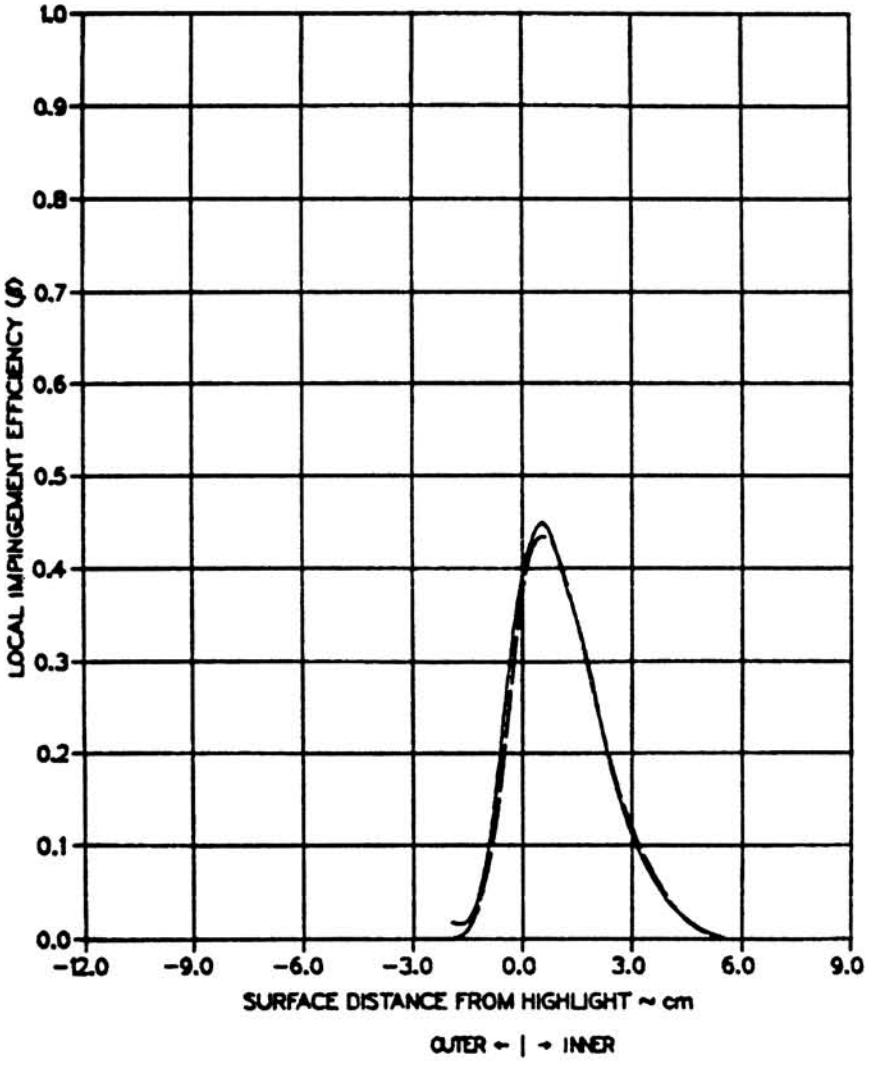

MVD = 16.45 MICRONS $\theta = 0°$

FIGURE 6.15

TEST REPEATABILITY FOR AXISYMMETRIC INLET:
$\alpha = 15°$, MASS FLOW = 22.96 LBM/SEC (PAGE 1 OF 3).

TEST RUN ID: 092185-7,9CG-AXI-15 AXISYMMETRIC INLET

TRUE AIR SPEED	=	76.45 m/s	(171.00 mph)
TUNNEL TOTAL TEMP	=	11.7 C	(53.1 F)
TUNNEL STATIC PRESSURE	=	95.44 kPa	(13.85 psia)
AIR/WATER PRESSURE RATIO	=	0.80	
COLLECTOR EFFICIENCY	=	0,86	

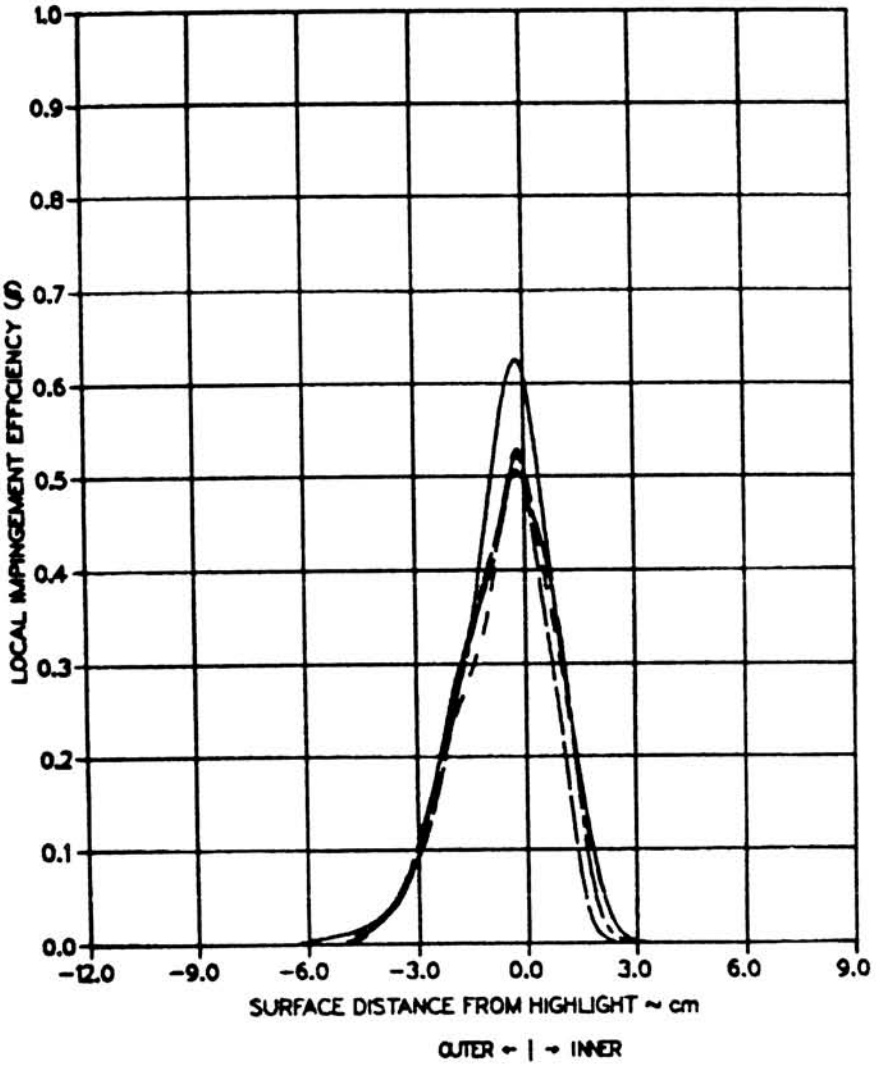

MVD = 16.45 MICRONS θ = 90°, 270°

FIGURE 6.15

TEST REPEATABILITY FOR AXISYMMETRIC INLET:
α = 15°, MASS FLOW = 22.96 LBM/SEC (PAGE 2 OF 3)

TEST RUN ID: 092185-7,9A-AXI-15 AXISYMMETRIC INLET

TRUE AIR SPEED	=	76.45 m/s	(171.00 mph)
TUNNEL TOTAL TEMP	=	11.7 C	(53.1 F)
TUNNEL STATIC PRESSURE	=	95.44 kPa	(13.85 psia)
AIR/WATER PRESSURE RATIO	=	0.80	
COLLECTOR EFFICIENCY	=	0,86	

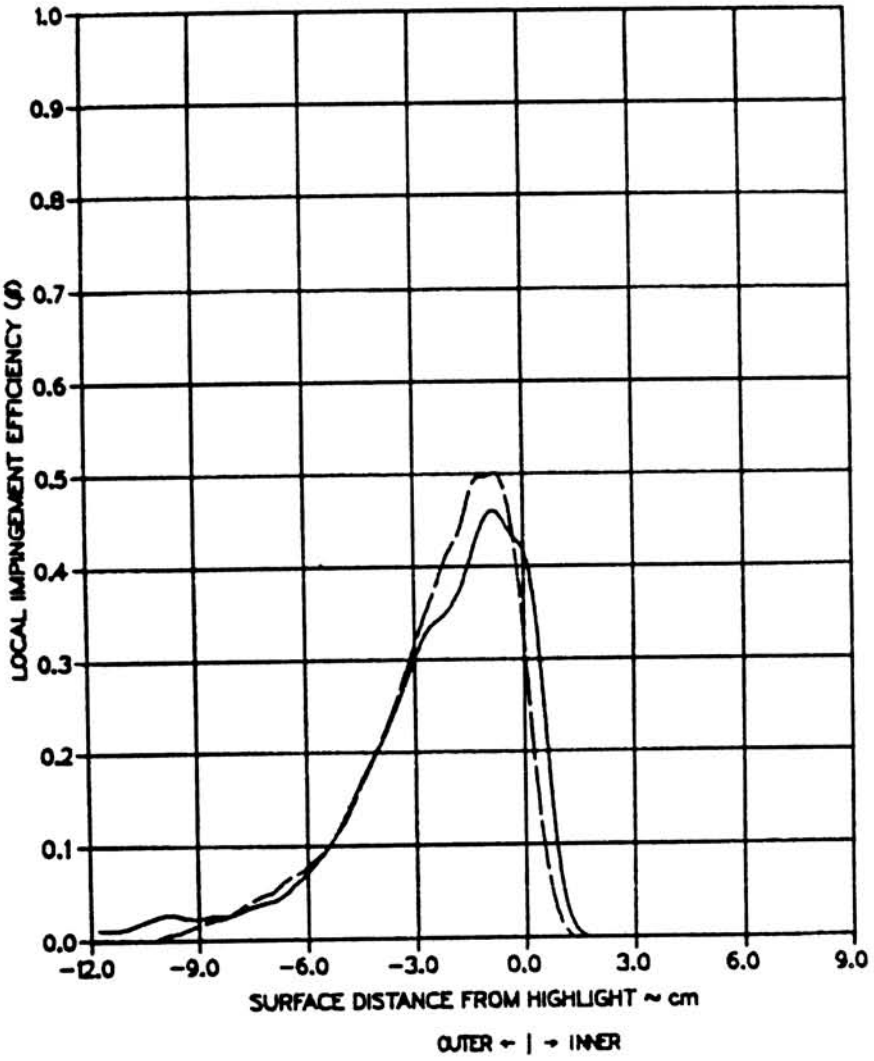

MVD = 16.45 MICRONS θ = 180°

FIGURE 6.15

TEST REPEATABILITY FOR AXISYMMETRIC INLET:
α = 15°, MASS FLOW = 22.96 LBM/SEC (PAGE 3 OF 3)

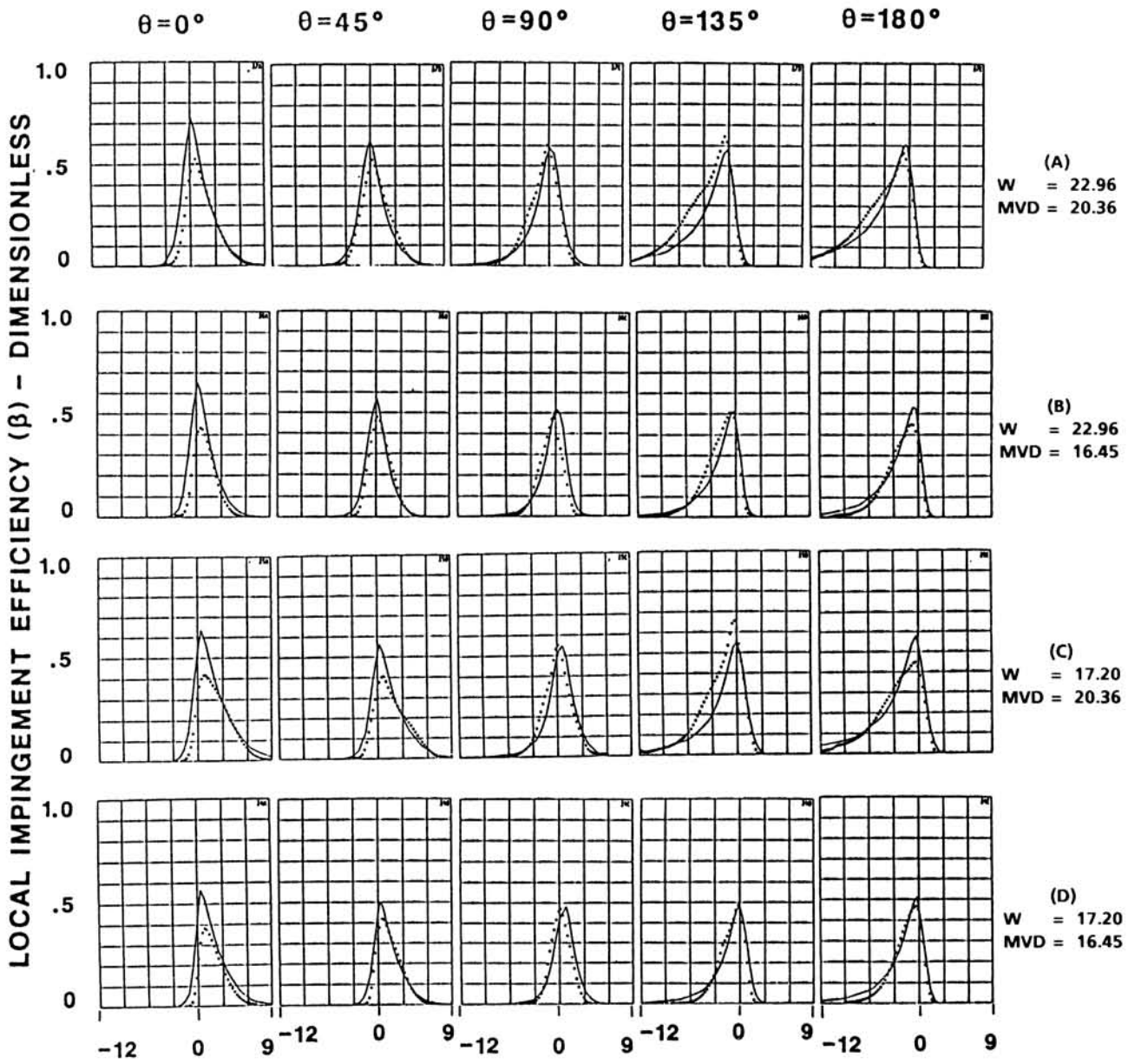

NOTE: W ~ LBM / SEC, MVD ~ μm
NEGATIVE SURFACE DISTANCE – OUTER SURFACE
POSITIVE SURFACE DISTANCE – INNER SURFACE

■ TEST DATA
——— THEORY

SUMMARY OF RESULTS

FIGURE 6.16

AVERAGED LOCAL WATER IMPINGEMENT EFFICIENCY DATA FOR AXISYMMETRIC INLET AT α = 15° (PAGE 1 OF 21).

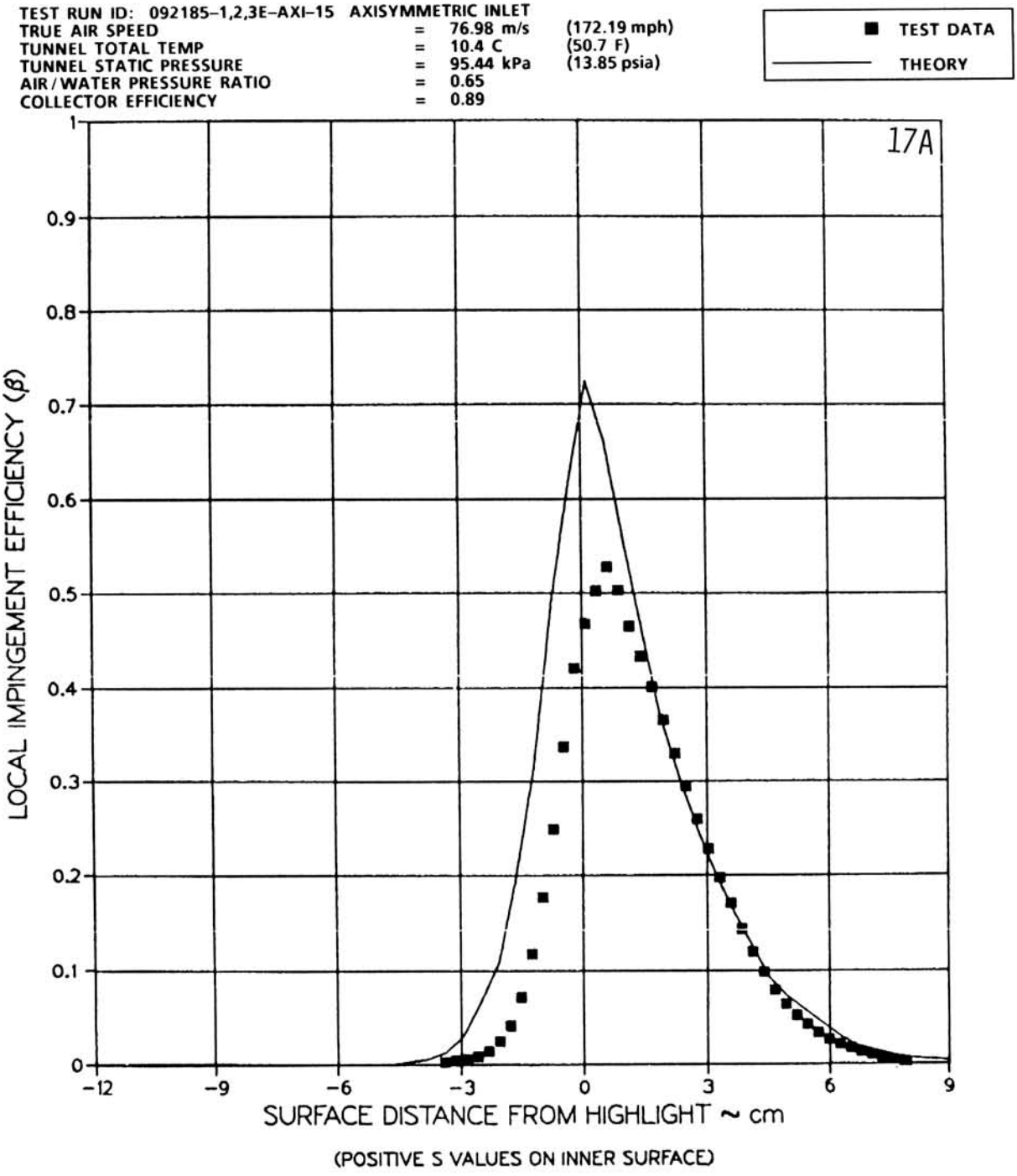

(A1) MVD = 20.36 MICRONS, MASS FLOW = 22.96 LBM/SEC, $\theta = 0°$

FIGURE 6.16

AVERAGED LOCAL WATER IMPINGEMENT EFFICIENCY DATA FOR AXISYMMETRIC INLET AT $\alpha = 15°$ (PAGE 2 OF 21).

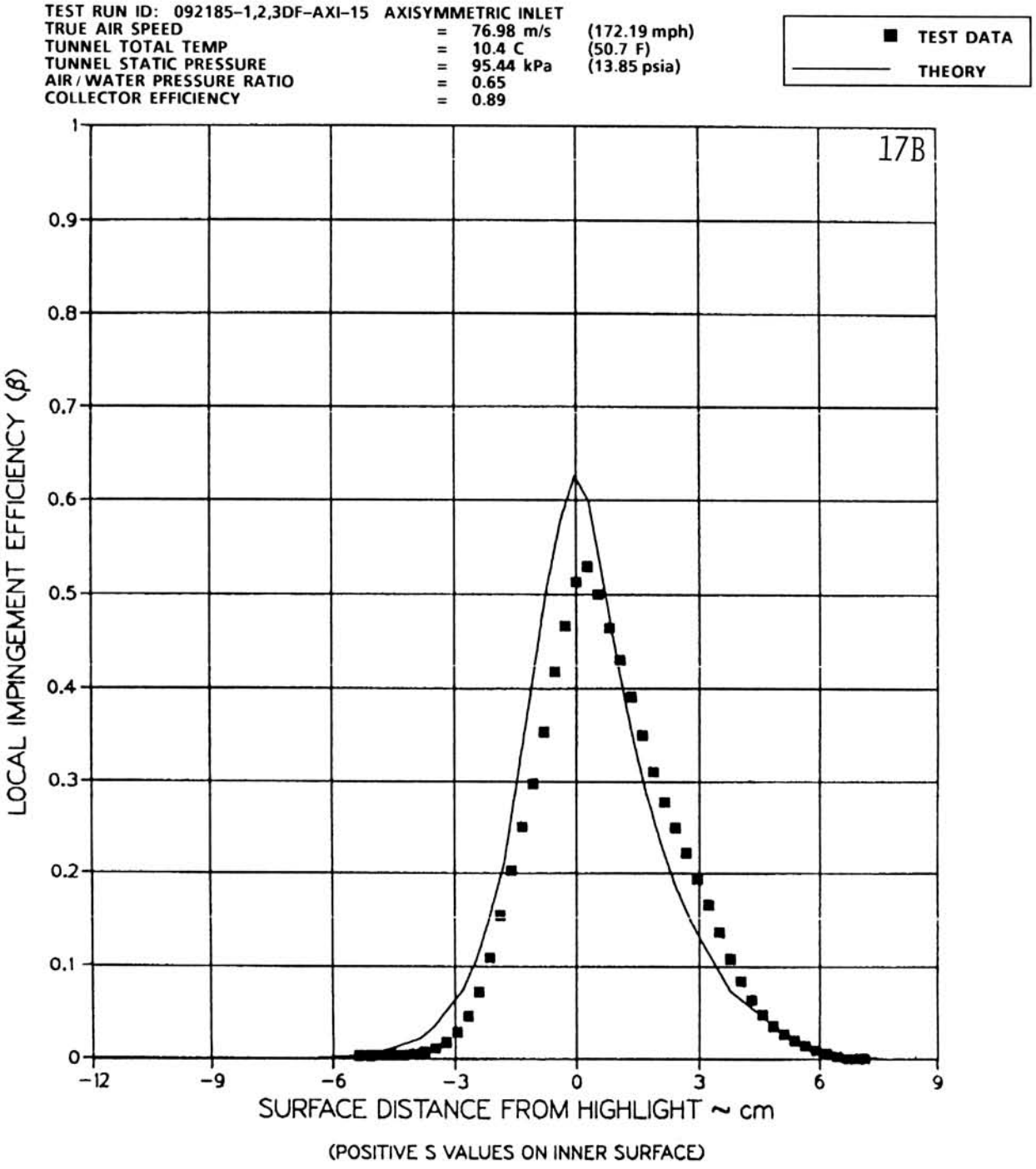

(A2) MVD = 20.36 MICRONS, MASS FLOW = 22.96 LBM / SEC, θ = 45°

FIGURE 6.16

AVERAGED LOCAL WATER IMPINGEMENT EFFICIENCY DATA FOR AXISYMMETRIC INLET AT α = 15° (PAGE 3 OF 21).

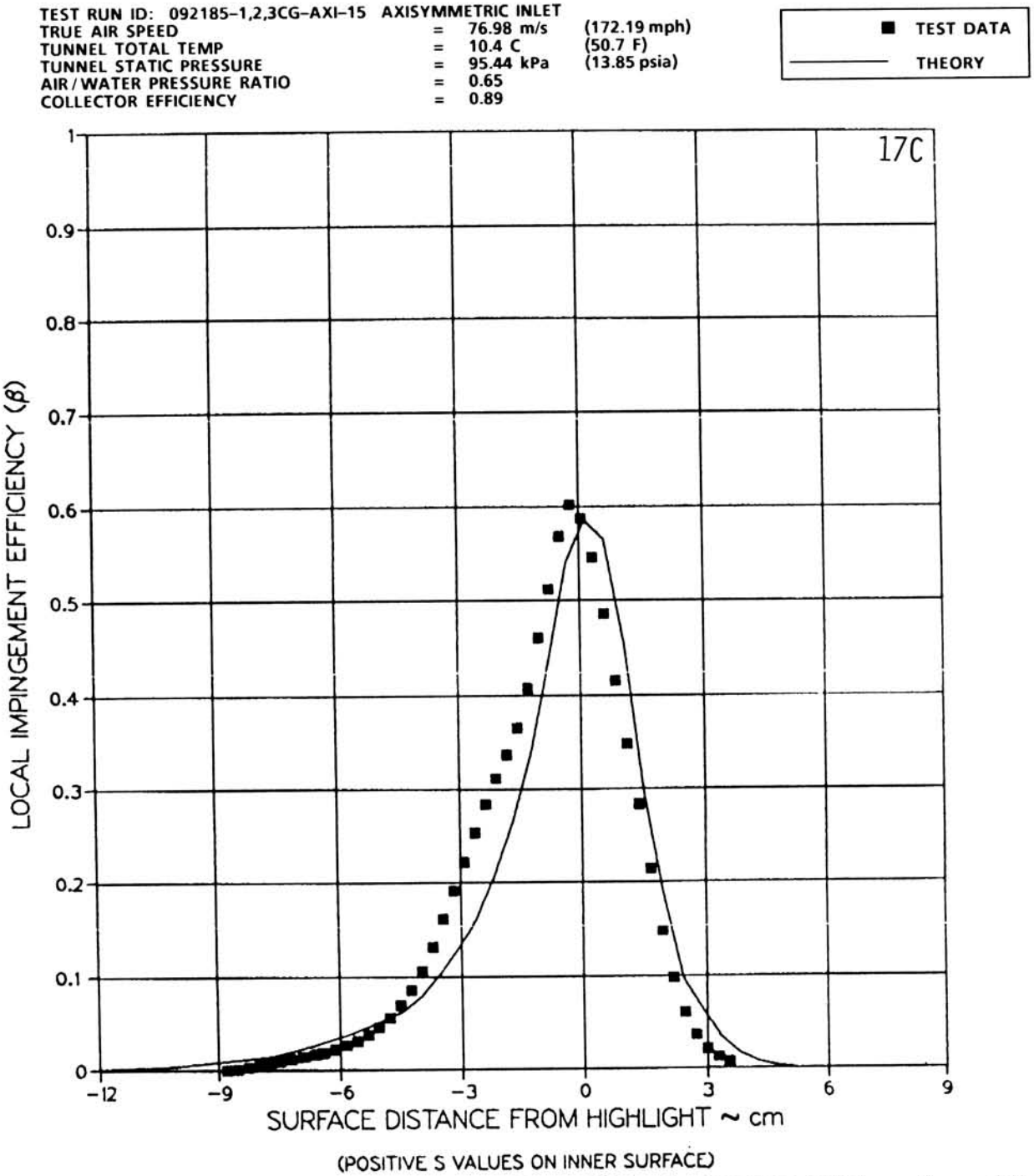

(A3) MVD = 20.36 MICRONS, MASS FLOW = 22.96 LBM/SEC, θ = 90°

FIGURE 6.16

AVERAGED LOCAL WATER IMPINGEMENT EFFICIENCY DATA FOR AXISYMMETRIC INLET AT α = 15° (PAGE 4 OF 21).

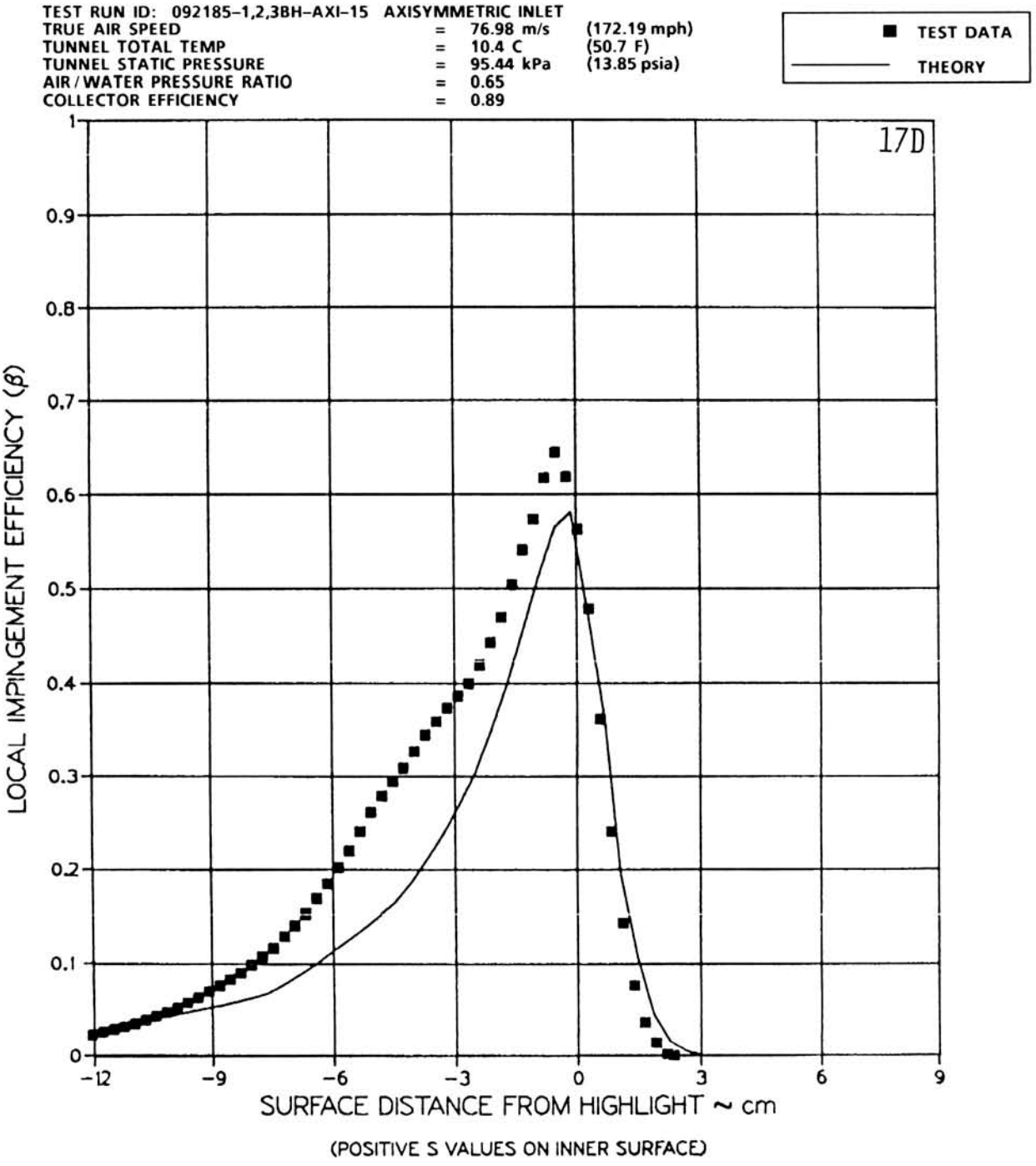

(A4) MVD = 20.36 MICRONS, MASS FLOW = 22.96 LBM / SEC, θ = 135°

FIGURE 6.16

AVERAGED LOCAL WATER IMPINGEMENT EFFICIENCY DATA FOR AXISYMMETRIC INLET AT α = 15° (PAGE 5 OF 21).

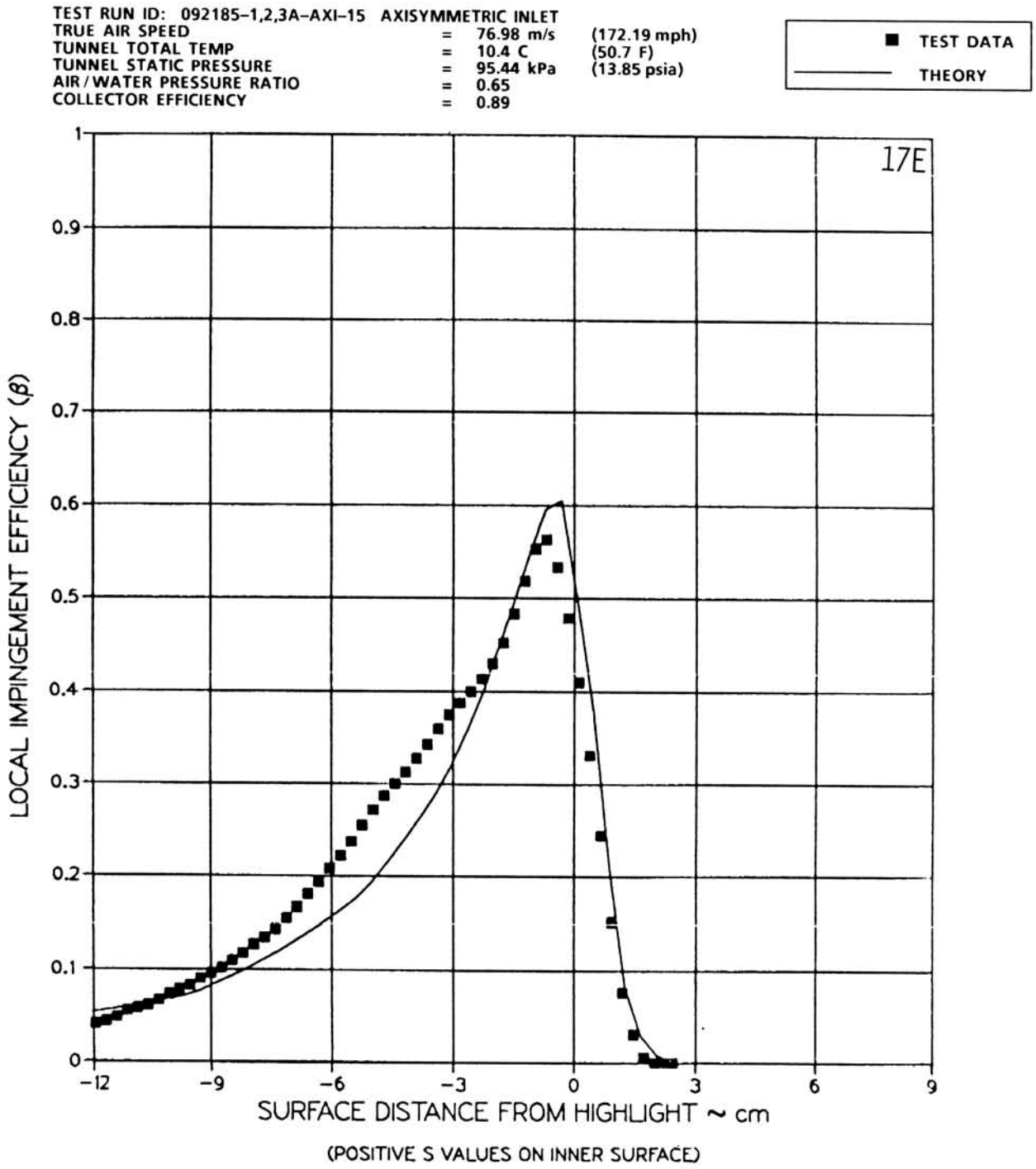

(A5) MVD = 20.36 MICRONS, MASS FLOW = 22.96 LBM/SEC, θ = 180°

FIGURE 6.16

AVERAGED LOCAL WATER IMPINGEMENT EFFICIENCY DATA FOR AXISYMMETRIC INLET AT α = 15° (PAGE 6 OF 21).

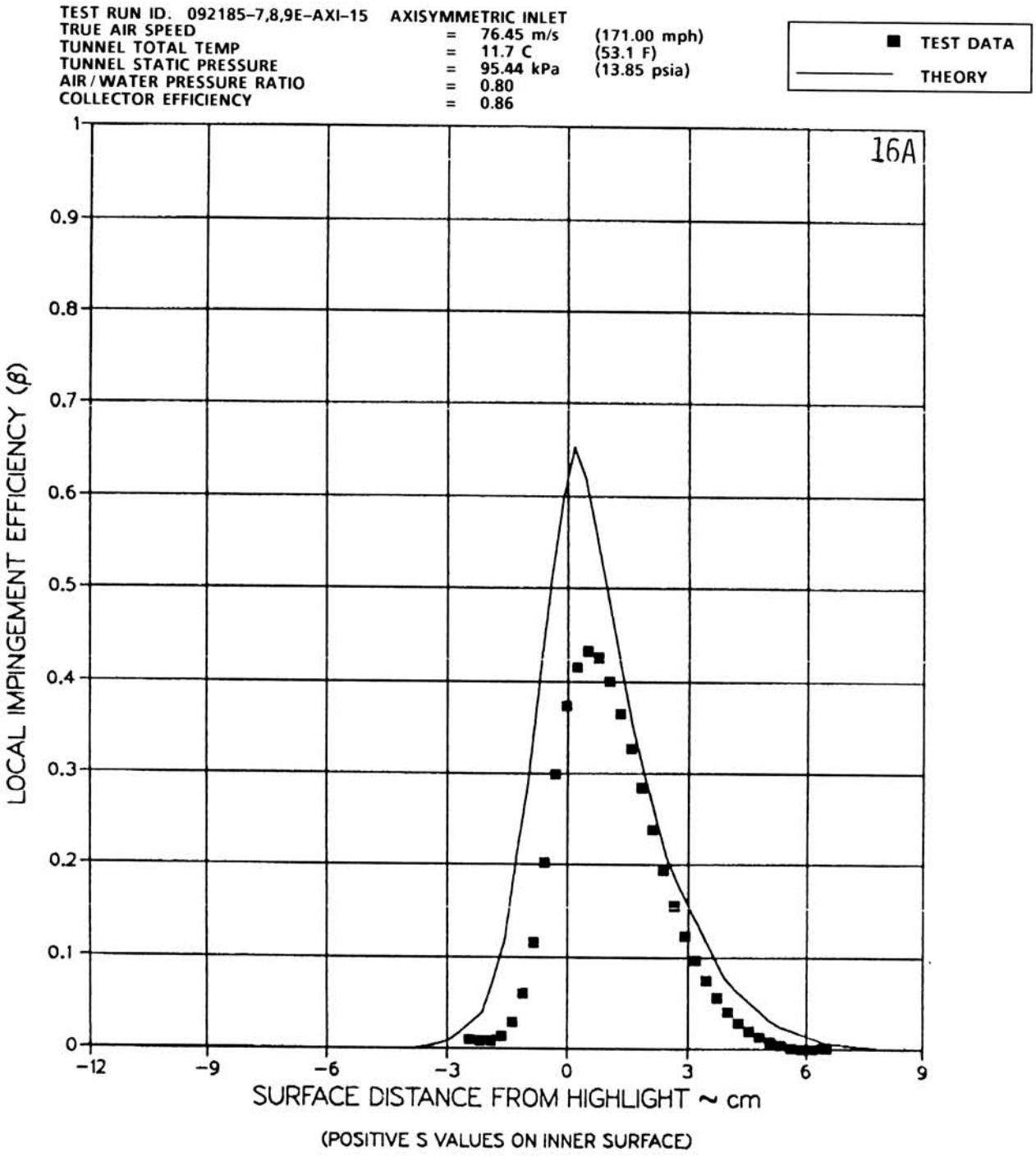

(B1) MVD = 16.45 MICRONS, MASS FLOW = 22.96 LBM/SEC, $\theta = 0°$

FIGURE 6.16

AVERAGED LOCAL WATER IMPINGEMENT EFFICIENCY DATA FOR AXISYMMETRIC INLET AT $\alpha = 15°$ (PAGE 7 OF 21).

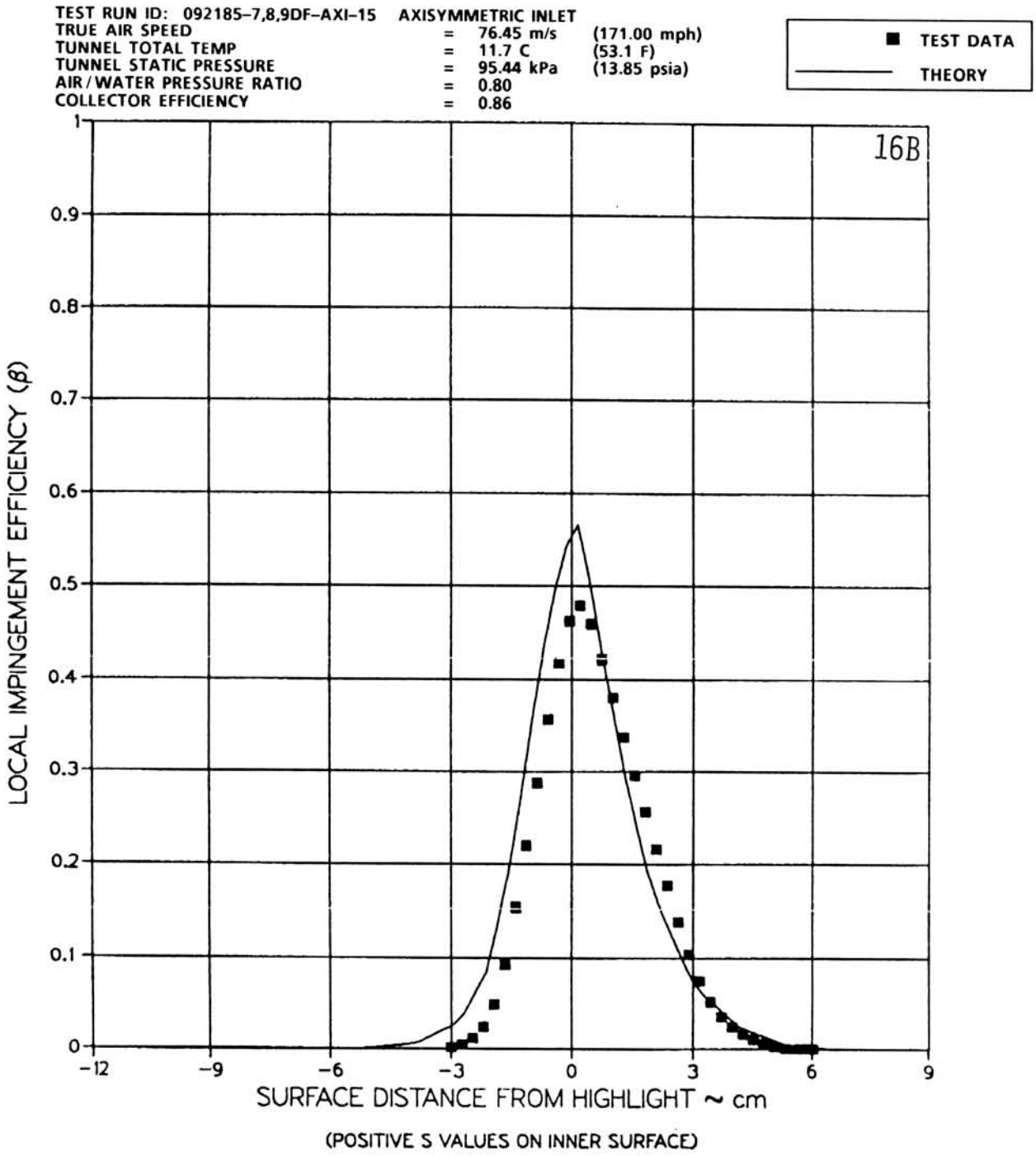

(B2) MVD = 16.45 MICRONS, MASS FLOW = 22.96 LBM/SEC, θ = 45°

FIGURE 6.16

AVERAGED LOCAL WATER IMPINGEMENT EFFICIENCY DATA FOR AXISYMMETRIC INLET AT α = 15° (PAGE 8 OF 21).

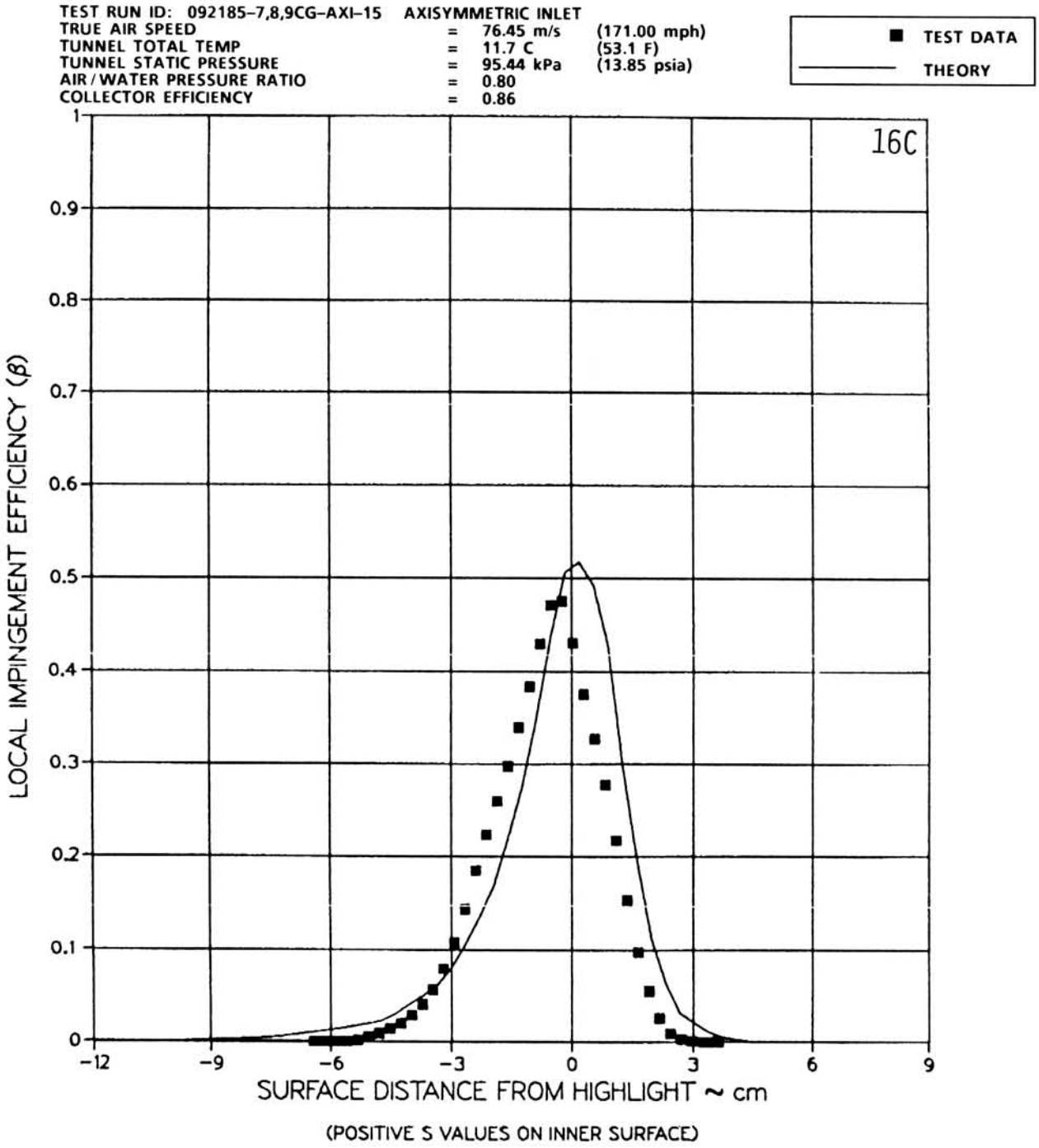

(B3) MVD = 16.45 MICRONS, MASS FLOW = 22.96 LBM/SEC, θ = 90°

FIGURE 6.16

AVERAGED LOCAL WATER IMPINGEMENT EFFICIENCY DATA FOR AXISYMMETRIC INLET AT α = 15° (PAGE 9 OF 21).

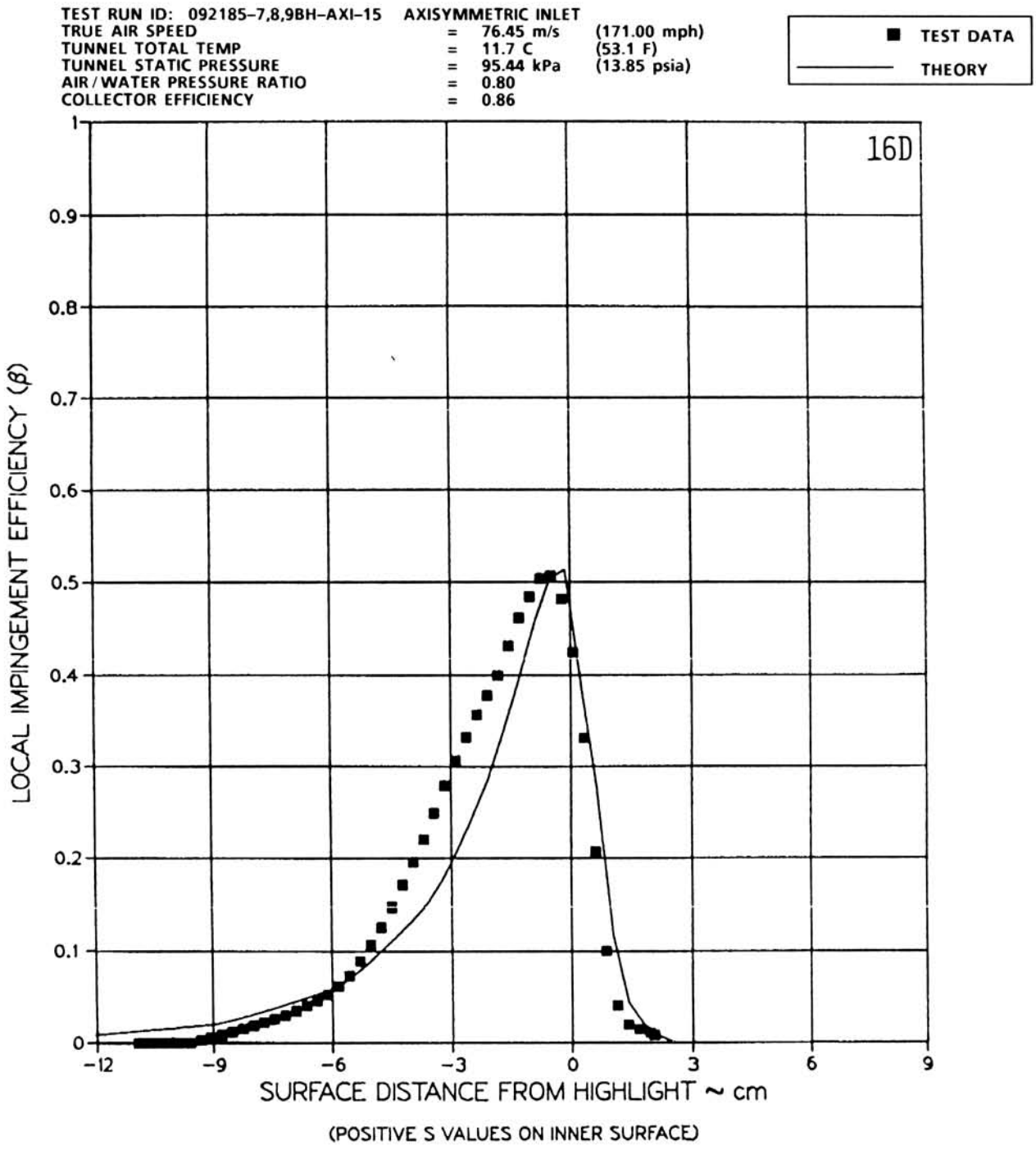

(B4) MVD = 16.45 MICRONS, MASS FLOW = 22.96 LBM/SEC, θ = 135°

FIGURE 6.16

AVERAGED LOCAL WATER IMPINGEMENT EFFICIENCY DATA FOR AXISYMMETRIC INLET AT α = 15° (PAGE 10 OF 21).

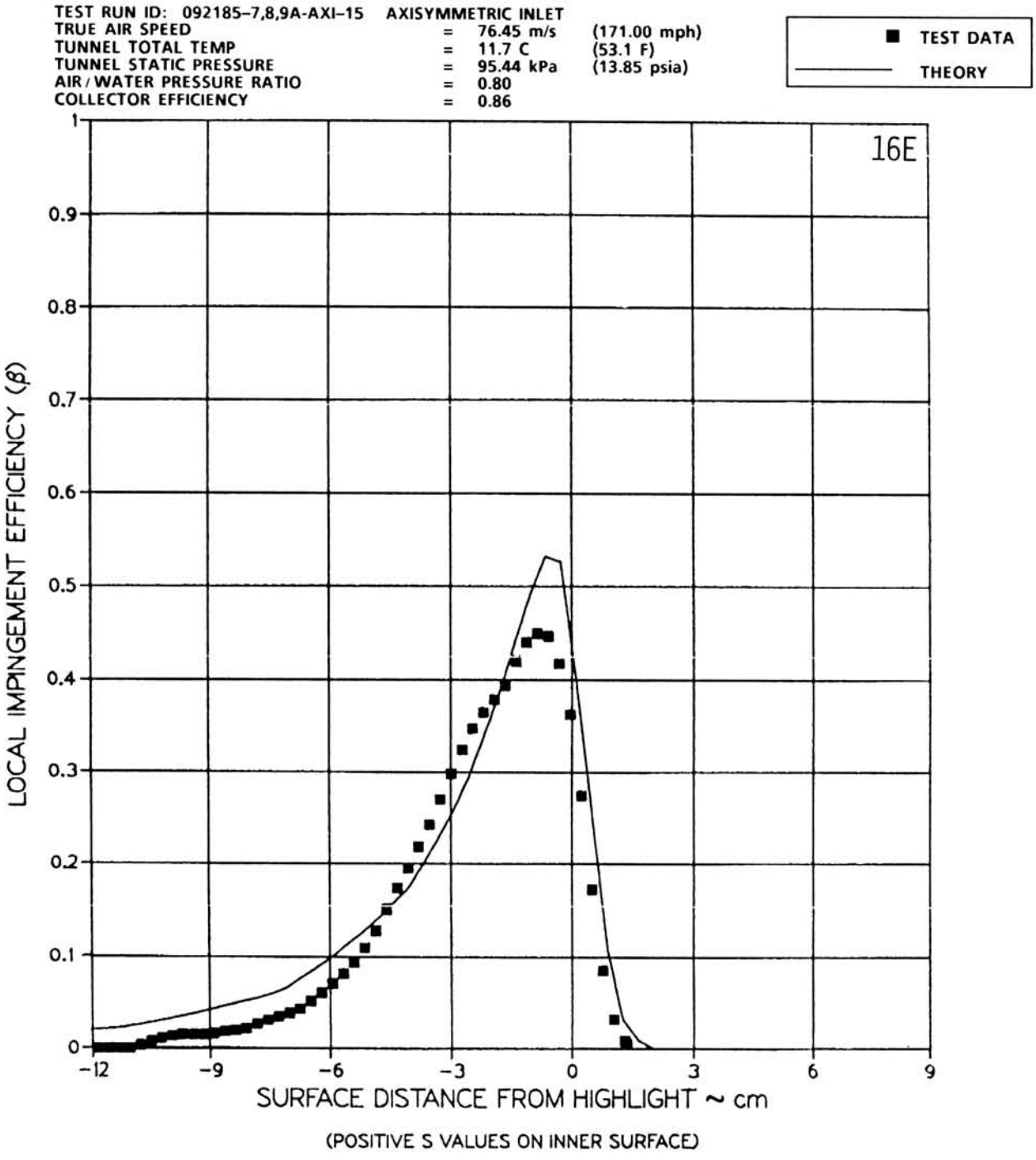

(B5) MVD = 16.45 MICRONS, MASS FLOW = 22.96 LBM / SEC, θ = 180°

FIGURE 6.16

AVERAGED LOCAL WATER IMPINGEMENT EFFICIENCY DATA FOR AXISYMMETRIC INLET AT α = 15° (PAGE 11 OF 21).

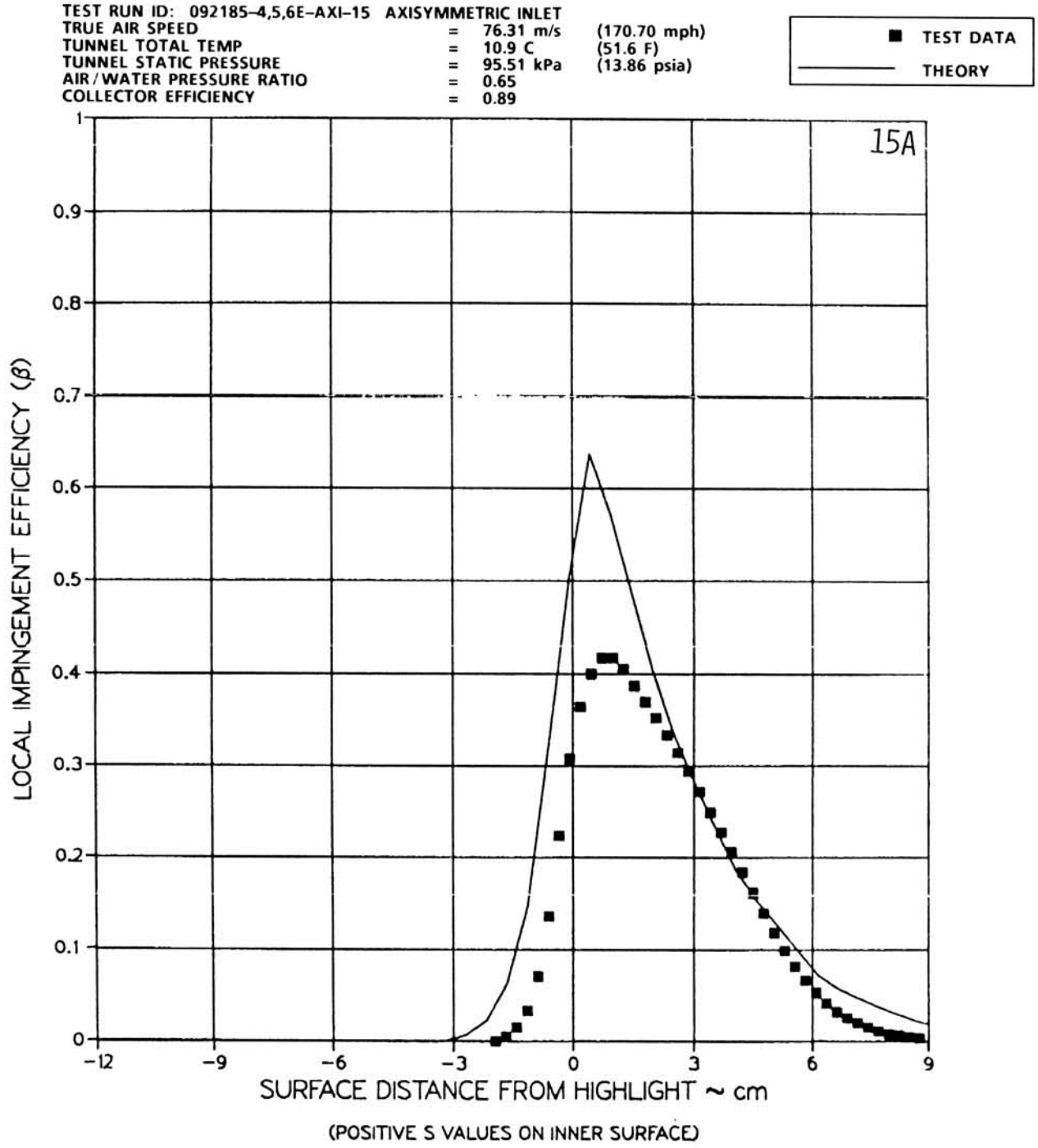

(C1) MVD = 20.36 MICRONS, MASS FLOW = 17.20 LBM/SEC, $\theta = 0°$

FIGURE 6.16

AVERAGED LOCAL WATER IMPINGEMENT EFFICIENCY DATA FOR AXISYMMETRIC INLET AT $\alpha = 15°$ (PAGE 12 OF 21).

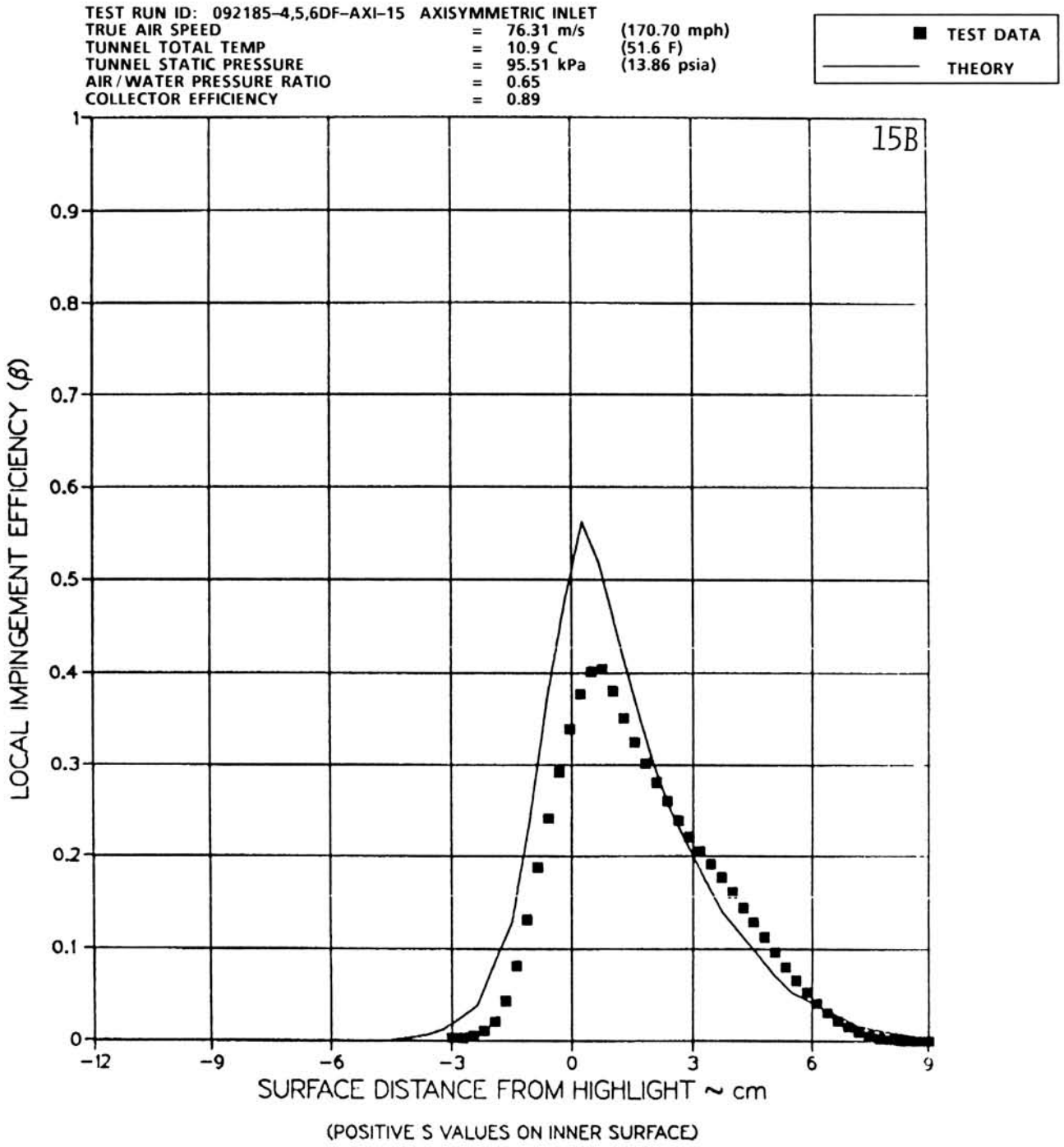

(C2) MVD = 20.36 MICRONS, MASS FLOW = 17.20 LBM/SEC, θ = 45°

FIGURE 6.16

AVERAGED LOCAL WATER IMPINGEMENT EFFICIENCY DATA FOR AXISYMMETRIC INLET AT α = 15° (PAGE 13 OF 21).

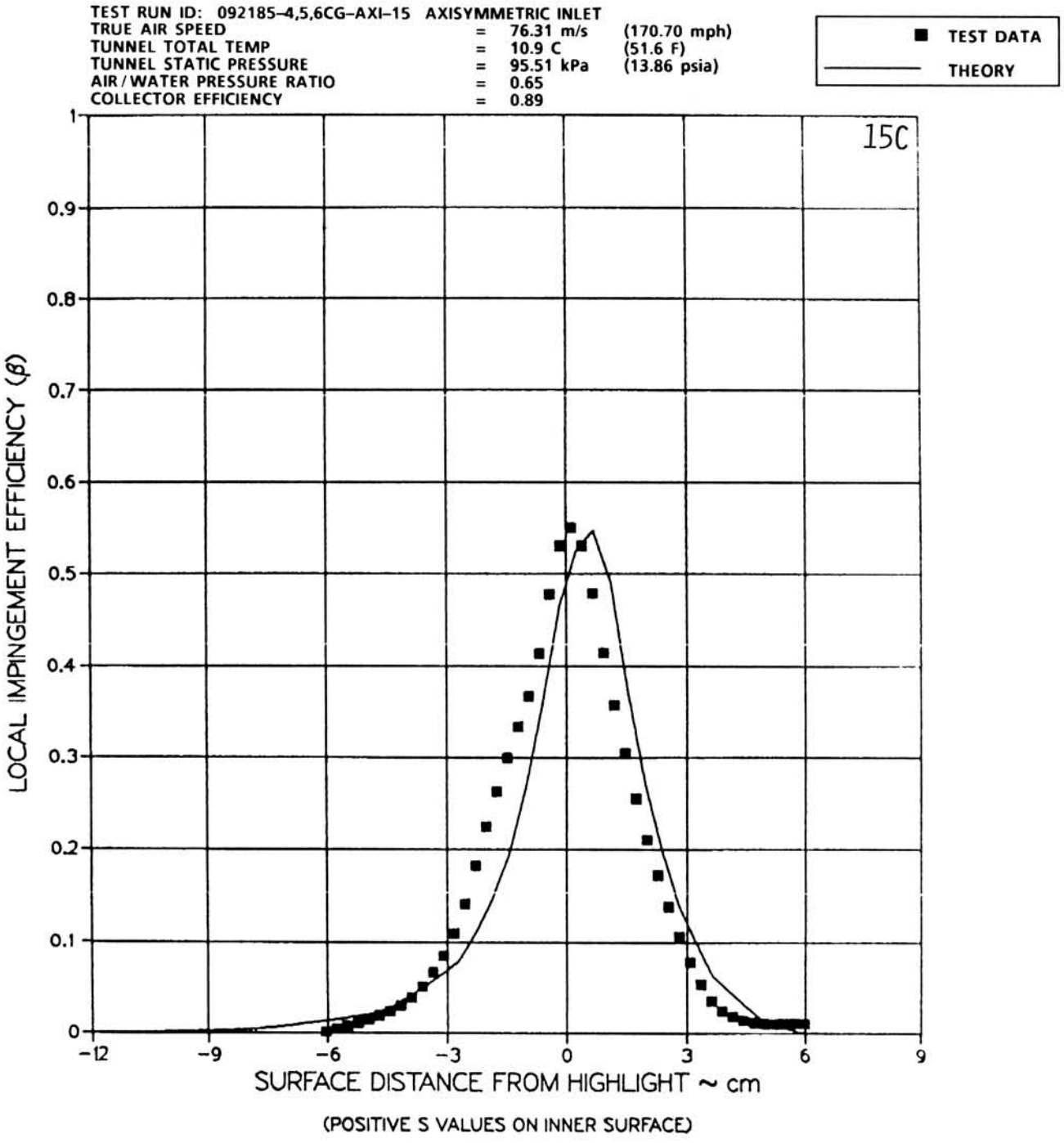

(C3) MVD = 20.36 MICRONS, MASS FLOW = 17.20 LBM/SEC, θ = 90°

FIGURE 6.16

AVERAGED LOCAL WATER IMPINGEMENT EFFICIENCY DATA FOR AXISYMMETRIC INLET AT α = 15° (PAGE 14 OF 21).

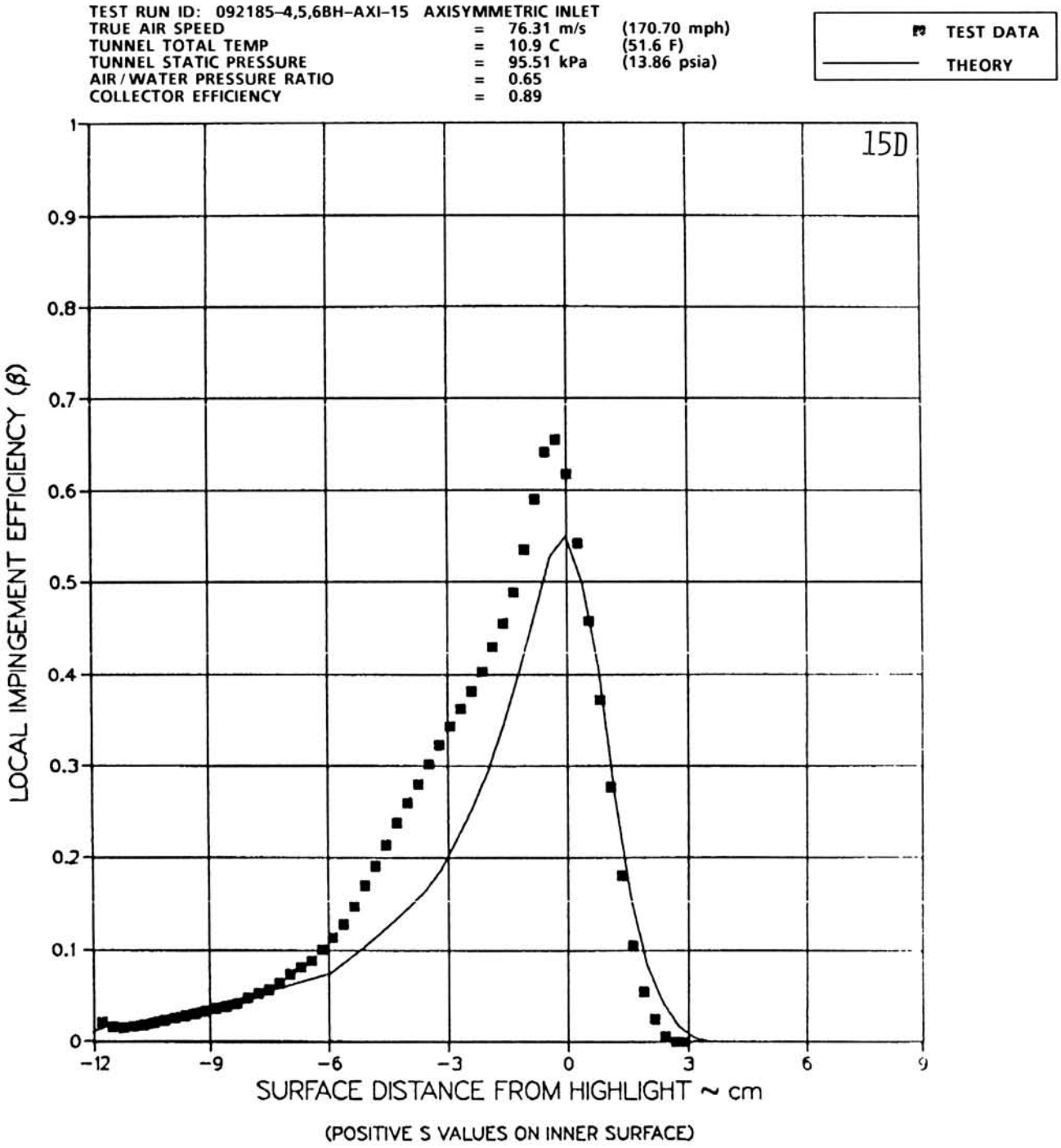

(C4) MVD = 20.36 MICRONS, MASS FLOW = 17.20 LBM/SEC, θ = 135°

FIGURE 6.16

AVERAGED LOCAL WATER IMPINGEMENT EFFICIENCY DATA FOR AXISYMMETRIC INLET AT α = 15° (PAGE 15 OF 21).

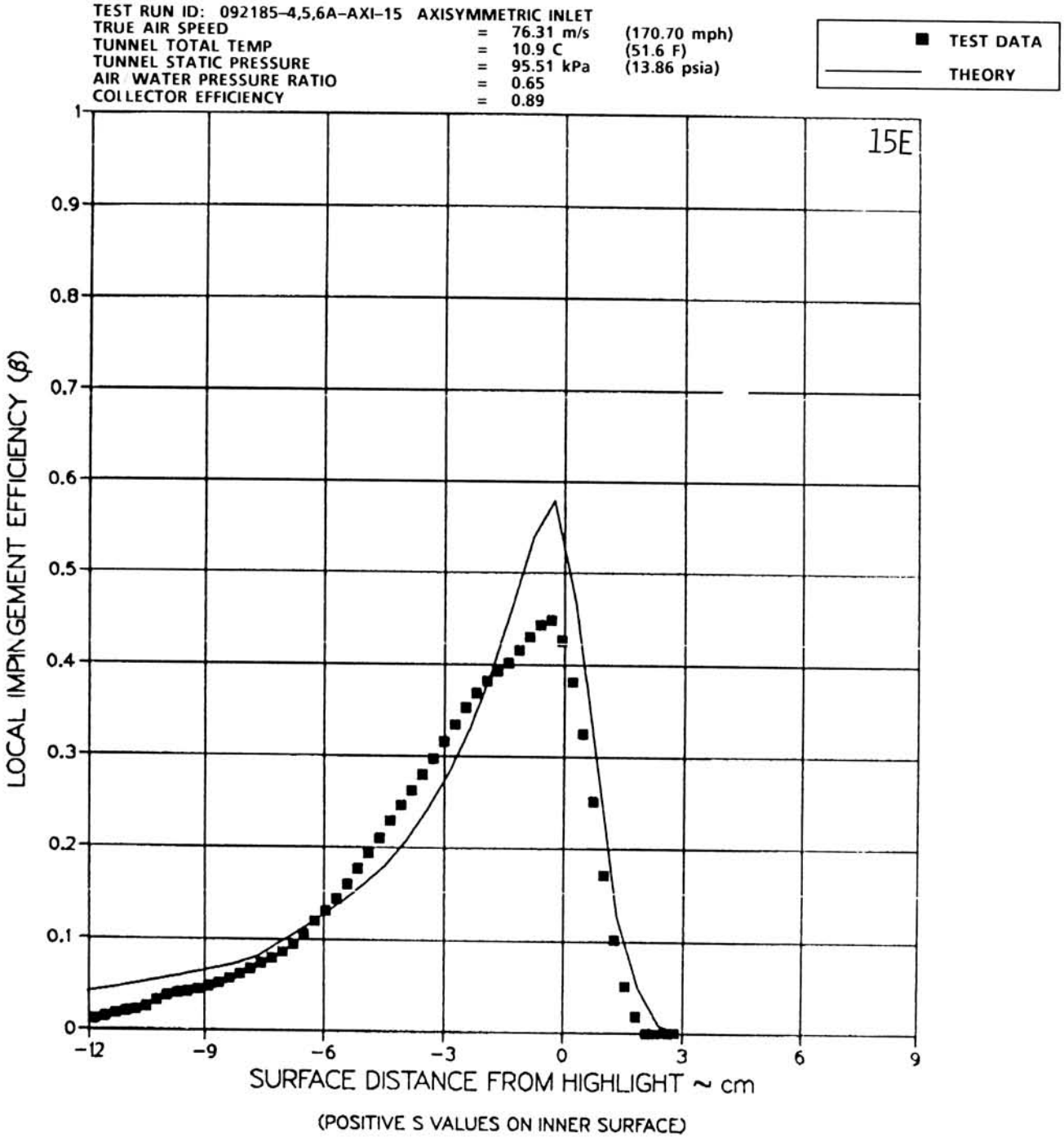

(C5) MVD = 20.36 MICRONS, MASS FLOW = 17.20 LBM / SEC, θ = 180°

FIGURE 6.16

AVERAGED LOCAL WATER IMPINGEMENT EFFICIENCY DATA FOR AXISYMMETRIC INLET AT α = 15° (PAGE 16 OF 21).

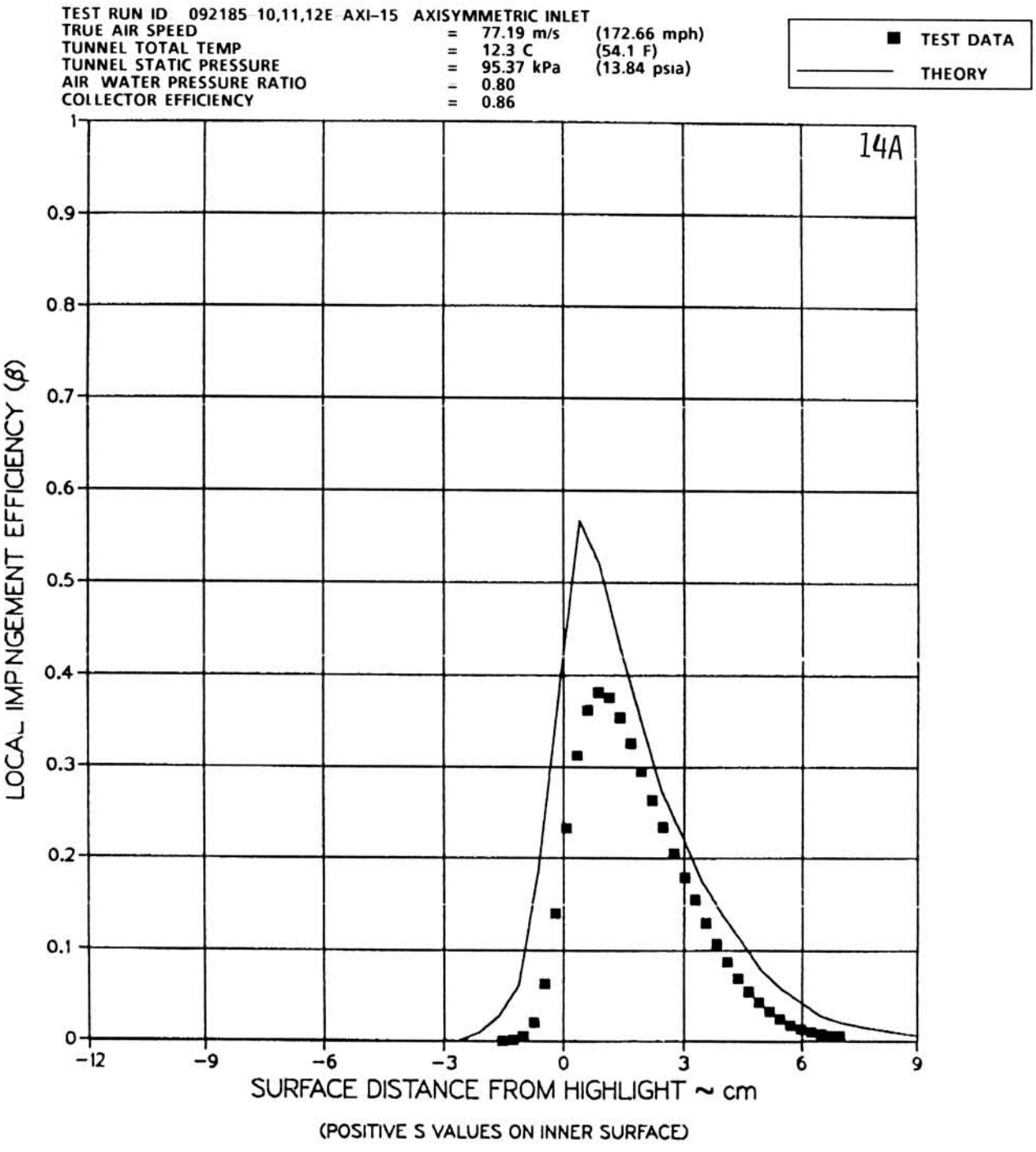

(D1) MVD = 16.45 MICRONS, MASS FLOW = 17.20 LBM / SEC, $\theta = 0°$

FIGURE 6.16

AVERAGED LOCAL WATER IMPINGEMENT EFFICIENCY DATA FOR AXISYMMETRIC INLET AT $\alpha = 15°$ (PAGE 17 OF 21).

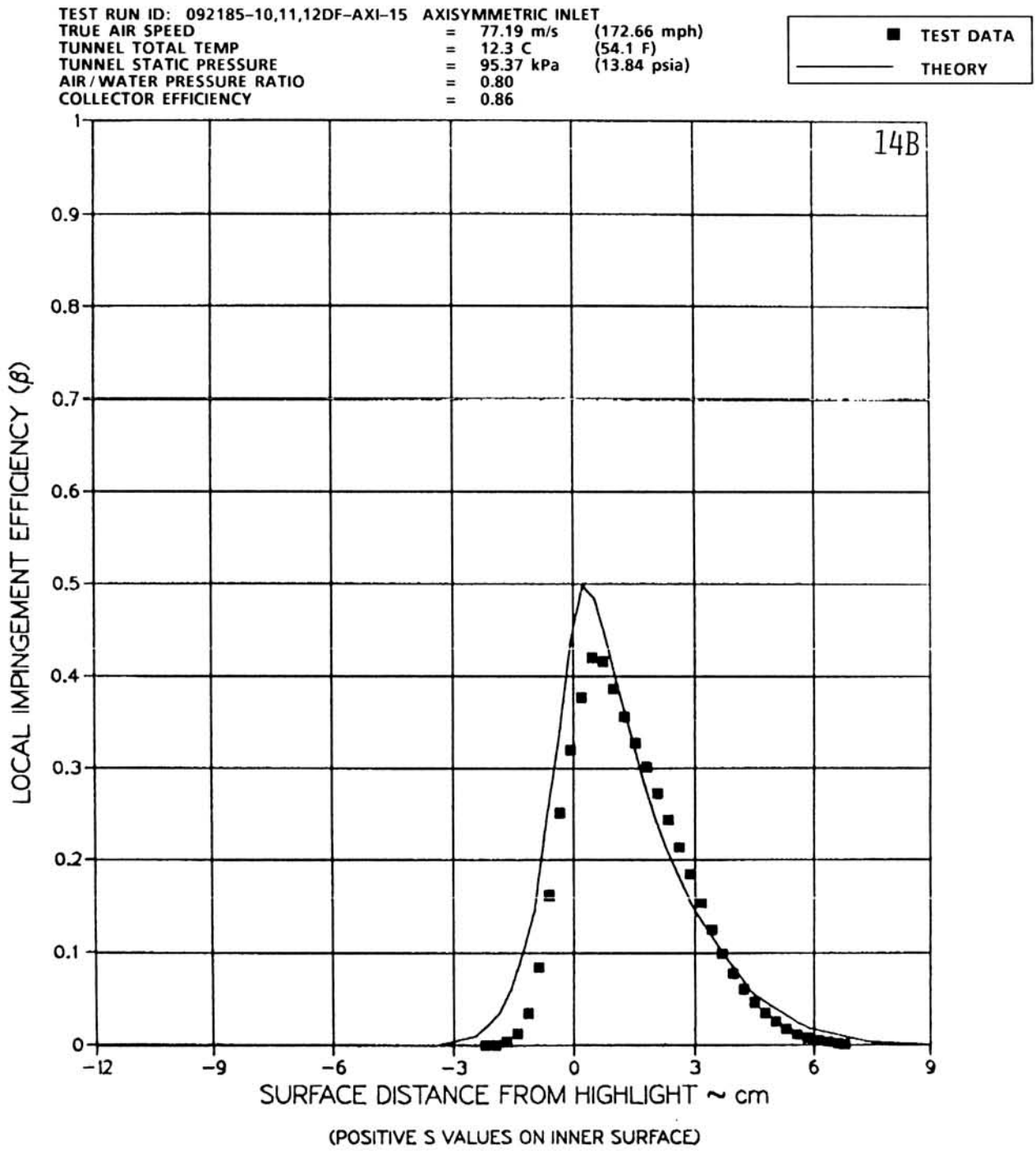

(D2) MVD = 16.45 MICRONS, MASS FLOW = 17.20 LBM/SEC, θ = 45°

FIGURE 6.16

AVERAGED LOCAL WATER IMPINGEMENT EFFICIENCY DATA FOR AXISYMMETRIC INLET AT α = 15° (PAGE 18 OF 21).

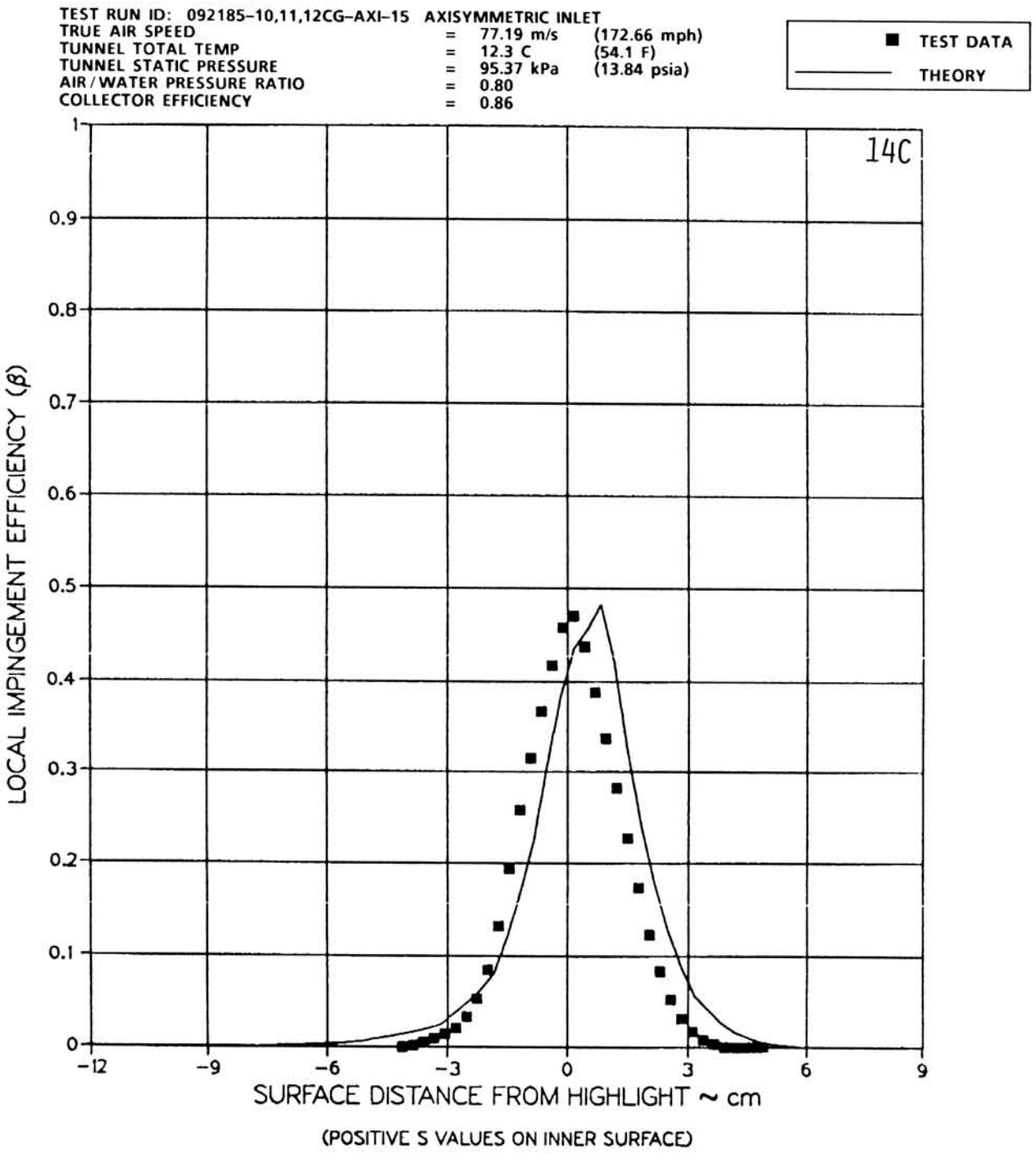

(D3) MVD = 16.45 MICRONS, MASS FLOW = 17.20 LBM/SEC, θ = 90°

FIGURE 6.16

AVERAGED LOCAL WATER IMPINGEMENT EFFICIENCY DATA FOR AXISYMMETRIC INLET AT α = 15° (PAGE 19 OF 21).

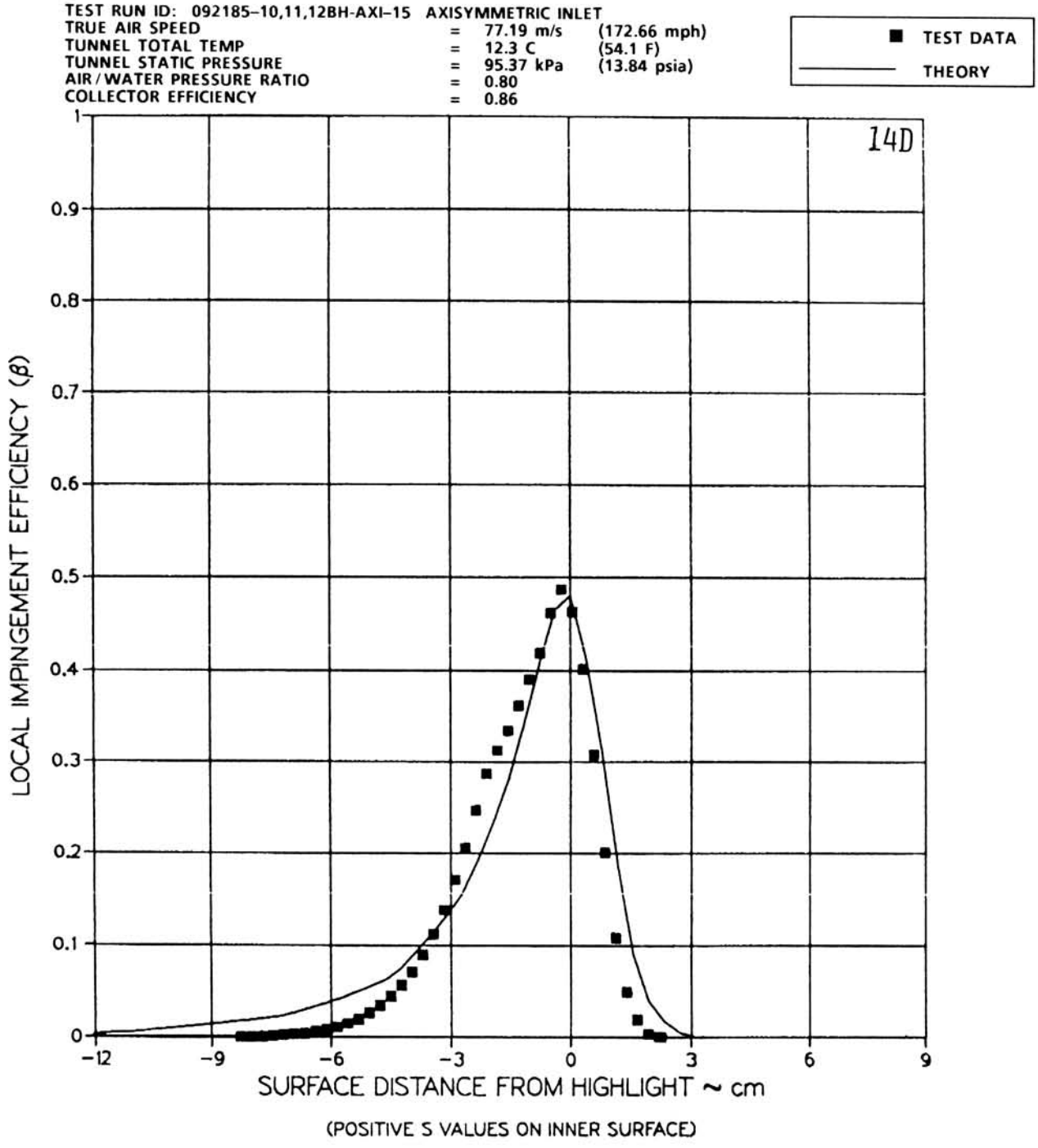

(D4) MVD = 16.45 MICRONS, MASS FLOW = 17.20 LBM/SEC, θ = 135°

FIGURE 6.16

AVERAGED LOCAL WATER IMPINGEMENT EFFICIENCY DATA FOR AXISYMMETRIC INLET AT α = 15° (PAGE 20 OF 21).

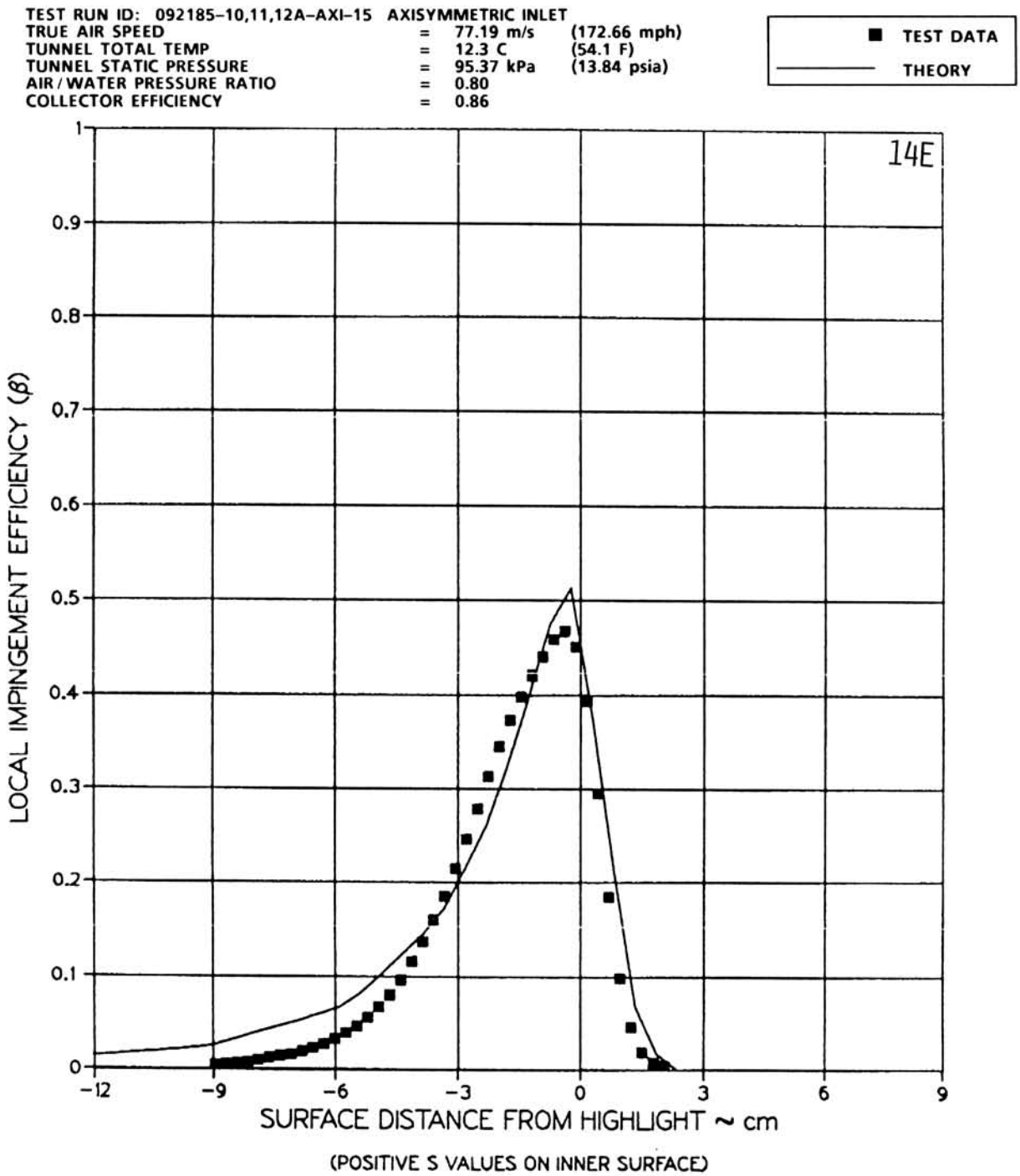

(D5) MVD = 16.45 MICRONS, MASS FLOW = 17.20 LBM/SEC, θ = 180°

FIGURE 6.16

AVERAGED LOCAL WATER IMPINGEMENT EFFICIENCY DATA FOR AXISYMMETRIC INLET AT α = 15° (PAGE 21 OF 21).

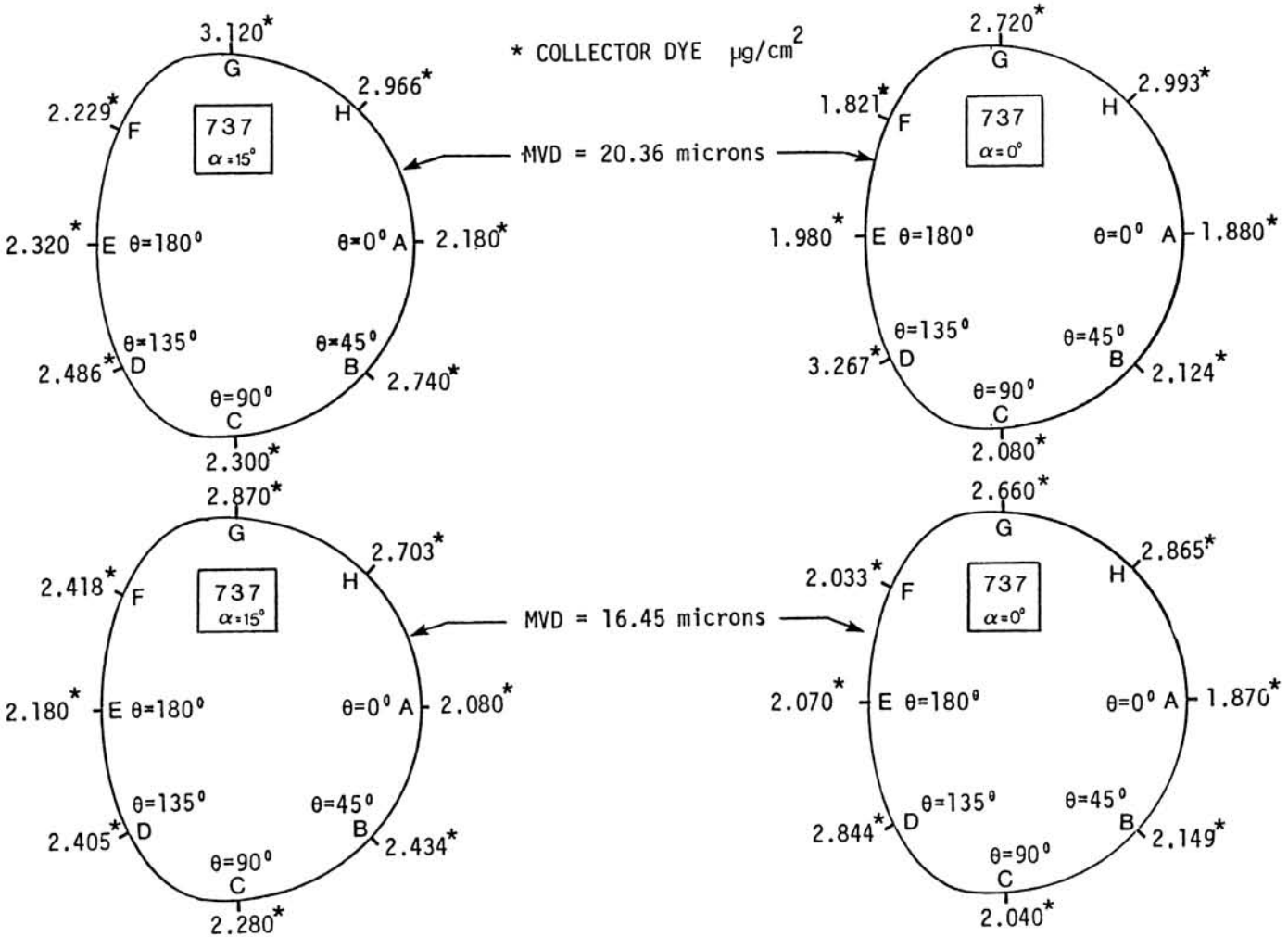

FIGURE 6.17

BLOTTER STRIP LOCATIONS, REFERENCE COLLECTOR DYE MASS, HIGHLIGHT MARK AND SURFACE DISTANCE CONVENTION FOR BOEING 737-300 INLET (PAGE 1 OF 2).

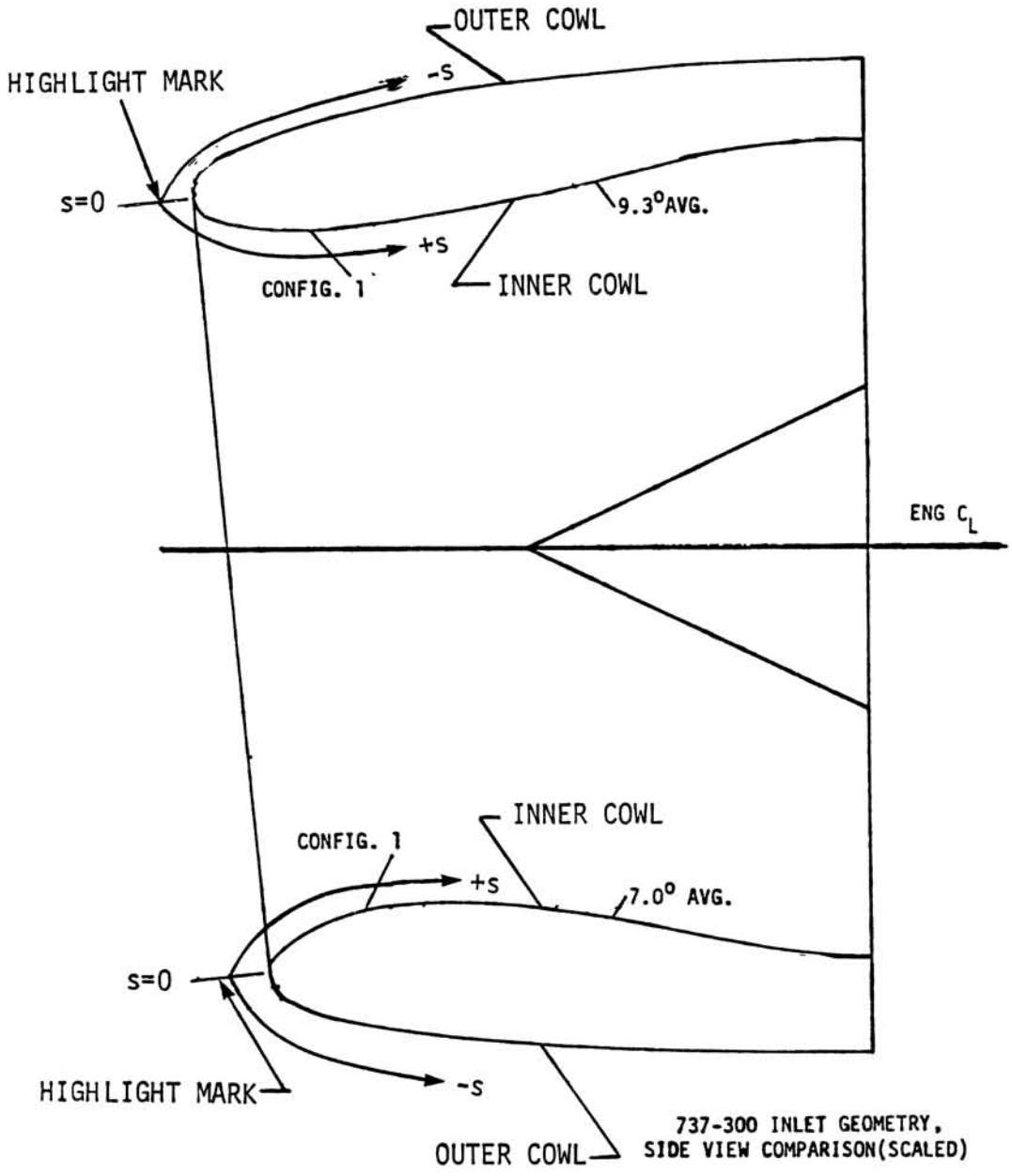

FIGURE 6.17

BLOTTER STRIP LOCATIONS, REFERENCE COLLECTOR DYE MASS, HIGHLIGHT MARK AND SURFACE DISTANCE CONVENTION FOR BOEING 737-300 INLET (PAGE 2 OF 2).

TEST RUN ID: 092385—2,3A-737-0 737-300 INLET

TRUE AIR SPEED	=	77.49 m/s	(173.33 mph)
TUNNEL TOTAL TEMP	=	15.0 C	(59.0 F)
TUNNEL STATIC PRESSURE	=	94.61 kPa	(13.73 psia)
AIR/WATER PRESSURE RATIO	=	0.65	
COLLECTOR EFFICIENCY	=	0.89	

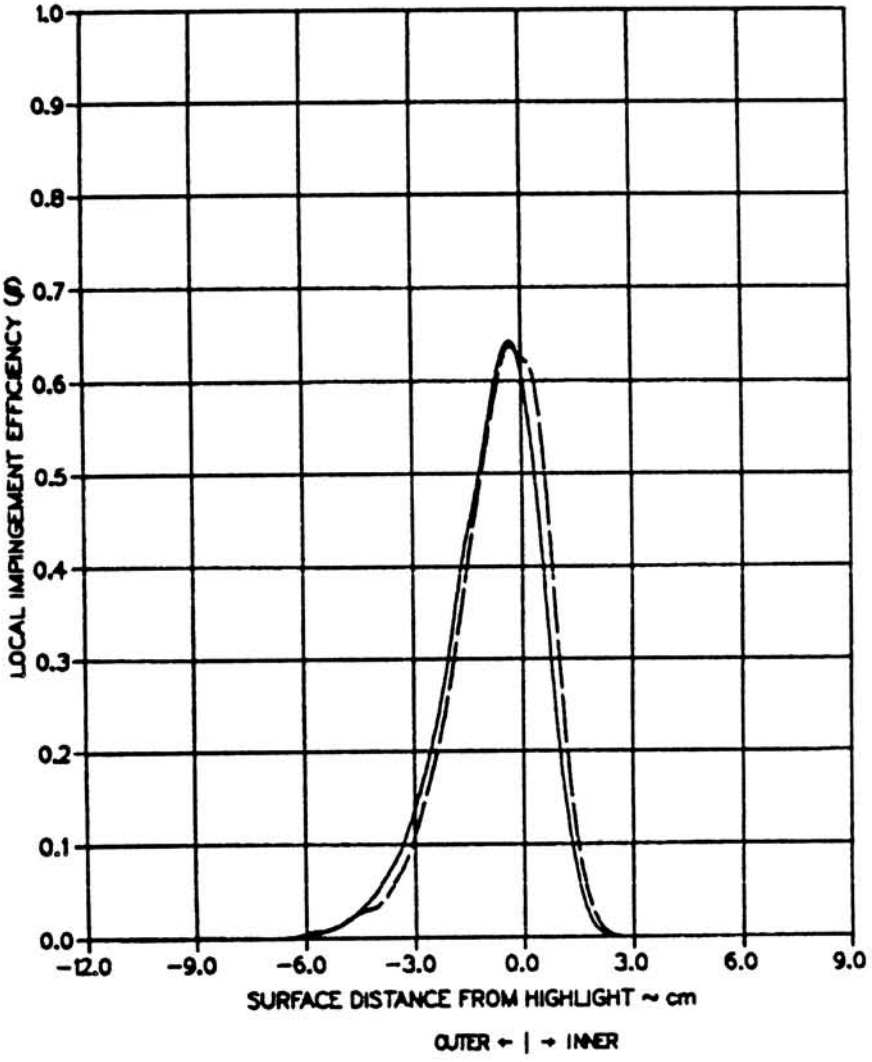

MVD = 20.36 MICRONS θ = 0°

FIGURE 6.18

TEST REPEATABILITY FOR BOEING 737-300 INLET:
α = 0°, MASS FLOW = 22.96 LBM/SEC (PAGE 1 OF 3).

TEST RUN ID: 092385-2,3CG-737-0 737-300 INLET

TRUE AIR SPEED	=	77.49 m/s	(173.33 mph)
TUNNEL TOTAL TEMP	=	15.0 C	(59.0 F)
TUNNEL STATIC PRESSURE	=	94.61 kPa	(13.73 psia)
AIR/WATER PRESSURE RATIO	=	0.65	
COLLECTOR EFFICIENCY	=	0.89	

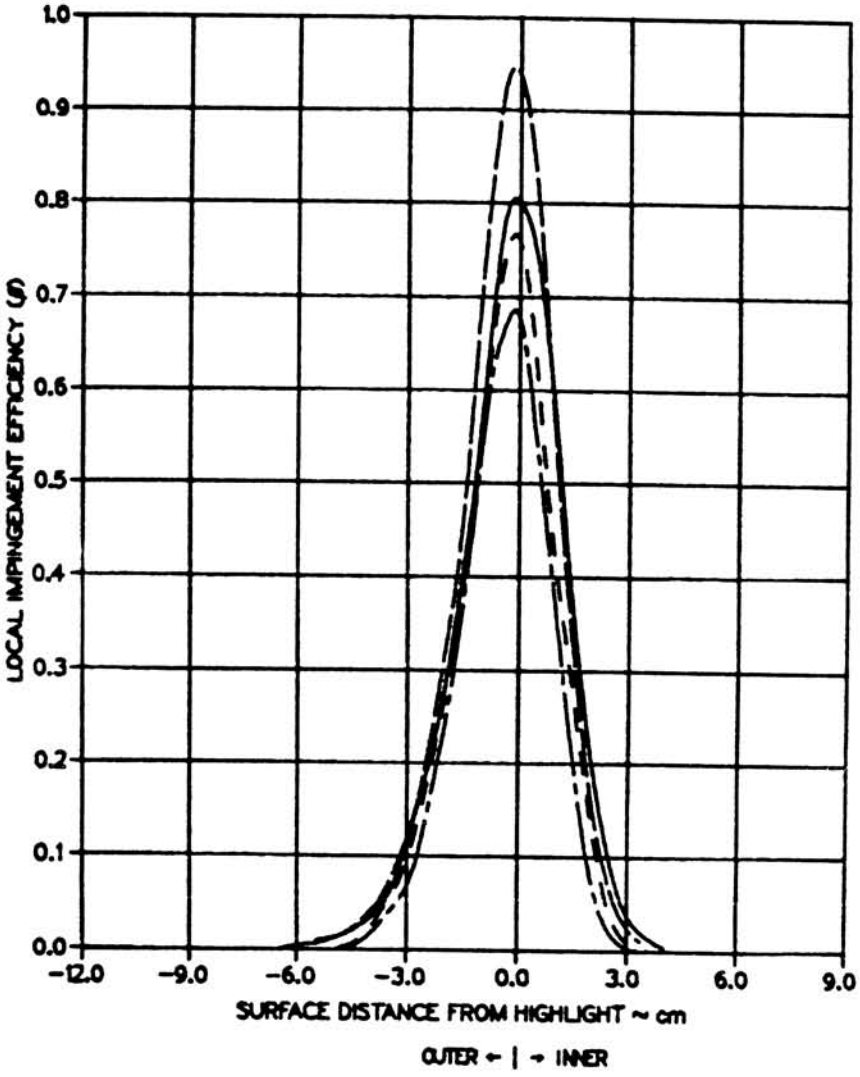

MVD = 20.36 MICRONS θ = 90°, 270°

FIGURE 6.18

TEST REPEATABILITY FOR BOEING 737-300 INLET:
α = 0°, MASS FLOW = 22.96 LBM/SEC (PAGE 2 OF 3).

TEST RUN ID: 092385-2,3E-737-0 737-300 INLET

TRUE AIR SPEED	=	77.49 m/s	(173.33 mph)
TUNNEL TOTAL TEMP	=	15.0 C	(59.0 F)
TUNNEL STATIC PRESSURE	=	94.61 kPa	(13.73 psia)
AIR/WATER PRESSURE RATIO	=	0.65	
COLLECTOR EFFICIENCY	=	0.89	

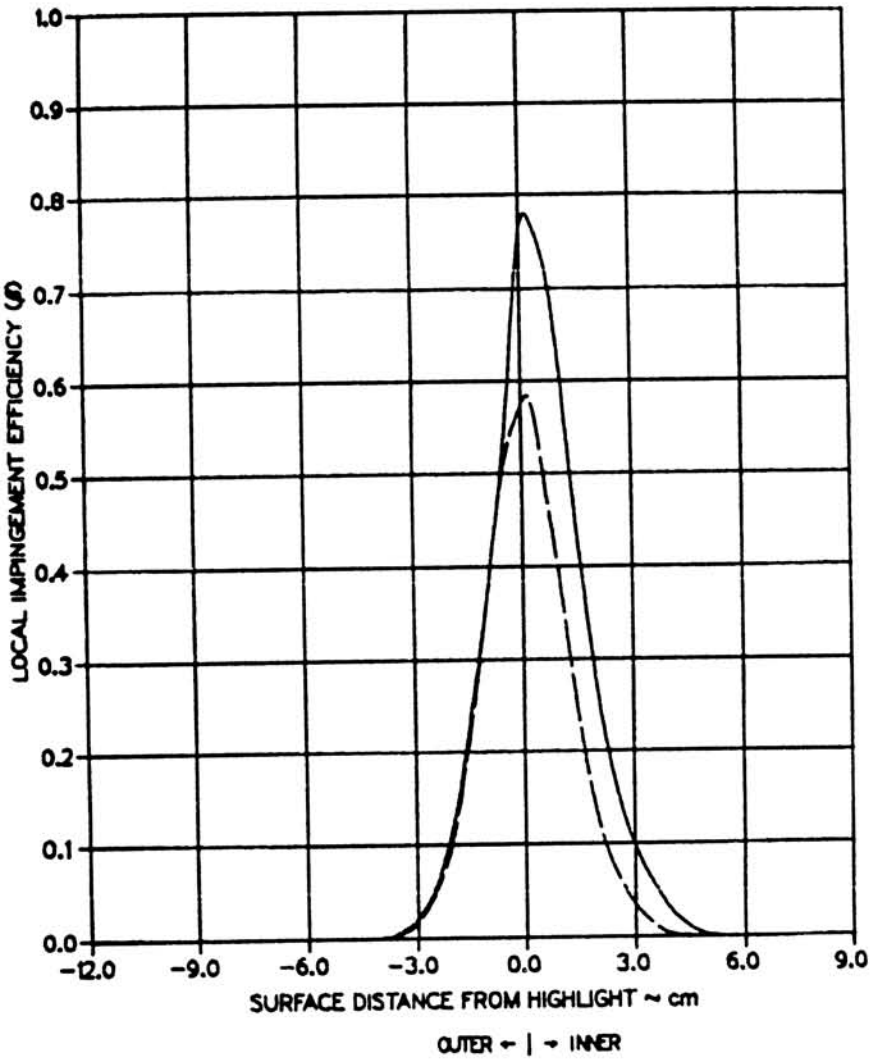

MVD = 20.36 MICRONS θ = 180°

FIGURE 6.18

TEST REPEATABILITY FOR BOEING 737-300 INLET:
α = 0°, MASS FLOW = 22.96 LBM/SEC (PAGE 3 OF 3).

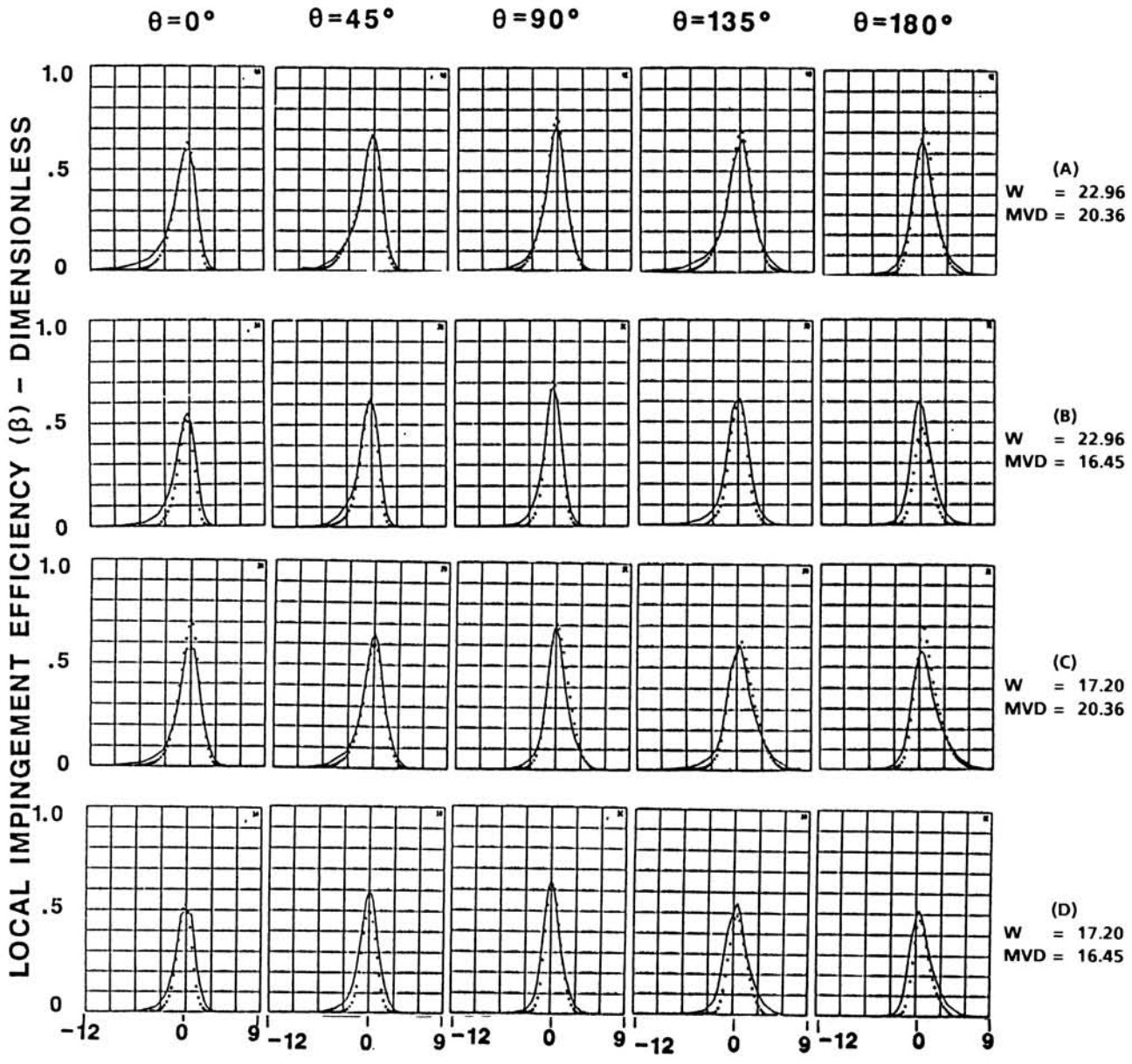

NOTE: W ~ LBM / SEC, MVD ~ μm
NEGATIVE SURFACE DISTANCE – OUTER SURFACE
POSITIVE SURFACE DISTANCE – INNER SURFACE

■ TEST DATA
——— THEORY

SUMMARY OF RESULTS

FIGURE 6.19

AVERAGED LOCAL WATER IMPINGEMENT EFFICIENCY DATA FOR BOEING 737-300 INLET AT $\alpha = 0°$ (PAGE 1 OF 21).

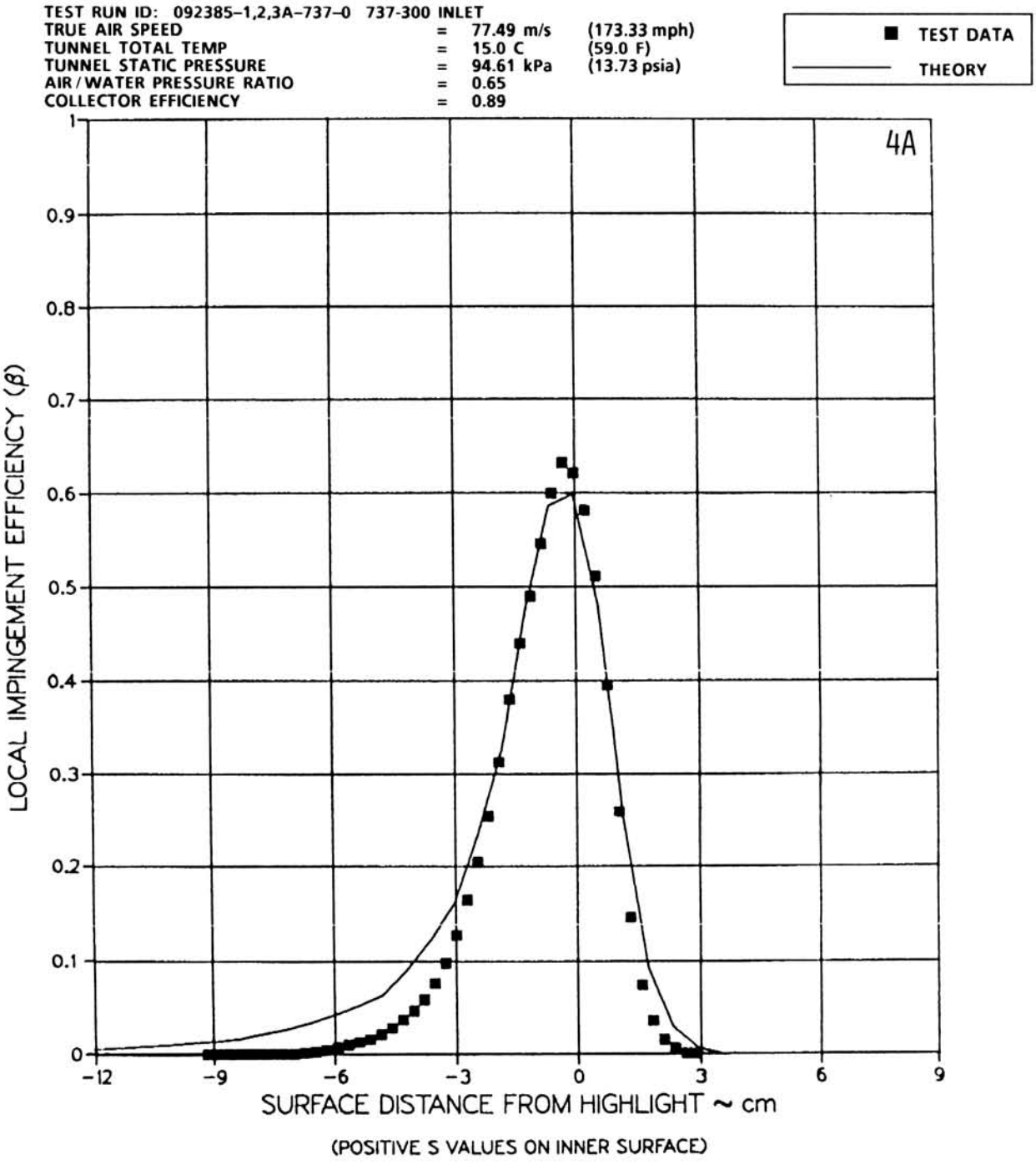

(A1) MVD = 20.36 MICRONS, MASS FLOW = 22.96 LBM / SEC, $\theta = 0°$

FIGURE 6.19

AVERAGED LOCAL WATER IMPINGEMENT EFFICIENCY DATA FOR BOEING 737-300 INLET AT $\alpha = 0°$ (PAGE 2 OF 21).

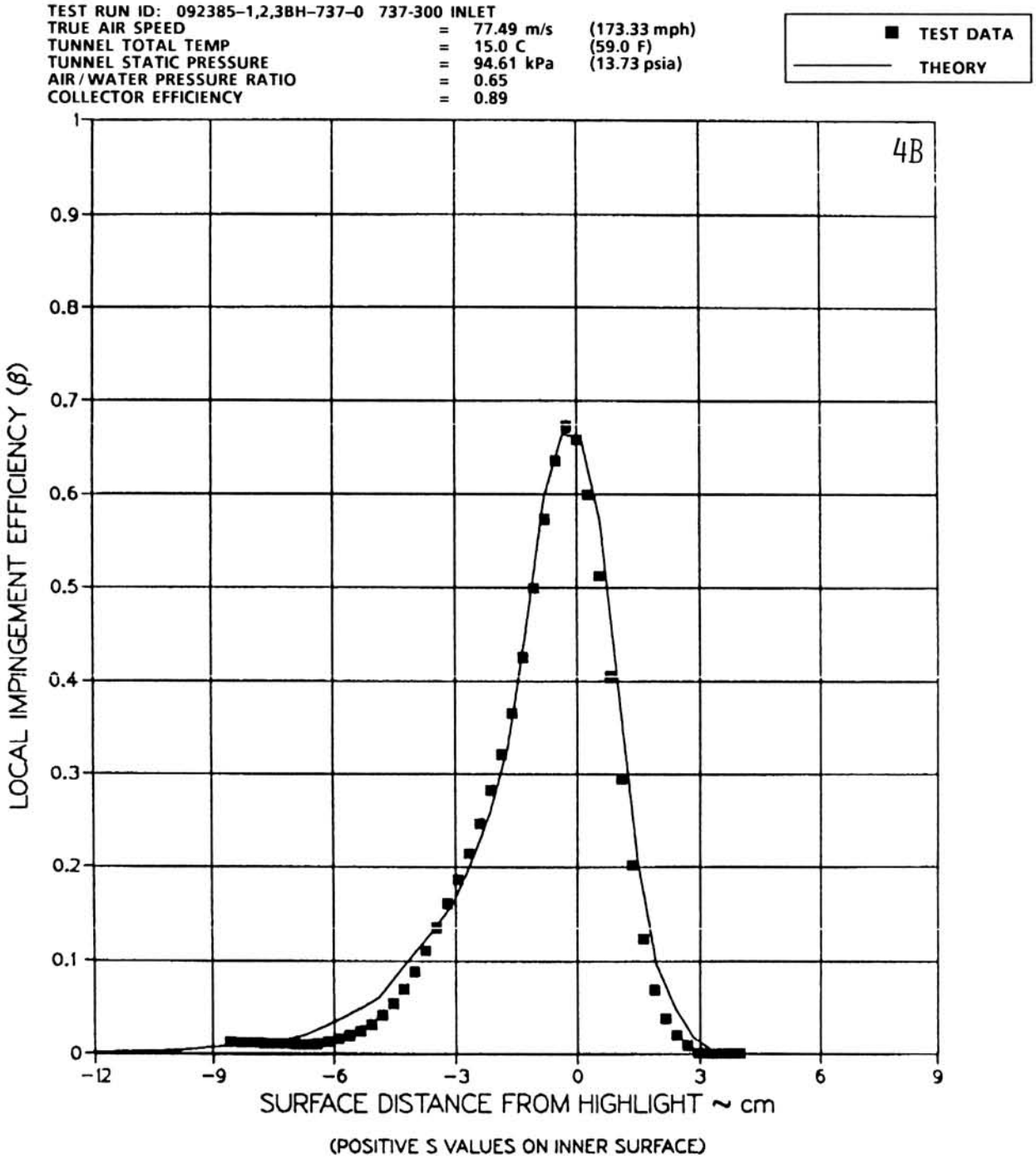

(A2) MVD = 20.36 MICRONS, MASS FLOW = 22.96 LBM / SEC, $\theta = 45°$

FIGURE 6.19

AVERAGED LOCAL WATER IMPINGEMENT EFFICIENCY DATA FOR BOEING 737-300 INLET AT $\alpha = 0°$ (PAGE 3 OF 21).

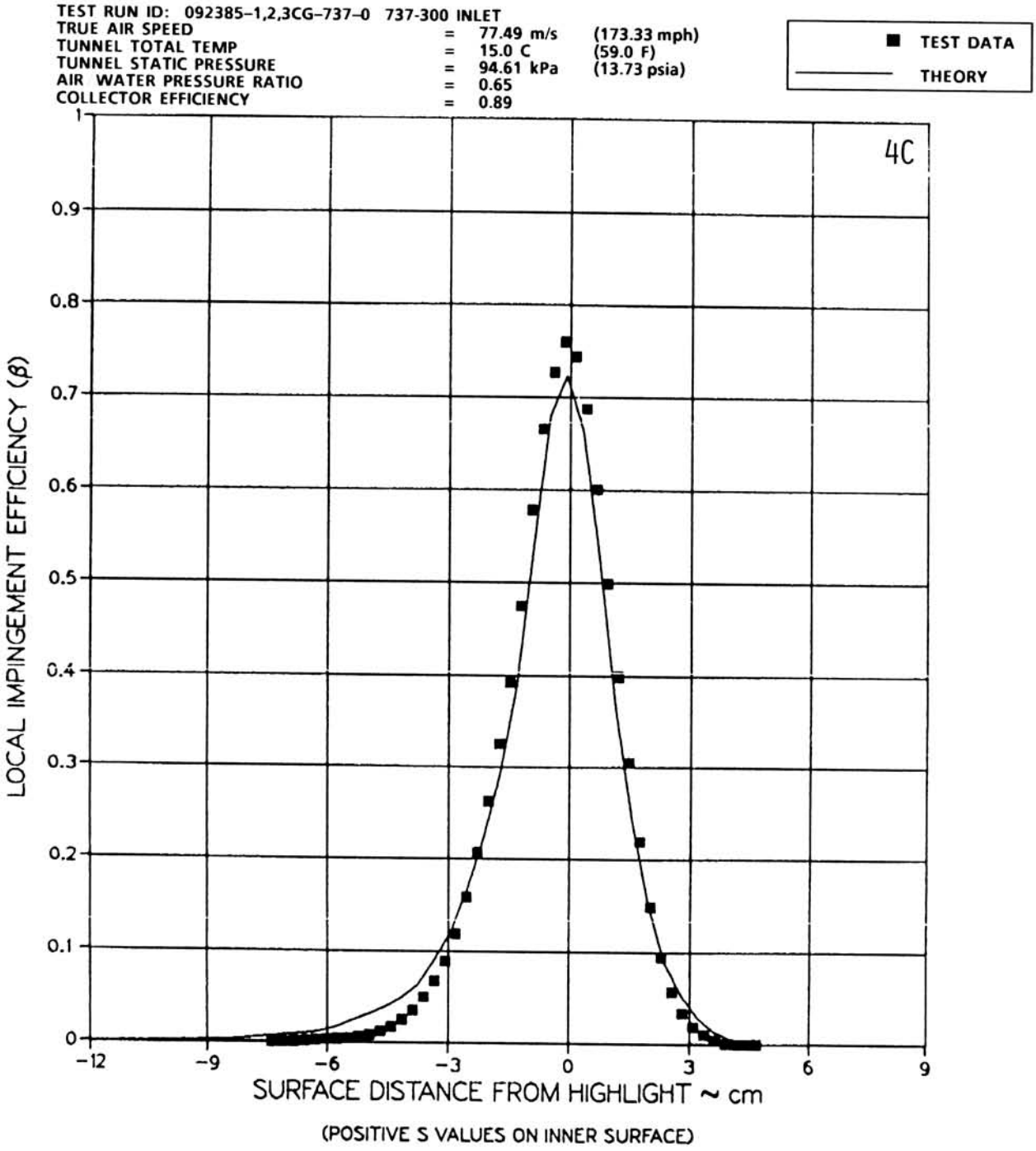

(A3) MVD = 20.36 MICRONS, MASS FLOW = 22.96 LBM / SEC, $\theta = 90°$

FIGURE 6.19

AVERAGED LOCAL WATER IMPINGEMENT EFFICIENCY DATA FOR BOEING 737-300 INLET AT $\alpha = 0°$ (PAGE 4 OF 21).

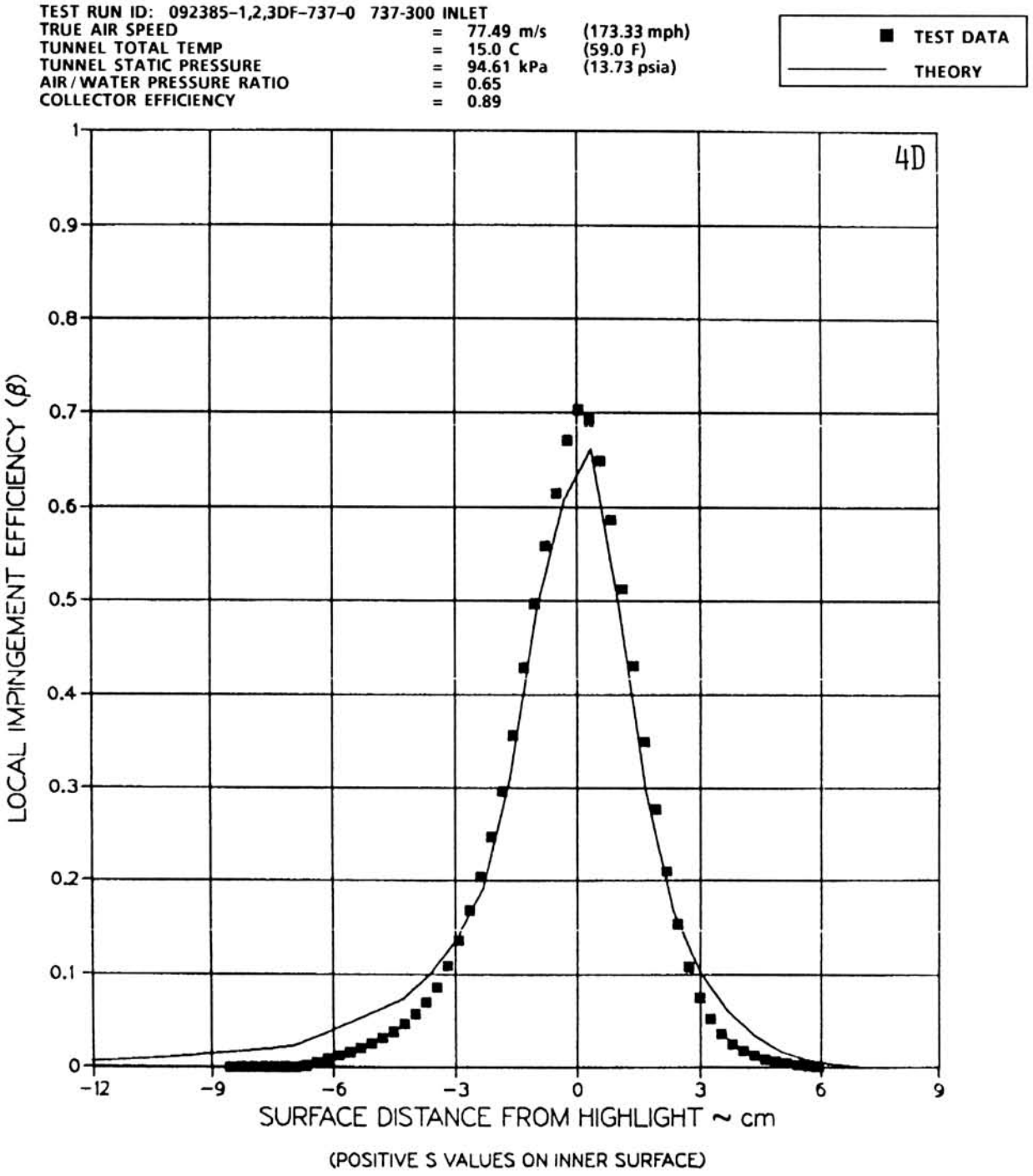

(A4) MVD = 20.36 MICRONS, MASS FLOW = 22.96 LBM/SEC, θ = 135°

FIGURE 6.19

AVERAGED LOCAL WATER IMPINGEMENT EFFICIENCY DATA FOR BOEING 737-300 INLET AT α = 0° (PAGE 5 OF 21).

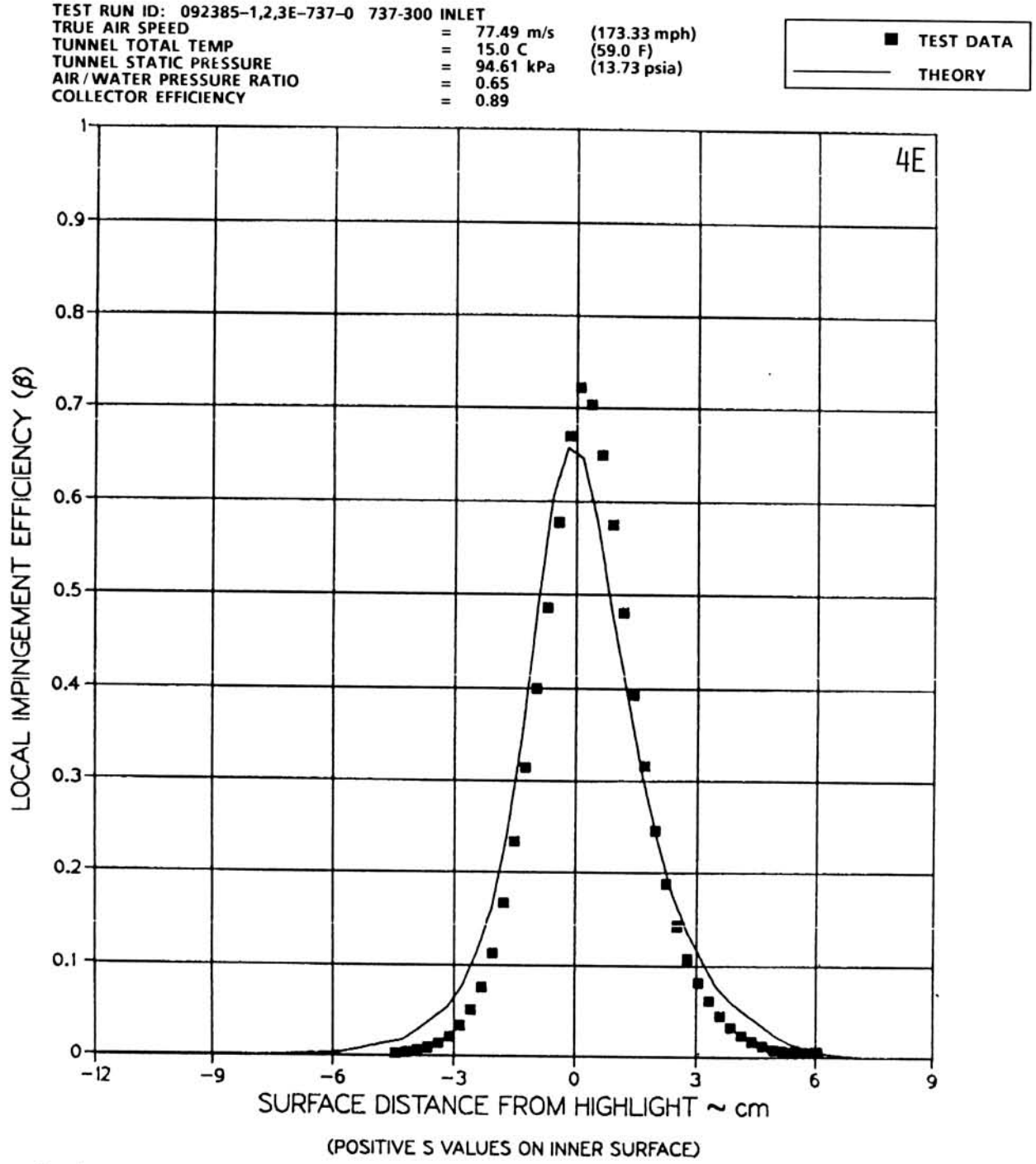

(A5) MVD = 20.36 MICRONS, MASS FLOW = 22.96 LBM / SEC, $\theta = 180°$

FIGURE 6.19

AVERAGED LOCAL WATER IMPINGEMENT EFFICIENCY DATA FOR BOEING 737-300 INLET AT $\alpha = 0°$ (PAGE 6 OF 21).

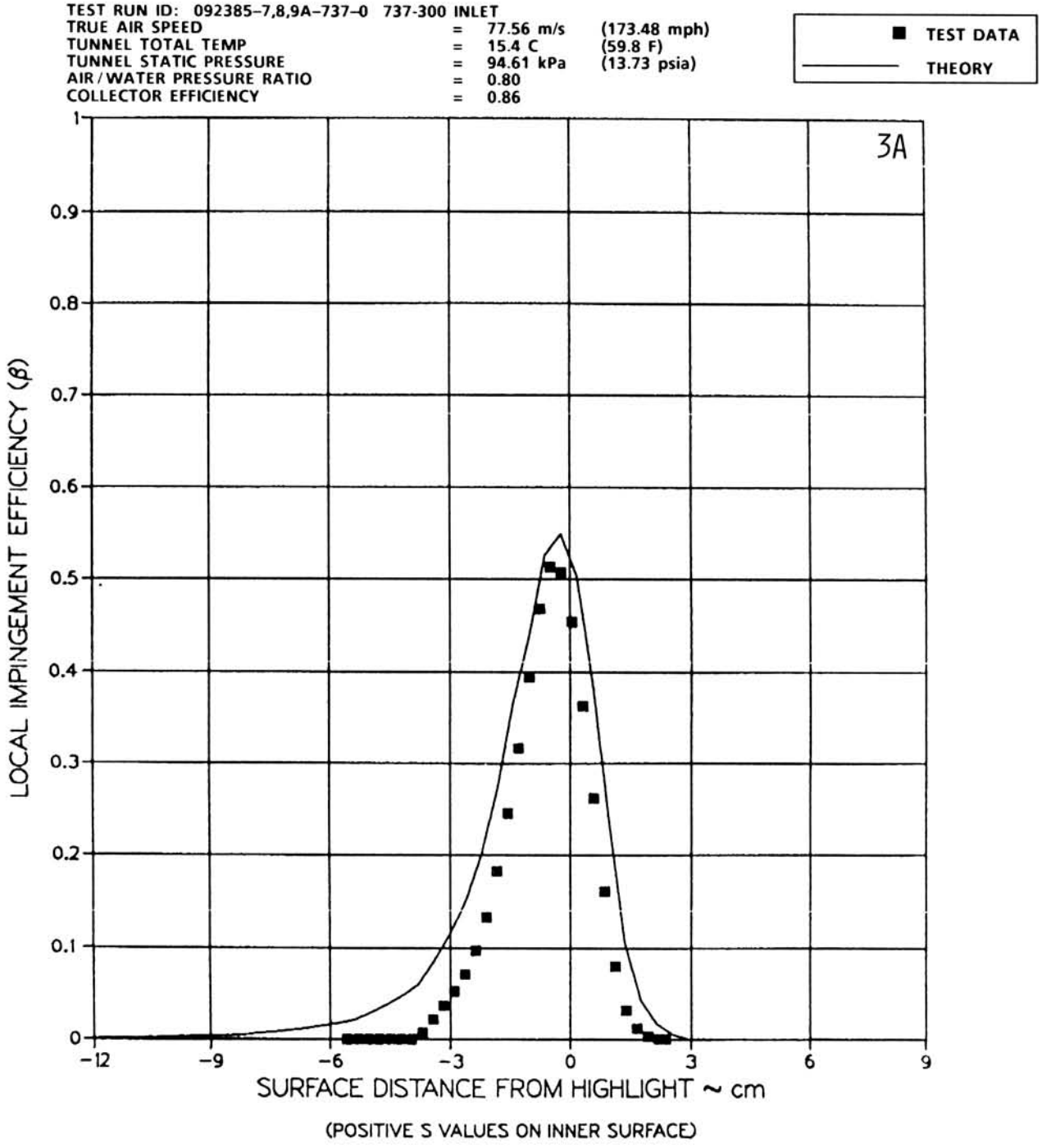

(B1) MVD = 16.45 MICRONS, MASS FLOW = 22.96 LBM/SEC, $\theta = 0°$

FIGURE 6.19

AVERAGED LOCAL WATER IMPINGEMENT EFFICIENCY DATA FOR BOEING 737-300 INLET AT $\alpha = 0°$ (PAGE 7 OF 21).

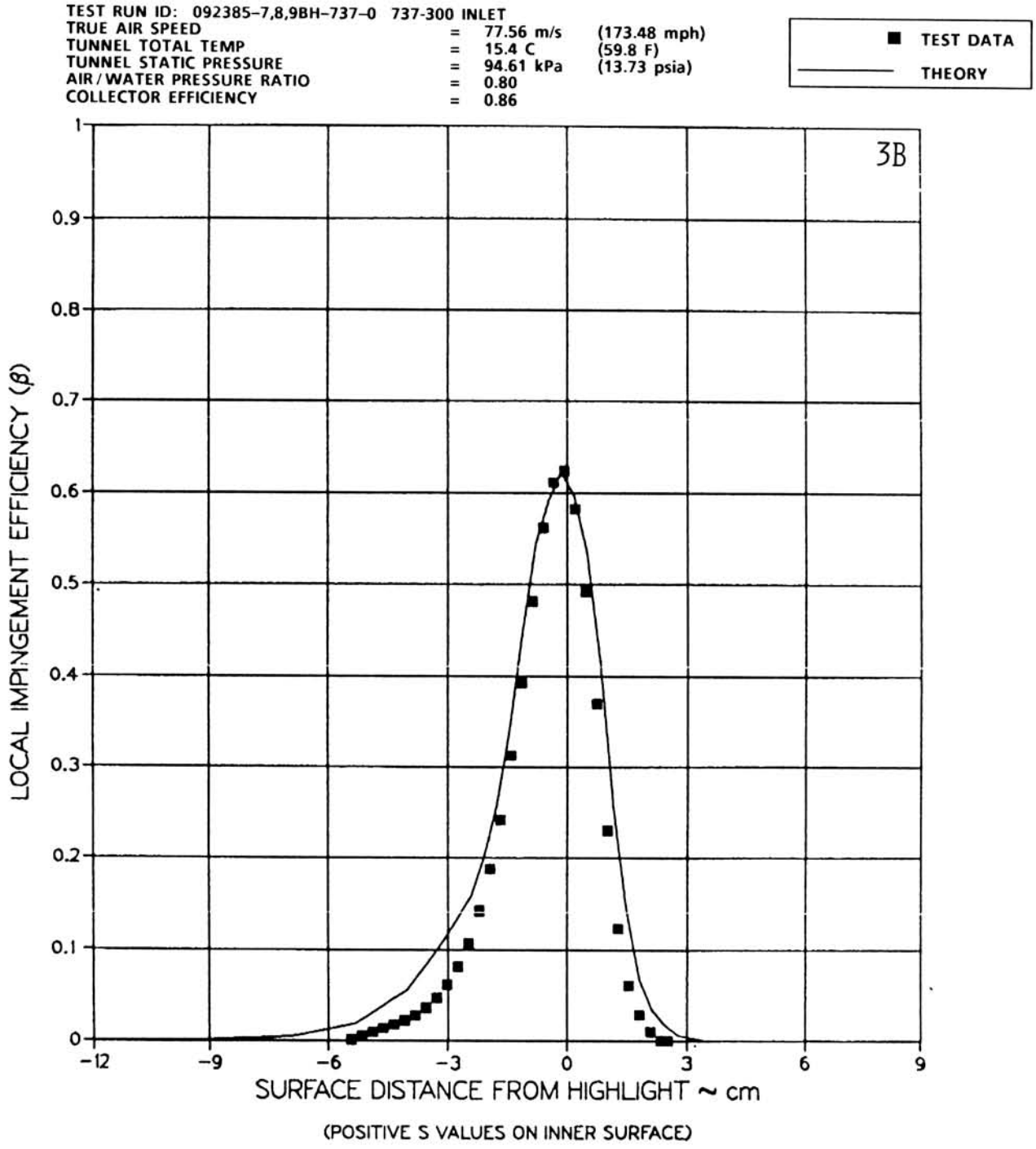

(B2) MVD = 16.45 MICRONS, MASS FLOW = 22.96 LBM/SEC, $\theta = 45°$

FIGURE 6.19

AVERAGED LOCAL WATER IMPINGEMENT EFFICIENCY DATA FOR BOEING 737-300 INLET AT $\alpha = 0°$ (PAGE 8 OF 21).

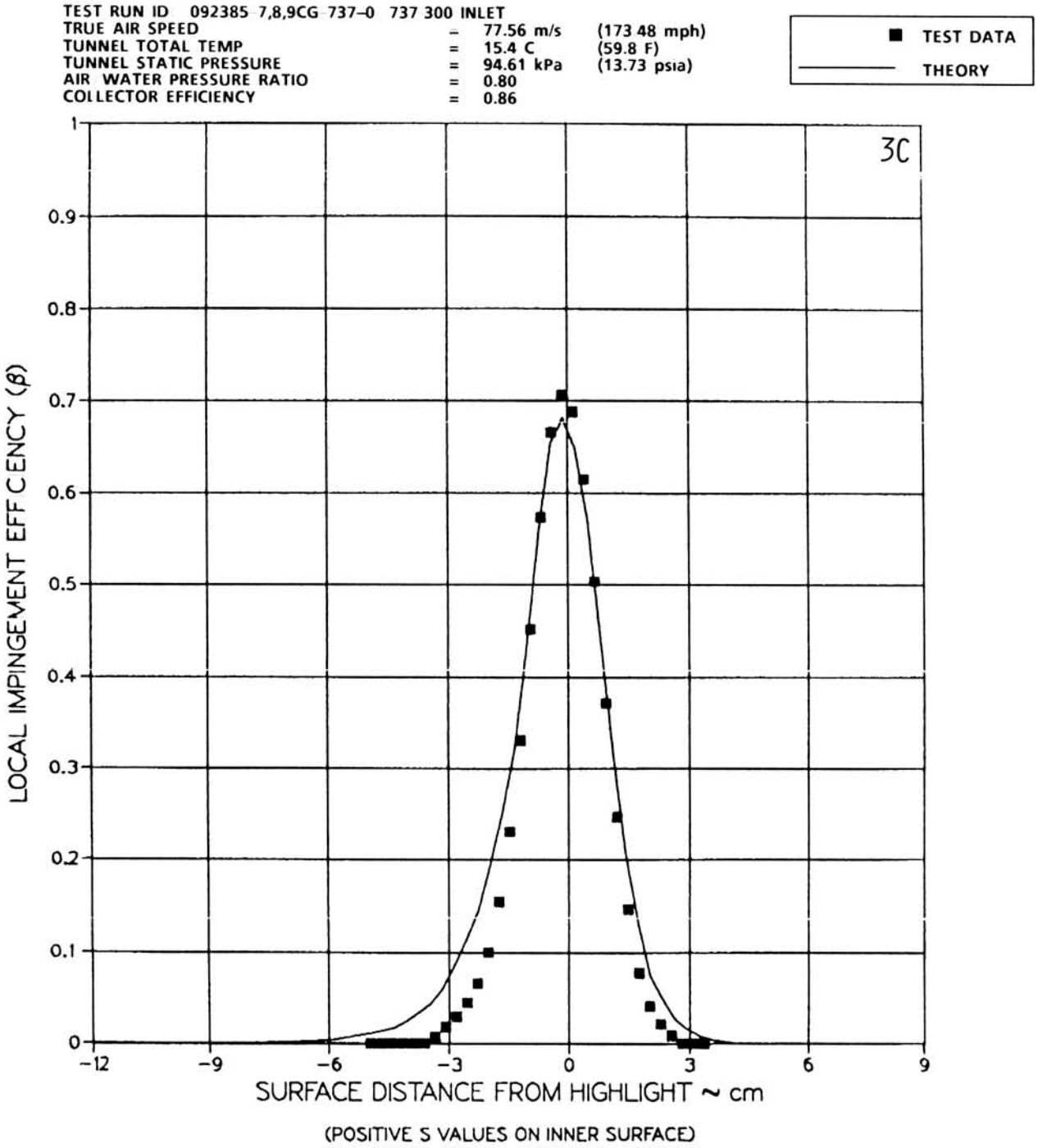

(B3) MVD = 16.45 MICRONS, MASS FLOW = 22.96 LBM / SEC, $\theta = 90°$

FIGURE 6.19

AVERAGED LOCAL WATER IMPINGEMENT EFFICIENCY DATA FOR BOEING 737-300 INLET AT $\alpha = 0°$ (PAGE 9 OF 21).

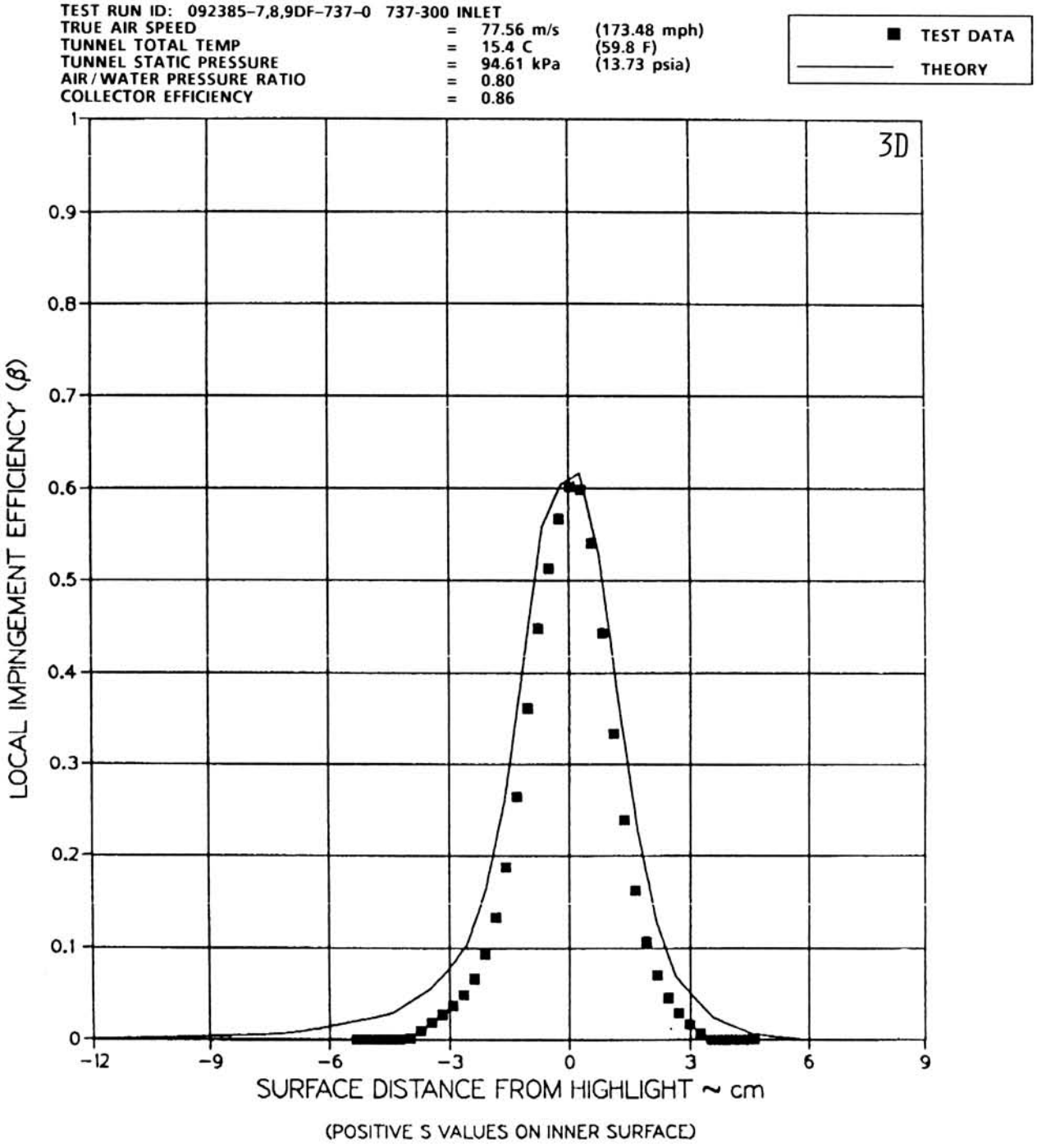

(B4) MVD = 16.45 MICRONS, MASS FLOW = 22.96 LBM/SEC, $\theta = 135°$

FIGURE 6.19

AVERAGED LOCAL WATER IMPINGEMENT EFFICIENCY DATA FOR BOEING 737-300 INLET AT $\alpha = 0°$ (PAGE 10 OF 21).

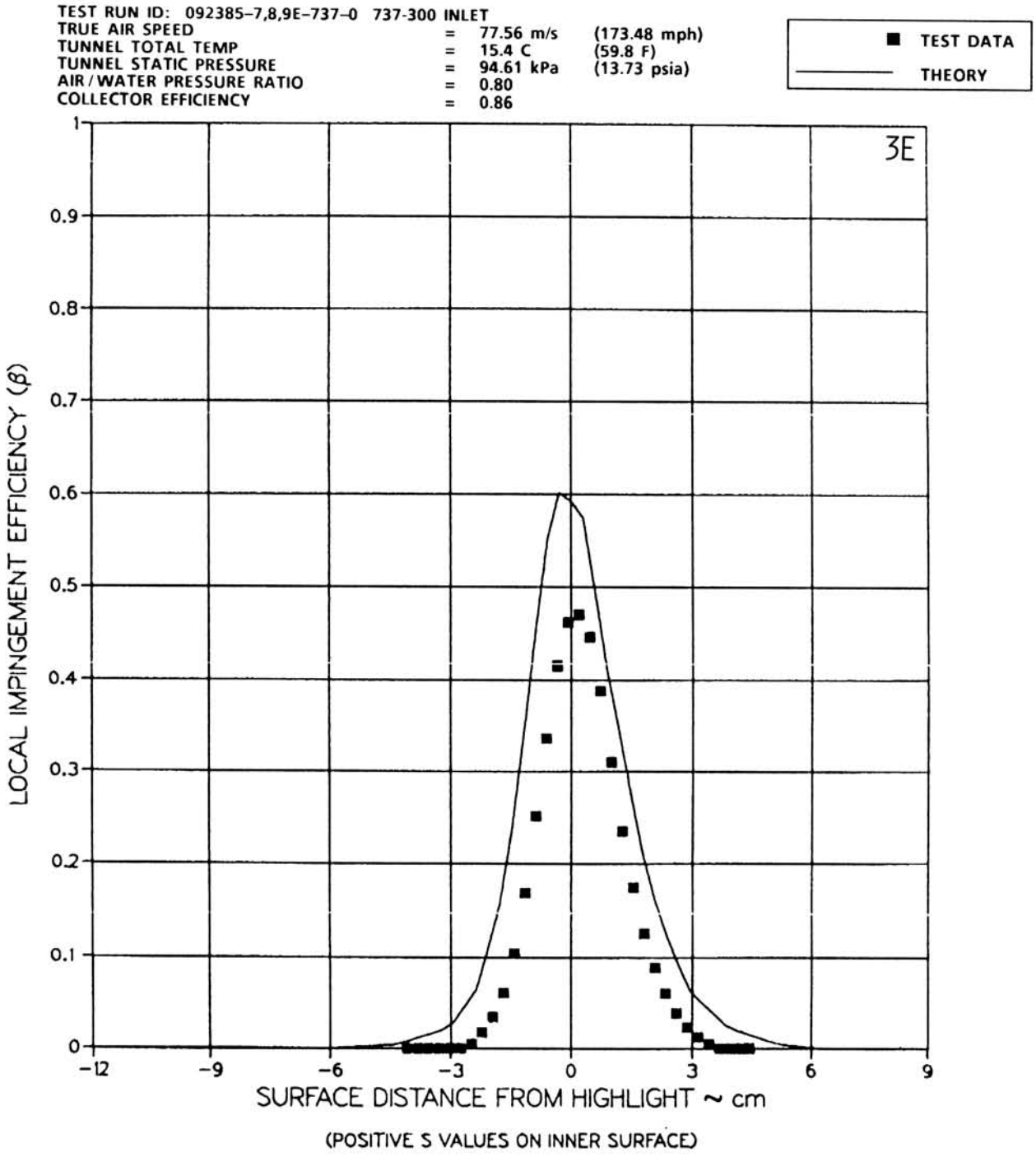

(B5) MVD = 16.45 MICRONS, MASS FLOW = 22.96 LBM/SEC, $\theta = 180°$

FIGURE 6.19

AVERAGED LOCAL WATER IMPINGEMENT EFFICIENCY DATA FOR BOEING 737-300 INLET AT $\alpha = 0°$ (PAGE 11 OF 21).

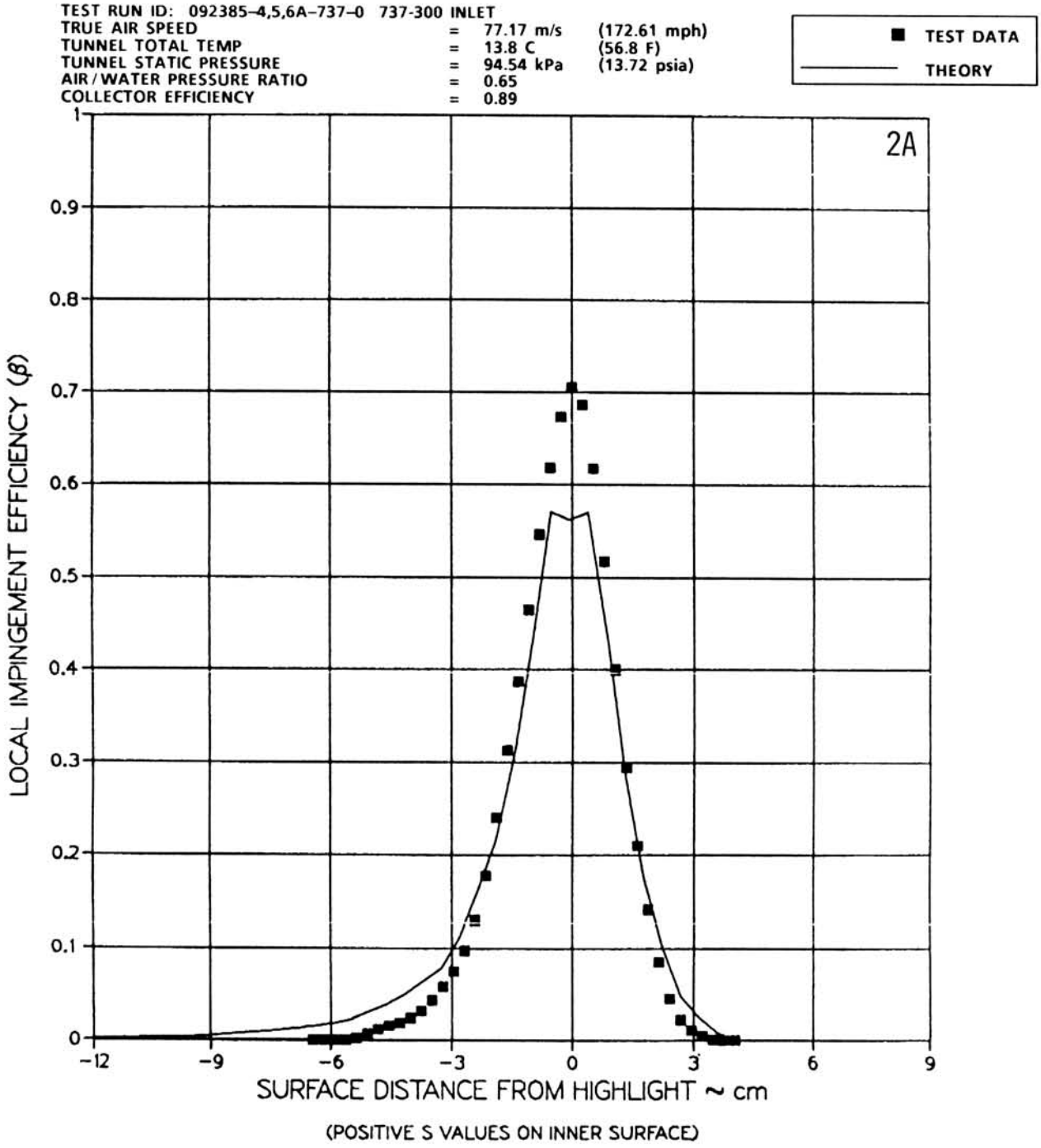

(C1) MVD = 20.36 MICRONS, MASS FLOW = 17.20 LBM / SEC, $\theta = 0°$

FIGURE 6.19

AVERAGED LOCAL WATER IMPINGEMENT EFFICIENCY DATA FOR BOEING 737-300 INLET AT $\alpha = 0°$ (PAGE 12 OF 21).

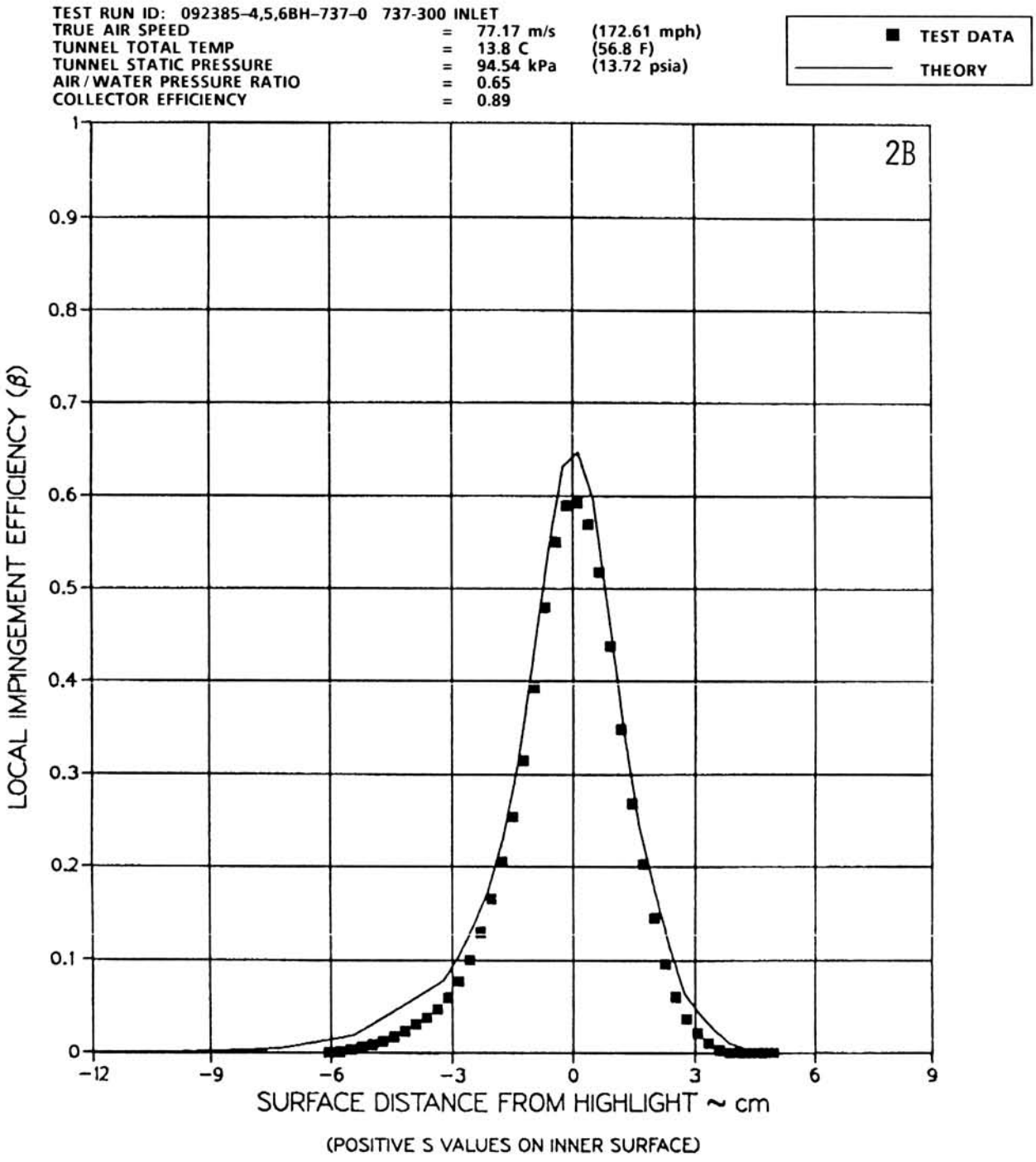

(C2) MVD = 20.36 MICRONS, MASS FLOW = 17.20 LBM/SEC, $\theta = 45°$

FIGURE 6.19

AVERAGED LOCAL WATER IMPINGEMENT EFFICIENCY DATA FOR BOEING 737-300 INLET AT $\alpha = 0°$ (PAGE 13 OF 21).

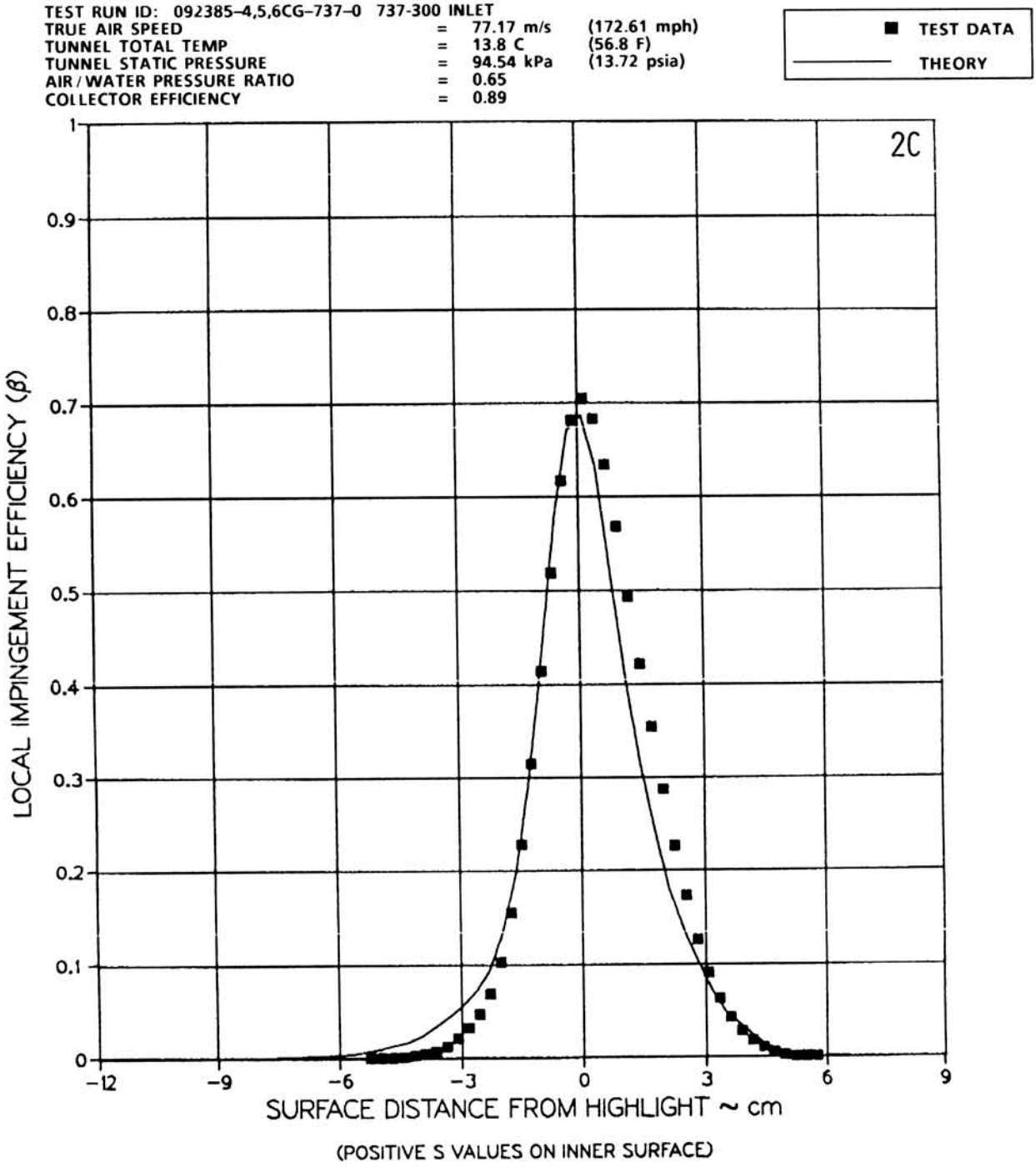

(C3) MVD = 20.36 MICRONS, MASS FLOW = 17.20 LBM / SEC, $\theta = 90°$

FIGURE 6.19

AVERAGED LOCAL WATER IMPINGEMENT EFFICIENCY DATA FOR BOEING 737-300 INLET AT $\alpha = 0°$ (PAGE 14 OF 21).

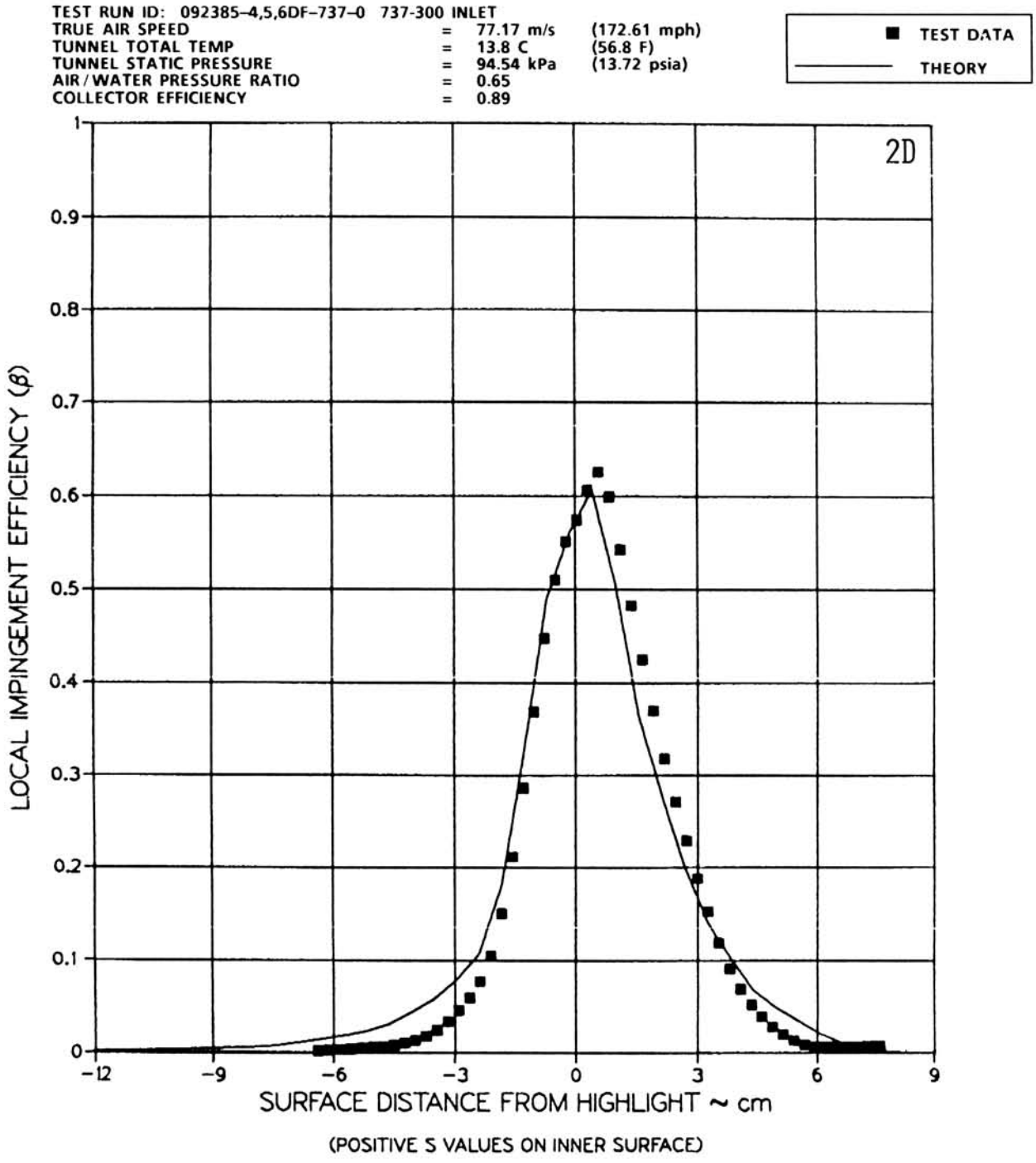

(C4) MVD = 20.36 MICRONS, MASS FLOW = 17.20 LBM/SEC, θ = 135°

FIGURE 6.19

AVERAGED LOCAL WATER IMPINGEMENT EFFICIENCY DATA FOR BOEING 737-300 INLET AT α = 0° (PAGE 15 OF 21).

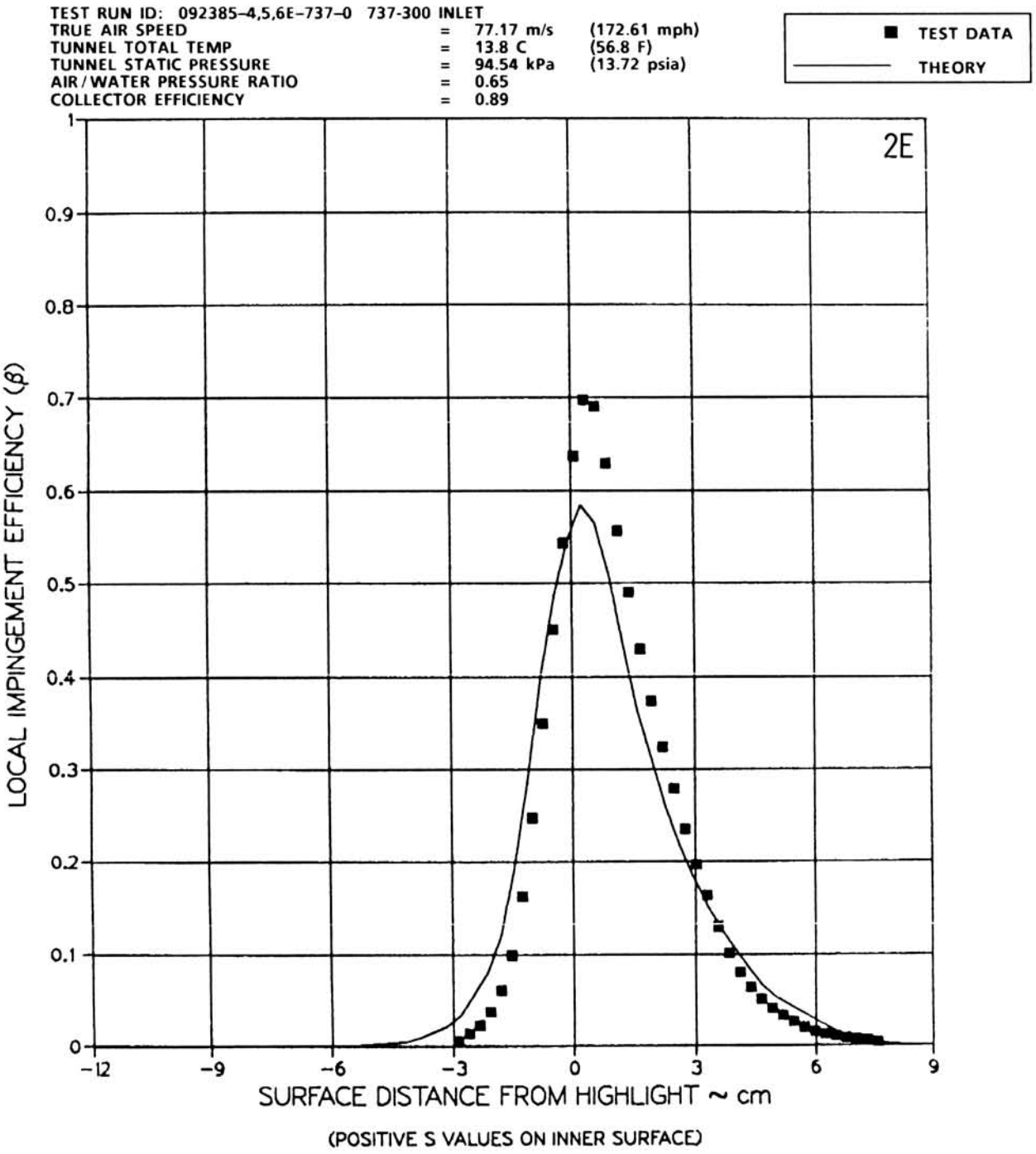

(C5) MVD = 20.36 MICRONS, MASS FLOW = 17.20 LBM/SEC, θ = 180°

FIGURE 6.19

AVERAGED LOCAL WATER IMPINGEMENT EFFICIENCY DATA FOR BOEING 737-300 INLET AT α = 0° (PAGE 16 OF 21).

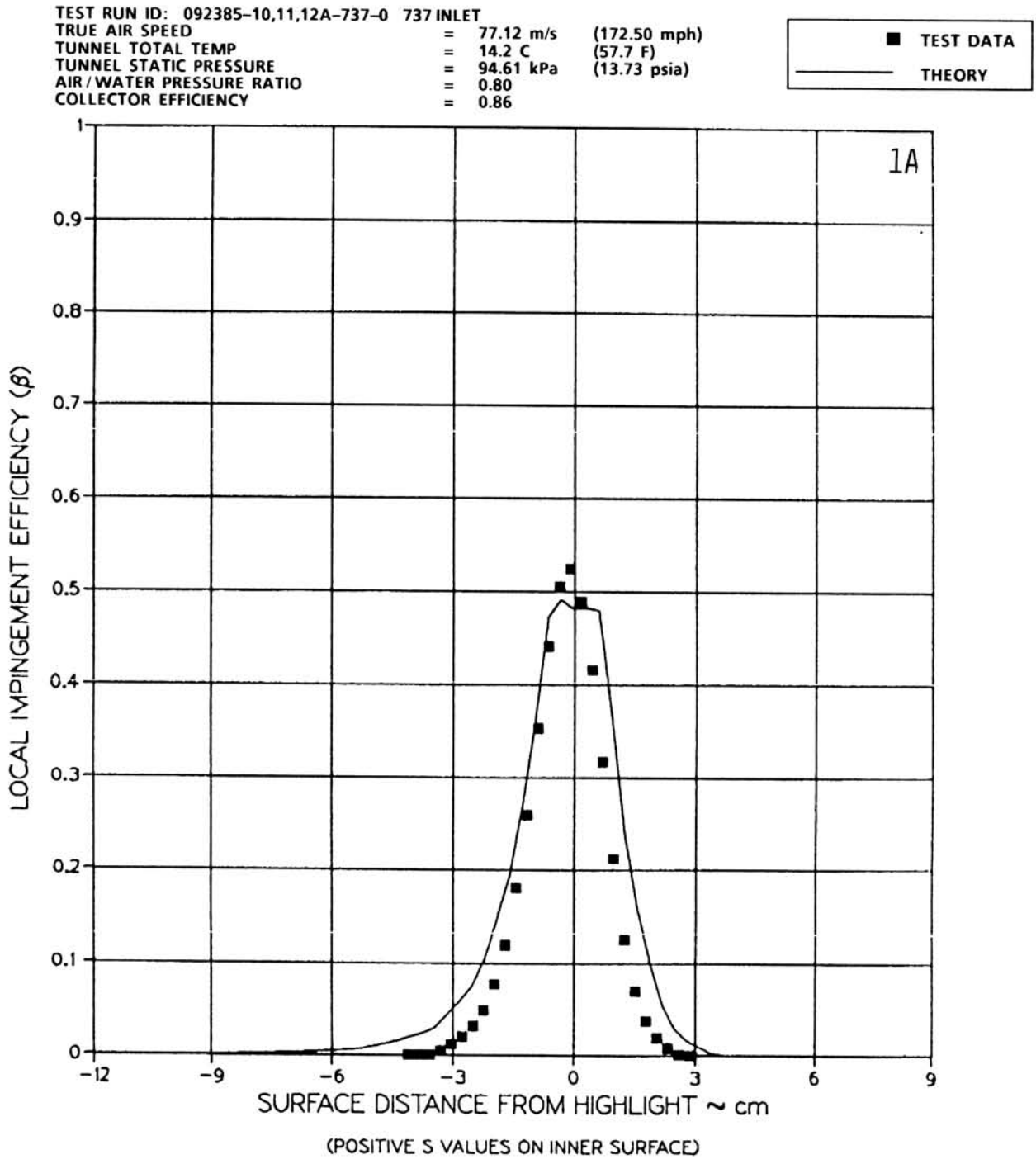

(D1) MVD = 16.45 MICRONS, MASS FLOW = 17.20 LBM / SEC, $\theta = 0°$

FIGURE 6.19

AVERAGED LOCAL WATER IMPINGEMENT EFFICIENCY DATA FOR BOEING 737-300 INLET AT $\alpha = 0°$ (PAGE 17 OF 21).

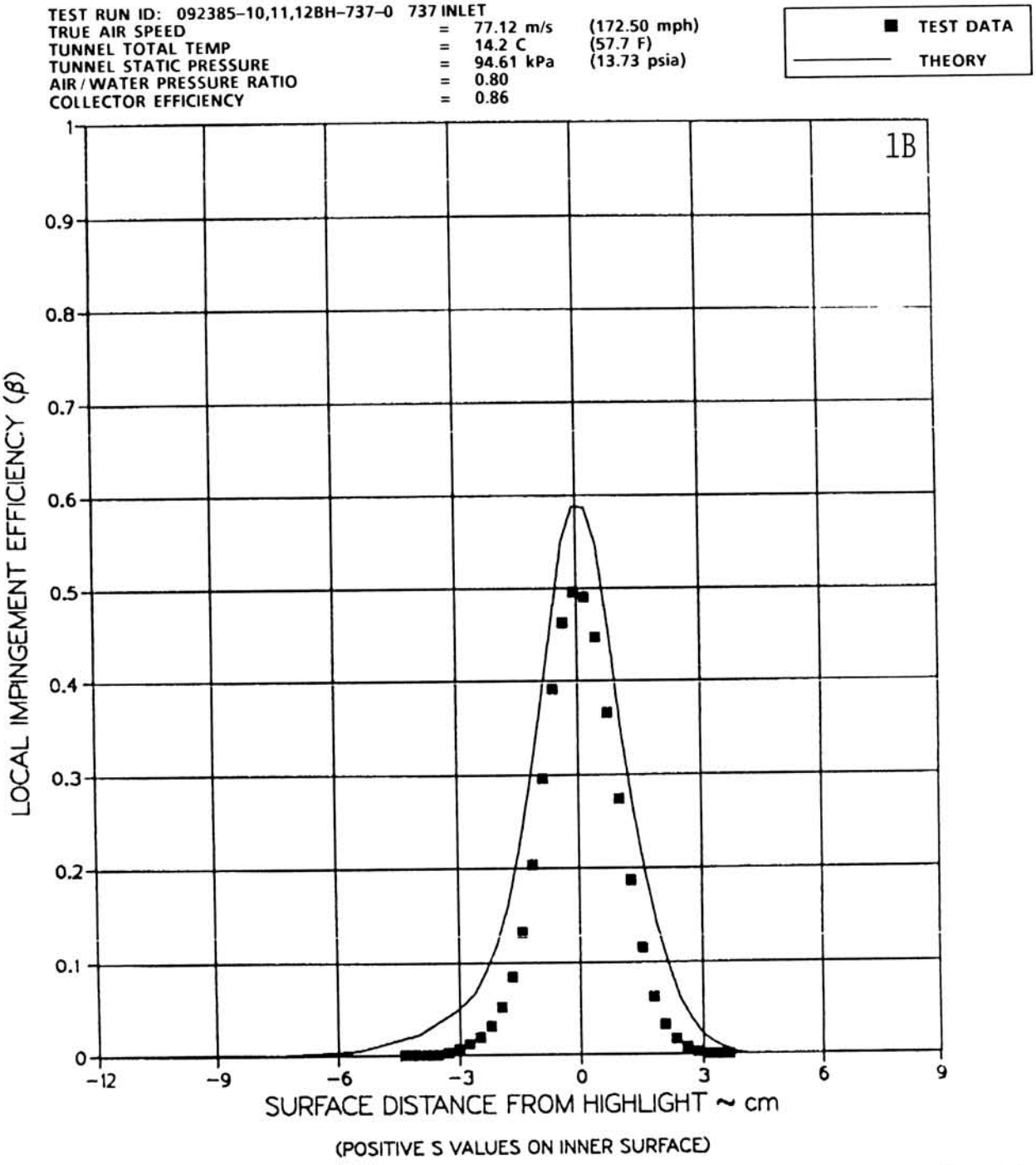

(D2) MVD = 16.45 MICRONS, MASS FLOW = 17.20 LBM / SEC, $\theta = 45°$

FIGURE 6.19

AVERAGED LOCAL WATER IMPINGEMENT EFFICIENCY DATA FOR BOEING 737-300 INLET AT $\alpha = 0°$ (PAGE 18 OF 21).

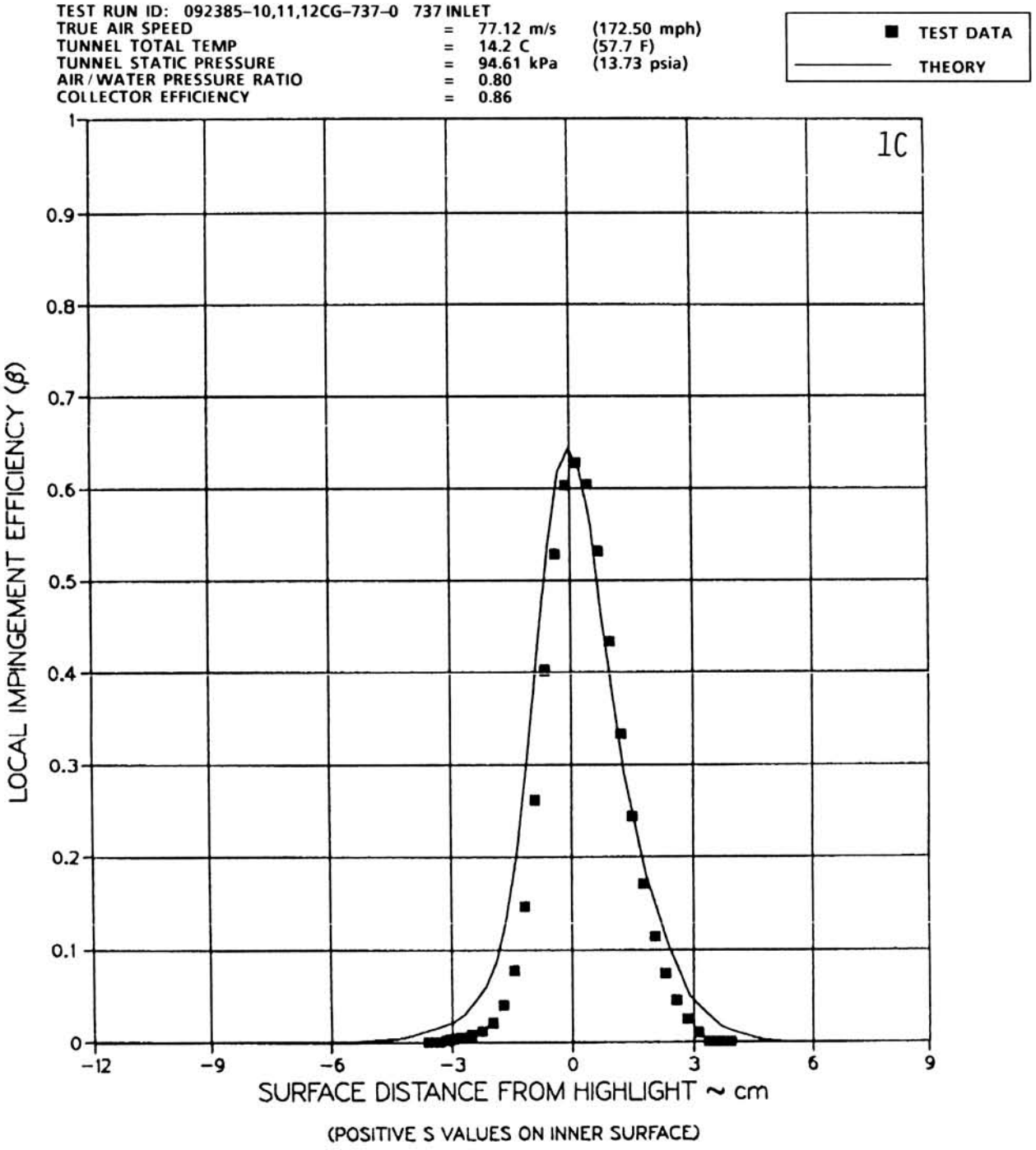

(D3) MVD = 16.45 MICRONS, MASS FLOW = 17.20 LBM/SEC, $\theta = 90°$

FIGURE 6.19

AVERAGED LOCAL WATER IMPINGEMENT EFFICIENCY DATA FOR BOEING 737-300 INLET AT $\alpha = 0°$ (PAGE 19 OF 21).

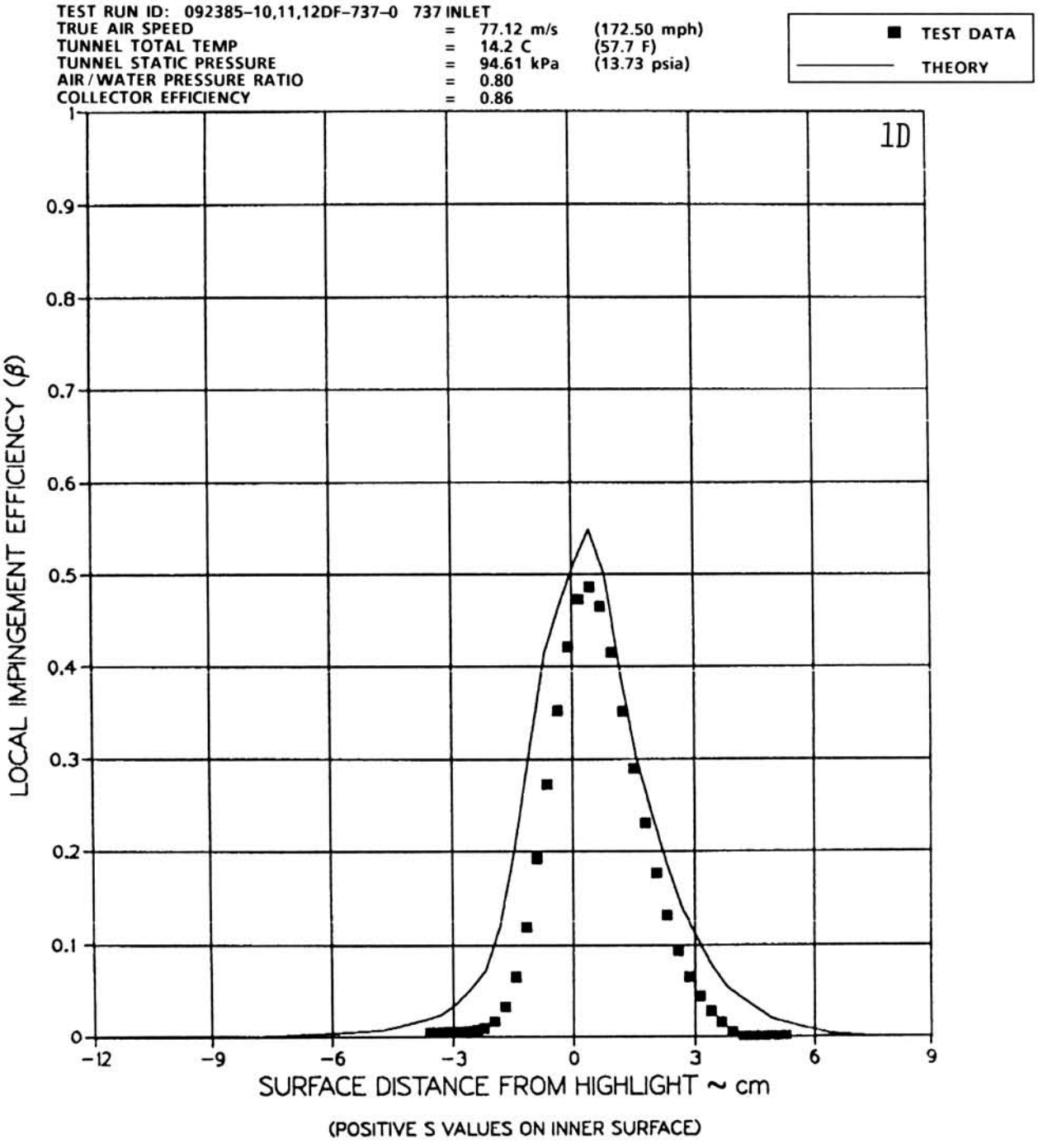

(D4) MVD = 16.45 MICRONS, MASS FLOW = 17.20 LBM / SEC, θ = 135°

FIGURE 6.19

AVERAGED LOCAL WATER IMPINGEMENT EFFICIENCY DATA FOR BOEING 737-300 INLET AT α = 0° (PAGE 20 OF 21).

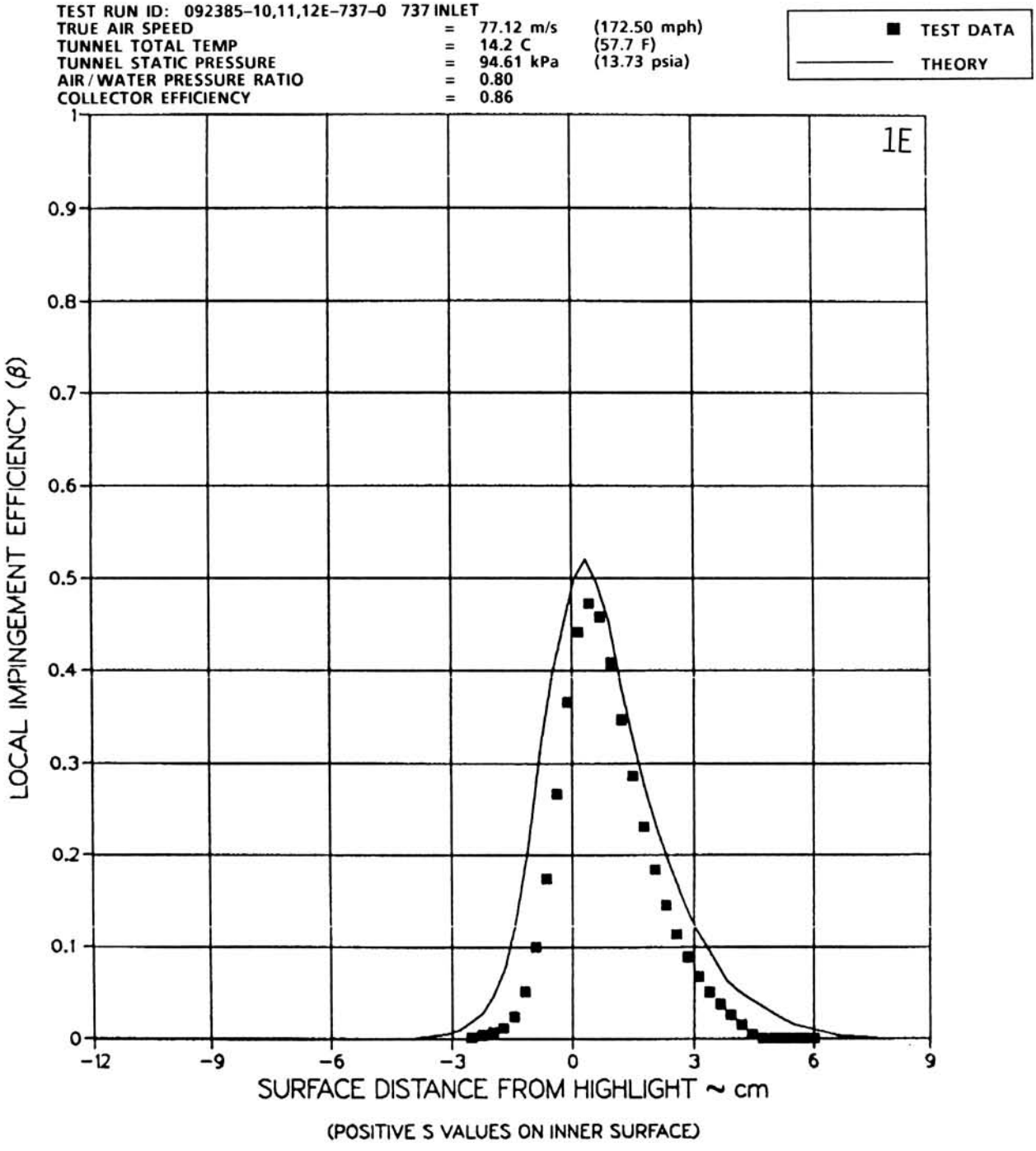

(D5) MVD = 16.45 MICRONS, MASS FLOW = 17.20 LBM/SEC, $\theta = 180°$

FIGURE 6.19

AVERAGED LOCAL WATER IMPINGEMENT EFFICIENCY DATA FOR BOEING 737-300 INLET AT $\alpha = 0°$ (PAGE 21 OF 21).

TEST RUN ID: 092385-17,18A-737-15 737-300 INLET

TRUE AIR SPEED	=	77.24 m/s	(172.77 mph)
TUNNEL TOTAL TEMP	=	13.9 C	(57.1 F)
TUNNEL STATIC PRESSURE	=	94.68 kPa	(13.74 psia)
AIR/WATER PRESSURE RATIO	=	0.65	
COLLECTOR EFFICIENCY	=	0.89	

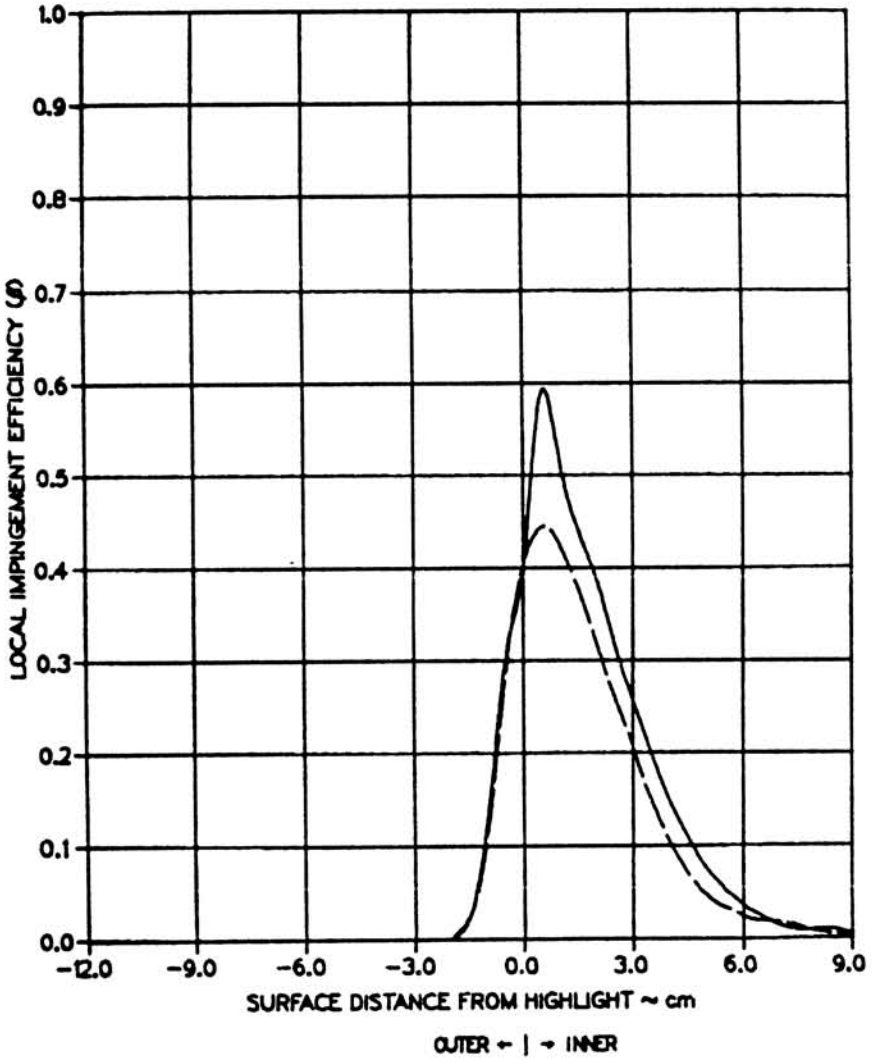

MVD = 20.36 MICRONS θ = 0°

FIGURE 6.20

TEST REPEATABILITY FOR BOEING 737-300 INLET:
α = 15°, MASS FLOW = 17.20 LBM/SEC (PAGE 1 OF 3).

TEST RUN ID: 092385-17,18CG-737-15 737-300 INLET

TRUE AIR SPEED	=	77.24 m/s	(172.77 mph)
TUNNEL TOTAL TEMP	=	13.9 C	(57.1 F)
TUNNEL STATIC PRESSURE	=	94.68 kPa	(13.74 psia)
AIR/WATER PRESSURE RATIO	=	0.65	
COLLECTOR EFFICIENCY	=	0.89	

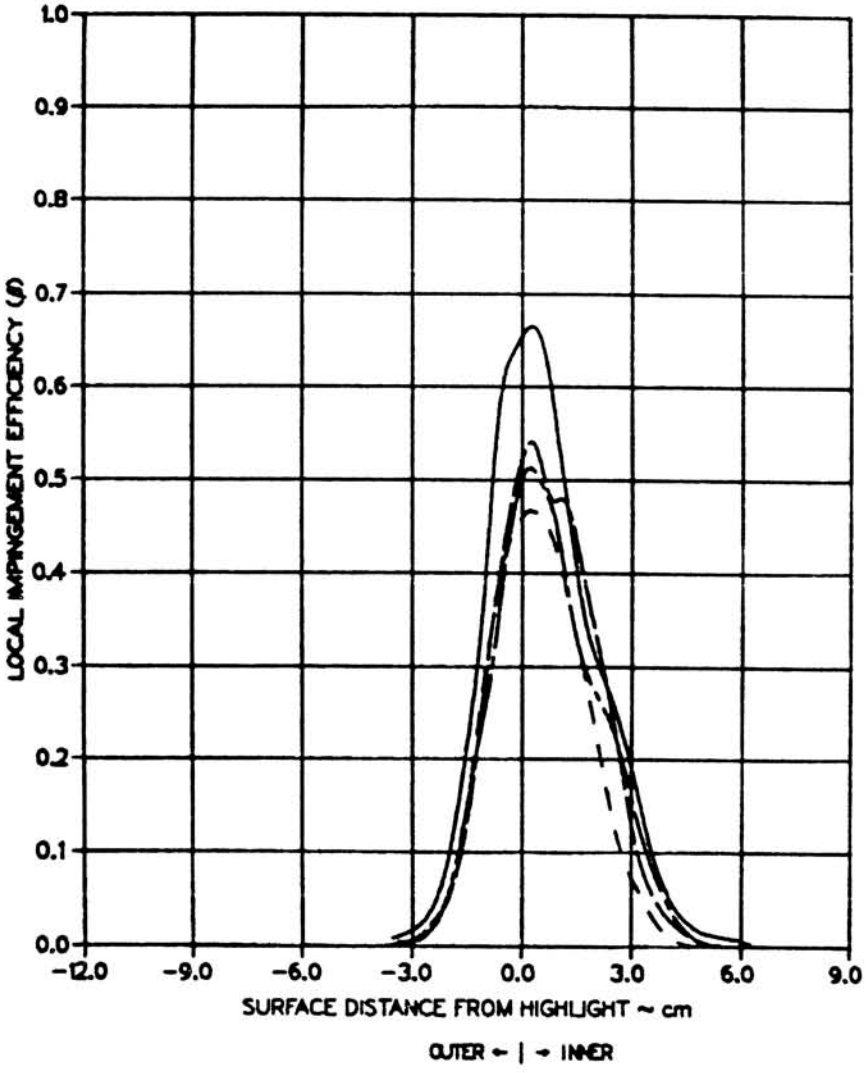

MVD = 20.36 MICRONS θ = 90°, 270°

FIGURE 6.20

TEST REPEATABILITY FOR BOEING 737-300 INLET:
α = 15°, MASS FLOW = 17.20 LBM/SEC (PAGE 2 OF 3).

TEST RUN ID: 092385-17,18E-737-15 737-300 INLET

TRUE AIR SPEED	=	77.24 m/s	(172.77 mph)
TUNNEL TOTAL TEMP	=	13.9 C	(57.1 F)
TUNNEL STATIC PRESSURE	=	94.68 kPa	(13.74 psia)
AIR/WATER PRESSURE RATIO	=	0.65	
COLLECTOR EFFICIENCY	=	0.89	

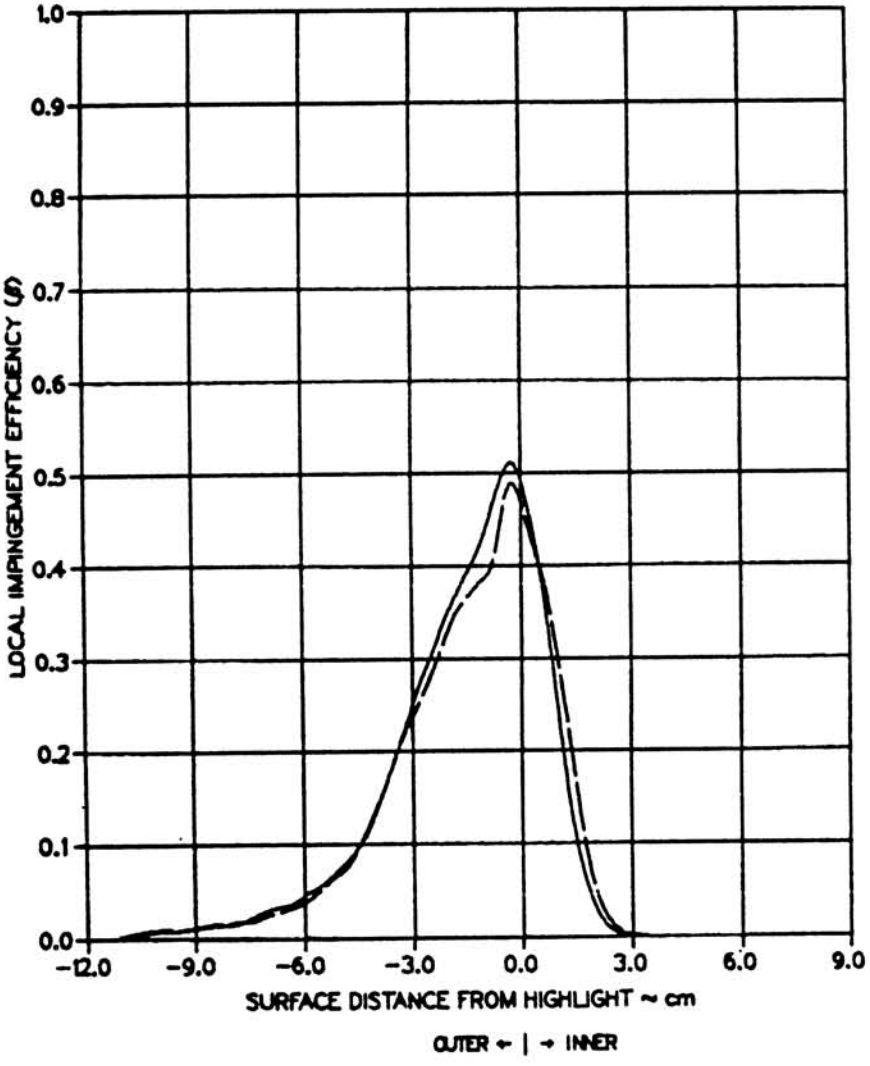

MVD = 20.36 MICRONS θ = 180°

FIGURE 6.20

TEST REPEATABILITY FOR BOEING 737-300 INLET:
α = 15°, MASS FLOW = 17.20 LBM/SEC (PAGE 3 OF 3).

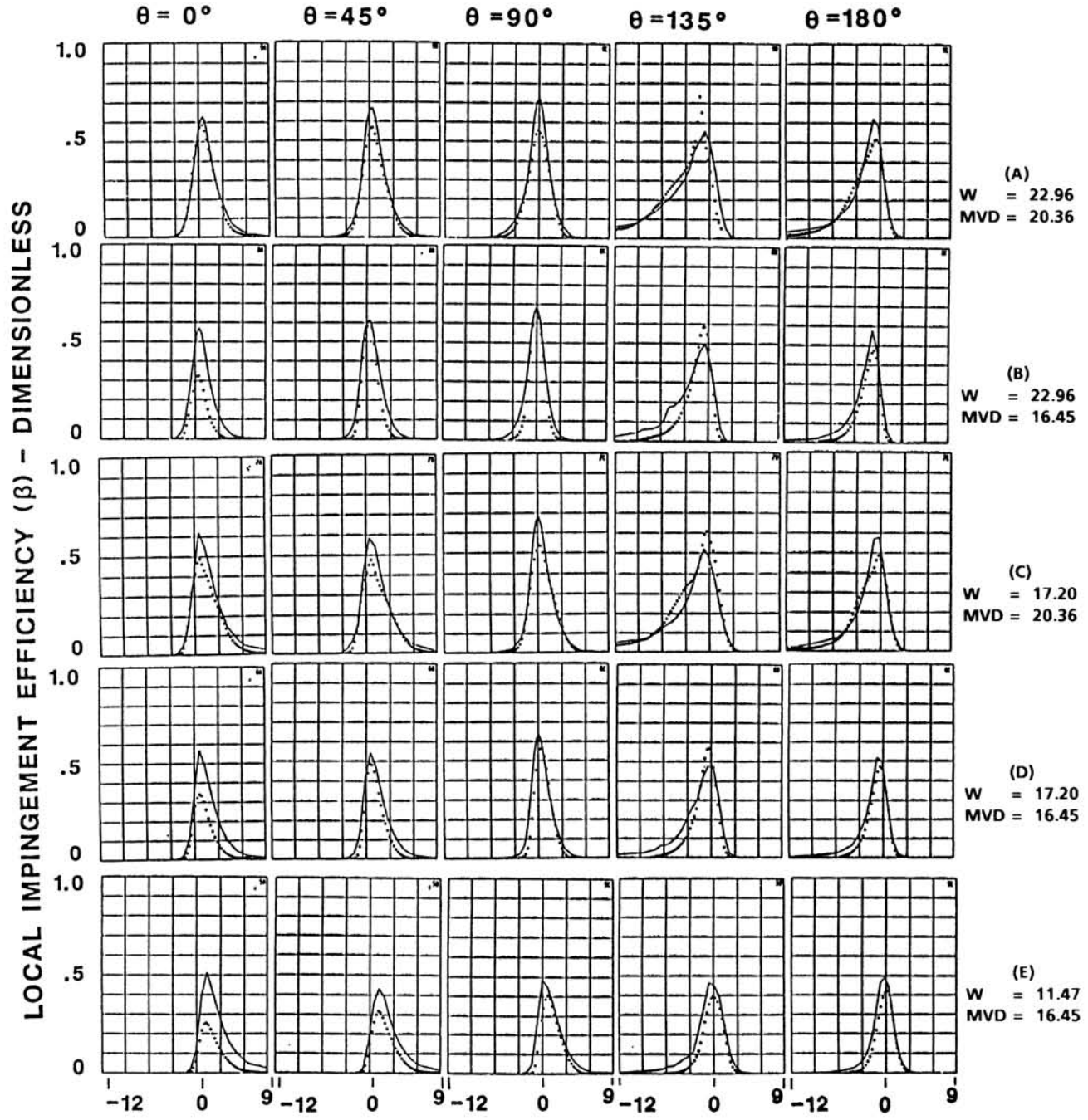

NOTE: W ~ LBM / SEC, MVD ~ μm
NEGATIVE SURFACE DISTANCE – OUTER SURFACE
POSITIVE SURFACE DISTANCE – INNER SURFACE

■ TEST DATA
——— THEORY

SUMMARY OF RESULTS

FIGURE 6.21

AVERAGED LOCAL WATER IMPINGEMENT EFFICIENCY DATA FOR BOEING 737-300 INLET AT α = 15° (PAGE 1 OF 26).

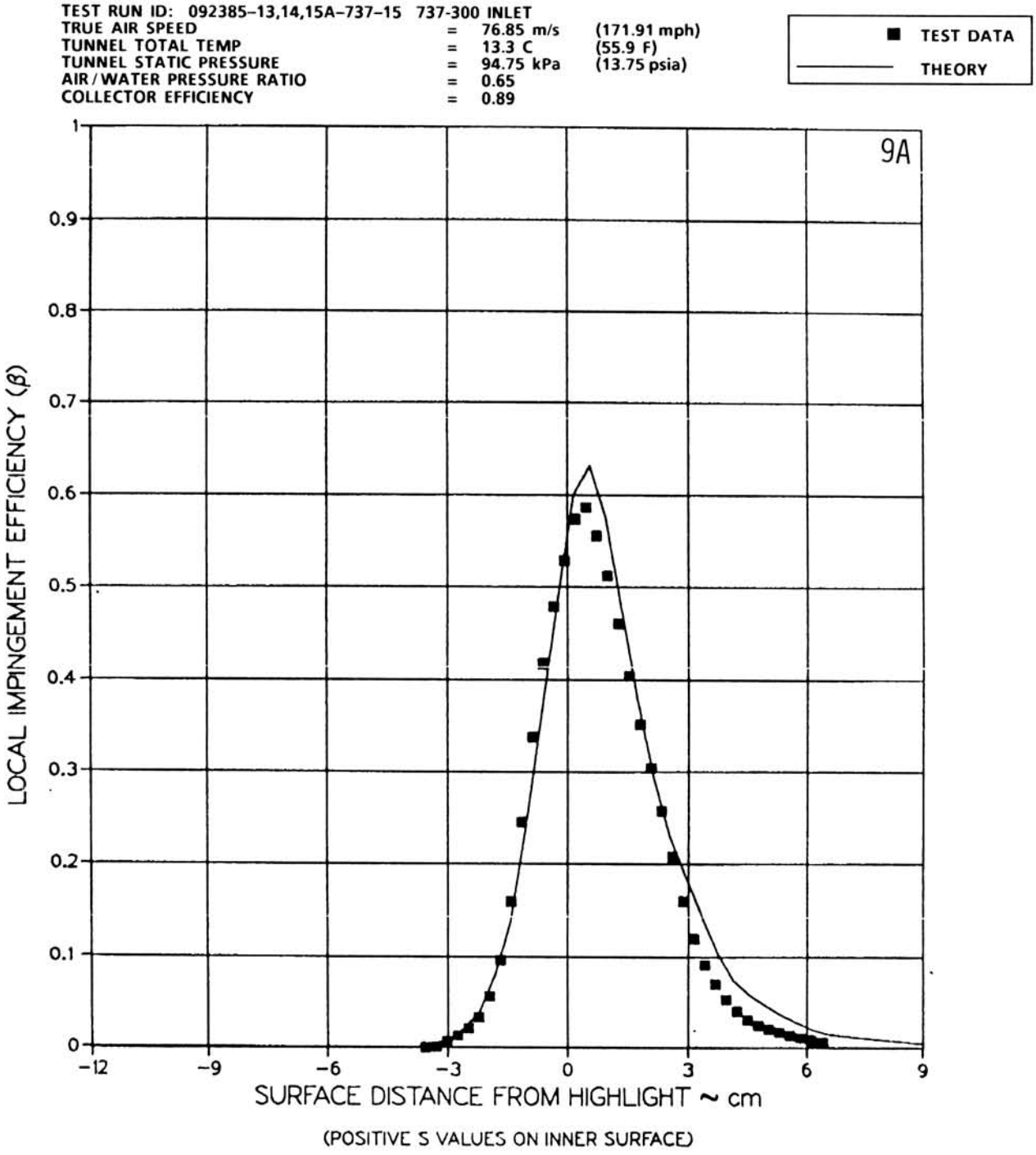

(A1) MVD = 20.36 MICRONS, MASS FLOW = 22.96 LBM / SEC, $\theta = 0°$

FIGURE 6.21

AVERAGED LOCAL WATER IMPINGEMENT EFFICIENCY DATA FOR BOEING 737-300 INLET AT $\alpha = 15°$ (PAGE 2 OF 26).

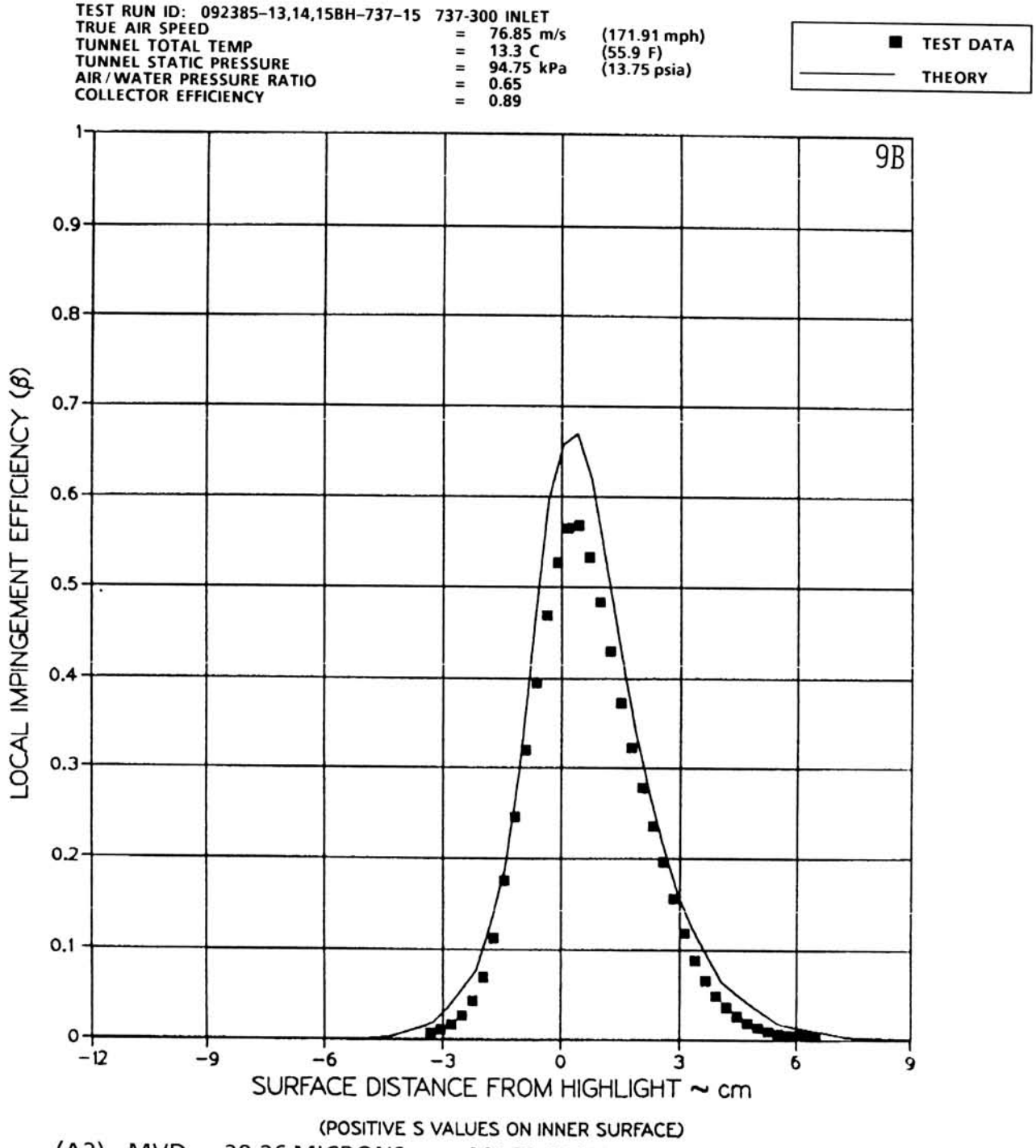

(A2) MVD = 20.36 MICRONS, MASS FLOW = 22.96 LBM/SEC, θ = 45°

FIGURE 6.21

AVERAGED LOCAL WATER IMPINGEMENT EFFICIENCY DATA FOR BOEING 737-300 INLET AT α = 15° (PAGE 3 OF 26).

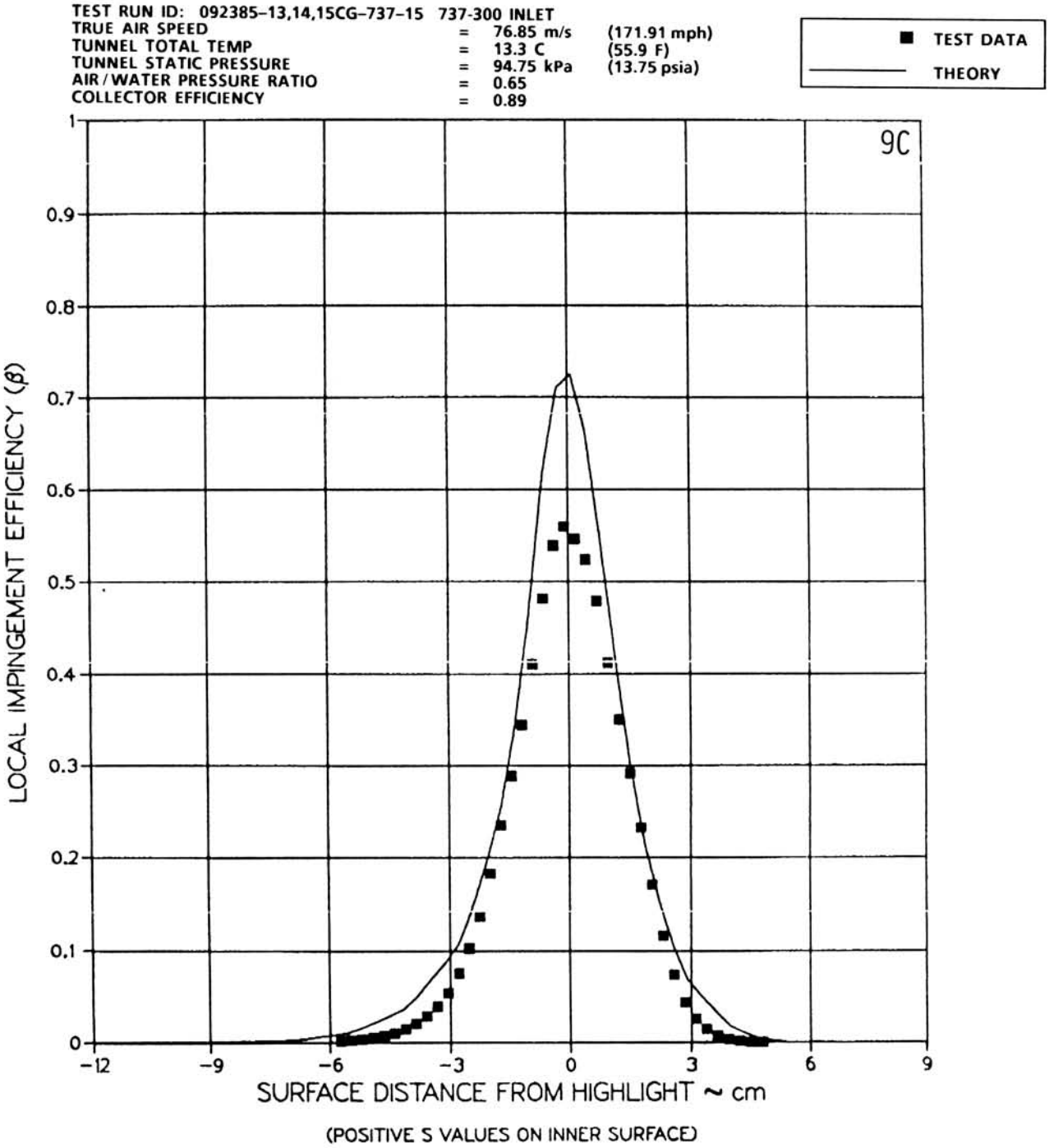

(A3) MVD = 20.36 MICRONS, MASS FLOW = 22.96 LBM / SEC, θ = 90°

FIGURE 6.21

AVERAGED LOCAL WATER IMPINGEMENT EFFICIENCY DATA FOR BOEING 737-300 INLET AT α = 15° (PAGE 4 OF 26).

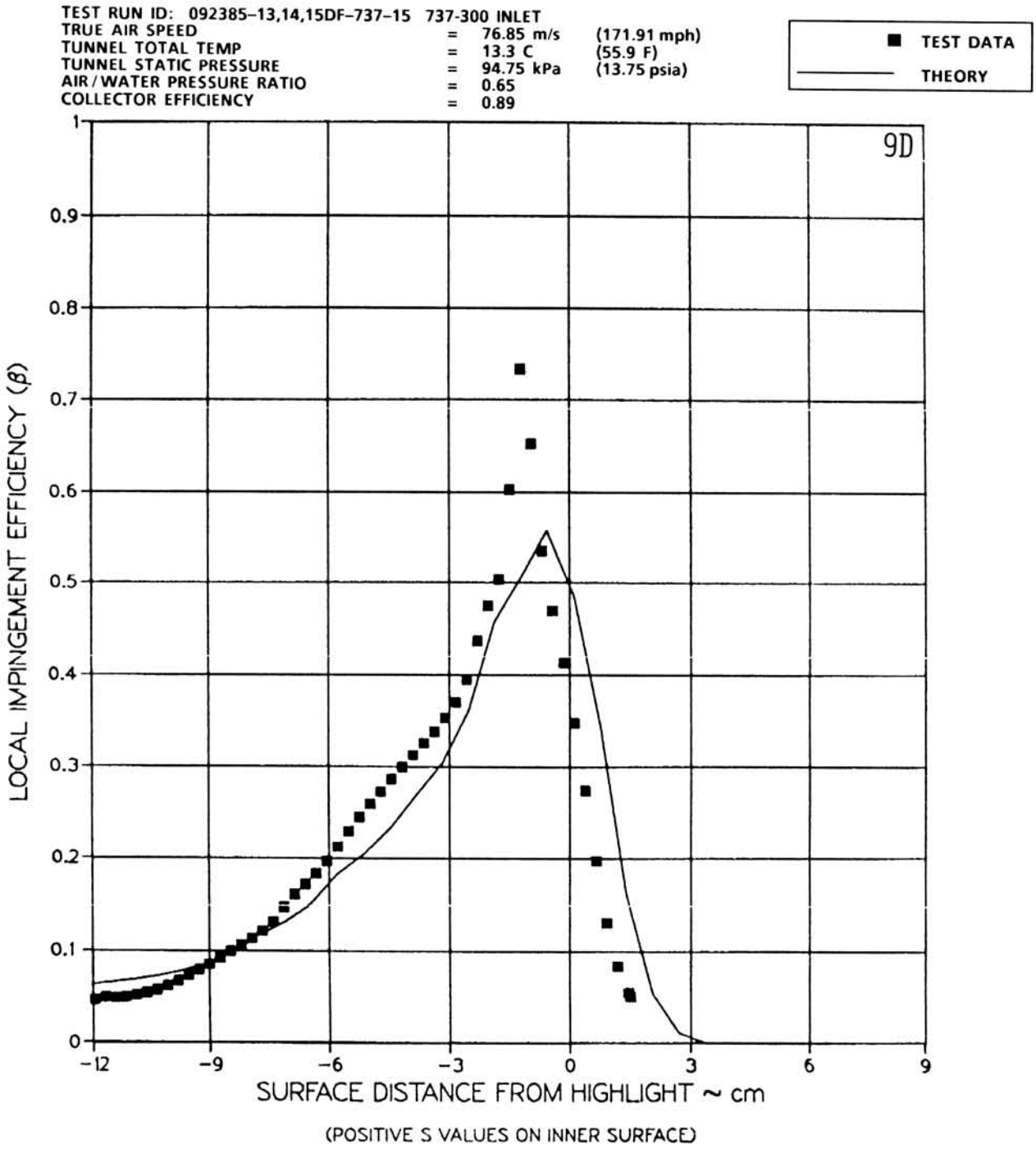

(A4) MVD = 20.36 MICRONS, MASS FLOW = 22.96 LBM/SEC, θ = 135°

FIGURE 6.21

AVERAGED LOCAL WATER IMPINGEMENT EFFICIENCY DATA FOR BOEING 737-300 INLET AT α = 15° (PAGE 5 OF 26).

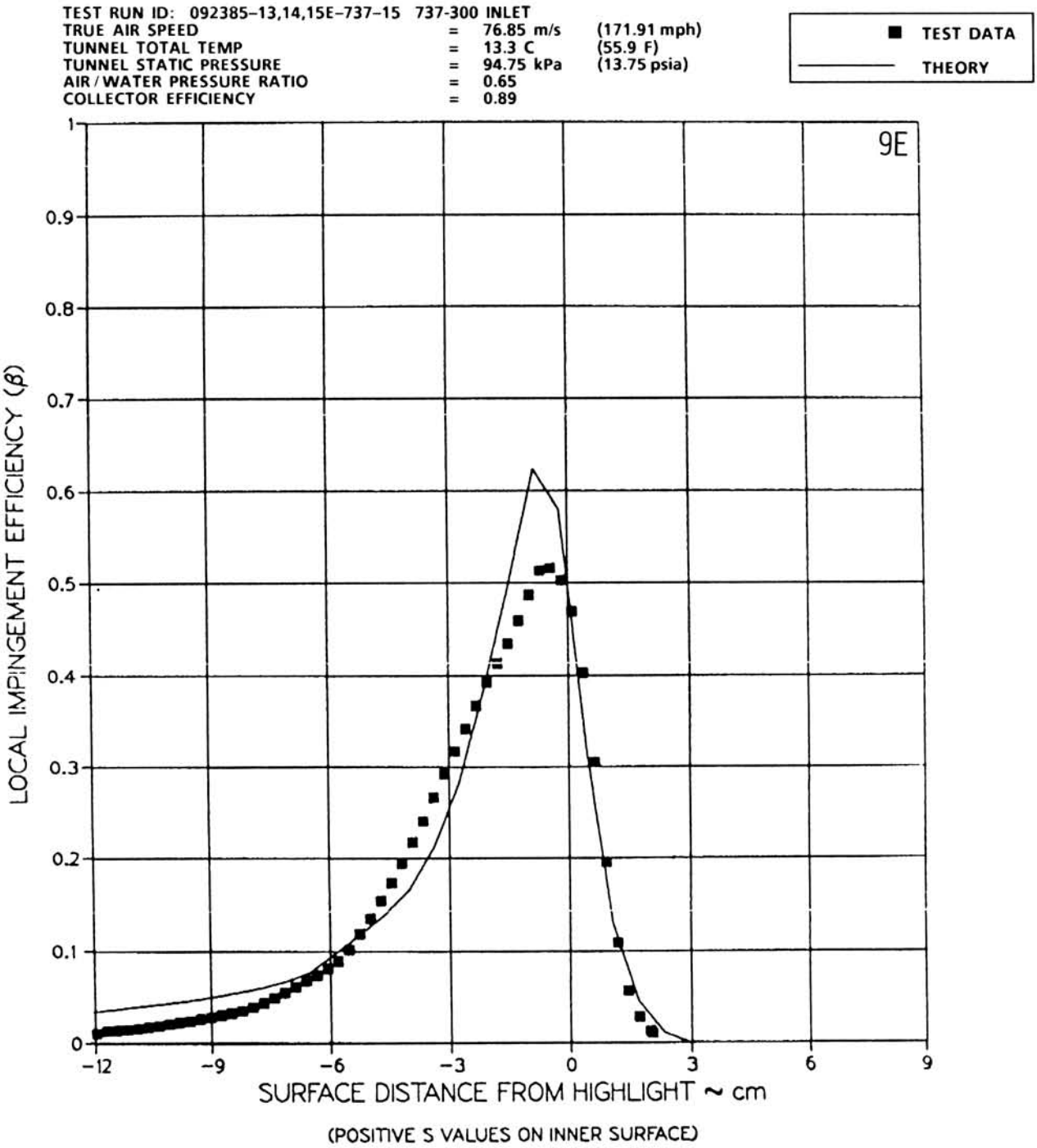

(A5) MVD = 20.36 MICRONS, MASS FLOW = 22.96 LBM/SEC, θ = 180°

FIGURE 6.21

AVERAGED LOCAL WATER IMPINGEMENT EFFICIENCY DATA FOR BOEING 737-300 INLET AT α = 15° (PAGE 6 OF 26).

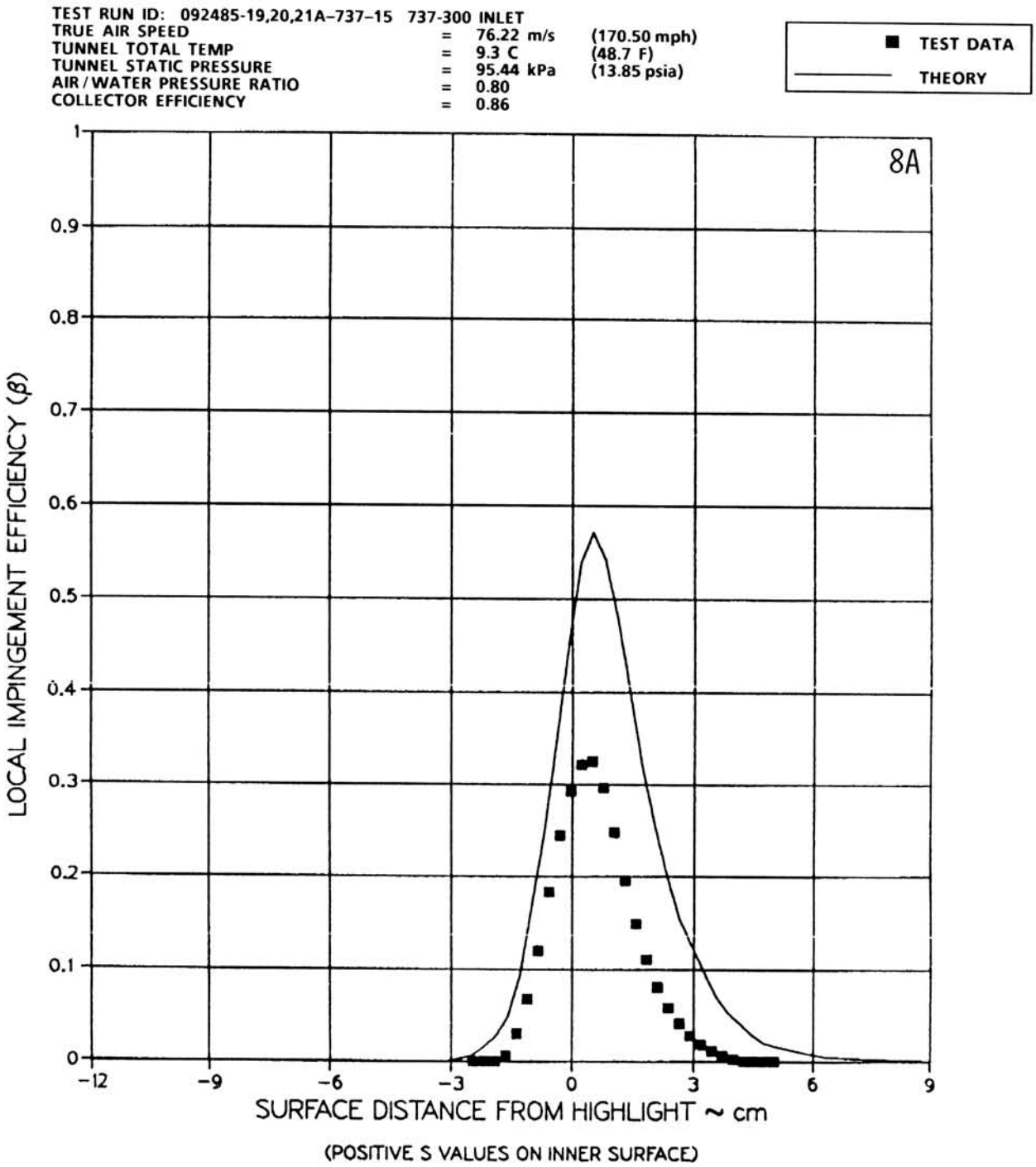

(B1) MVD = 16.45 MICRONS, MASS FLOW = 22.96 LBM/SEC, θ = 0°

FIGURE 6.21

AVERAGED LOCAL WATER IMPINGEMENT EFFICIENCY DATA FOR BOEING 737-300 INLET AT α = 15° (PAGE 7 OF 26).

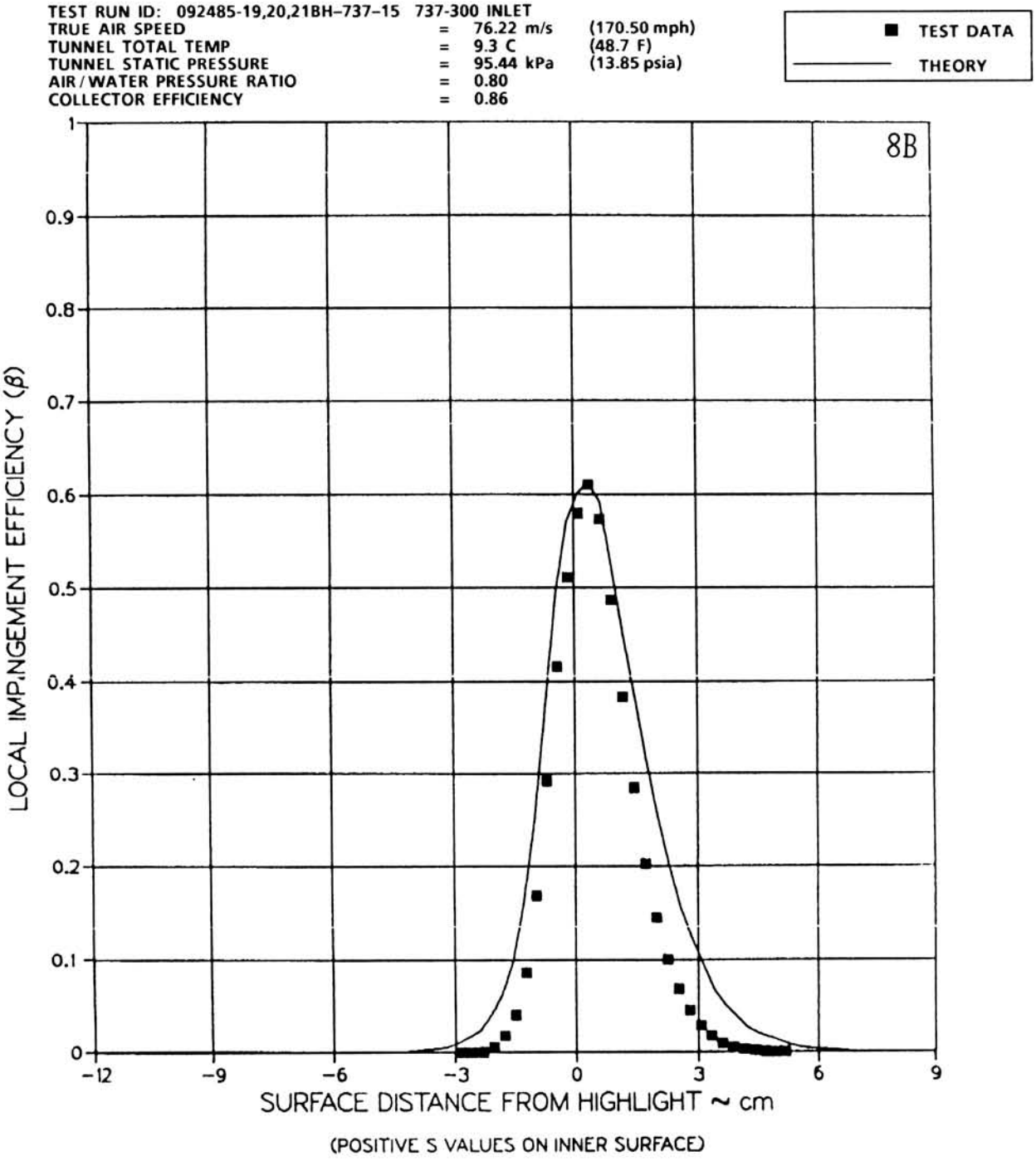

(B2) MVD = 16.45 MICRONS, MASS FLOW = 22.96 LBM / SEC, θ = 45°

FIGURE 6.21

AVERAGED LOCAL WATER IMPINGEMENT EFFICIENCY DATA FOR BOEING 737-300 INLET AT α = 15° (PAGE 8 OF 26).

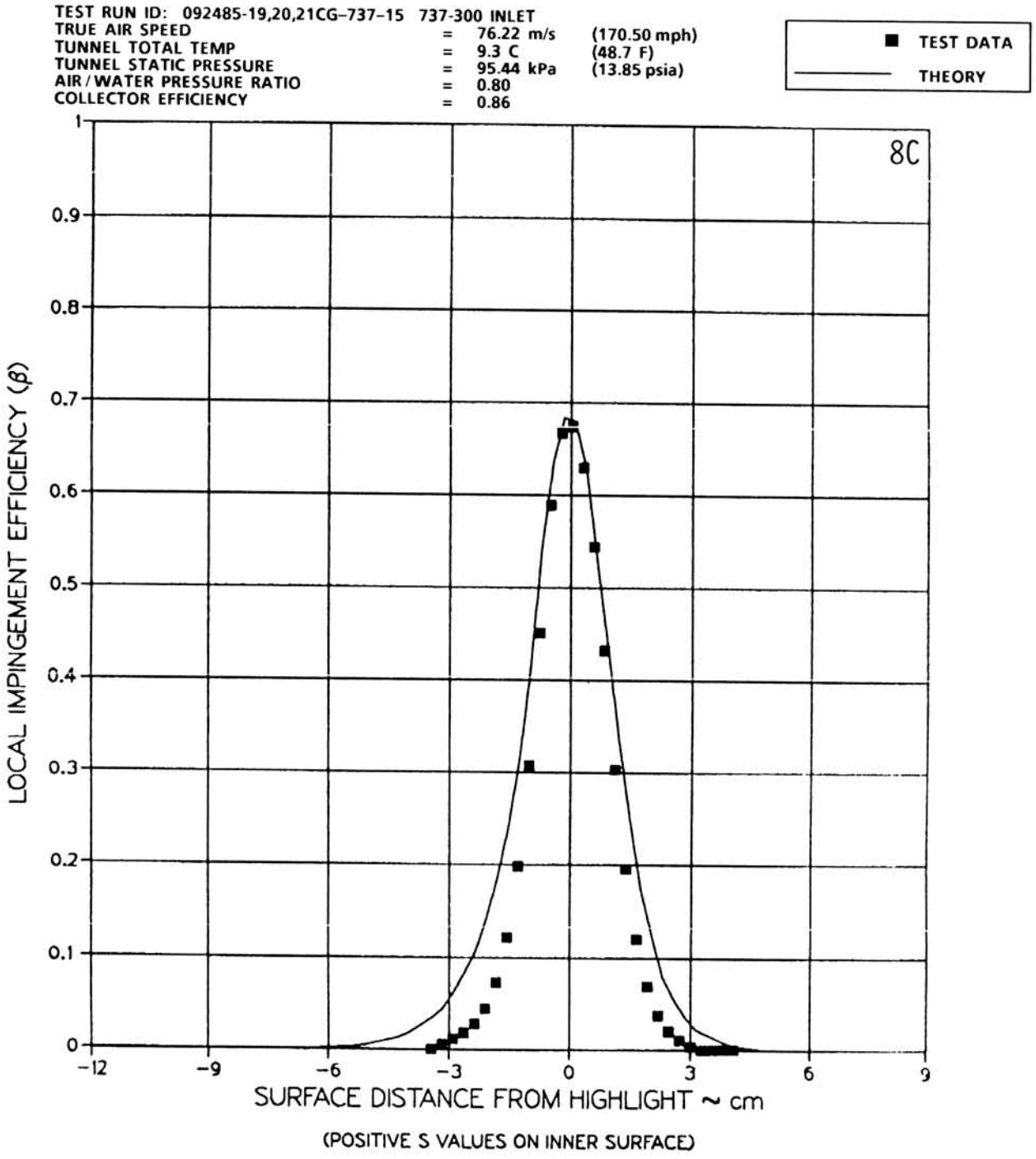

(B3) MVD = 16.45 MICRONS, MASS FLOW = 22.96 LBM/SEC, θ = 90°

FIGURE 6.21

AVERAGED LOCAL WATER IMPINGEMENT EFFICIENCY DATA FOR BOEING 737-300 INLET AT α = 15° (PAGE 9 OF 26).

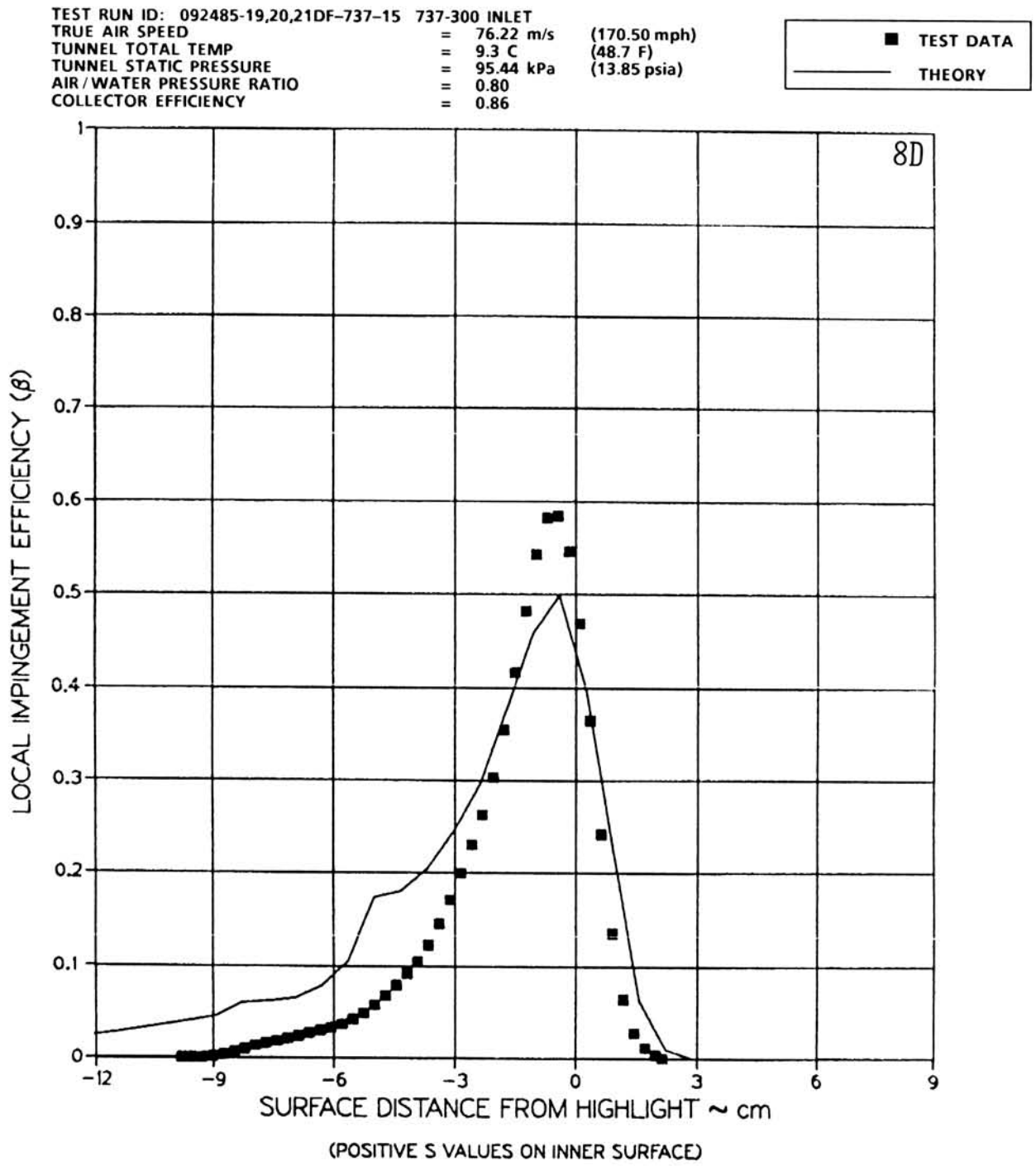

(B4) MVD = 16.45 MICRONS, MASS FLOW = 22.96 LBM / SEC, θ = 135°

FIGURE 6.21

AVERAGED LOCAL WATER IMPINGEMENT EFFICIENCY DATA FOR BOEING 737-300 INLET AT α = 15° (PAGE 10 OF 26).

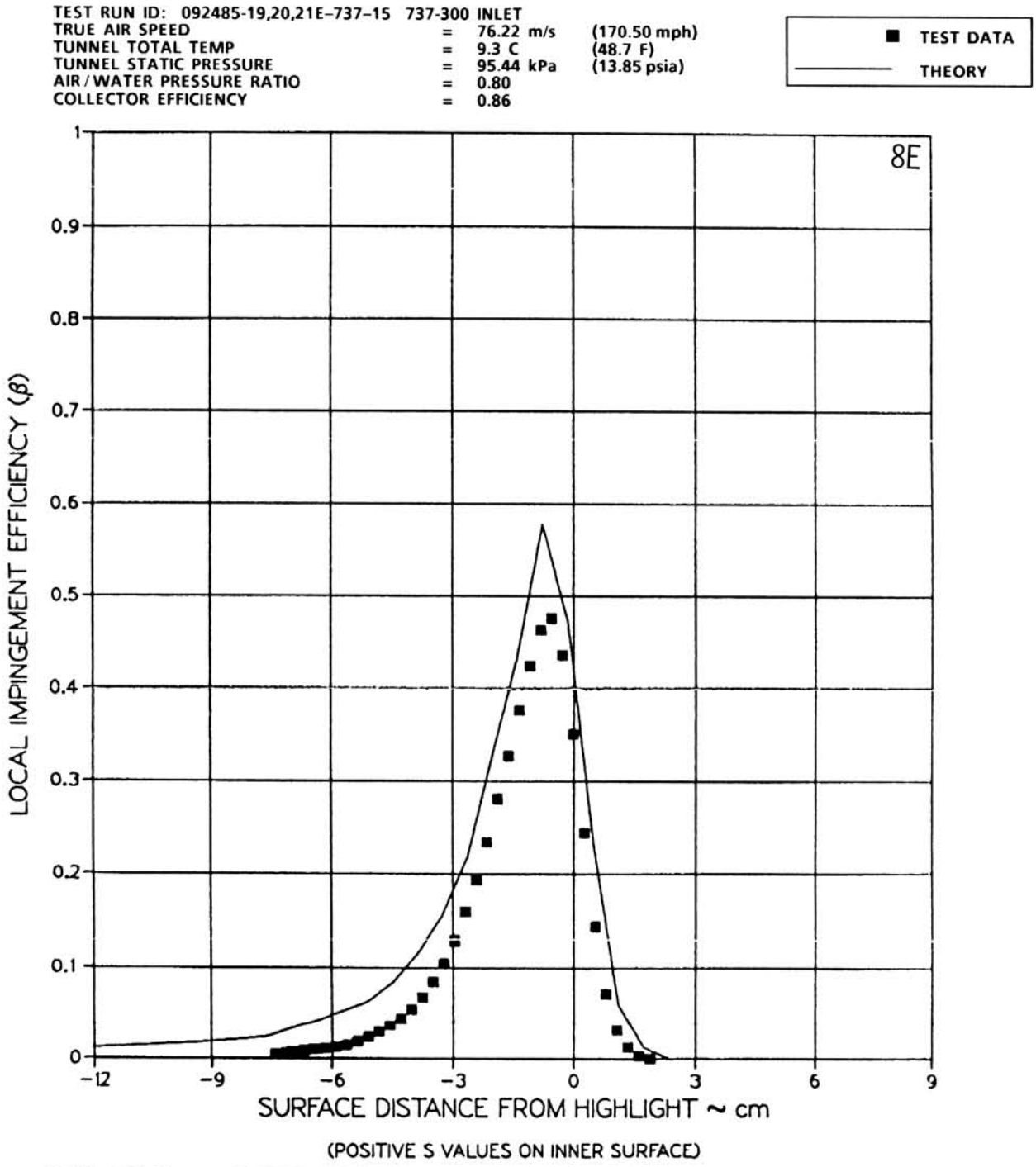

(B5) MVD = 16.45 MICRONS, MASS FLOW = 22.96 LBM/SEC, θ = 180°

FIGURE 6.21

AVERAGED LOCAL WATER IMPINGEMENT EFFICIENCY DATA FOR BOEING 737-300 INLET AT α = 15° (PAGE 11 OF 26).

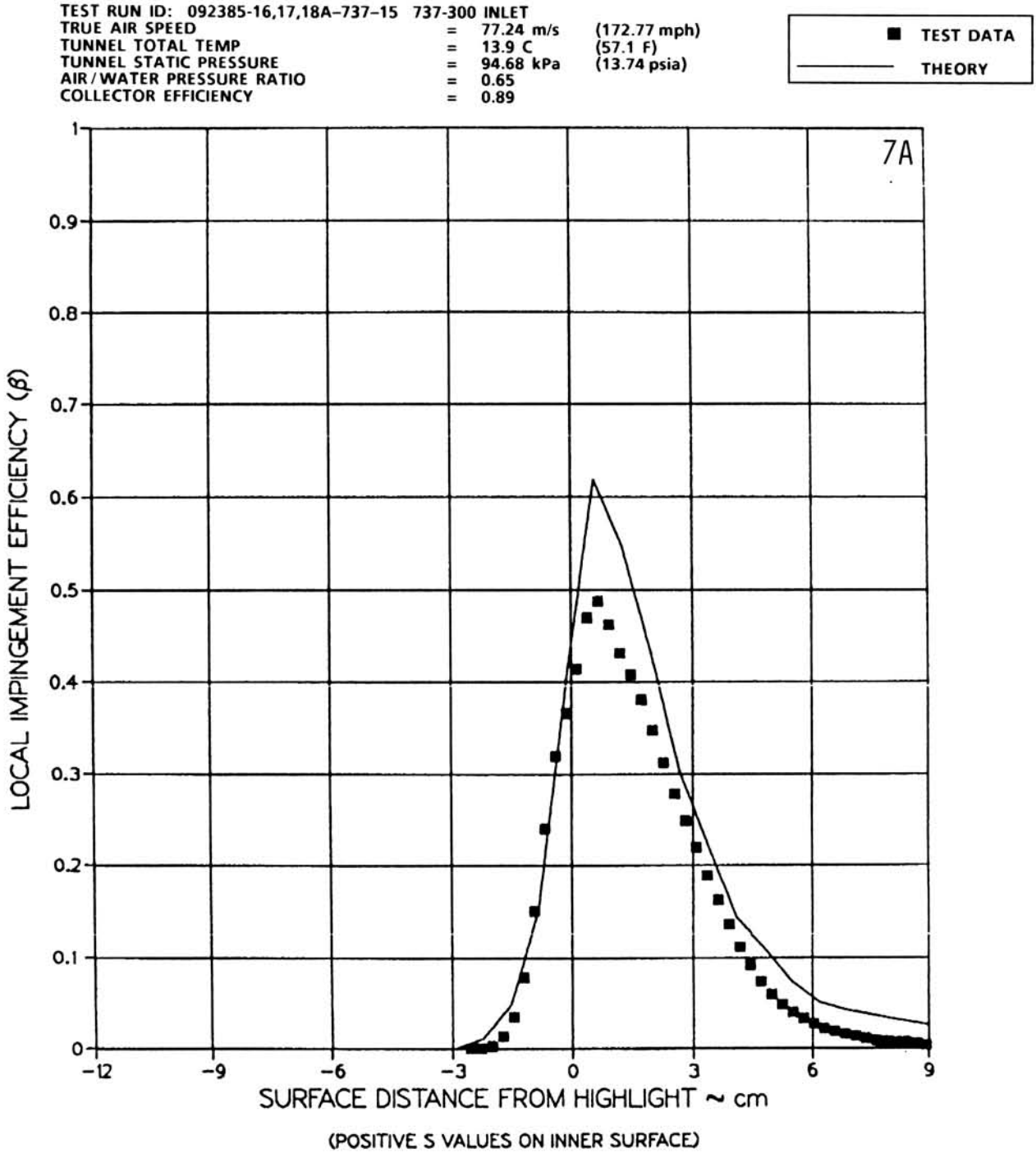

(C1) MVD = 20.36 MICRONS, MASS FLOW = 17.20 LBM/SEC, θ = 0°

FIGURE 6.21

AVERAGED LOCAL WATER IMPINGEMENT EFFICIENCY DATA FOR BOEING 737-300 INLET AT α = 15° (PAGE 12 OF 26).

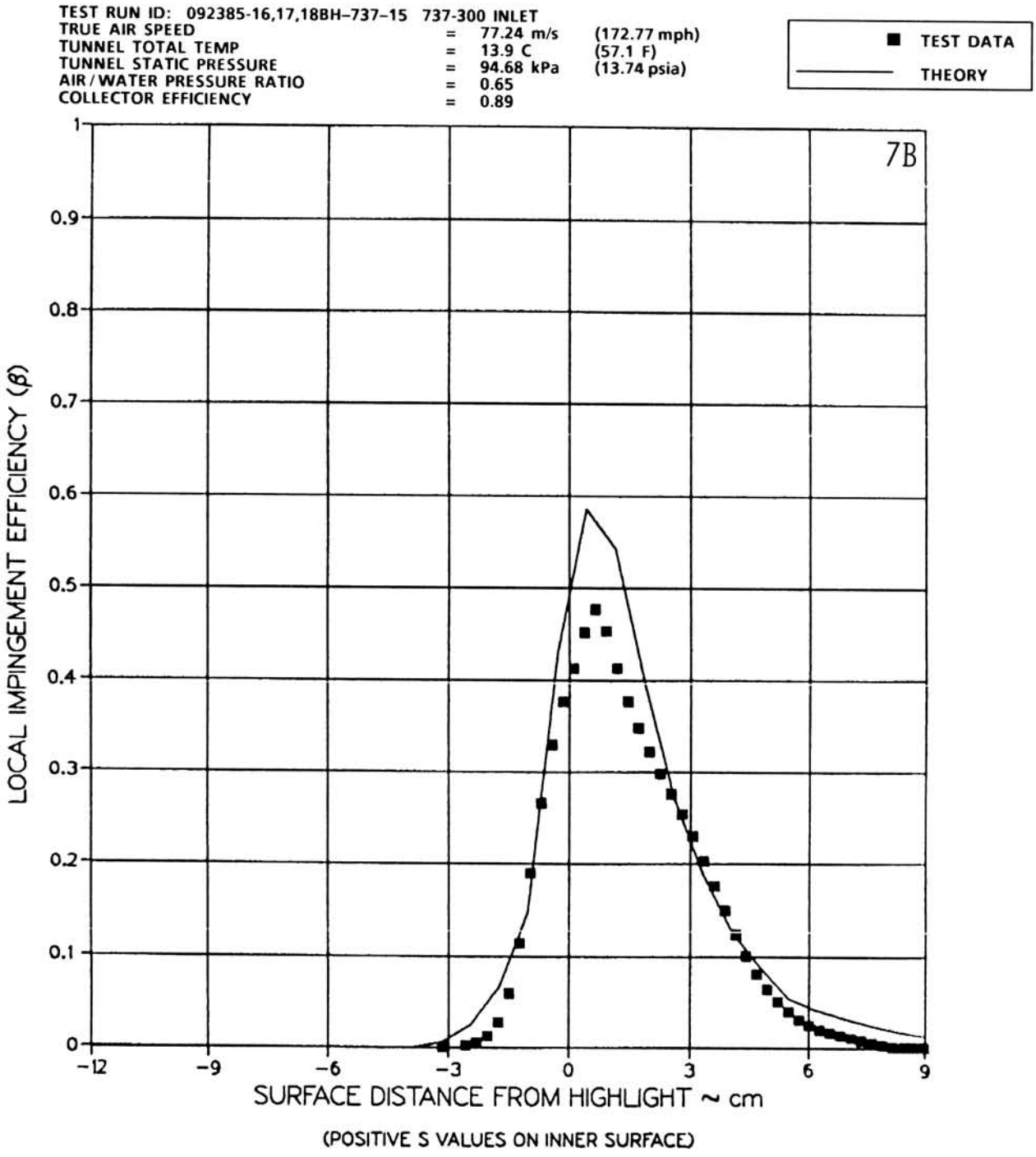

(C2) MVD = 20.36 MICRONS, MASS FLOW = 17.20 LBM/SEC, θ = 45°

FIGURE 6.21

AVERAGED LOCAL WATER IMPINGEMENT EFFICIENCY DATA FOR BOEING 737-300 INLET AT α = 15° (PAGE 13 OF 26).

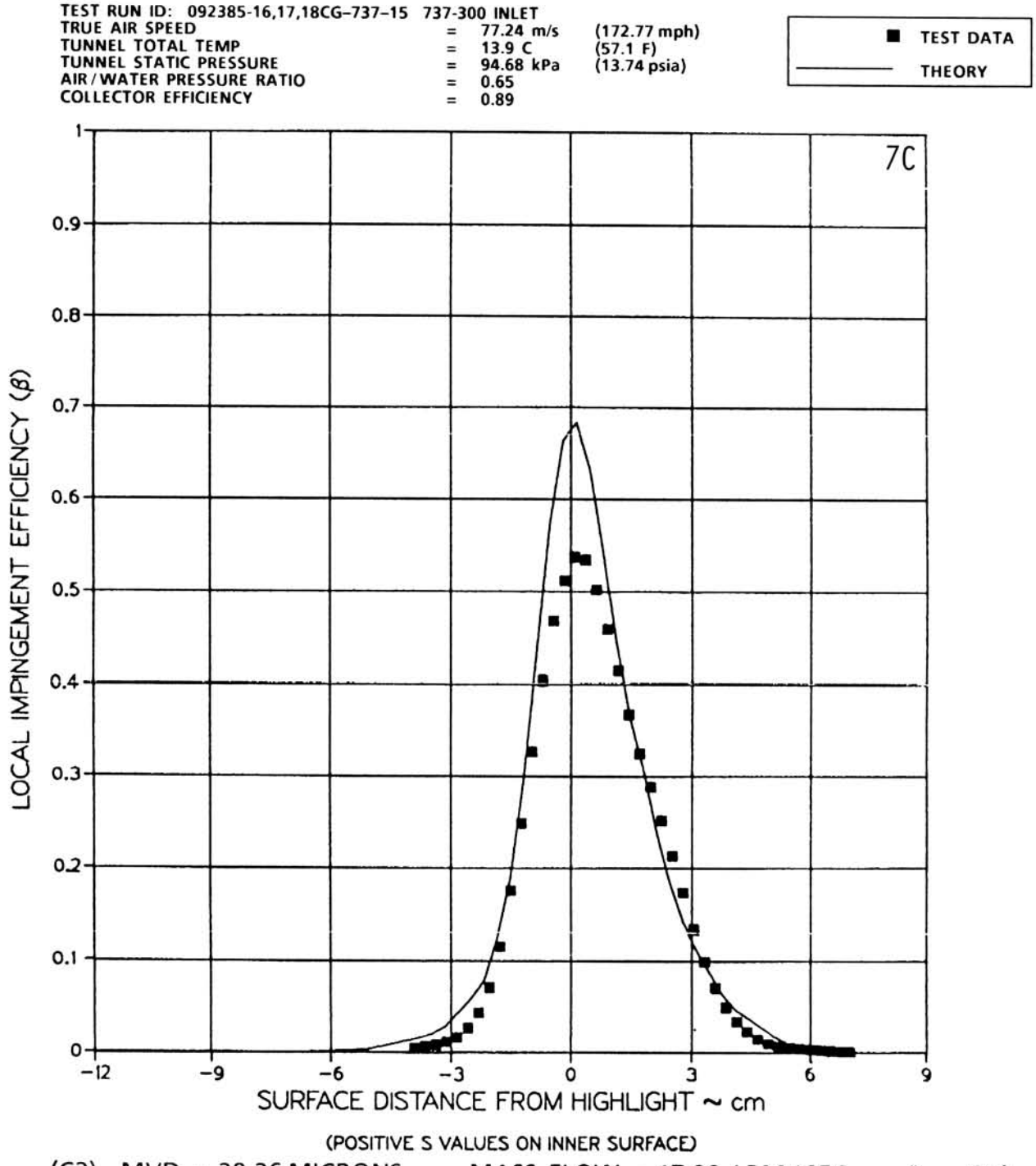

(C3) MVD = 20.36 MICRONS, MASS FLOW = 17.20 LBM/SEC, θ = 90°

FIGURE 6.21

AVERAGED LOCAL WATER IMPINGEMENT EFFICIENCY DATA FOR BOEING 737-300 INLET AT α = 15° (PAGE 14 OF 26).

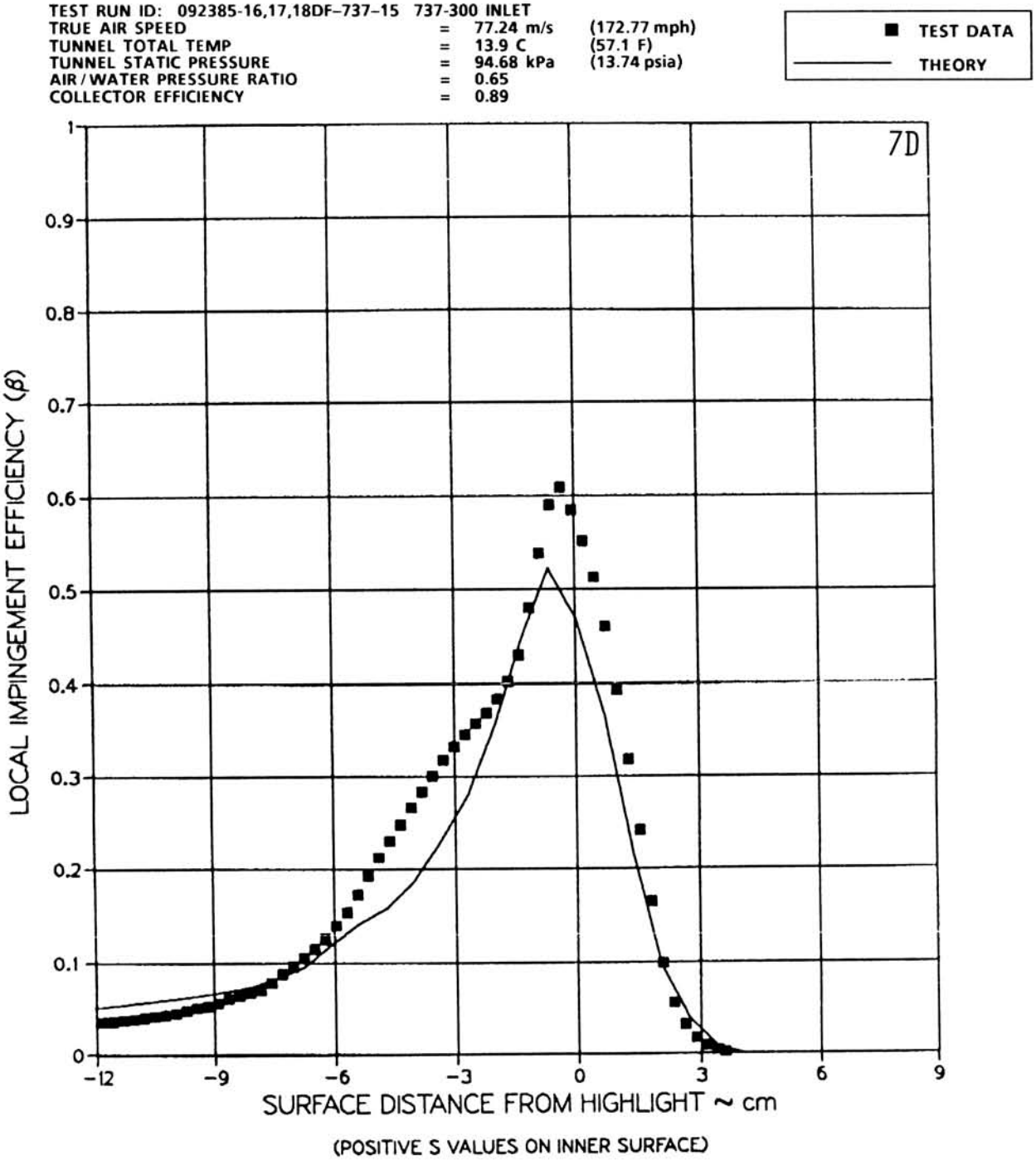

(C4) MVD = 20.36 MICRONS, MASS FLOW = 17.20 LBM/SEC, θ = 135°

FIGURE 6.21

AVERAGED LOCAL WATER IMPINGEMENT EFFICIENCY DATA FOR BOEING 737-300 INLET AT α = 15° (PAGE 15 OF 26).

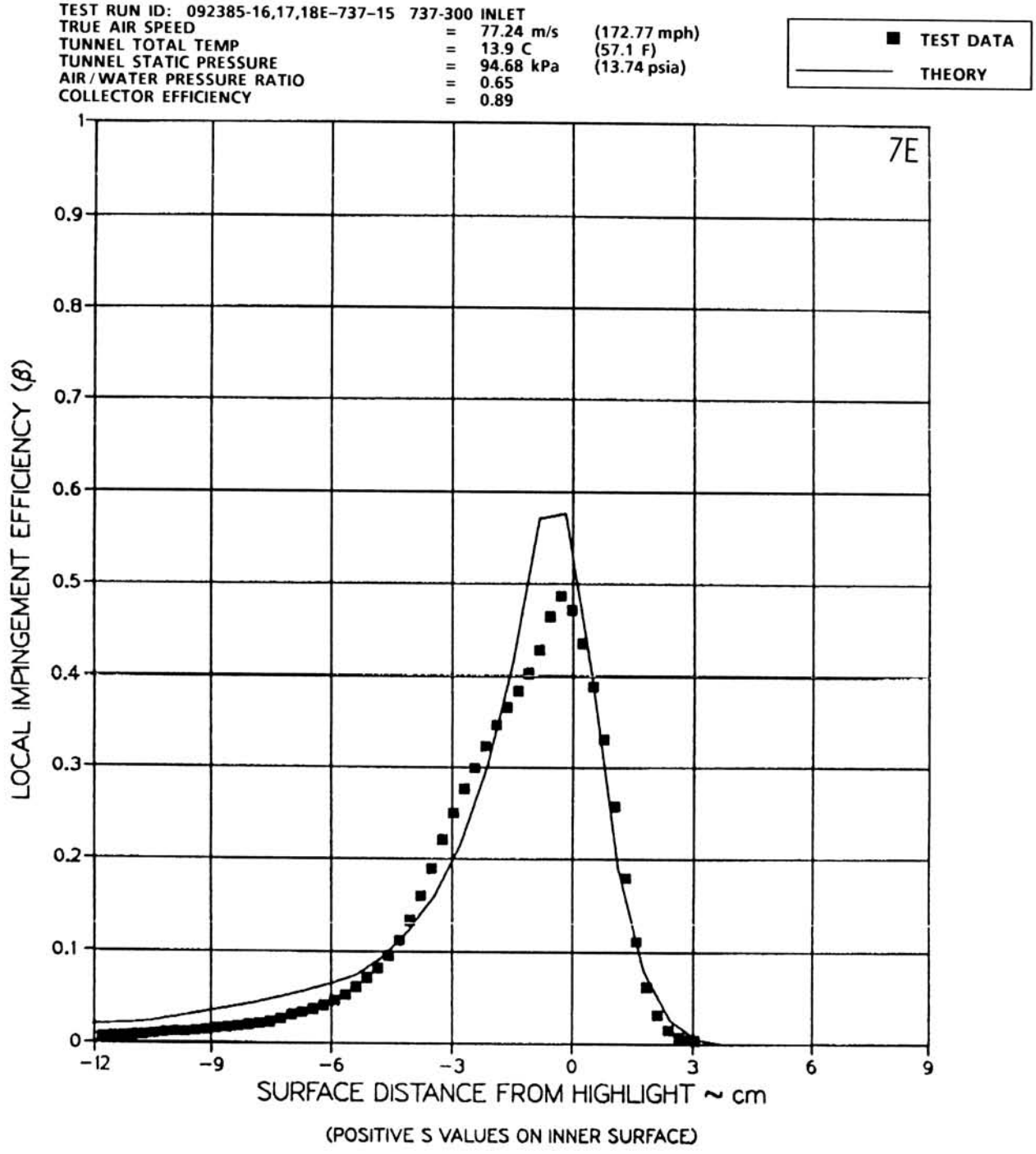

(C5) MVD = 20.36 MICRONS, MASS FLOW = 17.20 LBM / SEC, θ = 180°

FIGURE 6.21

AVERAGED LOCAL WATER IMPINGEMENT EFFICIENCY DATA FOR BOEING 737-300 INLET AT α = 15° (PAGE 16 OF 26).

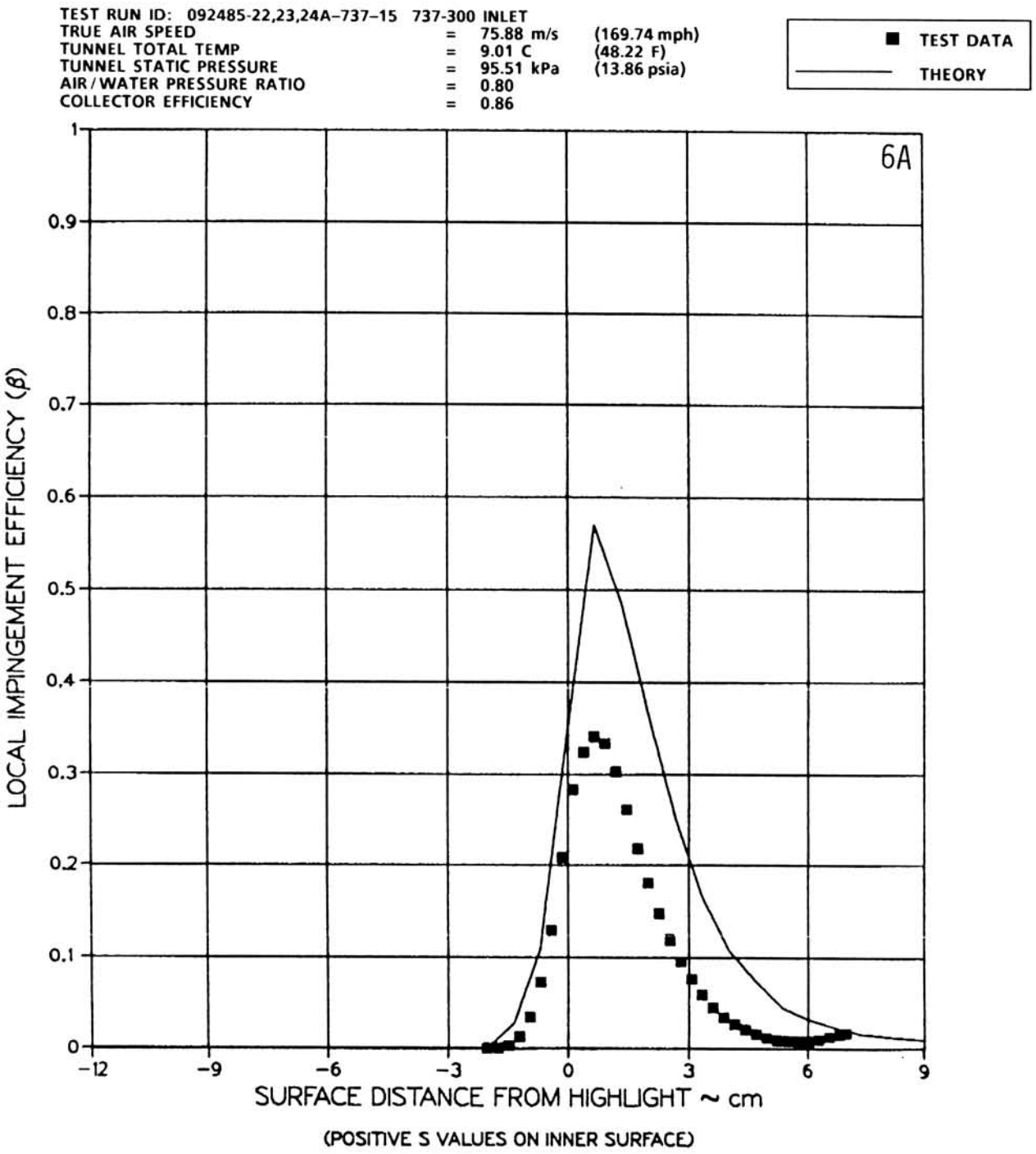

(D1) MVD = 16.45 MICRONS, MASS FLOW = 17.20 LBM/SEC, $\theta = 0°$

FIGURE 6.21

AVERAGED LOCAL WATER IMPINGEMENT EFFICIENCY DATA FOR BOEING 737-300 INLET AT $\alpha = 15°$ (PAGE 17 OF 26).

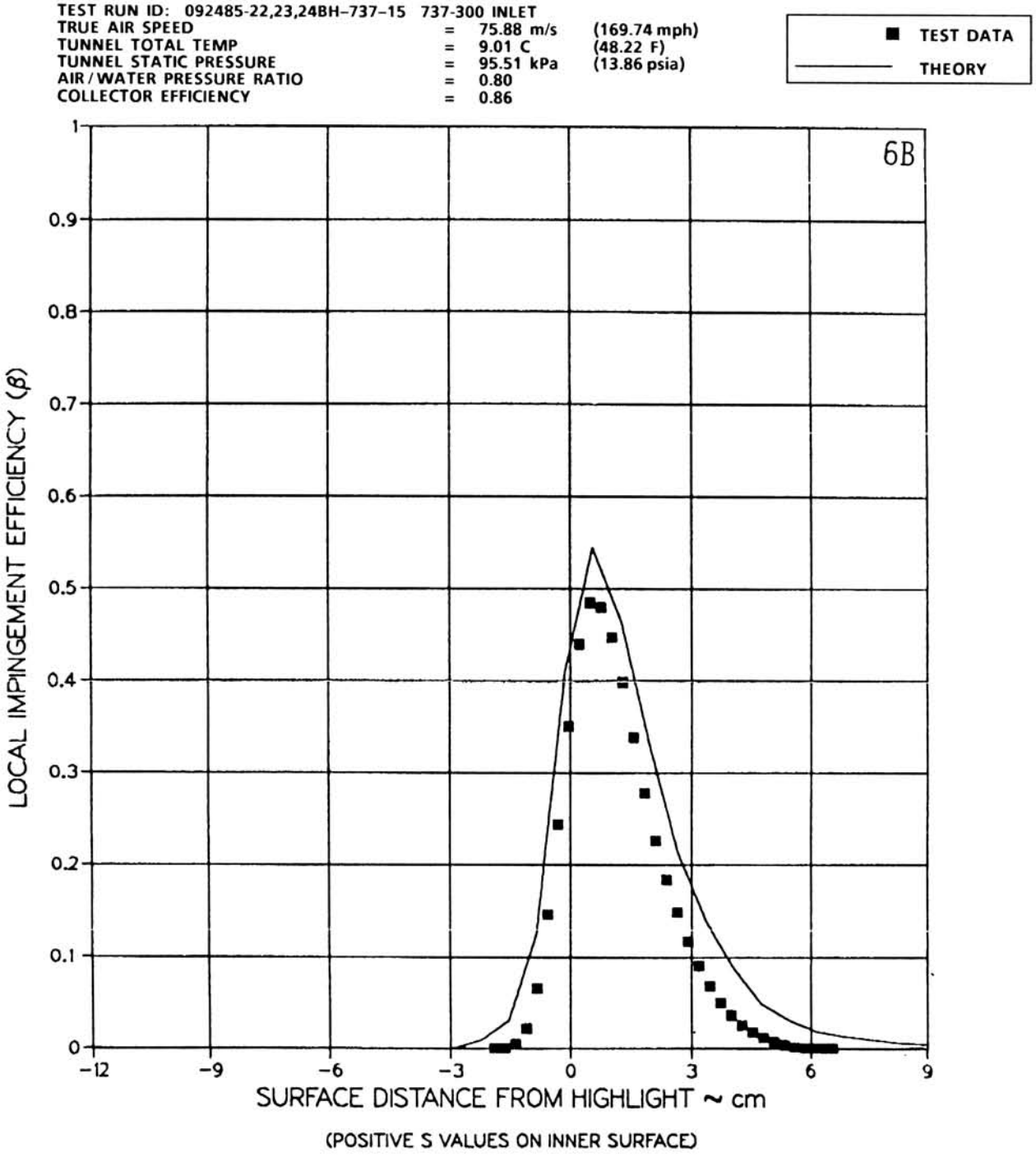

(D2) MVD = 16.45 MICRONS, MASS FLOW = 17.20 LBM / SEC, θ = 45°

FIGURE 6.21

AVERAGED LOCAL WATER IMPINGEMENT EFFICIENCY DATA FOR BOEING 737-300 INLET AT α = 15° (PAGE 18 OF 26).

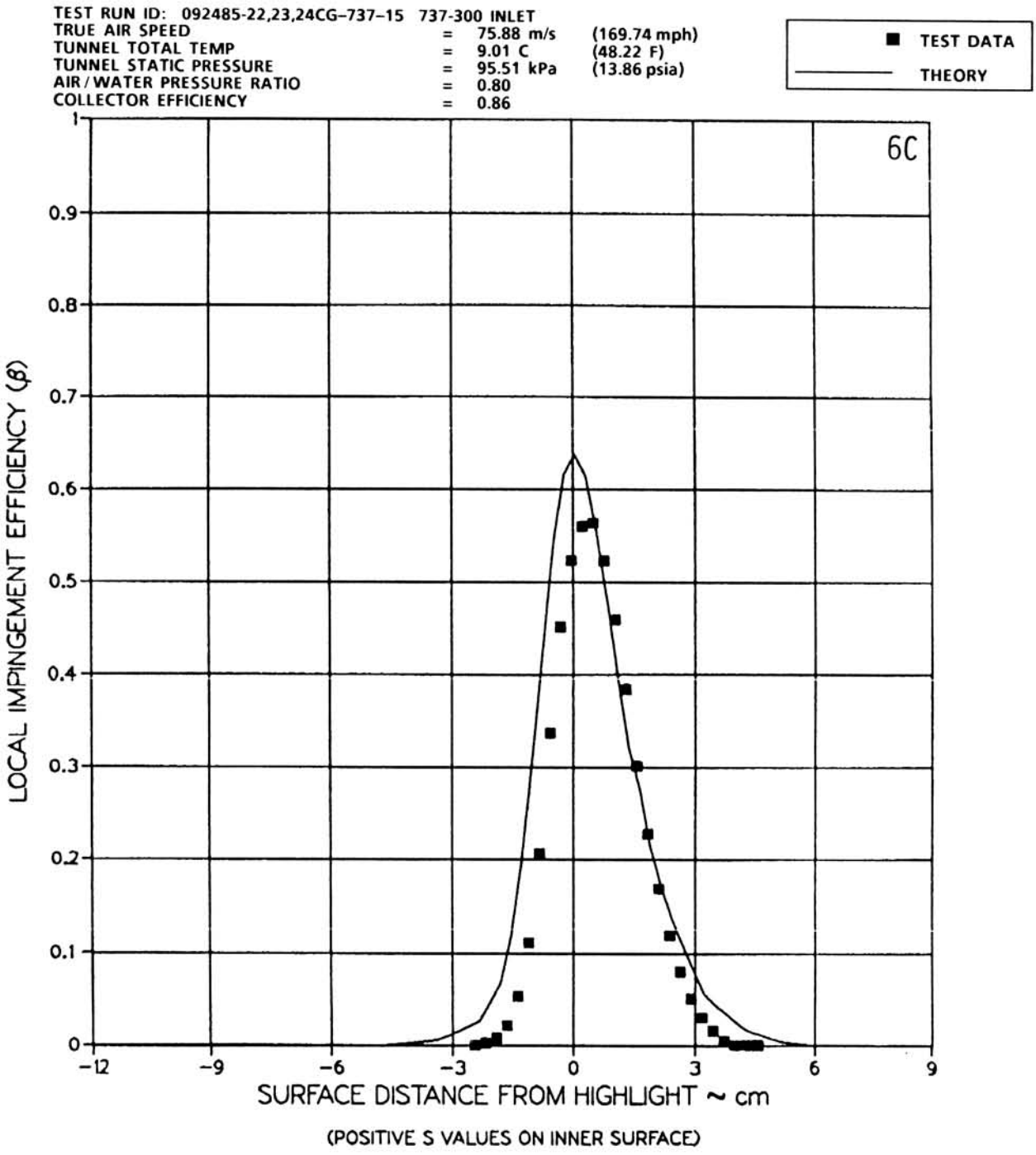

(D3) MVD = 16.45 MICRONS, MASS FLOW = 17.20 LBM/SEC, θ = 90°

FIGURE 6.21

AVERAGED LOCAL WATER IMPINGEMENT EFFICIENCY DATA FOR BOEING 737-300 INLET AT α = 15° (PAGE 19 OF 26).

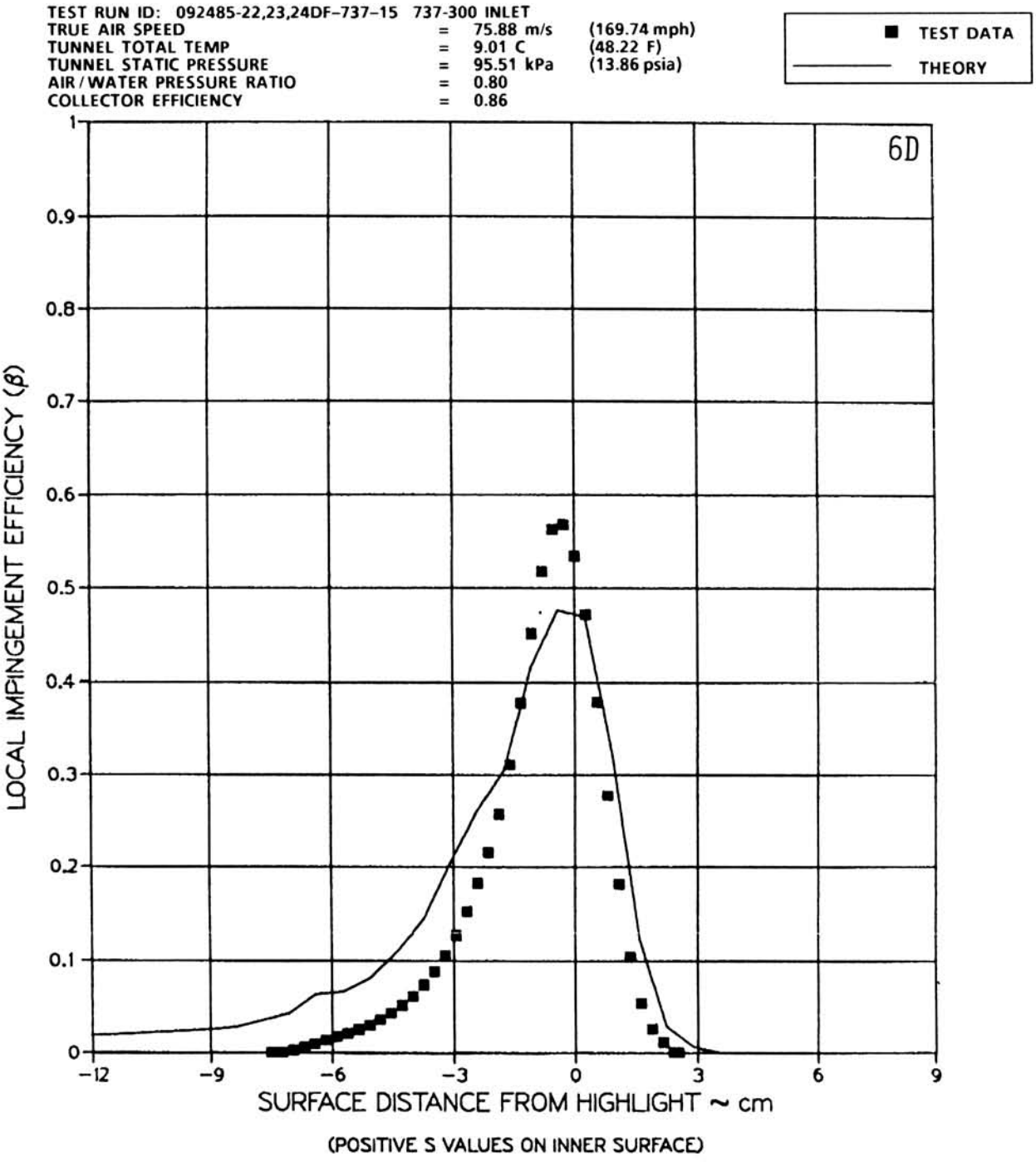

(D4) MVD = 16.45 MICRONS, MASS FLOW = 17.20 LBM/SEC, θ = 135°

FIGURE 6.21

AVERAGED LOCAL WATER IMPINGEMENT EFFICIENCY DATA FOR BOEING 737-300 INLET AT α = 15° (PAGE 20 OF 26).

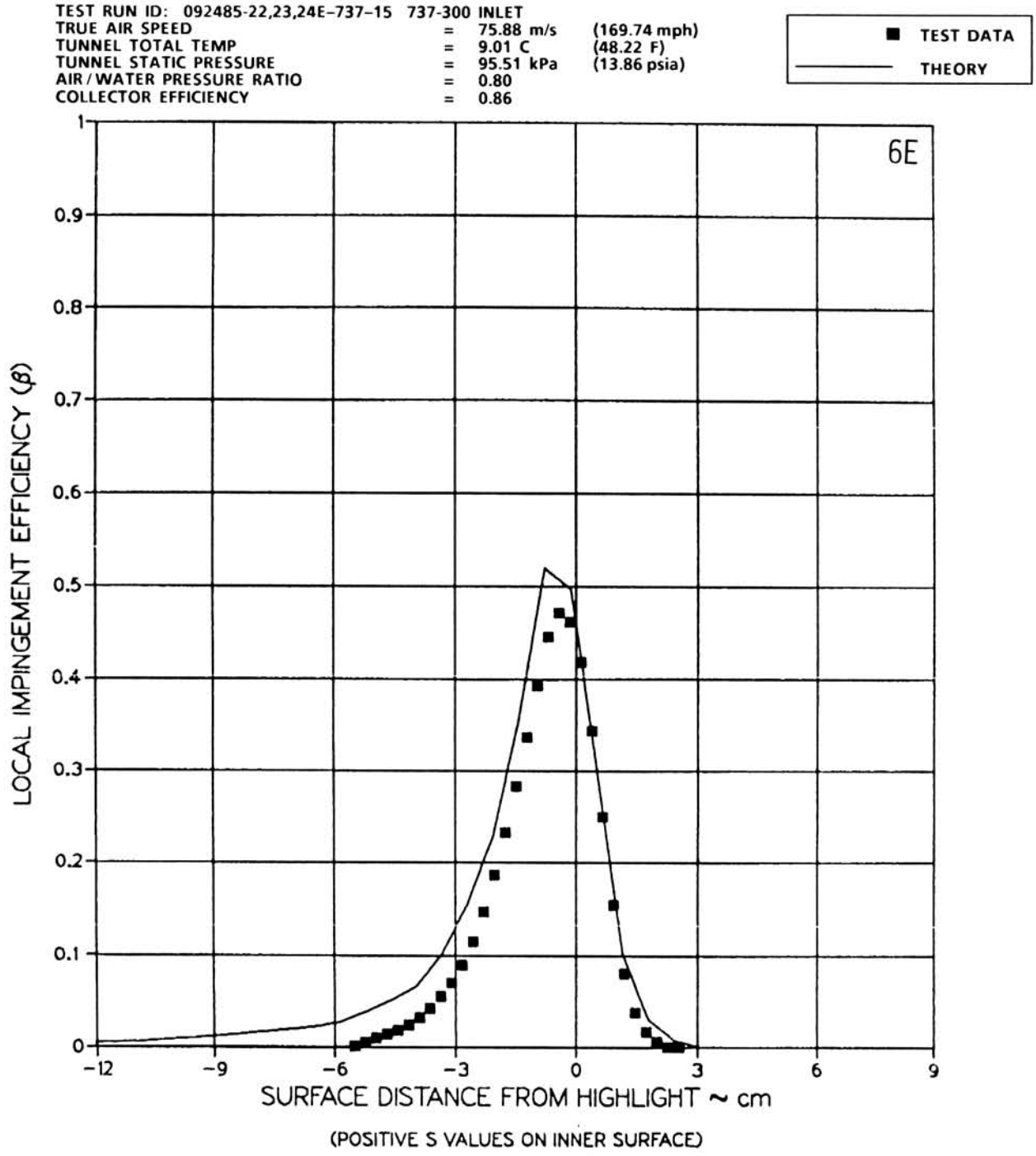

(D5) MVD = 16.45 MICRONS, MASS FLOW = 17.20 LBM/SEC, θ = 180°

FIGURE 6.21

AVERAGED LOCAL WATER IMPINGEMENT EFFICIENCY DATA FOR AT BOEING 737-300 INLET α = 15° (PAGE 21 OF 26).

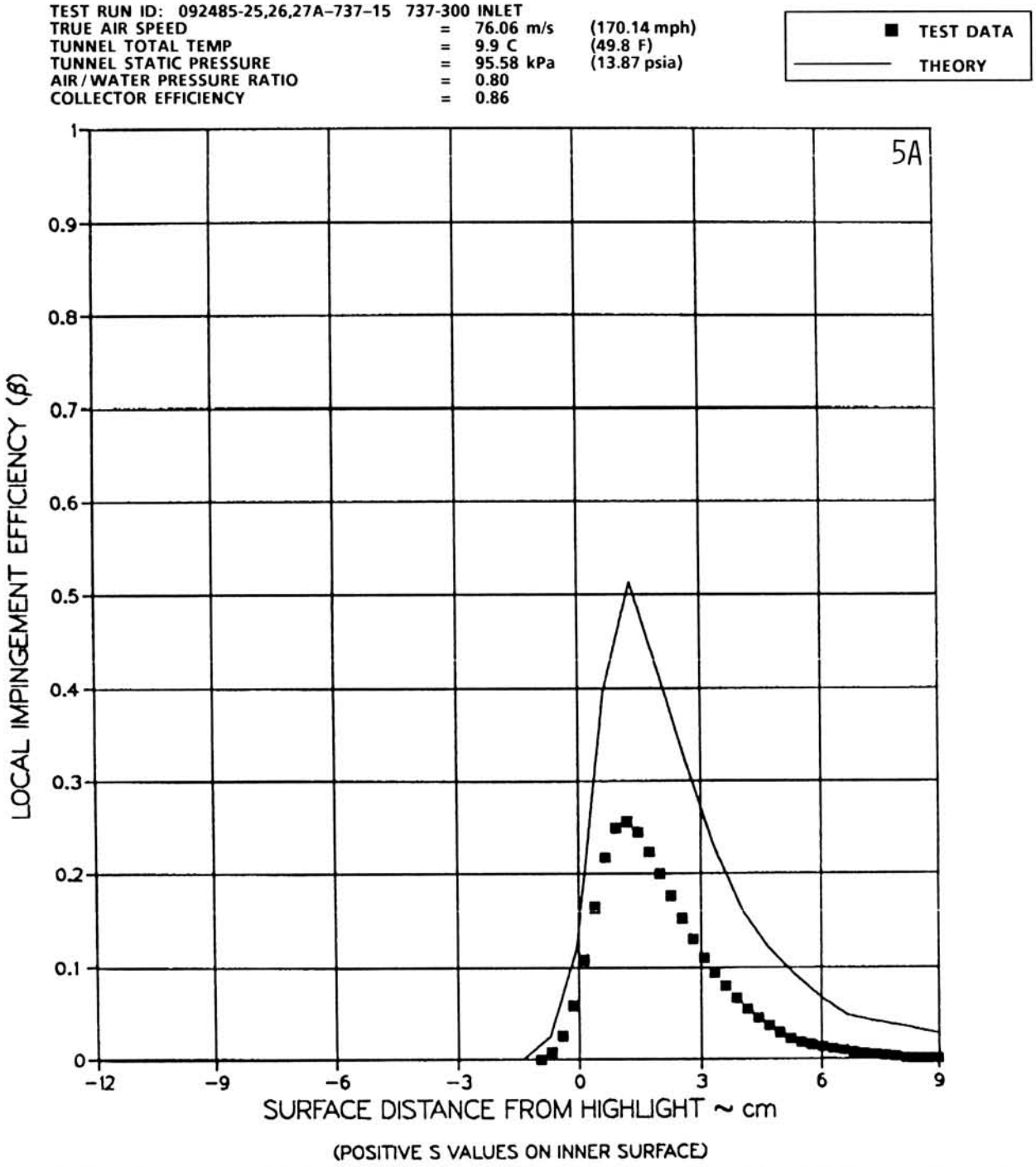

(E1) MVD = 16.45 MICRONS, MASS FLOW = 11.47 LBM/SEC, θ = 0°

FIGURE 6.21

AVERAGED LOCAL WATER IMPINGEMENT EFFICIENCY DATA FOR BOEING 737-300 INLET AT α = 15° (PAGE 22 OF 26).

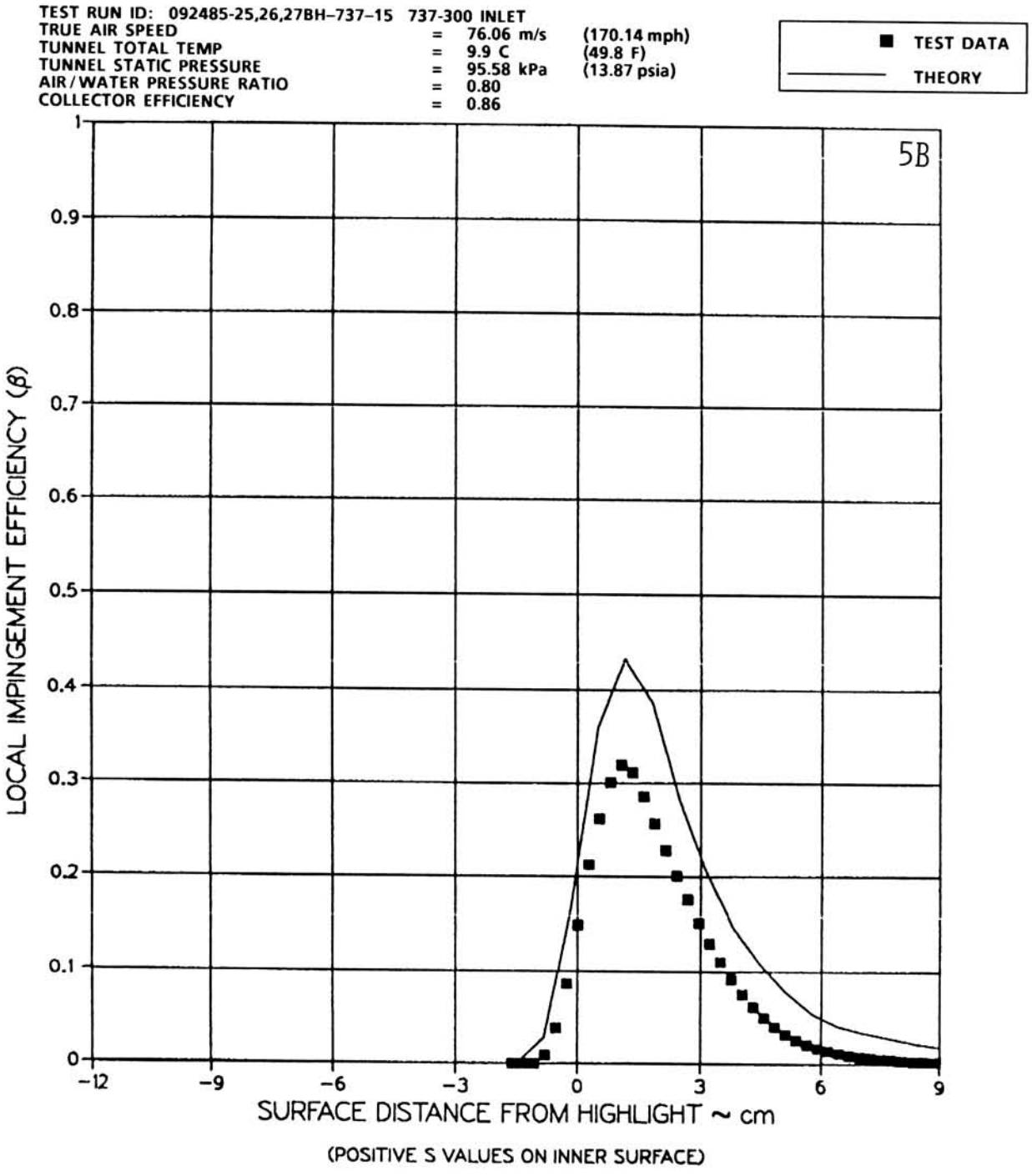

(E2) MVD = 16.45 MICRONS, MASS FLOW = 11.47 LBM / SEC, θ = 45°

FIGURE 6.21

AVERAGED LOCAL WATER IMPINGEMENT EFFICIENCY DATA FOR BOEING 737-300 INLET AT α = 15° (PAGE 23 OF 26).

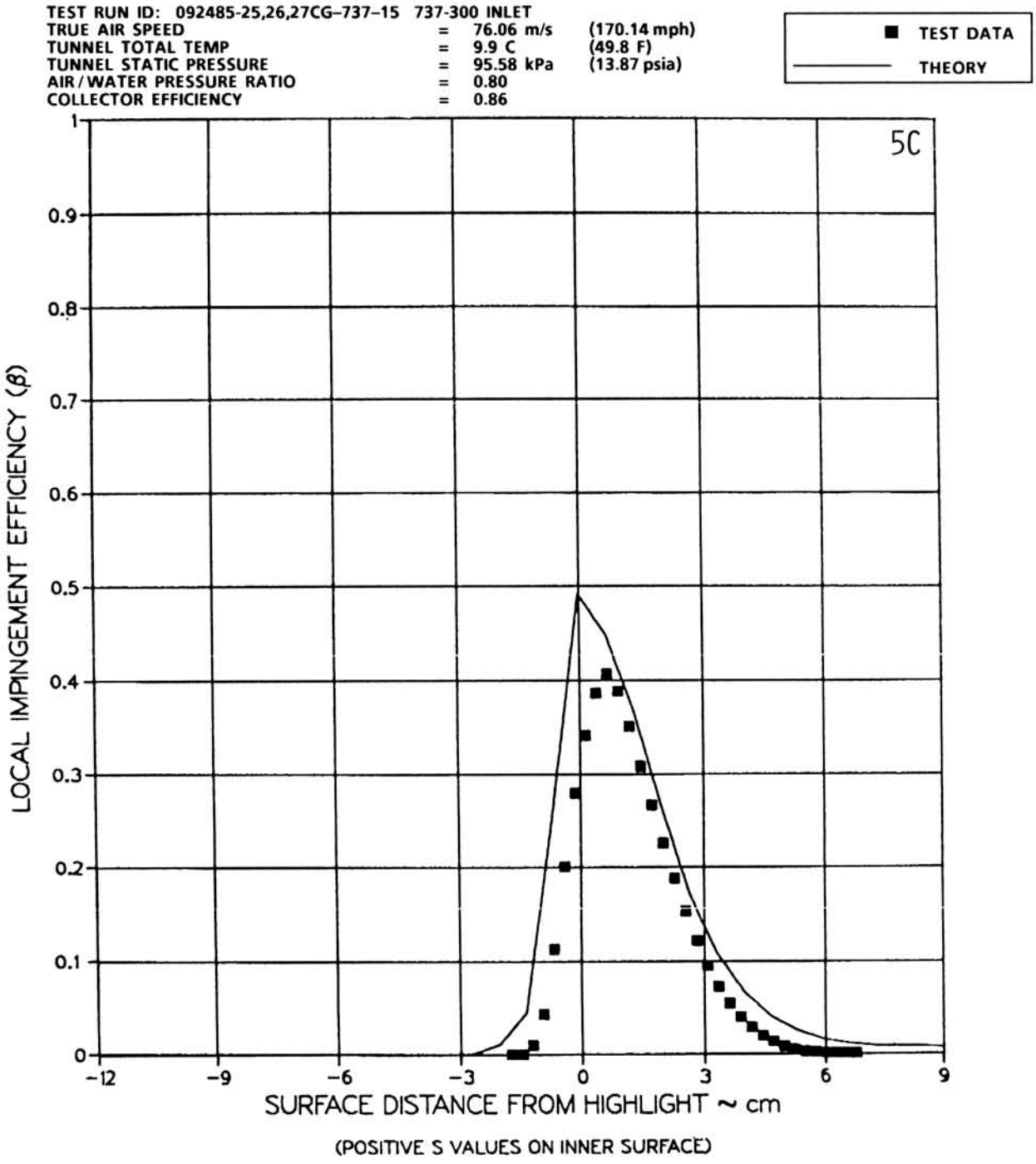

(E3) MVD = 16.45 MICRONS, MASS FLOW = 11.47 LBM/SEC, θ = 90°

FIGURE 6.21

AVERAGED LOCAL WATER IMPINGEMENT EFFICIENCY DATA FOR BOEING 737-300 INLET AT α = 15° (PAGE 24 OF 26).

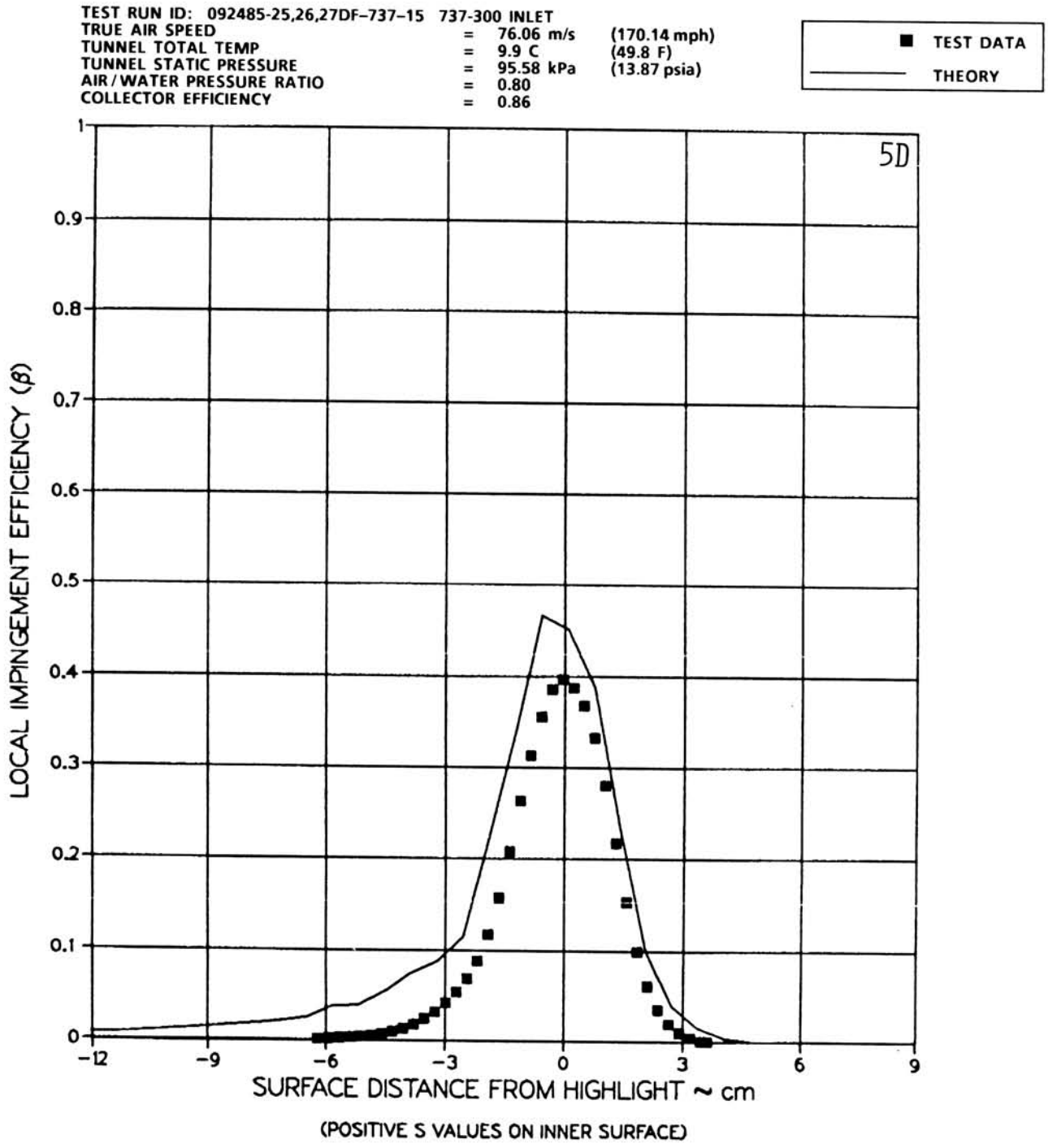

(E4) MVD = 16.45 MICRONS, MASS FLOW = 11.47 LBM/SEC, θ = 135°

FIGURE 6.21

AVERAGED LOCAL WATER IMPINGEMENT EFFICIENCY DATA FOR BOEING 737-300 INLET AT α = 15° (PAGE 25 OF 26).

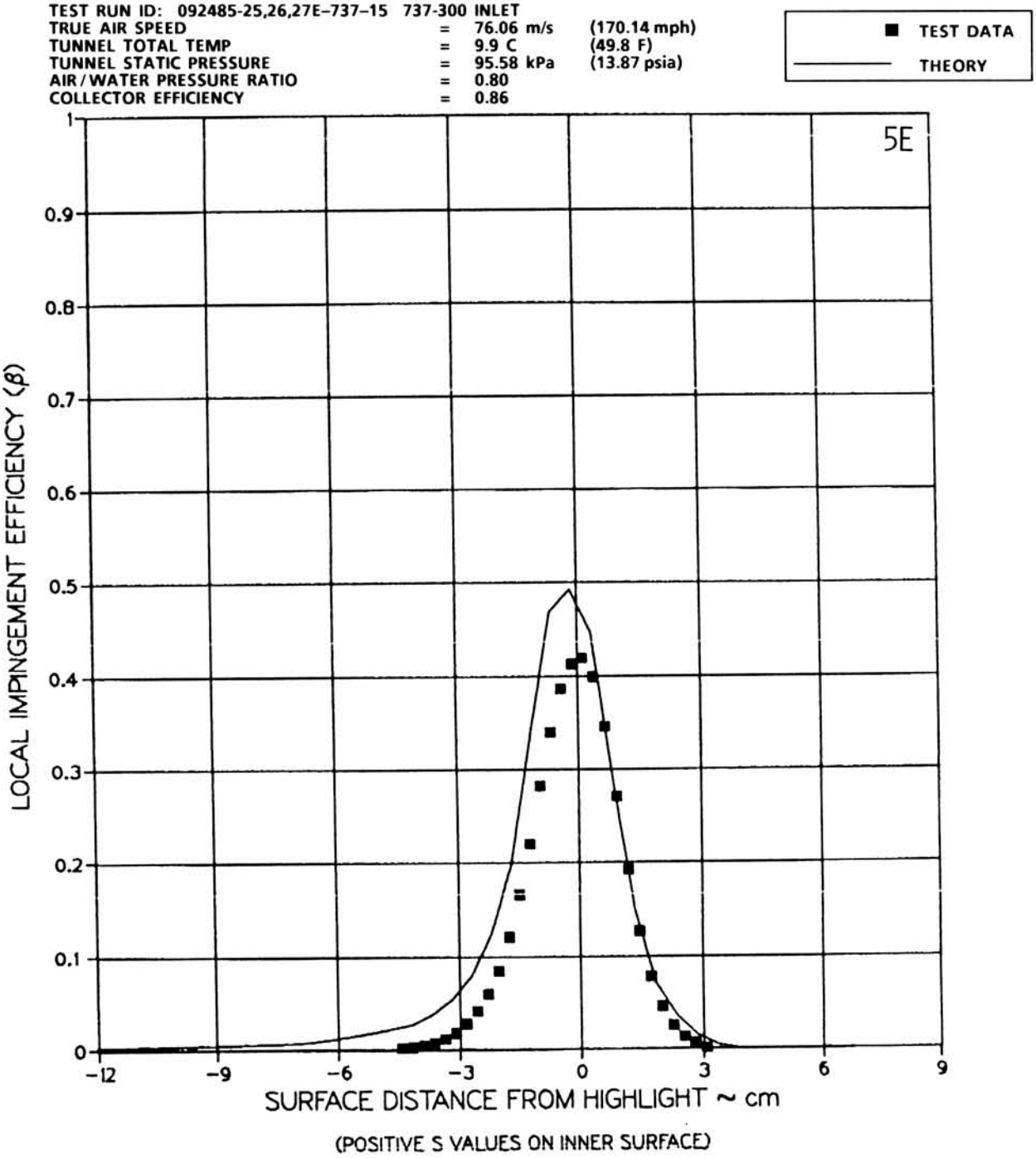

(E5) MVD = 16.45 MICRONS, MASS FLOW = 11.47 LBM/SEC, θ = 180°

FIGURE 6.21

AVERAGED LOCAL WATER IMPINGEMENT EFFICIENCY DATA FOR BOEING 737-300 INLET AT α = 15° (PAGE 26 OF 26).

7.0 CONCLUSIONS

An accurate and efficient method of measuring the local impingement efficiency on two and three-dimensional aerodynamic surfaces has been developed. Based on the results presented, the following conclusions can be made:

1. This investigation represents the first successful experimental determination of detailed water droplet efficiency distribution on a three-dimensional engine inlet surface.

2. A large number of water droplet impingement test data in the form of dye-traced blotter strips has been obtained for a variety of geometries, flow conditions and drop size distributions.

3. The laser reflectance method is accurate and repeatable. It is also considerably more efficient than colorimetric analysis. Unlike colorimetric analysis, the reflectance method allows data to be extracted from the blotter strips without destroying the blotter strips.

4. Accurate droplet size distribution data are essential for correlating theoretical and experimental data.

5. Determination of local LWC values using the reference collector mechanism improved the accuracy of the data by reducing the error due to nonuniform spray distribution.

6. Accurate suction flow measurements for engine inlet models are very important when correlating test and analytical results.

7. Agreement between test and analysis is good for most test configurations. Agreement is particularly good for the cylinder, for the airfoils at $\alpha = 0^{o}$ and for both engine inlets at $\alpha = 0^{o}$.

8. In most cases, test repeatability between test runs for a given test configuration was found to be $\pm$ 10 percent from the mean.

APPENDIX A: SPRAY SYSTEM DETAILS AND OPERATION PROCEDURES

A.1 Spray System Detail Description

The spray system consists of the following main components (see Figure A.1):

a. Supply tank and tank air pressure line
b. Air by-pass line
c. Dyed water manifold line
d. Air manifold line
e. Twelve nozzle assemblies

a. Supply Tank and Tank Air Pressure Line

A 9 gallon tank made out of aluminum alloy is used to supply dyed water under pressure to the nozzles via hoses and brass fittings. The tank is a cylindrical vessel with semispherical ends which is capable of withstanding pressures up to 300 psig. Filtered air is supplied to the inlet of the tank (upper end) from a 120 psig pressure source. The tank air pressure line consists of a hose (3/4" ID), a shut-off valve, a pressure regulating valve and a T-fitting which directs air to both the supply tank and the air by-pass line. An oil-filled pressure gauge mounted on the air regulating valve is used to read the pressure in the tank air line (usually 106 psig). A cross-fitting at the tank inlet is used to connect the air inlet, an oil filled pressure gauge and a pressure transducer, to the tank. The pressure transducer is employed to monitor tank pressure fluctuations during a droplet impingement test. A photograph of the tank and its main components is shown on Figure A.2.

Dyed water is supplied to the dyed water manifold from the tank outlet (lower side) via a hose, a 50 micron water filter and a shut-off valve. A T-fitting is used to connect the air by-pass line, the dyed water manifold and the tank outlet line. A drain line (DL1) is attached to the tank outlet line by means of a T-fitting.

b. Air By-Pass Line

The air by-pass line is utilized to remove water residues from water hoses and spray nozzles without having to empty the dyed water supply tank. The by-pass line consists of a hose and a shut-off valve, normally in the off position. Further details on the use of the by-pass line are given under spray system operation procedures.

c. Dyed Water Manifold Line

The manifold consists of 1/2 inch ID hose, a number of cross and T-fittings and drain lines as shown on Figure A.1. The manifold distributes pressurized water to 12 spray nozzles through individual hoses (1/2 inch ID). The three drain lines DL2, DL3 and DL4 have shut-off valves which are normally closed.

d. Air Manifold Line

Pressurized air is supplied to each nozzle where it mixes with the pressurized water to form a spray. Filtered air from a pressure source (maximum pressure is 120 psig) passes through an on/off control solenoid valve, a shut-off valve and a regulating valve to the manifold line which distributes air via individual hoses to each nozzle assembly. The design of the air manifold line is similar to the water manifold line. However, to reduce pressure losses, 3/4 inch ID hoses are used. The air volume flow is much higher than the water volume flow so air velocities in the hoses are greater than water velocities. Therefore, friction loses would be high if 1/2 inch ID hoses are used. Two oil-filled pressure gauges are installed on the pressure regulating valve to help monitor and adjust the pressure as shown in Figure A.3. The air pressures for the test were 65 and 80 psig.

e. Nozzle Assemblies

There are 12 nozzle assemblies in the spray system. The main components of a nozzle assembly are:

1. On/off control solenoid valve
2. Nozzle housing
3. NASA Lewis standard icing spray nozzle

Items 2 and 3 above make up the spray unit. Some nozzle assemblies have an adjustable valve and an oil filled pressure gauge or a pressure transducer. Two such assemblies are shown in Figure A.1.

The nozzles were located in the IRT plenum chamber and were mounted on the tunnel spray bars. The difference in elevation between nozzles resulted in a hydrostatic pressure differential. For optimum spray distribution, all nozzles should operate at approximately the same water pressure (100 $\pm$ 1 psig). To equalize the pressure between nozzles, an adjustable valve was employed during the design stage for all nozzles at the lower elevation. However, after the nozzles were mounted on the tunnel spray bar, the maximum hydrostatic pressure differential between nozzles was found to be 2 psig. The difference was reduced to $\pm$ 1 psig by considering the nominal operating pressure to be the mean of the nozzle elevations. This eliminated the need for the adjustable valves and saved time during the system set up period.

To monitor the pressure at the nozzles, pressure gauges or transducers were employed on some nozzle assemblies. A total of four transducers and three oil-filled pressure gauges were strategically distributed among the twelve nozzles. The transducers were wired to LED displays in the tunnel control room and were used during each test to monitor pressure fluctuations. The pressure gauges were employed for monitoring and adjusting pressures between wind tunnel tests. The pressures had to be adjusted manually between tests at the plenum chamber where the pressure regulators were located.

Figure A.4 shows a section of the main components of a nozzle assembly. The control solenoid valve is connected to the nozzle housing by means of a union connector. To minimize the internal volume between the solenoid outlet and the nozzle housing inlet, a small metal tube of approximately 1/8 inch ID was inserted in the available space and the rest of the volume was filled with epoxy as shown in the Figure A.4. This design minimizes air bubbles in the flow passage so that the water spray shuts off in a very short time (0.66 sec) after the solenoid valve is de-energized. The solenoid is shown in the de-energized (closed) mode of operation in this figure. The solenoid is a two way normally closed type (for more details see Reference 26).

The NASA Lewis standard icing spray nozzle is also shown in Figure A.4. This nozzle produces a narrow spray angle of finely atomized droplets. The atomizing air is introduced at a pressure above the choking condition for the exit orifice. The air leaves the nozzle and interacts with the water jet at sonic speeds. The atomizing air interacts both with the water spray and the tunnel air in the wake of the nozzle face to form a complicated flow configuration (see Figure A.4). The droplets breakup by going through the violence of a normal shock at the exit of the nozzle.

Each NASA standard nozzle carries an identification number which is used to obtain information regarding the measured spray characteristics of the nozzle (Nussle, R., Personal Communication, NASA, Lewis Research Center). The identification numbers of the nozzles used and their corresponding position in the present spray system are given in Figure A.5.

These nozzles were chosen because they have very similar spray characteristics at the operating pressures of this test.

A.2 Spray Nozzle Assemblies Location

The spray nozzle assemblies were mounted on the spray bars located in the IRT plenum chambers. There are 6 spray bars in the IRT at various elevations as shown in Figure A.5. The spray bars house multiple NASA standard nozzles which are employed in icing tests. These nozzles were not used in the present droplet impingement tests.

A bracket made out of solid aluminum was designed which clamps onto a spray bar with its axis parallel to the streamwise direction. A clamp built into the downstream end of the aluminum bracket holds a 3 ft long, 3/4 inch ID steel pipe perpendicular to the spray bar. One end of the pipe is connected to the air inlet of the nozzle housing and the other end is connected to a hose supplying pressurized air from the air manifold of the spray system. The pipe supports the nozzle housing and provides a means for adjusting nozzle height. Referring to Figures A.5 and 3.5, the solid aluminum bracket is used to move a nozzle in the Y direction while the steel pipe is used to move the nozzle along the Z-axis and/or rotate the nozzle about the Z-axis.

The Y and Z locations of all nozzle discharge orifices are given in Figure A.5. The Y, Z axes and the tunnel center line (X-axis) form an orthogonal system. The positive X-axis direction is taken downstream.

All nozzle discharge orifices are on the same vertical (YZ) plane which is located 36 feet (11 m) upstream of the tunnel test section entrance.

A.3 Spray System Operation Procedures

Three procedures will be discussed in this section:

a. Testing the spray system
b. Operation of the spray system
c. Draining the spray system

The following abbreviations are used throughout this section:

ACSV Air Control Solenoid Valve
APG Air Pressure Gauge
APR Air Pressure Regulating Valve (Air Pressure Regulator)
ASH Air Supply Hose
ASV Air Shut-off Valve
WAV Water Adjustable Valve
WCSV Water Control Solenoid Valve
WF Water Filter
WPG Water Pressure Gauge
WPRV Water Pressure Regulating Valve
WPT Water Pressure Transducer
WSH Water Supply Hose
WST Water Supply Tank
WSV Water Shut-off Valve

a. Testing the Spray System

Testing of the spray system should be performed after its installation in the tunnel plenum chamber. The following procedure is recommended. (Refer to Figure A.1).

Step 1:

Remove the cross-fitting from the tank inlet port. Fill the water supply tank with dyed-water solution (concentration 0.5 gram of dye per 1000 grams of water). Refit the cross-fitting to the inlet port and tighten.

Step 2:

Set ASV1 to the off position and make sure that APRV1 is closed. Connect the tank air pressure line to the air pressure source. Make sure that WSV1, WSV2 and ASV2 are in the off position. Slowly, open ASV1 and then open the regulating valve (APRV1) and begin to pressurize

the water in the tank. Watch the pressure gauges WPG1 and that installed on APRV1. When the required pressure (usually 100 psig) has been reached, lock the turning handle of the APRV1. At this point, check the tank lines for leaks and tighten the fittings as necessary.

Step 3:

Make sure all control solenoid valves are closed and remove all spray nozzles from their housing. Set ASV3 to the off position so that no air is supplied to the nozzles. Also, make sure that all the shut-off valves in the drain lines DL1, DL2, DL3 and DL4 are closed. Check all the adjustable valves (WAV1 through WAV12) in the nozzle assemblies and make sure they are fully open.

Step 4:

Open WSV2 slowly and let the pressurized water flow to the nozzles. At this point, check for possible leaks. When all hoses are filled with dyed-water and the flow has stopped, energize all the solenoid valves and spray for about 10 seconds. This will remove any small particles from the spray system which are likely to clog the spray nozzles.

Step 5:

De-energize (close) the solenoid valves and replace the spray nozzles in the nozzle housing and tighten them lightly. Energize (open) the solenoids once again for 30 to 40 seconds to spray through the nozzles and watch for any clogged spray nozzles. If all nozzles are spraying well, proceed to step 6. Otherwise, remove and very carefully clean the clogged nozzle(s).

Step 6:

With all solenoid valves closed, remove all the spray nozzles from their housings and replace all three O-rings in each nozzle with new ones. Refit nozzles back to their housings. With both ASV3 and APRV2 closed, energize ACSV3. Open ASV3 slowly and adjust APRV2 until the operating pressure (normally 60-80 psig) is reached. Pressurized air is now flowing through all the nozzle discharge orifices.

Step 7:

Energize all the control solenoid valves in the nozzle assemblies and watch the spray pattern for 10 to 20 seconds to make sure that the spray pattern is continuous and that all nozzles spray uniformly. Turn all solenoid valves off including ACSV3 so that both air and dyed-water stop to flow. If all the above steps have been completed successfully, the system is ready to go. As a final check, read all the pressure gauges on the nozzle assemblies to see if all nozzles operate at the required pressure.

b. Operation of the Spray System

Table A.1 gives the air and dyed water pressure settings for each pressure ratio used in this test. The water pressures given in this table are set at the nozzle inlet. The pressure at the supply tank should be higher than 100 psig to compensate for the hydrostatic pressure difference, which depends on the elevation of the nozzles. In this test, the pressure difference was 6 psig. So, the tank pressure was set at 106 psig.

TABLE A.1

AIR AND DYED WATER PRESSURE SETTING
FOR DROPLET TRAJECTORY TESTS

PRESSURE RATIO	DYED WATER PRESSURE AT NOZZLE INLET	AIR PRESSURE ~ PSIG
0.65	100 ± 1	65
0.80	100 ± 1	80

Operation of the spray system involves the following steps:

Step 1:

Fill up the supply tank with 9 gallons of dyed water as described in the system testing procedure. Set APRV1 until the pressure gauge on the tank reads the desired pressure (usually 106 psig). This should be done with WSV1, WSV2 and ASV2 in the off position as described earlier.

Step 2:

Set all control solenoid values (air and water) to off (closed). Make sure that all the shut-off valves in the drain lines (DL1 through DL4) are set to the off position. Open slowly the shut off valve WSV2 and let dyed water flow to the nozzles. It takes about 2 gallons (7.7 liters) of dyed water to fill up all the hoses if they are completely empty. This will cause a temporary pressure fluctuation in the tank. Check the pressure in the tank to make sure that it returns back to its original setting and adjust the regulating valves if necessary.

Step 3:

Check the readings of the gauges and transducers on the nozzles to see if nozzles are set at the correct pressure (see Table A.1). The transducer readings are displayed in the tunnel control room.

Step 4:

Set the electronic timer which activates all the water solenoid valves, to 5 seconds. The timer is located in the tunnel control room.

Activate the timer and observe the spray nozzles to see if all of them are spraying. It is very important that all nozzles spray since the cloud uniformity will be altered considerably if any one nozzle fails to spray. This check should be done prior to each wind tunnel test.

Step 5:

With the control solenoid valve ACSV3 in the open position and the ASV3 shut-off valve in the on position, set the pressure regulating valve APRV2 until the two pressure gauges on it read the required pressure (see Table A.1).

Step 6:

Start the tunnel and set the electronic timer to the desired spraying time. Make sure the air control solenoid valve is on and air flows through the nozzles before the timer is activated. Spraying time settings vary between 1 and 3 seconds depending on pressure ratio and dye concentration used. The greater the concentration or the smaller the pressure ratio, the shorter the spraying time should be. Examples of spray time duration can be found in Appendix G.

Once the spray is over, de-activate ACSV3. The supply tank should be inspected once in a while to see if there is sufficient solution in it. It is good practice not to let the tank run below 1/5th of its capacity. If additional solution needs to be added, set the shut-off valve WSV2 in the off position (ASV2 should always remain closed) and release the pressure in the tank by closing the regulator valve APRV1 until the gauge on it indicates zero pressure. Remove the cross-fitting and fill the tank with dyed solution. Pressurize the tank as described in step 1. After the tank is pressurized, set WSV2 in the on position before spraying again.

c. Draining the Spray System

The spray system needs to be drained whenever an icing test is performed while the water impingement spray system is installed in the tunnel. This is necessary as freezing of water in the system can cause considerable damage to the system components.

To drain the system, follow the steps below:

Step 1: Empty the supply tank

To empty the tank, close WSV2 and set the pressure in the tank to about 10 psig by adjusting APRV1 Clean the end of the drain hose DL1 and insert it in a five gallon container. Open WSV1 very slowly to allow dyed water to flow from the tank into the container. If the tank is full, two containers are required.

Step 2: Drain water hoses

Close WSV1 and increase the tank pressure to 60 psig by adjusting APRV1. Make sure that all water control solenoid valves are closed. Open WSV2 to pressurize the water in the hoses and then close WSV2. Clean the end of hose DL2 and insert it in a five gallon container. Open WSV3 slowly to drain lines WL1, WL2, WL11 and WL12.

Repeat the above operation with drain lines DL3 and DL4. Finally, with WSV1 through WSV5 closed, open WSV2 and activate all the water control solenoid valves and spray the remaining water through the spray nozzles.

The air by-pass line is used whenever the water hoses need to be drained without emptying the tank. This is done as described above but WSV2 remains closed and ASV2 is set to the on position in order to by-pass high pressure air to the hoses directly from the tank air pressure line.

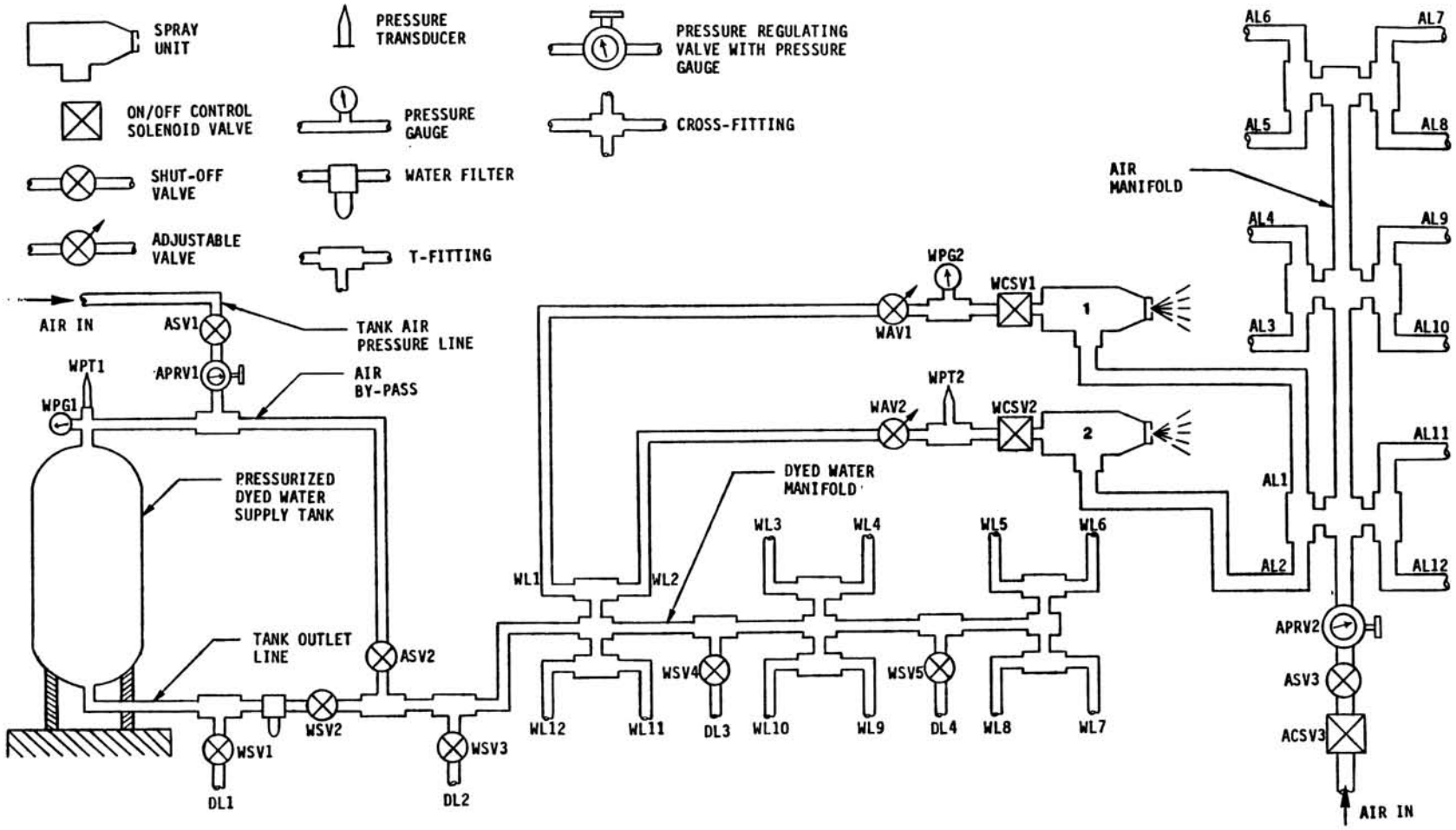

FIGURE A.1

DETAILED SCHEMATIC DIAGRAM OF SPRAY SYSTEM.

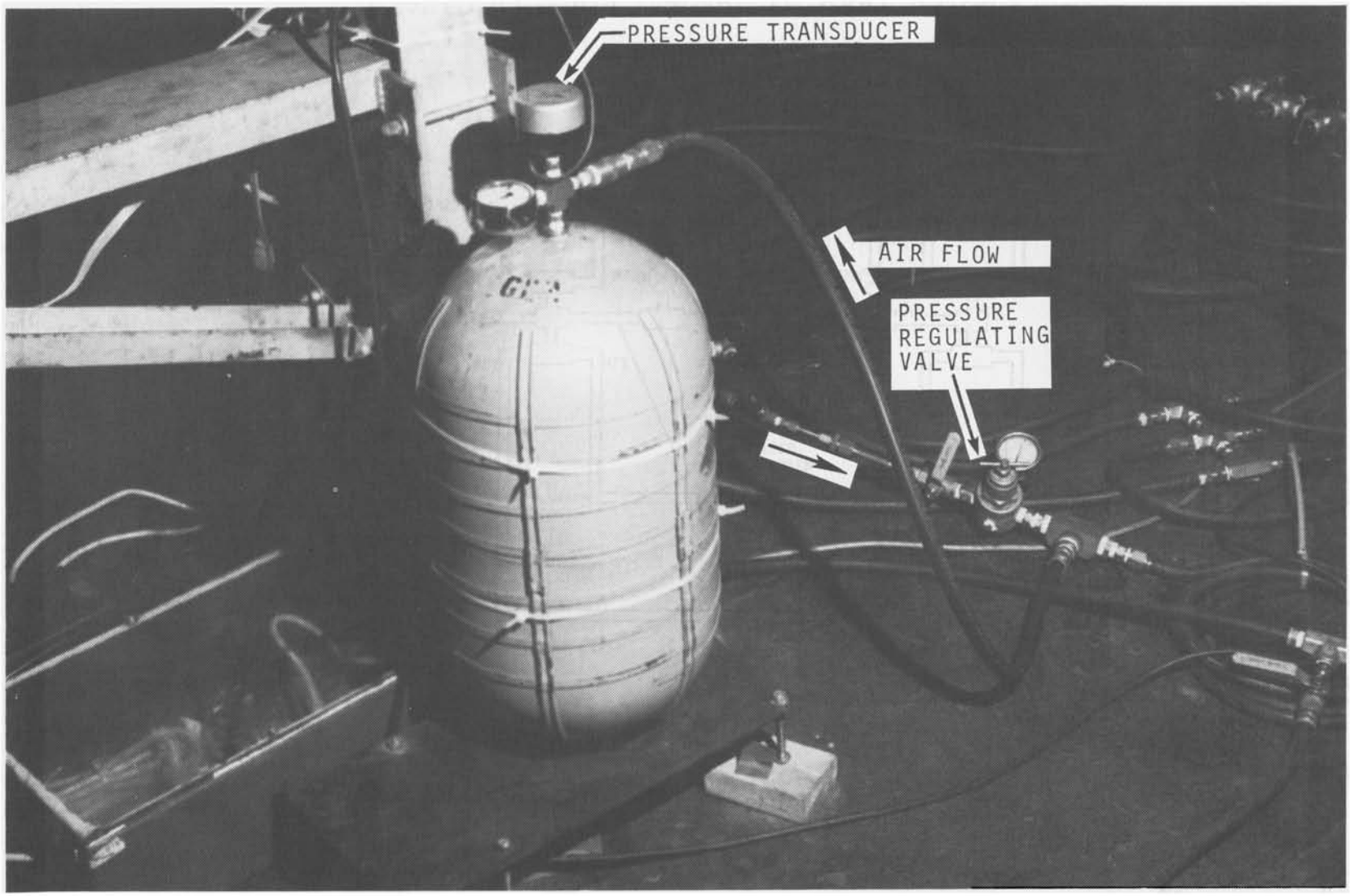

FIGURE A.2

PRESSURIZED DYED WATER SUPPLY TANK.

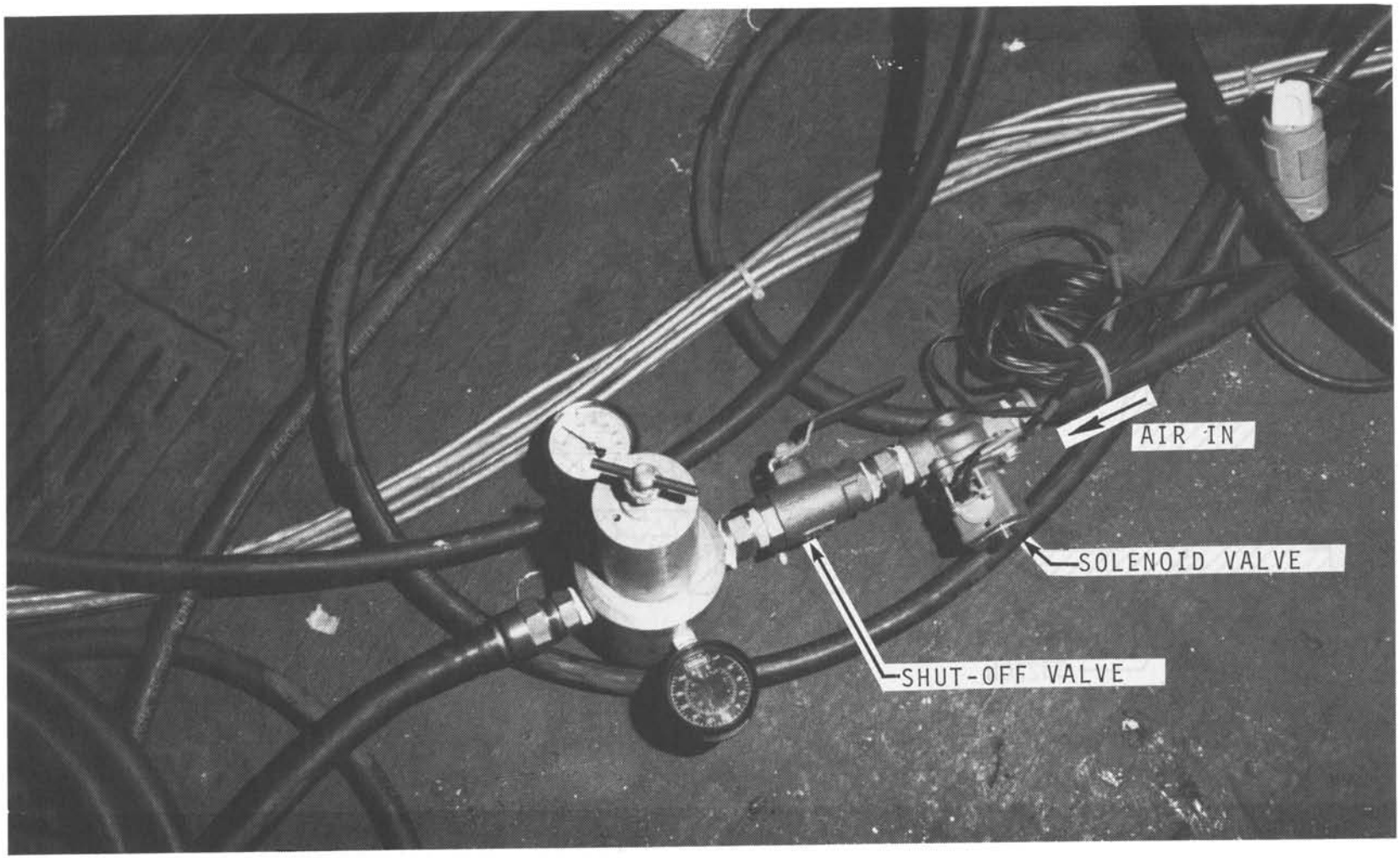

FIGURE A.3

PRESSURE REGULATING VALVE FOR AIR MANIFOLD.

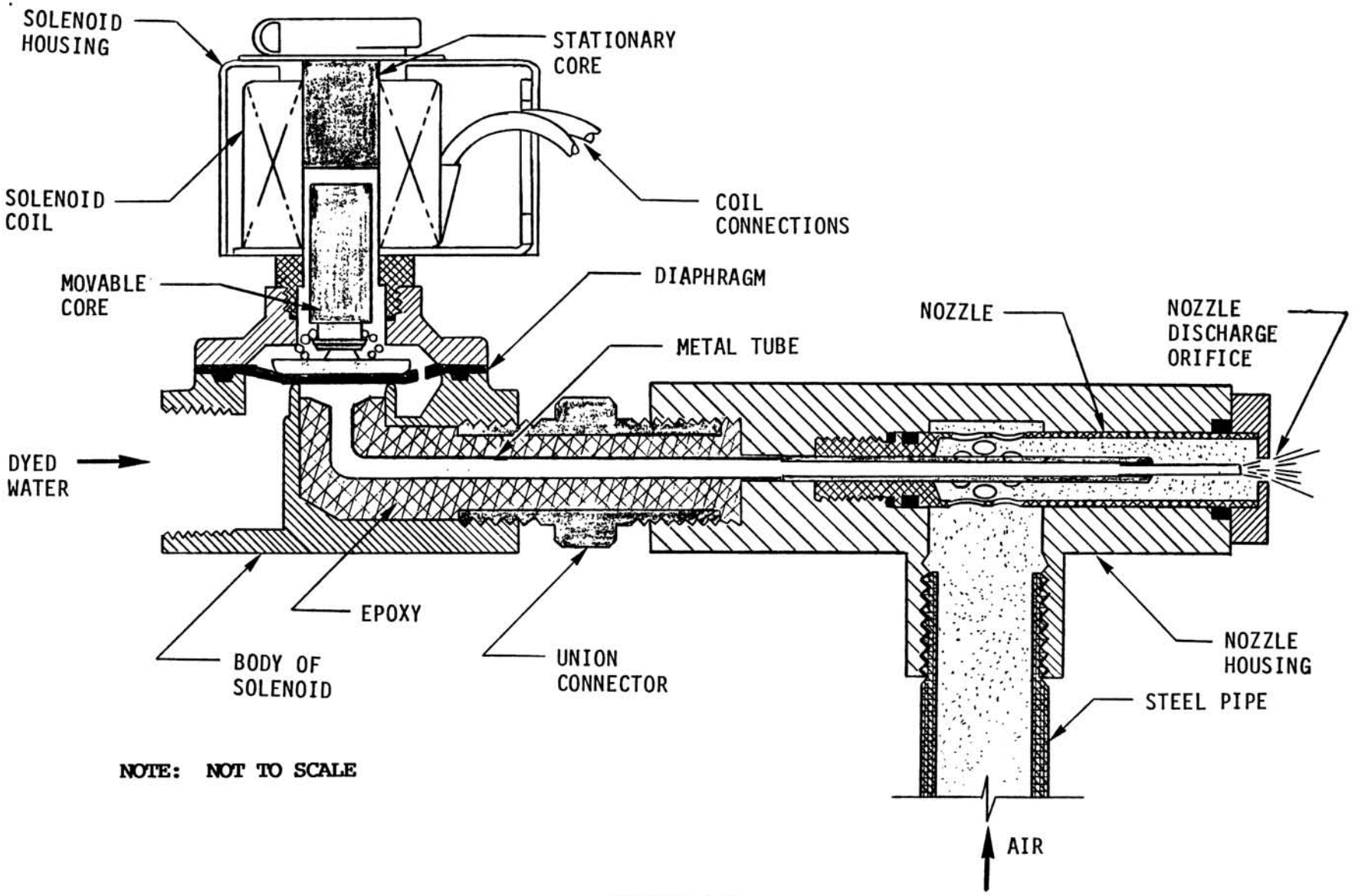

FIGURE A.4

DIAGRAM OF NOZZLE ASSEMBLY COMPONENTS.

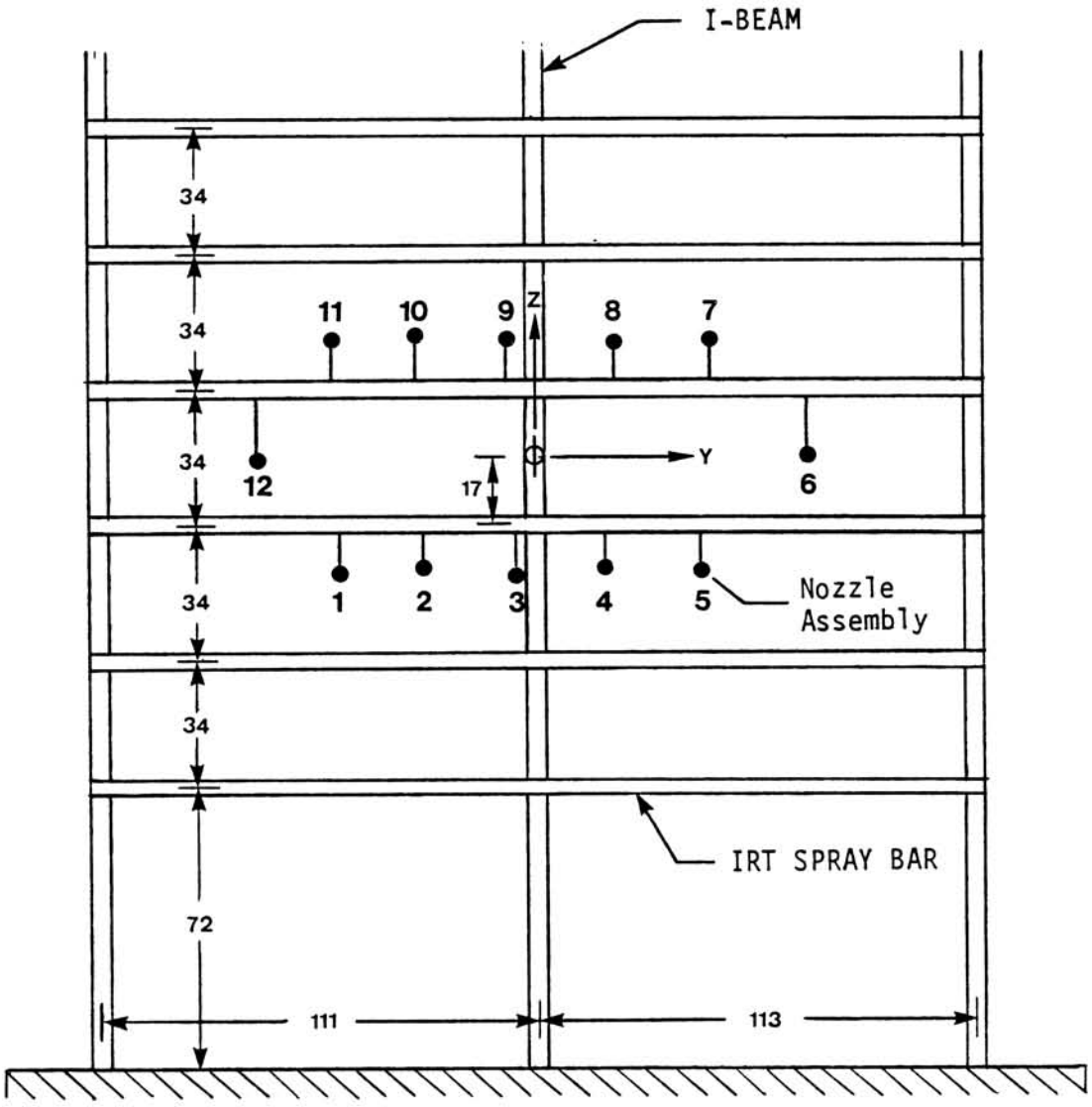

All dimensions in inches

Nozzle Assembly #	NASA Standard Nozzle #	Nozzle location Coordinates in inches Y , Z
1	40	-50.250 , -29.750
2	86	-29.000 , -28.625
3	16	- 5.000 , -30.125
4	115	17.500 , -28.625
5	43	43.500 , -29.500
6	50	69.000 , 0.500
7	75	45.000 , 30.500
8	107	19.000 , 29.750
9	112	- 7.625 , 30.500
10	111	-30.750 , 31.500
11	21	-52.000 , 30.750
12	13	-72.000 , - 1.000

FIGURE A.5

SPRAY NOZZLE LAYOUT IN IRT PLENUM CHAMBER.

APPENDIX B: CALIBRATION OF ENGINE INLET MASS FLOW SYSTEM

Accurate mass flow measurements for engine inlet tests are essential for comparing analytical and experimental inlet aerodynamic and impingement data. To measure the suction mass flow, a temperature compensated velocity probe manufactured by Kurz Instruments Inc. was installed in the NASA 24 inch ID suction pipe. This probe was calibrated utilizing a precalibrated 16 ft long, 8 in. ID duct with pitot tube, wall static tap and thermocouple instrumentation. The calibration of the duct was done at the Boeing pneumatics laboratory facility.

B.1 8 in. ID Duct Calibration

The set up for the 16 ft (192 in.) long, 8 in. ID duct calibration is shown in Figure B.1. The 8 in. duct is shown in Figure B.2. An ASME calibrated venturi tube was installed in the 4.026 in. ID duct. The venturi throat diameter was 2.996 inches. A regulating valve upstream of the venturi was used to adjust the air mass flow. A divergent duct downstream of the venturi connected the 4.026 in. ID duct to the 8 in. ID duct to be calibrated. The 8 in. ID duct consisted of two parts joined together by a flange. The first part was 120 inches long (15 duct diameters) and contained the fixed pitot tube, the wall static tap and the thermocouple. The length of the duct upstream of the fixed pitot tube was 112 inches (14 duct diameters). Duct lengths of at least 10 duct diameters upstream and 10 duct diameters downstream of the pitot tube location are required to allow the flow in the duct to reach a fully developed velocity profile near the pitot. The second part of the duct was 72 inches long (9 duct diameters). However, since the pitot was located 1 duct diameter upstream of the flange, the effective flow length downstream of the pitot was 80 inches (10 duct diameters). At the end of the second part of the duct, a divergent duct was welded to it which connected the 8 in. ID duct to a 1 ft long, 12 in. ID duct.

To calibrate the 8 in. ID duct, the air regulating valve upstream of the venturi was adjusted to the desired level and the static pressure drop ΔP_{SV} between the wall static tap and the static tap at the venturi throat was recorded. From the ASME venturi calibration curve, the mass flow corresponding to ΔP_{SV} was determined. Using the instrumentation installed in the 8 in. duct, the flow static pressure (P_{WS}), the flow velocity pressure (P_V) and the flow total temperature (T_t) were recorded. The procedure was repeated for mass flows varying from 400 lbm/min to 800 lbm/min and a total of 11 sets of measurements were obtained. From these measurements, the calibration curve of Figure B.3 was produced. The product of σP_V (in Hg) was plotted versus mass flow W (lbm/min) on log-log paper. The variable σ represents the density ratio ρ_{local}/ρ_{std} and is found from:

$$\sigma = \frac{\rho_{local}}{\rho_{std}} = \frac{P_{st}/RT_{st}}{\rho_{std}} = 35.3\left(\frac{P_{st}}{T_{st}}\right)$$

R = the gas constant (53.35241 ft lbf/lbm °R)

P_{st} = the wall static (P_{ws}) in psia

T_{st} = the static flow temperature. However, since the thermocouple measures total temperature, T_t is used in place of T_{st}

ρ_{std} = standard air density (0.0765 lbm/ft^3 at P_{st} = 14.696 psia and T_{st} = 520 °R).

The variable P_v represents the flow velocity pressure and is equal to the difference between the flow static pressure P_{ws} and the flow total pressure P_t.

B.2 Calibration of the NASA Suction Flow System

A schematic of the set up used for the calibration of the NASA Icing Research Tunnel suction system is shown in Figure B.4. The NASA suction system consisted of remote vacuum pumps which draw air from a large vacuum tank located on the side of the tunnel building (Figure B.5). A long 24 in. ID duct on top of the building with a remotely controlled regulating valve connected this tank to a shorter S-shaped 18 in. ID duct which terminated above the tunnel test section.

A 12 in. ID duct with an elbow welded to it, connected the 18 in. ID duct to the precalibrated 8 in. ID duct. The precalibrated duct was located inside the wind tunnel at the test section.

To measure the air mass flow in the NASA suction system, a Kurz probe was installed at approximately the two-thirds length point of the 24 in. ID duct. The duct length was greater than 10 duct diameters both upstream and downstream of the Kurz probe (Figures B.5 and B.6). These lengths provide for a fully developed flow velocity profile at the probe. The Kurz probe was connected to a digital voltmeter located in the tunnel control room.

To calibrate the Kurz probe, the following procedure was used:

The air regulating valve in the 24 in. ID duct was adjusted to provide a low mass flow through the system. When conditions were stable, the probe voltage was recorded. The wall static pressure (P_{ws}), flow velocity pressure (P_v) and flow total temperature (T_t) in the 8 in. ID precalibrated duct were recorded. Using P_{ws}, P_v and T_t, the product σP_v was obtained as explained in the previous section. From the calibration curve shown in Figure B.3, the mass flow rate corresponding to the σP_v was read. Next, the air mass flow in lbm/min was plotted versus the voltage indicated by the Kurz probe. The procedure was repeated for higher mass flows until a sufficient number of points were obtained to define the Kurz probe calibration curve. The raw Kurz probe calibration data are shown in Table B.1. The Kurz calibration curve is shown in Figure B.7.

TABLE B.1

RAW CALIBRATION DATA FOR THE KURZ PROBE

NO	P_S GAUGE ~ IN. Hg	P_S PSIA	T ~ °F	σ	P_V ~ IN. Hg	σP_V ~ IN. Hg	W $\frac{LBM}{MIN}$	W $\frac{LBM}{SEC}$	V ~ VOLTS
1	−1.10	13.919	75.2	0.923	0.60	0.554	242.0	(4.00)	0.91
2	−2.16	13.399	74.1	0.891	1.25	1.113	344.0	(5.70)	1.30
3	−3.25	12.864	72.0	0.858	1.97	1.691	425.0	(7.10)	1.62
4	−4.10	12.446	70.3	0.833	2.50	2.083	472.0	(7.90)	1.79
5	−5.00	12.004	69.2	0.805	3.17	2.553	523.0	(8.70)	2.00
6	−6.10	11.464	67.1	0.772	3.85	2.973	564.5	(9.40)	2.15
7	−7.40	10.825	61.5	0.737	4.70	3.463	609.5	(10.20)	2.34
8	−8.50	10.285	60.7	0.701	5.50	3.857	643.4	(10.70)	2.45
9	−9.00	10.040	62.6	0.682	6.15	4.194	671.1	(11.20)	2.51
10	−10.00	9.548	60.1	0.652	6.75	4.399	687.4	(11.50)	2.58
11	−11.15	8.984	58.0	0.616	7.90	4.864	723.0	(12.00)	2.65
12	−11.23	8.944	58.3	0.613	7.80	4.778	716.0	(11.90)	2.67
	CALIBRATION CURVE CHECK AFTER INLET IMPINGEMENT TESTS WERE COMPLETED								
13	−2.13	13.374	58.4	0.916	1.30	1.191	356.0	(5.90)	1.33
14	−5.02	11.954	54.0	0.826	3.13	2.584	526.0	(8.76)	2.02
15	−8.00	10.491	45.7	0.737	5.30	3.903	647.3	(10.78)	2.45
16	−11.31	8.865	44.9	0.623	8.30	5.173	745.7	(12.40)	2.70

Once the probe was calibrated, the precalibrated duct was removed and the engine inlet was connected to the NASA suction system as shown in Figure B.8. To provide the required air mass flow through the inlet, the regulating valve was adjusted until the voltage corresponding to this mass flow was indicated by the Kurz probe.

It is important that the location of the probe remains fixed after it has been calibrated. The calibration of the probe was checked after all engine inlet tests were completed.

B.3 Kurz Probe Details

The probe used to measure engine inlet mass flow in this test was a 415-4 Kurz "Duraflo" velocity sensor. The sensor consisted of a single probe containing mass velocity (R_p) and ambient temperature (R_{tc}) sensing elements (Figure B.9).

The velocity sensor is heated and operated as a constant-temperature thermal anemometer which responds to "standard" velocity (referenced to 25 °C and 760 mm Hg) or mass flow, by sensing the cooling effect of the air as it passes over the heated velocity sensor. The temperature sensor accurately compensates for a wide range of ambient temperature variations.

A schematic of the probe, typical installation and electronic control box are shown in Figure B.9. For displaying the velocity measurements, a Digital Panel Meter is used. The electronic control box contains a linearizing circuit which uses a breakpoint circuit to approximate the non-linear curve obtained from thermal anemometers. The two-wire current mode converts the probe velocity signal into a current which is virtually independent of cable length between probe and remote electronics.

The range of inlet mass flows required for this test was 0 -30 lbm/sec. The corresponding air velocity range in the 24 in. ID duct where the probe was installed was 0 - 100 ft/sec (0 - 68 mph). To obtain accurate mass flow measurements, the probe sensitivity had to be high at low flow velocities. Figure B.10 shows the signal output of the 415-4 sensor versus flow. Both axes in the diagram are normalized to 1. The Kurz sensor has a logarithmic response which means it is most sensitive at lower flows. The sensor can measures flows with gas velocities as low as 0.17 ft/sec accurately. For comparison, the response of differential pressure devices such as orifice plates, pitot tubes, insertion multiport pitot-static devices is also shown in the diagram. These devices have a quadratic response, therefore, are less sensitive to low gas velocities. Other advantages of the Kurz probe are: it is large, insensitive to dirt and easily cleaned. It is not fragile like "hot" wire anemometers. This is important since blotter strips may come loose during a test and can easily damage a hot wire anemometer. This would require recalibration of the system and could cause considerable delay.

ALL DIMENSIONS IN INCHES

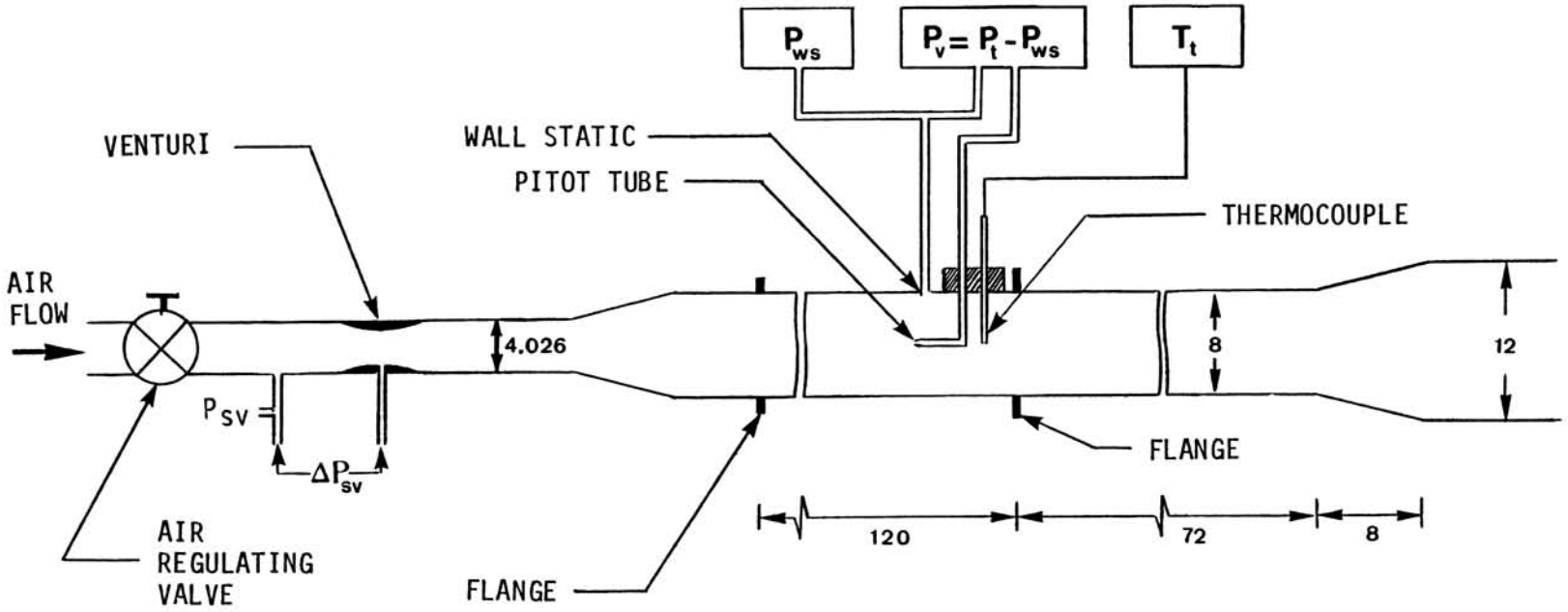

FIGURE B.1

EXPERIMENTAL SET UP FOR THE 8 INCH ID DUCT CALIBRATION AT THE BOEING PNEUMATICS LAB.

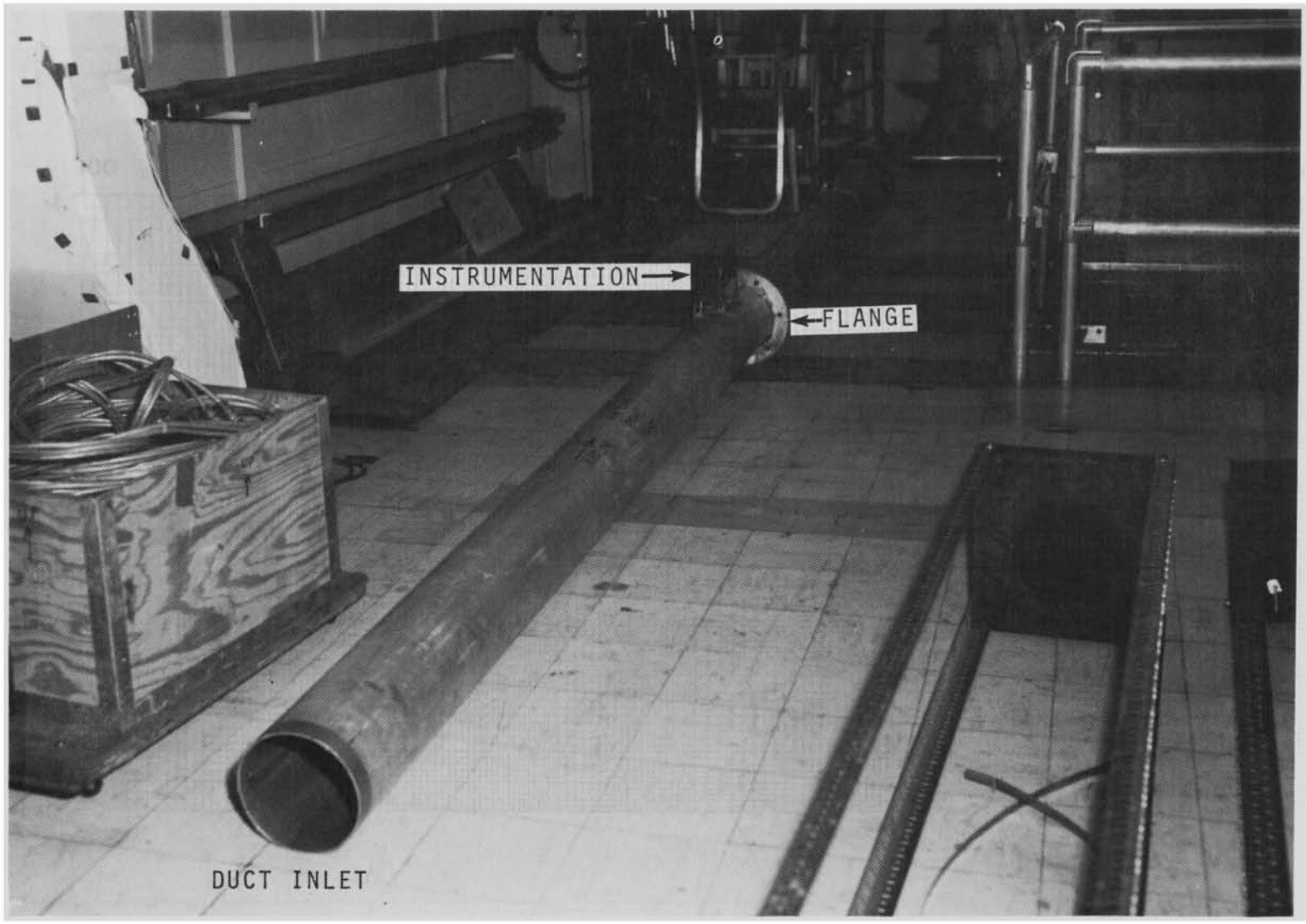

FIGURE B.2

PRECALIBRATED 8 INCH ID DUCT.

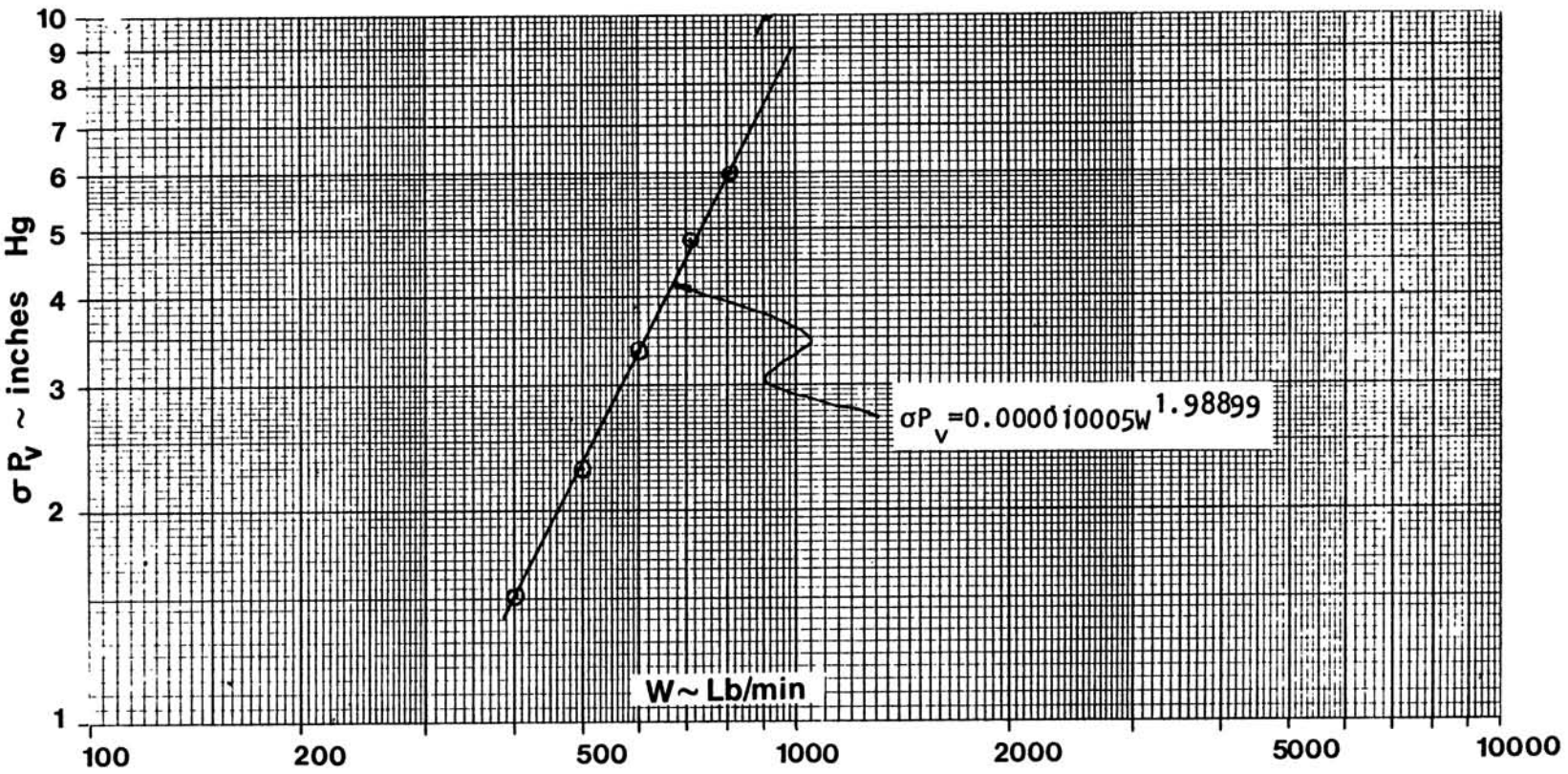

FIGURE B.3

MASS FLOW CALIBRATION CURVE FOR THE 8 INCH ID DUCT.

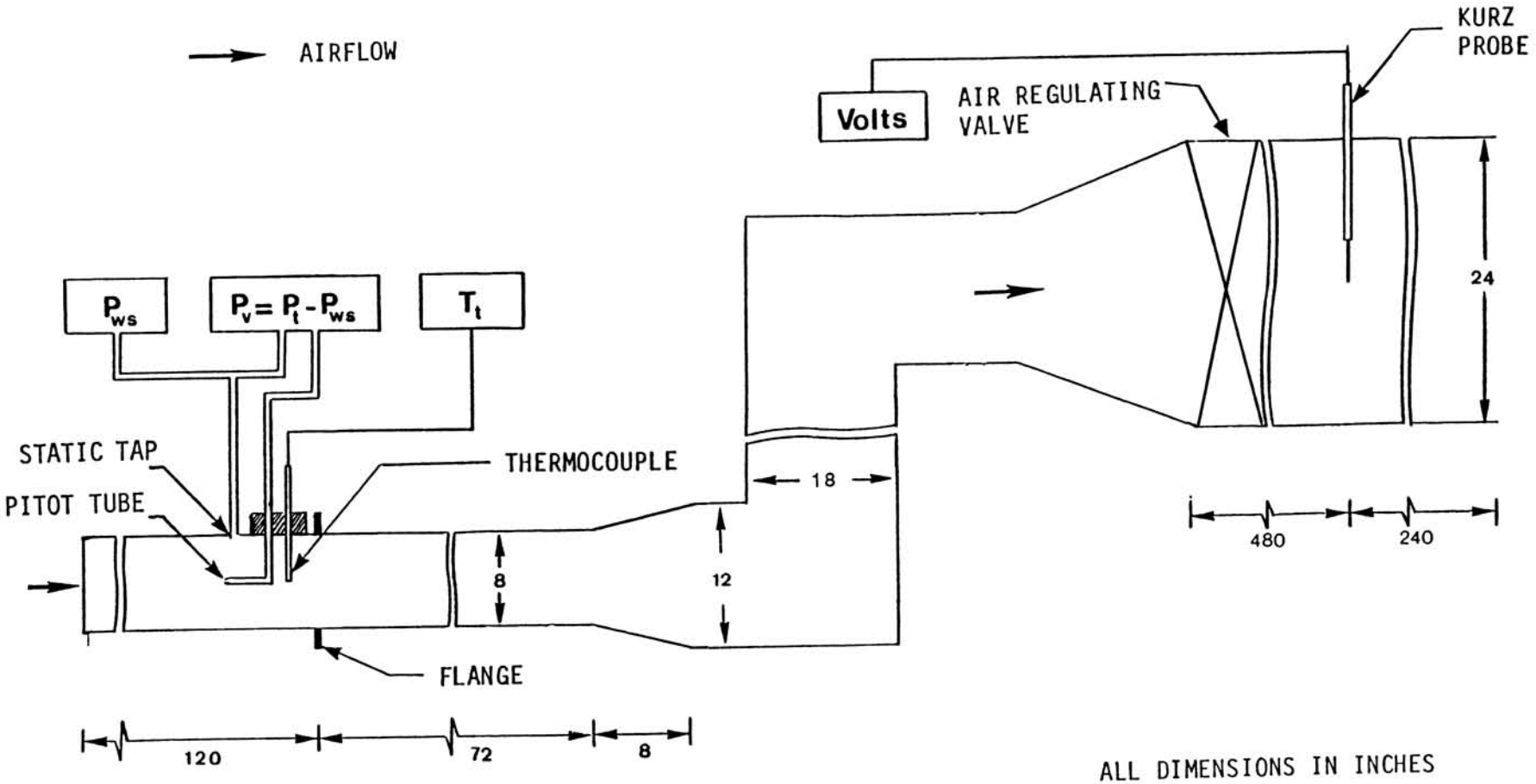

FIGURE B.4

EXPERIMENTAL SET UP FOR THE CALIBRATION OF THE NASA SUCTION FLOW SYSTEM.

FIGURE B.5

VACUUM TANK AND 24 INCH ID DUCT OF THE NASA SUCTION SYSTEM.

FIGURE B.6

INSTALLATION OF KURZ PROBE.

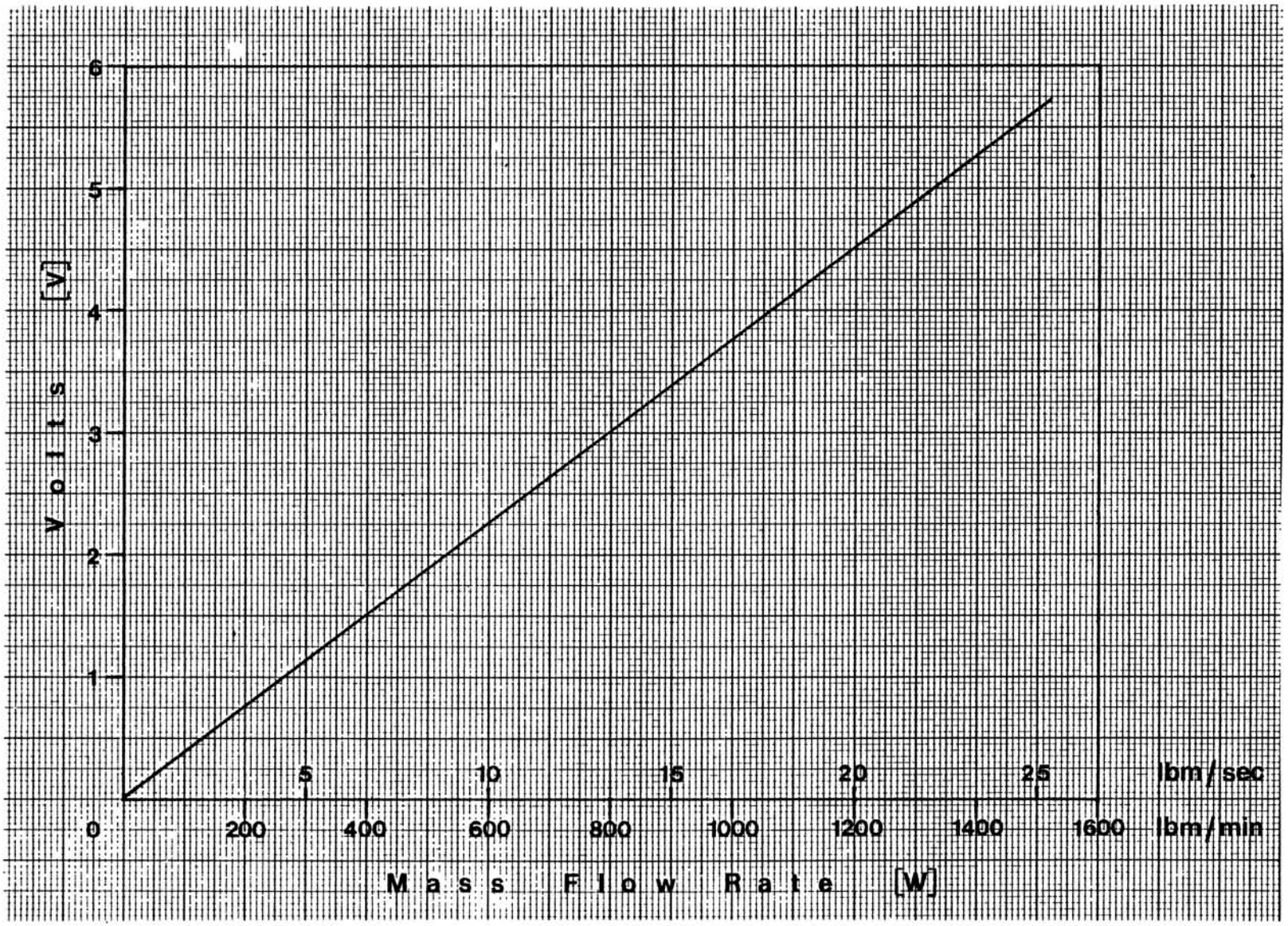

FIGURE B.7

KURZ PROBE CALIBRATION CURVE.

FIGURE B.8

ENGINE INLET CONNECTED TO THE NASA SUCTION SYSTEM.

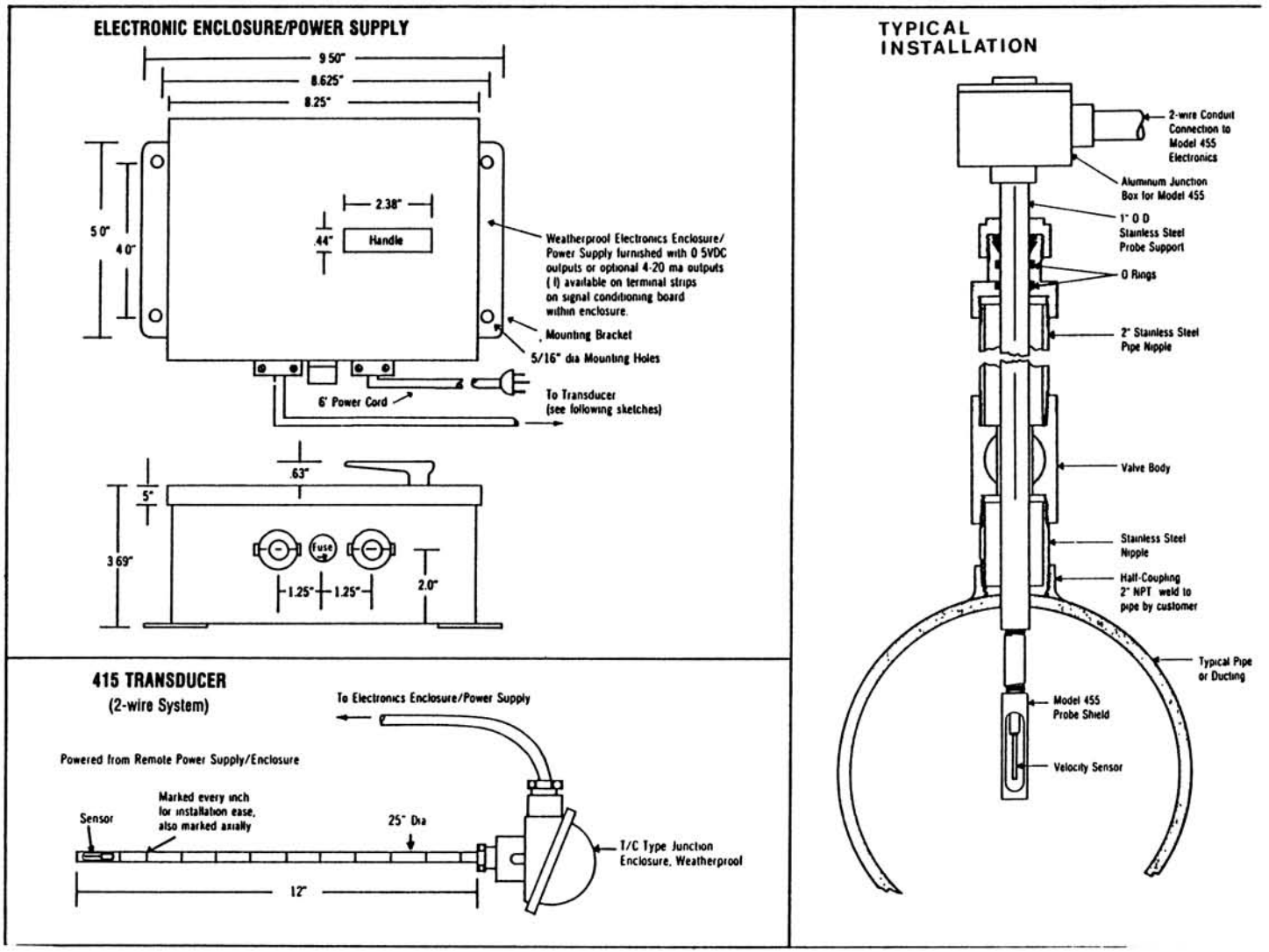

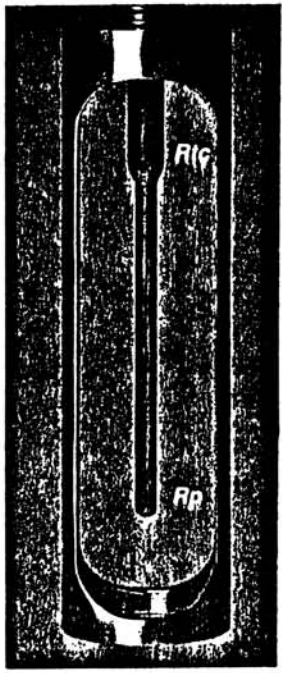

Probe Velocity and Temperature Sensor

FIGURE B.9

KURZ PROBE DETAILS.

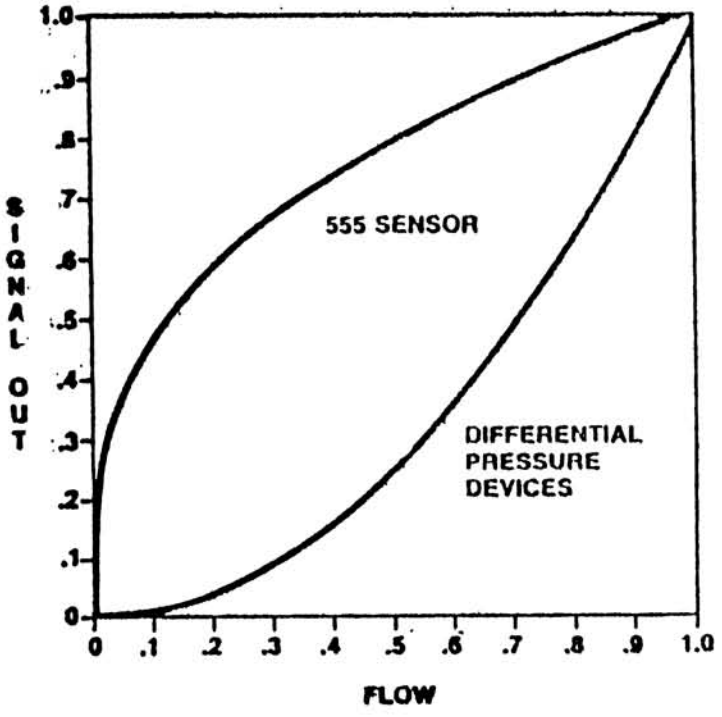

FIGURE B.10

SIGNAL OUTPUT OF KURZ PROBE COMPARED TO THAT OF DIFFERENTIAL PRESSURE DEVICES.

APPENDIX C: DATA REDUCTION METHOD DETAILS

Additional information on the various components of the reflectometer and data acquisition system is given in this appendix. A typical output of the digital data acquisition system and a table for the standard normalized reflectivity calibration curve are also presented.

C.1 Components of Automated Data Reduction System

C.1.1 Components of Automated Reflectometer

Laser	One 5 mW Hughes 3225H-PC He-Ne polarized laser. Beam diameter 1 mm, 10 degrees from normal.
Drum	The drum is cylindrical in shape, 136.6 mm in diameter, 63 mm high and is machined out of Polyvinal Chloride (PVC) tube.
Lens	Convergent lens, 37 mm in diameter positioned 244.6 mm from the drum surface. Focal length = 73 mm.
Photodetector	One EG&G FND-100 silicon photodiode powered from a 15 V DC source. The detector is positioned 90 mm behind the lens. The detector output voltage varies linearly with the intensity of the incident beam.
Stepper Motor	USM Responsyn Motor HDML-150, 800 steps/rev, powered from a 24 V DC source. The motor is driven by the computer through a HP 82940A GP-IO interface.
Linear Actuator	AMSI 601 AM model, travel range 3 in, 0.0254 mm/step. Powered from a 12 V DC source. The actuator is also driven by the computer through a HP 82940A GP-IO interface.
Optical Feedback	Consists of an EG&G FND-100 silicon photodiode powered from 15 V DC source. The detector is mounted on the end of the laser tube. A glass plate 1 mm thick at 45 to the beam directs part of the laser beam onto the detector.

C.1.2 Components of Digital Data Acquisition System

Microcomputer	HP-85 model with 8 bit processor. The computer drives the stepper motor and linear actuator, triggers and samples the digital voltmeters connected to the photodetectors, stores, processes, prints and plots the data.
Data Storage	A HP 82901M 5 1/4 dual floppy disk drive is used to store the voltage from the two photodectors. The location on the blotter strip is also stored.

Digital Voltmeter

A HP 3478A liquid crystal display digital multimeter is connected to the output of the photodetector which measures the amount of laser light reflected from the blotter strip. The signal from the detector is passed through an active filter before it is fed to the voltmeter. The active filter consists of a 741 operational amplifier with a gain of 500/1, and a low-pass filter (Figure C.1).

A Fluke 8520A LED display digital voltmeter is connected to the output of the photodetector of the optical feedback system. The signal from the detector is passed through a low pass active filter before it is fed to the voltmeter. The 741 operational amplifier of this filter has a gain of 10 to 1.

Both voltmeters are triggered simultaneously by the computer through a HP 10833A IO line and are sampled simultaneously through an IEEE-488 line.

Printer

A HP THINKJET printer is used to print the processed data. The printer is connected to the computer with a HP 82939A serial interface. A HP 9872A pen plotter is used. The plotter is connected to the computer using a HP 10833A IO line.

A schematic diagram of the automated reflectometer and data acquisition is shown on Figure 5.9 of Section 5.

C.2 Typical Output of Automated Data Reduction System

A typical output of the raw and processed data is shown in Figure C.2. The output includes results for each individual scan for the NACA 65_2015 airfoil section at $\alpha = 0^o$, exposed to a cloud with Mean Volumetric Diameter of 16.45 microns. The indicated tunnel speed was 175 mph.

The first line of the output is the identification for the test showing the date (092685) of the test, the run number (4), the last three digits (015) of the five digits airfoil number, the angle of attack (0) and the strip position (B). The next seven lines of the output (CHORD LENGTH to DROPLET SIZE) present information regarding model geometry, tunnel and spray cloud conditions for the test. The reference COLLECTOR DYE/UNIT AREA is a measure of liquid water content and the reference COLLECTOR EFFICIENCY is the theoretical value of the collector impingement efficiency for the droplet spray cloud of the test.

The next six lines of the output give positional data for the blotter strip. The NUMBER OF NEGATIVE STEPS (60) and the NUMBER OF POSITIVE STEPS (60) indicate the increments of the horizontal length of

each scan on either side of the highlight. This length is also given in mm. The NUMBER of SCAN is usually 3 and the vertical location of each of the three scans, measured from the upper edge of the blotter strip, is given in steps and in mm (see Figure C.3). The next line, RATIO USED FOR BARE PAPER, is a measure of the reflectance of the blotter paper without dye. The output continues with the results of the first scan (H1). There are 121 locations (-60 to +60) for each scan in this example. The step number and the corresponding length in mm, measured from the highlight mark are given in the first and second columns, respectively. The third column (DIRECT), shows the voltage output (V1) of the photodetector, which measures the amount of laser light reflected from the blotter strip at a given location. The fourth column (SPLIT) is the voltage output (V2) of the photodetector used in the optical feedback to monitor the laser power output. The fifth column (RATIO) is the ratio of voltage (V1) divided by the voltage (V2). Dividing this ratio value (V1/V2) by the value of the bare paper ratio, 1.145 in this case, gives column six (REFL). This is the value of the normalized reflectivity at a given location (STEP) on the blotter strip.

Next the program uses linear interpolation and the table presented in Section C.3 to find the dye mass density ($\mu g/cm^2$) shown in column seven (MASS). Finally, this mass is divided by the collector mass (2.52 $\mu g/cm^2$) and is multiplied by the collector efficiency (0.86) to give the value of the impingement efficiency. The impingement efficiency values (b) are shown in column eight.

Example:

Consider the location on the blotter strip corresponding to step -55 (-29.5 mm) from the highlight mark.

V1 = -2.6110
V2 = -2.4175

Therefore,

$$\text{RATIO} = \frac{V1}{V2} = \frac{-2.6110}{-2.4175} = 1.0800$$

$$\text{REFL} = \frac{1.0800}{1.1450} = 0.9433$$

From Table C.1, MASS = 0.0537.

$$\text{Impingement efficiency (b)} = \frac{0.0537}{2.52} * 0.86 = 0.0183$$

The results for scans #2 and #3 are also shown in Figure C.2. The average RATIO, REFL, MASS and b of all three scans are also presented.

In Figure C.3, the average values of Reflectivity, Dye Mass $\mu g/cm^2$ and impingement efficiency are plotted versus surface distance measured from the highlight mark. At the point where reflectivity is minimum, the dye mass and impingement efficiency reach their maximum values. Typically, only the impingement efficiency versus surface distance is plotted using averaged data. The maximum value of impingement efficiency for this test model at $\alpha = 0^0$ corresponds to the highlight location. The highlight, however, cannot always be marked accurately on the blotter paper. This results in the $\bar{\beta}$-curve being slightly shifted with respect to the highlight location.

C.3 Standard Normalized Refelctivity Table

The standard normalized reflectivity curve is given in tabulated form in Table C.1. This table is used by the computer program to calculate the dye mass corresponding to a given normalized reflectivity value. These data are plotted in Figure 5.5.

TABLE C.1

STANDARD NORMALIZED REFLECTIVITY TABLE

DYE-MASS μg CM^2	NORMAL REFL	DYE-MASS μg CM^2	NORMAL REFL	DYE-MASS μg·CM^2	NORMAL REFL	DYE-MASS μg CM^2	NORMAL REFL	DYE-MASS μg CM^2	NORMAL REFL
0 0000	1 00000	0 4500	0 62470	0 9000	0 44006	1 3500	0 37351	1 8600	0 34506
0 0100	0 98932	0 4600	0 61876	0 9100	0 43758	1 3600	0 37278	1 9000	0 34265
0.0200	0 97865	0 4700	0.61292	0 9200	0 43516	1 3700	0 37208	1 9400	0 34020
0 0300	0 96810	0 4800	0 60717	0 9300	0 43280	1 3800	0 37139	1 9800	0 33773
0 0400	0 95766	0 4900	0 60152	0 9400	0 43049	1 3900	0 37072	2 0200	0 33525
0 0500	0 94735	0 5000	0 59596	0 9500	0 42824	1 4000	0 37006	2 0600	0 33275
0 0600	0 93714	0 5100	0 59049	0 9600	0 42604	1 4100	0 36943	2 1000	0 33026
0.0700	0 92705	0 5200	0.58512	0 9700	0 42390	1 4200	0 36880	2 1400	0.32779
0.0800	0 91708	0.5300	0 57983	0 9800	0 42180	1 4300	0 36820	2 1800	0 32533
0.0900	0 90722	0 5400	0 57463	0 9900	0 41976	1 4400	0.36760	2 2200	0.32291
0.1000	0.89747	0 5500	0.56952	1 0000	0 41777	1 4500	0 36702	2 2600	0.32053
0 1100	0 88784	0 5600	0 56450	1 0100	0 41583	1 4600	0 36645	2 3000	0 31820
0 1200	0 87831	0.5700	0 55957	1 0200	0 41394	1 4700	0 36589	2 3400	0.31593
0.1300	0 86890	0 5800	0 55472	1 0300	0 41210	1 4800	0 36534	2 3800	0.31373
0 1400	0 85961	0 5900	0 54996	1.0400	0 41030	1 4900	0 36480	2 4200	0.31162
0 1500	0 85042	0.6000	0 54528	1.0500	0 40855	1 5000	0.36427	2 4500	0.31008
0.1600	0 84135	0.6100	0 54069	1.0600	0 40685	1 5100	0.36375	2 5000	0.30763
0.1700	0 83238	0.6200	0.53618	1.0700	0 40519	1 5200	0 36324	2 5500	0 30528
0.1800	0.82353	0.6300	0.53175	1.0800	0 40357	1 5300	0 36272	2 6000	0 30301
0.1900	0.81478	0 6400	0 52740	1.0900	0.40200	1 5400	0 36222	2 6500	0.30078
0 2000	0.80615	0.6500	0 52313	1 1000	0 40047	1 5500	0 36172	2 7000	0 29857
0.2100	0.79762	0.6600	0.51894	1 1100	0.39899	1 5600	0 36122	2 7500	0.29635
0 2200	0 78921	0.6700	0.51483	1 1200	0 39754	1.5700	0 36073	2 8000	0.29410
0 2300	0.78090	0.6800	0.51080	1.1300	0.39613	1 5800	0 36023	2 8500	0.29178
0 2400	0 77270	0.6900	0 50685	1 1400	0.39476	1.5900	0 35974	2 9000	0 28936
0 2500	0 76461	0 7000	0 50297	1 1500	0 39343	1.6000	0 35925	2 9500	0.28683
0.2600	0 75662	0.7100	0 49916	1.1600	0.39214	1.6100	0 35876	3 0000	0.28415
0 2700	0 74874	0.7200	0 49543	1 1700	0 39088	1 6200	0 35826	3 0500	0 28129
0 2800	0 74097	0 7300	0 49178	1 1800	0.38966	1 6300	0 35777	3 1000	0.27822
0 2900	0 73330	0.7400	0 48820	1 1900	0.38847	1 6400	0 35727	3 1500	0.27493
0 3000	0.72574	0.7500	0.48468	1 2000	0 38732	1 6500	0 35676	3 2000	0.27137
0.3100	0.71829	0.7600	0 48124	1 2100	0 38620	1 6600	0 35625	3.2500	0.26752
0.3200	0.71093	0.7700	0 47787	1 2200	0 38511	1.6700	0 35574	3 3000	0.26336
0.3300	0 70369	0.7800	0.47457	1 2300	0.38405	1 6800	0 35522	3.3500	0.25886
0.3400	0 69654	0.7900	0 47134	1 2400	0.38303	1 6900	0.35469	3.4000	0.25398
0.3500	0 68951	0 8000	0 46817	1 2500	0 38203	1 7000	0 35416	3 4500	0.24870
0.3600	0 68257	0.8100	0 46508	1 2600	0 38106	1 7100	0.35362	3.5000	0.24312
0.3700	0 67574	0.8200	0 46204	1.2700	0.38012	1 7200	0 35308		
0 3800	0 66900	0.8300	0 45908	1 2800	0.37921	1 7300	0 35254		
0 3900	0 66238	0.8400	0 45617	1 2900	0 37833	1 7400	0.35199		
0 4000	0 65585	0 8500	0 45333	1 3000	0.37746	1 7500	0 35143		
0.4100	0 64942	0.8600	0 45056	1 3100	0.37663	1 7600	0.35087		
0 4200	0.64309	0.8700	0.44784	1 3200	0.37581	1 7700	0.35031		
0 4300	0.63686	0 8800	0.44519	1.3300	0.37502	1 7800	0 34974		
0 4400	0.63073	0 8900	0.44259	1.3400	0.37426	1.8200	0 34743		

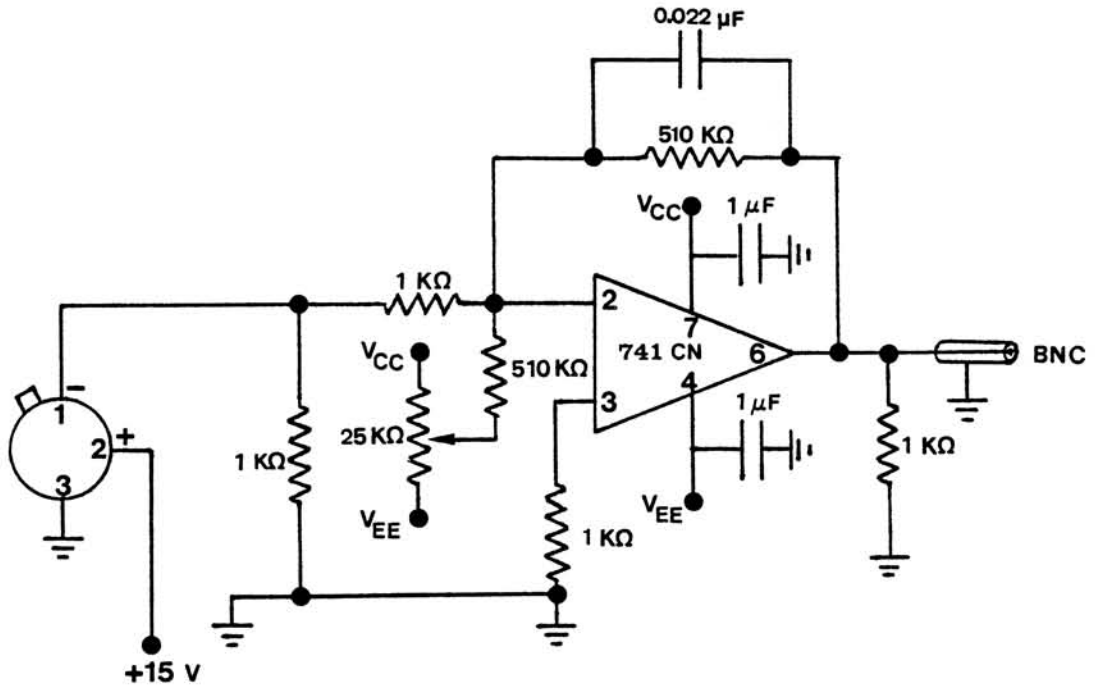

(A) FOR DIRECT OPTICAL SIGNAL ; AMPLIFIER GAIN 500:1

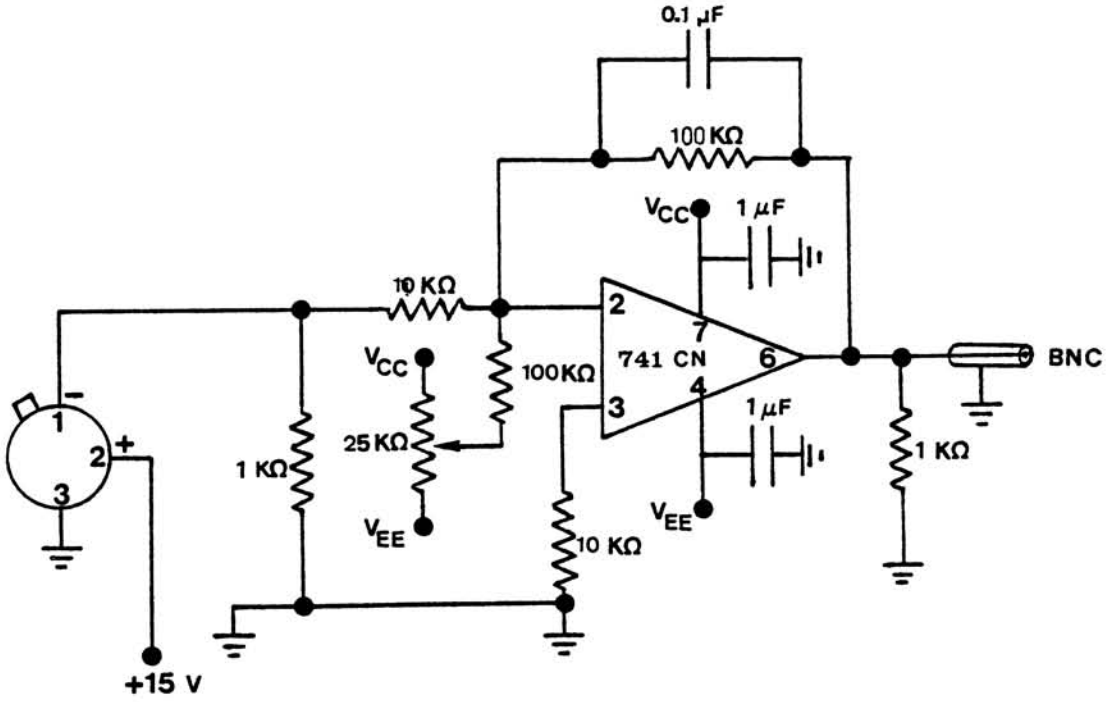

(B) FOR OPTICAL FEED-BACK SIGNAL ; AMPLIFIER GAIN 10:1

FIGURE C.1

SCHEMATIC DIAGRAM OF ACTIVE FILTERS

RUN ID : 092685-4B-015-0 NACA 652015 PAGE 1

CHORD LENGTH	33.02 cm	(13.00 in)
ANGLE OF ATTACK	0.00 deg	
TRUE AIR SPEED	81.75 m/s	(182.88 mph)
TUNNEL TOTAL TEMP	10.39 C	(50.70 F)
TUNNEL STATIC PRESSURE	94.48 kpa	(13.71 psia)
AIR/WATER PRESSURE RATIO	0.80	
DROPLET SIZE	16.45 microns	
COLLECTOR DYE/UNIT AREA	2.52 µgm/cm2	
COLLECTOR EFFICIENCY	0.86	

NUMBER OF NEGATIVE STEPS	60	SPANNING 32.18 mm	UPPER SURFACE
NUMBER OF POSITIVE STEPS	60	SPANNING 32.18 mm	LOWER SURFACE
NUMBER OF SCANS	3		
POSITION OF H1	8.04 mm	(304 LINEAR ACTUATOR STEPS)	
POSITION OF H2	18.10 mm	(684 LINEAR ACTUATOR STEPS)	
POSITION OF H3	28.15 mm	(1064 LINEAR ACTUATOR STEPS)	

RATIO USED FOR BARE PAPER IS 1.1450

DATA FOR SCAN H1

STEP	(mm)	DIRECT	SPLIT	RATIO	REFL	MASS	b	
-60	-32.2	-2.5950	-2.4162	+1.0740	0.9380	0.0590	0.0201	:
-59	-31.6	-2.5660	-2.4166	+1.0618	0.9274	0.0696	0.0238	:
-58	-31.1	-2.5800	-2.4173	+1.0673	0.9321	0.0649	0.0221	:
-57	-30.6	-2.5660	-2.4178	+1.0613	0.9269	0.0701	0.0239	:
-56	-30.0	-2.5770	-2.4177	+1.0659	0.9309	0.0661	0.0226	:
-55	-29.5	-2.6110	-2.4175	+1.0800	0.9433	0.0537	0.0183	:
-54	-29.0	-2.6090	-2.4171	+1.0794	0.9427	0.0543	0.0185	:
-53	-28.4	-2.6270	-2.4169	+1.0869	0.9493	0.0477	0.0163	:
-52	-27.9	-2.5600	-2.4164	+1.0594	0.9253	0.0717	0.0245	:
-51	-27.3	-2.5350	-2.4162	+1.0492	0.9163	0.0807	0.0275	:*
-50	-26.8	-2.5220	-2.4160	+1.0439	0.9117	0.0853	0.0291	:*
-49	-26.3	-2.4420	-2.4157	+1.0109	0.8829	0.1151	0.0393	:*
-48	-25.7	-2.4130	-2.4154	+0.9990	0.8725	0.1263	0.0431	:*
-47	-25.2	-2.4690	-2.4151	+1.0223	0.8929	0.1049	0.0358	:*
-46	-24.7	-2.4720	-2.4149	+1.0236	0.8940	0.1036	0.0354	:*
-45	-24.1	-2.5060	-2.4148	+1.0378	0.9063	0.0907	0.0309	:*
-44	-23.6	-2.5270	-2.4145	+1.0466	0.9141	0.0829	0.0283	:*
-43	-23.1	-2.4820	-2.4145	+1.0280	0.8978	0.0994	0.0339	:*
-42	-22.5	-2.4170	-2.4143	+1.0011	0.8743	0.1242	0.0424	:*
-41	-22.0	-2.4010	-2.4140	+0.9946	0.8687	0.1305	0.0445	:*
-40	-21.5	-2.4270	-2.4139	+1.0054	0.8781	0.1201	0.0410	:*
-39	-20.9	-2.4220	-2.4137	+1.0034	0.8764	0.1220	0.0416	:*
-38	-20.4	-2.3570	-2.4138	+0.9765	0.8528	0.1472	0.0502	:*
-37	-19.8	-2.4030	-2.4139	+0.9955	0.8694	0.1296	0.0442	:*
-36	-19.3	-2.4180	-2.4142	+1.0016	0.8747	0.1238	0.0422	:*
-35	-18.8	-2.3610	-2.4141	+0.9780	0.8542	0.1458	0.0498	:*
-34	-18.2	-2.3500	-2.4144	+0.9733	0.8501	0.1499	0.0512	:*
-33	-17.7	-2.3430	-2.4144	+0.9704	0.8475	0.1527	0.0521	:*
-32	-17.2	-2.2730	-2.4146	+0.9414	0.8221	0.1814	0.0619	:*
-31	-16.6	-2.2260	-2.4149	+0.9218	0.8050	0.2009	0.0686	:*
-30	-16.1	-2.1200	-2.4147	+0.8780	0.7668	0.2472	0.0844	: *
-29	-15.6	-2.1740	-2.4145	+0.9004	0.7864	0.2234	0.0762	: *
-28	-15.0	-2.2000	-2.4143	+0.9112	0.7958	0.2120	0.0723	:*
-27	-14.5	-2.0220	-2.4141	+0.8376	0.7315	0.2920	0.0997	: *
-26	-13.9	-2.0560	-2.4140	+0.8517	0.7438	0.2760	0.0942	: *

FIGURE C.2

TYPICAL OUTPUT OF AUTOMATED DATA REDUCTION SYSTEM (PAGE 1 OF 9).

RUN ID : 092685-4-015-0B NACA 652015 PAGE 2

-25	-13.4	-1.9720	-2.4141	+0.8169	0.7134	0.3162	0.1079
-24	-12.9	-1.9400	-2.4143	+0.8035	0.7018	0.3325	0.1135
-23	-12.3	-1.8450	-2.4150	+0.7640	0.6672	0.3824	0.1305
-22	-11.8	-1.7640	-2.4154	+0.7303	0.6378	0.4285	0.1462
-21	-11.3	-1.7600	-2.4155	+0.7286	0.6364	0.4308	0.1470
-20	-10.7	-1.7370	-2.4156	+0.7191	0.6280	0.4444	0.1517
-19	-10.2	-1.5970	-2.4155	+0.6611	0.5774	0.5349	0.1825
-18	-9.7	-1.5740	-2.4158	+0.6515	0.5690	0.5509	0.1880
-17	-9.1	-1.5560	-2.4160	+0.6440	0.5625	0.5640	0.1925
-16	-8.6	-1.4980	-2.4159	+0.6201	0.5415	0.6086	0.2077
-15	-8.0	-1.4870	-2.4159	+0.6155	0.5376	0.6174	0.2107
-14	-7.5	-1.4410	-2.4158	+0.5965	0.5210	0.6548	0.2235
-13	-7.0	-1.3320	-2.4157	+0.5514	0.4816	0.7586	0.2589
-12	-6.4	-1.2800	-2.4154	+0.5299	0.4628	0.8177	0.2791
-11	-5.9	-1.2540	-2.4153	+0.5192	0.4534	0.8500	0.2901
-10	-5.4	-1.2460	-2.4152	+0.5159	0.4506	0.8600	0.2935
-9	-4.8	-1.2530	-2.4150	+0.5188	0.4531	0.8510	0.2904
-8	-4.3	-1.1780	-2.4147	+0.4878	0.4261	0.9605	0.3278
-7	-3.8	-1.1460	-2.4147	+0.4746	0.4145	1.0182	0.3475
-6	-3.2	-1.1150	-2.4147	+0.4618	0.4033	1.0830	0.3696
-5	-2.7	-1.0770	-2.4147	+0.4460	0.3895	1.1814	0.4032
-4	-2.1	-1.0690	-2.4146	+0.4427	0.3867	1.2084	0.4124
-3	-1.6	-1.0440	-2.4147	+0.4324	0.3776	1.3022	0.4444
-2	-1.1	-1.0180	-2.4146	+0.4216	0.3682	1.4339	0.4894
-1	-0.5	-0.9780	-2.4145	+0.4051	0.3538	1.7036	0.5814
0	0.0	-0.9080	-2.4145	+0.3761	0.3284	2.1298	0.7268
1	0.5	-0.9560	-2.4145	+0.3959	0.3458	1.8456	0.6298
2	1.1	-0.9860	-2.4145	+0.4084	0.3567	1.6486	0.5626
3	1.6	-0.9620	-2.4145	+0.3984	0.3480	1.8091	0.6174
4	2.1	-0.9940	-2.4146	+0.4117	0.3595	1.5939	0.5440
5	2.7	-0.9860	-2.4147	+0.4083	0.3566	1.6492	0.5628
6	3.2	-0.9430	-2.4148	+0.3905	0.3411	1.9253	0.6570
7	3.8	-1.0280	-2.4147	+0.4257	0.3718	1.3774	0.4701
8	4.3	-1.0370	-2.4146	+0.4295	0.3751	1.3349	0.4556
9	4.8	-1.0490	-2.4148	+0.4344	0.3794	1.2789	0.4364
10	5.4	-1.0410	-2.4149	+0.4311	0.3765	1.3167	0.4494
11	5.9	-1.0610	-2.4150	+0.4393	0.3837	1.2362	0.4219
12	6.4	-1.1070	-2.4148	+0.4584	0.4004	1.1007	0.3757
13	7.0	-1.1500	-2.4151	+0.4762	0.4159	1.0109	0.3450
14	7.5	-1.2030	-2.4151	+0.4981	0.4350	0.9208	0.3143
15	8.0	-1.2110	-2.4152	+0.5014	0.4379	0.9088	0.3101
16	8.6	-1.2860	-2.4151	+0.5325	0.4651	0.8103	0.2765
17	9.1	-1.2940	-2.4151	+0.5358	0.4679	0.8008	0.2733
18	9.7	-1.3340	-2.4152	+0.5523	0.4824	0.7563	0.2581
19	10.2	-1.3900	-2.4153	+0.5755	0.5026	0.7012	0.2393
20	10.7	-1.4850	-2.4151	+0.6149	0.5370	0.6186	0.2111
21	11.3	-1.4970	-2.4153	+0.6198	0.5413	0.6091	0.2079
22	11.8	-1.5790	-2.4153	+0.6537	0.5710	0.5472	0.1867
23	12.3	-1.6430	-2.4153	+0.6802	0.5941	0.5036	0.1719
24	12.9	-1.7710	-2.4153	+0.7332	0.6404	0.4244	0.1448
25	13.4	-1.7760	-2.4153	+0.7353	0.6422	0.4215	0.1438
26	13.9	-1.8630	-2.4152	+0.7714	0.6737	0.3728	0.1272
27	14.5	-1.9300	-2.4151	+0.7991	0.6979	0.3379	0.1153
28	15.0	-1.9440	-2.4151	+0.8049	0.7030	0.3308	0.1129
29	15.6	-2.0100	-2.4151	+0.8323	0.7269	0.2981	0.1017
30	16.1	-2.0290	-2.4150	+0.8402	0.7338	0.2891	0.0987
31	16.6	-2.0190	-2.4151	+0.8360	0.7301	0.2938	0.1003
32	17.2	-2.0640	-2.4149	+0.8547	0.7465	0.2726	0.0930

FIGURE C.2

TYPICAL OUTPUT OF AUTOMATED DATA REDUCTION SYSTEM (PAGE 2 OF 9).

33	17.7	-2.1500	-2.4151	+0.8902	0.7775	0.2340	0.0799	: *
34	18.2	-2.2090	-2.4149	+0.9147	0.7989	0.2083	0.0711	:*
35	18.8	-2.2240	-2.4150	+0.9209	0.8043	0.2019	0.0689	:*
36	19.3	-2.2700	-2.4151	+0.9399	0.8209	0.1829	0.0624	:*
37	19.8	-2.2800	-2.4150	+0.9441	0.8245	0.1786	0.0609	:*
38	20.4	-2.3060	-2.4150	+0.9549	0.8339	0.1677	0.0572	:*
39	20.9	-2.3550	-2.4151	+0.9751	0.8516	0.1484	0.0506	:*
40	21.5	-2.3780	-2.4149	+0.9847	0.8600	0.1400	0.0478	:*
41	22.0	-2.3590	-2.4149	+0.9769	0.8531	0.1469	0.0501	:*
42	22.5	-2.4310	-2.4149	+1.0067	0.8792	0.1189	0.0406	:*
43	23.1	-2.3730	-2.4150	+0.9826	0.8582	0.1418	0.0484	:*
44	23.6	-2.4270	-2.4148	+1.0051	0.8778	0.1204	0.0411	:*
45	24.1	-2.4450	-2.4149	+1.0125	0.8842	0.1138	0.0388	:*
46	24.7	-2.4740	-2.4149	+1.0245	0.8947	0.1028	0.0351	:*
47	25.2	-2.4290	-2.4148	+1.0059	0.8785	0.1197	0.0408	:*
48	25.7	-2.4900	-2.4147	+1.0312	0.9006	0.0964	0.0329	:*
49	26.3	-2.5070	-2.4146	+1.0383	0.9068	0.0902	0.0308	:*
50	26.8	-2.5450	-2.4147	+1.0540	0.9205	0.0765	0.0261	:*
51	27.3	-2.5820	-2.4148	+1.0692	0.9338	0.0632	0.0216	:
52	27.9	-2.5840	-2.4148	+1.0701	0.9346	0.0624	0.0213	:
53	28.4	-2.6040	-2.4147	+1.0784	0.9418	0.0552	0.0188	:
54	29.0	-2.5870	-2.4147	+1.0714	0.9357	0.0613	0.0209	:
55	29.5	-2.5790	-2.4146	+1.0681	0.9328	0.0642	0.0219	:
56	30.0	-2.5850	-2.4147	+1.0705	0.9350	0.0620	0.0212	:
57	30.6	-2.5660	-2.4146	+1.0627	0.9281	0.0689	0.0235	:
58	31.1	-2.5900	-2.4146	+1.0726	0.9368	0.0602	0.0205	:
59	31.6	-2.6290	-2.4147	+1.0887	0.9509	0.0462	0.0158	:
60	32.2	-2.6240	-2.4146	+1.0867	0.9491	0.0479	0.0163	:

DATA FOR SCAN H2

STEP	(mm)	DIRECT	SPLIT	RATIO	REFL	MASS	b	
-60	-32.2	-2.5430	-2.4145	+1.0532	0.9198	0.0772	0.0263	:*
-59	-31.6	-2.5360	-2.4145	+1.0503	0.9173	0.0797	0.0272	:*
-58	-31.1	-2.6160	-2.4146	+1.0834	0.9462	0.0508	0.0173	:
-57	-30.6	-2.6320	-2.4145	+1.0901	0.9520	0.0452	0.0154	:
-56	-30.0	-2.5670	-2.4145	+1.0632	0.9285	0.0685	0.0234	:
-55	-29.5	-2.6290	-2.4146	+1.0888	0.9509	0.0462	0.0158	:
-54	-29.0	-2.6180	-2.4145	+1.0843	0.9470	0.0500	0.0171	:
-53	-28.4	-2.5610	-2.4146	+1.0606	0.9263	0.0707	0.0241	:
-52	-27.9	-2.5920	-2.4145	+1.0735	0.9376	0.0594	0.0203	:
-51	-27.3	-2.5210	-2.4145	+1.0441	0.9119	0.0851	0.0290	:*
-50	-26.8	-2.5190	-2.4146	+1.0432	0.9111	0.0859	0.0293	:*
-49	-26.3	-2.5380	-2.4146	+1.0511	0.9180	0.0790	0.0270	:*
-48	-25.7	-2.5010	-2.4146	+1.0358	0.9046	0.0924	0.0315	:*
-47	-25.2	-2.5390	-2.4146	+1.0515	0.9184	0.0786	0.0268	:*
-46	-24.7	-2.5760	-2.4148	+1.0668	0.9317	0.0653	0.0223	:
-45	-24.1	-2.5200	-2.4148	+1.0436	0.9114	0.0856	0.0292	:*
-44	-23.6	-2.4680	-2.4149	+1.0220	0.8926	0.1052	0.0359	:*
-43	-23.1	-2.4890	-2.4149	+1.0307	0.9002	0.0968	0.0330	:*
-42	-22.5	-2.4160	-2.4150	+1.0004	0.8737	0.1249	0.0426	:*
-41	-22.0	-2.4590	-2.4150	+1.0182	0.8893	0.1087	0.0371	:*
-40	-21.5	-2.5200	-2.4151	+1.0434	0.9113	0.0857	0.0292	:*
-39	-20.9	-2.4240	-2.4150	+1.0037	0.8766	0.1217	0.0415	:*
-38	-20.4	-2.2810	-2.4151	+0.9445	0.8249	0.1782	0.0608	:*
-37	-19.8	-2.3230	-2.4151	+0.9619	0.8401	0.1609	0.0549	:*
-36	-19.3	-2.3460	-2.4151	+0.9714	0.8484	0.1518	0.0518	:*

FIGURE C.2

TYPICAL OUTPUT OF AUTOMATED DATA REDUCTION SYSTEM (PAGE 3 OF 9).

-35	-18.8	-2.3470	-2.4152	+0.9718	0.8487	0.1514	0.0517
-34	-18.2	-2.2690	-2.4153	+0.9394	0.8205	0.1834	0.0626
-33	-17.7	-2.4070	-2.4152	+0.9966	0.8704	0.1286	0.0439
-32	-17.2	-2.2620	-2.4154	+0.9365	0.8179	0.1863	0.0636
-31	-16.6	-2.3320	-2.4154	+0.9655	0.8432	0.1575	0.0537
-30	-16.1	-2.1780	-2.4154	+0.9017	0.7875	0.2220	0.0758
-29	-15.6	-2.2220	-2.4155	+0.9199	0.8034	0.2029	0.0693
-28	-15.0	-2.1560	-2.4156	+0.8925	0.7795	0.2316	0.0790
-27	-14.5	-2.0660	-2.4155	+0.8553	0.7470	0.2719	0.0928
-26	-13.9	-2.0240	-2.4157	+0.8379	0.7317	0.2917	0.0996
-25	-13.4	-1.9480	-2.4157	+0.8064	0.7043	0.3290	0.1123
-24	-12.9	-1.9680	-2.4158	+0.8146	0.7115	0.3189	0.1088
-23	-12.3	-1.8770	-2.4159	+0.7769	0.6785	0.3660	0.1249
-22	-11.8	-1.9390	-2.4158	+0.8026	0.7010	0.3336	0.1139
-21	-11.3	-1.8400	-2.4158	+0.7617	0.6652	0.3857	0.1316
-20	-10.7	-1.8260	-2.4159	+0.7558	0.6601	0.3938	0.1344
-19	-10.2	-1.6890	-2.4160	+0.6991	0.6106	0.4741	0.1618
-18	-9.7	-1.6310	-2.4161	+0.6751	0.5896	0.5118	0.1747
-17	-9.1	-1.6330	-2.4161	+0.6759	0.5903	0.5105	0.1742
-16	-8.6	-1.5820	-2.4162	+0.6547	0.5718	0.5455	0.1862
-15	-8.0	-1.5720	-2.4162	+0.6506	0.5682	0.5526	0.1886
-14	-7.5	-1.4880	-2.4162	+0.6158	0.5379	0.6167	0.2105
-13	-7.0	-1.2780	-2.4162	+0.5289	0.4619	0.8206	0.2800
-12	-6.4	-1.2420	-2.4162	+0.5140	0.4489	0.8660	0.2956
-11	-5.9	-1.2510	-2.4162	+0.5178	0.4522	0.8543	0.2916
-10	-5.4	-1.2420	-2.4161	+0.5141	0.4490	0.8660	0.2955
-9	-4.8	-1.1780	-2.4162	+0.4875	0.4258	0.9617	0.3282
-8	-4.3	-1.1630	-2.4163	+0.4813	0.4204	0.9873	0.3369
-7	-3.8	-1.1390	-2.4162	+0.4714	0.4117	1.0330	0.3525
-6	-3.2	-1.1200	-2.4163	+0.4635	0.4048	1.0736	0.3664
-5	-2.7	-1.0380	-2.4164	+0.4296	0.3752	1.3338	0.4552
-4	-2.1	-1.0530	-2.4164	+0.4358	0.3806	1.2655	0.4319
-3	-1.6	-1.0620	-2.4164	+0.4395	0.3838	1.2349	0.4214
-2	-1.1	-1.0650	-2.4165	+0.4407	0.3849	1.2249	0.4180
-1	-0.5	-1.0520	-2.4166	+0.4353	0.3802	1.2692	0.4331
0	0.0	-1.0360	-2.4166	+0.4287	0.3744	1.3436	0.4585
1	0.5	-0.9570	-2.4166	+0.3960	0.3459	1.8445	0.6295
2	1.1	-0.9000	-2.4167	+0.3724	0.3252	2.1824	0.7448
3	1.6	-0.9730	-2.4167	+0.4026	0.3516	1.7441	0.5952
4	2.1	-0.9610	-2.4167	+0.3976	0.3473	1.8205	0.6213
5	2.7	-0.9600	-2.4167	+0.3972	0.3469	1.8266	0.6234
6	3.2	-0.9840	-2.4167	+0.4072	0.3556	1.6685	0.5694
7	3.8	-0.9840	-2.4167	+0.4072	0.3556	1.6685	0.5694
8	4.3	-0.9920	-2.4168	+0.4105	0.3585	1.6139	0.5508
9	4.8	-1.0390	-2.4169	+0.4299	0.3754	1.3302	0.4539
10	5.4	-1.0170	-2.4169	+0.4208	0.3675	1.4470	0.4938
11	5.9	-1.0550	-2.4169	+0.4365	0.3812	1.2594	0.4298
12	6.4	-1.1000	-2.4170	+0.4551	0.3975	1.1217	0.3828
13	7.0	-1.1510	-2.4170	+0.4762	0.4159	1.0107	0.3449
14	7.5	-1.2080	-2.4170	+0.4998	0.4365	0.9147	0.3122
15	8.0	-1.2940	-2.4171	+0.5354	0.4676	0.8021	0.2737
16	8.6	-1.3490	-2.4172	+0.5581	0.4874	0.7423	0.2533
17	9.1	-1.3550	-2.4171	+0.5606	0.4896	0.7361	0.2512
18	9.7	-1.4050	-2.4172	+0.5813	0.5076	0.6881	0.2348
19	10.2	-1.4690	-2.4172	+0.6077	0.5308	0.6323	0.2158
20	10.7	-1.5840	-2.4173	+0.6553	0.5723	0.5446	0.1859
21	11.3	-1.6390	-2.4173	+0.6780	0.5922	0.5071	0.1731
22	11.8	-1.6620	-2.4173	+0.6875	0.6005	0.4921	0.1680

FIGURE C.2

TYPICAL OUTPUT OF AUTOMATED DATA REDUCTION SYSTEM (PAGE 4 OF 9).

23	12.3	-1.6950	-2.4172	+0.7012	0.6124	0.4709	0.1607	: * :
24	12.9	-1.7490	-2.4173	+0.7235	0.6319	0.4379	0.1495	: * :
25	13.4	-1.8870	-2.4173	+0.7806	0.6818	0.3613	0.1233	: * :
26	13.9	-1.9600	-2.4173	+0.8108	0.7081	0.3236	0.1104	: * :
27	14.5	-1.9640	-2.4173	+0.8125	0.7096	0.3216	0.1097	: * :
28	15.0	-2.0320	-2.4174	+0.8406	0.7341	0.2886	0.0985	: * :
29	15.6	-2.0220	-2.4173	+0.8365	0.7305	0.2933	0.1001	: * :
30	16.1	-1.9900	-2.4174	+0.8232	0.7190	0.3085	0.1053	: * :
31	16.6	-2.1430	-2.4175	+0.8865	0.7742	0.2380	0.0812	: * :
32	17.2	-2.2090	-2.4176	+0.9137	0.7980	0.2094	0.0715	:* :
33	17.7	-2.1920	-2.4176	+0.9067	0.7919	0.2168	0.0740	:* :
34	18.2	-2.2520	-2.4176	+0.9315	0.8135	0.1911	0.0652	:* :
35	18.8	-2.2280	-2.4177	+0.9215	0.8048	0.2012	0.0687	:* :
36	19.3	-2.3130	-2.4178	+0.9567	0.8355	0.1659	0.0566	:* :
37	19.8	-2.3270	-2.4177	+0.9625	0.8406	0.1603	0.0547	:* :
38	20.4	-2.3300	-2.4177	+0.9637	0.8417	0.1591	0.0543	:* :
39	20.9	-2.4110	-2.4177	+0.9972	0.8709	0.1280	0.0437	:* :
40	21.5	-2.4390	-2.4178	+1.0088	0.8810	0.1170	0.0399	:* :
41	22.0	-2.5090	-2.4177	+1.0378	0.9063	0.0907	0.0309	:* :
42	22.5	-2.4720	-2.4176	+1.0225	0.8930	0.1047	0.0357	:* :
43	23.1	-2.4420	-2.4177	+1.0101	0.8821	0.1159	0.0395	:* :
44	23.6	-2.5190	-2.4177	+1.0419	0.9100	0.0870	0.0297	:* :
45	24.1	-2.5150	-2.4176	+1.0403	0.9085	0.0885	0.0302	:* :
46	24.7	-2.4550	-2.4176	+1.0155	0.8869	0.1111	0.0379	:* :
47	25.2	-2.5380	-2.4176	+1.0498	0.9169	0.0801	0.0274	:* :
48	25.7	-2.5760	-2.4177	+1.0655	0.9305	0.0665	0.0227	: :
49	26.3	-2.5400	-2.4178	+1.0505	0.9175	0.0795	0.0271	:* :
50	26.8	-2.5980	-2.4179	+1.0745	0.9384	0.0586	0.0200	: :
51	27.3	-2.5770	-2.4180	+1.0658	0.9308	0.0662	0.0226	: :
52	27.9	-2.5970	-2.4180	+1.0740	0.9380	0.0590	0.0201	: :
53	28.4	-2.6100	-2.4181	+1.0794	0.9427	0.0543	0.0185	: :
54	29.0	-2.6090	-2.4182	+1.0789	0.9423	0.0547	0.0187	: :
55	29.5	-2.5950	-2.4183	+1.0731	0.9372	0.0598	0.0204	: :
56	30.0	-2.6230	-2.4185	+1.0846	0.9472	0.0498	0.0170	: :
57	30.6	-2.5560	-2.4185	+1.0569	0.9230	0.0740	0.0252	:* :
58	31.1	-2.5690	-2.4186	+1.0622	0.9277	0.0693	0.0237	: :
59	31.6	-2.6440	-2.4186	+1.0932	0.9548	0.0427	0.0146	: :
60	32.2	-2.6590	-2.4186	+1.0994	0.9602	0.0378	0.0129	: :

DATA FOR SCAN H3

STEP	(mm)	DIRECT	SPLIT	RATIO	REFL	MASS	b	
-60	-32.2	-2.5640	-2.4178	+1.0605	0.9262	0.0708	0.0242	: :
-59	-31.6	-2.5690	-2.4183	+1.0623	0.9278	0.0692	0.0236	: :
-58	-31.1	-2.6350	-2.4180	+1.0897	0.9517	0.0454	0.0155	: :
-57	-30.6	-2.6690	-2.4181	+1.1038	0.9640	0.0340	0.0116	: :
-56	-30.0	-2.6380	-2.4180	+1.0910	0.9528	0.0445	0.0152	: :
-55	-29.5	-2.5960	-2.4179	+1.0737	0.9377	0.0593	0.0202	: :
-54	-29.0	-2.5690	-2.4180	+1.0624	0.9279	0.0691	0.0236	: :
-53	-28.4	-2.5180	-2.4180	+1.0414	0.9095	0.0875	0.0299	:* :
-52	-27.9	-2.5690	-2.4179	+1.0625	0.9279	0.0691	0.0236	: :
-51	-27.3	-2.5620	-2.4180	+1.0596	0.9254	0.0716	0.0244	: :
-50	-26.8	-2.5030	-2.4178	+1.0352	0.9041	0.0929	0.0317	:* :
-49	-26.3	-2.5200	-2.4179	+1.0422	0.9102	0.0868	0.0296	:* :
-48	-25.7	-2.4580	-2.4178	+1.0166	0.8879	0.1101	0.0376	:* :
-47	-25.2	-2.4410	-2.4177	+1.0096	0.8818	0.1162	0.0397	:* :
-46	-24.7	-2.5180	-2.4177	+1.0415	0.9096	0.0874	0.0298	:* :

FIGURE C.2

TYPICAL OUTPUT OF AUTOMATED DATA REDUCTION SYSTEM (PAGE 5 OF 9).

RUN ID : 092685-4-015-0B NACA 652015 PAGE 6

-45	-24.1	-2.5100	-2.4175	+1.0383	0.9068	0.0902	0.0308
-44	-23.6	-2.5630	-2.4176	+1.0601	0.9259	0.0711	0.0243
-43	-23.1	-2.5490	-2.4175	+1.0544	0.9209	0.0761	0.0260
-42	-22.5	-2.4950	-2.4175	+1.0321	0.9014	0.0956	0.0326
-41	-22.0	-2.4570	-2.4176	+1.0163	0.8876	0.1104	0.0377
-40	-21.5	-2.4480	-2.4176	+1.0126	0.8843	0.1137	0.0388
-39	-20.9	-2.4500	-2.4175	+1.0134	0.8851	0.1129	0.0385
-38	-20.4	-2.4370	-2.4178	+1.0079	0.8803	0.1177	0.0402
-37	-19.8	-2.5230	-2.4184	+1.0433	0.9111	0.0859	0.0293
-36	-19.3	-2.4630	-2.4185	+1.0184	0.8894	0.1086	0.0371
-35	-18.8	-2.4290	-2.4184	+1.0044	0.8772	0.1211	0.0413
-34	-18.2	-2.3940	-2.4181	+0.9900	0.8647	0.1349	0.0460
-33	-17.7	-2.4450	-2.4181	+1.0111	0.8831	0.1149	0.0392
-32	-17.2	-2.3740	-2.4180	+0.9818	0.8575	0.1425	0.0486
-31	-16.6	-2.3270	-2.4180	+0.9624	0.8405	0.1605	0.0548
-30	-16.1	-2.2960	-2.4181	+0.9495	0.8293	0.1729	0.0590
-29	-15.6	-2.1950	-2.4182	+0.9077	0.7928	0.2157	0.0736
-28	-15.0	-2.1850	-2.4183	+0.9035	0.7891	0.2201	0.0751
-27	-14.5	-2.1500	-2.4183	+0.8891	0.7765	0.2352	0.0803
-26	-13.9	-2.0710	-2.4183	+0.8564	0.7479	0.2707	0.0924
-25	-13.4	-2.0760	-2.4180	+0.8586	0.7498	0.2682	0.0915
-24	-12.9	-1.9040	-2.4178	+0.7875	0.6878	0.3524	0.1202
-23	-12.3	-1.9380	-2.4168	+0.8019	0.7003	0.3345	0.1142
-22	-11.8	-1.8620	-2.4168	+0.7704	0.6729	0.3740	0.1276
-21	-11.3	-1.8740	-2.4168	+0.7754	0.6772	0.3679	0.1256
-20	-10.7	-1.8460	-2.4168	+0.7638	0.6671	0.3827	0.1306
-19	-10.2	-1.9330	-2.4168	+0.7998	0.6985	0.3371	0.1150
-18	-9.7	-1.7800	-2.4168	+0.7365	0.6432	0.4198	0.1433
-17	-9.1	-1.6220	-2.4169	+0.6711	0.5861	0.5184	0.1769
-16	-8.6	-1.4550	-2.4168	+0.6020	0.5258	0.6437	0.2197
-15	-8.0	-1.3700	-2.4168	+0.5669	0.4951	0.7213	0.2462
-14	-7.5	-1.4000	-2.4168	+0.5793	0.5059	0.6926	0.2364
-13	-7.0	-1.3530	-2.4169	+0.5598	0.4889	0.7380	0.2519
-12	-6.4	-1.2540	-2.4167	+0.5189	0.4532	0.8509	0.2904
-11	-5.9	-1.2510	-2.4166	+0.5177	0.4521	0.8546	0.2917
-10	-5.4	-1.2530	-2.4166	+0.5185	0.4528	0.8521	0.2908
-9	-4.8	-1.1980	-2.4168	+0.4957	0.4329	0.9297	0.3173
-8	-4.3	-1.1770	-2.4169	+0.4870	0.4253	0.9640	0.3290
-7	-3.8	-1.1180	-2.4168	+0.4626	0.4040	1.0785	0.3681
-6	-3.2	-1.0620	-2.4168	+0.4394	0.3838	1.2355	0.4216
-5	-2.7	-1.0340	-2.4168	+0.4278	0.3737	1.3534	0.4619
-4	-2.1	-1.0410	-2.4167	+0.4308	0.3762	1.3204	0.4506
-3	-1.6	-1.0030	-2.4167	+0.4150	0.3625	1.5395	0.5254
-2	-1.1	-1.0170	-2.4166	+0.4208	0.3675	1.4462	0.4935
-1	-0.5	-1.0280	-2.4167	+0.4254	0.3715	1.3814	0.4714
0	0.0	-1.0000	-2.4166	+0.4138	0.3614	1.5592	0.5321
1	0.5	-0.9290	-2.4167	+0.3844	0.3357	2.0118	0.6866
2	1.1	-0.9350	-2.4167	+0.3869	0.3379	1.9769	0.6746
3	1.6	-0.9490	-2.4167	+0.3927	0.3430	1.8933	0.6461
4	2.1	-1.0270	-2.4166	+0.4250	0.3712	1.3859	0.4730
5	2.7	-0.9530	-2.4167	+0.3943	0.3444	1.8691	0.6379
6	3.2	-0.9230	-2.4169	+0.3819	0.3335	2.0471	0.6986
7	3.8	-0.9760	-2.4170	+0.4038	0.3527	1.7243	0.5884
8	4.3	-1.0010	-2.4170	+0.4141	0.3617	1.5537	0.5302
9	4.8	-1.0230	-2.4169	+0.4233	0.3697	1.4071	0.4802
10	5.4	-1.0340	-2.4170	+0.4278	0.3736	1.3538	0.4620
11	5.9	-1.0870	-2.4169	+0.4497	0.3928	1.1563	0.3946
12	6.4	-1.1220	-2.4169	+0.4642	0.4054	1.0698	0.3651

FIGURE C.2

TYPICAL OUTPUT OF AUTOMATED DATA REDUCTION SYSTEM (PAGE 6 OF 9).

RUN ID : 092685-4-015-0B NACA 652015 PAGE 7

13	7.0	-1.1820	-2.4170	+0.4890	0.4271	0.9556	0.3261	: * :
14	7.5	-1.2220	-2.4170	+0.5056	0.4416	0.8941	0.3051	: * :
15	8.0	-1.3530	-2.4170	+0.5598	0.4889	0.7381	0.2519	: * :
16	8.6	-1.3320	-2.4170	+0.5511	0.4813	0.7593	0.2591	: * :
17	9.1	-1.3940	-2.4169	+0.5768	0.5037	0.6983	0.2383	: * :
18	9.7	-1.4670	-2.4169	+0.6070	0.5301	0.6338	0.2163	: * :
19	10.2	-1.5760	-2.4169	+0.6521	0.5695	0.5500	0.1877	: * :
20	10.7	-1.6030	-2.4170	+0.6632	0.5792	0.5315	0.1814	: * :
21	11.3	-1.6490	-2.4171	+0.6822	0.5958	0.5005	0.1708	: * :
22	11.8	-1.7420	-2.4170	+0.7207	0.6295	0.4419	0.1508	: * :
23	12.3	-1.8810	-2.4172	+0.7782	0.6796	0.3645	0.1244	: * :
24	12.9	-1.8970	-2.4171	+0.7848	0.6854	0.3558	0.1214	: * :
25	13.4	-1.8320	-2.4171	+0.7579	0.6620	0.3909	0.1334	: * :
26	13.9	-1.9740	-2.4172	+0.8166	0.7132	0.3165	0.1080	: * :
27	14.5	-2.0600	-2.4170	+0.8523	0.7444	0.2753	0.0940	: * :
28	15.0	-2.0220	-2.4170	+0.8366	0.7306	0.2932	0.1001	: * :
29	15.6	-2.0470	-2.4170	+0.8469	0.7397	0.2814	0.0960	: * :
30	16.1	-2.0950	-2.4170	+0.8668	0.7570	0.2596	0.0886	: * :
31	16.6	-2.2170	-2.4169	+0.9173	0.8011	0.2056	0.0702	:* :
32	17.2	-2.1740	-2.4170	+0.8995	0.7856	0.2243	0.0766	: * :
33	17.7	-2.1900	-2.4170	+0.9061	0.7913	0.2174	0.0742	:* :
34	18.2	-2.1670	-2.4169	+0.8966	0.7831	0.2273	0.0776	: * :
35	18.8	-2.3200	-2.4169	+0.9599	0.8383	0.1628	0.0556	:* :
36	19.3	-2.3150	-2.4169	+0.9578	0.8365	0.1648	0.0562	:* :
37	19.8	-2.3390	-2.4172	+0.9676	0.8451	0.1554	0.0530	:* :
38	20.4	-2.3280	-2.4173	+0.9631	0.8411	0.1598	0.0545	:* :
39	20.9	-2.4160	-2.4176	+0.9993	0.8728	0.1259	0.0430	:* :
40	21.5	-2.4410	-2.4177	+1.0096	0.8818	0.1162	0.0397	:* :
41	22.0	-2.4500	-2.4178	+1.0133	0.8850	0.1130	0.0386	:* :
42	22.5	-2.4220	-2.4179	+1.0017	0.8748	0.1237	0.0422	:* :
43	23.1	-2.4080	-2.4180	+0.9959	0.8698	0.1293	0.0441	:* :
44	23.6	-2.4430	-2.4178	+1.0104	0.8825	0.1155	0.0394	:* :
45	24.1	-2.5160	-2.4176	+1.0407	0.9089	0.0881	0.0301	:* :
46	24.7	-2.5310	-2.4175	+1.0469	0.9144	0.0826	0.0282	:* :
47	25.2	-2.5530	-2.4174	+1.0561	0.9224	0.0746	0.0255	:* :
48	25.7	-2.5320	-2.4173	+1.0474	0.9148	0.0822	0.0281	:* :
49	26.3	-2.5300	-2.4173	+1.0466	0.9141	0.0829	0.0283	:* :
50	26.8	-2.5510	-2.4172	+1.0554	0.9217	0.0753	0.0257	:* :
51	27.3	-2.5650	-2.4171	+1.0612	0.9268	0.0702	0.0240	: :
52	27.9	-2.5720	-2.4170	+1.0641	0.9294	0.0676	0.0231	: :
53	28.4	-2.6060	-2.4169	+1.0782	0.9417	0.0553	0.0189	: :
54	29.0	-2.5700	-2.4168	+1.0634	0.9287	0.0683	0.0233	: :
55	29.5	-2.5850	-2.4167	+1.0696	0.9342	0.0628	0.0214	: :
56	30.0	-2.6060	-2.4166	+1.0784	0.9418	0.0552	0.0188	: :
57	30.6	-2.5860	-2.4166	+1.0701	0.9346	0.0624	0.0213	: :
58	31.1	-2.5840	-2.4167	+1.0692	0.9338	0.0632	0.0216	: :
59	31.6	-2.5850	-2.4166	+1.0697	0.9342	0.0628	0.0214	: :
60	32.2	-2.5970	-2.4165	+1.0747	0.9386	0.0584	0.0199	: :

AVERAGE OF ALL SCANS

STEP	(mm)	DIRECT	SPLIT	RATIO	REFL	MASS	b	
-60	-32.2			+1.0626	0.9280	0.0690	0.0235	: :
-59	-31.6			+1.0582	0.9242	0.0728	0.0249	: :
-58	-31.1			+1.0802	0.9434	0.0536	0.0183	: :
-57	-30.6			+1.0850	0.9476	0.0494	0.0168	: :
-56	-30.0			+1.0733	0.9374	0.0596	0.0203	: :

FIGURE C.2

TYPICAL OUTPUT OF AUTOMATED DATA REDUCTION SYSTEM (PAGE 7 OF 9).

RUN ID : 092685-4-015-0B NACA 652015 PAGE 8

-55	-29.5	+1.0808	0.9440	0.0530	0.0181	:
-54	-29.0	+1.0754	0.9392	0.0578	0.0197	:
-53	-28.4	+1.0630	0.9284	0.0686	0.0234	:
-52	-27.9	+1.0651	0.9303	0.0667	0.0228	:
-51	-27.3	+1.0509	0.9179	0.0791	0.0270	:*
-50	-26.8	+1.0408	0.9090	0.0880	0.0300	:*
-49	-26.3	+1.0347	0.9037	0.0933	0.0318	:*
-48	-25.7	+1.0171	0.8883	0.1097	0.0374	:*
-47	-25.2	+1.0278	0.8977	0.0996	0.0340	:*
-46	-24.7	+1.0440	0.9118	0.0852	0.0291	:*
-45	-24.1	+1.0399	0.9082	0.0888	0.0303	:*
-44	-23.6	+1.0429	0.9108	0.0862	0.0294	:*
-43	-23.1	+1.0377	0.9063	0.0907	0.0310	:*
-42	-22.5	+1.0112	0.8831	0.1149	0.0392	:*
-41	-22.0	+1.0097	0.8818	0.1162	0.0396	:*
-40	-21.5	+1.0205	0.8912	0.1066	0.0364	:*
-39	-20.9	+1.0069	0.8794	0.1187	0.0405	:*
-38	-20.4	+0.9763	0.8527	0.1473	0.0503	:*
-37	-19.8	+1.0002	0.8735	0.1251	0.0427	:*
-36	-19.3	+0.9971	0.8708	0.1281	0.0437	:*
-35	-18.8	+0.9847	0.8600	0.1400	0.0478	:*
-34	-18.2	+0.9676	0.8451	0.1554	0.0530	:*
-33	-17.7	+0.9927	0.8670	0.1323	0.0451	:*
-32	-17.2	+0.9532	0.8325	0.1692	0.0578	:*
-31	-16.6	+0.9499	0.8296	0.1725	0.0589	:*
-30	-16.1	+0.9097	0.7945	0.2136	0.0729	:*
-29	-15.6	+0.9093	0.7942	0.2140	0.0730	:*
-28	-15.0	+0.9024	0.7882	0.2212	0.0755	: *
-27	-14.5	+0.8606	0.7517	0.2660	0.0908	: *
-26	-13.9	+0.8486	0.7412	0.2795	0.0954	: *
-25	-13.4	+0.8273	0.7225	0.3037	0.1037	: *
-24	-12.9	+0.8019	0.7003	0.3345	0.1142	: *
-23	-12.3	+0.7809	0.6820	0.3609	0.1232	: *
-22	-11.8	+0.7678	0.6706	0.3772	0.1287	: *
-21	-11.3	+0.7552	0.6596	0.3946	0.1347	: *
-20	-10.7	+0.7462	0.6517	0.4064	0.1387	: *
-19	-10.2	+0.7200	0.6288	0.4430	0.1512	: *
-18	-9.7	+0.6877	0.6006	0.4919	0.1679	: *
-17	-9.1	+0.6637	0.5796	0.5307	0.1811	: *
-16	-8.6	+0.6256	0.5464	0.5979	0.2041	: *
-15	-8.0	+0.6110	0.5336	0.6260	0.2136	: *
-14	-7.5	+0.5972	0.5216	0.6534	0.2230	: *
-13	-7.0	+0.5467	0.4775	0.7708	0.2631	: *
-12	-6.4	+0.5210	0.4550	0.8446	0.2882	: *
-11	-5.9	+0.5182	0.4526	0.8530	0.2911	: *
-10	-5.4	+0.5161	0.4508	0.8593	0.2932	: *
-9	-4.8	+0.5007	0.4373	0.9114	0.3110	: *
-8	-4.3	+0.4854	0.4239	0.9706	0.3312	: *
-7	-3.8	+0.4695	0.4101	1.0416	0.3555	: *
-6	-3.2	+0.4549	0.3973	1.1230	0.3833	: *
-5	-2.7	+0.4345	0.3795	1.2781	0.4362	: *
-4	-2.1	+0.4364	0.3811	1.2602	0.4301	: *
-3	-1.6	+0.4290	0.3746	1.3407	0.4575	: *
-2	-1.1	+0.4277	0.3736	1.3548	0.4623	: *
-1	-0.5	+0.4219	0.3685	1.4289	0.4876	: *
0	0.0	+0.4062	0.3548	1.6847	0.5750	: *
1	0.5	+0.3921	0.3425	1.9016	0.6490	: *
2	1.1	+0.3892	0.3399	1.9441	0.6635	: *

FIGURE C.2

TYPICAL OUTPUT OF AUTOMATED DATA REDUCTION SYSTEM (PAGE 8 OF 9).

3	1.6	+0.3979	0.3475	1.8167	0.6200	: * :
4	2.1	+0.4114	0.3593	1.5978	0.5453	: * :
5	2.7	+0.4000	0.3493	1.7865	0.6097	: * :
6	3.2	+0.3932	0.3434	1.8859	0.6436	: * :
7	3.8	+0.4122	0.3600	1.5845	0.5407	: * :
8	4.3	+0.4180	0.3651	1.4914	0.5090	: * :
9	4.8	+0.4292	0.3748	1.3381	0.4567	: * :
10	5.4	+0.4266	0.3725	1.3680	0.4669	: * :
11	5.9	+0.4419	0.3859	1.2155	0.4148	: * :
12	6.4	+0.4593	0.4011	1.0963	0.3741	: * :
13	7.0	+0.4805	0.4196	0.9910	0.3382	: * :
14	7.5	+0.5012	0.4377	0.9097	0.3104	: * :
15	8.0	+0.5322	0.4648	0.8112	0.2768	: * :
16	8.6	+0.5472	0.4779	0.7694	0.2626	: * :
17	9.1	+0.5577	0.4871	0.7431	0.2536	: * :
18	9.7	+0.5802	0.5067	0.6905	0.2357	: * :
19	10.2	+0.6118	0.5343	0.6246	0.2131	: * :
20	10.7	+0.6445	0.5628	0.5633	0.1922	: * :
21	11.3	+0.6600	0.5764	0.5368	0.1832	: * :
22	11.8	+0.6873	0.6003	0.4925	0.1681	: * :
23	12.3	+0.7199	0.6287	0.4432	0.1512	: * :
24	12.9	+0.7472	0.6526	0.4051	0.1383	: * :
25	13.4	+0.7580	0.6620	0.3908	0.1334	: * :
26	13.9	+0.7996	0.6984	0.3373	0.1151	: * :
27	14.5	+0.8213	0.7173	0.3108	0.1061	: * :
28	15.0	+0.8274	0.7226	0.3036	0.1036	: * :
29	15.6	+0.8386	0.7324	0.2909	0.0993	: * :
30	16.1	+0.8434	0.7366	0.2855	0.0974	: * :
31	16.6	+0.8799	0.7685	0.2450	0.0836	: * :
32	17.2	+0.8893	0.7767	0.2350	0.0802	: * :
33	17.7	+0.9010	0.7869	0.2227	0.0760	: * :
34	18.2	+0.9143	0.7985	0.2088	0.0713	:* :
35	18.8	+0.9341	0.8158	0.1886	0.0644	:* :
36	19.3	+0.9515	0.8310	0.1709	0.0583	:* :
37	19.8	+0.9581	0.8367	0.1646	0.0562	:* :
38	20.4	+0.9605	0.8389	0.1622	0.0554	:* :
39	20.9	+0.9906	0.8651	0.1344	0.0459	:* :
40	21.5	+1.0010	0.8743	0.1243	0.0424	:* :
41	22.0	+1.0093	0.8815	0.1165	0.0398	:* :
42	22.5	+1.0103	0.8823	0.1157	0.0395	:* :
43	23.1	+0.9962	0.8700	0.1290	0.0440	:* :
44	23.6	+1.0191	0.8901	0.1079	0.0368	:* :
45	24.1	+1.0312	0.9006	0.0964	0.0329	:* :
46	24.7	+1.0290	0.8987	0.0985	0.0336	:* :
47	25.2	+1.0373	0.9059	0.0911	0.0311	:* :
48	25.7	+1.0480	0.9153	0.0817	0.0279	:* :
49	26.3	+1.0451	0.9128	0.0842	0.0287	:* :
50	26.8	+1.0613	0.9269	0.0701	0.0239	: :
51	27.3	+1.0654	0.9305	0.0665	0.0227	: :
52	27.9	+1.0694	0.9340	0.0630	0.0215	: :
53	28.4	+1.0787	0.9421	0.0549	0.0187	: :
54	29.0	+1.0712	0.9356	0.0614	0.0210	: :
55	29.5	+1.0703	0.9347	0.0623	0.0213	: :
56	30.0	+1.0778	0.9413	0.0557	0.0190	: :
57	30.6	+1.0632	0.9286	0.0684	0.0234	: :
58	31.1	+1.0680	0.9328	0.0642	0.0219	: :
59	31.6	+1.0839	0.9466	0.0504	0.0172	: :
60	32.2	+1.0869	0.9493	0.0477	0.0163	: :

FIGURE C.2

TYPICAL OUTPUT OF AUTOMATED DATA REDUCTION SYSTEM (PAGE 9 OF 9).

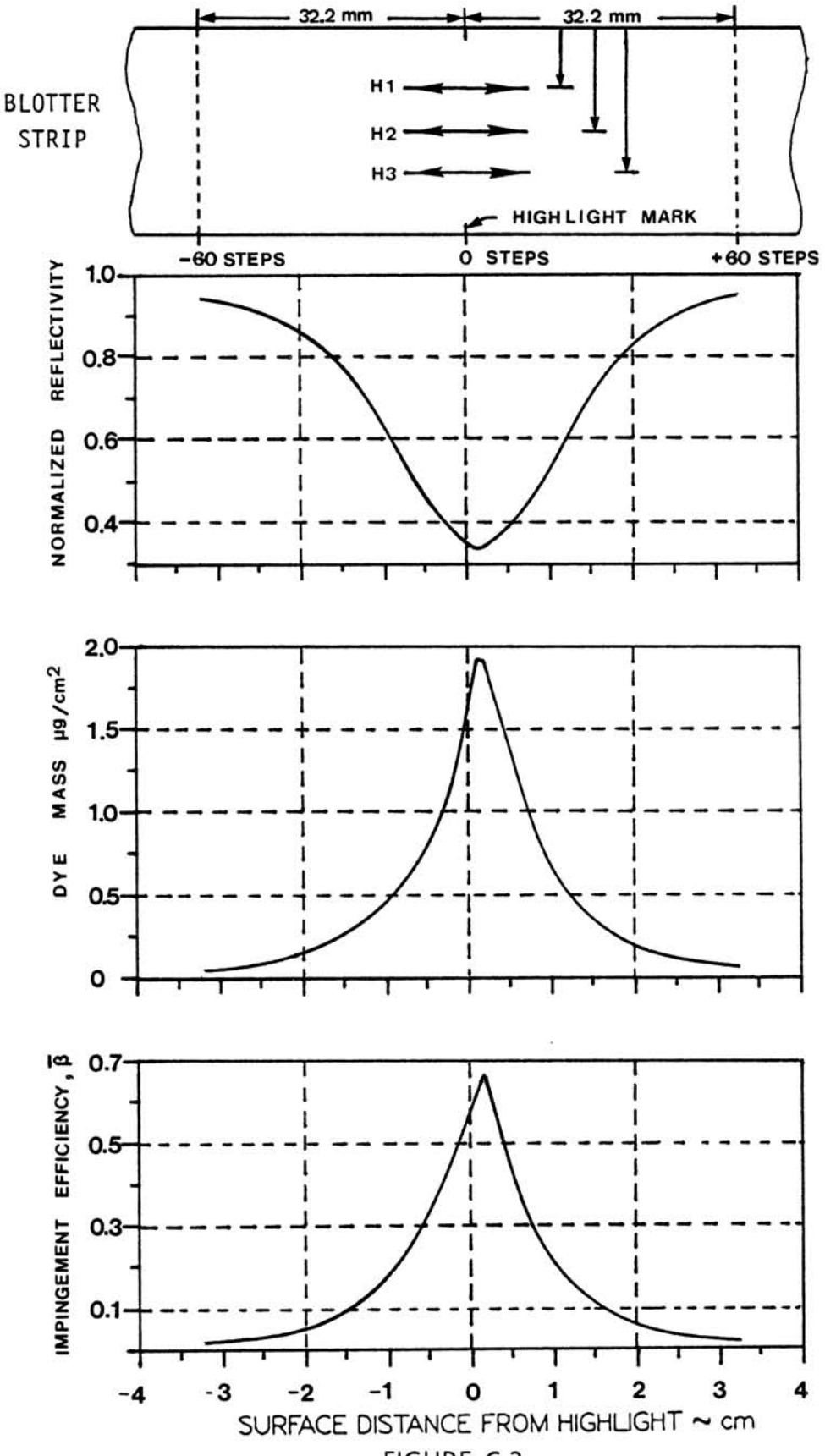

FIGURE C.3

PLOT OF AVERAGE OUTPUT DATA VS. SURFACE DISTANCE.

APPENDIX D: DERIVATION OF THE TRAJECTORY EQUATION (2-1)

The derivation below is based on that found in Reference 4.

$$dU_i/dt = C_D(R_v) \cdot R_v \cdot (V_i - U_i)/(24K) - (1-\sigma)gL\delta_{i2}/V_r^2 \qquad \text{(D-1)}$$

A vector diagram of the forces acting on the particle is shown on Figure D.1.

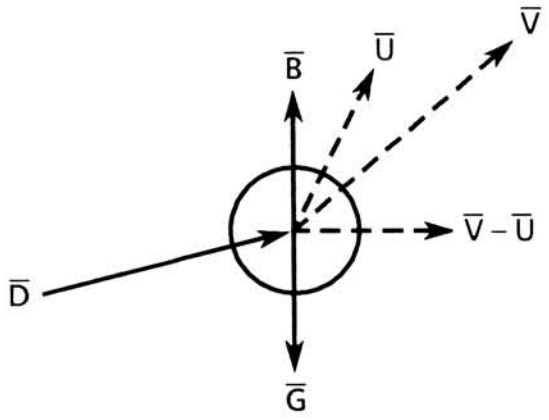

FIGURE D.1

FORCES ACTING ON PARTICLE AND VELOCITIES AT CENTER OF PARTICLE

Drag force, $\overline{D}$, is given by

$$D_i = C_D(R_v) \cdot q \cdot a \cdot \cos(i,n) \qquad \text{(D-2)}$$

where:

$R_v = \rho\,|\overline{V} - \overline{U}|\,d/\mu$,

C_D = sphere drag coefficient,

$q = \rho\,|\overline{V} - \overline{U}|^2/2$, velocity head experienced by the particle in the flow field,

$a = \pi d^2/4$, projected area of spherical particle,

$\overline{V}$ = flow velocity,

$\overline{U}$ = particle velocity,

$\cos(i,n) = (\overline{V} - \overline{U})_i/|\overline{V} - \overline{U}|$, direction cosine between the unit vectors $\bar{i}$ (parallel to i–axis) and $\bar{n}$ (parallel to $\overline{V} - \overline{U}$).

Using the definitions, (D-2) becomes

$$D_i = \frac{1}{2}\rho C_D(R_v)\cdot a\cdot|\bar{V}-\bar{U}|\cdot(\bar{V}-\bar{U})_i \qquad (D\text{-}3)$$

Buoyancy and gravity forces are

$$B_i = \rho g\tau\delta_{i2} \qquad (D\text{-}4)$$

$$G_i = -\rho_p g\tau\delta_{i2} \;;\quad \tau \equiv \pi d^3/6 \text{ , volume of spherical particle}$$

where the gravity force is assumed to act along the negative y(i=2) axis.

Summing the forces ($\Sigma F = ma$),

$$d\bar{U}_i/d\bar{t} = \frac{1}{2}\sigma C_D(R_v)\cdot(a/\tau)\cdot|\bar{V}-\bar{U}|\cdot(\bar{V}-\bar{U})_i - (1-\sigma)g\delta_{i2} \qquad (D\text{-}5)$$

Introducing the inertia parameter,

$$K \equiv \rho_p d^2 V_\infty/(18\mu L)$$

where L is the characteristic dimension of the boundary surface, the coefficient of $|\bar{V}-\bar{U}|\cdot(\bar{V}-\bar{U})_i$ term in (D-5) can be written as

$$\frac{1}{2}\sigma C_D(R_v)(a/\tau) = \rho C_D(R_v)\cdot(\pi d^2/4)\cdot(2\rho_p\pi d^3/6)^{-1}$$

$$= 3\rho C_D(R_v)\cdot(4\rho_p d)^{-1}$$

$$= \frac{3\rho C_D(R_v)}{4\left(\frac{\rho_p d^2 V_\infty}{18\mu L}\right)\left(\frac{18\mu L}{V_\infty d}\right)}$$

$$= \frac{C_D(R_v)}{24KL}\cdot\frac{\rho V_\infty d}{\mu}$$

$$= \frac{C_D(R_v)R}{24KL}$$

where $R = \rho V_\infty d/\mu$ (Reynolds number based on d).

Equation (D-5) thus becomes

$$d\bar{U}_i/d\bar{t} = \frac{C_D(R_v)\cdot R\cdot|\bar{V}-\bar{U}|\cdot(\bar{V}-\bar{U})_i}{24KL} - g(1-\sigma)\delta_{i2} \qquad \text{(D-6)}$$

Non-dimensionalizing (D-6)

$$\frac{d[\bar{U}_i/V_\infty]}{d[\bar{t}/(L/V_\infty)]} = \frac{C_D(R_v)\cdot R_v\cdot(\bar{V}_i/V_\infty - \bar{U}_i/V_\infty)}{24K} - (1-\sigma)gL\delta_{i2}/V_\infty^2$$

which is

$$dU_i/dt = \frac{C_D(R_v)\cdot R_v\cdot(V_i - U_i)}{24K} - (1-\sigma)gL\delta_{i2}/V_\infty^2$$

where $U_i = \bar{U}_i/V_\infty$, $V_i \equiv \bar{V}_i/V_\infty$ and $t = \bar{t}/(L/V_\infty)$.

APPENDIX E: DROPLET DISTRIBUTION DATA

Cloud droplet mean volumetric diameter (MVD) and distribution data are required inputs in trajectory codes. The droplet distributions and MVD's of the Icing Research Tunnel spray clouds used in these tests are presented here. These data have been provided by NASA Lewis and have been obtained from a series of single nozzle tests performed by the Air Force's Arnold Engineering Development Center (AEDC).

The droplet size and distribution test was done in a small wind tunnel with a 12 inch diameter section at a speed of 145 mph. A single NASA Lewis standard nozzle was used and measurements were performed 12 ft downstream of the nozzle, along the tunnel axis, using a laser droplet sizing instrument. Details of the laser instrumentation are given in Reference 17. Table E.1 summarizes the spray system pressures and corresponding spray cloud MVD's for the AEDC tests.

TABLE E.1

SUMMARY OF AEDC DROPLET TEST PERFORMED ON 2/28/84

P_{WATER}	P_{AIR}	SPRAY DURATION	MVD	PRESSURE RATIO
~ PSIA	~ PSIA	~ SEC	~ MICRONS	$\frac{\text{AIR} \sim \text{PSIG}}{\text{WATER} \sim \text{PSIG}}$
114.9	95	11.2	14.849	0.80
114.9	95	10.4	14.808	
114.9	85	13.2	17.211	0.70
115.2	75	12.2	20.895	0.60
115.2	75	12.1	20.968	

The raw data for the above tests are given in Figures E.1 -E.5. According to NASA (Shaw, R.J., Personal Communication, NASA, Lewis Research Center) all measurements regarding droplet size should be increased by 1/2 bin width (3.239/2 = 1.6195 microns). This correction also applies to the MVD of each of the five clouds produced.

For the trajectory tests performed during September 1985, the spray system air and water pressures used are given in Table E.2.

TABLE E.2

AIR AND WATER PRESSURES FOR TRAJECTORY TESTS

P_{WATER} ~ PSIG	P_{AIR} ~ PSIG	AIR / WATER
100	80	0.80
100	65	0.65

The droplet distribution and MVD for the 0.8 pressure ratio were calculated by taking the average distribution and average MVD of the results obtained by AEDC for two runs at the same pressure ratio. The droplet distribution and MVD for the 0.65 pressure ratio were calculated from the data provided for the 0.7 and 0.6 pressure ratios. Details of the method used to find the MVD and droplet distribution for the 0.65 pressure ratio are given later in this appendix.

The computer code used to provide the analytical data requires that the droplet distribution is given in cumulative fraction of LWC as a function of normalized droplet diameter with respect to MVD. The computer program at the end of this appendix was employed to transform the raw data into cumulative distributions. The average values of the two sets of raw data for the 0.6 and 0.8 pressure ratio are used to calculate the corresponding cumulative distributions. The program corrects all droplet diameters by 1.6195 microns as NASA suggested. The output of the program consists of tabulated cumulative distribution data for pressure ratios of 0.8, 0.7, 0.6 and 0.65 shown in Table E.3. Plots of the cumulative distributions are shown in Figures E.6 -E.9. A cumulative Langmuir "D" distribution is also shown in each figure for comparison.

To calculate the distribution and MVD for the 0.65 pressure ratio, the following procedure is used in the computer program.

Step 1: Calculate the average of the two sets of raw data provided for the 0.6 pressure ratio (Figures E.4 and E.5).

Step 2: Find the average of the distribution produced in step 1 and that provided for the 0.7 pressure ratio (Figure E.3).

Step 3: Correct the resulting distribution from step 2 by adding 3.239/2 microns to each diameter D(I) and to the MVD of

TABLE E.3

CUMULATIVE DROPLET DISTRIBUTIONS FOR 0.80, 0.70, 0.60 AND 0.65 PRESSURE RATIOS

0.80 PRESSURE RATIO		0.70 PRESSURE RATIO		0.60 PRESSURE RATIO		0 65 PRESSURE RATIO	
D(i) , MVD	CUMULATIVE % LWC	D(I) / MVD	CUMULATIVE % LWC	D(I) , MVD	CUMULATIVE % LWC	D(I) / MVD	CUMULATIVE % LWC
0 2953790	98.32819	0.2580190	98.68748	0 2154429	98.97092	0 2386062	98 82920
0.4922982	90.46082	0.4300317	92.51092	0.3590714	94.12818	0.3976770	93.31956
0 6892176	74.84180	0 6020444	80 24863	0.5027000	84.51393	0.5567479	82 38 29
0.8861369	59.37648	0.7740571	67.590421	0.6463286	74.79851	0.7158187	71.19447
1.083056	43.16064	0.9460697	53.90426	0.7899571	63.93088	0.8748895	58.91758
1.279975	29.23878	1.118082	41.46152	0.9335856	53.70710	1 033960	47.57932
1 476895	20.33694	1.290095	32.71413	1.077214	45.69329	1.193031	39.20372
1.673814	15.28073	1.462108	26.28095	1.220843	38.92984	1.352102	32.60540
1.870733	11.51724	1.634120	21.50757	1.364471	33.41702	1.511173	27.46231
2.067652	8.220558	1.806133	16.66058	1.508100	27.86952	1.670244	22.26506
2.264572	5.565914	1.978146	12.86013	1.651729	23.31952	1.829314	18.08983
2.461491	4.153376	2.150158	9.776473	1.795357	19.21533	1.988385	14.49591
2.658410	3.257207	2.322171	7.834065	1.938986	16.05081	2.147456	11.94245
2.855330	2.382298	2.494184	6.232542	2.082614	13.44551	2.306527	9.839032
3.052249	1.631782	2.666196	4.991240	2.226243	10.98659	2.465598	7.988926
3.249168	1.158577	2.838209	3.667184	2.369871	9.207335	2 624669	6.437269
3.446088	1.116045	3.010222	2.712564	2.513500	7.484468	2.783739	5.098525
3.643007	0.8158388	3.182234	1.967782	2.657128	6.440475	2.942810	4.204138
3.839926	0.5280015	3.354247	1.378164	2.800757	5.188847	3.101881	3.283514
4.036846	0.2672109	3.526260	0.8515505	2.944386	4.078660	3.260952	2.465114
4.233765	0.1201023	3.698272	0.7646593	3.088014	3.399748	3.420022	2.082213
4.430685	0.1201023	3.870285	0.6635161	3.231643	2.873332	3.579094	1.768433
4.627604	0.1201023	4.042298	0.4255998	3.375271	2.098275	3.738164	1.261947
4.824523	1.3589859E-05	4.214311	1.0401011E-05	3.518900	1.604837	3.897235	0.8024331
5.021442	1.3589859E-05	4.386323	1.0401011E-05	3.662529	1.150697	4 056306	0.5753630
5.218361	1.3589859E-05	4.558336	1.0401011E-05	3.806157	0.8686840	4.215376	0.4343565
5.415281	1.3589859E-05	4.730349	1.0401011E-05	3.949786	0.5061671	4.374448	0.2530980
5.612200	1.3589859E-05	4.902361	1.0401011E-05	4.093414	-1.0192394E-05	4.533518	9.3877316E-06
5.809119	1.3589859E-05	5.074374	1.0401011E-05	4.237043	-1.0192394E-05	4.692589	9.3877316E-06
6.006039	1.3589859E-05	5.246387	1.0401011E-05	4.380671	-1.0192394E-05	4.851660	9.3877316E-06

the distribution. At this point, a distribution for the 0.65 pressure ratio has been obtained.

Step 4: Using the distribution for the 0.65 pressure ratio calculated in step 3, the program applies linear interpolation to find the droplet diameter corresponding to 50percent LWC. This diameter is, by definition, the MVD of the distribution.

Step 5: Once the MVD has been calculated, a cumulative distribution is produced by the program. This distribution is shown in Figure E.9.

The trajectory code uses a seven drop discrete cumulative distribution. This is done by taking the values of D(I)/MVD at cumulative percent LWC values of 97.5, 90.0, 75.0, 50.0, 25.0, 10.0 and 2.5. These cumulative percent LWC values are the midpoints of the histogram values shown in Figure 2.5 and correspond to 5, 10, 20, 30, 20, 10 and 5 percent LWC.

Tables E.4 and E.5 show the discrete cumulative distributions used for the 0.8 and 0.65 pressure ratios.

TABLE E.4

DISCRETE CUMULATIVE DISTRIBUTION FOR 0.80 PRESSURE RATIO

CUMULATIVE % LWC	% LWC	D(I) / MVD FROM FIGURE E6
97.5	5	0.3161
90.0	10	0.4981
75.0	20	0.6872
50.0	30	1.0000
25.0	20	1.3737
10.0	10	1.9614
2.5	5	2.8288

MVD = 16.448 MICRONS

TABLE E.5

DISCRETE CUMULATIVE DISTRIBUTION FOR 0.65 PRESSURE RATIO

CUMULATIVE % LWC	% LWC	D(I) / MVD FROM FIGURE E6
97.5	5	0.2770
90.0	10	0.4460
75.0	20	0.6617
50.0	30	1.0000
25.0	20	1.5865
10.0	10	2.2943
2.5	5	3.2542

MVD = 20.362 MICRONS

D(I) µm	% LWC
3.239	1.687883E+000
6.478	7.942978E+000
9.717	1.576915E+001
12.956	1.511042E+001
16.195	1.623314E+001
19.434	1.368531E+001
22.673	8.070545E+000
25.912	5.336116E+000
29.151	4.012055E+000
32.390	3.269081E+000
35.629	2.735521E+000
38.868	1.371539E+000
42.107	9.612656E-001
45.346	8.653451E-001
48.585	8.537557E-001

D(I) µm	% LWC
51.824	3.736093E-001
55.063	8.506283E-002
58.302	3.879789E-001
61.541	3.327458E-001
64.780	3.821004E-001
68.019	2.942173E-001
71.258	0.000000E+000
74.497	0.000000E+000
77.736	2.401774E-001
80.975	0.000000E+000
84.214	0.000000E+000
87.453	0.000000E+000
90.692	0.000000E+000
93.931	0.000000E+000
97.170	0.000000E+000

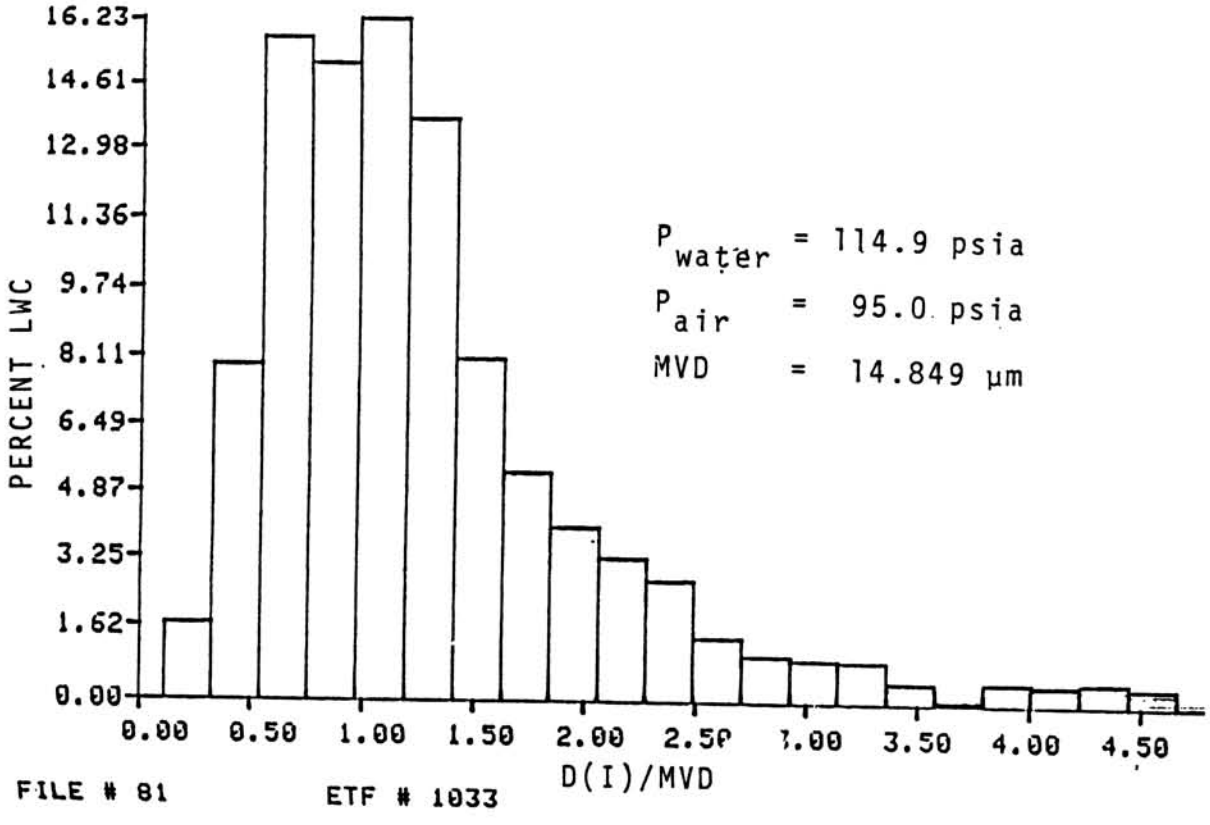

FIGURE E.1

FIRST SET OF AEDC DROPLET DISTRIBUTION DATA
FOR 0.80 PRESSURE RATIO.

D(I) µm	%-LWC
3.239	1.655746E+000
6.478	7.791748E+000
9.717	1.546891E+001
12.956	1.582021E+001
16.195	1.619854E+001
19.434	1.415841E+001
22.673	9.733140E+000
25.912	4.776305E+000
29.151	3.514914E+000
32.390	3.324291E+000
35.629	2.573768E+000
38.868	1.453536E+000
42.107	8.310727E-001
45.346	8.844719E-001

D(I) µm	%LWC
48.585	6.472778E-001
51.824	5.728009E-001
55.063	0.000000E+000
58.302	2.124339E-001
61.541	2.429289E-001
64.780	1.394807E-001
68.019	0.000000E+000
71.258	0.000000E+000
74.497	0.000000E+000
77.736	0.000000E+000
80.975	0.000000E+000
84.214	0.000000E+000
87.453	0.000000E+000
90.692	0.000000E+000

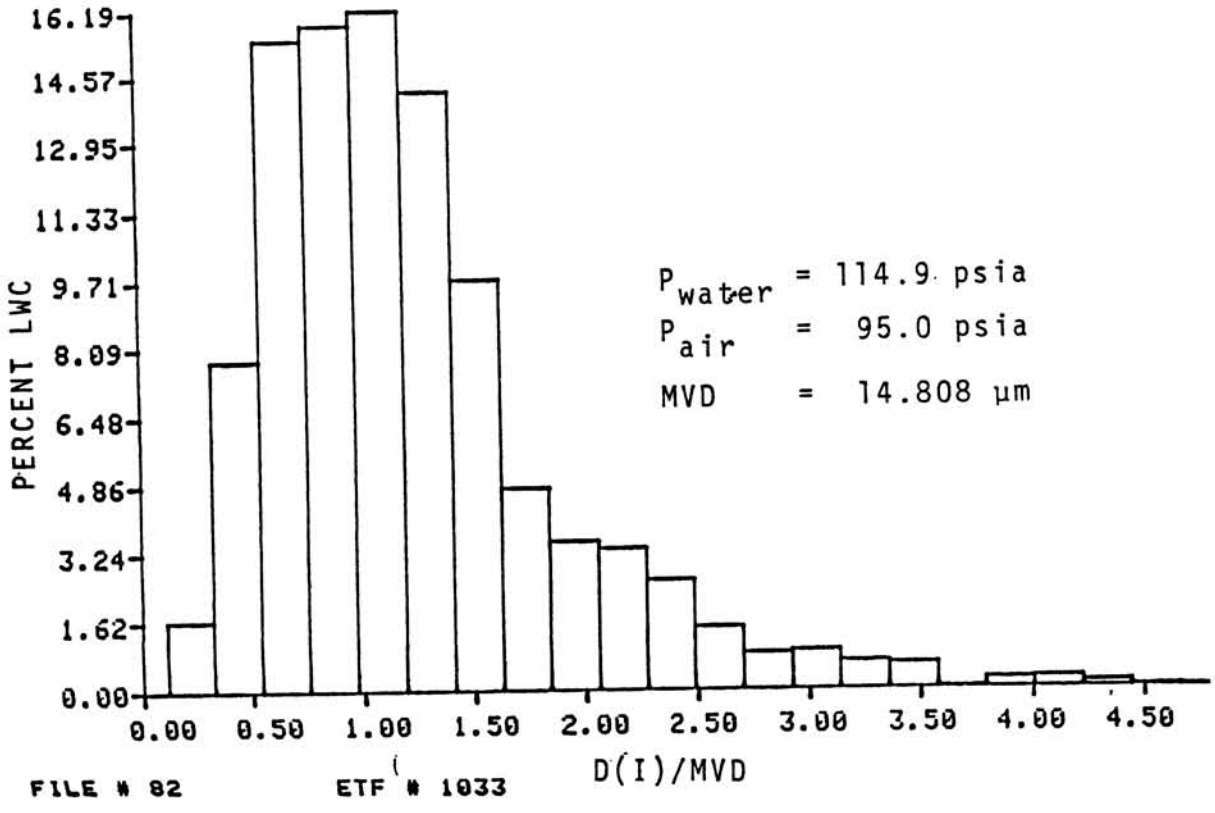

FIGURE E.2

SECOND SET OF AEDC DROPLET DISTRIBUTION DATA
FOR 0.80 PRESSURE RATIO.

D(I) µm	% LWC
3.239	1.312520E+000
6.478	6.176563E+000
9.717	1.226229E+001
12.956	1.265822E+001
16.195	1.368615E+001
19.434	1.245274E+001
22.673	8.737389E+000
25.912	6.433184E+000
29.151	4.773372E+000
32.390	4.846990E+000
35.629	3.800454E+000
38.868	3.083656E+000
42.107	1.942408E+000
45.346	1.601523E+000
48.585	1.241302E+000

D(I) µm	% LWC
51.824	1.324056E+000
55.063	9.546206E-001
58.302	7.447814E-001
61.541	5.896186E-001
64.780	5.266131E-001
68.019	8.689116E-002
71.258	1.011432E-001
74.497	2.379163E-001
77.736	4.255894E-001
80.975	0.000000E+000
84.214	0.000000E+000
87.453	0.000000E+000
90.692	0.000000E+000
93.931	0.000000E+000
97.170	0.000000E+000

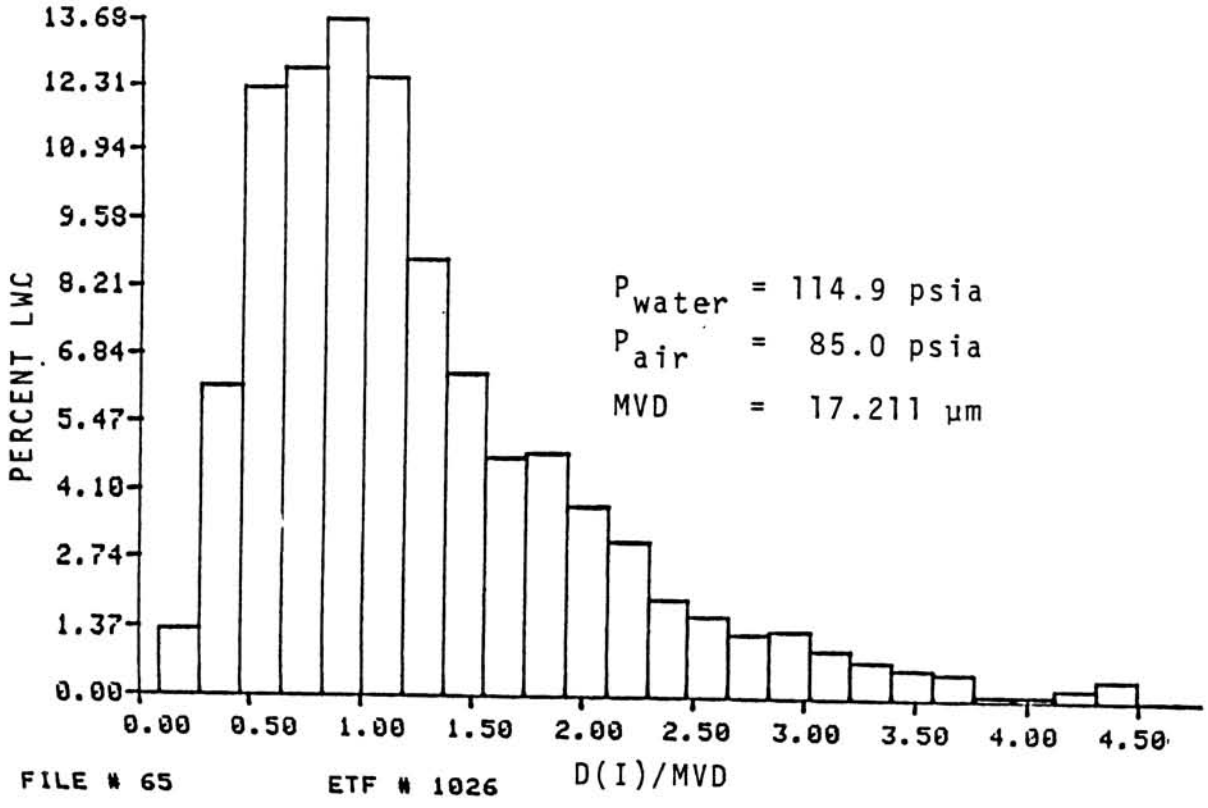

FIGURE E.3

AEDC DROPLET DISTRIBUTION DATA FOR 0.70 PRESSURE RATIO.

D(I) µm	% LWC
3.239	1.029511E+000
6.478	4.844757E+000
9.717	9.618267E+000
12.956	9.735176E+000
16.195	1.086081E+001
19.434	1.035628E+001
22.673	7.879408E+000
25.912	7.237892E+000
29.151	5.630361E+000
32.390	5.962796E+000
35.629	4.517730E+000
38.868	4.334715E+000
42.107	2.821173E+000
45.346	2.495355E+000
48.585	2.258865E+000

D(I) µm	% LWC
51.824	1.440806E+000
55.063	1.551544E+000
58.302	9.098646E-001
61.541	1.156052E+000
64.780	9.956430E-001
68.019	6.133161E-001
71.258	4.461956E-001
74.497	7.347016E-001
77.736	5.006662E-001
80.975	7.605607E-001
84.214	3.796719E-001
87.453	2.464217E-001
90.692	6.814623E-001
93.931	0.000000E+000
97.170	0.000000E+000

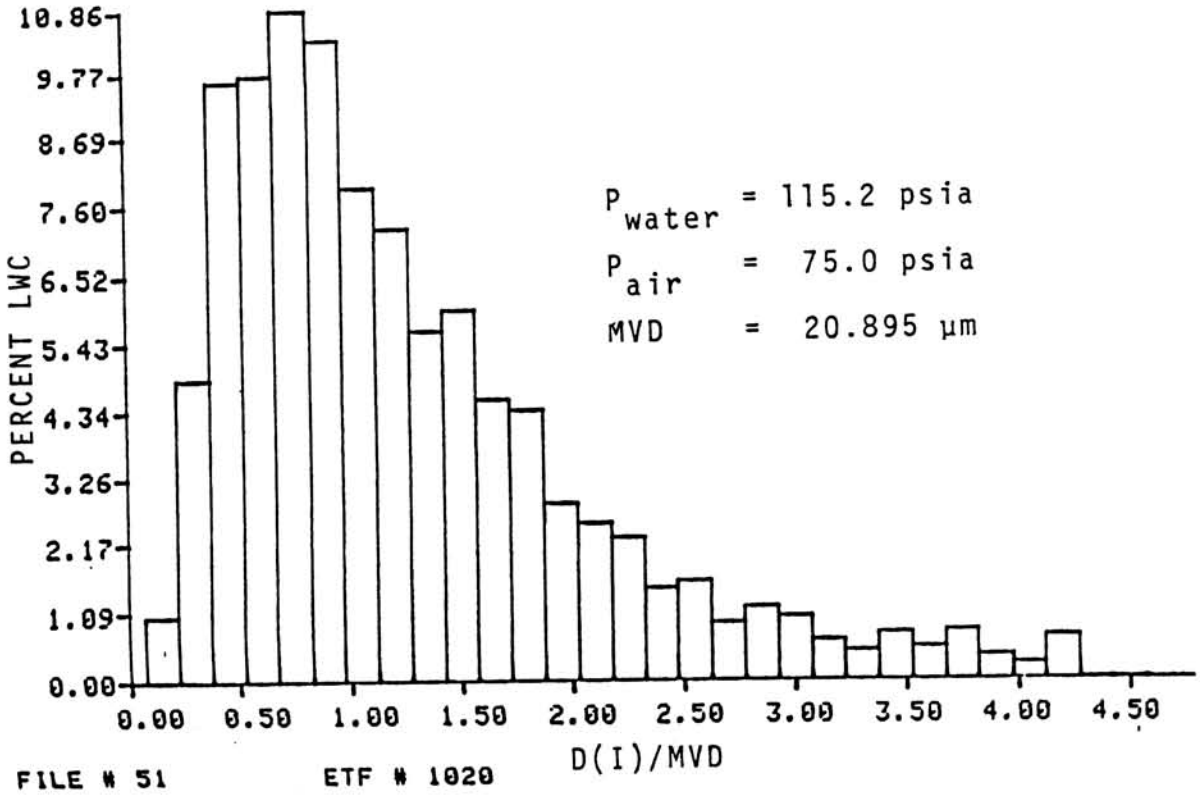

FIGURE E.4

FIRST SET OF AEDC DROPLET DISTRIBUTION DATA
FOR 0.60 PRESSURE RATIO.

D(I) µm	% LWC
3.239	1.028650E+000
6.478	4.840707E+000
9.717	9.610227E+000
12.956	9.695670E+000
16.195	1.087445E+001
19.434	1.009127E+001
22.673	8.148223E+000
25.912	6.289009E+000
29.151	5.395264E+000
32.390	5.132207E+000
35.629	4.582268E+000
38.868	3.873679E+000
42.107	3.507853E+000
45.346	2.715263E+000
48.585	2.658956E+000

D(I) µm	% LWC
51.824	2.117711E+000
55.063	1.894190E+000
58.302	1.178122E+000
61.541	1.347204E+000
64.780	1.224731E+000
68.019	7.445077E-001
71.258	6.066359E-001
74.497	8.154132E-001
77.736	4.862091E-001
80.975	1.477198E-001
84.214	1.843543E-001
87.453	4.786121E-001
90.692	3.308923E-001
93.931	0.000000E+000
97.170	0.000000E+000

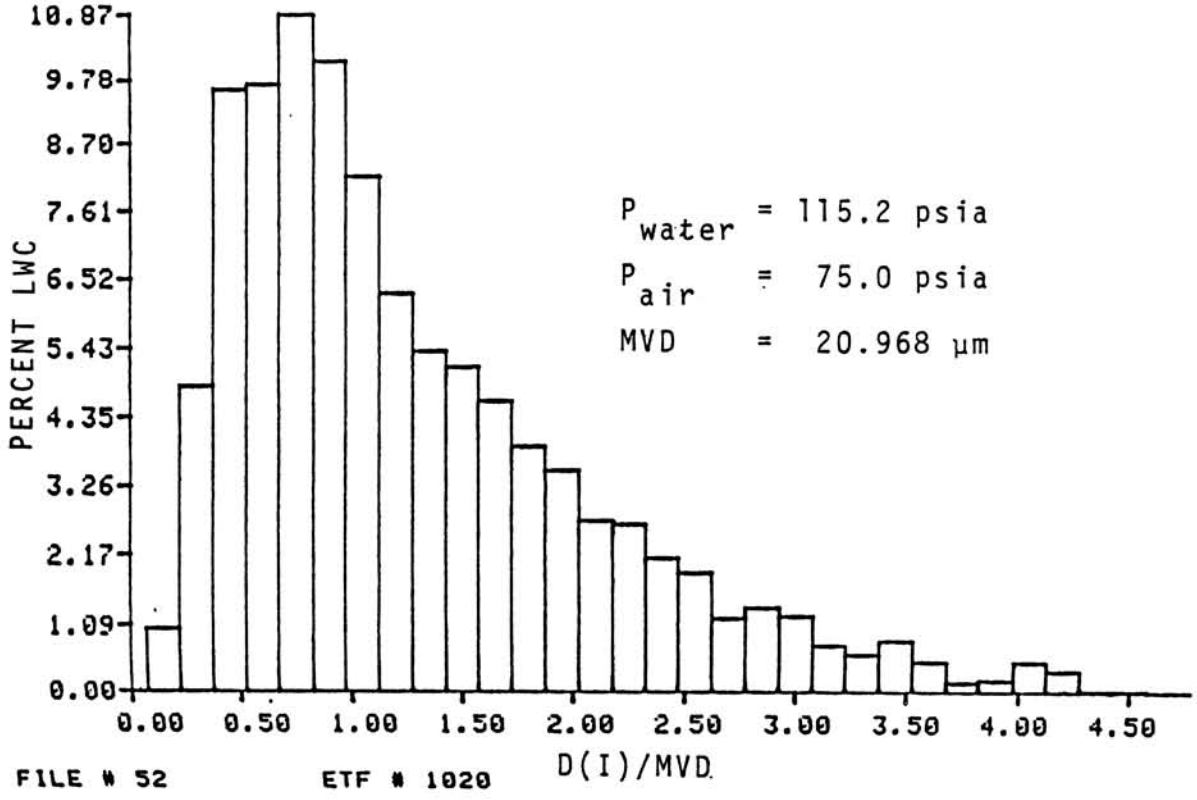

FIGURE E.5

SECOND SET OF AEDC DROPLET DISTRIBUTION DATA
FOR 0.60 PRESSURE RATIO.

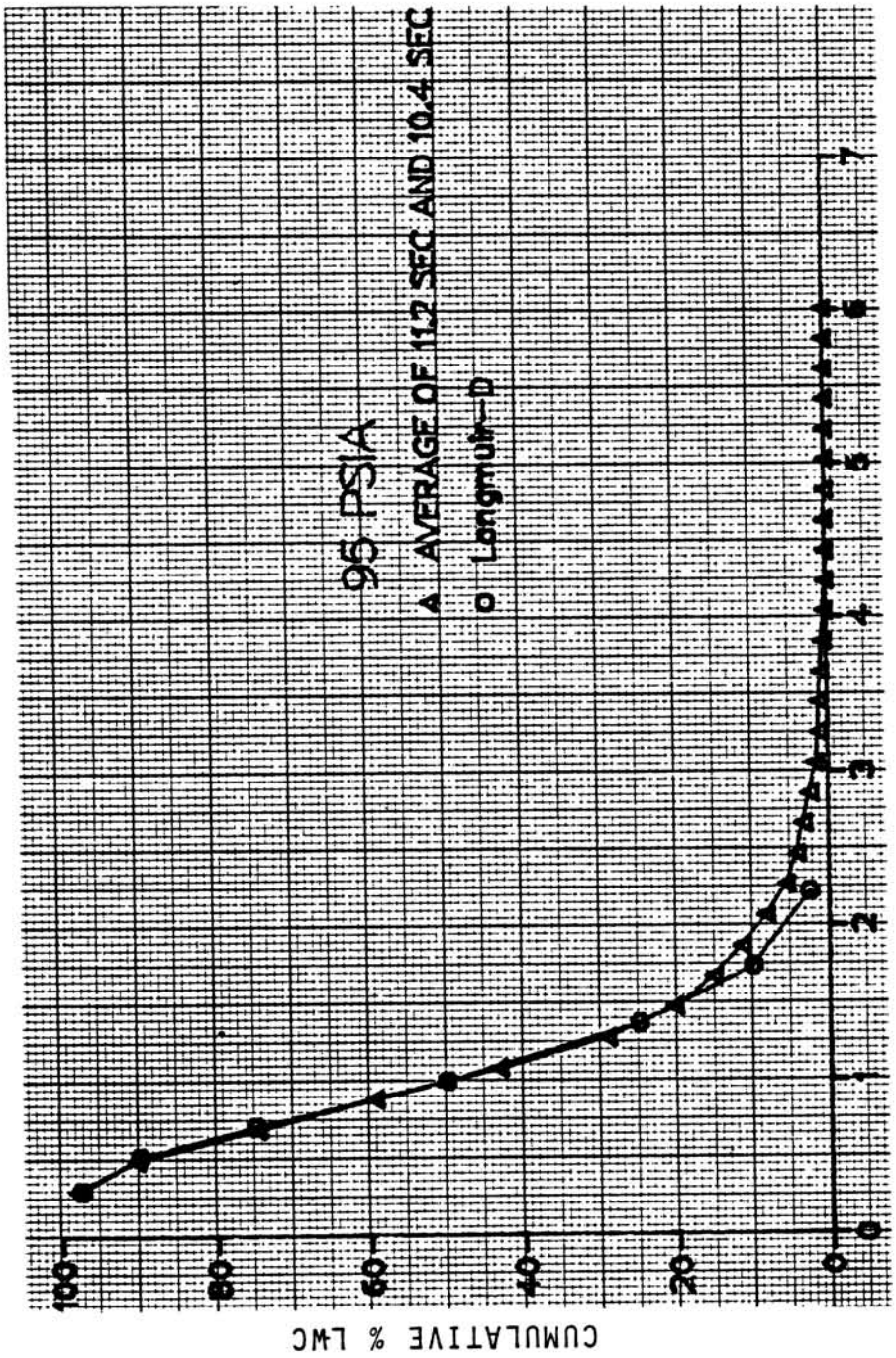

FIGURE E.6

CUMULATIVE DROPLET DISTRIBUTION FOR 0.80 PRESSURE RATIO.

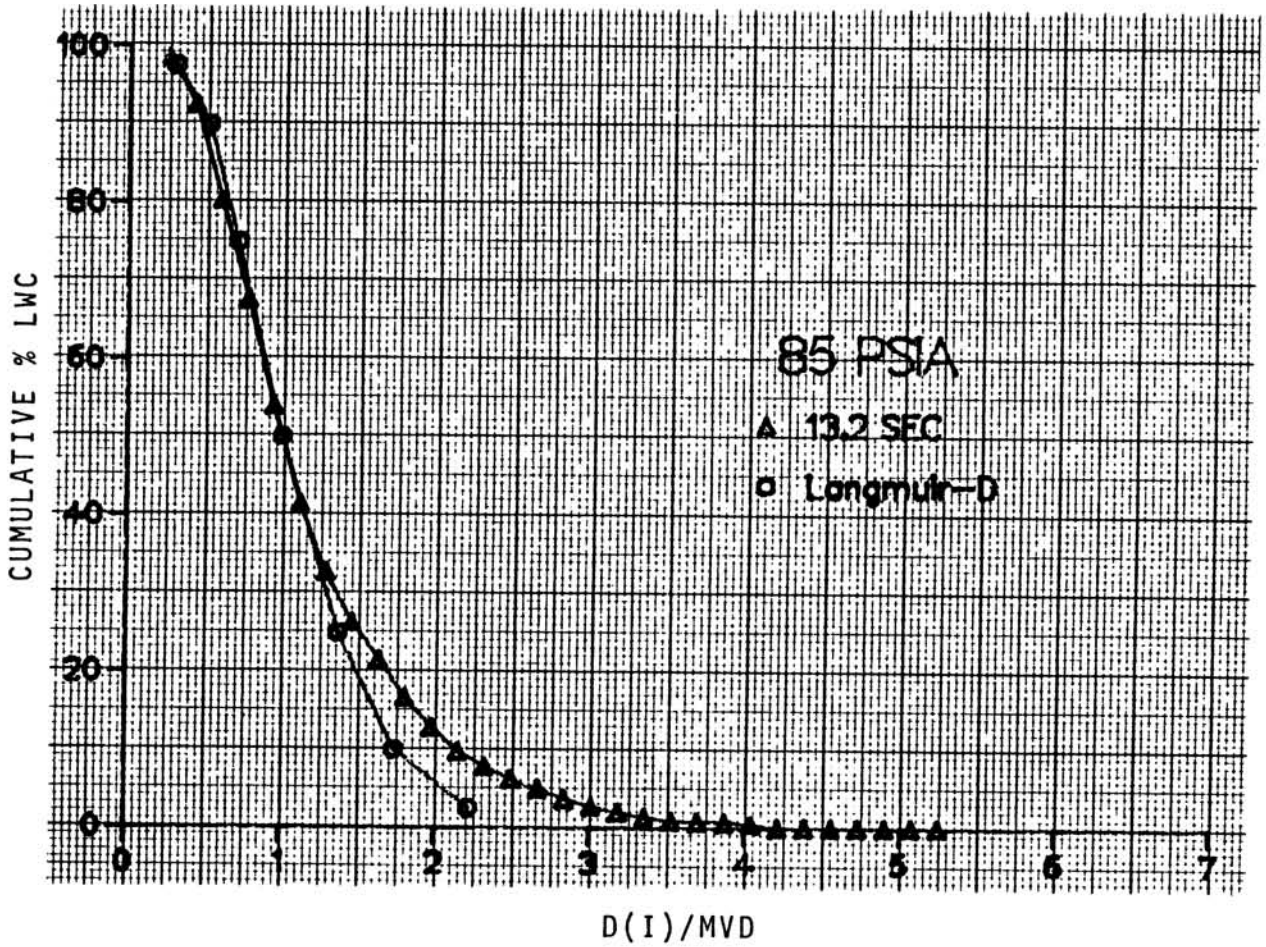

FIGURE E.7

CUMULATIVE DROPLET DISTRIBUTION FOR 0.70 PRESSURE RATIO.

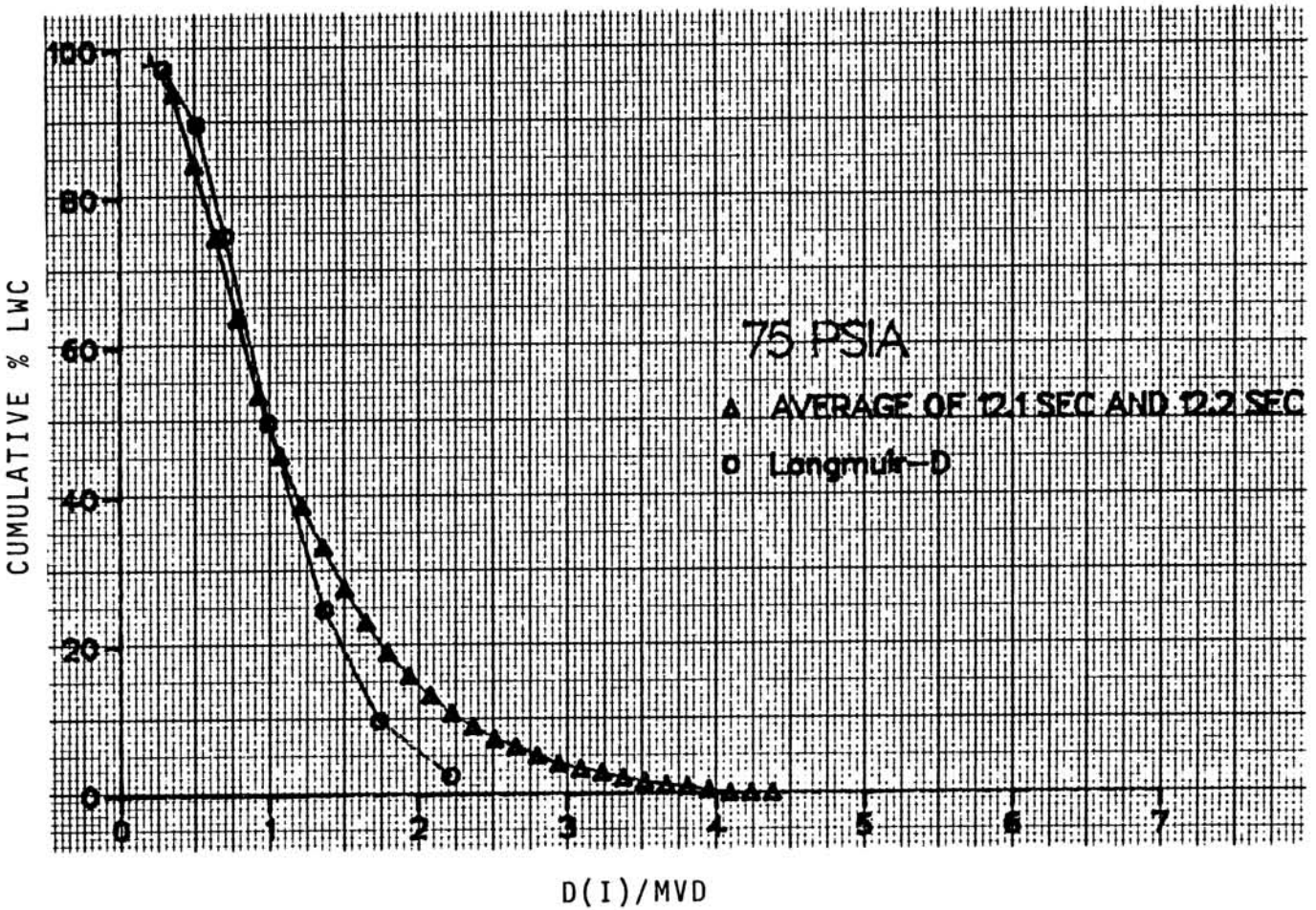

FIGURE E.8

CUMULATIVE DROPLET DISTRIBUTION FOR 0.60 PRESSURE RATIO.

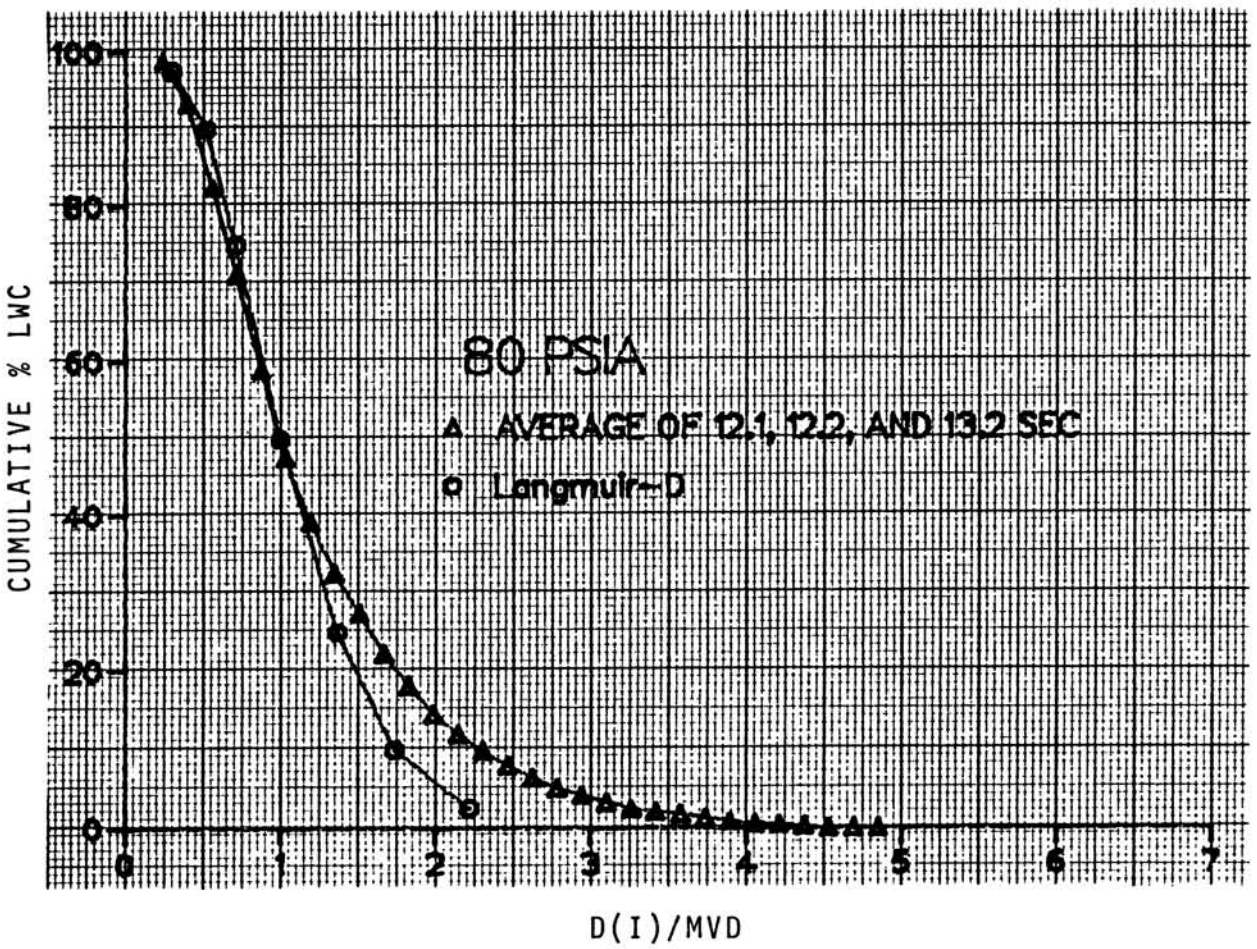

FIGURE E.9

CUMULATIVE DROPLET DISTRIBUTION FOR 0.65 PRESSURE RATIO.

Computer Program to Transform the AEDC Raw Data
into Cumulative Distributions.

```
      REAL X2(30),X3(30),X4(30),X12(30),X34(30),X6(30)
      REAL DM1,DM2,DM3,DM4,DM5,DM12,DM34,DM6
      REAL X,X1(30),Y1(30),Y2(30),Y3(30),X5(30)
      REAL Y4(30),Y5(30),Y12(30),Y34(30),Y6(30)
      REAL Y12S(30),Y34S(30),Y5S(30),Y6S(30)
      REAL X12S(30),X34S(30),X5S(30),X6S(30)
C  READ IN DATA
      READ (15,*) X,DM1
      WRITE (6,*) DM1
      DO 10 I=1,30
      READ (15,*) X1(I),Y1(I)
 10   CONTINUE
      READ (15,*) X,DM2
      WRITE (6,*) DM2
      DO 20 I=1,30
      READ (15,*) X2(I),Y2(I)
 20   CONTINUE
      READ (15,*) X,DM3
      WRITE (6,*) DM3
      DO 30 I=1,30
      READ (15,*) X3(I),Y3(I)
 30   CONTINUE
      READ (15,*) X,DM4
      WRITE (6,*) DM4
      DO 40 I=1,30
      READ (15,*) X4(I),Y4(I)
 40   CONTINUE
      READ (15,*) X,DM5
      WRITE (6,*) DM5
      DO 50 I=1,30
      READ (15,*) X5(I),Y5(I)
 50   CONTINUE
C  AVERAGE THE DM's
      DM12 = ((DM1+DM2)/2.0)+(3.239/2.0)
      DM34 = ((DM3+DM4)/2.0)+(3.239/2.0)
      DM5  = DM5+(3.239/2.0)
      DM6  = 20.362
C  AVERAGE THE Y's AND THE X's
C  CHANGE Y's TO % AND SHIFT THE X's 1/2 BIN WIDTH
      DO 11 I=1,30
      Y12(I) = (Y1(I)+Y2(I))/2.0
      X12(I) = (X1(I)+X2(I))/2.0
      Y34(I) = (Y3(I)+Y4(I))/2.0
      X34(I) = (X3(I)+X4(I))/2.0
      Y6(I)  = (Y34(I)+Y5(I))/2.0
      X6(I)  = (X34(I)+X5(I))/2.0
 11   CONTINUE
```

```
      Y12S(1) = 100.0 - Y12(1)
      X12S(1) = ((3.239/2.0)+X12(1))/DM12
      Y34S(1) = 100.0 - Y34(1)
      X34S(1) = ((3.239/2.0)+X34(1))/DM34
      Y5S(1)  = 100.0 - Y5(1)
      X5S(1)  = (X5(1)+(3.239/2.0))/DM5
      Y6S(1)  = 100.0 - Y6(1)
      X6S(1)  = ((3.239/2.0)+X6(1))/DM6
      DO 22 I=2,30
      Y12S(I) = Y12S(I-1) - Y12(I)
      X12S(I) = ((3.239/2.0)+X12(I))/DM12
      Y34S(I) = Y34S(I-1) - Y34(I)
      X34S(I) = ((3.239/2.0)+X34(I))/DM34
      Y5S(I)  = Y5S(I-1) - Y5(I)
      X5S(I)  = (X5(I)+(3.239/2.0))/DM5
      Y6S(I)  = Y6S(I-1) - Y6(I)
      X6S(I)  = ((3.239/2.0)+X6(I))/DM6
   22 CONTINUE
      DO 60 I=1,30
      WRITE (16,*) X12S(I),Y12S(I)
      WRITE (17,*) X34S(I),Y34S(I)
      WRITE (18,*) X5S(I),Y5S(I)
      WRITE (19,*) X6S(I),Y6S(I)
   60 CONTINUE
      STOP
      END
```

APPENDIX F: DERIVATION OF EQUATION (5–3) – REFLECTIVITY CURVE ERROR ANALYSIS

F.1 Derivation of Equation (5–3).

Consider the system of linear differential equations

$$-\frac{di}{Sdx} = -ai + j$$

$$\frac{dj}{Sdx} = -aj + i \qquad \text{(F-1)}$$

where $a = \frac{S+K}{S}$ with boundary conditions,

$$x = 0,\ r = R_g$$

$$x = X,\ r = R \qquad \text{(F-2)}$$

Letting $r = \frac{j}{i}$ and differentiating with respect to x,

$$\frac{dr}{dx} = \frac{idj/dx - jdi/dx}{i^2} \qquad \text{(F-3)}$$

Dividing both sides of Equation (F–3) by S,

$$\frac{dr}{Sdx} = \frac{idj/Sdx - jdi/Sdx}{i^2}$$

Using Equations (F-1)

$$\frac{dr}{Sdx} = \frac{i(-aj+i)+j(-ai+j)}{i^2}$$

$$= \frac{-aij + i^2 + j^2 - aij}{i^2}$$

$$= 1 + r^2 - 2ar \qquad \text{(F-4)}$$

Integrating (F–4),

$$s\int_0^X dx = \int_{R_g}^{R} \frac{dr}{r^2-2ar+1}$$

From Reference 27, page 296, Integral 110,

$$S[X-0] = \left[\frac{-2}{\sqrt{-4\,(1-a^2)}} \tanh^{-1} \frac{2r-2a}{\sqrt{-4(1-a^2)}} \right]_{R_g}^{R}$$

Let $b = \sqrt{a^2-1}$ $(b^2 = a^2-1,\ a^2 = b^2+1)$

$$SX = \left| \frac{-1}{b} \tanh^{-1} \frac{r-a}{b} \right|_{R_g}^{R}$$

$$SX = \left| \frac{-1}{b} \tanh^{-1} \frac{R-a}{b} - \tanh^{-1} \frac{R_g-a}{b} \right|$$

From Reference 27, page 233,

$$\tanh^{-1}x - \tanh^{-1}y = \tanh^{-1}\left(\frac{x-y}{1-xy} \right)$$

Using the above result

$$SX = \frac{-1}{b} \tanh^{-1} \left[\frac{\frac{R-a}{b} - \frac{R_g-a}{b}}{1-\left(\frac{R-a}{b} \right)\left(\frac{R_g-a}{b} \right)} \right]$$

$$\tanh(bSX) = -\frac{(R-R_g)/b}{\left[b^2-(R-a)(R_g-a) \right]/b^2}$$

$$= -\frac{b\,(R-R_g)}{b^2-(R-a)(R_g-a)}$$

$$\tanh(bSX)\left|b^2-\left(RR_g-Ra-R_ga+a^2\right)\right|=-b(R-R_g)$$

$$\tanh(bSX)(b^2-RR_g+Ra+R_ga-a^2)=-b(R-R_g)$$

$$\tanh(bSX)(a^2-1-RR_g+Ra+R_ga-a^2)=-b(R-R_g)$$

$$\tanh(bSX)(R_ga+R(a-R_g)-1)=-bR+bR_g$$

$$\tanh(bSX)(R_ga-1)-bR_g=-bR-R(a-R_g)\tanh(bSX)$$

$$R=\frac{-bR_g+\tanh(bSX)(R_ga-1)}{-(b+(a-R_g)\tanh(bSX))}$$

$$=\frac{R_g(-b+a\tanh(bSX))-\tanh(bSX))}{-(b+(a-R_g)\tanh(bSX))}$$

dividing by $\tanh(bSX)$

$$R=\frac{R_g(-b\coth(bSX)+a)-1}{-(a+b\coth(bSX)-R_g)}$$

$$=\frac{1-R_g(a-b\coth(bSX))}{a+b\coth(bSX)-R_g}$$

F.2 Reflectivity Curve Error Analysis.

Let $K = a \cdot c$ where c is the dye concentration and a is a constant. Using the above equation for K,

$$a = \frac{ac + S}{S}$$

$$b = \frac{\sqrt{ac\,(ac + 2S)}}{SX} \qquad \text{(F-5)}$$

Let $R = \frac{N}{D}$ where,

$$N = 1 - R_g\,(a - b\coth(bSX))$$

$$D = a + b\coth(bSX) - R_g \qquad \text{(F-6)}$$

Differentiating R with respect to c,

$$\frac{dR}{dc} = \frac{D\frac{dN}{dc} - N\frac{dD}{dc}}{D^2} = \frac{1}{D}\frac{dN}{dc} - \frac{N}{D^2}\frac{dD}{dc} = F(c) \qquad \text{(F-7)}$$

where,

$$\frac{dN}{dc} = 0 - R_g\left|\frac{da}{dc} - \coth(bSX)\frac{db}{dc} - b\frac{d}{dc}\coth(bSX)\right|$$

$$\frac{dD}{dc} = \frac{da}{dc} + \coth(bSX)\frac{db}{dc} + b\frac{d}{dc}\coth(bSX) - 0$$

$$\frac{da}{dc} = \frac{a}{S}$$

$$\frac{db}{dc} = \frac{1}{S}\,\frac{a\,(ac + 2S) + a^2c}{2\sqrt{ac\,(ac + 2S)}} = \frac{a\,(ac + S)}{S\sqrt{ac\,(ac + 2S)}}$$

$$\frac{d}{dc}\coth(bSX) = -\frac{d(bSX)}{dc}\,\mathrm{csch}^2(bSX) = \frac{-SX}{\sinh^2(bSX)}\,\frac{db}{dc}$$

Multiplying both sides of Equation (F 7)

$$\frac{dR}{dc}\,\frac{c}{R} = \frac{c}{R}\,F(c)$$

Rearranging

$$\frac{dR}{R} = \frac{c}{R}\,F(c)\,\frac{dc}{c}$$

where dc/c is the relative error in dye concentration due to an error dR in the value of reflectivity.

Solving for dc/c and normalizing the reflectance with respect to ε, the reflectance value corresponding to $c = 0$, (zero dye concentration) yields

$$\frac{dc}{c} = \frac{R}{\varepsilon c}\,\frac{1}{F(c)}\,\frac{dR}{R} \qquad \text{(F-9)}$$

where,

$$\varepsilon = \frac{1}{2 - R_g}$$

Program 1 at the end of this appendix evaluates dc/c as a function of R given values for dR , KX , SX and R_g. To calculate dc/c Equation (F-9) is used. Program 2 calculates dc/c as a function of R, given a value for dR , using the standard normalized reflectivity data given in Table C.1 (Appendix C).

```
C     PROGRAM #1
C
C     The Program Calculates the Relative Error in Dye Concentration
C     dc/c  Corresponding to an Error of dR in Reflectance.
C
C
      REAL KX , N
C
      NPOINT = 150
C
      WRITE(6,200)
200   FORMAT(' ENTER KX  SX  RG  DYECON  DR(EG 0.01)'/)
      READ(5,*)KX,SX,RG,DYECON,DR
C
C     X       = Layer Thickness.
C     KX      = Absorption coefficient multiplied by X.
C     SX      = Scattering Coefficient multiplied by X.
C     RG      = Reflectance of Backing.
C     DYECON  = Dye Concentration Increment.
C     DR      = Reflectance Error.
C
      ALPHA = KX
      EPSILN = 1/(2-RG)
C
      WRITE(2,220)KX,SX,RG
220   FORMAT('KUBELKA - EXPERIMENT   KX=',F5.2,' SX=',F5.2,' RG=',F5.2/
     &,'1,148'/,'REFL')
C
      DO 2 ICOUNT = 2 , NPOINT
      I=ICOUNT-1
      C = I*DYECON
C
C     C = Dye Concentration at Step  I.
C
      A = (SX+C*KX)/SX
      B = SQRT(ALPHA*C*(ALPHA*C+2*SX))/SX
C
      SINHBS = SINH(B*SX)
      COTHBS = 1/TANH(B*SX)
C
      N = 1 - RG*(A-B*COTHBS)
      D = A + B*COTHBS - RG
C
      R = N / D
      RNORM = R / EPSILN
C
C     R     = Reflectance
C     RNORM = Normalized Reflectance.
C
      DADC = ALPHA / SX
      DBDC = ALPHA*(ALPHA*C+SX)/(SX*SQRT(ALPHA*C*(ALPHA*C+2*SX)))
      DCOTDC = -DBDC*SX/(SINHBS*SINHBS)
      DNDC = -RG*(DADC-COTHBS*DBDC-B*DCOTDC)
      DDDC = DADC + COTHBS*DBDC + B*DCOTDC
      FC = (DNDC - N*DDDC/D)/D
```

```
C
C       DADC    = da/dc
C       DBDC    = db/dc
C       DCOTDC  = dcoth(bSX)/dc
C       DNDC    = dN/dc
C       DDDC    = dD/dc
C       FC      = F(c)
C
        DCOC    = -DR* 100/(C*FC*EPSILN)
        DCOCN   = -DCOC
C
C       DCOC    =  dc/c * 100%
C       DCOCN   = -dc/c * 100%
C
        WRITE(1,205)C,RNORM
        WRITE(2,206)RNORM,DCOC,DCOCN
2       CONTINUE
C
205     FORMAT(2F9.4)
206     FORMAT(3F9.3)
        STOP
        END
```

```
C       PROGRAM #2.
C
C       The Program Calculates dc/c for a Given dR from the Standard
C       Normalized Reflectivity Calibration Curve.
C
        REAL  ERROR(100,3), REFTBL(250) , MASTBL(250) ,MMDRD2,MR,MPDRD2
        REAL  RS(100)
        COMMON/BLOCK1/NTABLE
C
        READ(3,*)NTABLE
C
C       NTABLE = 217 ( Number of Entries in Table C.1)
C
        DO 6 I = 1 , NTABLE
        READ(3,*)MASTBL(I),REFTBL(I)
6       CONTINUE
C
C       MASTBL = Array for Dye-Mass per Square cm  (Table C.1).
C       REFTBL = Array for Normalized Reflectivity (Table C.1).
C
        NPOINT = 62
C
C       62 Points are Used to Define the Error Curve.
C
        WRITE(1,202)NPOINT
202     FORMAT('EROR CURVE DR=.01'/,'3,',I3/,'ER01'/,'ER02'/,'ER03')
C
C       Repeat the ERROR Calculation for DR = 0.01 , 0.02 , 0.03
C
        DO 3 J = 1 , 3
        DR = .01*J
        DRD2 = DR/2.
C
        DO 2 I = 1, NPOINT
        R = 1-.01*I
        RS(I)=R
C
C       Calculate Dye-Mass at R-dR/2
C
        CALL LININT(R-DRD2,MMDRD2,1,REFTBL,MASTBL)
C
C       Calculate Dye-Mass at R
C
        CALL LININT(R     ,MR    ,1,REFTBL,MASTBL)
C
C       Calculate Dye-Mass at R+dR/2
C
        CALL LININT(R+DRD2,MPDRD2,1,REFTBL,MASTBL)
C
C       % ERROR=100 * dc/c
C              =100*(Dye-Mass at R-dR/2 - Dye-Mass at R+dR)/Dye-Mass at R)
C
        ERROR(I,J) = 100 *(MMDRD2-MPDRD2)/MR
2       CONTINUE
C
```

```
3       CONTINUE
        DO 5 I = 1,NPOINT
5       WRITE(1,200)RS(I),(ERROR(I,J),J=1,3)
200     FORMAT(4F10.4)
C
C
        STOP
        END
C
        SUBROUTINE LININT(RH,MH,N,REFTBL,MASTBL)
        REAL MASTBL(250),MJ,MJP1,REFTBL(250),MH
        COMMON/BLOCK1/NTABLE
C
C       Finds the Mass of Dye per Square cm Corresponding to a given
C       Reflectivity Value. Table C.1 of Appendix C is used.
C
        RSAVE = RH
C
        DO 38 J = 1 , NTABLE
        IF(RSAVE.LE.REFTBL(J))GOTO 38
        JSAVE = J
        GOTO 110
38      CONTINUE
C
110     CONTINUE
C
        RJ = REFTBL(JSAVE)
        MJ = MASTBL(JSAVE)
        RJP1 = REFTBL(JSAVE+1)
        MJP1 = MASTBL(JSAVE+1)
        SLOPE = (MJ-MJP1)/(RJ-RJP1)
        BCONST = (RJ*MJP1-RJP1*MJ)/(RJ-RJP1)
        MH    =SLOPE*RH+BCONST
36      CONTINUE
        RETURN
        END
```

APPENDIX G: RAW TUNNEL CONDITIONS AND SPRAY SYSTEM DATA

The Test Log Sheets are presented in this Appendix. The following are recorded:

Date: Date of the Test.

P : Atmospheric pressure.

Dye Concentration: Dye - Mass in a given mass of water. Usually 0.0005 grams of dye per cubic centimeter of water (0.5 g/l).

Psychrometer Readings - Not recorded.

Relative Humidity - Not recorded.

Run No: The number of a test run.

Run ID: An identification for each model tested. This Run ID is also placed on each blotter strip.

TUNNEL CONDITIONS

Air Temp : Tunnel total temperature, during a test, average of three readings at three different tunnel locations.

I.A.S : Indicated Air Speed.

P_∞ : Tunnel static pressure during a test.

Q : Tunnel dynamic pressure.

Dew Point: Indicates the humidity level in the air stream.

SUPPLY PRESSURE

P_{air}/P_{H_2O}: Spray System Air Pressure (psig)/Spray System Water Pressure (psig).

P_{air} : Required spray system air pressure.
P_{H_2O} : Required spray system water pressure measured at nozzle inlet.

PLENUM PRESSURE

P_{air} : Air pressure setting of Air Regulating valve located at Tunnel Plenum (Figure A.3, Appendix A).

P_{H_2O} : Water pressure setting at water supply tank located at Tunnel Plenum chamber (Figure A.2, Appendix A). This pressure is usually 6 psig higher than the

supply pressure to account for the hydrostatic pressure difference between the tank level and the nozzle level.

TRANSDUCER READING

Tank Press: The reading of the transducer located at the top of the tank. This reading is always lower than that given by the oil filled pressure gauge due to transducer calibration. The transducer was used to monitor tank pressure fluctuation during a test.

TIME

Spray: Spray system timer setting + 0.66 sec. The 0.66 sec have been added to the actual time because the nozzles take 0.66 sec to stop spraying after the solenoid valve is closed. In reality, the nozzles flow rate is not constant during this 0.66 second period. Assuming a linear decrease in flow rate after the solenoid valve is closed, the time spray duration is equal to spray system timer setting + 0.33 second. Therefore, actual spray time is the time shown minus 0.33 second.

TABLE – II

■ Spray Uniformity Test, 2 Droplet Sizes

DATE: Sept. 12, 1985, Thursday

P_{BAR} = 14.48 PSIA

DYE CONCENTRATION = 0.0002 grm/cc

PSYCHROMETER READINGS = ___ °F DB

= 60.0 °F WB

RELATIVE HUMIDITY = ___ PERCENT

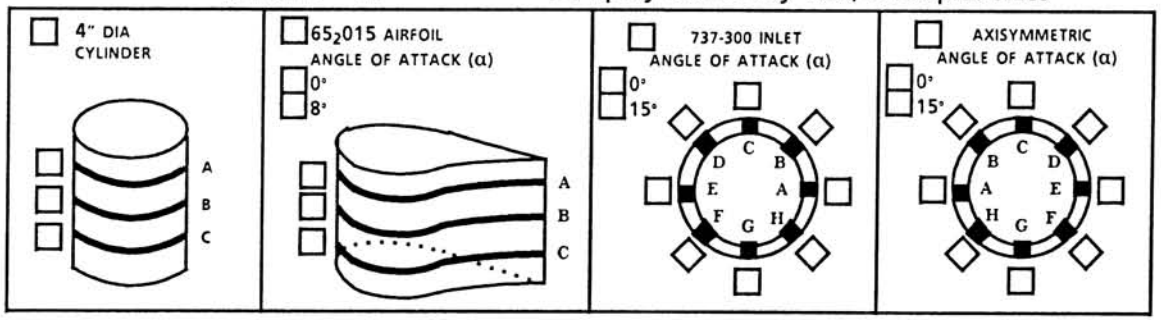

RUN NO.	RUN ID	TUNNEL CONDITIONS					SPRAY CONDITIONS											TIME (SEC.)		REMARKS
							SUPPLY PRESSURE			PLENUM PRESSURE		TRANSDUCER READINGS								
		AIR TEMP (°F)	I.A.S. (MPH)	P_α (PSIA)	Q (IN H_2O)	DEW POINT (F°)	$\frac{P_{AIR}}{P_{H_2O}}$	P_{AIR} (PSIG)	P_{H_2O} (PSIG)	P_{AIR} (PSIG)	P_{H_2O} (PSIG)	tank pres.	2	4	5	7	8	SPRAY (sec)	REF (sec)	
1	Unif-1	63.00	175	13.89	15.8	no reading	65/100	65	100	65	106							2.17	N/A	35 blotter strips
2	Unif-2	53.00	175	13.90	15 7	32.6	65.100	65	100	65	106							1.71	N'A	"
3	Unif-3	48.50	175	13.90	15.8	37.9	65.100	65	100	65	106							1.37	N A	"
4	Unif-4	45.30	175	13.90	15.7	40.1	80 100	80	100	80	106							1.71	N A	"
5	Unif-5	46.00	175	13.90	15.6	41.8	80 100	80	100	80	106							1.69	N A	"
																				"
6	Unif-6	55.00	175	13.89	15.8	43.0	80 100	80	100	80	106							1.69	N'A	"
7	Unif-7	51.00	175	13.90	15.6	43.1	80 100	80	100	80	106							1.97	N A	"
8	Unif-8	50.00	175	13.90	15 8	43.1	80 100	80	100	80	106							2.16	N A	"
9	Unif-9	49.00	175	13.90	15.6	43.4	65 100	65	100	65	106							1.37	N A	"
10	Unif-10	49.00	175	13.90	15.6	43.9	65 100	65	100	65	106							1.68	N'A	35 blotter strips

TABLE – II

■ Spray Uniformity Test, 1 Droplet Size

DATE: Sept. 13, 1985, Friday

P_{BAR} = 14.60 PSIA

DYE CONCENTRATION = ___ grm/cc

PSYCHROMETER READINGS = ___ °F DB

= 59.0 °F WB

RELATIVE HUMIDITY = ___ PERCENT

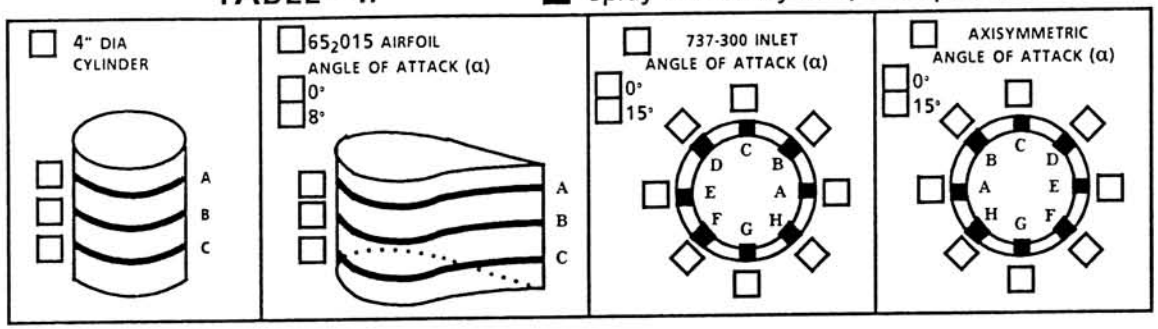

RUN NO.	RUN ID	TUNNEL CONDITIONS					SPRAY CONDITIONS											TIME (SEC.)		REMARKS
							SUPPLY PRESSURE			PLENUM PRESSURE		TRANSDUCER READINGS								
		AIR TEMP (°F)	I.A.S. (MPH)	P_α (PSIA)	Q (IN H_2O)	DEW POINT (F°)	$\frac{P_{AIR}}{P_{H_2O}}$	P_{AIR} (PSIG)	P_{H_2O} (PSIG)	P_{AIR} (PSIG)	P_{H_2O} (PSIG)	tank pres.	2	4	5	7	8	SPRAY (sec)	REF (sec)	
1	Unif-1	46.00	175	14.03	15.3	36.9	65/100	65	100	65	106							2.13	N/A	nozzles adjusted for these runs
2	Unif-2	46.30	175	14.01	15.7	37.4	65/100	65	100	65	106							1.73	N/A	nozzles adjusted for these runs
3	Unif-3	47.60	175	14.02	15.6	38.2	65/100	65	100	65	106							1.74	N/A	nozzles adjusted for these runs
																				break to scan samples
4	Unif-4	45.70	175	14.02	15.4	45.1	65 100	65	100	65	106							1.73	N A	
5	Unif-5	48.30	175	14.01	15.7	43.7	65/100	65	100	65	106							1.74	N A	
6	Unif-6	45.30	175	14.02	15.5	42.7	65/100	65	100	65	106							1.74	N A	

TABLE – II

■ Spray Uniformity and Droplet Sizing, 2 Droplet Sizes

DATE: Sept. 16, 1985, Monday

P_{BAR} = 14.44 PSIA

DYE CONCENTRATION = 0.0002 grm/cc
0.0004

PSYCHROMETER READINGS = ___ °F DB

= 69.0 °F WB
runs 9-12 73.0

RELATIVE HUMIDITY = ___ PERCENT

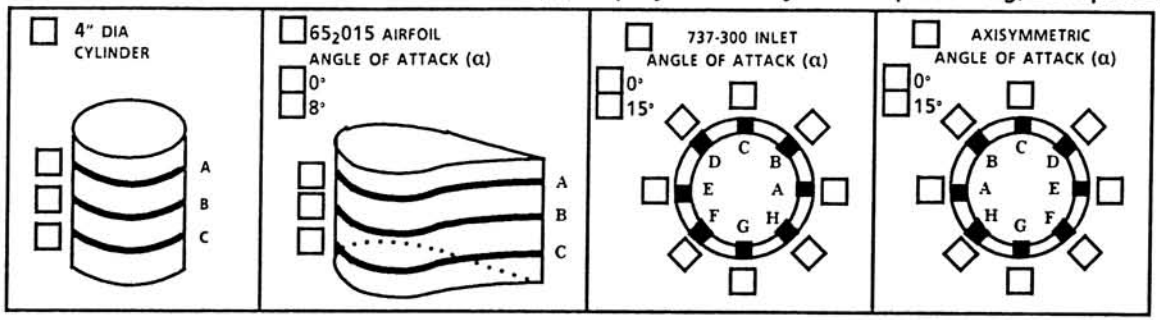

RUN NO.	RUN ID	TUNNEL CONDITIONS					SPRAY CONDITIONS											TIME (SEC.)		REMARKS
							SUPPLY PRESSURE			PLENUM PRESSURE		TRANSDUCER READINGS								
		AIR TEMP (°F)	I.A.S. (MPH)	P_α (PSIA)	Q (IN H_2O)	DEW POINT (F°)	$\frac{P_{AIR}}{P_{H_2O}}$	P_{AIR} (PSIG)	P_{H_2O} (PSIG)	P_{AIR} (PSIG)	P_{H_2O} (PSIG)	tank pres.	2	4	5	7	8	SPRAY (sec)	REF (sec)	
1	Unif-1	55.00	175	13.88	15.6	52.8	65/100	65	100	65	106							1.75	N/A	C = 0.0002
2	Unif-2	54.00	175	13.88	15.5	52.2	65/100	65	100	65	106							1.74	N/A	C = 0.0002
3	Drop-1	49.60	120	14.19	7.4	30.8	65/100	65	100	65	106							--	N/A	C = 0.0002 no good
4	Drop-2	49.60	120	14.19	7.4	31.1	65/100	65	100	65	106							--	N/A	C = 0.0002
5	Drop-3	48.30	120	14.19	7.3	23.1	80/100	80	100	80	106							--	N/A	C = 0.0002
6	Unif-3	49.00	175	13.89	15.3	48.2	80/100	80	100	80	106							--	N/A	C = 0.0002 no good
7	Unif-4	46.00	175	13.88	15.4	50.0	80/100	80	100	80	106							2.18	N/A	C = 0.0002
8	Unif-5	51.60	175	13.87	15.6	48.0	80/100	80	100	80	106							2.23	N/A	C = 0.0002
9	Unif-6	49.60	175	13.85	15.4	40.5	80/100	80	100	80	106							2.23	N/A	C = 0.0004
10	Unif-7	49.30	175	13.85	15.3	39.6	80/100	80	100	80	106							2.22	N/A	C = 0.0004
11	Unif-8	49.00	175	13.83	15.6	39.4	65/100	65	100	65	106							1.72	N/A	C = 0.0004
12	Unif-9	49.60	175	13.84	15.5	39.7	65/100	65	100	65	106							1.71	N/A	C = 0.0004

TABLE – II

■ Spray Uniformity Test, 2 Droplet Sizes

DATE: Sept. 16, 1985, Monday

P_{BAR} = 14.44 PSIA

DYE CONCENTRATION = 0.0002 / 0.0004 grm/cc

PSYCHROMETER READINGS = ___ °F DB

= 69.0 °F WB

runs 7 - 12 73.0° F WB

RELATIVE HUMIDITY = ___ PERCENT

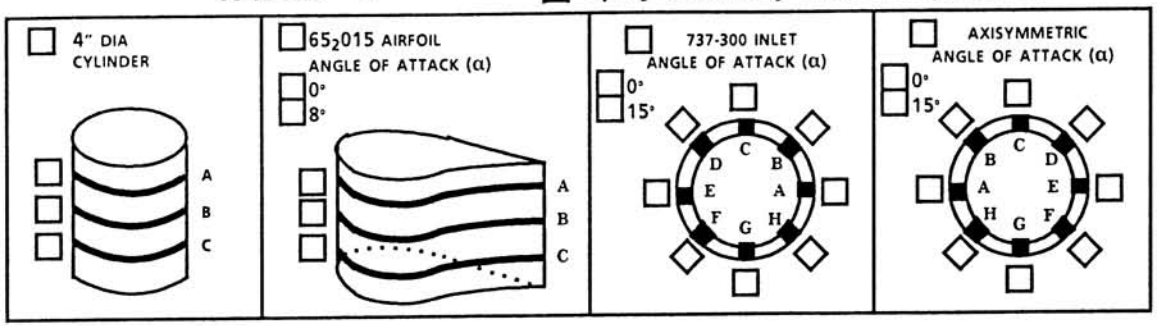

RUN NO.	RUN ID	TUNNEL CONDITIONS					SPRAY CONDITIONS												TIME (SEC.)		REMARKS
							SUPPLY PRESSURE			PLENUM PRESSURE		TRANSDUCER READINGS									
		AIR TEMP (°F)	I.A.S. (MPH)	P_α (PSIA)	Q (IN H_2O)	DEW POINT (F°)	$\frac{P_{AIR}}{P_{H_2O}}$	P_{AIR} (PSIG)	P_{H_2O} (PSIG)	P_{AIR} (PSIG)	P_{H_2O} (PSIG)	tank pres.	2	4	5	7	8	SPRAY (sec)	REF (sec)	
1	Unif-1	55.00	175	13.88	15.6	52.8	65/100	65	100	65	106							1.75	N/A	blotter at normal position for tests 1-2
2	Unif-2	54.00	175	13.88	15.5	52.2	65/100	65	100	65	106							1.74	N/A	blotter at normal position for tests 1-2
3	Drop-1	49.60	120	14.19	7.4	30.8	65/100	65	100	65	106							10.06	N/A	Droplet sizing test
4	Drop-2	49.60	120	14.19	7.4	31.1	65/100	65	100	65	106								N/A	
5	Drop-3	48.30	120	14.19	7.3	23.1	80/100	80	100	80	106								N/A	
6	Unif-3	49.00	175	13.89	15.3	48.2	80/100	80	100	80	106								N/A	bad spray water press. down to 80psi
7	Unif-4	46.00	175	13.88	15.4	50.0	80/100	80	100	80	106							2.18	N/A	no good
8	Unif-5	51.60	175	13.87	15.6	48.0	80/100	80	100	80	106							2.23	N/A	no good
9	Unif-6	49.60	175	13.85	15.4	40.5	80/100	80	100	80	106							2.23	N/A	Concentration = 0.0004grm/cc
10	Unif-7	49.30	175	13.85	15.3	39.6	80/100	80	100	80	106							2.22	N/A	Concentration = 0.0004grm/cc
11	Unif-8	49.00	175	13.83	15.6	39.4	65/100	65	100	65	106							1.72	N/A	Concentration = 0.0004grm/cc
12	Unif-9	49.600	175	13.84	15.5	39.7	65/100	65	100	65	106							1.71	N/A	Concentration = 0.0004grm/cc

TABLE – II

■ Spray Uniformity Test, 2 Droplet Sizes

DATE: Sept. 17, 1985, Tuesday

P_{BAR} = 14.4 PSIA

DYE CONCENTRATION = 0.0005 grm/cc

PSYCHROMETER READINGS = ___ °F DB

= 76.0 °F WB

RELATIVE HUMIDITY = ___ PERCENT

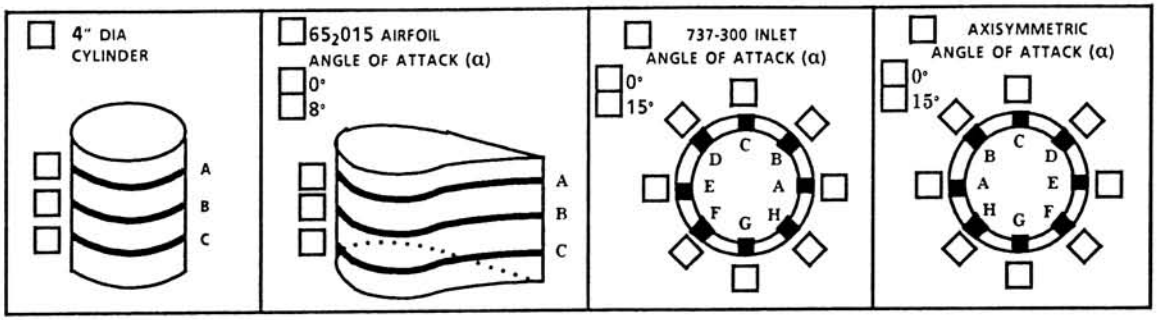

RUN NO.	RUN ID	TUNNEL CONDITIONS					SPRAY CONDITIONS												TIME (SEC.)		REMARKS
							SUPPLY PRESSURE			PLENUM PRESSURE		TRANSDUCER READINGS									
		AIR TEMP (°F)	I.A.S. (MPH)	P_α (PSIA)	Q (IN H_2O)	DEW POINT (F°)	$\frac{P_{AIR}}{P_{H_2O}}$	P_{AIR} (PSIG)	P_{H_2O} (PSIG)	P_{AIR} (PSIG)	P_{H_2O} (PSIG)	tank pres.	2	4	5	7	8	SPRAY (sec)	REF (sec)	
1	Unif-1	48.00	175	13.81	15.7	34.8	65/100	65	100	65	106							1.73	N A	blotter at intermediate position
2	Unif-2	44.30	175	13.81	15.6	33.4	65/100	65	100	65	106							1.73	N A	blotter at position B
3	Unif-3	50.30	175	13.81	15.6	32.0	80/100	80	100	80	106							2.71	N A	blotter at position A
4	Unif-4	48.70	175	13.82	15.5	31.3	80/100	80	100	80	106							2.71	N/A	blotter at position B
5	Unif-5	49.00	175	13.80	15.9	30.9	80/100	80	100	80	106							1.64 on		
																		60.0 off	N/A	3 intermittent sprays
6	Unif-6	48.70	150	13.96	11.85	30.4	80/100	80	100	80	106							2.72	N.A	blotter at standard position

TABLE – II

■ Single Collector

DATE: Sept. 18, 1985, Wednesday

P_{BAR} = 14.45 PSIA

DYE CONCENTRATION = 0.0005 grm/cc

PSYCHROMETER READINGS = ___ °F DB

= 74.3 °F WB

RELATIVE HUMIDITY = ___ PERCENT

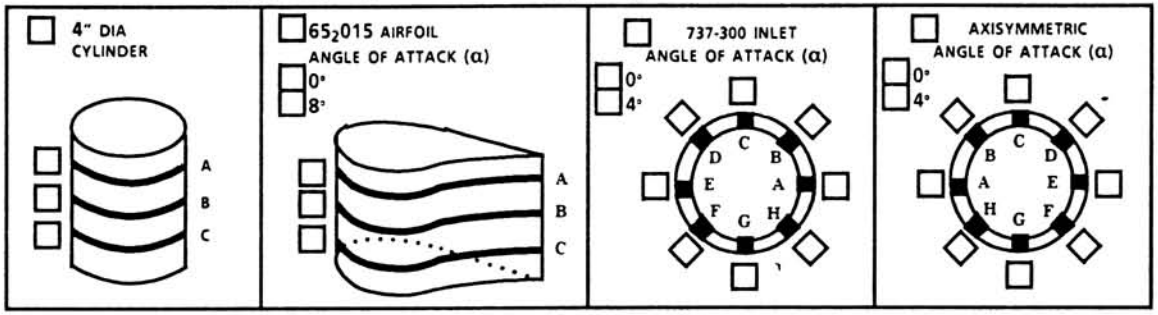

RUN NO.	RUN ID	TUNNEL CONDITIONS					SPRAY CONDITIONS											TIME (SEC.)		REMARKS
							SUPPLY PRESSURE			PLENUM PRESSURE		TRANSDUCER READINGS								
		AIR TEMP (°F)	I.A.S. (MPH)	P_∞ (PSIA)	Q (IN H_2O)	DEW POINT (°F)	$\frac{P_{AIR}}{P_{H_2O}}$	P_{AIR} (PSIG)	P_{H_2O} (PSIG)	P_{AIR} (PSIG)	P_{H_2O} (PSIG)	tank pres.	2	4	5	7	8	SPRAY (sec)	REF (sec)	
1	COL-1	45.33	175	13 90	15.30	41.3	0.65	65	100	65	106	96						3.69	N A	collector center 36" above tunnel floor
2	COL-2	44.70	175	13.90	15.50	40.8	0.65	65	100	65	106	95						3 20	N/A	"
3	COL-3	44.70	175	13.90	15.40	40.2	0.65	65	100	65	106	96						2.69	N.A	"
4	COL-4	46.70	175	13.89	15.35	39.6	0.65	65	100	65	106	95						2.14	N A	"
5	COL-5	47.30	175	13.89	15.40	39.0	0.65	65	100	65	106	96						1.64	N.A	"
6	COL-6	42.60	175	13.89	15.50	38.7	0.65	65	100	65	106	96						1.14	N.A	"
7	COL-7	42.70	175	13.89	15.50	37.9	0.80	80	100	80	106	95						1.15	N/A	"
8	COL-8	47.70	175	13.89	15.60	37.3	0.80	80	100	80	106	96						1.71	N A	"
9	COL-9	49 30	175	13 89	15 65	37 3	0 80	80	100	80	106	96						2 20	N/A	"
10	COL-10	48.67	175	13.89	15.40	37.3	0.80	80	100	80	106	96						2.69	N/A	"
11	COL-11	48.33	175	13.88	15.65	37.4	0.80	80	100	80	106	96						3.20	N A	"
12	COL-12	49 3	175	13.89	15.50	37.5	0.80	80	100	80	106	96						3.71	N A	collector center 36" above tunnel floor

TABLE – II

■ Single Collector (cont.)

DATE: Sept. 18, 1985, Wednesday

P_{BAR} = 14.45 PSIA

DYE CONCENTRATION = 0.0005 grm/cc

PSYCHROMETER READINGS = ___ °F DB

= 74.3 °F WB

RELATIVE HUMIDITY = ___ PERCENT

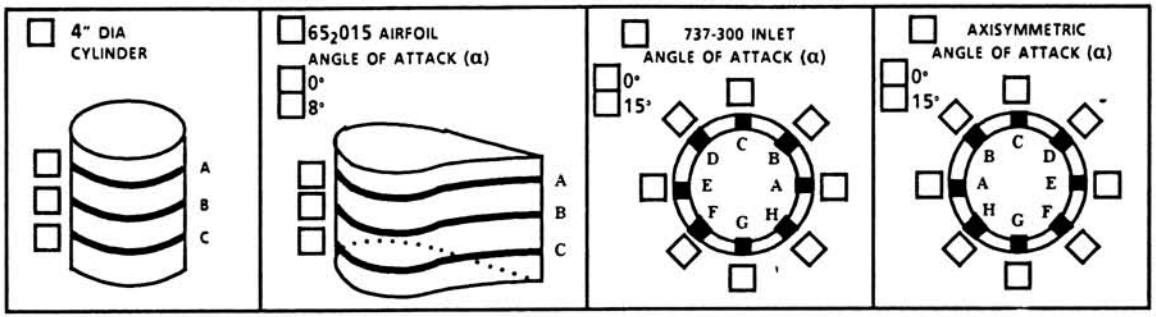

RUN NO.	RUN ID	TUNNEL CONDITIONS					SPRAY CONDITIONS											TIME (SEC.)		REMARKS
							SUPPLY PRESSURE			PLENUM PRESSURE		TRANSDUCER READINGS								
		AIR TEMP (°F)	I.A.S. (MPH)	P_∞ (PSIA)	Q (IN H_2O)	DEW POINT (°F)	$\frac{P_{AIR}}{P_{H_2O}}$	P_{AIR} (PSIG)	P_{H_2O} (PSIG)	P_{AIR} (PSIG)	P_{H_2O} (PSIG)	tank pres.	2	4	5	7	8	SPRAY (sec)	REF (sec)	
13	COL-13	47.33	175	13.87	15.40	37.6	0.65	65	100	65	106	96						3.70	N.A	collector center 32" above tunnel floor
14	COL-14	49.33	175	13.88	15.60	37.8	0.65	65	100	65	106	96						3.20	N.A	"
15	COL-15	49.00	175	13.89	15.30	38.1	0.65	65	100	65	106	96						2.67	N.A	"
16	COL-16	47.67	175	13.88	15.60	38.3	0.65	65	100	65	106	96						2.13	N.A	"
17	COL-17	48.67	175	13.87	15.50	38.4	0.65	65	100	65	106	96						1.70	N.A	"
18	COL-18	50.33	175	13.87	15.70	38.4	0.65	65	100	65	106	96						1.16	N.A	"
19	COL-19	48.33	175	13.87	15.50	38.4	0.80	80	100	80	106	96						1.15	N.A	"
20	COL-20	49.00	175	13.87	15.60	38.4	0.80	80	100	80	106	96						1.67	N.A	"
21	COL-21	49.33	175	13.87	15.70	38.4	0.80	80	100	80	106	96						2.17	N.A	"
22	COL-22	48.00	175	13.87	15.40	38.3	0.80	80	100	80	106	96						2.72?	N.A	possible time error "
23	COL-23	48.67	175	13.86	15.70	37.9	0.80	80	100	80	106	96						3.14	N.A	"
24	COL-24	50.33	175	13.86	15.90	38.2	0.80	80	100	80	106	96						3.64	N.A	collector center 32" above tunnel floor

TABLE – II

4 Inch Cylinder

DATE: Sept. 18, 1985, Wednesday

P_{BAR} = 14.45 PSIA

DYE CONCENTRATION = 0.0005 grm/cc

PSYCHROMETER READINGS = ___ °F DB

= 74.3 °F WB

RELATIVE HUMIDITY = ___ PERCENT

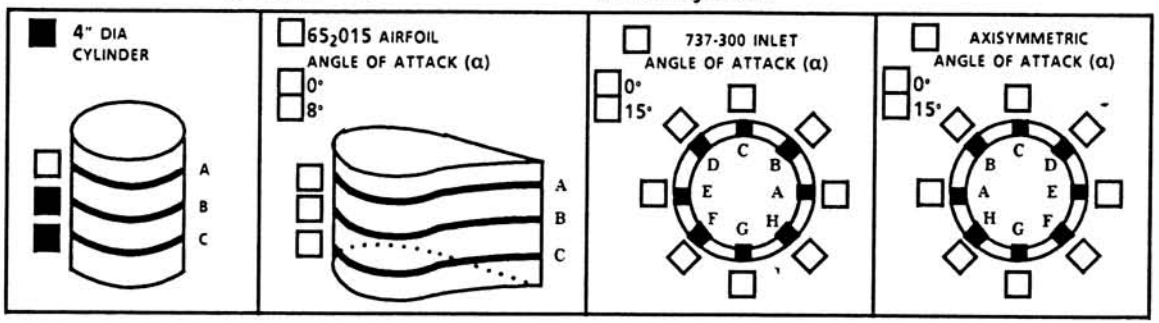

RUN NO.	RUN ID	TUNNEL CONDITIONS					SPRAY CONDITIONS											TIME (SEC.)		REMARKS
							SUPPLY PRESSURE			PLENUM PRESSURE		TRANSDUCER READINGS								
		AIR TEMP (°F)	I.A.S. (MPH)	P_∞ (PSIA)	Q (IN H_2O)	DEW POINT (°F)	$\frac{P_{AIR}}{P_{H_2O}}$	P_{AIR} (PSIG)	P_{H_2O} (PSIG)	P_{AIR} (PSIG)	P_{H_2O} (PSIG)	tank pres.	2	4	5	7	8	SPRAY (sec)	REF (sec)	
25	CYL - 1	46.00	175	13.87	15.90	37.8	0.65	65	100	65	106	95						2.18	N/A	2 strips VOID
26	CYL - 2	46.33	175	13.89	15.60	37.5	0.65	65	100	65	106	96						2.68	N/A	strip B (36")
27	CYL - 3	46.33	175	13.89	15.50	37.4	0.65	65	100	65	106	96						2.65	N/A	strip C (32")
28	CYL - 4	44.67	175	13.89	15.50	37.2	0.80	80	100	80	106	96						2.67	N/A	
29	CYL - 5	45.00	175	13.88	15.75	37.0	0.80	80	100	80	106	96						2.66	N.A	
30	CYL - 6	48.33	175	13.87	15.90	36.9	0.80	80	100	80	106	96						2.68	N/A	
31	CYL - 7	50.00	175	13.88	15.60	36.8	0.80	80	100	80	106	96						3.64	N/A	
32	CYL - 8	48.00	175	13.88	15.70	37.0	0.65	65	100	65	106	96						2.66	N/A	

TABLE – II

Axisymmetric Inlet α = 15°, 0°

DATE: Sept. 21, 1985, Saturday

P_{BAR} = 14.38 PSIA

DYE CONCENTRATION = 0.0005 grm/cc

PSYCHROMETER READINGS = ___ °F DB

= 66.33 °F WB

RELATIVE HUMIDITY = ___ PERCENT

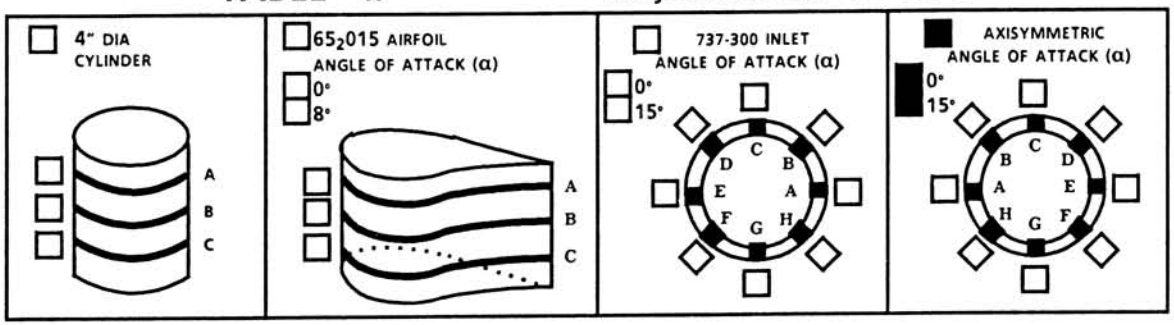

RUN NO.	RUN ID	TUNNEL CONDITIONS					SPRAY CONDITIONS											TIME (SEC.)		REMARKS
							SUPPLY PRESSURE			PLENUM PRESSURE		TRANSDUCER READINGS								
		AIR TEMP (°F)	I.A.S. (MPH)	P_∞ (PSIA)	Q (IN H_2O)	DEW POINT (°F)	$\frac{P_{AIR}}{P_{H_2O}}$	P_{AIR} (PSIG)	P_{H_2O} (PSIG)	P_{AIR} (PSIG)	P_{H_2O} (PSIG)	tank pres.		mass flow volts		mass flow lb s	α	SPRAY (sec)	REF (sec)	
1	1-AXI-15	48.66	165	13.85	14.4	46.8	0.65	65	100	65	106	96		5.2		22.96	15°	2.68	N/A	High Suction – 8 blotter strips
2	2-AXI-15	51.33	165	13.86	13.8	46.7	0.65	65	100	65	106	96		5.2		22.96	15°	2.56	N A	High Suction "
3	3-AXI-15	52.00	165	13.85	14.2	45.8	0.65	65	100	65	106	96		5.2		22.96	15°	2.66	N A	High Suction "
4	4-AXI-15	51.33	165	13.86	13.8	45.4	0.65	65	100	65	106	98		3.9		17.20	15°	2.67	N/A	Low Suction "
5	5-AXI-15	51.00	165	13.86	13.8	45.2	0.65	65	100	65	106	97		3.9		17.20	15°	2.67	N A	Low Suction "
6	6-AXI-15	52.33	165	13.86	14.0	45.0	0.65	65	100	65	106	96		3.9		17.20	15°	2.66	N/A	Low Suction "
7	7-AXI-15	53.00	165	13.86	13.9	45.1	0.80	80	100	80	106	98		5.2		22.96	15°	3.17	N/A	High Suction "
8	8-AXI-15	52.66	165	13.86	13.9	44.6	0.80	80	100	80	106	97		5.2		22.96	15°	3.16	N/A	High Suction "
9	9-AXI-15	53.66	165	13.84	13.8	44.5	0.80	80	100	80	106	99		5.2		22 96	15°	3.17	N/A	High Suction "
10	10-AXI-15	56.33	165	13.84	14.2	44.5	0.80	80	100	80	106	98		3.9		17.20	15°	3.16	N/A	Low Suction "
11	11-AXI-15	52.33	165	13.84	14.2	44.0	0.80	80	100	80	106	97		3.9		17.20	15°	3.16	N/A	Low Suction "
12	12-AXI-15	53.66	165	13.84	13.9	43.7	0.80	80	100	80	106	96		3.9		17.20	15°	3.18	N A	Low Suction – 8 blotter strips
13	13-AXI-0	55.33	165	13.84	13.9	44.0	0.65	65	100	65	106	97		5.2		22.96	0°	2.68	N/A	High Suction – 4 blotter strips
14	14-AXI-0	52.66	165	13.84	14.2	44.6	0.65	65	100	65	106	95		5.2		22.96	0°	2.64	N/A	High Suction – 4 blotter strips
																				last run for Saturday

TABLE – II

Axisymmetric Inlet $\alpha = 0°$

DATE: Sept. 23, 1985, Monday

P_{BAR} = 14.32 PSIA

DYE CONCENTRATION = 0.0005 grm/cc

PSYCHROMETER READINGS = ___ °F DB

= 73.33 °F WB

RELATIVE HUMIDITY = ___ PERCENT

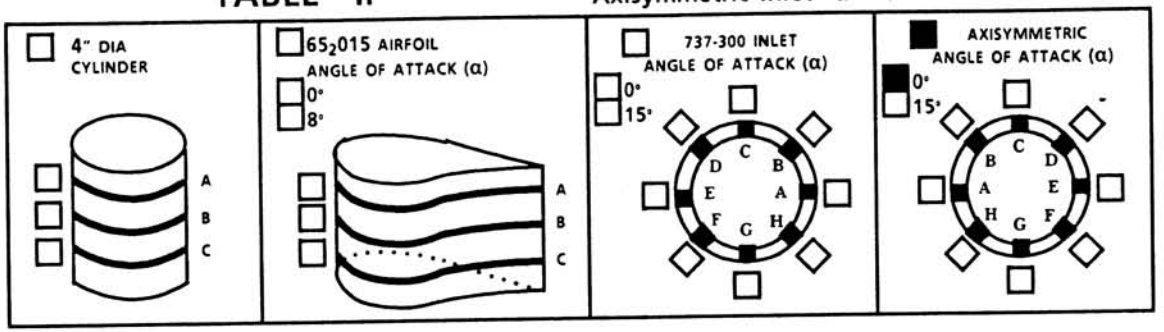

RUN NO.	RUN ID	TUNNEL CONDITIONS					SPRAY CONDITIONS											TIME (SEC.)		REMARKS
							SUPPLY PRESSURE			PLENUM PRESSURE		TRANSDUCER READINGS								
		AIR TEMP (°F)	I.A.S. (MPH)	P_∞ (PSIA)	Q (IN H_2O)	DEW POINT (°F)	$\frac{P_{AIR}}{P_{H_2O}}$	P_{AIR} (PSIG)	P_{H_2O} (PSIG)	P_{AIR} (PSIG)	P_{H_2O} (PSIG)	tank pres.		mass flow volts		mass flow lb s	α	SPRAY (sec)	REF (sec)	
15	15-AXI-0	55.66	165	13.77	14.0	44.4	0.65	65	100	65	106	96		5.2		22.96	0°	2.68	N/A	High Suction – 4 blotter strips
16	16-AXI-0	56.33	165	13.77	13.9	47.9	0.65	65	100	65	106	95		3.9		17.20	0°	2.69	N/A	Low Suction "
17	17-AXI-0	56.67	165	13.76	14.1	49.9	0.65	65	100	65	106	94		3.9		17.20	0°	2.69	N/A	Low Suction "
18	18-AXI-0	57.00	165	13.76	14.0	51.7	0.65	65	100	65	106	93		3.9		17.20	0°	2.69	N/A	Low Suction "
19	19-AXI-0	56.67	165	13.74	14.2	51.6	0.80	80	100	80	106	95		5.2		22.96	0°	3.19	N/A	High Suction "
20	20-AXI-0	57.67	165	13.74	14.0	51.6	0.80	80	100	80	106	95		5.2		22.96	0°	3.18	N/A	High Suction "
21	21-AXI-0	48.67	165	13.75	14.0	50.4	0.80	80	100	80	106	95		5.2		22.96	0°	3.18	N/A	High Suction "
22	22-AXI-0	51.67	165	13.74	14.0	47.7	0.80	80	100	80	106	95		3.9		17.20	0°	3.17	N/A	Low Suction "
23	23-AXI-0	54.33	165	13.74	13.9	45.8	0.80	80	100	80	106	97		3.9		17.20	0°	3.18	N/A	Low Suction "
24	24-AXI-0	53.67	165	13.74	13.8	45.8	0.80	80	100	80	106	97		3.9		17.20	0°	3.17	N/A	Low Suction – 4 blotter strips

TABLE – II

737–300 Engine Inlet $\alpha = 0°$

DATE: Sept. 23, 1985, Monday

P_{BAR} = 14.32 PSIA

DYE CONCENTRATION = 0.0005 grm/cc

PSYCHROMETER READINGS = ___ °F DB

= 57.7 °F WB

RELATIVE HUMIDITY = ___ PERCENT

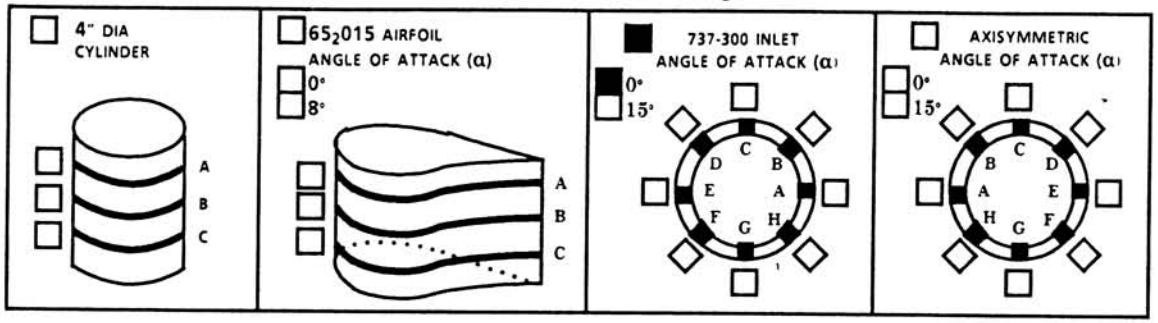

RUN NO.	RUN ID	TUNNEL CONDITIONS					SPRAY CONDITIONS											TIME (SEC.)		REMARKS
							SUPPLY PRESSURE			PLENUM PRESSURE		TRANSDUCER READINGS								
		AIR TEMP (°F)	I.A.S. (MPH)	P_∞ (PSIA)	Q (IN H_2O)	DEW POINT (°F)	$\frac{P_{AIR}}{P_{H_2O}}$	P_{AIR} (PSIG)	P_{H_2O} (PSIG)	P_{AIR} (PSIG)	P_{H_2O} (PSIG)	tank pres.		mass flow volts		mass flow lbs		SPRAY (sec)	REF (sec)	
1	1-737-0	59.33	165	13.73	14.00	50.0	0.65	65	100	65	106	98		5.2		22 96		2.68	N A	High Suction $\alpha = 0°$
2	2-737-0	58.66	165	13.74	14.10	50.6	0.65	65	100	65	106	98		5.2		22.96		2 68	N/A	High Suction $\alpha = 0°$
3	3-737-0	59.00	165	13.73	13.80	47.6	0.65	65	100	65	106	97		5.2		22.96		2.68	N A	High Suction $\alpha = 0°$
4	4-737-0	55.67	165	13.73	13.80	48.6	0.65	65	100	65	106	96		3.9		17.20		2.68	N.A	Low Suction $\alpha = 0°$
5	5-737-0	59.67	165	13.72	13.90	46.0	0.65	65	100	65	106	97		3.9		17 20		2 68	N A	Low Suction $\alpha = 0°$
6	6-737-0	55.00	165	13.72	14.00	48.2	0 65	65	100	65	106	96		3.9		17 20		2 68	N.A	Low Suction $\alpha = 0°$
7	7-737-0	60.67	165	13 73	14.00	47.1	0.80	80	100	80	106	97		5.2		22 96		3.18	N.A	High Suction $\alpha = 0°$
8	8-737-0	57.33	165	13.73	14.00	48.9	0.80	80	100	80	106	96		5.2		22 96		3.18	N A	High Suction $\alpha = 0°$
9	9-737-0	61.33	165	13.73	13.90	48.3	0.80	80	100	80	106	98		5.2		22.96		3.17	N A	High Suction $\alpha = 0°$
10	10-737-0	56.67	165	13.73	13.90	49.7	0.80	80	100	80	106	96		3.9		17.20		3.17	N A	Low Suction $\alpha = 0°$
11	11-737-0	62.33	165	13.73	13.90	48.4	0 80	80	100	80	106	97		3.9		17.20		3.17	N.A	Low Suction $\alpha = 0°$
12	12-737-0	53.67	165	13.73	13.80	49.9	0 80	80	100	80	106	96		3.9		17.20		3 17	N.A	Low Suction $\alpha = 0°$

TABLE – II

737–300 Engine Inlet α = 15°

DATE: Sept. 23, 1985, Monday

P_{BAR} = 14.32 PSIA

DYE CONCENTRATION = 0.0005 grm/cc

PSYCHROMETER READINGS = ___ °F DB

= 57.7 °F WB

RELATIVE HUMIDITY = ___ PERCENT

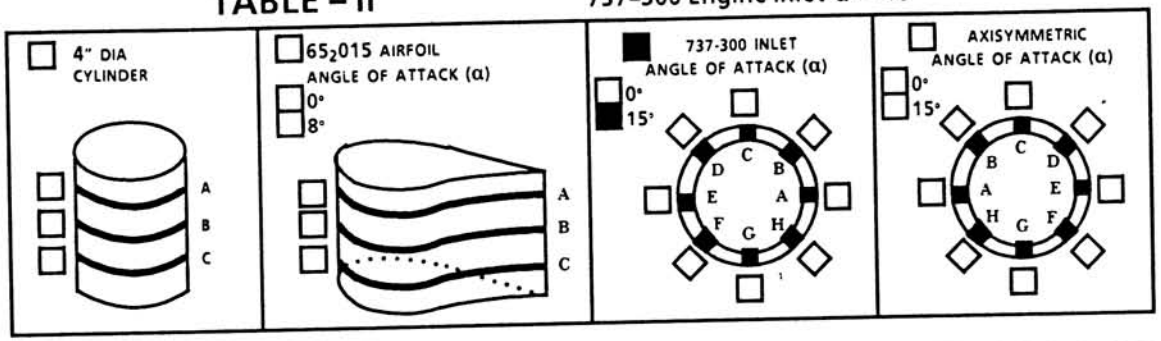

RUN NO.	RUN ID	TUNNEL CONDITIONS					SPRAY CONDITIONS											TIME (SEC.)		REMARKS
							SUPPLY PRESSURE			PLENUM PRESSURE		TRANSDUCER READINGS								
		AIR TEMP (°F)	I.A.S. (MPH)	P_∞ (PSIA)	Q (IN H_2O)	DEW POINT (°F)	$\frac{P_{AIR}}{P_{H_2O}}$	P_{AIR} (PSIG)	P_{H_2O} (PSIG)	P_{AIR} (PSIG)	P_{H_2O} (PSIG)	tank pres.		mass flow volts		mass flow lb/s		SPRAY (sec)	REF (sec)	
13	13-737-15	59.33	165	13.75	13.80	41.7	0.65	65	100	65	106	96		5.2		22.96		2.68	N/A	High Suction α = 15°
14	14-737-15	53.00	165	13.75	13.90	42.2	0.65	65	100	65	106	95		5.2		22.96		2.68	N/A	High Suction α = 15°
15	15-737-15	55.33	165	13.74	13.80	42.7	0.65	65	100	65	106	96		5.2		22.96		2.68	N/A	High Suction α = 15°
16	16-737-15	59.33	165	13.74	13.90	43.3	0.65	65	100	65	106	97		3.9		17.20		2.68	N/A	Low Suction α = 15°
17	17-737-15	56.33	165	13.74	14.00	45.5	0.65	65	100	65	106	97		3.9		17.20		2.68	N/A	Low Suction α = 15°
18	18-737-15	55.67	165	13.74	13.90	43.2	0.65	65	100	65	106	96		3.9		17.20		2.68	N/A	Low Suction α = 15°

TABLE – II

737–300 Engine Inlet α = 15°

DATE: Sept. 24, 1985, Tuesday

P_{BAR} = 14.34 PSIA

DYE CONCENTRATION = 0.0005 grm/cc

PSYCHROMETER READINGS = ___ °F DB

= 67.0 °F WB

RELATIVE HUMIDITY = ___ PERCENT

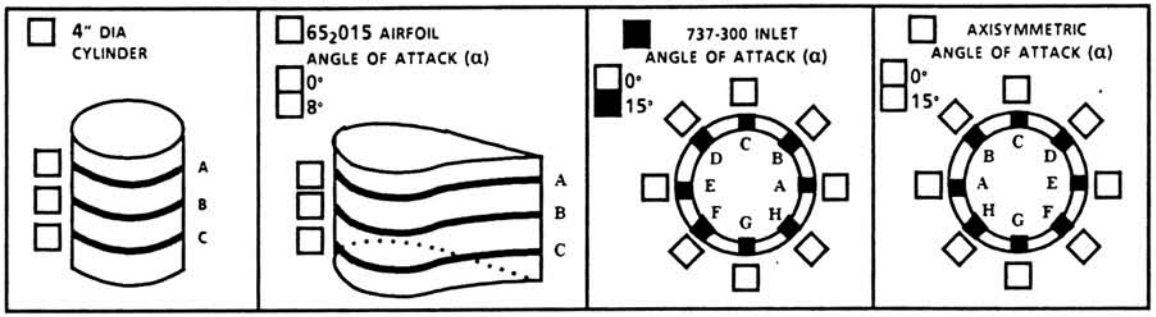

RUN NO.	RUN ID	TUNNEL CONDITIONS					SPRAY CONDITIONS												TIME (SEC.)		REMARKS
							SUPPLY PRESSURE			PLENUM PRESSURE		TRANSDUCER READINGS									
		AIR TEMP (°F)	I.A.S. (MPH)	P_∞ (PSIA)	Q (IN H_2O)	DEW POINT (°F)	$\frac{P_{AIR}}{P_{H_2O}}$	P_{AIR} (PSIG)	P_{H_2O} (PSIG)	P_{AIR} (PSIG)	P_{H_2O} (PSIG)	tank pres.		mass flow volts	cap-ture ratio	mass flow lb/s		SPRAY (sec)	REF (sec)	
19	19-737-15	46.33	165	13.84	13.90	34.9	0.80	80	100	80	106	98		5.2	1	22.96		3.19	N/A	High Suction α = 15°
20	20-737-15	53.00	165	13.85	13.90	32.9	0.80	80	100	80	106	98		5.2	1	22.96		3.19	N.A	High Suction α = 15°
21	21-737-15	46.67	165	13.85	13.90	35.1	0.80	80	100	80	106	97		5.2	1	22 96		3.19	N/A	High Suction α = 15°
22	22-737-15	47.33	165	13.85	13.80	34.1	0.80	80	100	80	106	97		3.9	.75	17.20		3.19	N A	Low Suction α = 15°
23	23-737-15	50.33	165	13.86	13.80	34.6	0.80	80	100	80	106	98		3.9	.75	17.20		3.19	N A	Low Suction α = 15°
24	24-737-15	47.00	165	13.87	13.80	36.0	0.80	80	100	80	106	97		3.9	.75	17.20		3.19	N.A	Low Suction α = 15°
25	25-737-15	53.00	165	13.86	13.90	34.4	0.80	80	100	80	106	98		2.6	.50	11.47		3.19	N/A	Lowest Suction α = 15°
26	26-737-15	48.00	165	13.87	13.90	34.9	0.80	80	100	80	106	97		2.6	.50	11.47		3.19	N/A	Lowest Suction α = 15°
27	27-737-15	48.33	165	13.88	13.70	32.4	0.80	80	100	80	106	97		2.6	.50	11.47		3.19	N.A	Lowest Suction α = 15°

TABLE – II

■ 4-Blade Reference Collector Calibration

DATE: Sept. 25, 1985, Wednesday

P_{BAR} = 14.40 PSIA

DYE CONCENTRATION = 0.0005 grm/cc

PSYCHROMETER READINGS = ___ °F DB

= ___ °F WB

RELATIVE HUMIDITY = ___ PERCENT

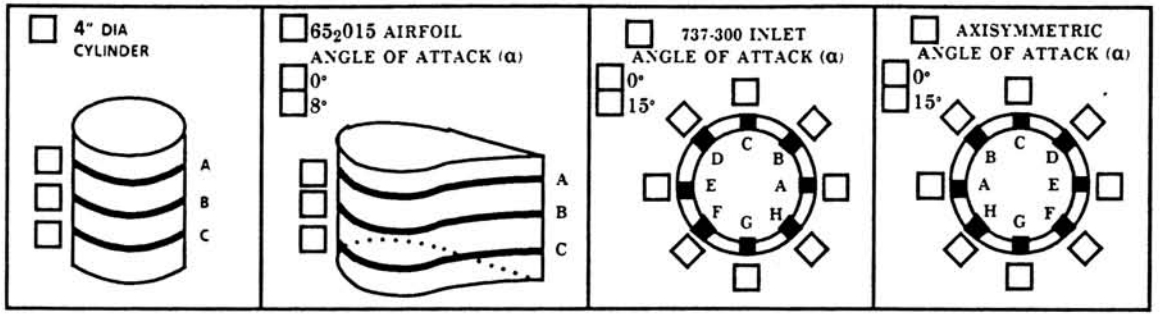

RUN NO.	RUN ID	TUNNEL CONDITIONS					SPRAY CONDITIONS											TIME (SEC.)		REMARKS
							SUPPLY PRESSURE			PLENUM PRESSURE		TRANSDUCER READINGS								
		AIR TEMP (°F)	I.A.S. (MPH)	P_∞ (PSIA)	Q (IN H_2O)	DEW POINT (°F)	$\frac{P_{AIR}}{P_{H_2O}}$	P_{AIR} (PSIG)	P_{H_2O} (PSIG)	P_{AIR} (PSIG)	P_{H_2O} (PSIG)	tank pres.	2	4	5	7	8	SPRAY (sec)	REF (sec)	
1	COL-1	43.00	165	13.845	13.70	33.2	0.65	65	100	65	106	94						2.68	N/A	for α = 15° engine inlet
2	COL-2	43.33	165	13.84	13.80	32.6	0.65	65	100	65	106	96						2.68	N/A	for α = 15° engine inlet
3	COL-3	45.66	165	13.85	13.70	32.3	0.65	65	100	65	106	96						2.68	N/A	for α = 15° engine inlet
4	COL-4	45.33	165	13.85	13.60	32.1	0.65	65	100	65	106	96						3.17	N/A	for α = 15° engine inlet
5	COL-5	46.33	165	13.84	13.60	32.1	0.65	65	100	65	106	96						3.17	N/A	for α = 15° engine inlet
6	COL-6	47.00	165	13.84	13.90	32.2	0.65	65	100	65	106	96						3.17	N/A	for α = 15° engine inlet
7	COL-7	45.66	165	13.84	13 90	32.5	0.65	65	100	65	106	96						3.17	N A	for α = 15° engine inlet
8	COL-8	44.33	165	13.84	13.85	32.8	0.80	80	100	80	106	97						3.17	N/A	for α = 15° engine inlet
9	COL-9	45.00	165	13.84	13 80	33.3	0 80	80	100	80	106	96						3.17	N/A	for α = 15° engine inlet
10	COL-10	44.33	165	13.84	13.80	33.3	0.80	80	100	80	106	96						3.17	N A	for α = 15° engine inlet
11	COL-11	44.00	165	13.83	14.00	33.4	0.80	80	100	80	106	96						3.66	N A	for α = 15° engine inlet
12	COL-12	43.00	165	13.83	13 80	33.3	0.80	80	100	80	106	96						3.66	N/A	for α = 15° engine inlet

TABLE – II

■ 4-Blade Reference Collector Calibration (cont.)

DATE: Sept. 25, 1985, Wednesday

P_{BAR} = 14.40 PSIA

DYE CONCENTRATION = 0.0005 grm/cc

PSYCHROMETER READINGS = ___ °F DB

= ___ °F WB

RELATIVE HUMIDITY = ___ PERCENT

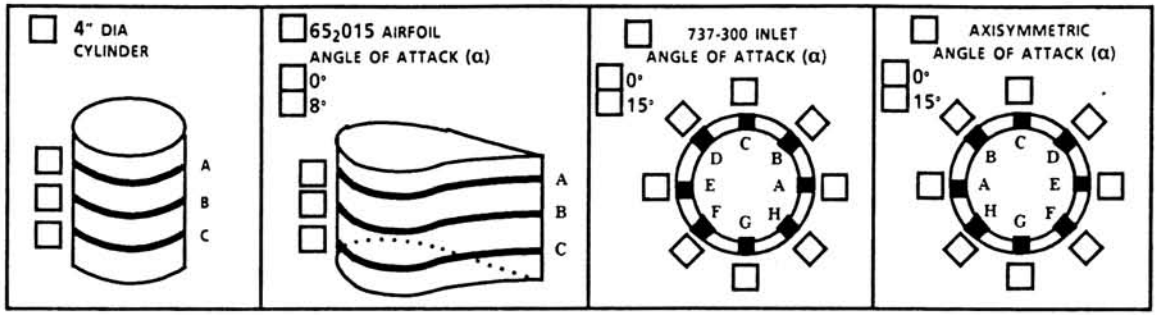

RUN NO.	RUN ID	TUNNEL CONDITIONS					SPRAY CONDITIONS											TIME (SEC.)		REMARKS
							SUPPLY PRESSURE			PLENUM PRESSURE		TRANSDUCER READINGS								
		AIR TEMP (°F)	I.A.S. (MPH)	P_∞ (PSIA)	Q (IN H_2O)	DEW POINT (°F)	$\frac{P_{AIR}}{P_{H_2O}}$	P_{AIR} (PSIG)	P_{H_2O} (PSIG)	P_{AIR} (PSIG)	P_{H_2O} (PSIG)	tank pres.	2	4	5	7	8	SPRAY (sec)	REF (sec)	
13	COL-13	44.66	165	13.83	13.80	33.0	0.65	65	100	65	106	97						2.68	N/A	for α = 0° engine inlet
14	COL-14	43 66	165	13.84	13.80	32.9	0.65	65	100	65	106	95						2.68	N/A	for α = 0° engine inlet
15	COL-15	44.00	165	13.83	13.90	33.0	0.65	65	100	65	106	96						2.68	N/A	for α = 0° engine inlet
16	COL-16	46.00	165	13.82	13.70	33.0	0.65	65	100	65	106	97						3.18	N/A	for α = 0° engine inlet
17	COL-17	45.66	165	13.80	13.80	33.0	0.65	65	100	65	106	97						3.18	N/A	for α = 0° engine inlet
18	COL-18	44.00	165	13.80	13.80	33.0	0.65	65	100	65	106	97						3.18	N/A	for α = 0° engine inlet
19	COL-19	46.66	165	13.80	13.80	33.2	0.80	80	100	80	106	96						3.18	N/A	for α = 0° engine inlet
20	COL-20	43 66	165	13 80	13.90	33 0	0 80	80	100	80	106	96						3.18	N/A	for α = 0° engine inlet
21	COL-21	43 66	165	13.81	13.90	32.7	0.80	80	100	80	106	96						3.18	N/A	for α = 0° engine inlet
22	COL-22	43.00	165	13.82	13.90	32.6	0.80	80	100	80	106	96						3.66	N/A	for α = 0° engine inlet
23	COL-23	44.33	165	13.81	13.90	32.4	0.80	80	100	80	106	96						3.66	N/A	for α = 0° engine inlet
24	COL-24	44.00	165	13.82	13.80	32.3	0.80	80	100	80	106	96						3 66	N/A	for α = 0° engine inlet

TABLE – II

■ Spray Uniformity Test, 2 Droplet Sizes

DATE: Sept. 25, 1985, Wednesday

P_{BAR} = ___ PSIA

DYE CONCENTRATION = ___ grm/cc

PSYCHROMETER READINGS = ___ °F DB

= ___ °F WB

RELATIVE HUMIDITY = ___ PERCENT

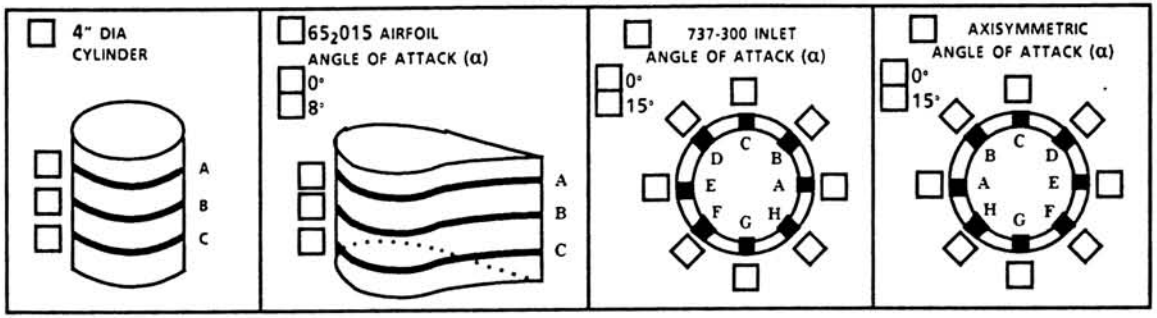

RUN NO.	RUN ID	TUNNEL CONDITIONS					SPRAY CONDITIONS											TIME (SEC.)		REMARKS
							SUPPLY PRESSURE			PLENUM PRESSURE		TRANSDUCER READINGS								
		AIR TEMP (°F)	I.A.S. (MPH)	P_∞ (PSIA)	Q (IN H_2O)	DEW POINT (°F)	$\frac{P_{AIR}}{P_{H_2O}}$	P_{AIR} (PSIG)	P_{H_2O} (PSIG)	P_{AIR} (PSIG)	P_{H_2O} (PSIG)	tank pres.	2	4	5	7	8	SPRAY (sec)	REF (sec)	
1	UNI-1	47.00	165	13.77	14.00	34.9	0.80	80	100	80	106	97						3.16	N/A	35 Blotter Strips
2	UNI-2	46.33	165	13.76	14.00	36.3	0.80	80	100	80	106	97						3.16	N/A	"
3	UNI-3	44.33	165	13.76	13.70	36.8	0.65	65	100	65	106	96						2 68	N/A	"
4	UNI-4	46.66	165	13.74	14.00	36.6	0.65	65	100	65	106	96						2.68	N A	35 Blotter Strips

TABLE – II

65_2015 Airfoil

DATE: Sept. 26, 1985, Thursday

P_{BAR} = 14.26 PSIA

DYE CONCENTRATION = 0.0005 grm/cc

PSYCHROMETER READINGS = ___ °F DB

= 67.00 °F WB

RELATIVE HUMIDITY = ___ PERCENT

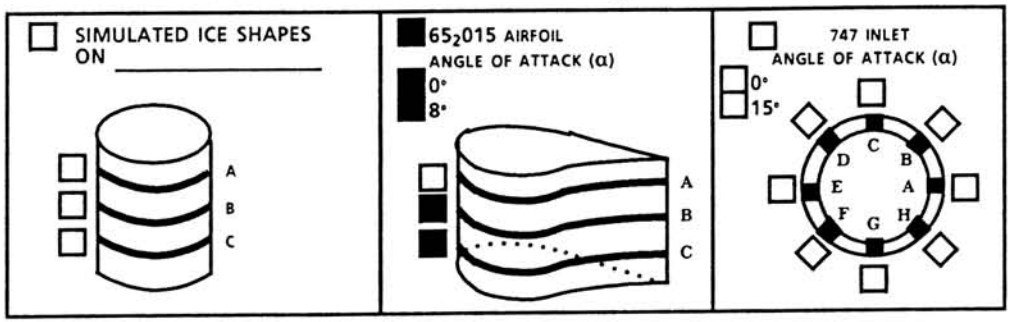

RUN NO.	RUN ID	TUNNEL CONDITIONS					SPRAY CONDITIONS												TIME (SEC.)		REMARKS
							SUPPLY PRESSURE			PLENUM PRESSURE		TRANSDUCER READINGS									
		AIR TEMP (°F)	I.A.S. (MPH)	P_∞ (PSIA)	Q (IN H_2O)	DEW POINT (°F)	$\frac{P_{AIR}}{P_{H_2O}}$	P_{AIR} (PSIG)	P_{H_2O} (PSIG)	P_{AIR} (PSIG)	P_{H_2O} (PSIG)	tank pres.	2	1	5	7	8	SPRAY (sec)	REF (sec)	
1	1-015-0	45.00	175	13.71	15.4	33.1	0.65	65	100	65	106	96						2.68	N/A	α = 0
2	2-015-0	51.00	175	13.72	15.5	34.8	0.65	65	100	65	106	96						2.68	N/A	α = 0
3	3-015-0	48.33	175	13.71	15.6	36.2	0.65	65	100	65	106	97						2.68	N/A	α = 0
4	4-015-0	50.66	175	13.71	15.8	37.0	0.80	80	100	80	106	96						3.18	N/A	α = 0
5	5-015-0	49.00	175	13.71	15.8	37.2	0.80	80	100	80	106	95						3.18	N/A	α = 0
6	6-015-0	47.30	175	13.70	15.7	37.2	0.80	80	100	80	106	96						3.18	N A	α = 0
7	7-015-8	49.00	175	13.72	15.8	37.8	0.65	65	100	65	106	96						2.68	N/A	α = 8
8	8-015-8	47.33	175	13.72	15.5	38.1	0.65	65	100	65	106	96						2.68	N/A	α = 8
9	9-015-8	50.33	175	13.72	15.5	38.0	0.65	65	100	65	106	96						2.68	N A	α = 8
10	10-015-8	48.00	175	13.73	15.4	38.0	0.80	80	100	80	106	96						3.18	N/A	α = 8
11	11-015-8	49.00	175	13.72	15.8	37.9	0.80	80	100	80	106	96						3.18	N/A	α = 8
12	12-015-8	50.66	175	13.72	15.8	37.9	0.80	80	100	80	106	96						3.18	N A	α = 8

TABLE – II

Supercritical Airfoil

DATE: Sept. 26, 1985, Thursday

P_{BAR} = 14.26 PSIA

DYE CONCENTRATION = 0.0005 grm/cc

PSYCHROMETER READINGS = ___ °F DB

= 67.00 °F WB

RELATIVE HUMIDITY = ___ PERCENT

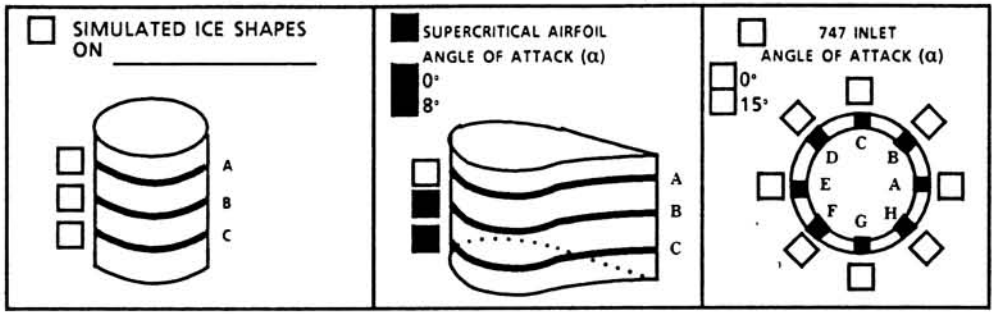

RUN NO.	RUN ID	TUNNEL CONDITIONS					SPRAY CONDITIONS											TIME (SEC.)		REMARKS
							SUPPLY PRESSURE			PLENUM PRESSURE		TRANSDUCER READINGS								
		AIR TEMP (°F)	I.A.S. (MPH)	P_x (PSIA)	Q (IN H_2O)	DEW POINT (°F)	$\frac{P_{AIR}}{P_{H_2O}}$	P_{AIR} (PSIG)	P_{H_2O} (PSIG)	P_{AIR} (PSIG)	P_{H_2O} (PSIG)	tank pres.	2	1	5	7	8	SPRAY (sec)	REF (sec)	
1	1-SUP-0	45.66	175	13.69	15.4	45.6	0.65	65	100	65	106	95						2.68	N/A	α = 0
2	2-SUP-0	46.66	175	13.70	15.6	44.7	0.65	65	100	65	106	95						2 68	N A	α = 0
3	3-SUP-0	48.00	175	13.69	15.6	44.3	0.65	65	100	65	106	96						2 68	N A	α = 0
4	4-SUP-0	49.67	175	13.70	15.5	43.1	0.80	80	100	80	106	96						3.18	N A	α = 0
5	5-SUP-0	49.33	175	13.68	15.7	42.4	0.80	80	100	82	106	96						3.18	N/A	α = 0
6	6-SUP-0	49.66	175	13.69	15.5	42.4	0.80	80	100	78	106	96						3.18	N A	α = 0
7	7-SUP-8	50.33	175	13.72	15.1	42.3	0.65	65	100	65	106	96						2.68	N/A	α = 8
8	8-SUP-8	49.33	175	13.71	15.4	42.2	0.65	65	100	65	106	96						2.68	N/A	α = 8
9	9-SUP-8	49.33	175	13.71	15.6	41.9	0.65	65	100	65	106	96						2.68	N A	α = 8
10	10-SUP-8	48.00	175	13.72	15.3	41.5	0.80	80	100	82	106	96						3.18	N/A	α = 8
11	11-SUP-8	51.33	175	13.72	15.5	41.2	0.80	80	100	78	106	96						3.18	N/A	α = 8
12	12-SUP-8	50.00	175	13.71	15.7	41.0	0.80	80	100	81	106	95						3.18	N A	α = 8
4A	4A-SUP-0	49.00	175	13.67	15.4	42.4	0 80	80	100	80	106	96						3.18	N A	α = 0

TABLE – II

Ice Shapes

DATE: Sept. 26, 1985, Thursday

P_{BAR} = 14.26 PSIA

DYE CONCENTRATION = 0.0005 grm/cc

PSYCHROMETER READINGS = ___ °F DB

= 67.00 °F WB

RELATIVE HUMIDITY = ___ PERCENT

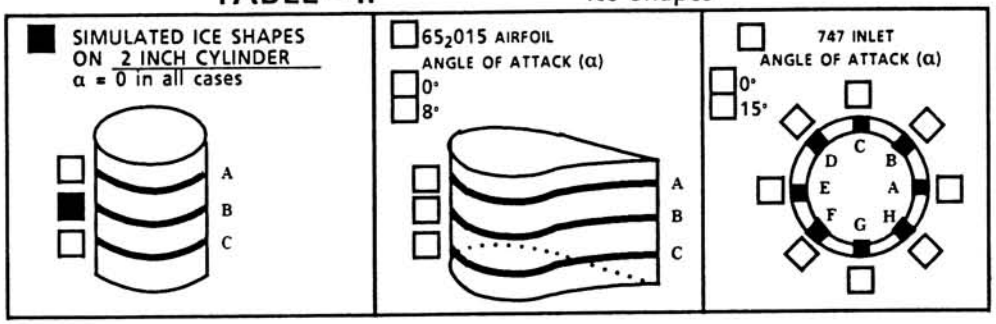

RUN NO.	RUN ID	TUNNEL CONDITIONS					SPRAY CONDITIONS											TIME (SEC.)		REMARKS
							SUPPLY PRESSURE			PLENUM PRESSURE		TRANSDUCER READINGS								
		AIR TEMP (°F)	I.A.S. (MPH)	P_∞ (PSIA)	Q (IN H_2O)	DEW POINT (°F)	$\frac{P_{AIR}}{P_{H_2O}}$	P_{AIR} (PSIG)	P_{H_2O} (PSIG)	P_{AIR} (PSIG)	P_{H_2O} (PSIG)	tank pres.	2	1	5	7	8	SPRAY (sec)	REF (sec)	
1	1-SG	46.30	175	13.71	15.5	40.2	0.65	65	100	65	106	94						2.68	N/A	Small glaze ice
2	2-SG	48.00	175	13.71	15.7	40.0	0.65	65	100	65	106	96						2.68	N.A	Small glaze ice
3	1-LG	51.33	175	13.72	15.5	39.3	0.65	65	100	65	106	96						2.68	N.A	Large glaze ice
4	1-RIME	51.00	175	13.71	15.6	39.9	0.65	65	100	65	106	96						2.68	N A	Rime ice
5	2-LG	49 66	175	13.70	15.6	40.2	0 65	65	100	65	106	95						2.68	N A	Large glaze ice
6	2-RIME	47.66	175	13.70	15.6	40.0	0.65	65	100	65	106	96						2.68	N'A	Rime ice
7	Olsen-1-SG	44.66	130	13.96	8.7	39.6	64 108	64	108	64	114	101						2.18	N A	Small glaze ice
8	Olsen-1-LG	48.00	130	13.96	8.8	39.2	64 108	64	108	64	114	104						2.18	N.A	Large glaze ice
9	Olsen-1-																			
	2' cylinder	48.00	130	13.96	8.7	39.3	64 108	64	108	64	114	104						2.18	N/A	2' cylinder
10	Olsen Rime	46.33	130	13 95	8.8	38.5	67.78	67	78	67	84	75						3.19	N/A	Olsen Rime
11	Olsen-2-																			
	2' cylinder	45.33	130	13.96	8.7	38.8	67 78	67	78	67	84	75						3.19	N/A	Olsen cylinder 2

APPENDIX H: REDUCTION OF TUNNEL CONDITIONS AND AERODYNAMIC DATA

MEASURED QUANTITIES

1) T ~ Temperature (°F)
2) $P_{s\infty}$ ~ Tunnel Static Pressure (PSIA)
3) Q ~ Tunnel Dynamic Pressure (in. H_2O)

CONSTANTS

Specific Heat Ratio: $\gamma = 1.4$

Gas constant: $R = 53.35241 \quad \dfrac{ft - lb_f}{lb_m - {}^\circ R}$

CONVERSION FACTORS

$$c = 27.678 \quad \frac{in\ H_2O}{lb_f / in^2}\ ; \quad g_c = 32.17405 \quad \frac{ft - lb_m}{lb_f - sec^2}$$

DATA REDUCTION

Symbols, in general, are defined in Appendix I.

a) Compute Air Density

$$\rho = \frac{P_{s\infty} * 144}{R * (T + 460)}\ lb_m / ft^3$$

b) Compute Mach Number (TRUE)

$$\frac{P_{s\infty}}{P_\infty} = \frac{1}{\left(1 + \dfrac{\gamma - 1}{2} M^2\right)^{\frac{\gamma}{(\gamma-1)}}}, \quad P_\infty = \text{Total Pressure}$$

Solving,

$$M^2 = \frac{2}{\gamma - 1}\left|\left(\frac{P_\infty}{P_{s\infty}}\right)^{\frac{\gamma-1}{\gamma}} - 1\right|$$

$$= \frac{2}{\gamma - 1}\left|\left(\frac{P_\infty - P_{s\infty} + P_{s\infty}}{P_{s\infty}}\right)^{\frac{\gamma-1}{\gamma}} - 1\right|$$

$$= \frac{2}{\gamma - 1}\left|\left(\frac{P_\infty - P_{s\infty}}{P_{s\infty}} + 1\right)^{\frac{\gamma-1}{\gamma}} - 1\right|$$

$$M = \sqrt{\frac{2}{\gamma - 1}\left[\left(\frac{Q}{cP_{s\infty}} + 1\right)^{\frac{\gamma-1}{\gamma}} - 1\right]}$$

c) Compute True Air Speed

$$V = \sqrt{\gamma g_c R(T + 460)}\ M$$

$$= 49.022325 \sqrt{(T + 460)}\ M \ \text{ft/sec}$$

$$\text{True Air Speed} = V\left(\frac{60}{88}\right) \text{ mph}$$

ENGINE INLET

Calculate surface Mach number from surface static pressure:

$$M_{sur} = \sqrt{\frac{2}{\gamma - 1}\left[\left(\frac{P_{\infty}}{P_s}\right)^{\frac{\gamma-1}{\gamma}} - 1\right]}$$

where,

$$P_{\infty} = P_s + \frac{Q}{27.678} \text{ (psia)}$$

P_s = static pressure at inlet surface (psia)

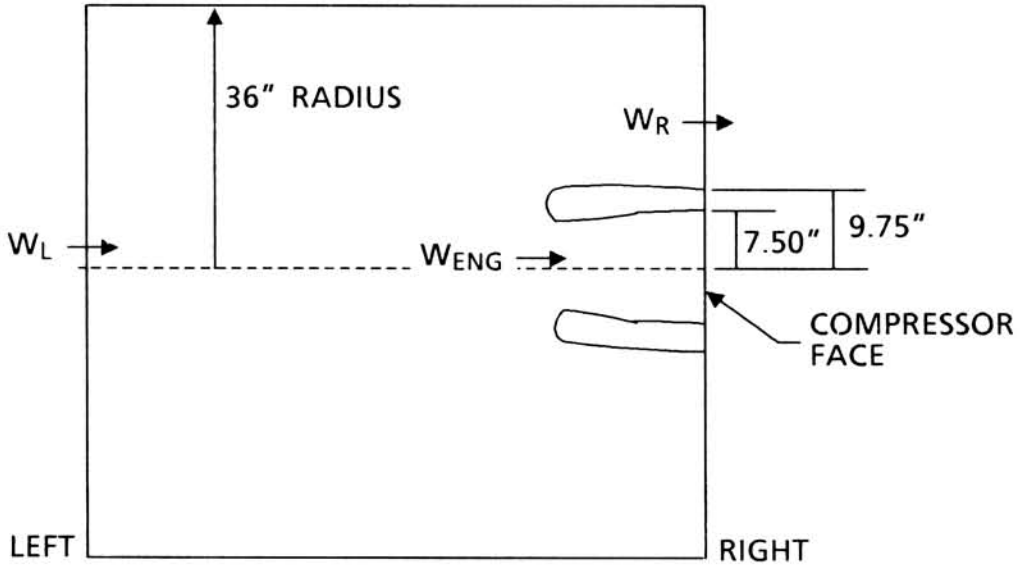

ENGINE INLET ANALYSIS COMPUTER PROGRAM INPUT GENERATION (FULL POTENTIAL)

FIGURE H.1

BOUNDARY CONDITIONS FOR ENGINE INLET FLOW FIELD ANALYSES

1) Area at left boundary

$$A_L = \pi r_o^2 = \pi \times 36^2 = 4071.50408 \text{ in}^2$$

2) Area at right boundary

$$A_R = \pi(r_o^2 - r_i^2) = \pi(36^2 - 9.75^2) = 3772.8564 \text{ in}^2$$

3) Compute mass flow at left boundary (W_L)

a) $$\rho_L = \frac{P_{s\infty} \times 144}{R \times (T + 460)} \Big| - \Big| \text{LBM/FT}^3$$

b) $$M_L = \sqrt{\frac{2}{\gamma - 1} \left| \left\{ \frac{Q}{cP_{s\infty}} + 1 \right\}^{\frac{\gamma - 1}{\gamma}} - 1 \right|}$$

c) $$V_L = 49.022325 \sqrt{(T + 460)}\, M_L \Big| = \Big| \text{FT/SEC}$$

d) $$W_L = \rho_L \times V_L \times A_L / 144.0 \Big| = \Big| \text{LBM/SEC}$$

4) Compute total pressure at the left boundary

$$P_{TL} = P_{s\infty} \left| 1 + \frac{\gamma - 1}{2} M_L^2 \right|^{\frac{\gamma}{\gamma - 1}}$$

5) Compute the conditions at the right boundary

a) $$W_R = W_L - W_{ENG}$$

b) $$P_{TR} = P_{TL}$$

c) $$T_{TR} = 460 + T \text{ (Measured at its plenum chamber)}$$

d) $$\frac{W_R \sqrt{T_{TR}}}{A_R P_{TR}} = \frac{M_R \sqrt{\frac{\gamma \times g_c}{R}}}{\left(1 + \frac{\gamma - 1}{2} M_R^2\right)^{(\gamma + 1)/\{2(\gamma - 1)\}}}, \quad W_R \Big| = \Big| \frac{\text{LBM}}{\text{SEC}}$$

Solve iteratively for M_R

e) $$P_{SR} = \frac{P_{TR}}{\left| 1 + \frac{\gamma - 1}{2} M_R^2 \right|^{\frac{\gamma}{\gamma - 1}}}$$

f) $$T_{SR} = \frac{T_{TR}}{\left| 1 + \frac{\gamma - 1}{2} M_R^2 \right|}$$

g) $$V_R = 49.022325 \sqrt{T_{SR}}\, M_R$$

6) Compressor Face Mach Number
Area of compressor face = A_c = 176.714587 in^2
Computer program calculated mass flow parameter (see examples of output and computer code at end of this appendix)

$$W_{ENG} = \rho_{CF} A_{CF} V_{CF}, \quad A_{CF}| = |IN^2$$

$$= \frac{P_{SCF} \times A_{CF}}{RT_{SCF}} M_{CF} \sqrt{\gamma g_C R T_{SCF}} \qquad \text{(1)}$$

$$\frac{T_{SR}}{T_{SCF}} = \frac{\left(1 + \frac{\gamma - 1}{2} M_{CF}^2\right)}{\left(1 + \frac{\gamma - 1}{2} M_R^2\right)}$$

$$\frac{1}{\sqrt{T_{SCF}}} = \frac{\left(1 + \frac{\gamma - 1}{2} M_{CF}^2\right)^{1/2}}{\left(1 + \frac{\gamma - 1}{2} M_R^2\right)^{1/2}} \frac{1}{\sqrt{T_{SR}}}$$

$$= \frac{\left(1 + \frac{\gamma - 1}{2} M_{CF}^2\right)^{1/2}}{\left(1 + \frac{\gamma - 1}{2} M_R^2\right)^{1/2}} \frac{1}{\sqrt{T_{SR}}} \frac{1}{M_R} \frac{V_R}{\sqrt{\gamma R g_c T_{SR}}} \qquad \text{(2)}$$

$$\frac{P_{SCF}}{P_{SR}} = \frac{\left(1 + \frac{\gamma - 1}{2} M_R^2\right)^{\gamma/(\gamma-1)}}{\left(1 + \frac{\gamma - 1}{2} M_{CF}^2\right)^{\gamma/(\gamma-1)}} \qquad \text{(3)}$$

Substituting (2) and (3) in (1)

$$W_{ENG} = \frac{A_{CF} M_{CF}}{M_R} \frac{1}{R} \frac{V_R P_{SR}}{T_{SR}} \frac{\left(1 + \frac{\gamma - 1}{2} M_R^2\right)^{\frac{\gamma}{\gamma-1} - \frac{1}{2}}}{\left(1 + \frac{\gamma - 1}{2} M_{CF}^2\right)^{\frac{\gamma}{\gamma-1} - \frac{1}{2}}}$$

$$= \frac{1}{R} \frac{P_{SR} V_R}{T_{SR}} \left| \frac{A_{CF} M_{CF}}{M_R} \left(\frac{1 + \frac{\gamma - 1}{2} M_R^2}{1 + \frac{\gamma - 1}{2} M_{CF}^2} \right)^{\frac{\gamma+1}{2(\gamma-1)}} \right| \qquad \text{(4)}$$

$$= \frac{1}{R} \frac{P_{SR} V_R}{T_{SR}} \left| \dot{m}_{P465C} \right|$$

NOTE: $\dot{m}_{P465C}$, as indicated above, is the parameter commonly checked by Reference 25 program users to check on program convergence and/or accuracy.

```
      IMPLICIT REAL*8 (A-H,O-Z)
      DIMENSION ALPHA(27),WENG(27),TEMP(27),PSINF(27),QH2O(27),
     +        RHO(27),ZMACH(27),VINF(27),WL(27),WR(27),PSR(27),TSR(27),
     +        ZMACHR(27),VINFR(27),ZMACHCF(27),P465M(27),WENGC(27)
      DATA ALPHA/0.0,0.0,0.0,0.0,0.0,0.0,0.0,0.0,0.0,0.0,0.0,0.0,0.0,
     +           15.0,15.0,15.0,15.0,15.0,15.0,15.0,15.0,15.0,15.0,
     +           15.0,15.0,15.0,15.0,15.0/
      DATA WENG/22.96,22.96,22.96,17.2,17.2,17.2,22.96,22.96,22.96,
     +          17.2,17.2,17.2,22.96,22.96,22.96,17.2,17.2,17.2,
     +          22.96,22.96,22.96,17.2,17.2,17.2,11.465,11.465,11.465/
      DATA TEMP/59.33,58.66,59.00,55.67,59.67,55.00,60.67,57.33,
     +          61.33,56.67,62.33,53.67,59.33,53.00,55.33,59.33,
     +          56.33,55.67,46.33,53.00,46.67,47.33,50.33,47.00,
     +          53.00,48.00,48.33/
      DATA PSINF/13.73,13.74,13.73,13.73,13.72,13.72,13.73,13.73,
     +           13.73,13.73,13.73,13.73,13.75,13.75,13.74,13.74,
     +           13.74,13.74,13.84,13.85,13.85,13.85,13.86,13.87,
     +           13.86,13.87,13.88/
      DATA QH2O/14.0,14.1,13.8,13.8,13.9,14.0,14.0,14.0,13.9,
     +          13.9,13.9,13.8,13.8,13.9,13.8,13.9,14.0,13.9,
     +          13.9,13.9,13.9,13.8,13.8,13.8,13.9,13.9,13.7/
      WRITE(6,100)
  100 FORMAT(15X,'737-300 ENGINE INLET MODEL, SEPT 23,1985(MONDAY)-',
     1 /,25X,'SEPT 24,1985 (TUESDAY) TEST DATA'/)
      WRITE(6,200)
  200 FORMAT(6X,'NO',2X,'ALPHA',2X,'WENG',5X,'TINF',3X,'PINF',3X,'QH2O'
     1,3X,'RHOINF',4X,'VINF',4X,'MPH',4X,'MACHL')
C
      G=1.4
      R=53.35241
      C=27.678
      GC=32.17405
      DO 10 I=1,27
      RHO(I)=PSINF(I)*144.0/R/(460.0+TEMP(I))
      ZMACH(I)=DSQRT(2./(G-1.)*((QH2O(I)/C/PSINF(I)+1.)**((G-1.)/G)-1.))
      VINF(I)=ZMACH(I)*49.022325*DSQRT(460.0+TEMP(I))
      ZMPH=VINF(I)*60.0/88.0
   10 WRITE(6,300)I,ALPHA(I),WENG(I),TEMP(I),PSINF(I),QH2O(I),RHO(I),
     1 VINF(I),ZMPH,ZMACH(I)
  300 FORMAT(5X,I3,1X,F5.1,2X,F6.2,2X,F6.2,1X,F6.2,1X,F6.2,1X,F9.6,1X,
     1 F7.3,1X,F7.3,1X,F7.4)
C
C     LEFT BOUNDARY DATA
C
      AL = 4071.50408
C
C     RIGHT BOUNDARY DATA
C
      AR=3756.71620
C
      WRITE(6,400)
  400 FORMAT(/6X,'NO',2X,'  WL ',2X,' WR ',5X,'TSR ',3X,'PSR',3X,'VINFR',
     1 4X,'MACHR',2X,'WENGC',3X,'P465M',4X,'MACHCF')
      DO 20 I=1,27
      WL(I) = RHO(I)*VINF(I)*AL/144.0
      WR(I) = WL(I) - WENG(I)
      PTL=PSINF(I)*(1.0+0.2*ZMACH(I)**2)**3.5
      TTR=460.0+TEMP(I)
      WFR=WR(I)*DSQRT(TTR)/AR/PTL
      CALL WFT(WR(I)*60.0,WFR,AMACH,PRR,TR,DUM)
```

```
      ZMACHR(I) = AMACH
      PSR(I) = PTL/PRR
      TSR(I) = TTR/TR
      VINFR(I) = ZMACHR(I)*49.022325*DSQRT(TSR(I))
C     WRITE(6,500)I,WL(I),WR(I),TSR(I),PSR(I),VINFR(I),ZMACHR(I)
   20 CONTINUE
  500 FORMAT(4X,I3,5X,F6.2,6X,F6.2,6X,F6.2,6X,F6.2,7X,F6.2,4X,F7.4)
C
C     COMPRESSOR FACE
C
      AC =  155.313743
C
C     WRITE(6,600)
  600 FORMAT(6X,'NO',5X,'WENGC',6X,'P465M',9X,'MACHCF')
      DO 40 I=1,27
C
      KOUNT=0
      XL = 0.05
      XH = 0.40
   30 CONTINUE
      KOUNT=KOUNT+1
      ZMACHCF(I)=(XL+XH)/2.0
      P465M(I) = AC*ZMACHCF(I)/ZMACHR(I)*((1.0+0.2*ZMACHR(I)**2)/
     1                                    (1.0+0.2*ZMACHCF(I)**2))**3.0
      WENGC(I) = 1.0/R*PSR(I)*VINFR(I)/TSR(I)*P465M(I)
      DB=DABS(WENGC(I)-WENG(I))
      IF(DB .LT. 0.00001 .OR. KOUNT .GT. 30)GO TO 35
      IF(WENGC(I) .LT. WENG(I)) XL = ZMACHCF(I)
      IF(WENGC(I) .GT. WENG(I)) XH = ZMACHCF(I)
      GO TO 30
   35 WRITE(6,700)I,WL(I),WR(I),TSR(I),PSR(I),VINFR(I),ZMACHR(I),
     + WENGC(I),P465M(I),ZMACHCF(I)
   40 CONTINUE
  700 FORMAT(5X,I3,1X,F6.2,2X,F6.2,2X,F6.2,F6.2,2X,F6.2,1X,F7.4,
     + 1X,F6.2,3X,F6.2,2X,F7.4)
      STOP
      END
```

737-300 ENGINE INLET MODEL, SEPT 23,1985(MONDAY)- SEPT 24,1985 (TUESDAY) TEST D
ATA

NO	ALPHA	WENG	TINF	PINF	QH2O	RHOINF
VINF	MPH	MACHL				
1	0.0	22.96	59.33	13.73	14.00	0.071357
254.631	173.612	0.2279				
2	0.0	22.96	58.66	13.74	14.10	0.071501
255.271	174.048	0.2286				
3	0.0	22.96	59.00	13.73	13.80	0.071402
252.749	172.329	0.2263				
4	0.0	17.20	55.67	13.73	13.80	0.071863
251.936	171.775	0.2263				
5	0.0	17.20	59.67	13.72	13.90	0.071258
253.906	173.118	0.2272				
6	0.0	17.20	55.00	13.72	14.00	0.071904
253.659	172.949	0.2280				
7	0.0	22.96	60.67	13.73	14.00	0.071173
254.959	173.836	0.2279				
8	0.0	22.96	57.33	13.73	14.00	0.071633
254.140	173.277	0.2279				
9	0.0	22.96	61.33	13.73	13.90	0.071083
254.220	173.332	0.2271				
10	0.0	17.20	56.67	13.73	13.90	0.071724
253.081	172.555	0.2271				
11	0.0	17.20	62.33	13.73	13.90	0.070947
254.463	173.498	0.2271				
12	0.0	17.20	53.67	13.73	13.80	0.072143
251.447	171.441	0.2263				
13	15.0	22.96	59.33	13.75	13.80	0.071461
252.647	172.259	0.2262				
14	15.0	22.96	53.00	13.75	13.90	0.072343
251.995	171.818	0.2270				
15	15.0	22.96	55.33	13.74	13.80	0.071963
251.763	171.656	0.2262				
16	15.0	17.20	59.33	13.74	13.90	0.071409
253.640	172.937	0.2270				
17	15.0	17.20	56.33	13.74	14.00	0.071824
253.803	173.048	0.2278				
18	15.0	17.20	55.67	13.74	13.90	0.071916
252.745	172.326	0.2270				
19	15.0	22.96	46.33	13.84	13.90	0.073775
249.551	170.148	0.2262				
20	15.0	22.96	53.00	13.85	13.90	0.072869
251.100	171.204	0.2261				
21	15.0	22.96	46.67	13.85	13.90	0.073779
249.546	170.145	0.2261				
22	15.0	17.20	47.33	13.85	13.80	0.073683
248.819	169.650	0.2253				
23	15.0	17.20	50.33	13.86	13.80	0.073303
249.465	170.090	0.2253				
24	15.0	17.20	47.00	13.87	13.80	0.073837
248.561	169.474	0.2252				
25	15.0	11.47	53.00	13.86	13.90	0.072921
251.010	171.143	0.2261				
26	15.0	11.47	48.00	13.87	13.90	0.073692
249.695	170.247	0.2260				
27	15.0	11.47	48.33	13.88	13.70	0.073697
247.907	169.027	0.2243				

NO	WL	WR	TSR	PSR	VINFR	MACHR
1	513.74	490.78	513.65	13.70	261.36	0.2352
2	516.07	493.11	512.94	13.71	262.06	0.2360
3	510.26	487.30	513.40	13.70	259.37	0.2335
4	511.91	494.71	509.97	13.69	261.81	0.2365
5	511.56	494.36	513.88	13.68	263.83	0.2374
6	515.70	498.50	509.22	13.67	263.64	0.2383

7	513.07	490.11	514.97	13.70	261.68	0.2352
8	514.73	491.77	511.67	13.70	260.88	0.2353
9	510.94	487.98	515.67	13.70	260.88	0.2344
10	513.24	496.04	510.91	13.68	263.01	0.2374
11	510.45	493.25	516.51	13.69	264.39	0.2373
12	512.90	495.70	507.99	13.69	261.32	0.2365
13	510.48	487.52	513.74	13.72	259.28	0.2333
14	515.45	492.49	507.43	13.72	258.72	0.2343
15	512.26	489.30	509.77	13.71	258.41	0.2335
16	512.11	494.91	513.55	13.69	263.57	0.2373
17	515.42	498.22	510.54	13.69	263.78	0.2381
18	513.92	496.72	509.93	13.69	262.67	0.2373
19	520.55	497.59	500.86	13.81	256.35	0.2337
20	517.34	494.38	507.47	13.82	257.86	0.2335
21	520.57	497.61	501.20	13.82	256.34	0.2336
22	518.38	501.18	501.76	13.80	258.70	0.2356
23	517.04	499.84	504.73	13.81	259.35	0.2355
24	518.92	501.72	501.44	13.82	258.45	0.2354
25	517.53	506.07	507.19	13.80	264.12	0.2392
26	520.26	508.80	502.25	13.81	262.77	0.2392
27	516.57	505.11	502.67	13.82	260.88	0.2374

NO	WENGC	P465M	MACHCF
1	22.96	175.75	0.2689
2	22.96	174.92	0.2684
3	22.96	177.00	0.2689
4	17.20	130.61	0.1969
5	17.20	130.70	0.1978
6	17.20	129.62	0.1968
7	22.96	175.99	0.2693
8	22.96	175.40	0.2683
9	22.96	176.76	0.2695
10	17.20	130.26	0.1970
11	17.20	131.00	0.1981
12	17.20	130.35	0.1965
13	22.96	176.93	0.2686
14	22.96	175.14	0.2668
15	22.96	176.28	0.2677
16	17.20	130.56	0.1974
17	17.20	129.69	0.1967
18	17.20	130.08	0.1967
19	22.96	173.34	0.2630
20	22.96	174.47	0.2647
21	22.96	173.34	0.2629
22	17.20	128.93	0.1935
23	17.20	129.27	0.1939
24	17.20	128.79	0.1931
25	11.47	85.11	0.1279
26	11.46	84.65	0.1272
27	11.46	85.27	0.1272

```
      IMPLICIT REAL*8 (A-H,O-Z)
      DIMENSION ALPHA(24),WENG(24),TEMP(24),PSINF(24),QH2O(24),
     +        RHO(24),ZMACH(24),VINF(24),WL(24),WR(24),PSR(24),TSR(24),
     +        ZMACHR(24),VINFR(24),ZMACHCF(24),P465M(24),WENGC(24)
      DATA ALPHA/15.0,15.0,15.0,15.0,15.0,15.0,15.0,15.0,15.0,15.0,
     +          15.0,15.0,0.0,0.0,0.0,0.0,0.0,0.0,0.0,0.0,0.0,0.0,
     +          0.0,0.0/
      DATA WENG/22.96,22.96,22.96,17.2,17.2,17.2,22.96,22.96,22.96,
     +         17.2,17.2,17.2,22.96,22.96,22.96,17.2,17.2,17.2,
     +         22.96,22.96,22.96,17.2,17.2,17.2/
      DATA TEMP/48.66,51.33,52.00,51.33,51.00,52.33,53.00,52.66,
     +         53.66,56.33,52.33,53.66,55.33,52.66,55.66,56.33,
     +         56.67,57.00,56.67,57.67,48.67,51.67,54.33,53.67/
      DATA PSINF/13.85,13.86,13.85,13.86,13.86,13.86,13.86,13.86,
     +          13.84,13.84,13.84,13.84,13.84,13.84,13.77,13.77,
     +          13.76,13.76,13.74,13.74,13.75,13.74,13.74,13.74/
      DATA QH2O/14.4,13.8,14.2,13.8,13.8,14.0,13.9,13.9,13.8,
     +         14.2,14.2,13.9,13.9,14.2,14.0,13.9,14.1,14.0,
     +         14.2,14.0,14.0,14.0,13.9,13.8/
      WRITE(6,100)
  100 FORMAT(15X,'AXISYME ENGINE INLET MODEL, SEPT 21,85(SATURDAY)-',
     1 /,25X,'SEPT 23,1985 (MONDAY) TEST DATA'/)
      WRITE(6,200)
  200 FORMAT(6X,'NO',2X,'ALPHA',2X,'WENG',5X,'TINF',3X,'PINF',3X,'QH2O'
     1,3X,'RHOINF',4X,'VINF',4X,'MPH',4X,'MACHL')
C
      G=1.4
      R=53.35241
      C=27.678
      GC=32.17405
      DO 10 I=1,24
      RHO(I)=PSINF(I)*144.0/R/(460.0+TEMP(I))
      ZMACH(I)=DSQRT(2./(G-1.)*((QH2O(I)/C/PSINF(I)+1.)**((G-1.)/G)-1.))
      VINF(I)=ZMACH(I)*49.022325*DSQRT(460.0+TEMP(I))
      ZMPH=VINF(I)*60.0/88.0
   10 WRITE(6,300)I,ALPHA(I),WENG(I),TEMP(I),PSINF(I),QH2O(I),RHO(I),
     1 VINF(I),ZMPH,ZMACH(I)
  300 FORMAT(5X,I3,1X,F5.1,2X,F6.2,2X,F6.2,1X,F6.2,1X,F6.2,1X,F9.6,1X,
     1 F7.3,1X,F7.3,1X,F7.4)
C
C     LEFT BOUNDARY DATA
C
      AL = 4071.50408
C
C     RIGHT BOUNDARY DATA
C
      AR=3772.85643
C
      WRITE(6,400)
  400 FORMAT(/6X,'NO',2X,'  WL ',2X,' WR ',5X,'TSR ',3X,'PSR',3X,'VINFR',
     1 4X,'MACHR'2X,'WENGC',3X,'P465M',4X,'MACHCF')
      DO 20 I=1,24
      WL(I) = RHO(I)*VINF(I)*AL/144.0
      WR(I) = WL(I) - WENG(I)
      PTL=PSINF(I)*(1.0+0.2*ZMACH(I)**2)**3.5
      TTR=460.0+TEMP(I)
      WFR=WR(I)*DSQRT(TTR)/AR/PTL
      CALL WFT(WR(I)*60.0,WFR,AMACH,PRR,TR,DUM)
      ZMACHR(I) = AMACH
      PSR(I) = PTL/PRR
```

```
      TSR(I) = TTR/TR
      VINFR(I) = ZMACHR(I)*49.022325*DSQRT(TSR(I))
C     WRITE(6,500)I,WL(I),WR(I),TSR(I),PSR(I),VINFR(I),ZMACHR(I)
   20 CONTINUE
  500 FORMAT(4X,I3,5X,F6.2,6X,F6.2,6X,F6.2,6X,F6.2,7X,F6.2,4X,F7.4)
C
C     COMPRESSOR FACE
C
      AC =  176.714587
C
C     WRITE(6,600)
  600 FORMAT(6X,'NO',5X,'WENGC',6X,'P465M',9X,'MACHCF')
      DO 40 I=1,24
C
      KOUNT=0
      XL = 0.05
      XH = 0.40
   30 CONTINUE
      KOUNT=KOUNT+1
      ZMACHCF(I)=(XL+XH)/2.0
      P465M(I) = AC*ZMACHCF(I)/ZMACHR(I)*((1.0+0.2*ZMACHR(I)**2)/
     1                                    (1.0+0.2*ZMACHCF(I)**2))**3.0
      WENGC(I) = 1.0/R*PSR(I)*VINFR(I)/TSR(I)*P465M(I)
      DB=DABS(WENGC(I)-WENG(I))
      IF(DB .LT. 0.00001 .OR. KOUNT .GT. 30)GO TO 35
      IF(WENGC(I) .LT. WENG(I)) XL = ZMACHCF(I)
      IF(WENGC(I) .GT. WENG(I)) XH = ZMACHCF(I)
      GO TO 30
   35 WRITE(6,700)I,WL(I),WR(I),TSR(I),PSR(I),VINFR(I),ZMACHR(I),
     + WENGC(I),P465M(I),ZMACHCF(I)
   40 CONTINUE
  700 FORMAT(5X,I3,1X,F6.2,2X,F6.2,2X,F6.2,F6.2,2X,F6.2,1X,F7.4,
     +  1X,F6.2,3X,F6.2,2X,F7.4)
      STOP
      END
```

AXISYME ENGINE INLET MODEL, SEPT 21,85(SATURDAY)-
SEPT 23,1985 (MONDAY) TEST DATA

NO	ALPHA	WENG	TINF	PINF	QH2O	RHOINF	VINF	MPH	MACHL
1	15.0	22.96	48.66	13.85	14.40	0.073490	254.435	173.478	0.2301
2	15.0	22.96	51.33	13.86	13.80	0.073159	249.709	170.256	0.2253
3	15.0	22.96	52.00	13.85	14.20	0.073011	253.513	172.850	0.2285
4	15.0	17.20	51.33	13.86	13.80	0.073159	249.709	170.256	0.2253
5	15.0	17.20	51.00	13.86	13.80	0.073207	249.629	170.201	0.2253
6	15.0	17.20	52.33	13.86	14.00	0.073017	251.735	171.638	0.2269
7	15.0	22.96	53.00	13.86	13.90	0.072921	251.010	171.143	0.2261
8	15.0	22.96	52.66	13.86	13.90	0.072970	250.927	171.087	0.2261
9	15.0	22.96	53.66	13.84	13.80	0.072722	250.456	170.766	0.2254
10	15.0	17.20	56.33	13.84	14.20	0.072346	254.673	173.641	0.2286
11	15.0	17.20	52.33	13.84	14.20	0.072911	253.685	172.967	0.2286
12	15.0	17.20	53.66	13.84	13.90	0.072722	251.351	171.375	0.2262
13	0.0	22.96	55.33	13.84	13.90	0.072487	251.759	171.654	0.2262
14	0.0	22.96	52.66	13.84	14.20	0.072864	253.767	173.023	0.2286
15	0.0	22.96	55.66	13.77	14.00	0.072074	253.366	172.749	0.2276
16	0.0	17.20	56.33	13.77	13.90	0.071981	252.635	172.251	0.2268
17	0.0	17.20	56.67	13.76	14.10	0.071881	254.598	173.589	0.2285
18	0.0	17.20	57.00	13.76	14.00	0.071835	253.786	173.036	0.2277
19	0.0	22.96	56.67	13.74	14.20	0.071776	255.671	174.321	0.2294
20	0.0	22.96	57.67	13.74	14.00	0.071638	254.132	173.272	0.2278
21	0.0	22.96	48.67	13.75	14.00	0.072958	251.823	171.698	0.2278
22	0.0	17.20	51.67	13.74	14.00	0.072478	252.655	172.265	0.2278
23	0.0	17.20	54.33	13.74	13.90	0.072103	252.417	172.102	0.2270
24	0.0	17.20	53.67	13.74	13.80	0.072196	251.357	171.380	0.2262

NO	WL	WR	TSR	PSR	VINFR	MACHR	WENGC	P465M	MACHCF
1	528.69	505.73	503.02	13.82	260.30	0.2367	22.96	171.29	0.2290
2	516.53	493.57	505.91	13.83	255.27	0.2315	22.96	175.51	0.2298
3	523.34	500.38	506.41	13.82	259.26	0.2350	22.96	173.12	0.2299
4	516.53	499.33	505.77	13.82	258.42	0.2344	17.20	129.96	0.1697
5	516.70	499.50	505.45	13.82	258.34	0.2344	17.20	129.92	0.1697
6	519.71	502.51	506.68	13.82	260.55	0.2361	17.20	129.14	0.1698
7	517.53	494.57	507.52	13.83	256.61	0.2324	22.96	175.15	0.2302
8	517.70	494.74	507.18	13.83	256.53	0.2324	22.96	175.09	0.2301
9	514.98	492.02	508.21	13.81	255.99	0.2316	22.96	176.06	0.2307
10	520.95	503.75	510.55	13.80	263.58	0.2380	17.20	128.82	0.1706
11	522.98	505.78	506.59	13.80	262.59	0.2380	17.20	128.30	0.1700
12	516.82	499.62	508.03	13.80	260.11	0.2354	17.20	129.88	0.1703
13	515.98	493.02	509.82	13.81	257.33	0.2325	22.96	175.70	0.2311
14	522.81	499.85	507.06	13.81	259.50	0.2351	22.96	173.30	0.2302
15	516.32	493.36	510.08	13.74	258.96	0.2339	22.96	175.58	0.2323
16	514.16	496.96	510.64	13.73	261.38	0.2359	17.20	130.58	0.1716
17	517.44	500.24	510.89	13.72	263.44	0.2377	17.20	129.72	0.1717
18	515.46	498.26	511.26	13.72	262.57	0.2369	17.20	130.24	0.1718
19	518.87	495.91	510.99	13.71	261.34	0.2358	22.96	174.68	0.2329
20	514.75	491.79	512.06	13.71	259.69	0.2341	22.96	176.14	0.2333
21	519.47	496.51	503.15	13.72	257.45	0.2341	22.96	174.47	0.2309
22	517.76	500.56	505.98	13.70	261.44	0.2371	17.20	129.64	0.1712
23	514.59	497.39	508.65	13.70	261.15	0.2362	17.20	130.47	0.1717
24	513.09	495.89	508.04	13.70	260.04	0.2353	17.20	130.86	0.1716

```
      SUBROUTINE WFT (W,WFF,AM,PR,TR,CHOKED)
C
C     PROGRAMMED BY W. SEIBEL
C
C     THIS ROUTINE SOLVES THE WEIGHT FLOW FUNCTION EQUATION FOR
C     THE MACH NUMBER.
C
C       ---- INPUT PARAMETERS----
C     NAME    DESCRIPTION                              DIMENSIONS
C
C     WFF     WEIGHT FLOW FUNCTION
C
C       ---- OUTPUT PARAMETERS----
C     NAME    DESCRIPTION                              DIMENSIONS
C
C     AM      MACH NUMBER
C     PR      PRESSURE RATIO
C     TR      TEMPERATURE RATIO
C
      IMPLICIT REAL*8 (A-H,O-Z)
      LOGICAL CHOKED
      DATA EPS /Z            2500/
C
C     GAMMA = 1.4
C     GC = 32.17405
C     R  = 53.35241
C     C1 = (GAMMA - 1.0)/2.0 = 0.2
C     C2 = GAMMA/(GAMMA - 1.0) = 3.5
C     C3 = (GAMMA + 1.0)/(2.0*GAMMA - 2.0) = 3.0
C     D = GAMMA*GC/R = 0.8442668288
C     E = SQRT(D) = 0.9188399364
C     F = D*D = 0.71278648
C     G = 2.0*D*C1 = 0.337707
C     H = 2.0*G = 0.67541346
C
      CHOKED = .FALSE.
      WFFMAX = 0.5317359
      IF (WFF .GT. 0.531735)  GO TO 130
      IF (WFF) 140,120,10
   10 B = 0.5
C     Z = 1.0 + 0.2*B*B
      Z = 1.05
C     ZZ = Z*Z
      ZZ = 1.1025
      WZ = WFF*Z
C     FB = E*B - WFF*(1.0 + C1*B*B)**C3
      FB = 0.4594199682 - 1.157625*WFF
      IF (FB) 30,90,20
   20 C = 0.0
      FC = -WFF
      GO TO 40
   30 C = 1.0
      FC = 0.9188399364 - 1.728*WFF
   40 A = C
      FA = FC
      KOUNT = 1
C
   50 IF (DSIGN(FB,FC) .NE. FB)  GO TO 60
      IF (DSIGN(FA,FB) .EQ. FA)  GO TO 140
      C = A
```

```
      FC = FA
   60 IF (DABS(FB) .LE. DABS(FC))  GO TO 70
      A = B
      B = C
      C = A
      FA = FB
      FB = FC
      FC = FA
   70 IF (DABS(C - B) .LT. EPS)  GO TO 90
      IF (KOUNT .GE. 30)  GO TO 140
      KOUNT = KOUNT + 1
      X = (B + C)/2.0
      S = 0.9188399364 - 1.2*B*WZ*Z
      IF (DABS(S) .LT. EPS)  GO TO 80
      S = B - FB/(0.9188399364 - 1.2*B*WZ*Z)
      IF (DABS(S - B) .LT. EPS) S = S + DSIGN(EPS,(C - B))
      IF ((S.GT.B .AND. S.LT.X) .OR. (S.GT.X .AND. S.LT.B))  X = S
   80 A = B
      FA = FB
      B = X
C     FB = E*B - WFF*(1.0 + C1*B*B)**C3
      Z = 1.0 + 0.2*B*B
      ZZ = Z*Z
      WZ = WFF*Z
      FB = 0.9188399364*B - WZ*ZZ
      FB = 0.9188399364*B - WFF*(1.0 + 0.2*B*B)**3
      IF (FB .NE. 0.0)  GO TO 50
   90 AM = B
      GO TO 110
C
      ENTRY WFS (W,WFF,AM,PR,TR)
C
      WFFMAX = 1.006536
      IF (WFF .GT. 1.00653)  GO TO 130
      IF (WFF) 140,120,100
C     AM = SQRT((SQRT(F + H*WFF*WFF) - D)/G)
  100 AM = SQRT(SQRT(0.71278648 + 0.67541346*WFF*WFF) - 0.844266)
     +                                                    /0.5811255
      IF (AM .GT. 1.0)  GO TO 130
C
C     TR = 1.0 + C1*AM*AM
  110 TR = 1.0 + 0.2*AM*AM
C     PR = TR**C2
      PR = TR**3.5
      RETURN
C
  120 AM = 0.0
      TR = 1.0
      PR = 1.0
      RETURN
C
  130 AM = 1.0
C     TR = 1.0 + C1
      TR = 1.2
C     PR = TR**C2
      PR = 1.892929159
      WC = 1.006545397*W/WFF
      CHOKED = .TRUE.
      RETURN
C
```

```
  140 WRITE (6,1000) W,WFF,WFFMAX,WC,AM,A,FA,B,FB,C,FC,KOUNT
 1000 FORMAT ('0***ERROR*** FAIL IN SUBROUTINE "WFT" (OR ENTRY "WFS")'/
     +         13X,'W      =',1PE15.7,', WFF    =',E15.7/
     +         13X,'WFFMAX =',1PE15.7,', WC     =',E15.7/
     +         13X,'AM     =',1PE15.7 /
     +         13X,'A      =',1PE15.7,', FA     =',E15.7/
     +         13X,'B      =',1PE15.7,', FB     =',E15.7/
     +         13X,'C      =',1PE15.7,', FC     =',E15.7/
     +         13X,'KOUNT  =',I15/
     +         13X,'RUN TERMINATED')
      STOP
C
      END
```

APPENDIX I: NOMENCLATURE

A_f	frontal area of a body, projected parallel to freestream velocity direction
A_{inlet}	area of inlet plane
$A_{\infty,m}$	area, perpendicular to freestream direction, defined by the tangent trajectories
a	projected area of spherical, particle, Equation (D-2)
a	$\frac{1}{2}\left(\frac{1}{K_\infty} + K_\infty\right)$, Equation (5-3)
$\overline{B}$	buoyancy force acting on a droplet
BNC	Berkeley's Nucleonics Corporation
b	$\frac{1}{2}\left(\frac{1}{K_\infty} - K_\infty\right)$, Equation (5-3)
C_D	droplet drag coefficient
$C_{D_{inc}}$	incompressible sphere drag coefficient
c	dye concentration, Equation (F-5)
$\overline{D}$	fluid dynamic drag force acting on the droplet
d	droplet diameter
d_i	droplet diameter, group i
dA_s	infinitesimal impingement area on body surface, Figure 2.1
dA_∞	infinitesimal freestream area corresponding to dA_s, Figure 2.1
E	total impingement efficiency in clouds of uniform droplet size, Equation (2-9)
$\overline{E}$	total impingement efficiency in clouds of nonuniform droplet size
G	Cunningham drag correction factor
$\overline{G}$	gravity force acting on a droplet
g	gravitational acceleration

He-Ne	Helium - Neon gas-type laser
IAS	Indicated Air Speed
IRT	Icing Research Tunnel
I_o	intensity of incident beam, Figure 5.2
i	intensity of light traveling inside a specimen towards its illuminated surface, Figure 5.2
$\bar{i}, \bar{j}, \bar{k}$	unit vectors // to x, y, z axis
J	intensity of reflected beam, Figure 5.2
j	intensity of light travelling inside a specimen towards its illuminated surface, Figure 5.2
K	inertia parameter, Equation (2-1)
K	dye absorption coefficient, Equation (5-2)
L	characteristic dimension of body
LWC_s	liquid water content at body surface
LWC_∞	liquid water content of droplet cloud at freestream
M	Mach number of air flow relative to droplet
M_{CF}	Mach number of air flow at compressor face
M_∞	Mach number of air flow at freestream
MVD	Mean Volumetric Diameter of the droplet cloud
N	number of droplet groups available in a discrete droplet distribution
n(x)	number of droplets for dropsize diameter x (or d)
$\bar{n}_s$	unit normal vector at body surface (pointing outward)
$\bar{n}_\infty$	unit vector parallel to $\bar{V}_\infty$
P_{AIR}	spray system air pressure
P_{st}	static pressure of air
P_t	total pressure of air
P_{WATER}	spray system water pressure

P_{ws}	wall static air pressure
Q	freestream dynamic pressure
q	velocity head experienced by a droplet in the flow field, Equation (D-2)
R	reflectivity, Equation (5-3)
R	gas constant
Re_{∞}	free stream Reynolds number with respect to droplet diameter
R_g	reflectivity of backing material, Equation (5-3)
R_v	Reynolds number of air flow relative to droplet
R_{∞}	reflectivity of specimen assuming infinite thickness
S	coefficient of scatter per unit depth of specimen
s	distance along surface from point of reference
s_m	distance along surface from point of reference to impingement limit (p), Figure 2.2
TAS	True Air Speed
T_{st}	static air temperature
T_t	total air temperature
t	time, dimensionless with L/V_{∞}
$\overline{t}$	time
U	droplet velocity, dimensionless with V_{∞}
$\overline{U}$	droplet velocity
V	potential flow velocity dimensionless with V_{∞}
$\overline{V}$	potential flow velocity
V_{CC}	collector voltage, Figure C.1
V_{EE}	emitter voltage, Figure C.1
$\overline{V}_{inlet}$	air velocity at inlet plane

V1	photodetector voltage output (reflected beam)
V2	photodetector voltage output (optical feedback)
V_∞	freestream airspeed
$\overline{V}_\infty$	freestream air velocity
W	engine inlet mass flow
$\overline{W}_\beta$	weighted local impingement rate
w_t	total liquid water content of droplet cloud
X	thickness of specimen, Equation (5-3)
x, r, θ	cylindrical coordinates
x, y, z	Cartesian coordinates
y_∞	ordinate of coordinate system perpendicular to freestream velocity direction at $x = -\infty$, Figure 2.2
$y_{\infty,m}$	y_∞ corresponding to tangent trajectory, Figure 2.2
α	angle of attack
β	local impingement efficiency for uniform droplet distribution, Equation (2-7)
$\overline{\beta}$	local impingement efficiency for clouds with non-uniform droplet size, Equations (2-12, 2-13)
γ	ratio of specific heats of air = 1.4
ΔP_{sv}	static pressure difference, Figure B.1
δ_{ij}	Kronecker delta
ε	reflectivity value for zero dye concentration (c = 0), Equation (F-9)
θ	central angle of cylinder measured from x-axis
θ_m	θ for tangent trajectory
μ	absolute air viscosity
ρ	density of air
ρ_p	particle (droplet) density

ρ_w	density of water
σ	density ratio
τ	volume of spherical particle

REFERENCES

1. Olsen, W., "Survey of Aircraft Icing Simulation Test facilities in North America," NASA TM 81707, February 1981.

2. Von Glahn, U.H., Gelder, T.F. and Smyers, W.H., "A Dye-Tracer Technique for Experimentally Obtaining Impingement Characteristics of Arbitrary Bodies and a Method for Determining Droplet Size Distribution," NACA TN 3338, March 1955.

3. Kim, J.J., Breer, M.D., Gass, J. and Kneeling, D., "Sand Separator Efficiency Calculation for the JVX Tilt Rotor Aircraft Inlet," American Helicopter Society, June 1986.

4. Kim, J.J., "Particle Trajectory Computation on a 3-Dimensional Engine Inlet," NASA CR 175023, January 1986.

5. Federal Aviation Regulation Part 25, Appendix C, 1974.

6. Schlichting, H., "Boundary - Layer Theory," 6th Edition, McGraw-Hill, 1968.

7. Gelder, T.F., Smyers, W.H. and Von Glahn, U., "Experimental Droplet Impingement on Several Two-Dimensional Airfoils with Thickness Ratios of 6 to 16 Percent," NACA TN 3839, December 1956.

8. Langmuir, I. and Blodgett, K.B., "A Mathematical Investigation of Water Droplet Trajectories," Army Air Forces Technical Report No. 5418, 1946.

9. Dorsch, R.G., Brun, R.J. and Gregg, J.L., "Impingement of Water Droplets on an Ellipsoid with Fineness Ratio 5 in Axisymmetric Flow," NACA TN 3099, 1954.

10. Dorsch, R.G., Saper, P.G. and Kadow, C.F., "Impingement of Water Droplets on a Sphere," NACA TN 3587, 1955.

11. Lewis, J.P. and Ruggeri, R.S., "Experimental Droplet Impingement on Four Bodies of Revolution," NACA TN 4092, 1957.

12. Gelder, T.F., "Droplet Impingement and Ingestion by Supersonic Nose Inlet in Subsonic Tunnel Conditions," NACA TN 4268, May 1958.

13. Brun, R.J., Gallagher, H.M. and Vogt, D.E., "Impingement of Water Droplets 5A004 Airfoil and Effect of Change in Airfoil Thickness from 12 to 4 Percent at 4 Angles of Attack," NACA TN 3047, 1953.

14. Ide, R.F. and Richter, G.P., "Comparison of Icing Cloud Instruments for 1982-1983 Icing Season Flight Program," NASA TM 83569, January 1984.

15. Reinmann, J.J., Shaw, R.J. and Olsen, W.A., "NASA Lewis Research Center's Program on Icing Research," NASA TM 83031, January 1983.

16. Hunt, J.D., "A Comparison of Particle Diagnostic Systems," AEDC-TR-80-33, August 1981, Arnold Engineering Development Center/DOT, Air Force Systems Command, Arnold Air Force Station, Tennessee 37389.

17. Bentley, H.T., "Fiber Optics Particle-Sizing System," AEDC-TR-73-111, September 1973, Arnold Engineering Development Center/DOT, Air Force Systems Command, Arnold Air Force Station, Tennessee 37389.

18. Breer, M.D., Seibel, W., "Particle trajectory Computer Program - User Manual," Boeing Document D3-9655-1, December 1974.

19. Breer, M.D., Seibel, W. and Lewis-Smith, F.A., "Potential Flow (ZEE921) and Data Preparation (ZEE911) Programs, Users Manual," Boeing Document D3-9821, July 1976.

20. Breer, M.D. and Schmidt, W.F., "Engine Inlet Anti-Icing Study - Proposed for 747," Boeing Document D6-13227, July 1967.

21. Wendlandt, W.M. and Hecht, H.G., "Reflectance Spectroscopy," Interscience Publishers, 1966.

22. Kubelka, P., "New Contributions to the Optics of Intensely Light-Scattering Materials. Part I," Journal of the Optical Society of America, Volume 38, No. 5, May 1948.

23. Goldman, J. and Goodall, R.R., "Quantitative Analysis of Thin Layer Chromatograms: A Theory for Light Absorption Methods with an Experimental Verification," Journal of Chromatography, Vol. 32, 1968.

24. Frei, R.W. and MacNeil, J.D., "Diffuse Reflectance Spectroscopy in Environmental Problem-Solving," CRC Press, 1973.

25. Reyhner, T.A., "Computation of Transonic Potential Flow About Three-Dimensional Inlets, Ducts, and Bodies," NASA CR-3514 (Boeing Document D6-49848, March 1982.

26. "ASCO Red-Hat Solenoid Valves," Catalog No. 31, Automatic Switch Co., Florham Park, New Jersey 07932.

27. Beyer, W.H., "CRC Standard Mathematical Tables," 26th Edition, CRC Press, Inc., 1983.

REPORT DOCUMENTATION PAGE

Form Approved
OMB No. 0704-0188

1. AGENCY USE ONLY (*Leave blank*)	2. REPORT DATE	3. REPORT TYPE AND DATES COVERED
	November 1989	Final Contractor Report

4. TITLE AND SUBTITLE

An Experimental Method for Measuring Water Droplet Impingement Efficiency on Two- and Three-Dimensional Bodies

5. FUNDING NUMBERS

WU–505–68–11
NAG3–566

6. AUTHOR(S)

M. Papadakis, R. Elangonan, G.A. Freund, Jr., M. Breer, G.W. Zumwalt, and L. Whitmer

7. PERFORMING ORGANIZATION NAME(S) AND ADDRESS(ES)

Wichita State University
Aerospace Engineering Department
Wichita, Kansas 67260–0044

8. PERFORMING ORGANIZATION REPORT NUMBER

E–4971

9. SPONSORING/MONITORING AGENCY NAME(S) AND ADDRESS(ES)

National Aeronautics and Space Administration
Lewis Research Center
Cleveland, Ohio 44135–3191
and
Federal Aviation Administration, Technical Center
Atlantic City International Airport, New Jersey 08405

10. SPONSORING/MONITORING AGENCY REPORT NUMBER

NASA CR–4257
DOT/FAA/CT–87/22

11. SUPPLEMENTARY NOTES

Prepared under Interagency Agreement DTFA03–81–A–00209 with the FAA Technical Center. M. Papadakis and G.W. Zumwalt, Wichita State University, Wichita, Kansas 67260–0044 (work funded by NASA Grant NAG3–566); R. Elangonan, G.A. Freund, Jr., M. Breer, and L. Whitmer, Boeing Military Airplanes, Wichita, Kansas. Project Managers, Colin S. Bidwell and Robert J. Shaw, Turbomachinery and Propulsion Systems Division, organization code RTI, 216–433–3947; and James T. Riley, Federal Aviation Administration, Technical Center, 609–485–4144.

12a. DISTRIBUTION/AVAILABILITY STATEMENT

Document Availability Change Notice

This document was published in November 1989 with a restriction. It was changed March 2005 to Unclassified/Unlimited per DAA modified March 30, 2005.

~~**For U.S. Government Agencies and U.S. Government Agency Contractors Only**~~

Unclassified - Unlimited
Subject Category 03
Available electronically at http://gltrs.grc.nasa.gov
This publication is available from the NASA Center for Aerospace Information, (301) 621–0390.

12b. DISTRIBUTION CODE

13. ABSTRACT ***(Maximum 200 words)***

An experimental method has been developed to determine the water droplet impingement characteristics on two- and three-dimensional bodies. The experimental results provide the essential droplet impingement data required to validate water droplet trajectory codes, which are used in the analysis of aircraft icing. A body, whose water droplet impingement characteristics are required, is covered at strategic locations by thin strips of moisture absorbing (blotter) paper, and is exposed to an air stream containing a water-dye solution spray cloud. Water droplet impingement data are extracted from the dyed blotter strips by measuring the optical reflectance of the dye deposit on the strips, using an automated reflectometer. Models tested include a 4-inch-diameter cylinder, a NACA 652015 airfoil section, a MS(1)–0317 supercritical airfoil section, three simulated ice shapes, an axisymmetric inlet and a Boeing 737–300 inlet model. Detailed descriptions of the dye-tracer technique, instrumentation, data reduction method and the results obtained are presented in this report. Analytical predictions of collection efficiency characteristics for most test configurations are included for comparison.

14. SUBJECT TERMS

Trajectory code validation; Water droplet trajectories; Experimental trajectory data; Impingement characteristics; Impingement data; Experimental impingement data; Trajectory codes

15. NUMBER OF PAGES

399

16. PRICE CODE

17. SECURITY CLASSIFICATION OF REPORT	18. SECURITY CLASSIFICATION OF THIS PAGE	19. SECURITY CLASSIFICATION OF ABSTRACT	20. LIMITATION OF ABSTRACT
Unclassified	Unclassified	Unclassified	